Instituto de Agroquímica y Tecnología de Alimentos

Grupo de Nuevos Materiales y Nanotecnología para Aplicaciones Alimentarias

Universidad Politécnica de Valencia

Doctorado en Ciencia, Tecnología y Gestión Alimentaria

Tesis Doctoral Internacional

DEVELOPMENT AND CHARACTERIZATION OF MONOLAYERS AND MULTILAYERS BASED ON BIODEGRADABLE MATERIALS DERIVED FROM WASTE AND BY-PRODUCTS OF INTEREST IN FOOD PACKAGING

DESARROLLO Y CARACTERIZACIÓN DE MONOCAPAS Y MULTICAPAS BASADOS EN MATERIALES BIODEGRADABLES DERIVADOS DE RESIDUOS Y SUBPRODUCTOS DE INTERÉS EN ENVASES ALIMENTARIOS

Beatriz Meléndez Rodríguez

Supervised by:

Dr. José María Lagarón

Dr. Sergio Torres Giner

Dr. Luis Cabedo Mas

Valencia, abril 2022

Dr. José María Lagarón Cabello, Investigador Científico del Consejo Superior de Investigaciones Científicas (CSIC) en el Instituto de Agroquímica y Tecnología de Alimentos (IATA), Dr. Sergio Torres Giner, Investigador Ramón y Cajal en la Universidad Politécnica de Valencia (UPV) y Dr. Luis Cabedo Mas, Profesor titular de la Universidad Jaume I (UJI)

CERTIFICAN

Que la presente memoria titulada "**Desarrollo y caracterización de monocapas y multicapas basados en materiales biodegradables derivados de residuos y subproductos de interés en envases alimentarios**" constituye la tesis doctoral de Beatriz Meléndez Rodríguez y reúne las condiciones adecuadas para su presentación. Asimismo, certifican haber dirigido y supervisado tanto los distintos aspectos del trabajo como la redacción.

Y para que así conste a los efectos oportunos, firmamos la presente en Valencia a abril de 2022.

Fdo. José María Lagarón Cabello

Fdo. Sergio Torres Giner

Fdo. Luis Cabedo Mas

A mis padres, Flori y José Manuel,

a mi hermana Flori y

a Damián,

por ser siempre mi apoyo incondicional.

AGRADECIMIENTOS

Parece increíble que haya llegado el momento de cerrar esta etapa de mi vida. Aquella que empezó hace algo más de cuatro años cuando, decidida a realizar el doctorado, me lancé a escribir a los investigadores cuyos proyectos me resultaron interesantes. Este viaje que parecía tan largo ha pasado en un abrir y cerrar de ojos. Gracias a la Vida, que me llevó de manera inesperada a esta tierra maravillosa, Valencia, la cual me enamoró desde el primer día y a la que siempre llevaré en mi corazón.

En primer lugar, agradecer a mis directores de tesis su apoyo durante estos años. A José María Lagarón, por abrirme las puertas de su laboratorio y confiar en mí tanto para la realización de esta tesis como para los diferentes proyectos que fueron surgiendo, dándome la oportunidad de visitar tantos lugares del mundo y conocer gente interesante. A Sergio Torres, por su ayuda y compromiso constantes. Sin ti estos años habrían sido más difíciles y menos divertidos. A Luis Cabedo, por su asistencia y colaboración cuando han sido necesarias, a pesar de la distancia.

Gracias a mis compañeros del mejor laboratorio, el 502, por hacer de él un lugar agradable y divertido que sentía como mi casa, y a las nuevas incorporaciones que a lo largo de estos años no hicieron más que mejorarlo. Kelly, Alberto, Cristina, Carmen, Zoran, María, Álvaro, Yuliana, gracias por los buenos momentos vividos tanto dentro como fuera del laboratorio, esta andadura no habría sido la misma sin vosotros. Tampoco sin Selomit, que siempre fue una más del grupo. Agradecer igualmente a todas las personas que han pasado por el laboratorio, que no han sido pocas, por contribuir también a enriquecer esta experiencia. Mención especial a Stella, Lorenzo y Laura, cuya implicación y colaboración se han visto reflejadas en algunas de las publicaciones científicas. No me olvido de nuestros compañeros de la Universitat Jaume I, Patricia, Abdulaziz, Estefanía, Jaume, quienes, además de ayudar con las mediciones, me han hecho pasar muy buenos momentos.

También, quiero agradecer a todo el personal que trabaja en el Instituto de Agroquímica y Tecnología de Alimentos su amabilidad y ayuda siempre que ha sido necesario. A los técnicos del SCSIE de la Universidad de Valencia, por su asistencia durante las largas horas de microscopía. A Chris Sammon, por la acogida en su grupo de Sheffield y su implicación y enseñanza durante mi estancia. Gracias también a Esther que me ofreció su ayuda y me abrió las puertas de su casa sin conocerme. Al personal de Gaiker, especialmente a Inmaculada Angulo, que siempre estuvieron dispuestos a colaborar y hacer de nuestras visitas unos días muy enriquecedores y productivos.

Por último, quiero darle las gracias y dedicar esta tesis a mi familia, sin la cual esta no habría sido posible. A mis padres, Flori y José Manuel, por su apoyo constante y su ejemplo de lucha, trabajo, humildad y cariño. Gracias por todo lo que hacéis día a día, sin una queja y siempre alegres y optimistas, sois mi modelo a seguir. A mi hermana Flori, por estar siempre dispuesta a ayudarme y ser el espejo en el que mirarme, por haber tenido que abrir camino y hacerlo todo mucho más fácil. Os quiero mucho. Finalmente, agradecer a mi compañero de vida, Damián, con quien la comparto desde la mitad de mi existencia, por acompañarme en esta aventura del doctorado desde el primer momento, y a su familia por el apoyo y cariño durante estos años. Damián gracias por estar ahí, apoyarme siempre y ser un ejemplo de superación. Deseando comenzar juntos este nuevo camino que empieza. Te quiero.

A todos gracias por haber formado parte de esta etapa tan bonita de mi vida.

ABSTRACT

The production and consumption of petroleum derived plastics that are not biodegradable has grown exponentially in recent decades, with the consequent impact on nature and organisms. The food packaging sector is today considered the main source of plastic contamination. Therefore, the study and development of new materials derived from renewable and biodegradable resources has emerged as a new field of great scientific, social, economic and political interest. The current PhD thesis focused on the development and characterization of polyhydroxyalkanoate (PHA) biopolymers derived from agro-industrial by-products (fruit pulp and cheese whey) and from the organic fraction of municipal wastewater, the municipal biowaste, synthesized by mixed microbial cultures (MMCs) and produced by electrospinning and melt compounding technologies. The resultant materials were particularly developed to obtain high-oxygen-barrier active monolayers and multilayers for use in Circular Bioeconomy-based food packaging.

In order to achieve the objectives, this PhD thesis has been divided into three blocks according to the technology used to obtain the materials. The first block consisted of the extraction of PHAs derived from agro-industrial waste for their optimal use in production processes. After this, the PHAs were then processed using the electrospinning technique, whereby polymeric fibers were obtained and thermally post-treated by an annealing process, at temperatures below the melting temperature of the polymer used, to form continuous and homogeneous films, also known as "biopapers". These monolayers showed good thermal and mechanical properties, as well as a high barrier to both vapors and gases. In addition, the fibers were functionalized with eugenol, an organic compound present in essential oils, to provide them with active antimicrobial function against foodborne microorganisms. On the other hand, the electrospinning of poly(ethylene-*co*-vinyl alcohol) (EVOH) copolymers, a synthetic polymer that is claimed to biodegrade under specific conditions and with high oxygen barrier, was performed. Cellulose nanocrystals (CNCs) were added to EVOH, to create high barrier more sustainable hybrid monolayers.

In the second block, the materials were processed using the melt compounding technique. For this purpose, the biomass derived PHAs extracted in the first block were blended with commercial PHAs as well as with cellulosic fillers, in this case rice husk flour (RHF), in order to form "green composites", where all the materials were based on renewable and biodegradable resources. After film formation by hot pressing, the blends showed excellent miscibility and optical properties, improved flexibility, as well as barrier properties similar to the neat biopolyester material.

Finally, in the third block, multilayer systems were produced using ad-hoc developed PHA blends, and PHA electrospun monolayer materials developed in the first block. They were based on the adhesive properties of the electrospun fibers after thermal treatment, which allowed the elimination of synthetic adhesive substances normally used in the industry, and on the use of the CNCs coatings as oxygen barrier interlayers. Thus, the multilayer systems developed were fully compostable, with high oxygen barrier, being potential candidates to replace current food packaging based on non-renewable petroleum-based materials.

Therefore, the materials developed herein are very promising bioadhesives showing antimicrobial and high barrier properties, as well as outer layers for structural or thin film purposes. Thus, by lamination, these materials can result in self-standing multilayer films, which can be used in rigid

or semirigid packaging as well as in flexible packaging. They are sustainable and environmentally friendly, as they are made from renewable sources or waste, and are biodegradable by composting, and, in some case, even biodegradable in the environment. Furthermore, they are potentially capable of providing comparable quality and food safety to those currently marketed from petrochemical sources.

RESUMEN

La producción y el consumo de plásticos derivados de petróleo ha crecido exponencialmente en las últimas décadas, con el consecuente impacto en la naturaleza y los seres vivos. El sector de los envases alimentarios es considerado actualmente la principal fuente de contaminación por plásticos. Por ello, el estudio y desarrollo de nuevos materiales derivados de recursos renovables y biodegradables ha emergido como un nuevo campo de gran interés tanto a nivel científico como social, económico y político. La presente tesis doctoral se enfocó en el desarrollo y caracterización de biopolímeros de polihidroxialcanoato (PHA) derivados de subproductos industriales (pulpa de frutas y suero de queso) y de la fracción orgánica de aguas residuales municipales, los residuos biológicos municipales, sintetizados por cultivos microbianos mixtos (MMCs) y producidos mediante las tecnologías de electroestirado y mezclado en fundido. Los materiales resultantes fueron desarrollados especialmente para obtener monocapas y multicapas activas y de alta barrera a oxígeno para su uso en envases alimentarios basados en la Bioeconomía Circular.

Para lograr los objetivos, esta tesis doctoral se ha dividido en tres bloques según la tecnología utilizada en la obtención de los materiales. El primer bloque consistió en la extracción de los PHAs derivados de residuos agro-industriales para su óptima utilización en los procesos de producción. Posteriormente, se realizó el procesado de los PHAs mediante la técnica de electroestirado, por la cual se obtuvieron fibras poliméricas que fueron tratadas térmicamente en un proceso de recocido, a temperaturas inferiores al punto de fusión del polímero utilizado, para formar films continuos y homogéneos, también denominados “biopapers”. Estas monocapas presentaron buenas propiedades térmicas y mecánicas, así como alta barrera tanto a vapores como a gases. Además, las fibras fueron funcionalizadas con eugenol, un compuesto orgánico presente en aceites esenciales, para proporcionarles una función antimicrobiana activa contra microorganismos trasmitidos por los alimentos. Por otro lado, se realizó el electroestirado de copolímeros de etileno-alcohol vinílico (EVOH), un polímero sintético que se afirma que se biodegrada en condiciones específicas y que posee alta barrera a oxígeno. Además, nanocristales de celulosa (CNCs) fueron añadidos al EVOH, para crear monocapas híbridas de alta barrera más sostenibles.

En el segundo bloque, los materiales se procesaron mediante la técnica de mezclado en fundido. Para ello, los PHAs derivados de biomasa extraídos en el primer bloque se mezclaron con PHAs comerciales, así como con cargas celulósicas, en este caso harina de cáscara de arroz (RHF), para formar “compuestos verdes”, en el que todos los materiales estaban basados en recursos renovables y biodegradables. Tras la formación de films por prensado en caliente, las mezclas mostraron buena miscibilidad y propiedades ópticas, una flexibilidad mejorada, así como propiedades de barrera similares a las del material de biopoliéster puro.

Finalmente, en el tercer bloque, se produjeron sistemas multicapas utilizando mezclas de PHA desarrolladas ad-hoc, y materiales monocapa de PHA electroestirado desarrollados en el primer bloque. Estas estructuras multicapas se basaron en las propiedades adhesivas que poseen las fibras electroestiradas tras aplicarles el tratamiento térmico, lo que permite eliminar las sustancias adhesivas sintéticas normalmente utilizadas en la industria, y en el uso de los revestimientos de CNCs como capas intermedias de barrera a oxígeno. Así, los sistemas multicapas desarrollados fueron totalmente compostables, con alta barrera a oxígeno, siendo potenciales candidatos para

sustituir a los actuales envases alimentarios basados en materiales no renovables provenientes del petróleo.

Por lo tanto, los materiales aquí desarrollados son tanto bioadhesivos muy prometedores que muestran propiedades antimicrobianas y de alta barrera, como capas exteriores con fines estructurales o para uso como films finos. Así, por laminación, estos materiales pueden dar lugar a films multicapas autoadhesivos, los cuales pueden ser empleados tanto en envases rígidos o semirrígidos como en envases flexibles. Estas estructuras son sostenibles y respetuosas con el medio ambiente, ya que provienen o de fuentes renovables o de residuos, y además son biodegradables mediante compostaje y, en algún caso, incluso biodegradables en el medio ambiente. Asimismo, son potencialmente capaces de proporcionar una calidad y seguridad alimentaria comparables a las que se comercializan actualmente a partir de fuentes petroquímicas.

RESUM

La producció i el consum de plàstics derivats de petroli ha crescut exponencialment en les últimes dècades, amb el conseqüent impacte en la naturalesa i els éssers vius. El sector dels envasos alimentaris és considerat actualment la principal font de contaminació per plàstics. Per això, l'estudi i desenvolupament de nous materials derivats de recursos renovables i biodegradables ha emergit com un nou camp de gran interés tant a nivell científic com social, econòmic i polític. La present tesi doctoral es va enfocar en el desenvolupament i caracterització de biopolímers de polihidroxialcanoato (PHA) derivats de subproductes industrials (polpa de fruites i sèrum de formatge) i de la fracció orgànica d'aigües residuals municipals, els residus biològics municipals, sintetitzats per cultius microbians mixtos (MMCs) i produïts mitjançant les tecnologies de electroestiratge i barrejat en fos. Els materials resultants van ser desenvolupats especialment per a obtindre monocapes i multicapes actives i d'alta barrera a oxigen per al seu ús en envasos alimentaris basats en la Bioeconomía Circular.

Per a aconseguir els objectius, aquesta tesi doctoral s'ha dividit en tres blocs segons la tecnologia utilitzada en l'obtenció dels materials. El primer bloc va consistir en l'extracció dels PHAs derivats de residus agro-industrials per a la seua òptima utilització en els processos de producció. Posteriorment, es va realitzar el processament dels PHAs mitjançant la tècnica de electroestiratge, per la qual es van obtindre fibres polimèriques que van ser tractades tèrmicament en un procés de recuita, a temperatures inferiors al punt de fusió del polímer utilitzat, per a formar films continus i homogenis, també denominats “biopapers”. Aquestes monocapes van presentar bones propietats tèrmiques i mecàniques, així com alta barrera tant a vapors com a gasos. A més, les fibres van ser funcionalitzats amb eugenol, un compost orgànic present en olis essencials, per a proporcionar-los una funció antimicrobiana activa contra microorganismes transmesos pels aliments. D'altra banda, es va realitzar el electroestirado de copolímers d'etilé-alcohol vinílic (EVOH), un polímer sintètic que s'afirma que es biodegrada en condicions específiques i que posseeix alta barrera a oxigen. A més, nanocristalls de cel·lulosa (CNCs) van ser afegits al EVOH, per a crear monocapes híbrides d'alta barrera més sostenibles.

En el segon bloc, els materials es van processar mitjançant la tècnica de barrejat en fos. Per a això, els PHAs derivats de biomassa extrets en el primer bloc es van mesclar amb PHAs comercials, així com amb càrregues cel·lulòsiques, en aquest cas farina de corfa d'arròs (RHF), per a formar “compostos verds”, en el qual tots els materials estaven basats en recursos renovables i biodegradables. Després de la formació de films per premsatge en calent, les mescles van mostrar bona miscibilitat i propietats òptiques, una flexibilitat millorada, així com propietats de barrera similars a les del material de biopolièster pur.

Finalment, en el tercer bloc, es van produir sistemes multicapes utilitzant mescles de PHA desenvolupades ad hoc, i materials monocape de PHA electroestirat desenvolupats en el primer bloc. Aquestes estructures multicapes es van basar en les propietats adhesives que posseeixen les fibres electroestirades després d'aplicar-los el tractament tèrmic, la qual cosa permet eliminar les substàncies adhesives sintètiques normalment utilitzades en la indústria, i en l'ús dels revestiments de CNCs com a capes intermèdies de barrera a oxigen. Així, els sistemes multicapes desenvolupats van ser totalment compostables, amb alta barrera a oxigen, sent potencials

candidats per a substituir als actuals envasos alimentaris basats en materials no renovables provinents del petroli.

Per tant, els materials ací desenvolupats són tant bioadhesius molt prometedors que mostren propietats antimicrobianes i d'alta barrera, com a capes exteriors amb finalitats estructurals o per a ús com a films fins. Així, per laminació, aquests materials poden donar lloc a films multicapes autoadhesius, els quals poden ser emprats tant en envasos rígids o semirígids com en envasos flexibles. Aquestes estructures són sostenibles i respectuoses amb el medi ambient, ja que provenen o de fonts renovables o de residus, i a més són biodegradables mitjançant compostatge i, en algun cas, fins i tot biodegradables en el medi ambient. Així mateix, són potencialment capaços de proporcionar una qualitat i seguretat alimentària comparables a les quals es comercialitzen actualment a partir de fonts petroquímiques.

INDEX

I. Introduction……...…1

1. Food packaging materials……...…...3

1.1. Current packaging status……...…….3

1.2. Polymers used in packaging…….…….4

1.3. Biopolymers as a new alternative…….…….…...….6

2. Polyhydroxyalkanoates for sustainable food packaging……8

2.1. Polyhydroxyalkanoates production through mixed microbial cultures using by-products…….….10

2.2. Circular Bioeconomy……...……13

3. High-oxygen-barrier materials……...….14

3.1. Poly(ethylene-*co*-vinyl alcohol) copolymers……...……16

3.2. Cellulose nanocrystals……...….18

4. Processing technologies in food packaging……...….21

4.1. Melt compounding…….……..….22

4.2. Electrospinning technology…….23

5. Multilayer structures……27

6. References…….…29

II. Objectives……51

General and specific objectives……53

III. Results……56

Block I: Development of interlayers based on polymeric fibers by electrospinning……62

Chapter I: Preparation and characterization of electrospun food biopackaging films of poly(3-hydroxybutyrate-*co*-3-hydroxyvalerate) derived from fruit pulp biowaste……64

Chapter II: Valorization of municipal biowaste into electrospun poly(3-hydroxybutyrate-*co*-3-hydroxyvalerate) biopapers for food packaging applications……94

Chapter III: Development and characterization of electrospun biopapers of poly(3-hydroxybutyrate-*co*-3-hydroxyvalerate) derived from cheese whey with varying 3-hydroxyvalerate contents……125

Chapter IV: Electrospun antimicrobial films of poly(3-hydroxybutyrate-*co*-3-hydroxyvalerate) containing eugenol essential oil encapsulated in mesoporous silica nanoparticles……164

Chapter V: Development and characterization of electrospun fiber-based poly(ethylene-*co*-vinyl alcohol) films of application interest as high-gas-barrier interlayers in food packaging……195

Block II: Development of PHA-based structural layers by melt compounding……234

Chapter VI: Reactive melt mixing of poly(3-hydroxybutyrate)/rice husk flour composites with purified biosustainably produced poly(3-hydroxybutyrate-*co*-3-hydroxyvalerate)……236

Chapter VII: Blends of poly(3-hydroxybutyrate-*co*-3-hydroxyvalerate) with fruit pulp biowaste derived poly(3-hydroxybutyrate-*co*-3-hydroxyvalerate-*co*-3-hydroxyhexanoate) for organic recycling food packaging……266

Block III: Development of barrier multilayer systems based on PHA……..….295

Chapter VIII: Barrier biopaper multilayers obtained by impregnation of electrospun poly(3-hydroxybutyrate-*co*-3-hydroxyvalerate) with protein and polysaccharide hydrocolloids……297

Chapter IX: High-oxygen-barrier multilayer films based on polyhydroxyalkanoates and cellulose nanocrystals…….320

IV. General discussion…….342

General discussion…….344

References…….350

Overall impact of research activities…….……351

V. Conclusions……353

VI. Annexes…….….358

Annex A: List of publications……360

Annex B: Additional works……...……369

I. INTRODUCTION

Introduction

1. Food packaging materials

1.1. Current packaging status

Plastics have been ubiquitous since their mass use began in the 1950s. The development of new technologies, their low cost, high strength and durability, have made plastics the fastest growing artificial material (Geyer, Jambeck, and Law 2017). Plastics production has increased from 1.5 million metric tons in 1950 to 368 million metric tons in 2019, with the largest producers being Asia 51 % (led by China with 31 %), North American Free Trade Agreement (NAFTA) 19 % and Europe 16 % (PlasticsEurope 2020) (**Figure 1a**). This expansion has been driven by the need to meet growing demand as the world's population increases. Plastics are present in all areas of society. **Figure 1b** depicts the plastics demand by segments in Europe in 2020, with 40 % used in packaging applications, of which 90 % correspond to uses related to food preservation, followed by 20 % building and construction, 10 % automotive and 30 % others sectors, which includes electronic, household, and agriculture, among others.

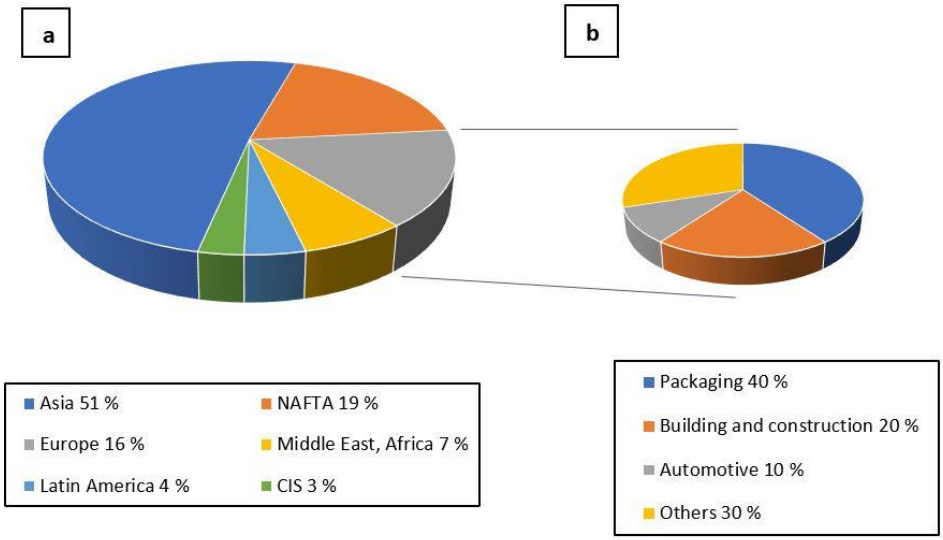

Figure 1. (a) Distribution of global plastics production and (b) plastics demand by segments in Europe in 2020. Source: PlasticsEurope Market Research Group (PEMRG) and Conversio Market & Strategy GmbH.

Therefore, within plastic applications, about one third is used for food packaging, replacing traditional materials such as paper and cardboard, metal and glass (Halonen et al. 2020). Thus, plastic food packaging has meant a great advance, since it increases food safety and quality as well as shelf life of foodstuff, and reduces food waste by improving transportation and preservation (Robertson 2012). However, the characteristics that make it so suitable, such as durability, versatility, strength and chemical resistance, are, at the same time, what have turned it

into one of the most serious global environmental problems (Barnes et al. 2009b). In addition, about 40 % of the plastics produced are single-use products, which increases the rate of waste generated and accumulated (Advisors et al. 2019). In Europe, with regard to plastic packaging, waste is mainly managed in three ways: recycling (42.0 %), energy recovery (39.5 %) and landfill (18.5 %) (PlasticsEurope 2020). However, more than one third of the waste is mismanaged, becoming pollution that mainly reaches the soil and freshwater masses (de Souza Machado et al. 2018). The rest, about 10 %, ends up in the oceans, where most of it accumulates on the ocean floor (Jambeck et al. 2015).

In addition to the above, approximately 90 % of the plastic used is of non-renewable source and it is not biodegradable, which further aggravates the situation. Thus, in the life cycle of plastics, represented in **Figure 2a**, the use of raw materials is constant, with a high dependence on petroleum resources, and a low reuse of those already produced through recycling, based on a linear economy, **Figure 2b**.

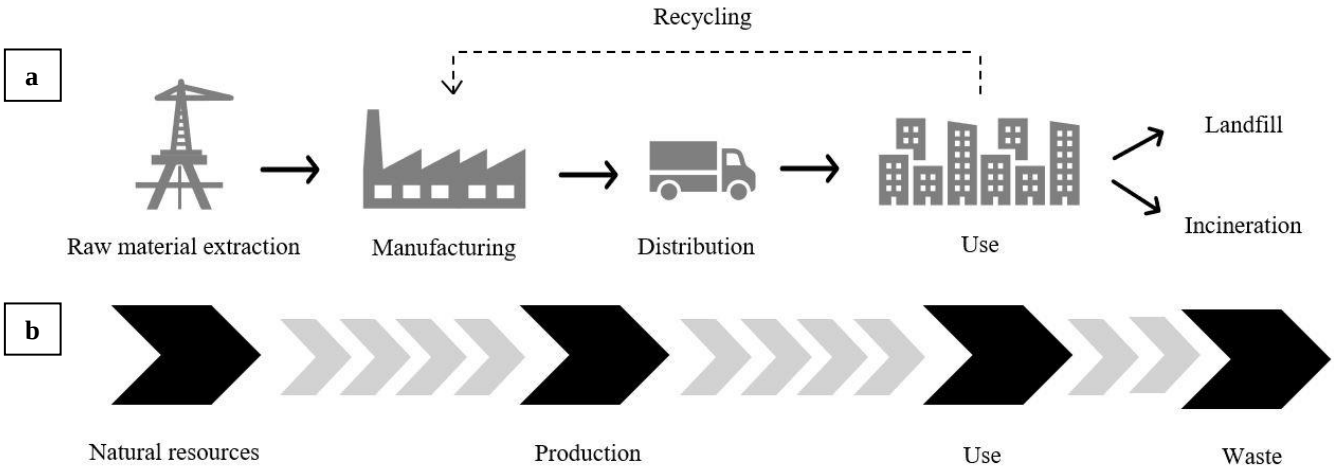

Figure 2. (a) Life cycle of plastics; (b) linear economy.

1.2. Polymers used in packaging

Polymers are macromolecules composed of molecules of long chains of small repetitive subunits called monomers. They can be inorganics, such as glass, or organics both natural, i.e. proteins and polysaccharides, and synthetic, to which most of the plastics used in industry belong (Simionescu and Ivanov 2014). Likewise, polymers can be divided into three categories: thermoplastics, thermosets, and elastomers (Council 2019). The difference between them lies in how they behave under load, influenced by the bonding of their chains. While thermosets do not admit deformation, as their chains are cross-linked by chemical bonds, elastomers are loosely cross-linked polymers that permit elastic deformation, and thermoplastics can be re-melted and re-solidified with similar mechanical properties, as their chains are linked by weak chemical forces (Van der Waals or hydrogen bonds) (Hahladakis and Iacovidou 2018). The latter can be divided into amorphous or semi-crystalline depending on whether they have a random or ordered structure.

The most commonly used plastics are: polyethylene (PE), polypropylene (PP), polyvinyl chloride (PVC), polystyrene (PS), polyethylene terephthalate (PET) and polyurethanes (PU), representing ca. 90 % of the overall (Ali et al. 2021). **Table 1** represents in which these materials are applied in everyday use.

Table 1. Common applications of conventional plastics used in packaging.

Plastic	Uses
Polyethylene terephthalate 1 **PET**	Mineral water and soft drink bottles Bottles of edible oils Detergent powder bottles Textile and carpet fibres 
High density polyethylene 2 **HDPE**	Containers Films Dairy packaging Toys Rigid pipe Bottle caps 
Polyvinyl chloride 3 **PVC**	Pipes Carpet backing Window frames Shampoo and vegetable oil bottles Credit cards Cable and wire sheathing Floor coverings Shoe soles 
Low density polyethylene 4 **LDPE**	Agricultural and packaging films Sacks Foams Flexible bottles 
Polypropylene 5 **PP**	Yoghurt containers Potato bags Straws Medicine pots Flower pots Car battery boxes 
Polystyrene 6 **PS**	Packaging pellets Yoghurt containers Fast food trays Disposable cutlery 

In the field of packaging, most of the plastics used belong to the thermoplastics group, as they can be shaped in the most suitable form according to their purpose, such as films, trays or bottles, being the more used PE, PP and PET. Based on their moldable nature, they might be thought to be recyclable and reusable. However, due to certain factors, this process is difficult to achieve, so their life cycle has a high environmental impact. Firstly, as their monomeric origin is petroleum-based, they are resistant to degradation at a very slow rate. They are almost inert to chemical and biological degradation, due to their high molecular weight, hydrophobicity and absence of functional groups that can be attacked by abiotic factors, such as light, humidity, heat, and atmosphere, as well as biotic, such as microbial enzymes (Chamas et al. 2020). Furthermore, due to the incomplete degradation they undergo, they remain in the form of microplastics, ranging in size from 1 μm to 5 mm (Barnes et al. 2009a), which are even more harmful to the environment, since, in this form, they are more easily transported by runoff from soils to the oceans or ingested by animals (Horton et al. 2017). In addition, it is common in the packaging industry that different types of plastics are blended or used in multilayers to improve the final characteristics of the material (Tartakowski 2010). This complicates their separation and recycling, resulting in a process that is costlier than manufacturing the new product from raw materials (Issifu and Sumaila 2020). Also, in most cases, they are used together with additives, such as plasticizers, colorants, or fibers, that hinder their recovery (Hahladakis et al. 2018).

Thus, both society and industry are seeking to replace petroleum derived materials with more sustainable processes and products that reduce greenhouse gas (GHG) emissions, solid waste, and pollution through bioalternative materials.

1.3. Biopolymers as a new alternative

Bioplastics are a large family of materials that includes bio-based or biodegradable materials or both. Bio-based materials are those derived from biomass source formed from totally or partially renewable resources, according to the European standard EN 16575, while biodegradable materials are those that can be degraded by microorganisms under aerobic or anaerobic conditions into water, gases (carbon dioxide and methane), and biomass, and depends on the chemical structure of the material and the environmental conditions (Van den Oever et al. 2017). Likewise, the fact that a material is biodegradable does not imply that it is industrial compostable, as this is regulated by standards, EN 13432 for packaging, which specifies the technical criteria. However, the use of bioplastics currently accounts for less than 1 % of the plastics market, although it is expected to reach 40 % within a decade (Bioplastics 2020a), with food packaging being its main application.

There are three main groups that belong to the bioplastics family, represented in **Figure 3**: plastics that are derived from fossil resources and are biodegradable, such as polybutylene adipate terephthalate (PBAT); bio-based or partly bio-based, non-biodegradable plastics such as bio-based PE, PP, or PET; and plastics that are both bio-based and biodegradable, such as polylactic acid (PLA) or polyhydroxyalkanoates (PHAs).

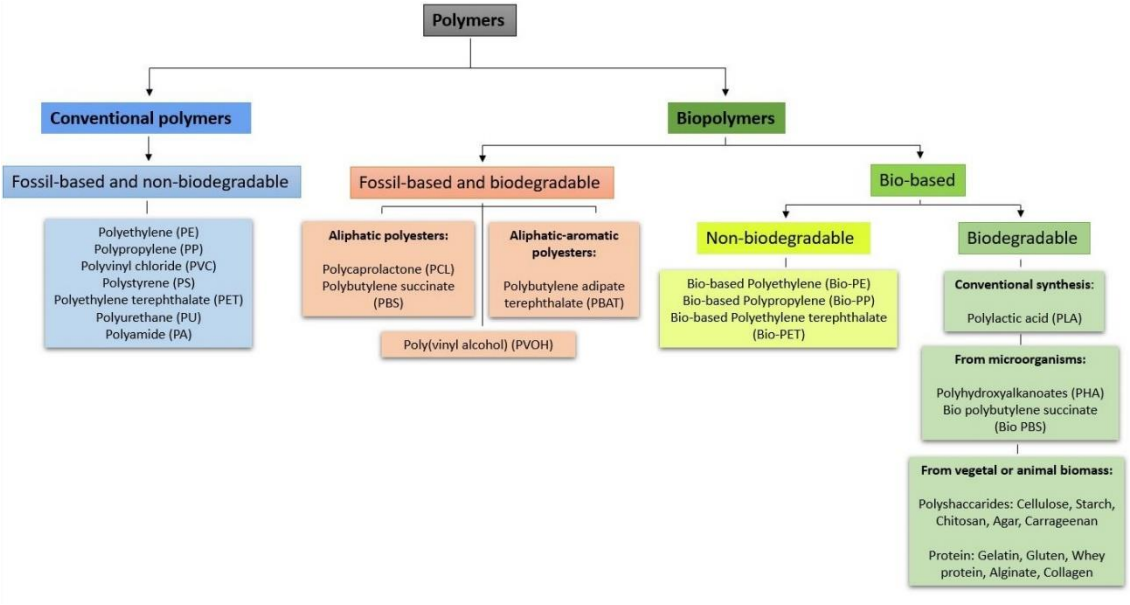

Figure 3. Classification of polymers according to their source and biodegradability.

Currently, most bioplastics derived from renewable resources are agro-based, i.e. they come from carbohydrate-rich plants such as corn, wheat or sugar cane, known as first-generation feedstocks. Although it might be thought that the use of these feedstocks competes with human or animal food, the percentage of agricultural area needed for the production of bioplastics is less than 0.02 % (Bioplastics 2020b). Moreover, this is the most efficient feedstock, since it produces the highest yield. The second and third generation, from non-food crops or waste and algae, respectively, are now under development and have not yet reached the commercialization stage (Ögmundarson et al. 2020).

Due to the diversity of bioplastics, they can be used in different applications depending on where they are most suitable. For example, bio-based PE or PET materials can be used in the same commodities that their petroleum-based counterparts do as they offer similar properties. Their advantages are that it is not necessary to invest in new knowledge or machinery for their production, since it is the same as that of the conventional ones (De Almeida Oroski, Chaves Alves, and Bomtempo 2014). Moreover, they reduce GHG emissions and, although they are not biodegradable, their similarity to fossil plastics allows them to be recycled in the same streams. Currently, they cover ca. 42 % of the bioplastic market (Bioplastics 2020b). In addition, a new biopolymer, called polyethylene furoate (PEF), is expected to be commercialized by 2023. It is a polymer similar to PET, but totally bio-based and with higher barrier properties (Coppola et al. 2021).

On the other hand, plastics that are based on fossil resources and are biodegradable, such as PBAT or polycaprolactone (PCL), are a smaller group and are mainly used in combination with starch or other bioplastics (Thakur et al. 2021). In these blends, these types of bioplastics provide advantages such as biodegradability and improved mechanical properties (Dammak et al. 2020).

Finally, biopolymers that are both bio-based and biodegradable such as PLA, PHA, or starch-based materials, are seen as a great alternative to petrochemical plastics, as they possess similar characteristics to them and can be processed in the same industrial equipment (Jaszkiewicz et al. 2014). Normally, they are used to short-lived, disposable products (Zhao, Cornish, and Vodovotz 2020). They allow less dependence on fossil resources and reduce waste. However, bioplastics show some limitations both in terms of their intrinsic properties such as barrier properties, brittleness, or low thermal resistance, as well as in terms of production costs and recycling in existing streams (Teck Kim, Min, and Won Kim 2014, Peelman et al. 2013). For this reason, they are used in blends with other biopolymers or fillers to enhance thermal, barrier and mechanical properties (Dasan, Bhat, and Ahmad 2017, Larsson, Markbo, and Jannasch 2016).

Among all bioplastics, PHAs have been seen as the most promising to replace existing synthetic plastics, especially for packaging applications, as they have the unique property of being compostable and biodegradable in both soil and marine environments (Suzuki, Tachibana, and Kasuya 2021).

2. Polyhydroxyalkanoates for sustainable food packaging

PHAs are linear polyesters synthesized by various bacteria, both Gram-positive and Gram-negative, such as *Cupriavidus necator*, *Pseudomonas oleovorans*, *Alcaligenes latus*, or *Escherichia coli*, and some extremely halophilic archaea, from the family *Halobacteriaceae* (Hermann-Krauss et al. 2013, Rydz et al. 2015) during fermentation of sugars or lipids to store carbon and energy under nutrient-limited conditions, such as nitrogen, phosphorus, oxygen, sulfur or magnesium, and excess of a carbon source (Lee 1996). PHAs accumulate in intracellular granules up to about 90 % (w/w) of the dry cell mass (shown in **Figure 4**) (Steinbüchel and Lütke-Eversloh 2003). Recently, transgenic plants cells have also been used for the production of PHAs. However, the accumulation capacity inside the plant cells was less than 10 % (w/w) of the dry weight, as high levels produced problems in plant growth and seed production (Dobrogojski et al. 2018, Bohmert et al. 2002).

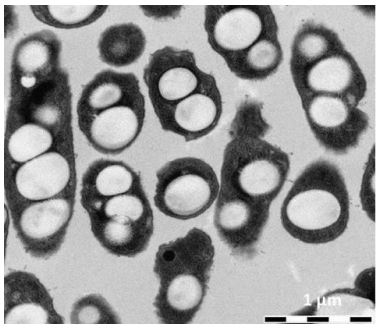

Figure 4. Polyhydroxyalkanoate (PHA) granules in the cells of the PHA-producing bacteria (Adapted from Obruca et al. (Obruca et al. 2020)).

The general structure of the PHAs is represented in **Figure 5**. PHAs are polyhydroxy acids with different monomeric units and side chain compositions can be produced by controlling the producing strain, fermentation conditions or feeding different carbon substrates or precursors during accumulation (Amstutz et al. 2019). More than 150 types of PHA monomers units have been identified (Zhang, Carlson, and Srienc 2006). Depending on the length of the side chain, R, PHAs can be classified into three types: short chain length-PHA (*scl*-PHA), when R contains 3-5 carbon atoms, medium chain length-PHA (*mcl*-PHA), from 6 to 14 carbon atoms, and long chain length-PHA (*lcl*-PHA), for more than 14 carbon atoms (Zinn, Witholt, and Egli 2001).

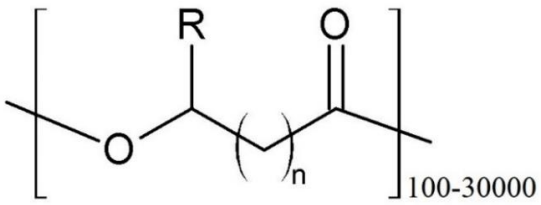

Figure 5. General structure of polyhydroxyalkanoates (PHAs).

They have been used in daily single-use products such as beverages and food, in the form of films, boxes or coating, in cosmetic and disposable personal hygiene articles, in biomedical applications such as temporary implants or drug delivery, as well as in agricultural films (Khalikova, Somersalo, and Korpela 2020, Mojaveryazdi et al. 2012). The differences in the many types of PHAs depend mainly on the composition of their monomers. The first PHA observed and widely studied is polyhydroxybutyrate (PHB). PHB has thermal and mechanical properties similar to conventional plastics, such as PP (Clifton-García et al. 2020). Furthermore, it is non-toxic and exhibits good moisture resistance and gas barrier properties (dos Santos et al. 2017). However, it is a brittle and stiff material, due to its crystalline nature, and has narrow processing temperature window, which limit its processability (Wang et al. 2013, Li et al. 2021). To overcome these drawbacks, the use of copolymers has been proposed. Thus, the incorporation of 3-hydroxyvalerate (3HV) or 4-hydroxybutyrate (4HB) units to PHB to obtain *scl*-copolymers such as poly(3-hydroxybutyrate-*co*-3-hydroxyvalerate) (PHBV) or poly(3-hydroxybutyrate-*co*-4-hydroxybutyrate) [P(3HB-*co*-4HB)] or *scl*-*mcl*-copolymers with the addition of 3-hydroxyhexanoate (3HHx) units to obtain poly(3-hydroxybutyrate-*co*-3-hydroxyhexanoate) [P(HB-*co*-HHx)] or poly(3-hydroxybutyrate-co-3-hydroxyvalerate-*co*-3-hydroxyhexanoate) [P(3HB-*co*-3HV-*co*-3HHx)], results in materials with low crystallinity and more elasticity (Sato et al. 2005, Madison and Huisman 1999). Typically, *scl*-PHA is fragile and rigid, while *mcl*-PHA is more flexible and easier to shape (Kabilan et al. 2012). PHBV has been more extensively used, since by varying the ratio of the 3-hydroxyvalerate (3HV) monomer, it can behave like PE, PP or PVC when the 3HV content is high, medium and low, respectively (Weng, Wang, and Wang 2011).

However, these changes in PHA monomers to adjust them according to the application result in an increase in production costs. Thus, although the demand for PHAs in the market is growing, its total industrialization and commercialization is still limited due to the fact that it is more costly than conventional plastics (Meereboer, Misra, and Mohanty 2020). Currently, the industrial

production of PHAs is based on pure cultures (wild type and recombinant bacteria), which requires sterile conditions, and on the use of specific carbon substrates such as glucose or sucrose, which accounts for about 50 % of the total production cost (Bugnicourt et al. 2014). In addition, the polymer fermentation process and the subsequent treatment, especially purification, contribute to its high manufacturing cost (Kourmentza et al. 2017). Consequently, the market price of PHAs is about 5 €/kg, while that of petroleum-based polymers is around 0.8–1.5 €/kg (Van den Oever et al. 2017).

Therefore, different strategies have been applied to turn the process more efficient and cheaper. For example, the use of waste streams and by-products as a carbon source in pure cultures has been developed in order to reduce production costs and revalorize waste products (Follonier et al. 2014, Ahn, Park, and Lee 2001). For instance, Rebocho et al. (Rebocho et al. 2020) produced natural PHB/*mcl*-PHA blend using co-culture of *C. necator* and *Pseudomonas Citronellolis* with apple pulp waste as the sole carbon source. Recently, the replacement of pure cultures by mixed microbial cultures (MMCs) together with the use of waste products is considered a better alternative for the scale-up of PHA production processes, since process costs are reduced, as sterile conditions are not necessary and higher yields are obtained (Nikodinovic-Runic et al. 2013, Kourmentza et al. 2015).

2.1. Polyhydroxyalkanoates production through mixed microbial cultures using by-products

The use of MMCs with low-cost feedstocks as a carbon source for the PHA production is advantageous over the use of pure cultures as they can better adapt to complex substrates (Reis et al. 2011). Thus, the consortium changes according to the carbon source provided, allowing the use of a broad range of feedstocks and the production of diverse of PHA copolymers compositions (Arroja et al. 2012, Mannina et al. 2020). In addition, as no axenic bioprocess or sterile conditions are required, the selection of the microorganism is based on its ability to accumulate PHA (Kourmentza et al. 2017). Several substrates have been employed in laboratory and pilot-scale experiments for the production of PHAs, including industrial and agricultural by-products, such as food waste (Moretto et al. 2020, Zhang, Wu, and Chen 2014), cheese whey (Colombo et al. 2016, Oliveira et al. 2018), molasses (Carvalho et al. 2014), olive and palm oil mill effluents (Ntaikou et al. 2014, Md. Din et al. 2012), as well as wastewaters (Pittmann and Steinmetz 2017, Morgan-Sagastume et al. 2013).

At laboratory and pilot-scale, the PHA production consists of three stages, represented in **Figure 6**: 1) acidogenic fermentation of the feedstocks to produce volatile fatty acids (VFAs), such as acetate, propionate, butyrate, and valerate, which are the precursors of PHA biosynthesis for MMCs. The configuration of these VFA-rich feedstocks affects the composition of PHA monomers as well as their molecular structure (Rodriguez-Perez et al. 2018). They can be modified by controlling some operating parameters, such as pH, the organic loading rate (OLR), hydraulic retention time (HRT) and temperature (Atasoy et al. 2018, Bertin et al. 2010). After the fermentation, a solid-liquid separation by centrifugation is performed. The liquid part is used in the following stages while the residual solid is converted into biogas by anaerobic digestion (Moretto et al. 2020). 2) Selection of microorganisms with high PHA storage by aerobic dynamic feeding (ADF) process, in sequencing batch reactors (SBRs), in which there is an alternation of substrate known as “feast and famine” regime (Dionisi, Beccari, et al. 2005). Therefore, due to

periods where the substrate is in excess (feast phase) and long periods of substrate starvation (famine phase), a selection pressure allows PHA-accumulating organisms to survive (Majone et al. 1996). Also, there are parameters that affect this step, such as the feedstock composition, OLR, sludge retention time (SRT) and the feast and famine ratio (Valentino et al. 2014, Dionisi et al. 2006). Several strains have been found constituting these MMCs, belonging to the genera *Thauera, Azoarcus, Alcaligenes, Acinetobacter, Comamonas, Achromobacter, Xanthobacter, Curtobacterium, Paracoccus, Kluyvera, Pseudomonas, Flavobacterium,* among others (Kourmentza et al. 2015, Albuquerque et al. 2013). 3) PHA production. In this stage, selected MMCs are fed with the fermented stream from stage 1, with the objective of accumulating PHA to their maximum capacity. The process is conducted in a fed-batch reactor where the MMCs are exposed to a large feast period with excess carbon while some nutrients are limited, such as nitrogen or phosphorous (Nielsen et al. 2017). The carbon to nutrient ratio (C/N and C/P) and pH are parameters that affect this stage (Johnson, Kleerebezem, and van Loosdrecht 2010, Montiel-Jarillo, Carrera, and Suárez-Ojeda 2017). PHA contents of 75 wt % have been achieved in MMCs with by-product substrates (Albuquerque, Torres, and Reis 2010), close to those obtained with synthetic substrates (75-90 wt %) (Johnson et al. 2009) or with pure cultures (90 wt %) (Passanha et al. 2013). Finally, the PHA-rich stream is subjected to an extraction and purification step (Dionisi, Carucci, et al. 2005).

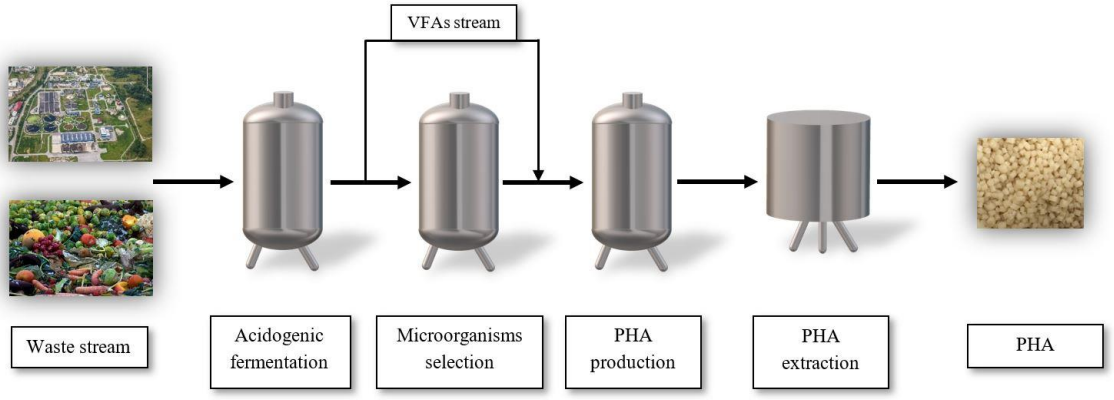

Figure 6. The three-stages polyhydroxyalkanoates (PHA) production process using mixed microbial cultures (MMCs).

After harvesting the biomass containing PHA by filtration, centrifugation, sedimentation, or flocculation (Koller, Niebelschütz, and Braunegg 2013), this must be stabilized before extraction to avoid polymer degradation by microorganisms. Two main approaches have been described: thermal drying or wet acidification of the biomass and lyophilization (Lorini, Martinelli, Pavan, et al. 2021). In addition, these pre-treatment steps enhance cell disruption (Jacquel et al. 2008). Afterwards, PHA recovery is performed. The method for PHA extraction is selected according to different criteria such as microbial production strain, since the MMCs cells are more resistant to hydrolysis than the pure ones (Samorì et al. 2015), type and composition of PHAs, purity requirements for the final application, impact on the PHAs properties, that is, thermal and

mechanical properties and the molecular weight, as well as cost and environmental risks (Mannina et al. 2019, Kunasundari and Sudesh 2011).

At laboratory and pilot scale, the PHA extraction process can be divided into two main categories: digestion of the non-PHA cell mass (NPCM) through chemical treatment or solvent extraction of PHA from the biomass. The latter is the most used method, in which chlorinated solvents such as chloroform, dichloromethane, and poly-chlorinated ethane are used in the dissolution phase (Kosseva and Rusbandi 2018). Then, the dissolved PHA is separated by evaporation or recovered in crystal form by adding a precipitating agent, such as methanol or ethanol, or water (Mannina et al. 2020). This method achieves high purity without altering the properties of the biopolymer (Ramsay et al. 1994). However, it implies high costs and environmental impact, due to the required amount of solvents, as well as their recovery, and because it is harmful to human health and nature (Madkour et al. 2013). For this reason, the use of halogen-free solvents such as alcohols, esters, amides, cyclic and acyclic ketones, etc, is gaining relevance as more sustainable alternative (Laycock et al. 2014, Kosseva and Rusbandi 2018). Also, dimethyl carbonate (DMC) has been reported to be a green solvent with high PHA recovery (Samorì et al. 2015). Regarding the digestion method, it consists in the disruption of the cell wall by the dissolution of the NPCM. Some of the chemicals used for the cellular lysis are oxidants, alkali, and surfactants such as sodium hydroxide (NaOH), sodium hypochlorite (NaClO), and sodium dodecyl sulphate (SDS) (Jiang et al. 2015, Mannina et al. 2019). Although this method presents high PHA recovery and has a lower cost than the solvent one, its main drawbacks are that wastewater treatment is required and that its use can lead to polymer degradation, since not only NPCM are dissolved (Kourmentza et al. 2017). This produces a decrease in the quality of the biopolymer, that is, its molecular weight. Therefore, the great challenge of PHAs recovery is to obtain high purity without compromising the quality of the polymer. For this reason, the combined use of both methods may be a useful option in which hypochlorite produces cell lysis while the released PHA is protected from degradation with chloroform (Hahn et al. 1993). On the other hand, other methods have been used to extract PHA from pure cultures. For instance, the use of enzymes to solubilize NPCM has allowed the extraction of PHA with high purity, although it is an expensive and complex process (Kapritchkoff et al. 2006). Its use for the recovery of PHAs from MMCs has not been reported, probably because it is not potent enough to overcome their high cellular resistance (Pagliano et al. 2021). Likewise, other cell disruption methods reported for pure cultures, such as mechanical disruption (bead mill disruption, high pressure homogenization, ultrasonication) (Gutt et al. 2016, Ishak et al. 2016), supercritical fluid (Hejazi, Vasheghani-Farahani, and Yamini 2003), cell fragility (Divyashree and Shamala 2010) or biological agents (Murugan et al. 2016, Ong et al. 2018), among others, have not yet been used for MMCs. Finally, a purification step can be performed if the final application requires it, for example, for medical use. For this purpose, the use of hydrogen peroxide or ozone has been reported (Kosseva and Rusbandi 2018).

Therefore, the production of PHAs bioplastics by MMCs through fermentation of by-products has great potential to replace petroleum-derived plastics. Future studies should focus on scaling up the process to a pre-industrial level to ensure the production and quality required for commercialization. This would allow the entry of these materials into the Circular Bioeconomy.

2.2. Circular Bioeconomy

The current concern about depletion of natural resources, environmental pollution and waste generated by the use of non-renewable resources and the growth in demand for products and energy has led to the development of international policies to address the problem. Society and industry must collaborate to solve this global challenge, which affects both human health and the environment. Thus, the European Union has developed several strategies focused on the transition from a linear to a circular economy, which consists of increasing the valorization of resource while minimizing waste and maintaining the value of the product for as long as possible, adopting the "closing the loop" philosophy (Commission 2015). The Circular Economy is based on the main principles of redesign, reduce, reuse, repair, remanufacture and recycle to ensure an efficient use of resources that satisfies economic, social and environmental needs (Maina, Kachrimanidou, and Koutinas 2017). Likewise, the Bioeconomy is focused on the conversion of renewable resources and by-products and wastes into value-added products such as food, feed, and bio-based products, including biopolymers, and bioenergy, in order to ensure food security, decrease dependence on fossil resources, and improve the economy and the environment (Commission 2012). From these two concepts, the term Circular Bioeconomy, represented in **Figure 7**, has recently emerged. It consists of enhancing the value of biomass by integrating it into the production process in order to exploit waste and residues to revalue them over time through cascading steps (Stegmann, Londo, and Junginger 2020).

New technologies are being developed to integrate this biomass into production chains in an economically and environmentally sustainable approach (Maina, Kachrimanidou, and Koutinas 2017). The valorization of waste, especially food and wastewater, as feedstock in bioprocesses to produce value-added products on the market has a large impact on the entire value chain. Therefore, different organic wastes have been reported for PHA production using MMCs. For instance, Lorini et al. used three different organic feedstocks, i.e. liquid slurry from municipal wastewater treatment, cellulosic primary sludge and fruit waste, for the production of PHAs by MMCs at pilot scale, obtaining biopolymers with varied monomer contents, good thermal and chemical characteristics and workability (Lorini, Martinelli, Capuani, et al. 2021). Similarly, wastewater effluents from a potato-starch factory were used as feedstock for MMCs on a pilot scale, producing PHA polymer blends by changing the composition of the accumulation feedstocks (Morgan-Sagastume et al. 2020). Other examples of such sustainable approaches have been established with the joint production of biomaterials and biofuels (Battista et al. 2020). For instance, pilot-scale biorefineries have been established at wastewater treatment plants (WWTPs) where anaerobic digestion of organic substrates has produced both biopolymers, such as PHA, and biogas (Valentino et al. 2018). This strategy represents the essence of the circular bioeconomy, eliminating the use of petroleum resources, thereby reducing GHG emissions and climate impacts, and increasing food security, based on a green and sustainable economic and environmental perspective (Leong et al. 2021).

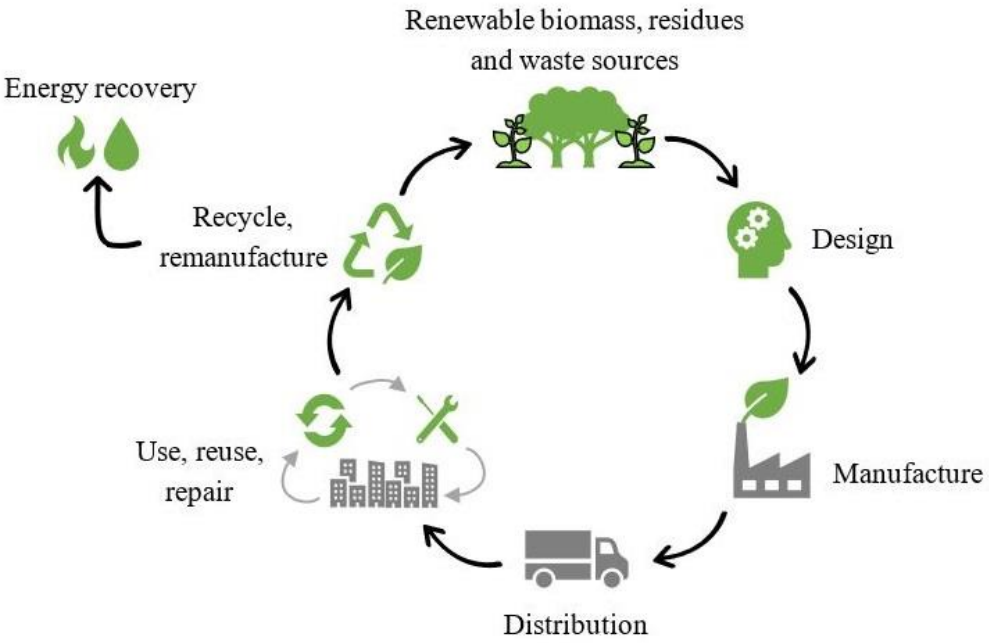

Figure 7. Circular Bioeconomy model.

3. High-oxygen-barrier materials

In the field of food packaging, barrier properties are one of the most important characteristics. This concept is based on the transport of gases and low molecular weight compounds, called permeants, from two sides with different concentrations. The permeation process is determined by tree steps: sorption of the permeant onto the polymer, diffusion through the material and desorption from the polymer surface. The schema of the process is represented in **Figure 8**.

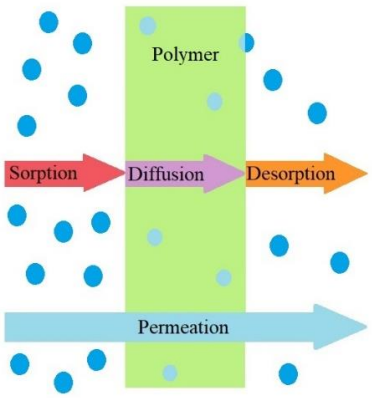

Figure 8. Mechanism of the permeation process (Adapted from Maes et al. (Maes et al. 2021)).

Thus, the permeability (P) coefficient of a material is determined, in turn, by two coefficients: the solubility (S), a thermodynamic constant which indicates the sorption of the permeant into the polymer, and the diffusion (D), a kinetic constant which describes the movement of the permeant through the polymer:

$$P = S \times D \quad (1)$$

The permeant includes gases (oxygen (O_2), carbon dioxide (CO_2)), water vapor, and aromas or odors. The barrier to these substances is necessary not only for food safety and quality, but also to extend shelf life. The barrier properties offered by polymers can be of different levels: poor, low, medium, high, and very high. Thus, depending on the final application of the packaging, the most suitable barrier material will be used. For instance, fresh fruit and vegetables continue to respire after harvesting, so packaging that allows gas exchange is required. Thus, a state of equilibrium must be reached between the amount of O_2 entering the package and the consumed it and the amount of CO_2 permeating out of the package and the develop by the packaged fruit (Giuggioli et al. 2015, Del Nobile et al. 2006). Similarly, an adequate water vapor barrier is necessary to obtain an equilibrium moisture content and to prevent water loss or dehydration (Auras, Singh, and Singh 2005). On the other hand, there are other applications such as meats and many beverages where high barriers are needed to meet their requirements (Michiels, Puyvelde, and Sels 2017).

High-oxygen-barrier polymers are those that offer low permeability similar to traditional packaging materials, such as glass or metals, and allow food preservation and shelf-life extension by delaying, for example, lipid oxidation, growth of microorganisms and other spoilage mechanisms (Gavara et al. 2016). To achieve this, these materials must have a low free volume and a high cohesive energy density. This is provided by materials of high crystallinity and high polarity, containing hydroxyl groups that allow high intra- and intermolecular bonding (Wang et al. 2018). Two materials that meet these attributes and have been widely used for this purpose are poly(ethylene-*co*-vinyl alcohol) (EVOH) and cellulose nanocrystals (CNCs). The former has been considered one of the highest oxygen barrier polymers and one of the most widely used in the packaging industry while CNCs have become more widespread in recent decades with the development of nanotechnology and the growing concern for the use of more environmentally friendly materials. However, these materials have some disadvantages, such as their great appetite for absorbing moisture in high relative humidity (RH) conditions, due to polar groups, which leads to the loss of high cohesions between their chains and increases the free volume and, consequently, the permeability to gases and other molecules. To overcome these issues, several approaches have been developed, such as the use of multilayers, blending with other polymers or coatings. The characteristics of these two polymers, as well as their benefits and drawbacks, are discussed in more detail below.

3.1. Poly(ethylene-*co*-vinyl alcohol) copolymers

EVOH copolymers are a family of resins with outstanding gas barrier properties. Its synthesis consists of two steps: the copolymerization of monomeric units of ethylene and vinyl acetate (EVA) and its hydrolysis to convert the acetoxy groups into a secondary alcohol (Iwanami and Hirai 1983). The EVOH obtained is a random branched structure. The synthesis and structure of EVOH copolymers are shown in **Figure 9** (Toit and Leonore 2013).

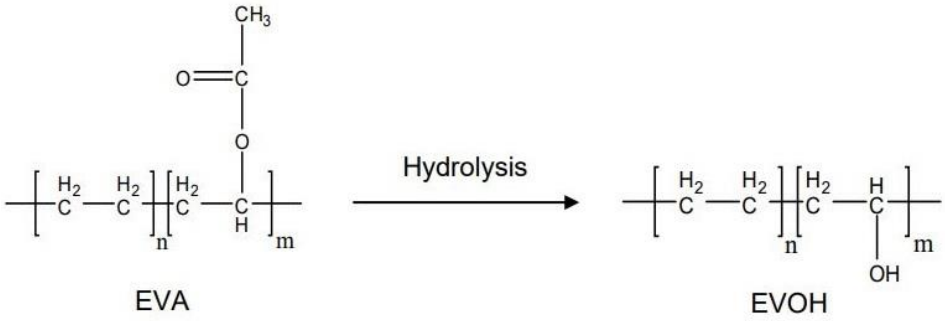

Figure 9. Formation and structure of poly(ethylene-*co*-vinyl alcohol) (EVOH) copolymers by hydrolysis of ethylene vinyl acetate (EVA) copolymer.

EVOH has a semi-crystalline structure in which the crystalline domains are dispersed in the amorphous matrix (Ezquerra et al. 2002). The size and distribution of these crystals are affected by the ratio of the content of the two monomers, PE and polyvinyl alcohol (PVOH). Thus, three types of crystalline structures have been described: monoclinic structure, for ethylene contents below 40 mol %, whose crystals are small and dense, with a degree of packaging like PVOH; hexagonal structure, for contents between 40-80 mol %, whose crystals are larger and less dense than the previous ones; and orthorhombic structure, for contents above 80 mol %, similar to those of PE (Cerrada et al. 1998). The composition of EVOH copolymers also confers different characteristics in terms of barrier and mechanical properties. Therefore, the outstanding barrier properties against gases are due to the high cohesion energy provided by the high inter- and intramolecular bonds of the hydroxyl groups of the PVOH units (Lagaron, Catalá, and Gavara 2004), while PE provides good water resistance but worse gas barrier. With respect to mechanical properties, a higher PVOH content hinders processability, due to its low thermal degradation point and its solubility in water, while PE provides processability and flexibility (Maes et al. 2019). Moreover, the vinyl alcohol content in the copolymers also affects their resistance to degradation under certain environmental conditions. Thus, several studies have reported the degradation of both homopolymer and copolymers with high vinyl alcohol content under different conditions using biological strains (Wu et al. 2019, Tomita, Kojoh, and Suzuki 1997, Kawai and Hu 2009).

Thus, the combination of both monomers offers a wide range of potential applications. EVOH has been used in such diverse sectors as rigid and flexible packaging, especially food, pharmaceutical and clinical articles, as well as in hydrocarbon containers, and heating pipes (McKeen 2012). This broad applicability is due to some of its good properties such as its excellent barrier to gases, not only to oxygen, but also to carbon dioxide, nitrogen and hydrogen

(Armstrong, Asme, and Spe 2009, Maes et al. 2021), and to organic substances such as aromatic compounds (López-Carballo et al. 2005), fuels (Zhao et al. 2015) and chemicals such as benzene, toluene, ethylbenzene and xylene isomers (BTEX) (McWatters and Rowe 2015, Lagaron, Powell, and Bonner 2001). EVOH also has other desirable qualities, such as chemical resistance and high transparency (Cabedo et al. 2017). Furthermore, it can be recycled in existing infrastructures for other polyolefins and does not contain substances harmful to the environment or human health, such as metals or chlorine, as is the case with polyvinylidene chloride (PVDC), which has a high barrier but is a contaminant (Wang 2019).

However, in addition to the monomer composition of the copolymers, other external factors affect the properties of the material. Thus, one of the main drawbacks of EVOH is its sensitivity to moisture due to its hydrophilic character, which confers a medium to poor barrier to water vapor (Aucejo, Catalá, and Gavara 2000). It easily absorbs water when exposed to high humid conditions, due to interactions between water molecules and polar hydroxyl groups (Iwamoto et al. 2006). At RH below 40 %, there is a reduction in oxygen permeability, as the free volume between the polymer chains decreases as it is filled with water molecules (Zhang, Britt, and Tung 2001). When the RH increases, plasticisation and swelling of the polymer occurs, which causes a weakening of the hydrogen bonds between its chains (self-association), leading to an increase in chain mobility and free volume (Zhang, Britt, and Tung 2001). This results in a reduction of the oxygen barrier, by a factor of 100-1000 from dry to humid conditions (López-Carballo et al. 2005), as well as of its mechanical and thermal properties, decreasing its tensile modulus and yield strength, and glass transition temperature (T_g), respectively (Zhang, Britt, and Tung 1999, Zhang, Lim, and Tung 2001). Similar effects occur with other substances such as methanol and ethanol (Cava, Sammon, and Lagaron 2007). For this reason, EVOH is normally used in multilayer structures, as a thin inner layer (usually far below 10 μm) sandwiched between hydrophobic materials, such as PP and PE, which also confer other improvements including abrasion resistance, heat sealability and strong printability (Mokwena and Tang 2012). However, it has some limitations such as increased production costs, difficulty in recycling and less transparency. Therefore, other strategies have been used to overcome shortcomings, such as blending with other polymers or adding fillers. The former is less complex and less costly than multilayer systems, although the final material properties are not exactly the same as for single materials, depending on the miscibility of the polymer, so it is difficult to predict the final characteristics (Chen et al. 2004). EVOH has been blended with polymers such as PVOH (Blanchard et al. 2021), polyamide (PA) (Lu et al. 2021, Yeh and Chen 2007), polyketone (PK) (Kim et al. 2020), thermoplastic starch (TPS) (Alves, Grande, and Carvalho 2019), among others, showing improvements in thermal, mechanical and barrier properties over neat polymers. A compatibilizer is often used to improve dispersivity between the polymers (Kim, Kim, and Lee 2021, Rahnama et al. 2017). On the other hand, the use of nanoparticles has also been developed in order to improve the limitations of EVOH. Among these nanofillers, it has been reported the use of nanoclays (Jeong, Kim, and Kim 2005, Cabedo et al. 2004), carbon nanotubes (Lee, Yoon, and Park 2012), graphene (Torres-Giner et al. 2018, González-Ruiz et al. 2016), CNCs (Orr and Shofner 2017, Martínez-Sanz, Lopez-Rubio, and Lagaron 2013), and mesoporous silica (Chiba and Tominaga 2012). In addition, nanoparticles can act as carriers for antimicrobials substances and antioxidants, such as metal-based nanoparticles or essential oils (EOs), enhancing polymer functionality, including active and smart food packaging (Cherpinski, Biswas, et al. 2019, Muriel-Galet et al. 2018).

3.2. Cellulose nanocrystals

Cellulose is the most abundant biopolymer in nature with an annual production of more than 7.5×10^{10} tons (Lunardi et al. 2021). It can be found in wood (Zhao et al. 2017, Fernandes et al. 2011), plants such as cotton, flax, hemp, or sisal (Barbash and Yashchenko 2020, Nam, Hillyer, and Condon 2020), in brown, green, and red algae species such as *Posidonia Oceanica*, *Cladophora*, *Valonia or Gelidium elegans* (Tarchoun, Trache, and Klapötke 2019, Pan et al. 2016), in tunicate marine animals (Zhu et al. 2018), in bacteria, including *Acetobacter*, *Agrobacterium*, *Rhizobiumm*, *Pseudomona*, among others (Campano et al. 2016, Anwar et al. 2021), and even in amoeba, such as *Acanthamoeba* or *Dictyostelium discoideum* (Garajová et al. 2019, Blanton et al. 2000). It is an attractive renewable resource due to characteristics such as environmental friendliness, low cost, biodegradability, biocompatibility, and non-toxicity (Du et al. 2019). Cellulose presents a multilevel structure, shown in **Figure 10**, consisting of aggregates of superfine fibrils. These, in turn, contain several cellulose chains, which are composed of large ordered (crystalline) domains and small disordered (amorphous) domains (Seddiqi et al. 2021). It is a linear homopolysaccharide composed by D-glucose units linked by 1,4-β-glycosidic bonds (Rebouillat 2013). The presence of interacting -OH groups tend to form intra- and intermolecular hydrogen bonds that provide strong self-association and an extended network. This network provides some of its relevant characteristics including stiffness and insolubility in common solvents and water (Kamel et al. 2020). In addition, these hydroxyl groups are active sites for chemical modifications, where they are replaced with functional groups such as chlorides, oxides or acids, in order to improve some characteristics or develop new ones (Giri and Adhikari 2012).

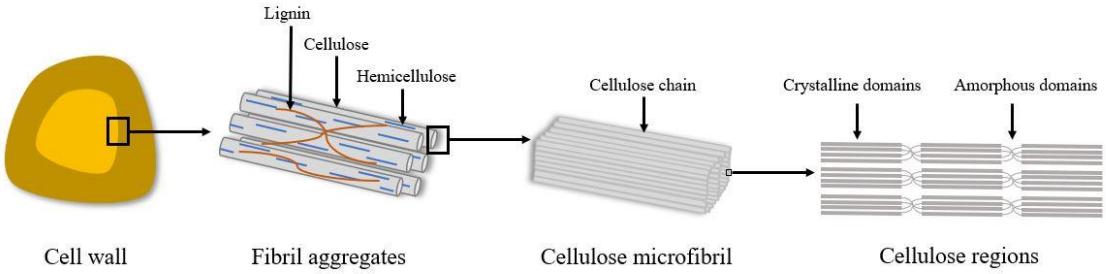

Figure 10. Schematic of the cellulose multilevel structure (Adapted from Seddiqi et al. (Seddiqi et al. 2021)).

The polymer chains form fibrous structures composed of microfibrils, where crystalline and amorphous regions are combined. The degree of crystallinity changes according to the source, extraction method or treatment (Lunardi et al. 2021), being higher for bacteria and tunicates (80-100 %) than for plants (40-60 %). Exist various types of interconvertible crystalline cellulose polymorphism (I, II, III, and IV). Cellulose I is the natural cellulose produced by organisms and has a metastable structure, triclinic or monoclinic, as it can be converted to Cellulose II or III. The former has a monocyclic structure and is produced by two possible process: chemical regeneration and mercerization. It is a more stable structure of technical importance, which is used to

manufacture transparent films (cellophane) and synthetic textile fibres (Wada, Ike, and Tokuyasu 2010). Cellulose III is produced by liquid ammonia treatments of Cellulose I or II. After thermal treatments, Cellulose IV is formed (Moon et al. 2011).

Furthermore, the development of cellulose nanomaterials (CNs) has gained attention in the last twenty years due to the improved properties over cellulose. Depending on the production conditions, these nanoparticles present different dimensions, morphologies and amount of amorphous fraction. There are two main types of nanocellulose: CNCs and cellulose nanofibers (CNFs). Thus, CNCs, also called cellulose nanowhiskers (CNWs) or nanocrystalline cellulose (NCCs), are produced by acid hydrolysis extraction, in which the amorphous part is dissolved while the crystalline part remains unaffected. These nanocrystals are elongated rod-shaped with diameters ranging between 3-50 nm and lengths of 100-500 nm (Nechyporchuk, Belgacem, and Bras 2016). On the other hand, CNFs, also known as nanofibrillated cellulose (NFCs) or microfibrillated cellulose (MFCs), are mainly produced by mechanical treatment of cellulosic fibers including microfluidization, ultrasonication, grinding, and high-pressure homogenization, the latter being the most commonly used (Jonoobi et al. 2015). Enzymatic and chemical pre-treatment (2,2,6,6-tetramethylpiperidine-1-oxyl (TEMPO) oxidation, acetylation, carboxymethylation) is sometimes carried out to reduce the high energy cost of the mechanical process (Tejado et al. 2012). CNFs present both crystalline and amorphous domains, and the nanofibers exhibit diameters of 5-50 nm and lengths of few micrometers (Nechyporchuk, Belgacem, and Bras 2016). CNFs present a higher flexibility than CNCs (Brinchi et al. 2013). There is another type of CNs, bacterial cellulose (BCs) which is a high purity and crystallinity nanofibers with diameters of 20-100 nm and lengths of several micrometers (Jozala et al. 2016). They are produced from low molecular weight sugars (bottom–up process). The process can take from few days to two weeks, making large-scale production a challenge (Gatenholm and Klemm 2010).

Focusing on CNCs, they have gained special relevance because of their intrinsic properties such as high surface area, low density, high Young's modulus and excellent strength, very low coefficient of thermal expansion, high thermal stability, and high transparency (Kargarzadeh et al. 2018). In addition, nanocrystals do not swell in water, at low RH, even though they have a hydrophilic surface (De France, Hoare, and Cranston 2017). They have been applied as barrier and antimicrobial film, packaging, drug delivery, biomedical implants, biosensors, etc (Moon et al. 2011). However, the main application of CNCs has been as reinforcement of polymeric matrices in nanocomposites. CNCs have been commercialized in aqueous solutions. However, they are also available in solid form, as this format is more suitable both for use in the dispersion of polymeric matrices and for lower transport costs (Khoshkava and Kamal 2014a). The process used for drying impacts on the morphology, surface energy, and thermostability of the CNCs and has the challenge of maintaining the nanodimension of the nanoparticles without producing agglomerations (Khoshkava and Kamal 2014a). Therefore, different methods have been proposed: air drying (AD), supercritical drying (SCD), freeze drying (FD), spray drying (SD) (**Figure 11**) and spray freeze drying (SFD), the latter two being the most common industrially used (Khoshkava and Kamal 2014b, Peng et al. 2013).

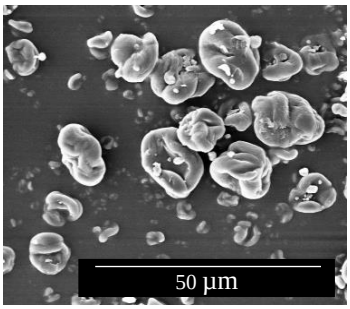

Figure 11. Scanning electron microscopy (SEM) image of spray-dried cellulose nanocrystals (CNCs).

CNCs have been shown to improve mechanical and barrier properties, due to the continuous network of nanocrystals governed by the mechanical percolation (Santos et al. 2014). This mechanism is based on the strong hydrogen bonding interactions between the nanoparticles and the short distance between them, which allows the formation of a three-dimensional network (Silvério et al. 2014). Below the percolation threshold, there are not enough particles to create strong interactions between them, and they are dispersed in the matrix. On the contrary, above the percolation threshold, the nanoparticles tend to aggregate, preventing a good dispersion through the polymeric matrix and, thus, diminishing their potential benefits. Therefore, it is import to consider the parameters that can affect this formation, some of which include the size, morphology and orientation of the nanocrystals, the processing method and the interaction between the matrix and the nanoparticles (Mariano, El Kissi, and Dufresne 2014). Regarding the processing method, casting and evaporation processes, which involve a slow drying procedure, provide an optimal rearrangement of the nanocrystals. The percolation network also affects the transparency of the films, being lower when agglomeration occurs, as it is able to scatter light (Boufi, Kaddami, and Dufresne 2014). Improvements in the mechanical properties of polymers have long been reported when CNCs have been incorporated into their matrices (Wang, Shankar, and Rhim 2017, Sukyai et al. 2018). For example, an increase in tensile modulus and strength of approximately 87.0 % and 25.3 %, respectively, was reported for a 5 wt % loading of CNCs on casting-prepared chitosan films compared to pure chitosan films (Khan et al. 2012). Similarly, a 24 % increase in Young's modulus and yield strength of solution cast polyethylene oxide (PEO)/CNCs films was reported when 7 wt % CNCs were incorporated into PEO matrix (Xu et al. 2013). However, Martinez-Sanz et al. did not find significant improvements in the mechanical properties of EVOH/CNCs nanocomposites prepared by melt compounding with the addition of up to 3 wt % CNCs, because the percolation threshold had not been reached at that nanocrystal content (Martínez-Sanz, Lopez-Rubio, and Lagaron 2013). In terms of barrier properties, CNCs have shown reduced permeability to water vapor and oxygen mostly related to the compact network that increases the tortuosity and diffusion path within the film, and also to their high crystallinity structure (Nair et al. 2014). Thus, several studies have reported reduced permeability of polymers in CNCs nanocomposites (Xiao et al. 2020, Chi and Catchmark 2018). For instance, a 10.6 % and 25.3 % reduction in water vapor and oxygen permeability, respectively, was obtained when 4 wt % CNCs were added to a gum arabic (GA) films (Kang et al. 2021). However, in that study, when the content of CNCs increased to 6 and 8 wt %, there was a decrease in barrier properties due to aggregation of the nanoparticles. In another study, a PLA/CNCs nanocomposite

showed an improvement in water vapor and oxygen barrier of 30 and 60 %, respectively, when 1 wt % CNCs was added to a pure PLA film (Karkhanis et al. 2018).

However, there are some drawbacks that limit their full use. Their hydrophilic character hinders their incorporation in hydrophobic polymeric matrices, as well as in non-polar solvents (Panchal, Ogunsona, and Mekonnen 2019). Moreover, the barrier properties of CNCs are affected by humidity conditions. Thus, at high RH (> 40 %), moisture can dissociate some hydrogen bonds, causing plasticisation and swelling of the structures, as is the case with synthetic polymers such as EVOH or PVOH, and allowing the oxygen molecules to diffuse more easily (Nair et al. 2014). Different strategies have been developed to induce hydrophobicity in nanocrystals. Some of these approaches include surface modification of CNCs through oxidations (Fraschini, Chauve, and Bouchard 2017), acetylations (Yuan et al. 2006), esterifications (Trinh and Mekonnen 2018), silylations (Goussé et al. 2002), among others (Eyley and Thielemans 2014), blending with other polymers (Popescu 2017, Fortunati et al. 2014), cross-linkers (Yin, Ahmad, and Amin 2014, Lim et al. 2014), and coating on hydrophobic polymers (Rampazzo et al. 2017). Also, the use of multilayer systems has been proposed a proper manner to protect the CNCs from moisture (Fotie, Limbo, and Piergiovanni 2020). Thus, the preservation of a CNCs layer between two layers of hydrophobic polymers such as PP, PET or PE allows to maintain their excellent mechanical and oxygen barrier properties as well as to obtain the benefits of the other polymers, such as water vapor barrier (Wang et al. 2020). In addition, their use in combination with biopolymers, such as PLA or PHAs, instead of petroleum-based materials turns the multilayer structure into a complete bio-based and biodegradable system (Koppolu et al. 2019, Figueroa-Lopez, Torres-Giner, et al. 2020). Furthermore, it has been reported that only a 1 μm thickness of the CNCs layer is sufficient to obtain the benefits of its high oxygen barrier properties, being even superior to commonly used synthetics such as EVOH or PVDC (Fotie et al. 2019, Fotie et al. 2020).

4. Processing technologies in food packaging

Various polymer processing methods have been applied both in the laboratory and on an industrial scale. They are used for the production of individual materials and for the blending of several components and/or fillers, the formation of nanocomposites, and the assembly of multilayers. Among those used for thermoplastics, melt-based processes including extrusion molding, compression molding, injection molding, and blow molding, are the most widely used in the industry. In these processes, the molten polymer flows into a mold or die to be shaped and then cools to solidify (Francis 2016). These are quite versatile processes in which polymers can adopt the form of films, tubes, fibers, or other complex shapes. However, when it is not possible or desirable to melt the polymer, solution processing has been employed. In this case, the polymer is dissolved in a solvent, poured into a mold and, after evaporation, solidifies to form a film (Rhim et al. 2006). Nevertheless, this method is less used industrially, due to the small quantity obtained and the fact that toxic solvents are sometimes used and have to be recovered afterwards, which makes the process more expensive (Siemann 2005). Emerging from the laboratory scale, other techniques are newly scaled-up and used to process polymers, such as electrospinning, which is also discussed below.

4.1. Melt compounding

Melt compounding is today the main industrial processing technology to mix polymeric materials to produce blends or polymeric materials with additives (Mokhena et al. 2018, Tanahashi 2010). On a laboratory scale, a mini melt mixer is often used, as it allows mixing small quantities of materials for rapid analysis. It consists of a mixer bowl, where the materials are fed, with two counter-rotating blades for mixing and three separate heating areas. Temperature, screw speed and time can be modified depending on the materials (Mokhena et al. 2018). Melt compounding has been used to blend at least two different polymers in order to improve their properties, creating a novel material whose properties have intermediate values between the materials used.

Polymer blending has been seen as a great method to obtain materials with enhanced properties and processability at a lower cost (Belabed et al. 2012). Therefore, polymers with poor mechanical, thermal, or barrier properties have been blended with others that have these improved qualities to enhance the final product and broaden their applications. For example, with regard to the PHBV, although it has many advantages, it also has poor thermal stability and brittleness, so blending with other polymers can improve these limitations (Nanda, Misra, and Mohanty 2011, Ju et al. 2014). However, the compatibility between the two or more materials used in the blend may not be adequate. Miscibility is a thermodynamic term describing the number of phases between polymers and the composition formed when mixed (Zeng, Li, and Du 2015). The interactions between polymers can range from strong to weak including hydrogen bonding, ion-dipole, dipole-dipole, donor-acceptor and Van der Waals interactions. This results in three types of blends: completely miscible, presenting a homogeneous morphology and a single T_g with a value between the T_g of the polymers used; partially miscible, showing two phases with one of the components dissolved in the other and two T_g, corresponding to the two phases but shifted from the pure components to the blends; and fully immiscible, showing a heterogeneous structure, with poor interphase adhesion and exhibiting T_g of the pure individual components used (El-Hadi 2014). Most polymer blends are immiscible, which implies the use of compatibilizers that allow the reduction of the interfacial tension coefficient, the improvement of adhesion between the different phases, and the formation and stabilisation of the required morphology. The compatibilization can be achieved by physical or chemical mechanisms, through the use of non-reactive and reactive compatibilizers, respectively (Ragaert, Delva, and Van Geem 2017). Non-reactive compatibilizers are based on the use of copolymers, usually block or grafted copolymers rather than random copolymers, which are compatible with the different phases of the blend and improve their interfacial adhesion. Some of the most commonly used are poly(styrene–ethylene/butylene–styrene) block copolymer (SEBS), styrene–butadiene copolymer rubber (SBR), ethylene propylene rubber (EPR), ethylene–propylene copolymer (EPM), EVA, among others (Nechifor et al. 2018). On the other hand, reactive compatibilizers establish effective bonds between the components of the blend through functional groups. Mainly used are: maleic anhydride (MA), glycidyl methacrylate (GMA), and acrylic acid (AA), which can be grafted onto the non-reactive compatibilizers or directly onto the components of the blend (Vilaplana and Karlsson 2008). Sometimes, the use of free-radical initiators, such as peroxides, in reactive processing is necessary to enhance the reaction rate. For instance, dicumyl peroxide (DCP) has been seen to induce the crosslinking within the matrix, improving the compatibility and the mechanical performance of the blends (Zhang, Misra, and Mohanty 2014, Dong et al. 2013).

Moreover, fillers are often used blended with polymers in order to improve mechanical properties, such as reinforcement, and to lower the price of the final product (Kuciel, Mazur, and Jakubowska 2019). The combination of fillers with polymer is termed composite. Natural fibers have been

used as polymer fillers and have proved to be a great alternative to traditionally used glass fibers, not only because they have excellent specific properties such as high strength and stiffness, but also because they are biodegradable, recyclable and environmentally friendly allowing the reuse of waste (Badia et al. 2014). They are derived mainly from plant lignocellulose and agricultural residues including hemp, cellulose, ramie, bamboo, flax, sisal, kenaf, jute, wood, pineapple, rice husk, wheat straw, and others (Berthet et al. 2015, Ahankari, Mohanty, and Misra 2011, Bassyouni and Waheed Ul Hasan 2015, Kittikorn et al. 2018). When these natural fibers are embedded in bio-based and biodegradable polymers, a "green composite" is formed. However, the inherent hydrophilic nature of these cellulosic fillers makes them sensitive to moisture absorption and hinders their dispersion in non-polar matrices (David et al. 2021). Thus, different strategies have been developed in order to chemically change the surface of the fillers for improving dispersibility and filler/polymer adhesion. Some of the approaches used are grafting, acetylation, alkali treatment, maleated coupling agents, among others (Li, Tabil, and Panigrahi 2007, Zhang, Zhong, and Ren 2017). Crosslinking agents such as triglycidyl isocyanurate (TGIC), a trifunctional epoxy compound, have also been used as a bonding agent between the fillers and the polymer matrix. TGIC improves interfacial adhesion through the reaction between its epoxy groups with the hydroxyl or carboxyl end groups of the fillers and polymers (Hao and Wu 2018, Guo et al. 2014).

Nanofillers have gained attention for use in polymer blends due to their unique optical, electrical and magnetic properties (Tanahashi 2010). They not only improve the mechanical, barrier and thermal properties of the polymer but also enhance the compatibility between the components of the blend (Mohammed Gumel and Annuar 2015). The most commonly used nanofillers are carbon nanotubes (CNTs), graphene nanoplatelets (GNPs) and nanosheets (GNSs), nanoclays (montmorillonite (MMT), halloysite nanotubes (HNTs)), starch nanocrystals (SNCs), CNCs, and metal nanoparticles (Pires et al. 2021, Sarfraz et al. 2021). Their nanoscale dimensions, with high aspect ratio and large surface area, allow their benefits to be obtained using small quantities (Mohammed Gumel and Annuar 2015). Their use has spread not only in the packaging industry, but also in energy, automotive and biomedical applications (Kausar 2021). Adequate dispersion of the nanofillers in the polymer matrix is required to obtain the improved properties. However, due to their high surface activity, these nanoparticles tend to agglomerate, losing some of their valuable benefits. Thus, different strategies have been applied in order to enhance their dispersion including the use of surfactants, sonication, microwaves, among others (Zubair and Ullah 2020). The method employed to process the nanocomposites is also important. The three most commonly applied are sol-gel polymerization, in situ polymerization, and melt compounding, the latter being the most efficient as it does not require the use of solvents and their removal, saving time and costs and being environmentally friendly, as well as being easier to scale up to an industrial level (Zhu, Abeykoon, and Karim 2021). In addition, the shear stress used during the mixing process induces the dispersive action of the agglomerates (Tanahashi et al. 2006).

4.2. Electrospinning technology

Electrohydrodynamic processing (EHDP) is a novel technique based on the production of fibers (known as electrospinning) or droplets (called electrospraying) from a polymeric liquid (a solution or melt) through the use of electrical force (Echegoyen et al. 2017). When fibers are

produced, their diameter dimensions range from a few micrometers to several nanometers and form continuous non-woven mats with large surface areas, while droplets develop non-continuous structures in the form of micro- and nanoparticles (capsules or beads) (Soares et al. 2018). The fibers and capsules obtained by EHDP are smaller than those obtained by traditional processes such as melt extrusion or SD, respectively, which confers extraordinary properties and functionalities (Torres-Giner, Pérez-Masiá, and Lagaron 2016).

The EHDP device consists of three components: power supply, syringe pump, and collector plate. In the process, the polymer liquid is electrically charged by the high voltage, repelling and accumulating charges on the surface. Above a certain electrical threshold, the charges exceed the surface tension, producing an unstable droplet, the so-called Taylor cone, from which the charged jet is emitted into the collector, where the fibers or particles are deposited in solid form as the solvent evaporates during the process (Xue et al. 2019). The schematic diagram of the main components of the electrospinning system is illustrated in **Figure 12**.

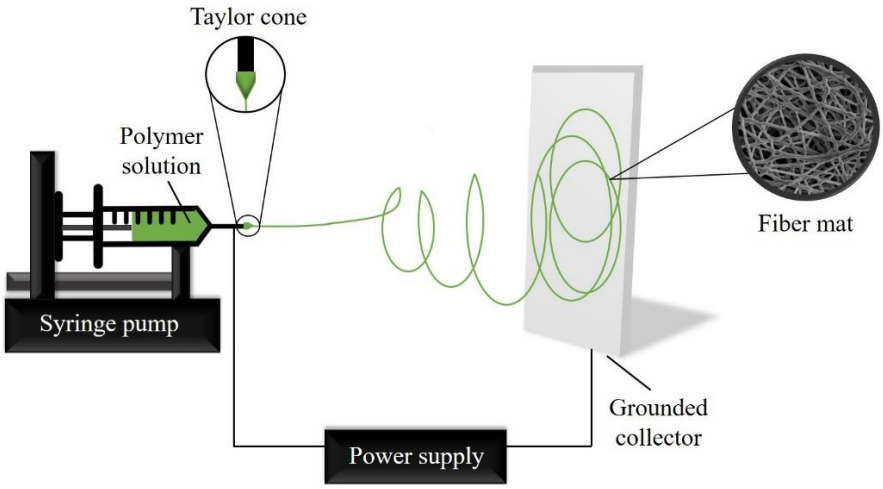

Figure 12. Schematic diagram of the electrospinning device.

The formation of these nanostructures is influenced by the parameters of the equipment, the properties of the polymer solution and environmental factors. Regarding the elements of the device, the applied voltage, the flow rate and the distance needle-collector are the critical factors. The voltage determines the fiber size and bead formation. The higher the voltage, the finer the fibers produced. However, when the voltage exceeds a critical value, bead formation occurs, attributed to a reduction of the Taylor cone and an increase in jet velocity (Haider, Haider, and Kang 2018). The flow rate also affects the morphology of the electrospun nanofibers and depends on the polymer solution used. Increasing it above a critical value, produces larger fiber diameters and induces the formation of beads, related to insufficient drying jet (Bhattarai et al. 2018). The needle-collector distance influences fiber diameter size and fiber/bead formation. The longer the distance, the smaller the fiber diameter and the fewer beads will be formed (Vlachou, Siamidi, and Kyriakou 2019).

The solution properties are controlled by polymer concentration, viscosity, molecular weight, surface tension, conductivity and solvent volatility. Concentration is affected by viscosity and surface tension. Thus, at low concentration, due to electric field and surface tension, the polymer chains break before reaching the collector, and nanoparticles are formed. At higher concentration, the viscosity increases and the polymer chains become entangled to form nanofibers. However, if the concentration increases above a critical value, clogging of the needle tip occurs due to excessive viscosity and dryness of the droplets. When this is removed, larger diameter beaded nanofibers are obtained (Pillay et al. 2013). The molecular weight of the polymer is also important as it affects the viscosity. Thus, a high molecular weight leads to increased viscosity and extensive chain entanglement, with the formation of beadless nanofiber (Bhattarai et al. 2018). Solution conductivity has a significant function in the formation of the Taylor cone and in controlling the size of the nanofibers. Low conductivities inhibit Taylor cone formation due to the lack of charge in the droplet. Beyond a critical value, Taylor cone will also be impeded, owing to the Coulombic forces between the charges on the fluid surface and the force of the external electric field (Vlachou, Siamidi, and Kyriakou 2019). Thus, a balance between surface tension and electric field (concentration, conductivity, and the viscosity) must be obtained as they affects the final morphology (Weng and Xie 2015). Finally, solvent volatility is a parameter that also affects the morphology of the nanofibers. The solvent should completely dissolve the polymer and have high evaporation rates and a moderate volatility profile, indicated by a moderate boiling point, in order to form smooth and beadless nanofibers (Xue et al. 2019).

Environmental parameters also have an impact on the electrospinning process and the formation of nanofibers. The two most influential are humidity and temperature. RH influences the diameters of the nanofibers and the formation of pores on the fibre surface, controlling the solidification process of the charged jet or the evaporation of solvent (Vlachou, Siamidi, and Kyriakou 2019). Temperature, on the other hand, acts through two opposite mechanisms, increasing the solvent evaporation rate and decreasing the viscosity, which leads to a reduction in fiber diameter (Haider, Haider, and Kang 2018).

Moreover, other modifications can be implemented in the electrospinning device that can change the final structure of the nanofiber mats. Thus, the collector unit is usually made of static aluminum plate. However, a rotating collector can be used to obtained aligned and drier fibers as they have more time to evaporate (Islam et al. 2019). In addition, the electrospinning setup can be operated horizontally and vertically, either top-down or bottom-up, with horizontal and bottom-up systems being preferable, as fewer defects are obtained in the final mats, as drips and stray fibers do not reach the collector (Suresh, Becker, and Glasmacher 2020). Furthermore, on a laboratory scale, the use of a single needle has been sufficient to obtain the desired product. However, on an industrial scale, in order to increase productivity and cover larger area, the use of multi-needles has been implemented (SalehHudin et al. 2018).

The growing interest in the use of this technique is due to its suitability for a wide range of polymeric materials and its use in many different applications due to the unique properties of electrospun nanofibers including high surface-to-volume ratio, porosity and uniform morphology (Ibrahim and Klingner 2020). Both synthetic and natural polymers as well as their blends have been successfully used in electrospinning. Natural polymers, including protein and polysaccharides such as collagen, gelatin, chitosan, elastin, and others, have been preferred because of their better biocompatibility and low toxicity (Law et al. 2017, Kalantari et al. 2019, Aoki, Miyoshi, and Yamagata 2015). However, they have some drawbacks such as higher costs, susceptibility to degradation, and lower mechanical performance (Hemmati et al. 2021). Synthetic

polymers, on the other hand, have certain advantages such as better electrospinnability and improved mechanical properties. Depending on the final application, different polymers are used. PS and PVC, for example, are suitable for environmental protection, while PCL, PLA, and poly(lactic-*co*-glycolic acid) (PLGA), being biocompatible and biodegradable, are used for biomedical applications (Xue et al. 2019). Other conductive (polyaniline (PANi), and polypyrrole (PPy)) and piezoelectric (poly(vinylidene fluoride) (PVDF)) polymers are used for electrical or mechanical applications (Nagam Hanumantharao and Rao 2019). In addition, the use of blends of natural and synthetic polymers provides new and improved properties. For instance, PCL/chitosan electrospun fibers showed a suitable scaffold function with good mechanical properties (Semnani et al. 2017). Similarly, when gelatin was blended both synthetic or natural polymers showed desirable biocompatibility and mechanical stability for scaffolds (Aldana and Abraham 2017).

Nanofibers have been applied in many different fields, focusing on biomedical sectors, such as wound dressing (Dong et al. 2020), medical implants (Al-Enizi, Zagho, and Elzatahry 2018), drug delivery (Stegmann, Londo, and Junginger 2020), tissue engineering scaffolds (Stafiej et al. 2017), but also in filtering membranes (Cho et al. 2020), enzyme immobilization (Fazel et al. 2016), protective textiles (Gorji, Bagherzadeh, and Fashandi 2017), and in the cosmetics and food industry (Yılmaz, Celep, and Tetik 2016, Zhao et al. 2020). Regarding food and packaging industry, the addition of nanoparticles in the polymer solution prior to electrospinning has resulted in the production of a large number of composites with extraordinary characteristics. In addition to reinforcing the polymer matrix, these nanoparticles provide additional properties, leading to the production of active packaging in which the substances interact with the food or the surrounding environment (Drago et al. 2020). These bioactive compounds can act as moisture or ethylene absorbers, oxygen scavengers, CO_2 absorbers/emitters, and antimicrobial or antioxidant agents (Cherpinski, Szewczyk, et al. 2019, Zhang et al. 2020). Thus, these substances limit or prevent the growth of microorganisms, ensuring food safety and prolonging shelf life (Zhao et al. 2020). Some of the most widely used are metals and metal oxide nanoparticles (Ag, Zn, Cu, Ti, Co, TiO_2, SiO_2, MgO, CaO) (Cherpinski, Szewczyk, et al. 2019, Quirós, Boltes, and Rosal 2016), natural extracts (NEs) (Figueroa-Lopez et al. 2019), and EOs (Ataei et al. 2020). These substances must be categorised as Generally Recognised as Safe (GRAS) by the US Food and Drug Administration (FDA) in order to be used in food packaging (Abd-Elsalam et al. 2017). Nevertheless, there are some limitations such as volatility, chemical instability, or possible interaction with packaged foods (Salević et al. 2019). For these reasons, the encapsulation of these substances by electrospinning technology allows to increase their stability and control their release, and, as electrospinning is performed at room temperature, the degradation of these compounds and their volatilization is avoided (Tang et al. 2019). Numerous examples have been published on the use of these substances for the prevention of food spoilage. For instance, *Allium ursinum L.* extract was encapsulated in electrospun PLA fibers, showing antibacterial activity as well as improved mechanical strength and a better water vapor barrier (Radusin et al. 2019). Carvacrol EO encapsulated in both zein and PLA electrospun fibers showed 99.6 and 91.3 % inhibition against mold and yeast and about 87 % inhibition against bacteria (Altan, Aytac, and Uyar 2018). In another study, electrospun ethylcellulose/gelatin nanofibers exhibited enhanced surface hydrophobicity, mechanical properties, water stability and antibacterial properties when ZnO nanoparticles were added to the fibers (Liu et al. 2018).

However, although embedding in the fibers protects the active substances, it is sometimes necessary to use other encapsulants prior to electrospinning. Cyclodextrins (CDs), cyclic

oligosaccharides produced by the enzymatic conversion of starch, are used as host molecule as they are able to form inclusion complexes with a variety of compounds through capture in their hydrophobic cavity (Celebioglu and Uyar 2021). They contribute to keeping the active substances stable and active in the electrospun nanofibers. For instance, eugenol/CD complex encapsulated in PVOH nanofibers presented higher thermal stability and slower release of eugenol compared to the non-encapsulated one (Kayaci, Ertas, and Uyar 2013). Mesoporous silica nanoparticles (MSNPs) have also been used to protect active substances against degradation or volatilization, thus allowing controlled and prolonged release. MSNPs have gained attention due to their variable properties such as particle size, pore size, volume, and structure, surface area, volume area, and surface functionality (Manzano and Vallet-Regí 2020). Also, they are accepted as GRAS. Encapsulation of different EOs in MSNPs was reported to increase their antimicrobial activity up to 10 times compared to free oils (Bravo Cadena et al. 2018).

Other electrospinning methods have been applied when encapsulating nanoparticles in polymeric fibers. In addition to the blending electrospinning described above, two other systems, coaxial electrospinning and emulsion electrospinning, are used in order to produce core/sheath structures. Coaxial electrospinning, also called co-electrospinning, is based on two polymer solutions flowing through two different pumps and syringes whose needles are one inside the other. The two liquids meet at the ends of the coaxial needle, forming the Taylor cone and a coaxial jet, whose nanofibers will have a different composition on the inside than on the outside (core/sheath nanofibers) (Xue et al. 2019). This method is useful for obtaining polymers with new properties, for polymers that are not electrospinnable by themselves, e.g. due to their low viscosity, and for encapsulating active substances, which are protected in the core from the environment and released in a more controlled form (Vlachou, Siamidi, and Kyriakou 2019). On the other hand, emulsion electrospinning is based on a solution of different liquid phases in which the continuous phase, usually an oil phase of the polymer solution, is the fiber shell and the droplet phase, an aqueous phase in which the active substance is dissolved, is the core. A surfactant is needed to disperse the two phases. In this case, no specific needle setup is required as in coaxial electrospinning (Wang et al. 2019). One of the advantages of this method is that there is no need for a common solvent between the polymer and the active substance, as in the case of blending electrospinning (Bhattarai et al. 2018).

In addition to the use of electrospinning for the fabrication of monolayer materials, nanofibers have arisen as a promising technology for the coating of interlayers in multilayer systems, to add new attributes such as adhesive properties. This is described in section 5.

5. Multilayer structures

Food packaging is essential for the maintenance, safety and quality of food, as it serves to transport and store it, to preserve it from contamination and microorganisms, to print and describe product characteristics and for marketing purposes to attract consumers to buy it. Depending on the packaged food, different materials are selected for the packaging according to their suitability to fit the required characteristics. Some of the basic specifications to be met are high barrier

(moisture, gas, light, odor), mechanical strength and sealability, heat and chemical resistance, optical qualities and antimicrobial properties (Anukiruthika et al. 2020).

However, the requirements of a food packaging are not possible to achieve with a single layer of a polymeric material. Therefore, the use of multilayer systems, typically 3 to 7 layers in food packaging, is a convenient solution to achieve these standards in an affordable and safe form. Polymeric multilayer systems produce thinner and lighter structures, as less material is needed than is used in conventional systems such as glass and metal (Ramos et al. 2015). In this structure, each layer has a specific function. Thus, the outer layer functions as a structural, moisture and light barrier layer, while the inner layers act as oxygen and active barriers, and as adhesive. **Figure 13** shows an example of a multilayer packaging structure showing the 4 main layers of the system: structural, barrier, active and food contact. The food contact layer must be inert and not react with food (Anukiruthika et al. 2020). The techniques commonly used to prepare these multilayer systems are coextrusion, lamination, coating, layer-by-layer assembly, coinjection with stretch blow molding, etc (Tyagi et al. 2021). However, electrospinning technology is emerging as a potential technique for the assembly of different layers, even with improved properties through the encapsulation of active substances, as discussed in section 4.2. Moreover, electrospun fiber mats have been very recently researched as hot-tack (HT) interlayers in multilayer systems due to their physico-chemical adhesive properties. These adhesive attributes allow the elimination of the petroleum-derived environmentally harmful synthetic tie layers that are normally used (Cerqueira et al. 2016). The assembly of the electrospun fiber layers is done by a thermal post-treatment, known as annealing, below the melting temperature (T_m) of the polymer, whereby the fibers coalesce and form a continuous structure without porosity, called biopapers (Cherpinski et al. 2018). The formation and structure of these biopapers are not well understood, and to provide an understanding is part of the academic objectives of this PhD thesis. These adhesive biopapers can offer improved optical, mechanical and barrier properties compared to their fibers and petroleum counterparts (Figueroa-Lopez, Cabedo, et al. 2020).

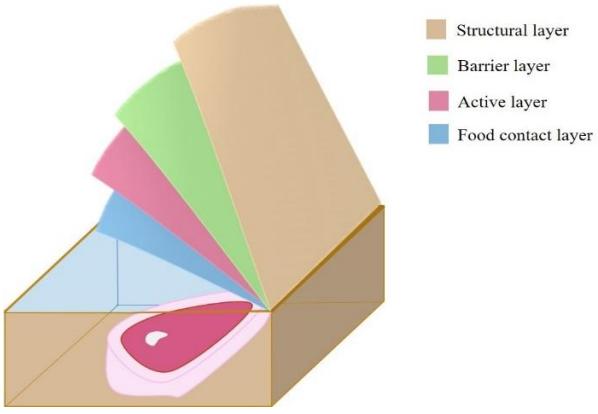

Figure 13. Structure of a multilayer packaging system.

6. References

Abd-Elsalam, Kamel A., Ayat F. Hashim, Mousa A. Alghuthaymi, and Ernest Said-Galiev. 2017. "10 - Nanobiotechnological strategies for toxigenic fungi and mycotoxin control." In *Food Preservation*, edited by Alexandru Mihai Grumezescu, 337-364. Academic Press.

Advisors, Dalberg, Wijnand de Wit, Adam Hamilton, Rafaella Scheer, Thomas Stakes, and Simon Allan. 2019. "Solving plastic pollution through accountability." *World Wide Fund For Nature report*.

Ahankari, Sandeep S., Amar K. Mohanty, and Manjusri Misra. 2011. "Mechanical behaviour of agro-residue reinforced poly(3-hydroxybutyrate-co-3-hydroxyvalerate), (PHBV) green composites: A comparison with traditional polypropylene composites." *Composites Science and Technology* 71 (5):653-657. doi: https://doi.org/10.1016/j.compscitech.2011.01.007.

Ahn, Woo Suk, Si Jae Park, and Sang Yup Lee. 2001. "Production of poly(3-hydroxybutyrate) from whey by cell recycle fed-batch culture of recombinant Escherichia coli." *Biotechnology Letters* 23 (3):235-240. doi: 10.1023/A:1005633418161.

Al-Enizi, Abdullah M., Moustafa M. Zagho, and Ahmed A. Elzatahry. 2018. "Polymer-Based Electrospun Nanofibers for Biomedical Applications." *Nanomaterials (Basel, Switzerland)* 8 (4):259. doi: 10.3390/nano8040259.

Albuquerque, M. G. E., C. A. V. Torres, and M. A. M. Reis. 2010. "Polyhydroxyalkanoate (PHA) production by a mixed microbial culture using sugar molasses: Effect of the influent substrate concentration on culture selection." *Water Research* 44 (11):3419-3433. doi: https://doi.org/10.1016/j.watres.2010.03.021.

Albuquerque, Maria G. E., Gilda Carvalho, Caroline Kragelund, Ana F. Silva, Maria T. Barreto Crespo, Maria A. M. Reis, and Per H. Nielsen. 2013. "Link between microbial composition and carbon substrate-uptake preferences in a PHA-storing community." *The ISME Journal* 7 (1):1-12. doi: 10.1038/ismej.2012.74.

Aldana, Ana A., and Gustavo A. Abraham. 2017. "Current advances in electrospun gelatin-based scaffolds for tissue engineering applications." *International Journal of Pharmaceutics* 523 (2):441-453. doi: https://doi.org/10.1016/j.ijpharm.2016.09.044.

Ali, Sameh Samir, Tamer Elsamahy, Eleni Koutra, Michael Kornaros, Mostafa El-Sheekh, Esraa A. Abdelkarim, Daochen Zhu, and Jianzhong Sun. 2021. "Degradation of conventional plastic wastes in the environment: A review on current status of knowledge and future perspectives of disposal." *Science of The Total Environment* 771:144719. doi: https://doi.org/10.1016/j.scitotenv.2020.144719.

Altan, Aylin, Zeynep Aytac, and Tamer Uyar. 2018. "Carvacrol loaded electrospun fibrous films from zein and poly(lactic acid) for active food packaging." *Food Hydrocolloids* 81:48-59. doi: https://doi.org/10.1016/j.foodhyd.2018.02.028.

Alves, Ana-Clara-Lancarovici, Rafael Grande, and Antonio-José-Felix Carvalho. 2019. "Thermal and Mechanical Properties of Thermoplastic Starch and Poly(Vinyl Alcohol-Co-Ethylene) Blends." *Journal of Renewable Materials* 7 (3):245--252.

Amstutz, Véronique, Nils Hanik, Julien Pott, Camila Utsunomia, and Manfred Zinn. 2019. "Chapter Four - Tailored biosynthesis of polyhydroxyalkanoates in chemostat cultures." In *Methods in Enzymology*, edited by Nico Bruns and Katja Loos, 99-123. Academic Press.

Anukiruthika, T., Priyanka Sethupathy, Anila Wilson, Kiran Kashampur, Jeyan Arthur Moses, and Chinnaswamy Anandharamakrishnan. 2020. "Multilayer packaging: Advances in preparation techniques and emerging food applications." *Comprehensive Reviews in Food Science and Food Safety* 19 (3):1156-1186. doi: https://doi.org/10.1111/1541-4337.12556.

Anwar, Budiman, Bunbun Bundjali, Yayan Sunarya, and I. Made Arcana. 2021. "Properties of Bacterial Cellulose and Its Nanocrystalline Obtained from Pineapple Peel Waste Juice." *Fibers and Polymers* 22 (5):1228-1236. doi: 10.1007/s12221-021-0765-8.

Aoki, Hiroyoshi, Hiromi Miyoshi, and Yutaka Yamagata. 2015. "Electrospinning of gelatin nanofiber scaffolds with mild neutral cosolvents for use in tissue engineering." *Polymer Journal* 47 (3):267-277. doi: 10.1038/pj.2014.94.

Armstrong, R., M. Asme, and M. Spe. 2009. "Improving indoor air quality by reducing radon and vapor intrusion through the use of ethylene vinyl alcohol (EVOH)."

Arroja, Luis, Isabel Capela, Maria Nadais, Luísa Serafim, and Flávio Silva. 2012. "Acidogenic Valorisation of High Strength Waste Products from Food Industry." In, 227-252.

Ataei, Shahla, Pedram Azari, Aziz Hassan, Belinda Pingguan-Murphy, Rosiyah Yahya, and Farina Muhamad. 2020. "Essential Oils-Loaded Electrospun Biopolymers: A Future Perspective for Active Food Packaging." *Advances in Polymer Technology* 2020:9040535. doi: 10.1155/2020/9040535.

Atasoy, Merve, Isaac Owusu-Agyeman, Elzbieta Plaza, and Zeynep Cetecioglu. 2018. "Bio-based volatile fatty acid production and recovery from waste streams: Current status and future challenges." *Bioresource Technology* 268:773-786. doi: https://doi.org/10.1016/j.biortech.2018.07.042.

Aucejo, S., R. Catalá, and R. Gavara. 2000. "Interactions between water and EVOH food packaging films / Interacciones entre el agua y películas de EVOH para el envasado de alimentos." *Food Science and Technology International* 6 (2):159-164. doi: 10.1177/108201320000600211.

Auras, Rafael A., S. Paul Singh, and Jagjit J. Singh. 2005. "Evaluation of oriented poly(lactide) polymers vs. existing PET and oriented PS for fresh food service containers." *Packaging Technology and Science* 18 (4):207-216. doi: https://doi.org/10.1002/pts.692.

Badia, J. D., T. Kittikorn, E. Strömberg, L. Santonja-Blasco, A. Martínez-Felipe, A. Ribes-Greus, M. Ek, and S. Karlsson. 2014. "Water absorption and hydrothermal performance of PHBV/sisal biocomposites." *Polymer Degradation and Stability* 108:166-174. doi: https://doi.org/10.1016/j.polymdegradstab.2014.04.012.

Barbash, V. A., and O. V. Yashchenko. 2020. "Preparation and application of nanocellulose from non-wood plants to improve the quality of paper and cardboard." *Applied Nanoscience* 10 (8):2705-2716. doi: 10.1007/s13204-019-01242-8.

Barnes, David, François Galgani, Richard Thompson, and Morton Barlaz. 2009a. "Accumulation and fragmentation of plastic debris in global environments." *Philosophical transactions of the Royal Society of London. Series B, Biological sciences* 364:1985-98. doi: 10.1098/rstb.2008.0205.

Barnes, David K. A., Francois Galgani, Richard C. Thompson, and Morton Barlaz. 2009b. "Accumulation and fragmentation of plastic debris in global environments." *Philosophical Transactions of the Royal Society B: Biological Sciences* 364 (1526):1985-1998. doi: doi:10.1098/rstb.2008.0205.

Bassyouni, M., and S. Waheed Ul Hasan. 2015. "13 - The use of rice straw and husk fibers as reinforcements in composites." In *Biofiber Reinforcements in Composite Materials*, edited by Omar Faruk and Mohini Sain, 385-422. Woodhead Publishing.

Battista, Federico, Nicola Frison, Paolo Pavan, Cristina Cavinato, Marco Gottardo, Francesco Fatone, Anna L Eusebi, Mauro Majone, Marco Zeppilli, Francesco Valentino, Debora Fino, Tonia Tommasi, and David Bolzonella. 2020. "Food wastes and sewage sludge as feedstock for an urban biorefinery producing biofuels and added-value bioproducts." *Journal of Chemical Technology & Biotechnology* 95 (2):328-338. doi: https://doi.org/10.1002/jctb.6096.

Belabed, Ch., Z. Benabdelghani, A. Granado, and A. Etxeberria. 2012. "Miscibility and specific interactions in blends of poly(4-vinylphenol-co-methyl methacrylate)/poly(styrene-co-4-vinylpyridine)." *Journal of Applied Polymer Science* 125 (5):3811-3819. doi: https://doi.org/10.1002/app.36343.

Berthet, M. A., H. Angellier-Coussy, V. Chea, V. Guillard, E. Gastaldi, and N. Gontard. 2015. "Sustainable food packaging: Valorising wheat straw fibres for tuning PHBV-based composites properties." *Composites Part A: Applied Science and Manufacturing* 72:139-147. doi: https://doi.org/10.1016/j.compositesa.2015.02.006.

Bertin, Lorenzo, Silvia Lampis, Daniela Todaro, Alberto Scoma, Giovanni Vallini, Leonardo Marchetti, Mauro Majone, and Fabio Fava. 2010. "Anaerobic acidogenic digestion of olive mill wastewaters in biofilm reactors packed with ceramic filters or granular activated carbon." *Water Research* 44 (15):4537-4549. doi: https://doi.org/10.1016/j.watres.2010.06.025.

Bhattarai, Rajan Sharma, Rinda Devi Bachu, Sai H. S. Boddu, and Sarit Bhaduri. 2018. "Biomedical Applications of Electrospun Nanofibers: Drug and Nanoparticle Delivery." *Pharmaceutics* 11 (1):5. doi: 10.3390/pharmaceutics11010005.

Bioplastics, European. 2020a. "Bioplastics market data." accessed 2021. https://www.european-bioplastics.org/market/.

Bioplastics, European. 2020b. "Renewable feedstock." accessed 2021. https://www.european-bioplastics.org/bioplastics/feedstock/.

Blanchard, Anthony, Flavien Melis, Fabrice Gouanvé, Jean-Matthieu Brouillat, and Eliane Espuche. 2021. "Influence of the PVOH molar mass on the morphology and functional properties of EVOH/PVOH films prepared by melt blending." *Journal of Polymer Science* 59 (1):70-83. doi: https://doi.org/10.1002/pol.20200370.

Blanton, R. L., D. Fuller, N. Iranfar, M. J. Grimson, and W. F. Loomis. 2000. "The cellulose synthase gene of Dictyostelium." *Proceedings of the National Academy of Sciences of the United States of America* 97 (5):2391-2396. doi: 10.1073/pnas.040565697.

Bohmert, Karen, Ilse Balbo, Alexander Steinbüchel, Gilbert Tischendorf, and Lothar Willmitzer. 2002. "Constitutive Expression of the β-Ketothiolase Gene in Transgenic Plants. A Major Obstacle for Obtaining Polyhydroxybutyrate-Producing Plants." *Plant Physiology* 128 (4):1282-1290. doi: 10.1104/pp.010615.

Boufi, Sami, Hamid Kaddami, and Alain Dufresne. 2014. "Mechanical Performance and Transparency of Nanocellulose Reinforced Polymer Nanocomposites." *Macromolecular Materials and Engineering* 299 (5):560-568. doi: https://doi.org/10.1002/mame.201300232.

Bravo Cadena, Marimar, Gail M. Preston, Renier A. L. Van der Hoorn, Helen E. Townley, and Ian P. Thompson. 2018. "Species-specific antimicrobial activity of essential oils and enhancement by encapsulation in mesoporous silica nanoparticles." *Industrial Crops and Products* 122:582-590. doi: https://doi.org/10.1016/j.indcrop.2018.05.081.

Brinchi, L., F. Cotana, E. Fortunati, and J. M. Kenny. 2013. "Production of nanocrystalline cellulose from lignocellulosic biomass: Technology and applications." *Carbohydrate Polymers* 94 (1):154-169. doi: https://doi.org/10.1016/j.carbpol.2013.01.033.

Bugnicourt, Elodie, Patrizia Cinelli, Vera Alvarez, and Andrea Lazzeri. 2014. "Polyhydroxyalkanoate (PHA): Review of synthesis, characteristics, processing and potential applications in packaging." *eXPRESS Polymer Letters* 8:791-808. doi: 10.3144/expresspolymlett.2014.82.

Cabedo, Lluís, Enrique Giménez, José M. Lagaron, Rafael Gavara, and Juan J. Saura. 2004. "Development of EVOH-kaolinite nanocomposites." *Polymer* 45 (15):5233-5238. doi: https://doi.org/10.1016/j.polymer.2004.05.018.

Cabedo, Luis, María Pilar Villanueva, José María Lagarón, and Enrique Giménez. 2017. "Development and characterization of unmodified kaolinite/EVOH nanocomposites by melt compounding." *Applied Clay Science* 135:300-306. doi: https://doi.org/10.1016/j.clay.2016.10.008.

Campano, Cristina, Ana Balea, Angeles Blanco, and Carlos Negro. 2016. "Enhancement of the fermentation process and properties of bacterial cellulose: a review." *Cellulose* 23 (1):57-91. doi: 10.1007/s10570-015-0802-0.

Carvalho, Gilda, Adrian Oehmen, Maria G. E. Albuquerque, and Maria A. M. Reis. 2014. "The relationship between mixed microbial culture composition and PHA production performance from fermented molasses." *New Biotechnology* 31 (4):257-263. doi: https://doi.org/10.1016/j.nbt.2013.08.010.

Cava, D., C. Sammon, and J. M. Lagaron. 2007. "Sorption-induced release of antimicrobial isopropanol in EVOH copolymers as determined by ATR-FTIR spectroscopy." *Journal of Applied Polymer Science* 103 (5):3431-3437. doi: https://doi.org/10.1002/app.25532.

Celebioglu, Asli, and Tamer Uyar. 2021. "Electrohydrodynamic encapsulation of eugenol-cyclodextrin complexes in pullulan nanofibers." *Food Hydrocolloids* 111:106264. doi: https://doi.org/10.1016/j.foodhyd.2020.106264.

Cerqueira, Miguel A., María José Fabra, Jinneth Lorena Castro-Mayorga, Ana I. Bourbon, Lorenzo M. Pastrana, António A. Vicente, and Jose M. Lagaron. 2016. "Use of Electrospinning to Develop Antimicrobial Biodegradable Multilayer Systems: Encapsulation of Cinnamaldehyde and Their Physicochemical Characterization." *Food and Bioprocess Technology* 9 (11):1874-1884. doi: 10.1007/s11947-016-1772-4.

Cerrada, María L., Ernesto Pérez, José M. Pereña, and Rosario Benavente. 1998. "Wide-Angle X-ray Diffraction Study of the Phase Behavior of Vinyl Alcohol−Ethylene Copolymers." *Macromolecules* 31 (8):2559-2564. doi: 10.1021/ma9705127.

Chamas, Ali, Hyunjin Moon, Jiajia Zheng, Yang Qiu, Tarnuma Tabassum, Jun Hee Jang, Mahdi Abu-Omar, Susannah L. Scott, and Sangwon Suh. 2020. "Degradation Rates of Plastics in the Environment." *ACS Sustainable Chemistry & Engineering* 8 (9):3494-3511. doi: 10.1021/acssuschemeng.9b06635.

Chen, Shiming, Li Tan, Furong Qiu, Xiuli Jiang, Min Wang, and Hongdong Zhang. 2004. "The study of poly(styrene-co-p-(hexafluoro-2-hydroxylisopropyl)-α-methyl-styrene)/poly(propylene carbonate) blends by ESR spin probe and Raman." *Polymer* 45 (9):3045-3053. doi: https://doi.org/10.1016/j.polymer.2004.02.049.

Cherpinski, Adriane, Atanu Biswas, Jose M. Lagaron, Alain Dufresne, Sanghoon Kim, Megan Buttrum, Eduardo Espinosa, and H. N. Cheng. 2019. "Preparation and evaluation of oxygen scavenging nanocomposite films incorporating cellulose nanocrystals and Pd nanoparticles in poly(ethylene-co-vinyl alcohol)." *Cellulose* 26 (12):7237-7251. doi: 10.1007/s10570-019-02613-8.

Cherpinski, Adriane, Piotr K. Szewczyk, Adam Gruszczyński, Urszula Stachewicz, and Jose M. Lagaron. 2019. "Oxygen-Scavenging Multilayered Biopapers Containing Palladium Nanoparticles Obtained by the Electrospinning Coating Technique." *Nanomaterials* 9 (2):262.

Cherpinski, Adriane, Sergio Torres-Giner, Luis Cabedo, Jose Alberto Méndez, and Jose M. Lagaron. 2018. "Multilayer structures based on annealed electrospun biopolymer coatings of interest in water and aroma barrier fiber-based food packaging applications." *Journal of Applied Polymer Science* 135 (24):45501. doi: https://doi.org/10.1002/app.45501.

Chi, Kai, and Jeffrey M. Catchmark. 2018. "Improved eco-friendly barrier materials based on crystalline nanocellulose/chitosan/carboxymethyl cellulose polyelectrolyte complexes." *Food Hydrocolloids* 80:195-205. doi: https://doi.org/10.1016/j.foodhyd.2018.02.003.

Chiba, Yuta, and Yoichi Tominaga. 2012. "Poly(ethylene-co-vinyl alcohol)/sulfonated mesoporous organosilicate composites as proton-conductive membranes." *Journal of Power Sources* 203:42-47. doi: https://doi.org/10.1016/j.jpowsour.2011.11.072.

Cho, Chia-Jung, Yu-Sheng Chang, Yan-Zhen Lin, Dai-Hua Jiang, Wei-Hung Chen, Wen-Yinn Lin, Chin-Wen Chen, Syang-Peng Rwei, and Chi-Ching Kuo. 2020. "Green electrospun nanofiber membranes filter prepared from novel biomass thermoplastic copolyester: Morphologies and filtration properties." *Journal of the Taiwan Institute of Chemical Engineers* 106:206-214. doi: https://doi.org/10.1016/j.jtice.2019.11.002.

Clifton-García, B., O. González-Reynoso, J.R. Robledo-Ortiz, J. Villafaña-Rojas, and Y. González-García. 2020. "Forest soil bacteria able to produce homo and copolymers of polyhydroxyalkanoates from several pure and waste carbon sources." *Letters in Applied Microbiology* 70 (4):300-309. doi: https://doi.org/10.1111/lam.13272.

Colombo, Bianca, Tommy Pepè Sciarria, Maria Reis, Barbara Scaglia, and Fabrizio Adani. 2016. "Polyhydroxyalkanoates (PHAs) production from fermented cheese whey by using a mixed microbial culture." *Bioresource Technology* 218:692-699. doi: https://doi.org/10.1016/j.biortech.2016.07.024.

Commission, European. 2012. "Communication from the Commission to the European Parliament, the Council, the European Economic and Social Committee and the Committee of the Regions. Innovating for Sustainable Growth: A Bioeconomy for

Europe." accessed 2021. https://op.europa.eu/es/publication-detail/-/publication/84e7a360-6970-4cb8-939d-8acbf33f0ae8/language-en.
Commission, European. 2015. "Closing the loop – an EU action plan for the Circular Economy." accessed 2021. https://eur-lex.europa.eu/legal-content/EN/TXT/?uri=CELEX%3A52015DC0614 (2015).
Coppola, Gerardo, Maria Teresa Gaudio, Catia Giovanna Lopresto, Vincenza Calabro, Stefano Curcio, and Sudip Chakraborty. 2021. "Bioplastic from Renewable Biomass: A Facile Solution for a Greener Environment." *Earth Systems and Environment*. doi: 10.1007/s41748-021-00208-7.
Council, AC. 2019. "The Basics: Polymer Definition and Properties." Retrieved from American Chemistry Council, accessed 2021. https://plastics.americanchemistry.com/plastics/The-Basics/.
Dammak, Mohamed, Yesmine Fourati, Quim Tarrés, Marc Delgado-Aguilar, Peré Mutjé, and Sami Boufi. 2020. "Blends of PBAT with plasticized starch for packaging applications: Mechanical properties, rheological behaviour and biodegradability." *Industrial Crops and Products* 144:112061. doi: https://doi.org/10.1016/j.indcrop.2019.112061.
Dasan, Y. K., A. H. Bhat, and Faiz Ahmad. 2017. "Polymer blend of PLA/PHBV based bionanocomposites reinforced with nanocrystalline cellulose for potential application as packaging material." *Carbohydrate Polymers* 157:1323-1332. doi: https://doi.org/10.1016/j.carbpol.2016.11.012.
David, Grégoire, Laurent Heux, Stéphanie Pradeau, Nathalie Gontard, and Hélène Angellier-Coussy. 2021. "Upcycling of Vine Shoots: Production of Fillers for PHBV-Based Biocomposite Applications." *Journal of Polymers and the Environment* 29 (2):404-417. doi: 10.1007/s10924-020-01884-8.
De Almeida Oroski, Fabio, Flávia Chaves Alves, and José Vitor Bomtempo. 2014. "Bioplastics Tipping Point: drop-in or non-drop-in?" *Journal of Business Chemistry* 11 (1).
De France, Kevin J., Todd Hoare, and Emily D. Cranston. 2017. "Review of Hydrogels and Aerogels Containing Nanocellulose." *Chemistry of Materials* 29 (11):4609-4631. doi: 10.1021/acs.chemmater.7b00531.
de Souza Machado, Anderson Abel, Werner Kloas, Christiane Zarfl, Stefan Hempel, and Matthias C. Rillig. 2018. "Microplastics as an emerging threat to terrestrial ecosystems." *Global Change Biology* 24 (4):1405-1416. doi: https://doi.org/10.1111/gcb.14020.
Del Nobile, M. A., A. Baiano, A. Benedetto, and L. Massignan. 2006. "Respiration rate of minimally processed lettuce as affected by packaging." *Journal of Food Engineering* 74 (1):60-69. doi: https://doi.org/10.1016/j.jfoodeng.2005.02.013.
Dionisi, D., G. Carucci, M. Petrangeli Papini, C. Riccardi, M. Majone, and F. Carrasco. 2005. "Olive oil mill effluents as a feedstock for production of biodegradable polymers." *Water Research* 39 (10):2076-2084. doi: https://doi.org/10.1016/j.watres.2005.03.011.
Dionisi, Davide, Mario Beccari, Simona Di Gregorio, Mauro Majone, Marco Petrangeli Papini, and Giovanni Vallini. 2005. "Storage of biodegradable polymers by an enriched microbial community in a sequencing batch reactor operated at high organic load rate." *Journal of Chemical Technology & Biotechnology* 80 (11):1306-1318. doi: https://doi.org/10.1002/jctb.1331.
Dionisi, Davide, Mauro Majone, Giovanni Vallini, Simona Di Gregorio, and Mario Beccari. 2006. "Effect of the applied organic load rate on biodegradable polymer production by mixed microbial cultures in a sequencing batch reactor." *Biotechnology and Bioengineering* 93 (1):76-88. doi: https://doi.org/10.1002/bit.20683.
Divyashree, M. S., and T. R. Shamala. 2010. "Extractability of polyhydroxyalkanoate synthesized by Bacillus flexus cultivated in organic and inorganic nutrient media." *Indian Journal of Microbiology* 50 (1):63-69. doi: 10.1007/s12088-010-0013-1.
Dobrogojski, Jędrzej, Maciej Spychalski, Robert Luciński, and Sławomir Borek. 2018. "Transgenic plants as a source of polyhydroxyalkanoates." *Acta Physiologiae Plantarum* 40 (9):162. doi: 10.1007/s11738-018-2742-4.
Dong, Weifu, Piming Ma, Shifeng Wang, Mingqing Chen, Xiaoxia Cai, and Yong Zhang. 2013. "Effect of partial crosslinking on morphology and properties of the poly(β-

hydroxybutyrate)/poly(d,l-lactic acid) blends." *Polymer Degradation and Stability* 98 (9):1549-1555. doi: https://doi.org/10.1016/j.polymdegradstab.2013.06.033.

Dong, Yuping, Yuqi Zheng, Keyan Zhang, Yueming Yao, Lihuan Wang, Xiaoran Li, Jianyong Yu, and Bin Ding. 2020. "Electrospun Nanofibrous Materials for Wound Healing." *Advanced Fiber Materials* 2 (4):212-227. doi: 10.1007/s42765-020-00034-y.

dos Santos, Antonio José, Luiz Veriano Oliveira Dalla Valentina, Andrey Alayo Hidalgo Schulz, and Marcia Adriana Tomaz Duarte. 2017. "From Obtaining to Degradation of PHB: Material Properties. Part I." *Ingeniería y Ciencia* 13:269-298.

Drago, Emanuela, Roberta Campardelli, Margherita Pettinato, and Patrizia Perego. 2020. "Innovations in Smart Packaging Concepts for Food: An Extensive Review." *Foods (Basel, Switzerland)* 9 (11):1628. doi: 10.3390/foods9111628.

Du, Haishun, Wei Liu, Miaomiao Zhang, Chuanling Si, Xinyu Zhang, and Bin Li. 2019. "Cellulose nanocrystals and cellulose nanofibrils based hydrogels for biomedical applications." *Carbohydrate Polymers* 209:130-144. doi: https://doi.org/10.1016/j.carbpol.2019.01.020.

Echegoyen, Y., M. J. Fabra, J. L. Castro-Mayorga, A. Cherpinski, and J. M. Lagaron. 2017. "High throughput electro-hydrodynamic processing in food encapsulation and food packaging applications: Viewpoint." *Trends in Food Science & Technology* 60:71-79. doi: https://doi.org/10.1016/j.tifs.2016.10.019.

El-Hadi, Ahmed. 2014. "The Effect of Additives Interaction on the Miscibility and Crystal Structure of Two Immiscible Biodegradable Polymers." *Polímeros* 24:1-8. doi: 10.4322/polimeros.2014.039.

Eyley, Samuel, and Wim Thielemans. 2014. "Surface modification of cellulose nanocrystals." *Nanoscale* 6 (14):7764-7779. doi: 10.1039/C4NR01756K.

Ezquerra, T. A., I. Šics, A. Nogales, Z. Denchev, and F. J. Baltá-Calleja. 2002. "Simultaneous crystalline-amorphous phase evolution during crystallization of polymer systems." *Europhysics Letters (EPL)* 59 (3):417-422. doi: 10.1209/epl/i2002-00211-3.

Fazel, Ramin, Seyed-Fakhreddin Torabi, Pooya Naseri-Nosar, Salehe Ghasempur, Seyed-Omid Ranaei-Siadat, and Khosro Khajeh. 2016. "Electrospun polyvinyl alcohol/bovine serum albumin biocomposite membranes for horseradish peroxidase immobilization." *Enzyme and Microbial Technology* 93-94:1-10. doi: https://doi.org/10.1016/j.enzmictec.2016.07.002.

Fernandes, Anwesha N., Lynne H. Thomas, Clemens M. Altaner, Philip Callow, V. Trevor Forsyth, David C. Apperley, Craig J. Kennedy, and Michael C. Jarvis. 2011. "Nanostructure of cellulose microfibrils in spruce wood." *Proceedings of the National Academy of Sciences* 108 (47):E1195. doi: 10.1073/pnas.1108942108.

Figueroa-Lopez, Kelly J., Luis Cabedo, Jose M. Lagaron, and Sergio Torres-Giner. 2020. "Development of Electrospun Poly(3-hydroxybutyrate-co-3-hydroxyvalerate) Monolayers Containing Eugenol and Their Application in Multilayer Antimicrobial Food Packaging." *Frontiers in Nutrition* 7 (140). doi: 10.3389/fnut.2020.00140.

Figueroa-Lopez, Kelly J., Sergio Torres-Giner, Inmaculada Angulo, Maria Pardo-Figuerez, Jose Manuel Escuin, Ana Isabel Bourbon, Luis Cabedo, Yuval Nevo, Miguel A. Cerqueira, and Jose M. Lagaron. 2020. "Development of Active Barrier Multilayer Films Based on Electrospun Antimicrobial Hot-Tack Food Waste Derived Poly(3-hydroxybutyrate-co-3-hydroxyvalerate) and Cellulose Nanocrystal Interlayers." *Nanomaterials* 10 (12):2356.

Figueroa-Lopez, Kelly J., António A. Vicente, Maria A.M. Reis, Sergio Torres-Giner, and Jose M. Lagaron. 2019. "Antimicrobial and Antioxidant Performance of Various Essential Oils and Natural Extracts and Their Incorporation into Biowaste Derived Poly(3-hydroxybutyrate-co-3-hydroxyvalerate) Layers Made from Electrospun Ultrathin Fibers." *Nanomaterials* 9 (2):144.

Follonier, Stéphanie, Miriam S. Goyder, Anne-Claire Silvestri, Simon Crelier, Franka Kalman, Roland Riesen, and Manfred Zinn. 2014. "Fruit pomace and waste frying oil as sustainable resources for the bioproduction of medium-chain-length polyhydroxyalkanoates." *International Journal of Biological Macromolecules* 71:42-52. doi: https://doi.org/10.1016/j.ijbiomac.2014.05.061.

Fortunati, E., F. Luzi, D. Puglia, F. Dominici, C. Santulli, J. M. Kenny, and L. Torre. 2014. "Investigation of thermo-mechanical, chemical and degradative properties of PLA-limonene films reinforced with cellulose nanocrystals extracted from Phormium tenax leaves." *European Polymer Journal* 56:77-91. doi: https://doi.org/10.1016/j.eurpolymj.2014.03.030.

Fotie, G, L Amoroso, S Limbo, G Muratore, and L Piergiovanni. 2019. "Food life extension by cellulose nanocrystals coatings." *Ital. J. Food Sci* 27:8-14.

Fotie, Ghislain, Stefano Gazzotti, Marco Aldo Ortenzi, and Luciano Piergiovanni. 2020. "Implementation of High Gas Barrier Laminated Films Based on Cellulose Nanocrystals for Food Flexible Packaging." *Applied Sciences* 10 (9):3201.

Fotie, Ghislain, Sara Limbo, and Luciano Piergiovanni. 2020. "Manufacturing of Food Packaging Based on Nanocellulose: Current Advances and Challenges." *Nanomaterials* 10 (9):1726.

Francis, Lorraine F. 2016. "Chapter 3 - Melt Processes." In *Materials Processing*, edited by Lorraine F. Francis, 105-249. Boston: Academic Press.

Fraschini, Carole, Grégory Chauve, and Jean Bouchard. 2017. "TEMPO-mediated surface oxidation of cellulose nanocrystals (CNCs)." *Cellulose* 24 (7):2775-2790. doi: 10.1007/s10570-017-1319-5.

Garajová, Mária, Martin Mrva, Naděžda Vaškovicová, Michal Martinka, Janka Melicherová, and Andrea Valigurová. 2019. "Cellulose fibrils formation and organisation of cytoskeleton during encystment are essential for Acanthamoeba cyst wall architecture." *Scientific Reports* 9 (1):4466. doi: 10.1038/s41598-019-41084-6.

Gatenholm, P., and D. Klemm. 2010. "Bacterial nanocellulose as a renewable material for biomedical applications." *MRS Bulletin* 35 (3):208-213. doi: 10.1557/mrs2010.653.

Gavara, Rafael, Ramon Catala, Gracia López-Carballo, Josep Pasqual Cerisuelo i Ferriols, Irene Domínguez, Virginia Muriel-Galet, and Pilar Hernandez-Muñoz. 2016. "Use of EVOH for Food Packaging Applications." In.

Geyer, Roland, Jenna R. Jambeck, and Kara Lavender Law. 2017. "Production, use, and fate of all plastics ever made." *Science Advances* 3 (7):e1700782. doi: 10.1126/sciadv.1700782.

Giri, Jyoti, and Rameshwar Adhikari. 2012. "A Brief review on extraction of nanocellulose and its application." *BIBECHANA* 9 (0):81-87. doi: 10.3126/bibechana.v9i0.7179.

Giuggioli, Nicole Roberta, Rossella Briano, Claudio Baudino, and Cristiana Peano. 2015. "Effects of packaging and storage conditions on quality and volatile compounds of raspberry fruits." *CyTA - Journal of Food* 13 (4):512-521. doi: 10.1080/19476337.2015.1011238.

González-Ruiz, Jesús, Lourde Yataco-Lazaro, Sueli Virginio, Maria das Graças da Silva-Valenzuela, Esperidiana Moura, and Francisco Valenzuela-Díaz. 2016. "Effects of Graphene Oxide Addition on Mechanical and Thermal Properties of Evoh Films." In *Characterization of Minerals, Metals, and Materials 2016*, edited by Shadia Jamil Ikhmayies, Bowen Li, John S. Carpenter, Jiann-Yang Hwang, Sergio Neves Monteiro, Jian Li, Donato Firrao, Mingming Zhang, Zhiwei Peng, Juan P. Escobedo-Diaz and Chenguang Bai, 667-674. Cham: Springer International Publishing.

Gorji, M., R. Bagherzadeh, and H. Fashandi. 2017. "21 - Electrospun nanofibers in protective clothing." In *Electrospun Nanofibers*, edited by Mehdi Afshari, 571-598. Woodhead Publishing.

Goussé, Cécile, Henri Chanzy, Gérard Excoffier, Ludiwine Soubeyrand, and Etienne Fleury. 2002. "Stable suspensions of partially silylated cellulose whiskers dispersed in organic solvents." *Polymer* 43 (9):2645-2651. doi: https://doi.org/10.1016/S0032-3861(02)00051-4.

Guo, Gang, Qiwu Shi, Yanbing Luo, Rangrang Fan, Liangxue Zhou, Zhiyong Qian, and Jie Yu. 2014. "Preparation and ageing-resistant properties of polyester composites modified with functional nanoscale additives." *Nanoscale Research Letters* 9 (1):215. doi: 10.1186/1556-276X-9-215.

Gutt, Beatrice, Karl Kehl, Qun Ren, and Luciano F. Boesel. 2016. "Using ANOVA Models To Compare and Optimize Extraction Protocols of P3HBHV from Cupriavidus necator."

Industrial & Engineering Chemistry Research 55 (39):10355-10365. doi: 10.1021/acs.iecr.6b02694.

Hahladakis, John N., and Eleni Iacovidou. 2018. "Closing the loop on plastic packaging materials: What is quality and how does it affect their circularity?" *Science of The Total Environment* 630:1394-1400. doi: https://doi.org/10.1016/j.scitotenv.2018.02.330.

Hahladakis, John N., Costas A. Velis, Roland Weber, Eleni Iacovidou, and Phil Purnell. 2018. "An overview of chemical additives present in plastics: Migration, release, fate and environmental impact during their use, disposal and recycling." *Journal of Hazardous Materials* 344:179-199. doi: https://doi.org/10.1016/j.jhazmat.2017.10.014.

Hahn, Sei, Yong Chang, Beom Soo Kim, Kyung Lee, and Ho Chang. 1993. "The Recovery of Poly(3-Hydroxybutyrate) by Using Dispersions of Sodium Hypochlorite Solution and Chloroform." *Biotechnol Tech* 7:209-212. doi: 10.1007/BF02566149.

Haider, Adnan, Sajjad Haider, and Inn-Kyu Kang. 2018. "A comprehensive review summarizing the effect of electrospinning parameters and potential applications of nanofibers in biomedical and biotechnology." *Arabian Journal of Chemistry* 11 (8):1165-1188. doi: https://doi.org/10.1016/j.arabjc.2015.11.015.

Halonen, Niina, Petra S. Pálvölgyi, Andrea Bassani, Cecilia Fiorentini, Rakesh Nair, Giorgia Spigno, and Krisztian Kordas. 2020. "Bio-Based Smart Materials for Food Packaging and Sensors – A Review." *Frontiers in Materials* 7 (82). doi: 10.3389/fmats.2020.00082.

Hao, Mingyang, and Hongwu Wu. 2018. "Effect of in situ reactive interfacial compatibilization on structure and properties of polylactide/sisal fiber biocomposites." *Polymer Composites* 39 (S1):E174-E187. doi: https://doi.org/10.1002/pc.24484.

Hejazi, Parisa, Ebrahim Vasheghani-Farahani, and Yadollah Yamini. 2003. "Supercritical Fluid Disruption of Ralstonia eutropha for Poly(β-hydroxybutyrate) Recovery." *Biotechnology Progress* 19 (5):1519-1523. doi: https://doi.org/10.1021/bp034010q.

Hemmati, Fatemeh, Akbar Bahrami, Afshin Faridi Esfanjani, Hedayat Hosseini, David Julian McClements, and Leonard Williams. 2021. "Electrospun antimicrobial materials: Advanced packaging materials for food applications." *Trends in Food Science & Technology* 111:520-533. doi: https://doi.org/10.1016/j.tifs.2021.03.014.

Hermann-Krauss, Carmen, Martin Koller, Alexander Muhr, Hubert Fasl, Franz Stelzer, and Gerhart Braunegg. 2013. "Archaeal Production of Polyhydroxyalkanoate (PHA) Co- and Terpolyesters from Biodiesel Industry-Derived By-Products." *Archaea* 2013:129268. doi: 10.1155/2013/129268.

Horton, Alice A., Alexander Walton, David J. Spurgeon, Elma Lahive, and Claus Svendsen. 2017. "Microplastics in freshwater and terrestrial environments: Evaluating the current understanding to identify the knowledge gaps and future research priorities." *Science of The Total Environment* 586:127-141. doi: https://doi.org/10.1016/j.scitotenv.2017.01.190.

Ibrahim, Hassan M., and Anke Klingner. 2020. "A review on electrospun polymeric nanofibers: Production parameters and potential applications." *Polymer Testing* 90:106647. doi: https://doi.org/10.1016/j.polymertesting.2020.106647.

Ishak, K. A., M. S. M. Annuar, T. Heidelberg, and A. M. Gumel. 2016. "Ultrasound-Assisted Rapid Extraction of Bacterial Intracellular Medium-Chain-Length Poly(3-Hydroxyalkanoates) (mcl-PHAs) in Medium Mixture of Solvent/Marginal Non-solvent." *Arabian Journal for Science and Engineering* 41 (1):33-44. doi: 10.1007/s13369-015-1833-4.

Islam, Md Shariful, Bee Chin Ang, Andri Andriyana, and Amalina Muhammad Afifi. 2019. "A review on fabrication of nanofibers via electrospinning and their applications." *SN Applied Sciences* 1 (10):1248. doi: 10.1007/s42452-019-1288-4.

Issifu, Ibrahim, and U. Rashid Sumaila. 2020. "A Review of the Production, Recycling and Management of Marine Plastic Pollution." *Journal of Marine Science and Engineering* 8 (11):945.

Iwamoto, Reikichi, Toshihiko Matsuda, Shigetoshi Amiya, and Tomoyuki Yamamoto. 2006. "Interactions of water with OH groups in poly(ethylene-co-vinyl alcohol)." *Journal of*

Polymer Science Part B: Polymer Physics 44 (17):2425-2437. doi: https://doi.org/10.1002/polb.20894.

Iwanami, T, and Y Hirai. 1983. "Ethylene vinyl alcohol resins for gas-barrier material." *Tappi journal* 66 (10):85-90.

Jacquel, Nicolas, Chi-Wei Lo, Yu-Hong Wei, Ho-Shing Wu, and Shaw S. Wang. 2008. "Isolation and purification of bacterial poly(3-hydroxyalkanoates)." *Biochemical Engineering Journal* 39 (1):15-27. doi: https://doi.org/10.1016/j.bej.2007.11.029.

Jambeck, Jenna R., Roland Geyer, Chris Wilcox, Theodore R. Siegler, Miriam Perryman, Anthony Andrady, Ramani Narayan, and Kara Lavender Law. 2015. "Plastic waste inputs from land into the ocean." *Science* 347 (6223):768-771. doi: 10.1126/science.1260352.

Jaszkiewicz, Adam, Andrzej K. Bledzki, Andrzej Duda, Andrzej Galeski, and Piotr Franciszczak. 2014. "Investigation of Processability of Chain-Extended Polylactides During Melt Processing – Compounding Conditions and Polymer Molecular Structure." *Macromolecular Materials and Engineering* 299 (3):307-318. doi: https://doi.org/10.1002/mame.201300115.

Jeong, Han Mo, Byeong Choon Kim, and Eun Ha Kim. 2005. "Structure and properties of EVOH/organoclay nanocomposites." *Journal of Materials Science* 40 (14):3783-3787. doi: 10.1007/s10853-005-3719-4.

Jiang, Yang, Gizela Mikova, Robbert Kleerebezem, Luuk A. M. van der Wielen, and Maria C. Cuellar. 2015. "Feasibility study of an alkaline-based chemical treatment for the purification of polyhydroxybutyrate produced by a mixed enriched culture." *AMB Express* 5 (1):5. doi: 10.1186/s13568-015-0096-5.

Johnson, Katja, Yang Jiang, Robbert Kleerebezem, Gerard Muyzer, and Mark C. M. van Loosdrecht. 2009. "Enrichment of a Mixed Bacterial Culture with a High Polyhydroxyalkanoate Storage Capacity." *Biomacromolecules* 10 (4):670-676. doi: 10.1021/bm8013796.

Johnson, Katja, Robbert Kleerebezem, and Mark C. M. van Loosdrecht. 2010. "Influence of the C/N ratio on the performance of polyhydroxybutyrate (PHB) producing sequencing batch reactors at short SRTs." *Water Research* 44 (7):2141-2152. doi: https://doi.org/10.1016/j.watres.2009.12.031.

Jonoobi, Mehdi, Reza Oladi, Yalda Davoudpour, Kristiina Oksman, Alain Dufresne, Yahya Hamzeh, and Reza Davoodi. 2015. "Different preparation methods and properties of nanostructured cellulose from various natural resources and residues: a review." *Cellulose* 22 (2):935-969. doi: 10.1007/s10570-015-0551-0.

Jozala, Angela Faustino, Leticia Celia de Lencastre-Novaes, André Moreni Lopes, Valéria de Carvalho Santos-Ebinuma, Priscila Gava Mazzola, Adalberto Pessoa-Jr, Denise Grotto, Marli Gerenutti, and Marco Vinicius Chaud. 2016. "Bacterial nanocellulose production and application: a 10-year overview." *Applied Microbiology and Biotechnology* 100 (5):2063-2072. doi: 10.1007/s00253-015-7243-4.

Ju, Dandan, Lijing Han, Fan Li, Shan Chen, and Lisong Dong. 2014. "Poly(ε-caprolactone) composites reinforced by biodegradable poly(3-hydroxybutyrate-co-3-hydroxyvalerate) fiber." *International Journal of Biological Macromolecules* 67:343-350. doi: https://doi.org/10.1016/j.ijbiomac.2014.03.048.

Kabilan, Sujatha, Mahalakshmi Ayyasamy, Sridhar Jayavel, and Gunasekaran Paramasamy. 2012. "Pseudomonas sp. as a Source of Medium Chain Length Polyhydroxyalkanoates for Controlled Drug Delivery: Perspective." *International Journal of Microbiology* 2012:317828. doi: 10.1155/2012/317828.

Kalantari, Katayoon, Amalina M. Afifi, Hossein Jahangirian, and Thomas J. Webster. 2019. "Biomedical applications of chitosan electrospun nanofibers as a green polymer – Review." *Carbohydrate Polymers* 207:588-600. doi: https://doi.org/10.1016/j.carbpol.2018.12.011.

Kamel, Rabab, Nahla A. El-Wakil, Alain Dufresne, and Nermeen A. Elkasabgy. 2020. "Nanocellulose: From an agricultural waste to a valuable pharmaceutical ingredient." *International Journal of Biological Macromolecules* 163:1579-1590. doi: https://doi.org/10.1016/j.ijbiomac.2020.07.242.

Kang, Shufang, Yaqing Xiao, Xinyu Guo, Aiyun Huang, and Huaide Xu. 2021. "Development of gum arabic-based nanocomposite films reinforced with cellulose nanocrystals for strawberry preservation." *Food Chemistry* 350:129199. doi: https://doi.org/10.1016/j.foodchem.2021.129199.

Kapritchkoff, Fernanda M., Alexandre P. Viotti, Rita C. P. Alli, Marisa Zuccolo, José G. C. Pradella, Alfredo E. Maiorano, Everson A. Miranda, and Antonio Bonomi. 2006. "Enzymatic recovery and purification of polyhydroxybutyrate produced by Ralstonia eutropha." *Journal of Biotechnology* 122 (4):453-462. doi: https://doi.org/10.1016/j.jbiotec.2005.09.009.

Kargarzadeh, Hanieh, Marcos Mariano, Deepu Gopakumar, Ishak Ahmad, Sabu Thomas, Alain Dufresne, Jin Huang, and Ning Lin. 2018. "Advances in cellulose nanomaterials." *Cellulose* 25 (4):2151-2189. doi: 10.1007/s10570-018-1723-5.

Karkhanis, Sonal S., Nicole M. Stark, Ronald C. Sabo, and Laurent M. Matuana. 2018. "Performance of poly(lactic acid)/ cellulose nanocrystal composite blown films processed by two different compounding approaches." *Polymer Engineering & Science* 58 (11):1965-1974. doi: https://doi.org/10.1002/pen.24806.

Kausar, Ayesha. 2021. "Progress in green nanocomposites for high-performance applications." *Materials Research Innovations* 25 (1):53-65. doi: 10.1080/14328917.2020.1728489.

Kawai, Fusako, and Xiaoping Hu. 2009. "Biochemistry of microbial polyvinyl alcohol degradation." *Applied Microbiology and Biotechnology* 84 (2):227-237. doi: 10.1007/s00253-009-2113-6.

Kayaci, Fatma, Yelda Ertas, and Tamer Uyar. 2013. "Enhanced Thermal Stability of Eugenol by Cyclodextrin Inclusion Complex Encapsulated in Electrospun Polymeric Nanofibers." *Journal of Agricultural and Food Chemistry* 61 (34):8156-8165. doi: 10.1021/jf402923c.

Khalikova, Elvira, Susanne Somersalo, and Timo Korpela. 2020. "Metabolites Produced by Alkaliphiles with Potential Biotechnological Applications." In *Alkaliphiles in Biotechnology*, edited by Gashaw Mamo and Bo Mattiasson, 157-193. Cham: Springer International Publishing.

Khan, Avik, Ruhul A. Khan, Stephane Salmieri, Canh Le Tien, Bernard Riedl, Jean Bouchard, Gregory Chauve, Victor Tan, Musa R. Kamal, and Monique Lacroix. 2012. "Mechanical and barrier properties of nanocrystalline cellulose reinforced chitosan based nanocomposite films." *Carbohydrate Polymers* 90 (4):1601-1608. doi: https://doi.org/10.1016/j.carbpol.2012.07.037.

Khoshkava, V., and M. R. Kamal. 2014a. "Effect of drying conditions on cellulose nanocrystal (CNC) agglomerate porosity and dispersibility in polymer nanocomposites." *Powder Technology* 261:288-298. doi: https://doi.org/10.1016/j.powtec.2014.04.016.

Khoshkava, Vahid, and Musa R. Kamal. 2014b. "Effect of Cellulose Nanocrystals (CNC) Particle Morphology on Dispersion and Rheological and Mechanical Properties of Polypropylene/CNC Nanocomposites." *ACS Applied Materials & Interfaces* 6 (11):8146-8157. doi: 10.1021/am500577e.

Kim, Jihun, Seijin Oh, Sung Min Cho, Jaeho Jun, and Soonjong Kwak. 2020. "Oxygen barrier properties of polyketone/EVOH blend films and their resistance to moisture." *Journal of Applied Polymer Science* 137 (47):49537. doi: https://doi.org/10.1002/app.49537.

Kim, Jung Soo, Dong Hyun Kim, and Youn Suk Lee. 2021. "Various properties of PP/EVOH blends applying itaconic acid based compatibilizer according to ethylene content in the EVOH." *Polymer-Plastics Technology and Materials* 60 (11):1176-1184. doi: 10.1080/25740881.2021.1882492.

Kittikorn, T., R. Malakul, E. Stromberg, M. Ek, and S. Karlsson. 2018. "Enhancement of mechanical, thermal and antibacterial properties of sisal/PHBV biocomposite by fibre modification." *Journal of Metals, Materials and Minerals* 28 (1).

Koller, Martin, Horst Niebelschütz, and Gerhart Braunegg. 2013. "Strategies for recovery and purification of poly[(R)-3-hydroxyalkanoates] (PHA) biopolyesters from surrounding biomass." *Engineering in Life Sciences* 13 (6):549-562. doi: https://doi.org/10.1002/elsc.201300021.

Koppolu, Rajesh, Johanna Lahti, Tiffany Abitbol, Agne Swerin, Jurkka Kuusipalo, and Martti Toivakka. 2019. "Continuous Processing of Nanocellulose and Polylactic Acid into Multilayer Barrier Coatings." *ACS Applied Materials & Interfaces* 11 (12):11920-11927. doi: 10.1021/acsami.9b00922.

Kosseva, Maria R., and Edy Rusbandi. 2018. "Trends in the biomanufacture of polyhydroxyalkanoates with focus on downstream processing." *International Journal of Biological Macromolecules* 107:762-778. doi: https://doi.org/10.1016/j.ijbiomac.2017.09.054.

Kourmentza, C., I. Ntaikou, G. Lyberatos, and M. Kornaros. 2015. "Polyhydroxyalkanoates from Pseudomonas sp. using synthetic and olive mill wastewater under limiting conditions." *International Journal of Biological Macromolecules* 74:202-210. doi: https://doi.org/10.1016/j.ijbiomac.2014.12.032.

Kourmentza, Constantina, Jersson Plácido, Nikolaos Venetsaneas, Anna Burniol-Figols, Cristiano Varrone, Hariklia N. Gavala, and Maria A. M. Reis. 2017. "Recent Advances and Challenges towards Sustainable Polyhydroxyalkanoate (PHA) Production." *Bioengineering (Basel, Switzerland)* 4 (2):55. doi: 10.3390/bioengineering4020055.

Kuciel, Stanislaw, Karolina Mazur, and Paulina Jakubowska. 2019. "Novel Biorenewable Composites Based on Poly (3-hydroxybutyrate-co-3-hydroxyvalerate) with Natural Fillers." *Journal of Polymers and the Environment* 27 (4):803-815. doi: 10.1007/s10924-019-01392-4.

Kunasundari, B., and K. Sudesh. 2011. "Isolation and recovery of microbial polyhydroxyalkanoates." *Express Polymer Letters* 5 (7):620-634. doi: 10.3144/expresspolymlett.2011.60.

Lagaron, J. M., R. Catalá, and R. Gavara. 2004. "Structural characteristics defining high barrier properties in polymeric materials." *Materials Science and Technology* 20 (1):1-7. doi: 10.1179/026708304225010442.

Lagaron, Jose M., Anthony K. Powell, and Graham Bonner. 2001. "Permeation of water, methanol, fuel and alcohol-containing fuels in high-barrier ethylene–vinyl alcohol copolymer." *Polymer Testing* 20 (5):569-577. doi: https://doi.org/10.1016/S0142-9418(00)00077-5.

Larsson, Matilda, Olivia Markbo, and Patric Jannasch. 2016. "Melt processability and thermomechanical properties of blends based on polyhydroxyalkanoates and poly(butylene adipate-co-terephthalate)." *RSC Advances* 6 (50):44354-44363. doi: 10.1039/C6RA06282B.

Law, Jia Xian, Ling Ling Liau, Aminuddin Saim, Ying Yang, and Ruszymah Idrus. 2017. "Electrospun Collagen Nanofibers and Their Applications in Skin Tissue Engineering." *Tissue engineering and regenerative medicine* 14 (6):699-718. doi: 10.1007/s13770-017-0075-9.

Laycock, Bronwyn, Monica V. Arcos-Hernandez, Alexandra Langford, Steven Pratt, Alan Werker, Peter J. Halley, and Paul A. Lant. 2014. "Crystallisation and fractionation of selected polyhydroxyalkanoates produced from mixed cultures." *New Biotechnology* 31 (4):345-356. doi: https://doi.org/10.1016/j.nbt.2013.05.005.

Lee, Eun-Ju, Jin-San Yoon, and Eun-Soo Park. 2012. "Preparation and properties of the highly porous poly(ethylene-co-vinyl alcohol)/multiwalled carbon nanotube nanocomposites prepared by a simple saponification method." *Journal of Applied Polymer Science* 125 (S1):E691-E704. doi: https://doi.org/10.1002/app.36537.

Lee, Sang Yup. 1996. "Bacterial polyhydroxyalkanoates." *Biotechnology and Bioengineering* 49 (1):1-14. doi: https://doi.org/10.1002/(SICI)1097-0290(19960105)49:1<1::AID-BIT1>3.0.CO;2-P.

Leong, Hui Yi, Chih-Kai Chang, Kuan Shiong Khoo, Kit Wayne Chew, Shir Reen Chia, Jun Wei Lim, Jo-Shu Chang, and Pau Loke Show. 2021. "Waste biorefinery towards a sustainable circular bioeconomy: a solution to global issues." *Biotechnology for Biofuels* 14 (1):87. doi: 10.1186/s13068-021-01939-5.

Li, Fang, Hou-Yong Yu, Yingzhan Li, Somia Yassin Hussain Abdalkarim, Jiaying Zhu, and Ying Zhou. 2021. "“Soft-rigid” synergistic reinforcement of PHBV composites with

functionalized cellulose nanocrystals and amorphous recycled polycarbonate." *Composites Part B: Engineering* 206:108542. doi: https://doi.org/10.1016/j.compositesb.2020.108542.

Li, Xue, Lope G. Tabil, and Satyanarayan Panigrahi. 2007. "Chemical Treatments of Natural Fiber for Use in Natural Fiber-Reinforced Composites: A Review." *Journal of Polymers and the Environment* 15 (1):25-33. doi: 10.1007/s10924-006-0042-3.

Lim, Lim Sze, Ishak Ahmad, Mohd Azwani Shah Mat Lazim, and Mohd. Cairul Iqbal Mohd Amin. 2014. "Chemical crosslinking of acrylic acid to form biocompatible pH sensitive hydrogel reinforced with cellulose nanocrystals (CNC)." *AIP Conference Proceedings* 1614 (1):366-370. doi: 10.1063/1.4895224.

Liu, Yuyu, Yang Li, Lingli Deng, Lin Zou, Fengqin Feng, and Hui Zhang. 2018. "Hydrophobic Ethylcellulose/Gelatin Nanofibers Containing Zinc Oxide Nanoparticles for Antimicrobial Packaging." *Journal of Agricultural and Food Chemistry* 66 (36):9498-9506. doi: 10.1021/acs.jafc.8b03267.

López-Carballo, Gracia, David Cava, Jose M. Lagarón, Ramón Catalá, and Rafael Gavara. 2005. "Characterization of the Interaction between Two Food Aroma Components, α-Pinene and Ethyl Butyrate, and Ethylene−Vinyl Alcohol Copolymer (EVOH) Packaging Films as a Function of Environmental Humidity." *Journal of Agricultural and Food Chemistry* 53 (18):7212-7216. doi: 10.1021/jf051041n.

Lorini, Laura, Andrea Martinelli, Giorgio Capuani, Nicola Frison, Maria Reis, Bruno Sommer Ferreira, Marianna Villano, Mauro Majone, and Francesco Valentino. 2021. "Characterization of Polyhydroxyalkanoates Produced at Pilot Scale From Different Organic Wastes." *Frontiers in Bioengineering and Biotechnology* 9 (52). doi: 10.3389/fbioe.2021.628719.

Lorini, Laura, Andrea Martinelli, Paolo Pavan, Mauro Majone, and Francesco Valentino. 2021. "Downstream processing and characterization of polyhydroxyalkanoates (PHAs) produced by mixed microbial culture (MMC) and organic urban waste as substrate." *Biomass Conversion and Biorefinery* 11 (2):693-703. doi: 10.1007/s13399-020-00788-w.

Lu, Weixin, Chong Lu, Jing Hu, Jingjing Wu, and Qinpeng Zhou. 2021. "Effects of the blending time on the properties and non-isothermal crystallization behavior of PA6/EVOH blends." *Polymer Engineering & Science* 61 (6):1719-1731. doi: https://doi.org/10.1002/pen.25695.

Lunardi, Valentino Bervia, Felycia Edi Soetaredjo, Jindrayani Nyoo Putro, Shella Permatasari Santoso, Maria Yuliana, Jaka Sunarso, Yi-Hsu Ju, and Suryadi Ismadji. 2021. "Nanocelluloses: Sources, Pretreatment, Isolations, Modification, and Its Application as the Drug Carriers." *Polymers* 13 (13):2052.

Madison, L. L., and G. W. Huisman. 1999. "Metabolic engineering of poly(3-hydroxyalkanoates): from DNA to plastic." *Microbiology and molecular biology reviews : MMBR* 63 (1):21-53. doi: 10.1128/MMBR.63.1.21-53.1999.

Madkour, Mohamed H., Daniel Heinrich, Mansour A. Alghamdi, Ibraheem I. Shabbaj, and Alexander Steinbüchel. 2013. "PHA Recovery from Biomass." *Biomacromolecules* 14 (9):2963-2972. doi: 10.1021/bm4010244.

Maes, Caroline, Maarten te Molder, Wout Luyten, Geert Herremans, Naomi Winckelmans, Roos Peeters, Robert Carleer, and Mieke Buntinx. 2021. "Determination of the nitrogen gas transmission rate (N2GTR) of ethylene vinyl alcohol copolymer, using a newly developed permeation measurement system." *Polymer Testing* 93:106979. doi: https://doi.org/10.1016/j.polymertesting.2020.106979.

Maes, Caroline, Giberto Mitsuyoshi Yuki Junior, Cynthia Teniers, Wout Luyten, Geert Herremans, Roos Peeters, Pieter Samyn, Robert Carleer, and Mieke Buntinx. 2019. "Ethylene Vinyl Alcohol Copolymer (EVOH) as a Functional Barrier against Surrogate Components Migrating from Paperboard." *Journal of Chemistry* 2019:4180708. doi: 10.1155/2019/4180708.

Maina, Sofia, Vasiliki Kachrimanidou, and Apostolis Koutinas. 2017. "A roadmap towards a circular and sustainable bioeconomy through waste valorization." *Current Opinion in*

Green and Sustainable Chemistry 8:18-23. doi: https://doi.org/10.1016/j.cogsc.2017.07.007.

Majone, M., P. Massanisso, A. Carucci, K. Lindrea, and V. Tandoi. 1996. "Influence of storage on kinetic selection to control aerobic filamentous bulking." *Water Science and Technology* 34 (5-6):223-232. doi: 10.2166/wst.1996.0554.

Mannina, Giorgio, Dario Presti, Gabriela Montiel-Jarillo, Julián Carrera, and María Eugenia Suárez-Ojeda. 2020. "Recovery of polyhydroxyalkanoates (PHAs) from wastewater: A review." *Bioresource Technology* 297:122478. doi: https://doi.org/10.1016/j.biortech.2019.122478.

Mannina, Giorgio, Dario Presti, Gabriela Montiel-Jarillo, and María Eugenia Suárez-Ojeda. 2019. "Bioplastic recovery from wastewater: A new protocol for polyhydroxyalkanoates (PHA) extraction from mixed microbial cultures." *Bioresource Technology* 282:361-369. doi: https://doi.org/10.1016/j.biortech.2019.03.037.

Manzano, Miguel, and María Vallet-Regí. 2020. "Mesoporous Silica Nanoparticles for Drug Delivery." *Advanced Functional Materials* 30 (2):1902634. doi: https://doi.org/10.1002/adfm.201902634.

Mariano, Marcos, Nadia El Kissi, and Alain Dufresne. 2014. "Cellulose nanocrystals and related nanocomposites: Review of some properties and challenges." *Journal of Polymer Science Part B: Polymer Physics* 52 (12):791-806. doi: https://doi.org/10.1002/polb.23490.

Martínez-Sanz, Marta, Amparo Lopez-Rubio, and Jose M. Lagaron. 2013. "Nanocomposites of ethylene vinyl alcohol copolymer with thermally resistant cellulose nanowhiskers by melt compounding (II): Water barrier and mechanical properties." *Journal of Applied Polymer Science* 128 (3):2197-2207. doi: https://doi.org/10.1002/app.38432.

McKeen, Laurence W. 2012. "10 - Polyvinyls and Acrylics." In *Film Properties of Plastics and Elastomers (Third Edition)*, edited by Laurence W. McKeen, 219-254. Boston: William Andrew Publishing.

McWatters, Rebecca S., and R. Kerry Rowe. 2015. "Permeation of Volatile Organic Compounds through EVOH Thin Film Membranes and Coextruded LLDPE/EVOH/LLDPE Geomembranes." *Journal of Geotechnical and Geoenvironmental Engineering* 141 (2):04014091. doi: doi:10.1061/(ASCE)GT.1943-5606.0001209.

Md. Din, Mohd Fadhil, Ponraj Mohanadoss, Zaini Ujang, Mark van Loosdrecht, Salmiati Muhd Yunus, Shreeshivadasan Chelliapan, Vasudeo Zambare, and Gustaf Olsson. 2012. "Development of Bio-PORec® system for polyhydroxyalkanoates (PHA) production and its storage in mixed cultures of palm oil mill effluent (POME)." *Bioresource Technology* 124:208-216. doi: https://doi.org/10.1016/j.biortech.2012.08.036.

Meereboer, Kjeld W., Manjusri Misra, and Amar K. Mohanty. 2020. "Review of recent advances in the biodegradability of polyhydroxyalkanoate (PHA) bioplastics and their composites." *Green Chemistry* 22 (17):5519-5558. doi: 10.1039/D0GC01647K.

Michiels, Youri, Peter Van Puyvelde, and Bert Sels. 2017. "Barriers and Chemistry in a Bottle: Mechanisms in Today's Oxygen Barriers for Tomorrow's Materials." *Applied Sciences* 7 (7):665.

Mohammed Gumel, Ahmad, and Mohamad Suffian Annuar. 2015. "Nanocomposites of polyhydroxyalkanoates (PHAs)." *RSC Green Chemistry* 2015:98-118.

Mojaveryazdi, Farzaneh, Nor Zain, Shahabaldin Rezania, and Hesam Kamyab. 2012. "Production of biodegradable polymers (PHA) through low cost carbon sources:Green Chemistry." *International Journal of Chemical and Environmental Engineering* 4 (3):185-189.

Mokhena, T. C., J. S. Sefadi, E. R. Sadiku, M. J. John, M. J. Mochane, and A. Mtibe. 2018. "Thermoplastic Processing of PLA/Cellulose Nanomaterials Composites." *Polymers* 10 (12):1363.

Mokwena, K. Khanah, and Juming Tang. 2012. "Ethylene Vinyl Alcohol: A Review of Barrier Properties for Packaging Shelf Stable Foods." *Critical Reviews in Food Science and Nutrition* 52 (7):640-650. doi: 10.1080/10408398.2010.504903.

Montiel-Jarillo, Gabriela, Julián Carrera, and María Eugenia Suárez-Ojeda. 2017. "Enrichment of a mixed microbial culture for polyhydroxyalkanoates production: Effect of pH and N and P concentrations." *Science of The Total Environment* 583:300-307. doi: https://doi.org/10.1016/j.scitotenv.2017.01.069.

Moon, Robert J., Ashlie Martini, John Nairn, John Simonsen, and Jeff Youngblood. 2011. "Cellulose nanomaterials review: structure, properties and nanocomposites." *Chemical Society Reviews* 40 (7):3941-3994. doi: 10.1039/C0CS00108B.

Moretto, Giulia, Ivan Russo, David Bolzonella, Paolo Pavan, Mauro Majone, and Francesco Valentino. 2020. "An urban biorefinery for food waste and biological sludge conversion into polyhydroxyalkanoates and biogas." *Water Research* 170:115371. doi: https://doi.org/10.1016/j.watres.2019.115371.

Morgan-Sagastume, F., F. Valentino, M. Hjort, D. Cirne, L. Karabegovic, F. Gerardin, P. Johansson, A. Karlsson, P. Magnusson, T. Alexandersson, S. Bengtsson, M. Majone, and A. Werker. 2013. "Polyhydroxyalkanoate (PHA) production from sludge and municipal wastewater treatment." *Water Science and Technology* 69 (1):177-184. doi: 10.2166/wst.2013.643.

Morgan-Sagastume, Fernando, Simon Bengtsson, Giulia De Grazia, Tomas Alexandersson, Luca Quadri, Peter Johansson, Per Magnusson, and Alan Werker. 2020. "Mixed-culture polyhydroxyalkanoate (PHA) production integrated into a food-industry effluent biological treatment: A pilot-scale evaluation." *Journal of Environmental Chemical Engineering* 8 (6):104469. doi: https://doi.org/10.1016/j.jece.2020.104469.

Muriel-Galet, Virginia, Édgar Pérez-Esteve, María Ruiz-Rico, Ramón Martínez-Máñez, José Manuel Barat, Pilar Hernández-Muñoz, and Rafael Gavara. 2018. "Anchoring Gated Mesoporous Silica Particles to Ethylene Vinyl Alcohol Films for Smart Packaging Applications." *Nanomaterials* 8 (10):865.

Murugan, Paramasivam, Lizhu Han, Chee-Yuen Gan, Frans H. J. Maurer, and Kumar Sudesh. 2016. "A new biological recovery approach for PHA using mealworm, Tenebrio molitor." *Journal of Biotechnology* 239:98-105. doi: https://doi.org/10.1016/j.jbiotec.2016.10.012.

Nagam Hanumantharao, Samerender, and Smitha Rao. 2019. "Multi-Functional Electrospun Nanofibers from Polymer Blends for Scaffold Tissue Engineering." *Fibers* 7 (7):66.

Nair, Sandeep S., J. Y. Zhu, Yulin Deng, and Arthur J. Ragauskas. 2014. "High performance green barriers based on nanocellulose." *Sustainable Chemical Processes* 2 (1):23. doi: 10.1186/s40508-014-0023-0.

Nam, Sunghyun, Matthew B. Hillyer, and Brian D. Condon. 2020. "Method for identifying the triple transition (glass transition-dehydration-crystallization) of amorphous cellulose in cotton." *Carbohydrate Polymers* 228:115374. doi: https://doi.org/10.1016/j.carbpol.2019.115374.

Nanda, Malaya R., Manjusri Misra, and Amar K. Mohanty. 2011. "The Effects of Process Engineering on the Performance of PLA and PHBV Blends." *Macromolecular Materials and Engineering* 296 (8):719-728. doi: https://doi.org/10.1002/mame.201000417.

Nechifor, Marioara, Fulga Tanasă, Carmen-Alice Teacă, and Mădălina Zănoagă. 2018. "Compatibilization strategies toward new polymer materials from re-/up-cycled plastics." *International Journal of Polymer Analysis and Characterization* 23 (8):740-757. doi: 10.1080/1023666X.2018.1509493.

Nechyporchuk, Oleksandr, Mohamed Naceur Belgacem, and Julien Bras. 2016. "Production of cellulose nanofibrils: A review of recent advances." *Industrial Crops and Products* 93:2-25. doi: https://doi.org/10.1016/j.indcrop.2016.02.016.

Nielsen, Chad, Asif Rahman, Asad Ur Rehman, Marie K. Walsh, and Charles D. Miller. 2017. "Food waste conversion to microbial polyhydroxyalkanoates." *Microbial Biotechnology* 10 (6):1338-1352. doi: https://doi.org/10.1111/1751-7915.12776.

Nikodinovic-Runic, Jasmina, Maciej Guzik, Shane T. Kenny, Ramesh Babu, Alan Werker, and Kevin E. O Connor. 2013. "Chapter Four - Carbon-Rich Wastes as Feedstocks for Biodegradable Polymer (Polyhydroxyalkanoate) Production Using Bacteria." In *Advances in Applied Microbiology*, edited by Sima Sariaslani and Geoffrey M. Gadd, 139-200. Academic Press.

Ntaikou, I., C. Valencia Peroni, C. Kourmentza, V. I. Ilieva, A. Morelli, E. Chiellini, and G. Lyberatos. 2014. "Microbial bio-based plastics from olive-mill wastewater: Generation and properties of polyhydroxyalkanoates from mixed cultures in a two-stage pilot scale system." *Journal of Biotechnology* 188:138-147. doi: https://doi.org/10.1016/j.jbiotec.2014.08.015.

Obruca, Stanislav, Petr Sedlacek, Eva Slaninova, Ines Fritz, Christina Daffert, Katharina Meixner, Zuzana Sedrlova, and Martin Koller. 2020. "Novel unexpected functions of PHA granules." *Applied Microbiology and Biotechnology* 104 (11):4795-4810. doi: 10.1007/s00253-020-10568-1.

Ögmundarson, Ólafur, Sumesh Sukumara, Alexis Laurent, and Peter Fantke. 2020. "Environmental hotspots of lactic acid production systems." *GCB Bioenergy* 12 (1):19-38. doi: https://doi.org/10.1111/gcbb.12652.

Oliveira, Catarina S. S., Marisa O. D. Silva, Carlos E. Silva, Gilda Carvalho, and Maria A. M. Reis. 2018. "Assessment of Protein-Rich Cheese Whey Waste Stream as a Nutrients Source for Low-Cost Mixed Microbial PHA Production." *Applied Sciences* 8 (10):1817.

Ong, Su Yean, Idris Zainab-L, Somarajan Pyary, and Kumar Sudesh. 2018. "A novel biological recovery approach for PHA employing selective digestion of bacterial biomass in animals." *Applied Microbiology and Biotechnology* 102 (5):2117-2127. doi: 10.1007/s00253-018-8788-9.

Orr, Matthew P., and Meisha L. Shofner. 2017. "Processing strategies for cellulose nanocrystal/polyethylene-co-vinyl alcohol composites." *Polymer* 126:211-223. doi: https://doi.org/10.1016/j.polymer.2017.08.043.

Pagliano, Giorgia, Paola Galletti, Chiara Samorì, Agnese Zaghini, and Cristian Torri. 2021. "Recovery of Polyhydroxyalkanoates From Single and Mixed Microbial Cultures: A Review." *Frontiers in Bioengineering and Biotechnology* 9 (54). doi: 10.3389/fbioe.2021.624021.

Pan, Ruijun, Ocean Cheung, Zhaohui Wang, Petter Tammela, Jinxing Huo, Jonas Lindh, Kristina Edström, Maria Strømme, and Leif Nyholm. 2016. "Mesoporous Cladophora cellulose separators for lithium-ion batteries." *Journal of Power Sources* 321:185-192. doi: https://doi.org/10.1016/j.jpowsour.2016.04.115.

Panchal, Prachiben, Emmanuel Ogunsona, and Tizazu Mekonnen. 2019. "Trends in Advanced Functional Material Applications of Nanocellulose." *Processes* 7 (1):10.

Passanha, Pearl, Sandra R. Esteves, Gopal Kedia, Richard M. Dinsdale, and Alan J. Guwy. 2013. "Increasing polyhydroxyalkanoate (PHA) yields from Cupriavidus necator by using filtered digestate liquors." *Bioresource Technology* 147:345-352. doi: https://doi.org/10.1016/j.biortech.2013.08.050.

Peelman, Nanou, Peter Ragaert, Bruno De Meulenaer, Dimitri Adons, Roos Peeters, Ludwig Cardon, Filip Van Impe, and Frank Devlieghere. 2013. "Application of bioplastics for food packaging." *Trends in Food Science & Technology* 32 (2):128-141. doi: https://doi.org/10.1016/j.tifs.2013.06.003.

Peng, Yucheng, Douglas J. Gardner, Yousoo Han, Alper Kiziltas, Zhiyong Cai, and Mandla A. Tshabalala. 2013. "Influence of drying method on the material properties of nanocellulose I: thermostability and crystallinity." *Cellulose* 20 (5):2379-2392. doi: 10.1007/s10570-013-0019-z.

Pillay, Viness, Clare Dott, Yahya E. Choonara, Charu Tyagi, Lomas Tomar, Pradeep Kumar, Lisa C. du Toit, and Valence M. K. Ndesendo. 2013. "A Review of the Effect of Processing Variables on the Fabrication of Electrospun Nanofibers for Drug Delivery Applications." *Journal of Nanomaterials* 2013:789289. doi: 10.1155/2013/789289.

Pires, João, Camila Damásio de Paula, Victor Gomes Lauriano Souza, Ana Luísa Fernando, and Isabel Coelhoso. 2021. "Understanding the Barrier and Mechanical Behavior of Different Nanofillers in Chitosan Films for Food Packaging." *Polymers* 13 (5):721.

Pittmann, Timo, and Heidrun Steinmetz. 2017. "Polyhydroxyalkanoate Production on Waste Water Treatment Plants: Process Scheme, Operating Conditions and Potential Analysis for German and European Municipal Waste Water Treatment Plants." *Bioengineering (Basel, Switzerland)* 4 (2):54. doi: 10.3390/bioengineering4020054.

PlasticsEurope. 2020. "Plastics - the Facts 2020. An analysis of European plastics production, demand and waste data." accessed 2021. https://www.plasticseurope.org/en/resources/publications/4312-plastics-facts-2020.

Popescu, Maria-Cristina. 2017. "Structure and sorption properties of CNC reinforced PVA films." *International Journal of Biological Macromolecules* 101:783-790. doi: https://doi.org/10.1016/j.ijbiomac.2017.03.168.

Quirós, Jennifer, Karina Boltes, and Roberto Rosal. 2016. "Bioactive Applications for Electrospun Fibers." *Polymer Reviews* 56 (4):631-667. doi: 10.1080/15583724.2015.1136641.

Radusin, Tanja, Sergio Torres-Giner, Alena Stupar, Ivan Ristic, Aleksandra Miletic, Aleksandra Novakovic, and Jose Maria Lagaron. 2019. "Preparation, characterization and antimicrobial properties of electrospun polylactide films containing Allium ursinum L. extract." *Food Packaging and Shelf Life* 21:100357. doi: https://doi.org/10.1016/j.fpsl.2019.100357.

Ragaert, Kim, Laurens Delva, and Kevin Van Geem. 2017. "Mechanical and chemical recycling of solid plastic waste." *Waste Management* 69:24-58. doi: https://doi.org/10.1016/j.wasman.2017.07.044.

Rahnama, Mohammadreza, Abdulrasoul Oromiehie, Shervin Ahmadi, and Ismaeil Ghasemi. 2017. "Investigation of polyethylene-grafted-maleic anhydride presence as a compatibilizer on various properties of nanocomposite films based on polyethylene/ethylene vinyl alcohol/ nanoclay." *Polymers for Advanced Technologies* 28 (4):449-462. doi: https://doi.org/10.1002/pat.3905.

Ramos, Marina, Arantzazu Valdés, Ana Cristina Mellinas, and María Carmen Garrigós. 2015. "New Trends in Beverage Packaging Systems: A Review." *Beverages* 1 (4):248-272.

Rampazzo, Riccardo, Derya Alkan, Stefano Gazzotti, Marco A. Ortenzi, Giulio Piva, and Luciano Piergiovanni. 2017. "Cellulose Nanocrystals from Lignocellulosic Raw Materials, for Oxygen Barrier Coatings on Food Packaging Films." *Packaging Technology and Science* 30 (10):645-661. doi: https://doi.org/10.1002/pts.2308.

Ramsay, J. A., E. Berger, R. Voyer, C. Chavarie, and B. A. Ramsay. 1994. "Extraction of poly-3-hydroxybutyrate using chlorinated solvents." *Biotechnology Techniques* 8 (8):589-594. doi: 10.1007/BF00152152.

Rebocho, Ana Teresa, João R. Pereira, Luísa A. Neves, Vítor D. Alves, Chantal Sevrin, Christian Grandfils, Filomena Freitas, and Maria A. M. Reis. 2020. "Preparation and Characterization of Films Based on a Natural P(3HB)/mcl-PHA Blend Obtained through the Co-culture of Cupriavidus Necator and Pseudomonas Citronellolis in Apple Pulp Waste." *Bioengineering* 7 (2):34.

Rebouillat, Serge. 2013. "State of the Art Manufacturing and Engineering of Nanocellulose: A Review of Available Data and Industrial Applications." *Journal of Biomaterials and Nanobiotechnology* 04:165-188. doi: 10.4236/jbnb.2013.42022.

Reis, M., M. Albuquerque, M. Villano, and M. Majone. 2011. "6.51 - Mixed Culture Processes for Polyhydroxyalkanoate Production from Agro-Industrial Surplus/Wastes as Feedstocks." In *Comprehensive Biotechnology (Second Edition)*, edited by Murray Moo-Young, 669-683. Burlington: Academic Press.

Rhim, Jong-Whan, Amar K. Mohanty, Sher P. Singh, and Perry K. W. Ng. 2006. "Effect of the processing methods on the performance of polylactide films: Thermocompression versus solvent casting." *Journal of Applied Polymer Science* 101 (6):3736-3742. doi: https://doi.org/10.1002/app.23403.

Robertson, Gordon L. . 2012. "Food packaging : principles and practice." *Taylor & Francis Group*.

Rodriguez-Perez, Santiago, Antonio Serrano, Alba A. Pantión, and Bernabé Alonso-Fariñas. 2018. "Challenges of scaling-up PHA production from waste streams. A review." *Journal of Environmental Management* 205:215-230. doi: https://doi.org/10.1016/j.jenvman.2017.09.083.

Rydz, Joanna, Wanda Sikorska, Mariya Kyulavska, and Darinka Christova. 2015. "Polyester-Based (Bio)degradable Polymers as Environmentally Friendly Materials for Sustainable Development." *International Journal of Molecular Sciences* 16 (1):564-596.

SalehHudin, Hanna Sofia, Edzrol Niza Mohamad, Wan Nor Liza Mahadi, and Amalina Muhammad Afifi. 2018. "Multiple-jet electrospinning methods for nanofiber processing: A review." *Materials and Manufacturing Processes* 33 (5):479-498. doi: 10.1080/10426914.2017.1388523.

Salević, Ana, Cristina Prieto, Luis Cabedo, Viktor Nedović, and Jose Maria Lagaron. 2019. "Physicochemical, Antioxidant and Antimicrobial Properties of Electrospun Poly(ε-caprolactone) Films Containing a Solid Dispersion of Sage (Salvia officinalis L.) Extract." *Nanomaterials* 9 (2):270.

Samorì, Chiara, Federica Abbondanzi, Paola Galletti, Loris Giorgini, Laura Mazzocchetti, Cristian Torri, and Emilio Tagliavini. 2015. "Extraction of polyhydroxyalkanoates from mixed microbial cultures: Impact on polymer quality and recovery." *Bioresource Technology* 189:195-202. doi: https://doi.org/10.1016/j.biortech.2015.03.062.

Santos, Talita M., Men de Sá M. Souza Filho, Carlos Alberto Caceres, Morsyleide F. Rosa, João Paulo S. Morais, Alaídes M. B. Pinto, and Henriette M. C. Azeredo. 2014. "Fish gelatin films as affected by cellulose whiskers and sonication." *Food Hydrocolloids* 41:113-118. doi: https://doi.org/10.1016/j.foodhyd.2014.04.001.

Sarfraz, Jawad, Tina Gulin-Sarfraz, Julie Nilsen-Nygaard, and Marit Kvalvåg Pettersen. 2021. "Nanocomposites for Food Packaging Applications: An Overview." *Nanomaterials* 11 (1):10.

Sato, Harumi, Jiří´ Dybal, Rumi Murakami, Isao Noda, and Yukihiro Ozaki. 2005. "Infrared and Raman spectroscopy and quantum chemistry calculation studies of C–H···O hydrogen bondings and thermal behavior of biodegradable polyhydroxyalkanoate." *Journal of Molecular Structure* 744-747:35-46. doi: https://doi.org/10.1016/j.molstruc.2004.10.069.

Seddiqi, Hadi, Erfan Oliaei, Hengameh Honarkar, Jianfeng Jin, Lester C. Geonzon, Rommel G. Bacabac, and Jenneke Klein-Nulend. 2021. "Cellulose and its derivatives: towards biomedical applications." *Cellulose* 28 (4):1893-1931. doi: 10.1007/s10570-020-03674-w.

Semnani, Dariush, Elham Naghashzargar, Mehdi Hadjianfar, Fahimeh Dehghan Manshadi, Sajjad Mohammadi, Saeed Karbasi, and Farshid Effaty. 2017. "Evaluation of PCL/chitosan electrospun nanofibers for liver tissue engineering." *International Journal of Polymeric Materials and Polymeric Biomaterials* 66 (3):149-157. doi: 10.1080/00914037.2016.1190931.

Siemann, Ulrich. 2005. "Solvent cast technology – a versatile tool for thin film production." In *Scattering Methods and the Properties of Polymer Materials*, edited by Norbert Stribeck and Bernd Smarsly, 1-14. Berlin, Heidelberg: Springer Berlin Heidelberg.

Silvério, Hudson, Wilson Flauzino Neto, Ingrid Silva, Joyce Rosa, Rosana Assunção, Hernane Barud, Sidney Ribeiro, and Daniel Pasquini. 2014. "Mechanical, Thermal, and Barrier Properties of Methylcellulose/Cellulose Nanocrystals Nanocomposites." *Polímeros* 24:683-688. doi: 10.1590/0104-1428.1691.

Simionescu, Bogdan C., and Daniela Ivanov. 2014. "Natural and Synthetic Polymers for Designing Composite Materials." In *Handbook of Bioceramics and Biocomposites*, edited by Iulian Vasile Antoniac, 1-54. Cham: Springer International Publishing.

Soares, Rosane M. D., Nataly M. Siqueira, Molamma P. Prabhakaram, and Seeram Ramakrishna. 2018. "Electrospinning and electrospray of bio-based and natural polymers for biomaterials development." *Materials Science and Engineering: C* 92:969-982. doi: https://doi.org/10.1016/j.msec.2018.08.004.

Stafiej, Piotr, Florian Küng, Daniel Thieme, Marta Czugala, Friedrich E. Kruse, Dirk W. Schubert, and Thomas A. Fuchsluger. 2017. "Adhesion and metabolic activity of human corneal cells on PCL based nanofiber matrices." *Materials Science and Engineering: C* 71:764-770. doi: https://doi.org/10.1016/j.msec.2016.10.058.

Stegmann, Paul, Marc Londo, and Martin Junginger. 2020. "The circular bioeconomy: Its elements and role in European bioeconomy clusters." *Resources, Conservation & Recycling: X* 6:100029. doi: https://doi.org/10.1016/j.rcrx.2019.100029.

Steinbüchel, Alexander, and Tina Lütke-Eversloh. 2003. "Metabolic engineering and pathway construction for biotechnological production of relevant polyhydroxyalkanoates in microorganisms." *Biochemical Engineering Journal* 16 (2):81-96. doi: https://doi.org/10.1016/S1369-703X(03)00036-6.

Sukyai, P., P. Anongjanya, N. Bunyahwuthakul, K. Kongsin, N. Harnkarnsujarit, U. Sukatta, R. Sothornvit, and R. Chollakup. 2018. "Effect of cellulose nanocrystals from sugarcane bagasse on whey protein isolate-based films." *Food Research International* 107:528-535. doi: https://doi.org/10.1016/j.foodres.2018.02.052.

Suresh, Sinduja, Alexander Becker, and Birgit Glasmacher. 2020. "Impact of Apparatus Orientation and Gravity in Electrospinning—A Review of Empirical Evidence." *Polymers* 12 (11):2448.

Suzuki, Miwa, Yuya Tachibana, and Ken-ichi Kasuya. 2021. "Biodegradability of poly(3-hydroxyalkanoate) and poly(ε-caprolactone) via biological carbon cycles in marine environments." *Polymer Journal* 53 (1):47-66. doi: 10.1038/s41428-020-00396-5.

Tanahashi, Mitsuru. 2010. "Development of Fabrication Methods of Filler/Polymer Nanocomposites: With Focus on Simple Melt-Compounding-Based Approach without Surface Modification of Nanofillers." *Materials* 3 (3):1593-1619.

Tanahashi, Mitsuru, Masaki Hirose, Jeong-Chang Lee, and Kunihiko Takeda. 2006. "Organic/inorganic nanocomposites prepared by mechanical smashing of agglomerated silica ultrafine particles in molten thermoplastic resin." *Polymers for Advanced Technologies* 17 (11-12):981-990. doi: https://doi.org/10.1002/pat.841.

Tang, Yadong, Ying Zhou, Xingzi Lan, Dongchao Huang, Tingting Luo, Junjie Ji, Zihui Mafang, Xiaomin Miao, Han Wang, and Wenlong Wang. 2019. "Electrospun Gelatin Nanofibers Encapsulated with Peppermint and Chamomile Essential Oils as Potential Edible Packaging." *Journal of Agricultural and Food Chemistry* 67 (8):2227-2234. doi: 10.1021/acs.jafc.8b06226.

Tarchoun, Ahmed Fouzi, Djalal Trache, and Thomas M. Klapötke. 2019. "Microcrystalline cellulose from Posidonia oceanica brown algae: Extraction and characterization." *International Journal of Biological Macromolecules* 138:837-845. doi: https://doi.org/10.1016/j.ijbiomac.2019.07.176.

Tartakowski, Zenon. 2010. "Recycling of packaging multilayer films: New materials for technical products." *Resources, Conservation and Recycling* 55 (2):167-170. doi: https://doi.org/10.1016/j.resconrec.2010.09.004.

Teck Kim, Young, Byungjin Min, and Kyung Won Kim. 2014. "Chapter 2 - General Characteristics of Packaging Materials for Food System." In *Innovations in Food Packaging (Second Edition)*, edited by Jung H. Han, 13-35. San Diego: Academic Press.

Tejado, Alvaro, Md Nur Alam, Miro Antal, Han Yang, and Theo G. M. van de Ven. 2012. "Energy requirements for the disintegration of cellulose fibers into cellulose nanofibers." *Cellulose* 19 (3):831-842. doi: 10.1007/s10570-012-9694-4.

Thakur, Mamta, Ishrat Majid, Shafat Hussain, and Vikas Nanda. 2021. "Poly(ε-caprolactone): A potential polymer for biodegradable food packaging applications." *Packaging Technology and Science* 34 (8):449-461. doi: https://doi.org/10.1002/pts.2572.

Toit, D., and Madeleine Leonore. 2013. "Incorporation of polysaccharide nanowhiskers into a poly(ethylene-co-vinyl alcohol) matrix."

Tomita, Kosuke, Kanehisa Kojoh, and Atsushi Suzuki. 1997. "Isolation of thermophiles assimilating poly(ethylene-co-vinyl alcohol)." *Journal of Fermentation and Bioengineering* 84 (5):400-402. doi: https://doi.org/10.1016/S0922-338X(97)81998-8.

Torres-Giner, Sergio, Yolanda Echegoyen, Roberto Teruel-Juanes, Jose D. Badia, Amparo Ribes-Greus, and Jose M. Lagaron. 2018. "Electrospun Poly(ethylene-co-vinyl alcohol)/Graphene Nanoplatelets Composites of Interest in Intelligent Food Packaging Applications." *Nanomaterials* 8 (10):745.

Torres-Giner, Sergio, Rocío Pérez-Masiá, and Jose M. Lagaron. 2016. "A review on electrospun polymer nanostructures as advanced bioactive platforms." *Polymer Engineering & Science* 56 (5):500-527. doi: https://doi.org/10.1002/pen.24274.

Trinh, Binh Minh, and Tizazu Mekonnen. 2018. "Hydrophobic esterification of cellulose nanocrystals for epoxy reinforcement." *Polymer* 155:64-74. doi: https://doi.org/10.1016/j.polymer.2018.08.076.

Tyagi, Preeti, Khandoker Samaher Salem, Martin A. Hubbe, and Lokendra Pal. 2021. "Advances in barrier coatings and film technologies for achieving sustainable packaging of food products – A review." *Trends in Food Science & Technology* 115:461-485. doi: https://doi.org/10.1016/j.tifs.2021.06.036.

Valentino, Francesco, Mario Beccari, Serena Fraraccio, Giulio Zanaroli, and Mauro Majone. 2014. "Feed frequency in a Sequencing Batch Reactor strongly affects the production of polyhydroxyalkanoates (PHAs) from volatile fatty acids." *New Biotechnology* 31 (4):264-275. doi: https://doi.org/10.1016/j.nbt.2013.10.006.

Valentino, Francesco, Marco Gottardo, Federico Micolucci, Paolo Pavan, David Bolzonella, Simona Rossetti, and Mauro Majone. 2018. "Organic Fraction of Municipal Solid Waste Recovery by Conversion into Added-Value Polyhydroxyalkanoates and Biogas." *ACS Sustainable Chemistry & Engineering* 6 (12):16375-16385. doi: 10.1021/acssuschemeng.8b03454.

Van den Oever, Martien, Karin Molenveld, Maarten Zee, and Harriëtte Bos. 2017. *Bio-based and biodegradable plastics – Facts and Figures. Focus on food packaging in the Netherlands*.

Vilaplana, Francisco, and Sigbritt Karlsson. 2008. "Quality Concepts for the Improved Use of Recycled Polymeric Materials: A Review." *Macromolecular Materials and Engineering* 293 (4):274-297. doi: https://doi.org/10.1002/mame.200700393.

Vlachou, Marilena, Angeliki Siamidi, and Sotiria Kyriakou. 2019. "Electrospinning and Drug Delivery." In *Electrospinning and Electrospraying*. IntechOpen.

Wada, Masahisa, Masakazu Ike, and Ken Tokuyasu. 2010. "Enzymatic hydrolysis of cellulose I is greatly accelerated via its conversion to the cellulose II hydrate form." *Polymer Degradation and Stability* 95 (4):543-548. doi: https://doi.org/10.1016/j.polymdegradstab.2009.12.014.

Wang, Chenyu, Jun Wang, Liangdan Zeng, Ziwen Qiao, Xiaochen Liu, He Liu, Jin Zhang, and Jianxun Ding. 2019. "Fabrication of Electrospun Polymer Nanofibers with Diverse Morphologies." *Molecules* 24 (5):834.

Wang, Jinwu, Douglas J. Gardner, Nicole M. Stark, Douglas W. Bousfield, Mehdi Tajvidi, and Zhiyong Cai. 2018. "Moisture and Oxygen Barrier Properties of Cellulose Nanomaterial-Based Films." *ACS Sustainable Chemistry & Engineering* 6 (1):49-70. doi: 10.1021/acssuschemeng.7b03523.

Wang, Lili. 2019. "Effect of regrind content on PP-EVOH sheets properties and effect of orientation on permeability of EVOH multilayer films." Master of Applied Science in Chemical Engineering, University of Montreal.

Wang, Long-Feng, Shiv Shankar, and Jong-Whan Rhim. 2017. "Properties of alginate-based films reinforced with cellulose fibers and cellulose nanowhiskers isolated from mulberry pulp." *Food Hydrocolloids* 63:201-208. doi: https://doi.org/10.1016/j.foodhyd.2016.08.041.

Wang, Lu, Cong Chen, Jinwu Wang, Douglas J. Gardner, and Mehdi Tajvidi. 2020. "Cellulose nanofibrils versus cellulose nanocrystals: Comparison of performance in flexible multilayer films for packaging applications." *Food Packaging and Shelf Life* 23:100464. doi: https://doi.org/10.1016/j.fpsl.2020.100464.

Wang, Yuanpeng, Ronghui Chen, JiYuan Cai, Zhenggui Liu, Yanmei Zheng, Haitao Wang, Qingbiao Li, and Ning He. 2013. "Biosynthesis and Thermal Properties of PHBV Produced from Levulinic Acid by Ralstonia eutropha." *PLOS ONE* 8 (4):e60318. doi: 10.1371/journal.pone.0060318.

Weng, Lin, and Jingwei Xie. 2015. "Smart electrospun nanofibers for controlled drug release: recent advances and new perspectives." *Current pharmaceutical design* 21 (15):1944-1959. doi: 10.2174/1381612821666150302151959.

Weng, Yun-Xuan, Xiu-Li Wang, and Yu-Zhong Wang. 2011. "Biodegradation behavior of PHAs with different chemical structures under controlled composting conditions." *Polymer Testing* 30 (4):372-380. doi: https://doi.org/10.1016/j.polymertesting.2011.02.001.

Wu, H. F., L. Z. Yue, S. L. Jiang, Y. Q. Lu, Y. X. Wu, and Z. Y. Wan. 2019. "Biodegradation of polyvinyl alcohol by different dominant degrading bacterial strains in a baffled anaerobic bioreactor." *Water Science and Technology* 79 (10):2005-2012. doi: 10.2166/wst.2019.202.

Xiao, Yaqing, Yingnan Liu, Shufang Kang, Kunhua Wang, and Huaide Xu. 2020. "Development and evaluation of soy protein isolate-based antibacterial nanocomposite films containing cellulose nanocrystals and zinc oxide nanoparticles." *Food Hydrocolloids* 106:105898. doi: https://doi.org/10.1016/j.foodhyd.2020.105898.

Xu, Xuezhu, Fei Liu, Long Jiang, J. Y. Zhu, Darrin Haagenson, and Dennis P. Wiesenborn. 2013. "Cellulose Nanocrystals vs. Cellulose Nanofibrils: A Comparative Study on Their Microstructures and Effects as Polymer Reinforcing Agents." *ACS Applied Materials & Interfaces* 5 (8):2999-3009. doi: 10.1021/am302624t.

Xue, Jiajia, Tong Wu, Yunqian Dai, and Younan Xia. 2019. "Electrospinning and Electrospun Nanofibers: Methods, Materials, and Applications." *Chemical Reviews* 119 (8):5298-5415. doi: 10.1021/acs.chemrev.8b00593.

Yeh, Jen-Taut, and Heng-Yi Chen. 2007. "Blending and oxygen permeation properties of the blown films of blends of modified polyamide and ethylene vinyl alcohol copolymer with varying vinyl alcohol contents." *Journal of Materials Science* 42 (14):5742-5751. doi: 10.1007/s10853-006-0555-0.

Yılmaz, Fulya, Gizem Celep, and Gamze Tetik. 2016. "Nanofibers in Cosmetics." In.

Yin, Ooi Shok, Ishak Ahmad, and Mohd. Cairul Iqbal Mohd Amin. 2014. "Synthesis of chemical cross-linked gelatin hydrogel reinforced with cellulose nanocrystals (CNC)." *AIP Conference Proceedings* 1614 (1):375-380. doi: 10.1063/1.4895226.

Yuan, Huihong, Yoshiharu Nishiyama, Masahisa Wada, and Shigenori Kuga. 2006. "Surface Acylation of Cellulose Whiskers by Drying Aqueous Emulsion." *Biomacromolecules* 7 (3):696-700. doi: 10.1021/bm050828j.

Zeng, Jian-Bing, Kun-Ang Li, and An-Ke Du. 2015. "Compatibilization strategies in poly(lactic acid)-based blends." *RSC Advances* 5 (41):32546-32565. doi: 10.1039/C5RA01655J.

Zhang, Bo, Ross Carlson, and Friedrich Srienc. 2006. "Engineering the monomer composition of polyhydroxyalkanoates synthesized in Saccharomyces cerevisiae." *Applied and environmental microbiology* 72 (1):536-543. doi: 10.1128/AEM.72.1.536-543.2006.

Zhang, Cen, Yang Li, Peng Wang, and Hui Zhang. 2020. "Electrospinning of nanofibers: Potentials and perspectives for active food packaging." *Comprehensive Reviews in Food Science and Food Safety* 19 (2):479-502. doi: https://doi.org/10.1111/1541-4337.12536.

Zhang, Kunyu, Manjusri Misra, and Amar K. Mohanty. 2014. "Toughened Sustainable Green Composites from Poly(3-hydroxybutyrate-co-3-hydroxyvalerate) Based Ternary Blends and Miscanthus Biofiber." *ACS Sustainable Chemistry & Engineering* 2 (10):2345-2354. doi: 10.1021/sc500353v.

Zhang, Longhe, Jing Zhong, and Xiaofeng Ren. 2017. "Natural Fiber-Based Biocomposites." In, 31-70.

Zhang, Mingmei, Haiyun Wu, and Hong Chen. 2014. "Coupling of polyhydroxyalkanoate production with volatile fatty acid from food wastes and excess sludge." *Process Safety and Environmental Protection* 92 (2):171-178. doi: https://doi.org/10.1016/j.psep.2012.12.002.

Zhang, Zhongbin, Ian J. Britt, and Marvin A. Tung. 1999. "Water absorption in EVOH films and its influence on glass transition temperature." *Journal of Polymer Science Part B: Polymer Physics* 37 (7):691-699. doi: https://doi.org/10.1002/(SICI)1099-0488(19990401)37:7<691::AID-POLB20>3.0.CO;2-V.

Zhang, Zhongbin, Ian J. Britt, and Marvin A. Tung. 2001. "Permeation of oxygen and water vapor through EVOH films as influenced by relative humidity." *Journal of Applied Polymer Science* 82 (8):1866-1872. doi: https://doi.org/10.1002/app.2030.

Zhang, Zhongbin, Loong-Tak Lim, and Marvin A. Tung. 2001. "Limonene transport and mechanical properties of EVOH and nylon 6,6 films as influenced by RH." *Journal of Applied Polymer Science* 79 (11):1949-1957. doi: https://doi.org/10.1002/1097-4628(20010314)79:11<1949::AID-APP1002>3.0.CO;2-F.

Zhao, Jing, Charbel Kanaan, Robert Clément, Benoît Brulé, Henri Lenda, and Anne Jonquières. 2015. "Permeability of EVOH Barrier Material Used in Automotive Applications: Metrology Development for Model Fuel Mixtures." *Oil Gas Sci. Technol. – Rev. IFP Energies nouvelles* 70 (2):353-366.

Zhao, Luying, Gaigai Duan, Guoying Zhang, Haoqi Yang, Shuijian He, and Shaohua Jiang. 2020. "Electrospun Functional Materials toward Food Packaging Applications: A Review." *Nanomaterials (Basel, Switzerland)* 10 (1):150. doi: 10.3390/nano10010150.

Zhao, Xiaoying, Katrina Cornish, and Yael Vodovotz. 2020. "Narrowing the Gap for Bioplastic Use in Food Packaging: An Update." *Environmental Science & Technology* 54 (8):4712-4732. doi: 10.1021/acs.est.9b03755.

Zhao, Yadong, Carl Moser, Mikael E. Lindström, Gunnar Henriksson, and Jiebing Li. 2017. "Cellulose Nanofibers from Softwood, Hardwood, and Tunicate: Preparation–Structure–Film Performance Interrelation." *ACS Applied Materials & Interfaces* 9 (15):13508-13519. doi: 10.1021/acsami.7b01738.

Zhu, Ge, Hui Xu, Alain Dufresne, and Ning Lin. 2018. "High-Adsorption, Self-Extinguishing, Thermal, and Acoustic-Resistance Aerogels Based on Organic and Inorganic Waste Valorization from Cellulose Nanocrystals and Red Mud." *ACS Sustainable Chemistry & Engineering* 6 (5):7168-7180. doi: 10.1021/acssuschemeng.8b01244.

Zhu, Jiayi, Chamil Abeykoon, and Nazmul Karim. 2021. "Investigation into the effects of fillers in polymer processing." *International Journal of Lightweight Materials and Manufacture* 4 (3):370-382. doi: https://doi.org/10.1016/j.ijlmm.2021.04.003.

Zinn, Manfred, Bernard Witholt, and Thomas Egli. 2001. "Occurrence, synthesis and medical application of bacterial polyhydroxyalkanoate." *Advanced Drug Delivery Reviews* 53 (1):5-21. doi: https://doi.org/10.1016/S0169-409X(01)00218-6.

Zubair, Muhammad, and Aman Ullah. 2020. "Recent advances in protein derived bionanocomposites for food packaging applications." *Critical Reviews in Food Science and Nutrition* 60 (3):406-434. doi: 10.1080/10408398.2018.1534800.

II. OBJECTIVES

General and specific objectives

Current concerns about the depletion of natural resources, as well as pollution caused by the inexorable growth in the use of non-renewable and non-biodegradable plastics, have generated scientific, social and political interest in the search for new materials to replace existing ones. Thus, biopolymers have emerged as a great alternative, as they come from renewable sources and can be biodegradable. Polyhydroxyalkanoates (PHAs) are one of the most promising bioplastics, as they are synthesised by microbial fermentation of renewable resources such as agro-industrial and urban waste, are biodegradable, biocompatible, non-toxic and possess certain properties comparable to their petroleum-based counterparts. In addition, the combined use of other substances, such as cellulose nanocrystals (CNCs) or essential oils (EOs), can improve some of their properties, such as their oxygen barrier or antimicrobial characteristics, respectively. All these facts propose them as suitable candidates for use in food packaging, where these features are critical to ensure food quality and safety, as well as to extend shelf life. In this context, the general objective of this PhD thesis was:

"The development and characterization of novel PHAs derived from agro-industry by-products and urban waste for use in high barrier and active monolayers and multilayers processed by electrospinning and melt compounding with application interest in food packaging".

To achieve this goal, specific objectives had to be sequentially accomplished:

1. Development of interlayers based on polymeric fibers by electrospinning.

1.1. Study of PHA extraction processes to obtain the optimum material to be processed by electrospinning and melt compounding.

1.2. Characterization of PHAs from agro-industrial by-products and urban waste with monomer contents and chemical compositions different from those commercially available in order to obtain materials with improved properties and processability for food packaging. Understand the mechanisms of thermally-induced interfiber coalescence process occurring in these materials.

1.3. Functionalization of PHA fibers by organic compounds present in EOs encapsulated in mesoporous silica nanoparticles (MSNPs) and their controlled release for the development of antimicrobial layers.

1.4. Characterization of active antimicrobial monolayers in open and closed systems to simulate food packaging conditions.

1.5. Electrospinning of synthetic polymers such as poly(ethylene-*co*-vinyl alcohol) (EVOH) copolymers, known for its high oxygen barrier. Addition of CNCs, nanoparticles of renewable

and biodegradable origin and also with high oxygen barrier, to EVOH solutions in order to obtain hybrid oxygen barrier materials with an eco-friendlier profile.

2. Development of PHA-based structural layers by melt compounding.

2.1. Blends of PHAs of agro-industrial by-product origin with commercial PHAs to obtain materials with improved properties and lower cost.

2.2. Addition of natural organic fillers for the formation of “green composites” to reduce further the production costs of biopolymers and revalue waste products.

2.3. Study of possible additives to improve the dispersion of PHA mixtures and fillers.

3. Development of barrier multilayer systems based on PHA.

3.1. Development of a simple methodology to impregnate PHA electrospun fibers with food hydrocolloids containing CNCs to obtain biodegradable high barrier multilayer materials.

3.2. Development of a fully compostable multilayer, with outer structural layers obtained by film blowing and containing PHA blended with poly(butylene adipate-*co*-terephthalate) (PBAT) and two inner layers, one of electrospun PHAs fibers with adhesive properties and one of CNCs with high oxygen barrier.

III. RESULTS

Results

This PhD thesis is a collection of research works that have been divided into three blocks, in which each chapter corresponds to published journal papers. The first block is focused on the preparation and characterization of polyhydroxyalkanoates (PHAs) derived from agro-industrial by-products and urban waste and the development of their monolayers by electrospinning. These PHAs were mostly poly(hydroxybutyrate-*co*-hydroxyvalerate) (PHBV), which had different 3-hydroxyvalerate (3HV) monomer contents from each other and from those normally commercialized. This makes them interesting to study, as many of their properties vary as a function of 3HV, such as their mechanical performance, as well as their processing window. The study of their morphologies and optical properties, as well as their crystallinity, thermal characteristics and mechanical and barrier performance are compiled in **Chapter I**, **Chapter II**, and **Chapter III**. In this block, the electrospun PHAs fibers were also prepared and functionalized with active substances, specifically with organic compounds present in essential oils encapsulated in mesoporous silica nanoparticles, to provide them with antimicrobial properties. The results of this work are presented in **Chapter IV**. Finally, the synthetic poly(ethylene-*co*-vinyl alcohol) (EVOH) copolymers was also processed by electrospinning, as despite its non-renewable origin, it can be biodegradable and has a high-oxygen barrier, which makes it widely used for food packaging. Cellulose nanocrystals (CNCs), nanoparticles of natural origin and biodegradable, which also have a high-oxygen barrier, were added to the EVOH solutions to produce very high-oxygen-barrier materials with a more environmentally friendly character. **Chapter V** gathers the results of this work.

The second block is dedicated to the development of PHA monolayers by melt compounding. In **Chapter VI**, the blend of a commercial PHA, polyhydroxybutyrate (PHB), with a PHBV from an agro-industrial by-product was developed. In addition, a natural organic filler, i.e. rice husk flour, was added to the composition to reduce the cost of the biopolymer production process, forming a "green composite". Moreover, the use of these fillers allows the manufacture of more sustainable materials, as they valorize agri-food waste, are biodegradable, and reduce pollutant emissions. To increase the compatibility between the biopolymers and the fillers, a compatibilizer, triglycidyl isocyanurate (TGIC) and an initiator, dicumyl peroxide (DCP), were added. On the other hand, a blend of two PHAs was also developed in **Chapter VII**. In this case, one of the biopolymers was a commercial PHBV, while the other was the biomass derived terpolymer poly(hydroxybutyrate-*co*-hydroxyvalerate-*co*-hydroxyhexanoate) [P(3HB-*co*-3HV-*co*-3HHx)]. No compatibilizers or initiators were needed for this mixture due to their high chemical affinity.

To conclude, the third block deals with development of multilayer systems based on the monolayers developed and characterized in the two previous blocks. Thus, in **Chapter VIII**, multilayers based on electrospun PHBV fibers were developed with CNCs impregnation as interlayers to create high barrier structures. In addition, various biopolymers, protein and polysaccharides, were added to the CNCs solution to improve certain properties. These hydrocolloids were also impregnated into the PHBV fibers. Finally, the last work carried out consisted of the development of a multilayer of a more industrial design, in which the outer structural layer was composed of a blend of PHB with poly(butylene adipate-*co*-terephthalate)

(PBAT) made by film blown extrusion, while the two inner layers were a layer of CNCs, which gave the high barrier properties to the system, and a layer of electrospun PHBV fibers that provided the adhesion between all the layers. The results of this work are presented in **Chapter IX**.

Block I: Development of interlayers based on polymeric fibers by electrospinning

Chapter I:

Beatriz Meléndez-Rodríguez, Jinneth L. Castro-Mayorga, Maria A. M. Reis, Chris Sammon, Luis Cabedo, Sergio Torres-Giner, and José María Lagarón. **Preparation and characterization of electrospun food biopackaging films of poly(3-hydroxybutyrate-*co*-3-hydroxyvalerate) derived from fruit pulp biowaste.** *Frontiers in Sustainable Food Systems* 2018, 2:38.

Chapter II:

Beatriz Meléndez-Rodríguez, Sergio Torres-Giner, Laura Lorini, Francesco Valentino, Chris Sammon, Luis Cabedo, and José María Lagarón. **Valorization of municipal biowaste into electrospun poly(3-hydroxybutyrate-*co*-3-hydroxyvalerate) biopapers for food packaging applications**. *Applied Bio Materials* 2020, 3, 9, 6110-6123.

Chapter III:

Beatriz Meléndez-Rodríguez, Maria A. M. Reis, Monica Carvalheira, Chris Sammon, Luis Cabedo, Sergio Torres-Giner, and José María Lagarón. **Development and characterization of electrospun biopapers of poly(3-hydroxybutyrate-*co*-3-hydroxyvalerate) derived from cheese whey with varying 3-hydroxyvalerate contents**. *Biomacromolecules* 2021, 22(7), 2935-2953.

Chapter IV:

Beatriz Meléndez-Rodríguez, Kelly J. Figueroa-López, Andrea Bernardos, Ramón Martínez-Máñez, Luis Cabedo, Sergio Torres-Giner, and José María Lagarón. **Electrospun antimicrobial films of poly(3-hydroxybutyrate-*co*-3-hydroxyvalerate) containing eugenol essential oil encapsulated in mesoporous silica nanoparticles**. *Nanomaterials* 2019, 9(2), 227.

Chapter V:

Beatriz Meléndez-Rodríguez, Sergio Torres-Giner, Lorenzo Zavagna, Chris Sammon, Luis Cabedo, Cristina Prieto and José María Lagarón. **Development and characterization of**

electrospun fiber-based poly(ethylene-*co*-vinyl alcohol) films of application interest as high-gas-barrier interlayers in food packaging. *Polymers* 2021, 13(13), 2061.

Block II: Development of PHA-based structural layers by melt compounding

Chapter VI:

Beatriz Meléndez-Rodríguez, Sergio Torres-Giner, Abdulaziz Aldureid, Luis Cabedo, and José María Lagarón. **Reactive melt mixing of poly(3-hydroxybutyrate)/rice husk flour composites with purified biosustainably produced poly(3-hydroxybutyrate-*co*-3-hydroxyvalerate)**. *Materials* 2019, 12(13), 2152.

Chapter VII:

Beatriz Meléndez-Rodríguez, Sergio Torres-Giner, Maria A. M. Reis, Fernando Silva, Mariana Matos, Luis Cabedo, and José María Lagarón. **Blends of poly(3-hydroxybutyrate-*co*-3-hydroxyvalerate) with fruit pulp biowaste derived poly(3-hydroxybutyrate-*co*-3-hydroxyvalerate-*co*-3-hydroxyhexanoate) for organic recycling food packaging**. *Polymers* 2021, 13(7), 1155.

Block III: Development of barrier multilayer systems based on PHA

Chapter VIII:

Beatriz Meléndez-Rodríguez, Marie-Stella M'Bengue, Sergio Torres-Giner, Luis Cabedo, Cristina Prieto, and José María Lagarón. **Barrier biopaper multilayers obtained by impregnation of electrospun poly(3-hydroxybutyrate-*co*-3-hydroxyvalerate) with protein and polysaccharide hydrocolloids.** *Carbohydrate Polymer Technologies and Applications* 2021, 100150.

Chapter IX:

Beatriz Meléndez-Rodríguez, Sergio Torres-Giner, Inmaculada Angulo, María Pardo-Figuerez, Loïc Hilliou, José Manuel Escuin, Luis Cabedo, Yuval Nevo, Cristina Prieto, and José María Lagarón. **High-oxygen-barrier multilayer films based on polyhydroxyalkanoates and cellulose nanocrystals.** *Nanomaterials* 2021, 11(6), 1443.

Block I: Development of interlayers based on polymeric fibers by electrospinning

Chapter I

Preparation and Characterization of Electrospun Food Biopackaging Films of Poly(3-hydroxybutyrate-*co*-3-hydroxyvalerate) Derived From Fruit Pulp Biowaste

Frontiers in Sustainable Food Systems 2018, 2:38

Beatriz Meléndez-Rodríguez[1], Jinneth L. Castro-Mayorga[1], Maria A. M. Reis[2], Chris Sammon[3], Luis Cabedo[4], Sergio Torres-Giner[1], and José María Lagarón[1]

[1] Novel Materials and Nanotechnology Group, Institute of Agrochemistry and Food Technology (IATA), Spanish Council for Scientific Research (CSIC), Paterna, Spain

[2] UCIBIO-REQUIMTE, Chemistry Department, Faculty of Sciences and Technology, Universidade NOVA de Lisboa, Caparica, Portugal

[3] Materials and Engineering Research Institute, Sheffield Hallam University, Sheffield, United Kingdom

[4] Polymers and Advanced Materials Group, Universitat Jaume I (UJI), Castellón, Spain

Abstract

In the present study, circular economy based and potentially low-cost poly(3-hydroxybutyrate-*co*-3-hydroxyvalerate) (PHBV) was produced by mixed microbial cultures derived from fruit pulp, an industrial by-product of the juice industry. Three different chemical routes, namely non-extraction, extraction with sodium hypochlorite (NaClO), and extraction with chloroform, in combination with filtering and centrifugation, were explored to purify the biopolymer and find the most optimal solution for its processing via electrospinning. The resultant ultrathin fiber mats of the different extracted PHBV materials were thermally post-processed at different temperatures in order to obtain continuous films adequate for food packaging applications. The resultant films were characterized in terms of morphology, crystallinity as well as thermal, mechanical, and barrier properties. The results showed that extraction with both chloroform and NaClO with a post-treatment of filtering and centrifugation of the PHBV-containing biomass were necessary refining steps to allow its processing by electrospinning. In particular, the PHBV extracted with chloroform presented the highest degree of purity, resulting in more transparent films with lower wettability and higher flexibility. The here-formulated electrospun films made of biomass derived from biowaste exhibit great potential as interlayers or coatings for food biopackaging applications.

Keywords: PHBV; electrospinning; packaging; biowaste; Circular Economy

1. Introduction

The growing concern for plastic waste disposal of petroleum-based materials has intensified the study and development of bio-based and biodegradable polymers, particularly those synthesized from agro-industrial residues (Babu, O'Connor, and Seeram 2013). Polyhydroxyalkanoates (PHAs) comprise a family of biodegradable biopolyesters synthesized by hundred species of Gram-positive (G+) and Gram-negative (G−) bacteria (Rehm 2003). PHAs provide a particularly good alternative to fossil-derived polymers, showing the highest potential to replace polyolefins in packaging applications (Fabra et al. 2014, Mutlu et al. 2018). The most widely studied PHA is poly(3-hydroxybutyrate) (PHB), which possesses similar thermal and mechanical properties than polystyrene (PS) and isotactic polypropylene (iPP) (Savenkova et al. 2000). PHB homopolyester has, however, excessive brittleness and a narrow processing temperature window, which limit its use for packaging applications (Reis et al. 2008). Instead, its copolymer with 3-hydroxyvalerate (HV), i.e., poly(3-hydroxybutyrate-*co*-3-hydroxyvalerate) (PHBV) has a much lower crystallinity, decreased stiffness, and lower melting temperature (Chen and Wang 2002, Martínez-Sanz et al. 2016).

The production of PHAs based on open mixed cultures is a sustainable alternative to reduce costs (Dias et al. 2006, Serafim et al. 2008). However, large investments are needed in the processes of fermentation, isolation, purification, etc. Nowadays, main research efforts currently focus on reducing the costs of the fermentation and downstream processes and make the PHAs' industrial production more competitive (Jacquel et al. 2007). In this sense, the production of PHA by mixed crops from renewable resources is both economically and environmentally attractive. In particular, the use of food waste as the raw material for the PHA production is a more economical and sustainable industrial form within the frame of the Circular Economy (Colombo et al. 2017). For example, fermented cheese whey (CW), whose potential due to high contents in proteins and sugars is mostly not fully valorized at present, can be used as the feeding solution for PHA production (Colombo et al. 2016, Domingos et al. 2018, Martínez-Abad et al. 2016). Nevertheless, the extraction methods should be optimized in order to properly extract the biopolymer from the cell walls, especially in mixed cultures, where is more complex due to these are more resistant to cell hydrolysis than pure cultures (Samorì et al. 2015). Moreover, the chemical digestion methods adopted to disrupt the cell wall and release PHAs can affect the purity and molecular weight (MW) of the obtained polymer (Kunasundari and Sudesh 2011) while the large amounts of chemicals used can also increase the recovery cost and make the process environmentally unfriendly. To address these issues, improvements in the methods of purification and extraction are being currently explored.

Electrospinning is a physical process used for the formation of continuous polymer fibers with ultrathin diameters, generally in the sub-micrometer range, through the action of an external high-voltage electric field. At a critical high voltage, typically 5–35 kV, the polymer solution droplets distort and form the so-called Taylor's cone. This erupts from the solution to form a charged polymer jet whose size and morphology are affected by the solution properties, mainly viscosity, surface tension, and conductivity of the polymer solution, and also by the process conditions, namely applied voltage, flow-rate, and tip-to-collector distance (Doshi and Reneker 1995, Torres-Giner, Gimenez, and Lagaron 2008). In the field of packaging, the electrospun fiber structure represents a good option from a point of view of mechanical reinforcement (Torres-Giner 2011), but it can also enhance the barrier performance of biopolymer matrices (Busolo, Torres-Giner, and Laaron 2009, Torres-Giner, Martinez-Abad, and Lagaron 2014). The use of electrospinning

in active food packaging by the incorporation into the fibers of both nanofillers or active substances can add an extra value to the final product, changing the packed food condition to extend the shelf life and improve safety and/or sensory properties (Torres-Giner, Pérez-Masiá, and Lagaron 2016).

Furthermore, the application of a thermal post-treatment below the biopolymer's melting temperature (T_m), habitually referred as to annealing, offers the possibility to produce continuous films of more application interest in packaging. This technology is particularly very promising to valorize forms of processing renewable polymers in the form of interlayers or coatings with enhanced flexibility and transparency while potentially retaining the barrier performance to gases and vapors of conventional films prepared by compression molding or extrusion (Echegoyen et al. 2017, Fabra, López-Rubio, and Lagaron 2016). In comparison with films obtained by compression molding, electrospun PHB films have showed better optical properties, similar barrier performance, and higher elongation at break and toughness (Cherpinski et al. 2017). In addition, electrospun PHA films have been recently applied as coatings on fiber-based packaging layers to improve their moisture resistance (Cherpinski et al. 2018). Other recent studies have been focused on the incorporation of antimicrobial ingredients in the electrospun PHA fibers, which can be thereafter integrated as active layers in packaging structures. For example, electrospun mats made of PHBV derived from CW and containing zinc oxide (ZnO) were thermally post-processed as coatings on PHBV films to develop antimicrobial nanocomposites (Castro-Mayorga et al. 2017). Similarly, in another study, copper oxide (CuO) nanoparticles were loaded into PHBV electrospun coatings to form antimicrobial coatings with increased capacity (Castro Mayorga et al. 2018).

The objective of this study is to assess different routes of extraction for PHBV-containing biomass derived from an industrial biowaste of fruit pulps for its optimal processing by electrospinning. Moreover, the obtained electrospun PHBV mats were subjected to a post-processing annealing treatment to prepare and characterize continuous films of relevance in food packaging applications.

2. Experimental

2.1. Materials

PHBV copolyester was produced at pilot-plant scale at Universidade NOVA (Lisboa, Portugal) using mixed microbial cultures fed with fermented fruits. These were obtained from fruit pulps supplied by SumolCompal S.A. (Portugal) as an industrial residue of the juice industry, which were taken from the stored barrels that did not comply with the criteria to be processed.

Commercial PHBV was ENMAT™ Y1000P, produced by Tianan Biologic Materials (Ningbo, China) and delivered in the form of pellets. According to the manufacturer, the molar fraction of HV in the commercial copolymer is 3 %.

2,2,2-trifluoroethanol (TFE), ≥ 99 % purity, and $_D$-limonene, with 98 % purity, were obtained from Sigma Aldrich S.A. (Madrid, Spain). Sodium hypochlorite, 10–15 % active chloride, was supplied by Scharlab, S.L. (Barcelona, Spain) while chloroform, stabilized with ethanol and 99.8

% purity, was purchased from Panreac S.A. (Barcelona, Spain). Sodium bicarbonate ($NaHCO_3$) was supplied by JMGS (Odivelas, Portugal).

2.2. Production of Unpurified PHBV Powder

PHBV was produced using mixed microbial cultures applying a three-stage process: (1) acidogenic fermentation of the agro-food waste to produce a mixture of fermentation products, i.e., the precursors for PHA biosynthesis; (2) culture selection, where microorganisms were selected based on their PHA storage ability through alternating periods of feast and famine; (3) PHA production, in which the selected microorganisms were fed with the fermentation products mixture resultant from the acidogenic step in order to accumulate PHA up to the culture's maximum capacity.

The experimental setup consisted of three pilot-scale reactors. The fruit pulp waste was first fermented in a 60-L up-flow anaerobic sludge blanket reactor (UASB) inoculated with anaerobic granules from a full-scale anaerobic digester. The acidogenic reactor operated using an organic loading rate (OLR) of 29 ± 2 g-COD·L^{-1}·d^{-1}, a hydraulic retention time (HRT) of 1 day, a pH value of 4.7 ± 0.1 (controlled by adding $NaHCO_3$ in the feed), and a temperature of 30 ± 1 °C. The obtained stream of fermentation products had an average composition of 5 ± 1 % lactate, 17 ± 1 % acetate, 7 ± 1 % propionate, 9 ± 1 % ethanol, 57 ± 2 % butyrate, and 5 ± 1 % valerate (% COD basis) and was further used to fed the two subsequent steps of the process. A 100-L aerobic sequencing batch reactor (SBR) inoculated with activated sludge from the Muleta Wastewater Treatment Plant, in Portugal, was used for the enrichment of the PHA-producing culture. The SBR operated at a feast and famine regime in 12 h cycles, comprising four periods: feeding (12 min), aeration (11 h), settling (45 min), and withdrawal (15 min). The OLR was maintained at 350 C-mM·d^{-1} and the HRT and SRT were 1 and 4 days, respectively. In the feeding phase, the stream obtained in the acidogenic reactor was fed as the carbon source together with a mineral solution (Serafim et al. 2004) to adjust the reactor's OLR. Nitrogen and phosphorus concentrations were adjusted, keeping the C/N/P molar ratio at 100/7/1. PHA production was performed in a 50-L aerobic fed-batch reactor inoculated with 25 L of biomass purged from the SBR at the end of famine phase (ca. 10.5 h from cycle started). The reactor was fed with the fermented fruit pulp waste in a pulse-wise mode controlled by the dissolved oxygen (DO) response. When DO increased, a new pulse of carbon source was provided until no DO response was observed, indicating that the culture reached its maximum capacity.

A PHBV cell content of ca. 70 % (wt %) was attained at the end of the accumulation assay. The molar fraction of HV in the copolymer was ca. 20 mol %, as determined by gas chromatography with flame ionization detector (GC-FID) according to the method described by Lanham et al. (Lanham et al. 2013). Samples were calibrated through standard curves with a solution made of a commercial copolymer of PHBV with 12 % HV molar content and heptadecane as internal standard, both supplied by Sigma Aldrich Química S.A. (Sintra, Portugal).

Finally, lyophilization of the PHA-containing medium was performed neutralizing the liquid material. Then, it was centrifuged at 4000 rpm during 15 min and the resultant pellet was washed three times with distilled water. The obtained material was stored at −80 °C for at least 3 h and freeze-dried for a week to produce the unpurified PHBV powder.

2.3. Processing Routes

The unpurified lyophilized PHBV powder was processed using three different routes. **Figure 1** gathers a schematic description of the here-employed procedures. **Table 1** summarizes the different PHBV solution samples used for electrospinning with their resultant yields determined using Equation (1):

$$Yield = (W_f/W_i) \times 100 \quad (1)$$

Where W_i is the initial dry weight (100 g) and W_f is the final weight obtained after drying the resultant solution samples at 110 °C for 24 h.

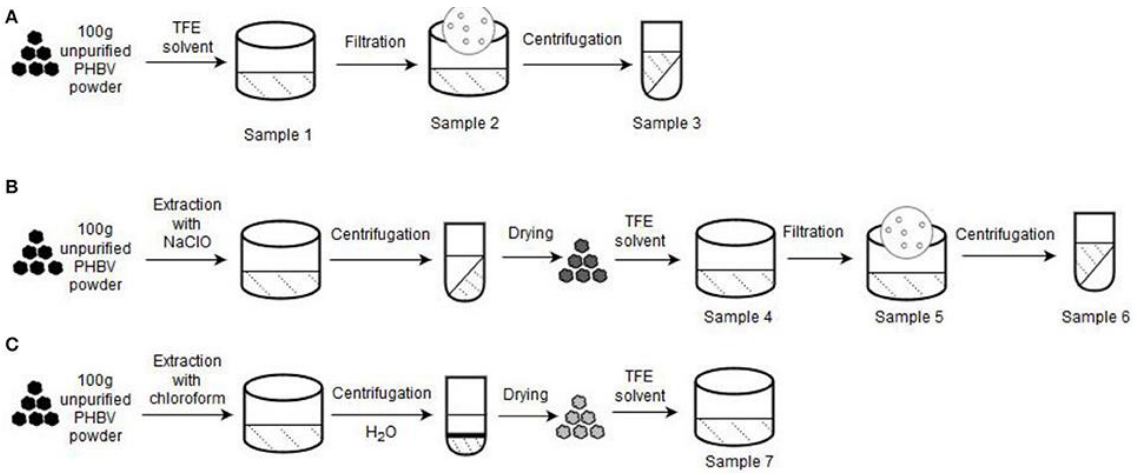

Figure 1. Processing routes for the preparation of the poly(3-hydroxybutyrate-*co*-3-hydroxyvalerate) (PHBV) solutions used for electrospinning: (A) Non-extraction; (B) Extraction with sodium hypochlorite (NaClO); (C) Extraction with chloroform. A starting sample of 100 g of unpurified PHBV powder was used in each process.

Table 1. Description and yield of the different poly(3-hydroxybutyrate-*co*-3-hydroxyvalerate) (PHBV) solutions used for electrospinning based on extraction routes with sodium hypochlorite (NaClO) and chloroform.

Sample	Description	Yield (%)
1	Unpurified PHBV	100
2	Unpurified PHBV after filtration	80
3	Unpurified PHBV after filtration and centrifugation	28
4	PHBV purified by NaClO	56
5	PHBV purified by NaClO after filtration	48
6	PHBV purified by NaClO after filtration and centrifugation	28
7	PHBV purified by chloroform	40

2.3.1. Non-Extraction Procedure

About 100 g of unpurified PHBV powder was dissolved in TFE at 8 wt % under magnetic stirring for 120 h at room temperature (sample 1). Then, part of this PHBV solution was filtered using Funnels Buchner Kartell disks, 2.5-mm mesh, from Scharlab S.L. (Barcelona, Spain) (sample 2). Finally, part of the filtered PHBV solution was additionally centrifugated at 13000 rpm for 5 min (sample 3) in an Avanti J-26S XP Centrifuge (Beckman Coulter).

2.3.2. Extraction Procedure with NaClO

Second route was based on the NaClO extraction method (Samorì et al. 2015, Villano et al. 2014). Briefly, 10 wt % unpurified PHBV powder was mixed with pre-diluted NaClO (5 % Cl_2). The mixture was stirred for 3 h at room temperature to degrade the non-PHA cellular material. The resultant PHBV solution was then centrifugated for 15 min at 6500 rpm and washed four times with distilled water. Afterwards, it was dried in 2 steps, first at 40 °C for 2 days, and then at 70 °C for 5 h. The resultant powder was dissolved in TFE at 8 wt % under magnetic stirring for 48 h at 50 °C (sample 4). After this, the resultant PHBV solution was filtered (sample 5) and also centrifuged at 13000 rpm for 5 min (sample 6).

2.3.3. Extraction Procedure with Chloroform

Third route followed a chloroform-based extraction method (Fiorese et al. 2009). For this, the unpurified PHBV powder was dissolved in chloroform at 5 wt %. The mixture was then stirred for 24 h at 50 °C to degrade the non-PHA cellular material. Later on, the solution was transferred to centrifugation tubes in which distilled water was added at 50 wt %. After shaking the tubes manually, these were centrifuged for 5 min at 4000 rpm. Afterwards, the PHBV suspension was recovered from the bottom of the tubes with a pipette and transferred to beakers, leaving them in the extractor hood until the solvent was completely evaporated. The resultant powder was dissolved in TFE at 2 wt % under magnetic stirring for 24 h at 50 °C (sample 7).

2.4. Characterization of PHBV Solutions

Prior to electrospinning, all the prepared PHBV solutions were characterized in terms of their viscosity, surface tension, and conductivity. The apparent viscosity (ηa) was determined at 100 s^{-1} using a rotational viscosity meter Visco BasicPlus L from Fungilab S.A. (San Feliu de Llobregat, Spain) equipped with a low-viscosity adapter (LCP). The surface tension was measured following the Wilhemy plate method using an EasyDyne K20 tensiometer from Krüss GmbH (Hamburg, Germany). The conductivity was evaluated using a conductivity meter XS Con6 from Lab-box (Barcelona, Spain). All measurements were carried out at room temperature in triplicate.

2.5. Electrospinning Process

All PHBV solutions were processed by electrospinning using a high-throughput dual polarization Fluidnatek® LE-500 pilot-plant device manufactured by Bioinicia S.L. (Valencia, Spain). The equipment was operated in the lab configuration mode by means of a motorized single needle injector, scanning horizontally toward a roll-to-roll collector. **Table 2** includes the different tested PHBV solutions in TFE with their final processing conditions, which were optimized for each solution. All experiments were carried out at room conditions, i.e., 25 °C and 40 % RH. The collected fiber mats were dried in a desiccator at 0 % RH for 15 days to completely remove the remaining solvent.

Table 2. Selected optimal conditions during electrospinning for the different poly(3-hydroxybutyrate-*co*-3-hydroxyvalerate) (PHBV) solutions.

Sample	Concentration (wt %)	Voltage (kV)	Flow-rate (ml/h)	Needle-to-collector distance (cm)	Time (h)
1	8	11.4	5	15	Not feasible
2	8	11.4	5	15	2.5
3	8	11.0	2	15	6.0
4	8	9.0	2	15	Not feasible
5	8	9.4	2	15	6.0
6	8	19.0	3	29	4.0
	2	19.0	4	22	6.0
7	4	22.0	4	25	6.0
	8	25.5	4	29	6.0
Commercial	10	19.0	6	15	2.0

2.6. Film Preparation

The resultant electrospun PHBV mats were subjected to annealing process in a 4122-model press from Carver, Inc. (Wabash, IN, USA). This was analyzed in the temperature range from 80 to 145 °C, for 10 s, without pressure. The post-processed samples had an average thickness of ~60 μm.

2.7. Characterization

2.7.1. Scanning Electron Microscopy

The morphologies of the electrospun PHBV fibers and resultant films were observed by scanning electron microscopy (SEM) using an S-4800 device from Hitachi (Tokyo, Japan). The samples were fixed to beveled holders using conductive double-sided adhesive tape and sputtered with a mixture of gold-palladium under vacuum prior to observation. An accelerating voltage of 10 kV was used and the estimation of the dimensions was performed by means of the Aperture software from Apple (Cupertino, CA, USA) using a minimum of 20 SEM micrographs in their original magnification.

2.7.2. Contact Angle Measurements

Measurements of contact angle were performed in a Video-Based Contact Angle Meter model Theta Lite TL 101 from Biolin Scientific (Espoo, Finland). Data were obtained by analyzing the shape of a distilled water drop of 5 µl, placed over the sample surface, taken after 10 s of the droplet-surface contact. Measurements were carried out at room conditions. Image analyses were carried out by the OneAttension software. At least, three replicates were made for each sample.

2.7.3. FTIR Spectroscopy

Fourier transform infrared (FTIR) spectra were collected coupling the attenuated total reflection (ATR) accessory Golden Gate of Specac, Ltd (Orpington, UK) to the Tensor 37 FTIR equipment (Bruker, Germany). Single spectra were collected in the wavelength range from 4000 to 600 cm^{-1} by averaging 20 scans at a resolution of 4 cm^{-1}.

Variable temperature FTIR was performed on a Nicolet Nexus FTIR instrument from Thermo Fisher Scientific Inc (Wilmington, DE, USA) coupled to a variable temperature single reflection diamond ATR sampling accessory of Specac Ltd. (Orpington, UK). Spectra were collected by averaging 64 scans at 4 cm^{-1} resolution using the blank ATR crystal at the same temperature as the background. Spectra were collected at 10 °C intervals from 30 to 100 °C and thereafter at 5 °C intervals up to 180 °C. To ensure the validity of the selected temperature, spectra were not collected until the digital reading on the temperature controller remained constant.

2.7.4. WAXD

Wide angle X-ray diffraction (WAXD) was performed using a Bruker AXS D4 ENDEAVOR diffractometer (Billerica, MA, USA). The samples were scanned, at room temperature, in the reflection mode using incident Cu K-alpha radiation (k = 1.54 Å), while the generator was set up at 40 kV and 40 mA. The data were collected over the range of scattering angles (2θ) comprised in the 2–40° range.

2.7.5. Thermal Analysis

Thermal transitions were studied by differential scanning calorimetry (DSC) on a DSC-7 analyzer from PerkinElmer, Inc. (Waltham, MA, USA), equipped with a cooling accessory Intracooler 2 also from PerkinElmer, Inc. A three-step program, under nitrogen atmosphere with a flow-rate of 20 ml/min, was applied: A first heating step from −30 to 180 °C, followed by a cooling step to −30 °C, and completed by a second heating to 200 °C. The heating and cooling rates were set as 10 °C/min and the typical sample weight was ~3 mg while an empty aluminium pan was used as reference. Calibration was performed using an indium sample. All tests were carried out, at least, in duplicate. The glass transition temperature (T_g), cold crystallization temperature (T_{cc}), enthalpy of cold crystallization (ΔH_{cc}), melting temperature (T_m), and enthalpy of melting (ΔH_m) were obtained from the heating scans, while the crystallization temperature from the melt (T_c) and enthalpy of crystallization (ΔH_c) were determined from the cooling scan.

Thermogravimetric analysis (TGA) was performed in a TG-STDA model TGA/STDA851e/LF/1600 thermobalance from Mettler-Toledo, LLC (Columbus, OH, USA). The samples, with a weight of about 15 mg, were heated from 50 to 900 °C, at a heating rate of 10 °C/min under a nitrogen flow-rate of 50 ml/min.

2.7.6. Mechanical Tests

Tensile tests of the PHBV films were performed according to ASTM standard method D638 using an Instron 4400 universal testing machine from Instron (Norwood, MA, USA) equipped with a 1-kN load cell. The tests were performed, at room conditions, with 115 × 16 mm^2 stamped dumb-bell shaped specimens using a cross-head speed of 10 mm/min. Samples were conditioned to the test conditions for 24 h prior to tensile assay. A minimum of six specimens were measured for each sample.

2.7.7. Permeability Tests

The water vapor permeability (WVP) of the film samples was determined using the gravimetric method ASTM E96-95 in triplicate. For this, 5 ml of distilled water was placed inside a Payne permeability cup (diameter of 3.5 cm) from Elcometer Sprl (Hermallesous-Argenteau, Belgium). The film was not in direct contact with water but exposed to 100 % RH on one side and secured with silicon rings. They were placed within a desiccator, sealed with dried silica gel, at 0 % RH cabinet at 25 °C. The control samples were cups with aluminum films to estimate solvent loss through the sealing. The cups were weighted periodically using an analytical balance (±0.0001 g). WVP was calculated from the regression analysis of weight loss data vs. time, and the weight loss was calculated as the total loss minus the loss through the sealing. The permeability was obtained by multiplying the permeance by the film thickness.

Similar as described above for WVP, limonene permeability (LP) was measured placing inside the Payne permeability cups 5 ml of $_D$-limonene. The cups containing the films were placed at controlled room conditions of 25 °C and 40 % RH. The limonene vapor permeation rates were estimated from the steady-state permeation slopes and the weight loss was calculated as the total cell loss minus the loss through the sealing. LP were calculated taking into account the average film thickness in each case. The samples were tested in triplicate.

The oxygen permeability coefficient was derived from the oxygen transmission rate (OTR) measurements that were recorded at 60 % RH and 25 °C, in duplicate, using an Oxygen Permeation Analyzer M8001 from Systech Illinois (Thame, UK). The humidity equilibrated samples were purged with nitrogen, before exposure to an oxygen flow of 10 ml/min. The exposure area during the test was 5 cm^2 for each sample. In order to obtain the oxygen permeability (OP), film thickness and gas partial pressure were considered.

2.8. Statistical Analysis

Statistical differences across solution and material properties were evaluated with a two-tailed unpaired t-test using GraphPad Prism 7.04 of GraphPad Software Company (La Jolla, CA, USA).

Mean values and standard deviations were also calculated. Significant differences were used at the 99 % confidence level ($p < 0.01$).

3. Results and Discussion

3.1. PHBV Powders

Figure 2 shows the appearance of the obtained powders of the various PHBV samples. As it can be seen in Figure 2.1, the unpurified PHBV powder presented a light brown color, indicating the presence of biomass impurities derived from the pulp fruits and the fermentation process. The PHBV powder processed without any purification method but filtered, shown in Figure 2.2, presented a similar color. However, when this sample was filtered and centrifugated, the brown color became more intense, as it can be observed in Figure 2.3. Nevertheless, it is possible that the powder developed a dark color during the drying process. In any case, this suggests that most of the impurities still remained in the unpurified PHBV samples. After treatment with NaClO, the powder became clearly whiter, as shown in Figure 2.4. This color change can be related to both the extraction of impurities of the pulp fruits and the intrinsic whitening effect of bleach. However, the PHBV sample again developed the brown color for both the sample filtered (Figure 2.5) and the sample filtered and centrifugated (Figure 2.6). This would confirm that the color development was favored during drying by most likely Maillard browning reactions. In the case of the PHBV powder extracted with chloroform, as seen in Figure 2.7, it presented a yellowish color.

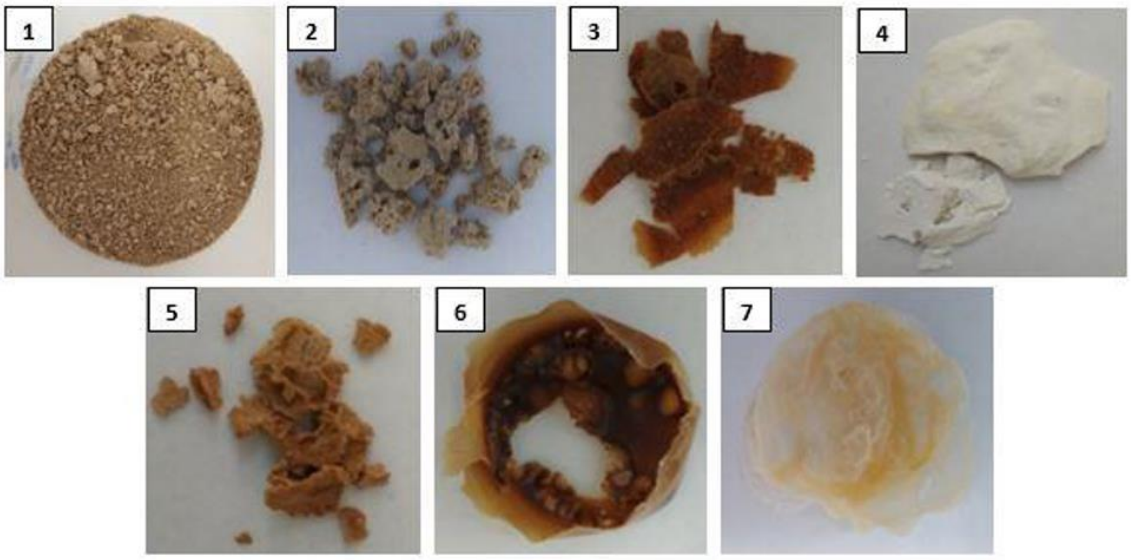

Figure 2. Pictures of the different poly(3-hydroxybutyrate-*co*-3-hydroxyvalerate) (PHBV) powders obtained after drying from the extraction routes of the different solutions from sample 1 to sample 7.

The visual aspect of here-obtained PHBV powders can be, therefore, related to the resultant content of biomass impurities derived from the pulp fruits and the fermentation process. As it can be seen in previous **Table 1**, the samples reached different yield values at each process, indicating that the removal of non-PHA material was achieved to different extends. In addition, one can observe that both the filtration and centrifugation processes further reduced the impurities content, producing a reduction of the yield values. For instance, the yield values of the NaClO- and chloroform-extracted powders were 56 and 40 %, respectively. However, since it was necessary for the PHBV powder processed with NaClO to be filtered and centrifugated, the final yields generated with this route ranged in values of 48–28 %.

3.2. Electrospun PHBV Fibers

All the here-prepared PHBV solutions were intended to be processed by electrospinning. However, due to their high impurities, samples 1 and 4 clogged the injector of the electrospinning device and hence could not be processed, being ruled out of the study. Samples 2, 3, 5, 6, and 7 were successfully processed by electrospinning and their optimal processing conditions are gathered in the cited **Table 2**.

Figure 3 shows the resultant electrospun mats obtained from the different PHBV solutions. In all cases, the electrospinning process generated a mat composed of non-woven fibers with different sizes. In particular, the mean diameters of the electrospun fibers obtained from the solution samples made of unpurified PHBV were 0.71 ± 0.12 μm (Figure 3A), after filtration (sample 2), and 0.75 ± 0.14 μm (Figure 3B), after filtration and centrifugation (sample 3). It is also worthy to mention that both samples, however, presented certain difficulties during electrospinning due to their high content of particles in suspension. For the solutions of PHBV extracted with NaClO, the fiber sizes significantly increased from 0.65 ± 0.24 μm (Figure 3C), after filtration (sample 5), to 1.91 ± 0.40 μm (Figure 3D), after filtration and centrifugation (sample 6). In the case of sample 7, i.e., the solution made of PHBV extracted with chloroform, the mean fiber diameter was 1.32 ± 1.12 μm (Figure 3E). The morphology of the electrospun fibers obtained from a solution made of commercial PHBV, processed in similar conditions, was also included for comparison purposes. These fibers presented a mean diameter of 1.21 ± 0.27 μm (Figure 3F).

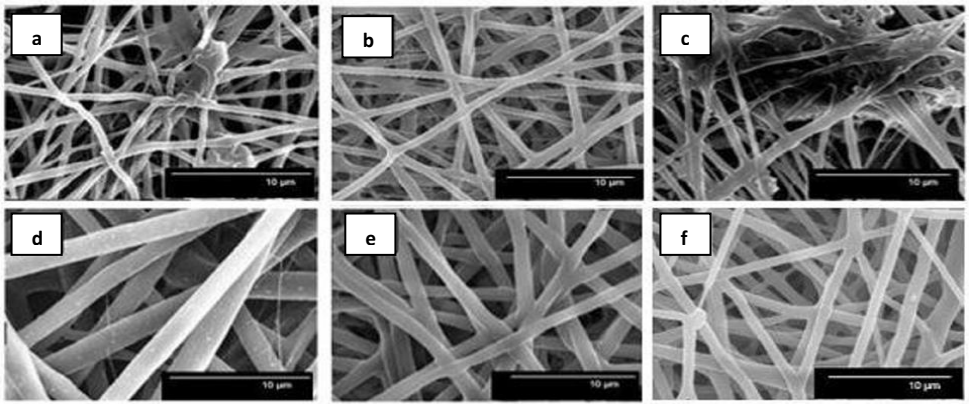

Figure 3. Scanning electron microscopy (SEM) images of poly(3-hydroxybutyrate-*co*-3-hydroxyvalerate) (PHBV) fibers of: (a) Sample 2, (b) Sample 3, (c) Sample 5, (d) Sample 6, (e) Sample 7, and (f) Commercial sample.

Therefore, the application of the extraction procedures increased the fiber size, which were further increased after centrifugation in the case of the NaClO route. This change in morphology suggests that the purity of the biopolymer improved, which in turn increased its content in the TFE solutions. The increase in fiber size with polymer content can be ascribed to an increase in the viscoelastic properties of the material processed by electrospinning (Torres-Giner, Gimenez, and Lagaron 2008). It is also worthy to mention that in the case of samples 2 and 5, i.e., samples that were not centrifugated, these solutions generated some beaded morphologies and/or big agglomerates. This fact can be related to the presence of remaining impurities in the PHBV solutions. Interestingly, these beaded-like structures were not observed in the case of sample 7, which was not centrifugated, suggesting that the extraction route with chloroform was more efficient than that with NaClO.

Due to the difficulties faced during electrospinning and the presence of beads in their fiber mats, the study was further continued only with samples 6 and 7. In order to correlate the obtained morphologies with the characteristics of each PHBV, the solution properties were characterized in terms of their viscosity, surface tension, and conductivity. In the case of sample 7, different PHBV concentrations were also tested in order to find out the best processing conditions for the materials. **Table 3** displays the values of viscosity, surface tension, and conductivity of samples 6 and 7 as well as the properties of the solution made of commercial PHBV. From this table, it can be observed that the solution made of PHBV extracted with chloroform, at a concentration of 8 wt %, presented a significantly higher viscosity, i.e., ~28300 cP, than the PHBV solution processed with NaClO at the same concentration, i.e., ~6300 cP. Indeed, sample 7 could not be electrospun at 8 or even 4 wt %, but it was processed at 2 wt %. This PHBV solution provided a viscosity value of ~300 cP. The viscosity of the commercial benchmark PHBV solution was ~690 cP, i.e., between the viscosity range of both extracted PHBV solutions. In this sense, it has been reported that relatively high viscosities are desirable to obtain uniform electrospun fibers from biopolymers, however excessively high viscosities can also yield low processability due to instabilities during electrospinning (Sreekumar et al. 2017). In the case of surface tension, all PHBV solutions presented similar values, i.e., in the 20–27 mN/m range. All PHBV solutions also presented similar values of conductivity, varying from 1 to 4 μS/cm, with the exception of sample 6. For the latter PHBV solution, conductivity was considerably higher, i.e., 162.5 μS/cm, which is a factor that limits its processability by electrospinning. The observed higher conductivity may be related to the presence of ions coming from the bleach treatment. Although solution properties can anticipate processability issues during electrospinning, habitually it is difficult to elucidate the effect of a single property without considering the impact of the other ones (Torres-Giner et al. 2017).

Table 3. Solution properties of the poly(3-hydroxybutyrate-*co*-3-hydroxyvalerate) (PHBV) samples.

Sample	Concentration (wt %)	Viscosity (cP)	Surface tension (mN/m)	Conductivity (μS/cm)
6	8	6362.3 ± 41.6^{b}	25.2 ± 0.2^{a}	162.50 ± 1.60^{b}
7	2	296.8 ± 1.2^{a}	20.5 ± 0.1^{a}	1.29 ± 0.01^{a}
	4	2783.4 ± 21.1^{b}	23.3 ± 0.1^{a}	1.44 ± 0.01^{a}
	8	28291.0 ± 98.3^{b}	26.5 ± 0.2^{a}	2.05 ± 0.01^{a}
Commercial	10	688.8 ± 5.4^{a}	21.9 ± 0.1^{a}	3.74 ± 0.02^{a}

Superscript letters in the same column indicate a statistically significant difference ($p < 0.01$) among the samples for each solution property.

3.3. Electrospun PHBV Films

The electrospun mats obtained from solution samples 6 and 7 were subjected to a thermal post-treatment in order to produce continuous films of more application interest in, for instance, packaging. In order to ascertain the film-forming process, the cryofracture surfaces of the electrospun mats after post-treatment at different temperatures were analyzed. **Figure 4** shows the SEM images, both taken at low, i.e. 1000x, and high magnifications, i.e., 5000x, of the cross-sections of the electrospun PHBV mats. As one can observe, up to 110 °C, the electrospun PHBV material preserved their original fiber-based morphology though the mat porosity was gradually reduced with increasing temperature. At a temperature of 125 °C, a compact packing rearrangement of the electrospun fibers was produced. This phenomenon successfully resulted in the formation of a continuous film with a very low porosity. However, at the highest tested temperature, i.e., 145 °C, the film integrity was lost and some large voids were formed probably due to partial material melting and/or degradation. Similar film cross-sections were recently observed by Cherpinski et al. (Cherpinski et al. 2017) for electrospun commercial PHB fibers post-processed at 160 °C, a temperature below the homopolyester melting point. It was reported that the morphology of the starting electrospun non-woven fibers mat was lost due to the ultrathin fiber coalescence during the annealing step.

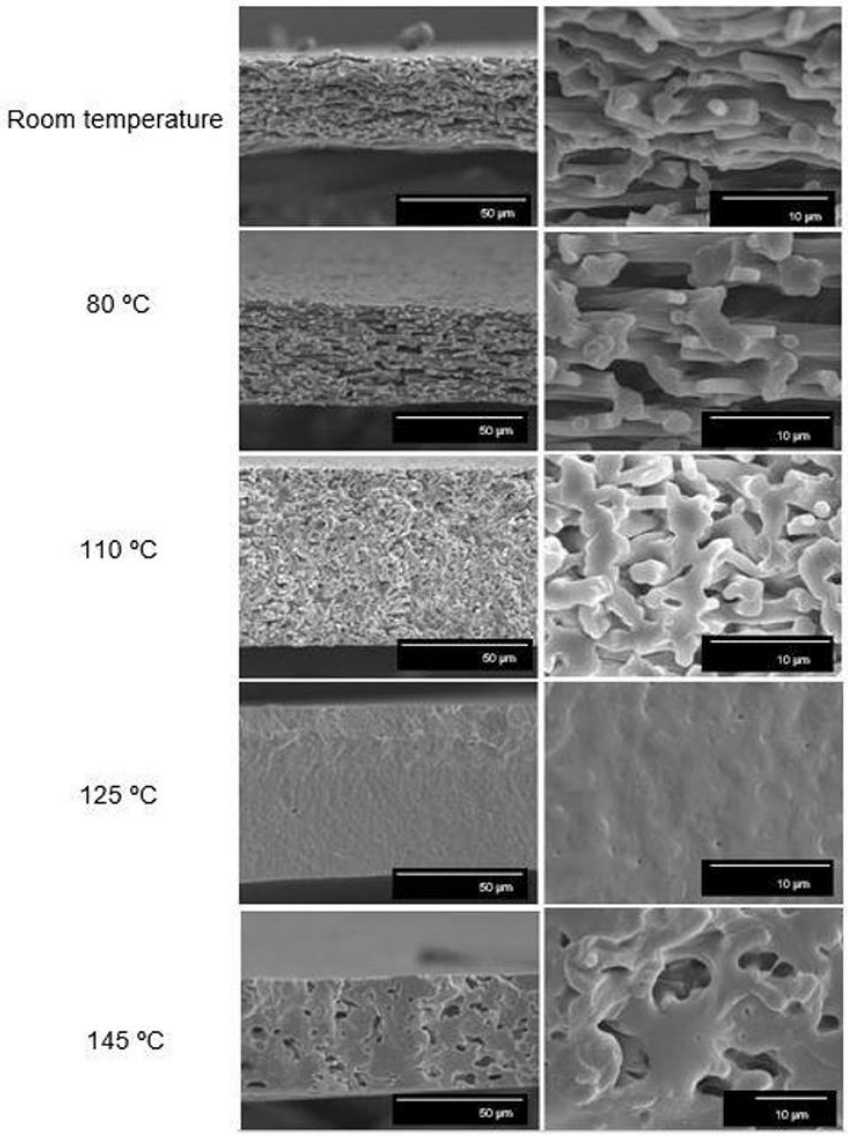

Figure 4. Scanning electron microscopy (SEM) images taken at 1000x (Left) and 5000x (Right) on the cross-sections of the electrospun poly(3-hydroxybutyrate-*co*-3-valerate) (PHBV) mats processed at different temperatures: Room temperature (25 °C), 80, 110, 125, and 145 °C. Scale markers of 50 and 10 µm.

Based on this observation, a post-processing temperature of 125 °C was selected for annealing the electrospun mats obtained from samples 6 and 7. **Figure 5** shows the visual aspect of both films to ascertain their contact transparency. Simple naked eye examination of this figure indicates that both PHBV materials generated films with similar surfaces but the contact transparency was higher in the film obtained from sample 7, i.e., in the film made of PHBV material purified with chloroform. This suggests that the latter film presented lower crystallinity and/or higher purity than the film produced with PHBV material extracted with NaClO.

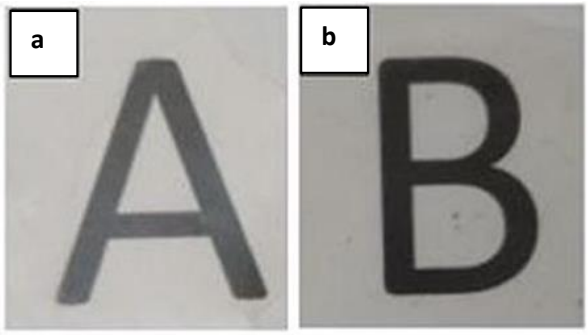

Figure 5. Visual aspect of the electrospun poly(3-hydroxybutyrate-*co*-3-valerate) (PHBV) films obtained from: (a) Sample 6 and (b) Sample 7.

3.4. Characterization of the Electrospun PHBV Materials

The PHBV films obtained from samples 6 and 7 were characterized in terms of their hydrophobicity and thermal, mechanical, and barrier performance. These properties were analyzed in order to ascertain their potential use in packaging applications.

3.4.1. Contact Angle

The water contact angle of the PHBV films obtained from samples 6 and 7 were determined. Both electrospun films presented similar values, i.e., 78.2° ± 1.6 and 85.6° ± 0.3 for sample 6 and 7, respectively. Therefore, both electrospun films were highly hydrophobic suggesting that polar biomass residues were efficiently removed. The higher contact value observed for sample 7, i.e., the film obtained from the electrospun fibers treated with chloroform, further supports the fact that this film presented higher purity. Electrospun films made of commercial PHB and PHBV were recently applied to coat nanopapers, resulting in contact angle values in the 75-85° range (Cherpinski et al. 2018).

3.4.2. Thermal Properties

Table 4 displays the thermal transitions, for the three-step program, carried out by DSC for the electrospun fibers and annealed films of the two different extracted PHBV materials. The DSC curves of all thermal steps are gathered for each sample in **Figure 6**. During the first heating, one can observe that cold crystallization was not unambiguously observed in the fibers or the films for both PHBV materials. Additionally, melting was produced in a single peak in the 136–144 °C range. Higher values of T_m were observed in the film samples in comparison to the fibers, suggesting that the films developed crystalline structures with thicker lamellae thickness or less defective crystals. In relation to the cooling step, it can be observed that both the fibers and film obtained from sample 6 crystallized from the melt in a single step, showing a clear T_c value at ~65.5 and 71 °C, respectively. For sample 7, however, both PHBV materials, i.e., fibers and film, cold crystallized to a significant extent during the second heating step, presenting values of T_{cc} at

~52 and 65.5 °C, respectively. Sample 7 did not exhibit a clear crystallization peak during the cooling step. These observations suggest that sample 6 was easier to crystallize during cooling than sample 7, probably because of the presence of more nucleating impurities in the former sample.

Table 4. Thermal properties of the poly(3-hydroxybutyrate-*co*-3-hydroxyvalerate) (PHBV) fibers and films. The glass transition temperature (T_g), melting temperature (T_m), enthalpy of melting (ΔH_m), cold crystallization temperature (T_{cc}) and enthalpy of the cold crystallization (ΔH_{cc}) were obtained from the differential scanning calorimetry (DSC) curves during the first and second heating scan while the crystallization temperature (T_c) and enthalpy of crystallization (ΔH_c) from the cooling scan.

Sample		First heating		Cooling		Second heating					
		T_m (°C)	ΔH_m (J/g)	T_c (°C)	ΔH_c (J/g)	T_g	T_{cc} (°C)	ΔH_{cc} (J/g)	Tm_1 (°C)	Tm_2 (°C)	ΔH_m (J/g)
6	Fibers	136.8 ± 1.0[a]	41.0 ± 0.4[a]	65.5 ± 0.1[a]	34.5 ± 4.3[a]	-0.8 ± 0.2[a]	-	-	126.1 ± 0.7[a]	141.4 ± 1.0[a]	31.0 ± 8.6[a]
	Film	143.1 ± 1.8[a]	36.7 ± 3.1[a]	71.2 ± 4.0[a]	33.9 ± 3.5[a]	2.7 ± 0.1[a]	-	-	136.7 ± 2.8[a]	149.3 ± 2.4[a]	46.3 ± 9.8[a]
7	Fibers	139.1 ± 0.2[a]	42.2 ± 1.5[a]	-	-	-4.4 ± 1.2[b]	52.3 ± 3.3[a]	39.6 ± 0.8[a]	128.1 ± 0.5[a]	143.8 ± 0.2[a]	57.8 ± 0.9[b]
	Film	141.8 ± 2.0[a]	37.8 ± 6.6[a]	-	-	-0.3 ± 1.3[b]	65.5 ± 1.5[a]	43.0 ± 1.9[a]	135.5 ± 2.3[a]	148.4 ± 2.1[a]	43.2 ± 2.0[a]

Superscript letters in the same column indicate a statistically significant difference ($p < 0.01$) among the samples for each thermal property.

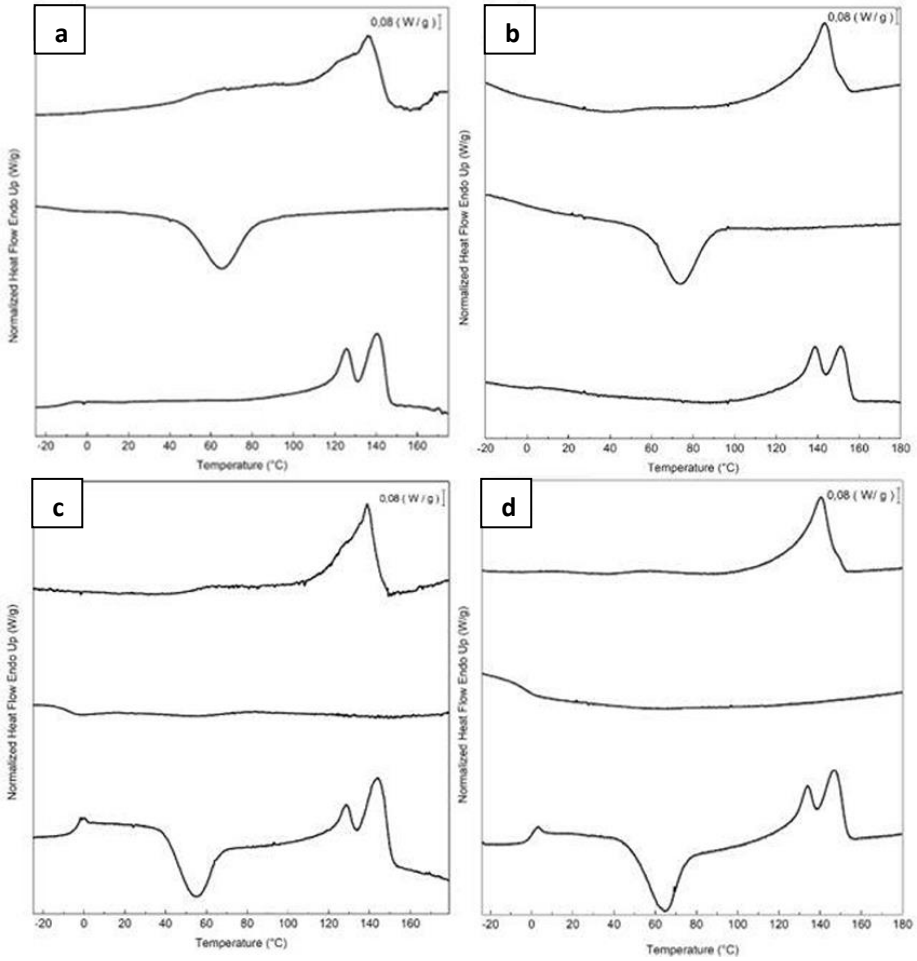

Figure 6. First heating, cooling, and second heating curves, shown from top to bottom, of the electrospun poly(3-hydroxybutyrate-*co*-3-valerate) (PHBV): (a) Fibers obtained from sample 6; (b) Film obtained from sample 6; (c) Fibers obtained from sample 7; (d) Film obtained from sample 7.

During the second heating, the glass transition of the PHBV was clearly observed, which occurred in the temperature range ranging from −5 to 3 °C for all samples. In the case of sample 7, a slight endothermic peak during the glass transition was also noticed. This can be ascribed to a stress relaxation process of the amorphous phase during the heating run. Briefly, the amorphous polymer chains may attain a lower-free energy state during cooling. As a result of this frozen segmental mobility, the sample presents smaller free volume, enthalpy, and potential energy (Cowie, Harris, and McEwen 1998). Therefore, when these materials are reheated, more energy is required to surpass the glass transition, resulting in a small endothermic peak associated with the change in heat capacity triggered by the T_g (Hutchinson et al. 1999). In addition, all samples showed a bimodal endothermic peak. A first melting temperature was observed in the range of 126–137 °C, followed by a more intense second melting temperature in the 141–150 °C range. Similar observations were previously found by Zhang et al. (Zhang, Misra, and Mohanty 2014) in a PHA copolyester, indicating that multiple melting peaks are linked to crystal reorganization upon melting by which imperfect crystals order into spherulites with thicker lamellar thicknesses and then melt at higher temperatures. In addition, the melting peaks at low temperatures could be also

ascribed to the crystalline phase of the HV-rich fractions due to the relatively high HV content, i.e., 20 mol %. Additionally, similar to the first heating, higher T_m values were observed in the films that in the fibers. For instance, in the PHBV materials obtained from sample 7, the T_m values were in range of 128.1–143.8 °C, for the fibers, whereas the values ranged in 135.5–148.4 °C, for the film.

In comparison with other previous studies, the here-studied PHBV films exhibited a lower melting profile than other PHBV films prepared by solving casting, i.e., T_m values at 145–157 °C for HV 12 mol % (Sanchez-Garcia, Gimenez, and Lagaron 2008). Similarly, PHBV materials with HVs of 3 and 18 mol % prepared by melt mixing also showed higher T_m values, i.e., 169.6 and 173.2 °C, and T_c values, i.e., 107.1 °C (Castro Mayorga et al. 2018). In relation to other electrospun films, Cherpinski et al. (Cherpinski et al. 2018) reported two melting points at 162.2 and 177.3 °C for PHB films while T_c was 110.4 °C. The lower values in the present study can be related to the higher HV content of the here-processed PHBV materials.

Table 5 shows the thermal stability obtained by TGA of the electrospun fibers and films obtained from samples 6 and 7. One can observe that both processes generated materials with a similar thermal stability though sample 6, i.e., the PHBV materials extracted with NaClO, presented slightly better thermal values. In particular, the onset degradation temperature ($T_{5\%}$) of both materials obtained from sample 6 occurred at 268 °C while the thermal decomposition of sample 7 started at 263 and 267 °C, for its fibers and film, respectively. In addition, the thermal degradation temperature (T_{deg}) was also higher in sample 6, i.e., 294 °C, with a mass loss of only around 61 %. In the case of sample 7, T_{deg} values were at 285 and 290 °C, for its fibers and film, respectively, presenting a mass loss of ~75 %. Finally, the amount of residual mass was lower in the chloroform-extracted PHBV materials, in the 3–3.5 % range, than the NaClO-extracted ones, i.e., 6–6.5 %.

Table 5. The onset degradation temperature, defined as the temperature at 5 % weight loss ($T_{5\%}$), degradation temperature (T_{deg}), and residual mass of the poly(3-hydroxybutyrate-*co*-3-hydroxyvalerate) (PHBV) fibers and films. Residual mass was measured at 800 °C.

Sample		$T_{5\%}$ (°C)	T_{deg} (°C)	Mass loss (%)	Residual mass (%)
6	Fibers	268 ± 1.0^a	294 ± 0.6^a	61.1 ± 0.7^a	6.4 ± 1.3^a
	Film	268 ± 0.7^a	294 ± 0.3^a	62.1 ± 0.4^a	5.8 ± 1.2^a
7	Fibers	263 ± 2.1^a	285 ± 2.4^b	74.6 ± 1.2^b	3.5 ± 0.2^b
	Film	267 ± 1.8^a	290 ± 3.0^a	77.2 ± 1.4^b	3.2 ± 0.3^b

Superscript letters in the same column indicate a statistically significant difference ($p < 0.01$) among the samples for each thermal property.

Previous electrospun PHBV films with a HV content of 3 mol % showed a $T_{5\%}$ value of 269 °C and a T_{deg} value of 290.8 °C with a residual mass of 5.1 % (Castro-Mayorga et al. 2017), which are relatively close to the ones obtained here. Interestingly, previously prepared PHBV films with a HV content of 18 mol % presented lower thermal stability, i.e., 249.8 °C (Castro-Mayorga,

Fabra, and Lagaron 2016), which is an indication that the here-obtained PHBV films could have less impurities since it is known that the thermal degradation mechanism in PHA is easily accelerated by the presence of fermentation residues (Hablot et al. 2008).

3.4.3. Crystallinity

WAXD experiments were conducted on both films and fiber mats obtained from samples 6 and 7 to assess their crystallinity since DSC, being a dynamic method, does not provide an accurate description of crystallinity for this biopolymer as discussed earlier (Castro Mayorga et al. 2018, Cherpinski et al. 2017). The diffractograms, included in **Figure 7**, presented two main peaks located at 13.5° and 16.9° (2θ), followed by three other minor reflections at ca. 22°, 25°, and 27° (2θ). These peaks can be found in the four plots, thus revealing a similar semicrystalline nature for all the samples. According to the literature, these peaks correspond to the (020), (110), (111), (130), and (040) lattice planes of the orthorhombic unit cell of PHB (Mottina et al. 2016). This is in agreement with previous literature reporting that the crystalline structure of PHBV with HV contents below 37 % is that of the PHB homopolymer (Kunioka, Tamaki, and Doi 1989).

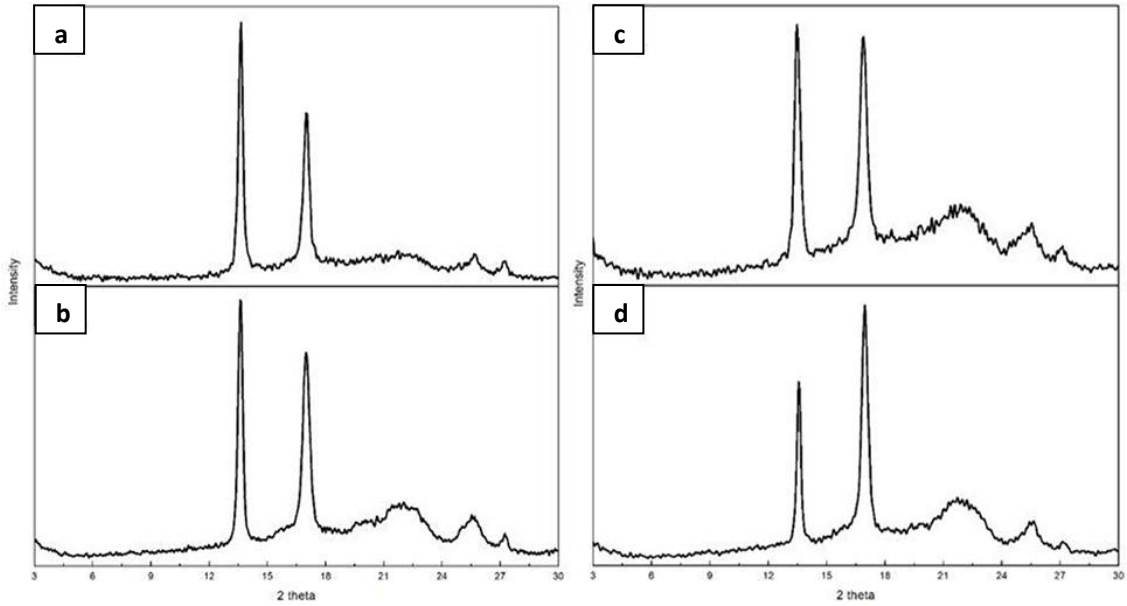

Figure 7. Wide angle X-ray diffraction (WAXD) patterns of the electrospun poly(3-hydroxybutyrate-*co*-3-valerate) (PHBV): (a) Fibers obtained from sample 6; (b) Film obtained from sample 6; (c) Fibers obtained from sample 7; (d) Film obtained from sample 7.

In regard to the crystallinity determined by WAXD, one can observe in **Table 6** that the materials obtained from sample 6 were seen to exhibit higher crystallinity than those obtained from sample 7 while the films tended to show slightly higher crystallinity than the fibers, albeit the differences were very small. DSC seemed thus unable to discriminate among the samples, since all materials exhibited similar enthalpies of melting (see previous **Table 4**). As a result, and based on our

previous study (Cherpinski et al. 2017), ATR-FTIR spectra as a function of temperature were recorded for the various materials with the aim of assessing their molecular order.

Table 6. WAXD crystallinity and ATR-FTIR 1720 cm^{-1} band width at half height.

Sample		WAXD	1720 cm^{-1} band width
6	Fibers	47	22.6
	Film	49	21.8
7	Fibers	36	27.5
	Film	39	25.0

Figure 8 gathers, as an example, two different view plots of the FTIR spectra taken across temperature of the electrospun fibers obtained from sample 7. Additionally, **Figure 9** shows the evolution with temperature of the ratio of absorbance of the bands 1230/1453 and the 1720 cm^{-1} band width at half height for the electrospun fibers obtained from samples 6, 7 and from the commercial PHBV solution. The latter two spectral features have been previously connected with the molecular order (crystallinity) in the polymer (Cherpinski et al. 2017). Thus, higher band ratios and lower 1720 cm^{-1} band widths were correlated with higher crystallinity in the biopolymer (Cherpinski et al. 2017). The strongest peak, seen at ca. 1720 cm^{-1}, has been assigned to the stretching vibration of the carbonyl group (C = O) in PHA copolyesters, corresponding to the intramolecular bonding of their crystalline state, while the complex and multiple peaks in the region from 1000 to 880 cm^{-1} have been related to the stretching bands of the carbon–carbon single bond (C–C) (Torres-Giner et al. 2016). Finally, the ester-related band was observed at ~1080 cm^{-1} and the band at ~1020 cm^{-1} is known to arise from C–O and C–O–C stretching vibrations of ester groups in biopolyesters (Torres-Giner et al. 2011). In **Figure 8** one can easily see that sample 7 underwent an increase in the intensity of the 1720 cm^{-1} carbonyl band, and also of other peaks, with increasing temperature up to a maximum at around 120 °C and then a decrease in band intensity, concomitant band broadening, and shift toward higher wavenumbers suggesting a decrease in molecular order and eventually melting. **Figure 9** more clearly depicts for the three materials the evolution of the cited two molecular order spectroscopic indexes used. From this figure, it can be easily appreciated that for the fibers at room temperature the fibers obtained from the commercial PHBV solution and sample 6 were more crystalline than those obtained from sample 7, in good agreement with the WAXD results. With increasing temperature, samples 6 and 7 underwent an increase in molecular order with maximum around 120 °C, in agreement with melting and recrystallization events suggested previously to explain crystallization, cold crystallization, and multiple melting endotherms during the DSC experiments.

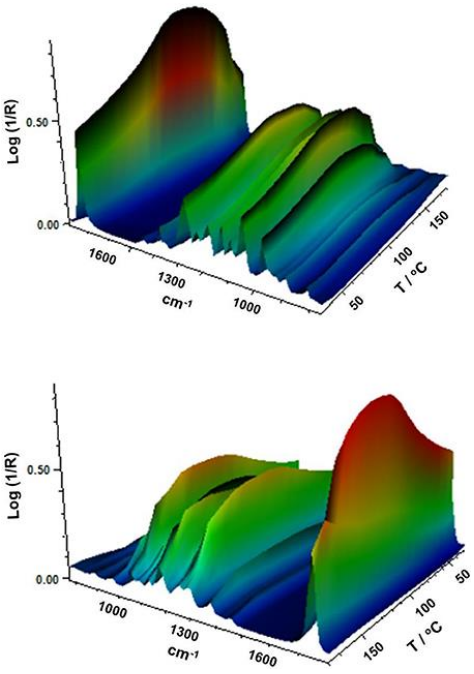

Figure 8. Fourier transform infrared (FTIR) spectra taken across temperature of the electrospun poly(3-hydroxybutyrate-*co*-3-hydroxyvalerate) (PHBV) fibers obtained from sample 7.

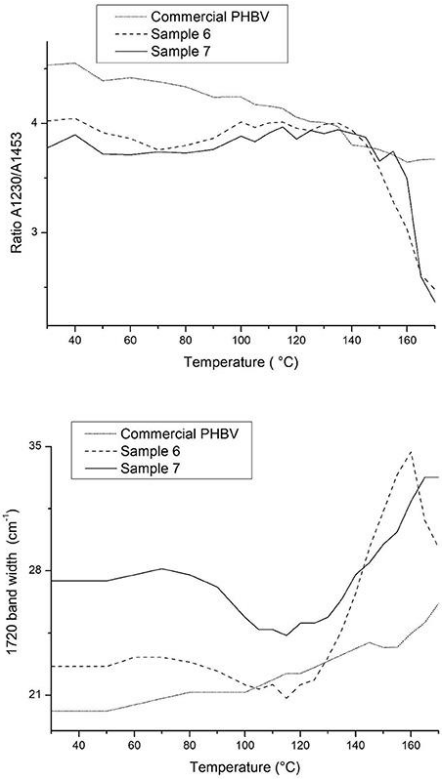

Figure 9. Evolution with temperature of the ratio of absorbance of the bands 1230/1453 and the 1720 cm^{-1} band width at half height for the electrospun poly(3-hydroxybutyrate-*co*-3-hydroxyvalerate) (PHBV) fibers obtained from samples 6, 7 and from the commercial PHBV solution.

Finally, **Table 6** also gathers the 1720 cm^{-1} band width for the fibers and films obtained from samples 6 and 7. This value was actually in good agreement with the WAXD results, again supporting that this simple and rapid method may be alternative to WAXD for rapid assessment of relative crystallinity among different samples, as opposed to the dynamic more commonly method often used based on DSC.

3.4.4. Mechanical Properties

Table 7 displays the values of the elastic modulus (E), tensile strength at break (σ_b), elongation at break (ε_b), and toughness (T) of the electrospun PHBV films calculated from their strain-stress curves. In general, both films presented characteristics of a brittle material associated to PHBV, showing low ε_b and T values, below 3 % and 0.5 mJ/m^3, respectively. However, in regard to the mechanical strength properties, the film samples presented a dissimilar performance. For the electrospun film obtained from sample 7, it can be observed that the specimens presented a relative low modulus, i.e., 434 MPa, while this was around three times higher for that obtained from sample 6. It is hypothesized that the presence of more impurities and higher crystallinity could be behind the higher rigidity associated to the film produced with sample 6.

Table 7. Mechanical properties in terms of tensile modulus (E), tensile strength at break (σ_b), elongation at break (ε_b), and toughness (T) of the electrospun poly(3-hydroxybutyrate-*co*-3-hydroxyvalerate) (PHBV) films obtained from samples 6 and 7.

Sample	E (MPa)	σ_b (MPa)	ε_b (%)	T (mJ/m^3)
6	1166 ± 120^a	18.9 ± 0.9^a	2.6 ± 0.2^a	0.3 ± 0.1^a
7	434 ± 2^b	7.1 ± 0.9^b	2.9 ± 0.4^a	0.4 ± 0.1^a

Superscript letters in the same column indicate a statistically significant difference ($p < 0.01$) among the samples for each mechanical property.

In comparison to PHB films prepared by conventional compression molding, it has been recently observed that equivalent annealed electrospun films exhibited higher elongation at break and toughness while similar mechanical strength (Cherpinski et al. 2017). Therefore, a more balanced mechanical performance can be achieved in biopolymer films prepared by electrospinning followed by optimal post-processing. The higher flexibility and toughness observed for the film produced with sample 7 makes it potentially more interesting for uses in flexible packaging applications.

3.4.5. Barrier Properties

Table 8 gathers the WVP, LP, and OP values of the electrospun PHBV films obtained from samples 6 and 7. From this table, it can be observed that the electrospun film obtained with the

PHBV treated with chloroform, i.e., sample 7, presented the lowest WVP value, of 5.25×10^{-15} $kg \cdot m \cdot m^{-2} \cdot Pa^{-1} \cdot s^{-1}$. This value was about 6 times lower than that observed for the PHBV film obtained from sample 6, i.e., 3.29 x 10^{-14} $kg \cdot m \cdot m^{-2} \cdot Pa^{-1} \cdot s^{-1}$. This suggests that, in spite of the film prepared with NaClO being more crystalline, the film sample prepared with chloroform presented lower wettability, free volume, and presumably also lower porosity, which can be related to the presence of impurities. The here-reported values are close to this of the benchmark petroleum derived polyethylene terephthalate (PET) films, i.e., 2.30×10^{-15} $kg \cdot m \cdot m^{-2} \cdot Pa^{-1} \cdot s^{-1}$ (Lagarón 2011), widely employed for medium barrier food packaging applications. Additionally, the here-prepared electrospun PHBV films showed lower WVP values than these of PHBV films prepared by solvent casting, i.e., 1.27×10^{-14} $kg \cdot m \cdot m^{-2} \cdot Pa^{-1} \cdot s^{-1}$ (Sanchez-Garcia, Gimenez, and Lagaron 2008), while these were higher but in the same range than these of compression-molded PHB films, i.e., 1.7×10^{-15} $kg \cdot m \cdot m^{-2} \cdot Pa^{-1} \cdot s^{-1}$ (Sanchez-Garcia, Gimenez, and Lagaron 2007).

Table 8. Values of water vapor permeability (WVP), D-limonene permeability (LP), and oxygen permeability (OP) of the electrospun poly(3-hydroxybutyrate-*co*-3-hydroxyvalerate) (PHBV) films obtained from samples 6 and 7.

Sample	WVP x 10^{14} ($kg \cdot m \cdot m^{-2} \cdot Pa^{-1} \cdot s^{-1}$)	LP x 10^{14} ($kg \cdot m \cdot m^{-2} \cdot Pa^{-1} \cdot s^{-1}$)	OP x 10^{19} ($m^3 \cdot m \cdot m^{-2} \cdot Pa^{-1} \cdot s^{-1}$)
6	3.29 ± 1.16^a	0.29 ± 0.27^a	1.02 ± 0.03^a
7	0.53 ± 0.51^b	3.54 ± 0.38^b	1.49 ± 0.54^a

Superscript letters in the same column indicate a statistically significant difference ($p < 0.01$) among the samples for each barrier property.

In relation to LP, a strong plasticizer for PHA polymers, the highest barrier performance was observed for the PHBV film prepared from sample 6. Thus, the LP value for the electrospun film obtained with PHBV treated with NaClO was 2.97×10^{-15} $kg \cdot m \cdot m^{-2} \cdot Pa^{-1} \cdot s^{-1}$, which is similar to that observed for a compression-molded PHB film, i.e., 8.8×10^{-15} $kg \cdot m \cdot m^{-2} \cdot Pa^{-1} \cdot s^{-1}$ (Sanchez-Garcia, Gimenez, and Lagaron 2007). LP reached a value of 3.54×10^{-14} $kg \cdot m \cdot m^{-2} \cdot Pa^{-1} \cdot s^{-1}$ for the film prepared with sample 7. This can be related to the higher purity of this film, resulting in higher uptake and hence permeation for this sample. This value was lower, i.e., higher barrier, than those previously reported by Sanchez-Garcia et al. (Sanchez-Garcia, Gimenez, and Lagaron 2008) for PHBV films with 12 mol % HV prepared by solvent casting, i.e., 1.99×10^{-13} $kg \cdot m \cdot m^{-2} \cdot Pa^{-1} \cdot s^{-1}$, and for PET films obtained by compression molding, i.e., 1.17×10^{-13} $kg \cdot m \cdot m^{-2} \cdot Pa^{-1} \cdot s^{-1}$.

Finally, both electrospun PHBV films presented a good barrier performance to oxygen. In particular, the OP values were 1.02×10^{-19} $m^3 \cdot m \cdot m^{-2} \cdot Pa^{-1} \cdot s^{-1}$, for the film obtained from sample 6, and 1.49×10^{-19} $m^3 \cdot m \cdot m{-}2 \cdot Pa^{-1} \cdot s^{-1}$, for the one obtained from sample 7. These values are slightly lower than the OP value reported by Cherpinski et al. (Cherpinski et al. 2018), i.e., 1.20×10^{-18} $m^3 \cdot m \cdot m^{-2} \cdot Pa^{-1} \cdot s^{-1}$, for an electrospun PHB film with a thickness of 142 μm. In this sense, it should be taken into account that OP is mainly a diffusivity-driven property since oxygen is a non-condensable small gas molecule and, hence, it is more sensitive to the material free volume,

defects, porosity, morphological differences, crystallinity, etc. This suggests that the here-obtained electrospun films presented a relatively good uniformity and low porosity. Resultant OP values are also slightly lower than these reported for conventional 100-μm PHB films prepared by Sanchez-Garcia et al. (Sanchez-Garcia, Gimenez, and Lagaron 2007) using compression molding, i.e., 2.24×10^{-19} $m^3 \cdot m \cdot m^{-2} \cdot Pa^{-1} \cdot s^{-1}$. In addition, in a more practical context for food packaging applications, the OP values of these electrospun PHBV films are in the range of PET films, i.e., 1.35×10^{-19} $m^3 \cdot m \cdot m^{-2} \cdot Pa^{-1} \cdot s^{-1}$ and two order of magnitude lower than those of low-density polyethylene (LDPE) films, i.e., 2.15×10^{-17} $m^3 \cdot m \cdot m^{-2} \cdot Pa^{-1} \cdot s^{-1}$ and only 1.5–2 higher than those of high-barrier ethylene–vinyl alcohol copolymer (EVOH) films, i.e., 7.7×10^{-20} $m^3 \cdot m \cdot m^{-2} \cdot Pa^{-1} \cdot s^{-1}$ (Lagarón 2011).

4. Conclusions

Circular economy and potentially low-cost PHBV-containing biomass, produced in a pilot plant scale from mixed microbial cultures fed with fruit pulp biowaste, was optimally subjected to two extraction process, namely NaClO and chloroform, and subsequently electrospun and post-processed by annealing to form continuous films with high transparency. The resultant PHBV films were seen to have differences in wettability, crystallinity, thermal stability, and mechanical and barrier properties depending on the route of purification applied. In view of the overall results, the biomass purified using chloroform resulted in lower crystallinity materials with higher toughness and barrier to moisture. Hence, this route seemed to be more favorable for the development of electrospun PHBV films as coatings or interlayers. The barrier data indicated that these new materials could potentially substitute their petroleum-based counterpart PET to applied in medium barrier food packaging applications.

5. References

Babu, R. P., K. O'Connor, and R. Seeram. 2013. "Current progress on bio-based polymers and their future trends." *Prog. Biomater.* 2 (8):1-16.

Busolo, M. A., S. Torres-Giner, and J. M. Laaron. 2009. "Enhancing the gas barrier properties of polylactic acid by means of electrospun ultrathin zein fibers." Annual Technical Conference - ANTEC, Conference Proceedings.

Castro-Mayorga, J. L., M. J. Fabra, and J. M. Lagaron. 2016. "Stabilized nanosilver based antimicrobial poly(3-hydroxybutyrate-co-3-hydroxyvalerate) nanocomposites of interest in active food packaging." *Innovative Food Science and Emerging Technologies* 33:524-533. doi: 10.1016/j.ifset.2015.10.019.

Castro-Mayorga, J. L., M. J. Fabra, A. M. Pourrahimi, R. T. Olsson, and J. M. Lagaron. 2017. "The impact of zinc oxide particle morphology as an antimicrobial and when incorporated in poly(3-hydroxybutyrate-co-3-hydroxyvalerate) films for food packaging and food contact surfaces applications." *Food and Bioproducts Processing* 101:32-44. doi: 10.1016/j.fbp.2016.10.007.

Castro Mayorga, J. L., M. J. Fabra Rovira, L. Cabedo Mas, G. Sánchez Moragas, and J. M. Lagarón Cabello. 2018. "Antimicrobial nanocomposites and electrospun coatings based on poly(3-hydroxybutyrate-co-3-hydroxyvalerate) and copper oxide nanoparticles for active packaging and coating applications." *Journal of Applied Polymer Science* 135 (2). doi: 10.1002/app.45673.

Chen, L. J., and M. Wang. 2002. "Production and evaluation of biodegradable composites based on PHB-PHV copolymer." *Biomaterials* 23 (13):2631-2639. doi: 10.1016/S0142-9612(01)00394-5.

Cherpinski, A., S. Torres-Giner, L. Cabedo, and J. M. Lagaron. 2017. "Post-processing optimization of electrospun submicron poly(3-hydroxybutyrate) fibers to obtain continuous films of interest in food packaging applications." *Food Additives and Contaminants - Part A Chemistry, Analysis, Control, Exposure and Risk Assessment* 34 (10):1817-1830. doi: 10.1080/19440049.2017.1355115.

Cherpinski, A., S. Torres-Giner, J. Vartiainen, M. S. Peresin, P. Lahtinen, and J. M. Lagaron. 2018. "Improving the water resistance of nanocellulose-based films with polyhydroxyalkanoates processed by the electrospinning coating technique." *Cellulose* 25 (2):1291-1307. doi: 10.1007/s10570-018-1648-z.

Colombo, B., F. Favini, B. Scaglia, T. P. Sciarria, G. D'Imporzano, M. Pognani, A. Alekseeva, G. Eisele, C. Cosentino, and F. Adani. 2017. "Enhanced polyhydroxyalkanoate (PHA) production from the organic fraction of municipal solid waste by using mixed microbial culture." *Biotechnology for Biofuels* 10 (1). doi: 10.1186/s13068-017-0888-8.

Colombo, B., T. P. Sciarria, M. Reis, B. Scaglia, and F. Adani. 2016. "Polyhydroxyalkanoates (PHAs) production from fermented cheese whey by using a mixed microbial culture." *Bioresource Technology* 218:692-699. doi: 10.1016/j.biortech.2016.07.024.

Cowie, J. M. G., S. Harris, and I. J. McEwen. 1998. "Physical aging in poly(vinyl acetate). 2. Relative rates of volume and enthalpy relaxation." *Macromolecules* 31 (8):2611-2615. doi: 10.1021/ma970287t.

Dias, J. M. L., P. C. Lemos, L. S. Serafim, C. Oliveira, M. Eiroa, M. G. E. Albuquerque, A. M. Ramos, R. Oliveira, and M. A. M. Reis. 2006. "Recent advances in polyhydroxyalkanoate production by mixed aerobic cultures: From the substrate to the final product." *Macromolecular Bioscience* 6 (11):885-906. doi: 10.1002/mabi.200600112.

Domingos, J. M. B., S. Puccio, G. A. Martinez, N. Amaral, M. A. M. Reis, S. Bandini, F. Fava, and L. Bertin. 2018. "Cheese whey integrated valorisation: Production, concentration and exploitation of carboxylic acids for the production of polyhydroxyalkanoates by a fed-batch culture." *Chemical Engineering Journal* 336:47-53. doi: 10.1016/j.cej.2017.11.024.

Doshi, J., and D. H. Reneker. 1995. "Electrospinning process and applications of electrospun fibers." *Journal of Electrostatics* 35 (2-3):151-160. doi: 10.1016/0304-3886(95)00041-8.

Echegoyen, Y., M. J. Fabra, J. L. Castro-Mayorga, A. Cherpinski, and J. M. Lagaron. 2017. "High throughput electro-hydrodynamic processing in food encapsulation and food packaging applications: Viewpoint." *Trends in Food Science and Technology* 60:71-79. doi: 10.1016/j.tifs.2016.10.019.

Fabra, M. J., A. López-Rubio, and J. M. Lagaron. 2016. "Use of the electrohydrodynamic process to develop active/bioactive bilayer films for food packaging applications." *Food Hydrocolloids* 55:11-18. doi: 10.1016/j.foodhyd.2015.10.026.

Fabra, M. J., G. Sánchez, A. López-Rubio, and J. M. Lagaron. 2014. "Microbiological and ageing performance of polyhydroxyalkanoate-based multilayer structures of interest in food packaging." *LWT - Food Science and Technology* 59 (2P1):760-767. doi: 10.1016/j.lwt.2014.07.021.

Fiorese, M. L., F. Freitas, J. Pais, A. M. Ramos, G. M. F. De Aragão, and M. A. M. Reis. 2009. "Recovery of polyhydroxybutyrate (PHB) from Cupriavidus necator biomass by solvent extraction with 1,2-propylene carbonate." *Engineering in Life Sciences* 9 (6):454-461. doi: 10.1002/elsc.200900034.

Hablot, E., P. Bordes, E. Pollet, and L. Avérous. 2008. "Thermal and thermo-mechanical degradation of poly(3-hydroxybutyrate)-based multiphase systems." *Polymer Degradation and Stability* 93 (2):413-421. doi: 10.1016/j.polymdegradstab.2007.11.018.

Hutchinson, J. M., S. Smith, B. Horne, and G. M. Gourlay. 1999. "Physical aging of polycarbonate: enthalpy relaxation, creep response, and yielding behavior." *Macromolecules* 32 (15):5046-5061. doi: 10.1021/ma981391t.

Jacquel, N., C. W. Lo, H. S. Wu, Y. H. Wei, and S. S. Wang. 2007. "Solubility of polyhydroxyalkanoates by experiment and thermodynamic correlations." *AIChE Journal* 53 (10):2704-2714. doi: 10.1002/aic.11274.

Kunasundari, B., and K. Sudesh. 2011. "Isolation and recovery of microbial polyhydroxyalkanoates." *Express Polymer Letters* 5 (7):620-634. doi: 10.3144/expresspolymlett.2011.60.

Kunioka, M., A. Tamaki, and Y. Doi. 1989. "Crystalline and Thermal Properties of Bacterial Copolyesters: Poly(3-hydroxybutyrate-co-3-hydroxyvalerate) and Poly(3-hydroxybutyrate-co-4-hydroxybutyrate)." *Macromolecules* 22 (2):694-697. doi: 10.1021/ma00192a031.

Lagarón, J. M. 2011. "Multifunctional and nanoreinforced polymers for food packaging." In *Multifunctional and Nanoreinforced Polymers for Food Packaging*, 1-28.

Lanham, A. B., A. R. Ricardo, M. G. E. Albuquerque, F. Pardelha, M. Carvalheira, M. Coma, J. Fradinho, G. Carvalho, A. Oehmen, and M. A. M. Reis. 2013. "Determination of the extraction kinetics for the quantification of polyhydroxyalkanoate monomers in mixed microbial systems." *Process Biochemistry* 48 (11):1626-1634. doi: 10.1016/j.procbio.2013.07.023.

Martínez-Abad, A., L. Cabedo, C. S. S. Oliveira, L. Hilliou, M. Reis, and J. M. Lagarón. 2016. "Characterization of polyhydroxyalkanoate blends incorporating unpurified biosustainably produced poly(3-hydroxybutyrate-co-3-hydroxyvalerate)." *Journal of Applied Polymer Science* 133 (2). doi: 10.1002/app.42633.

Martínez-Sanz, M., A. Lopez-Rubio, M. Villano, C. S. S. Oliveira, M. Majone, M. Reis, and J. M. Lagarón. 2016. "Production of bacterial nanobiocomposites of polyhydroxyalkanoates derived from waste and bacterial nanocellulose by the electrospinning enabling melt compounding method." *Journal of Applied Polymer Science* 133 (2). doi: 10.1002/app.42486.

Mottina, A. C., E. Ayres, R. L. Orefice, and J. J. D. Câmara. 2016. "What changes in poly(3-hydroxybutyrate) (PHB) when processed as electrospun nanofibers or thermo-compression molded film?" *Materials Research* 19 (1):57-66. doi: 10.1590/1980-5373-MR-2015-0280.

Mutlu, G., S. Calamak, K. Ulubayram, and E. Guven. 2018. "Curcumin-loaded electrospun PHBV nanofibers as potential wound-dressing material." *Journal of Drug Delivery Science and Technology* 43:185-193. doi: 10.1016/j.jddst.2017.09.017.

Rehm, B. H. A. 2003. "Polyester synthases: Natural catalysts for plastics." *Biochemical Journal* 376 (1):15-33. doi: 10.1042/BJ20031254.

Reis, K. C., J. Pereira, A. C. Smith, C. W. P. Carvalho, N. Wellner, and I. Yakimets. 2008. "Characterization of polyhydroxybutyrate-hydroxyvalerate (PHB-HV)/maize starch blend films." *Journal of Food Engineering* 89 (4):361-369. doi: 10.1016/j.jfoodeng.2008.04.022.

Samorì, C., F. Abbondanzi, P. Galletti, L. Giorgini, L. Mazzocchetti, C. Torri, and E. Tagliavini. 2015. "Extraction of polyhydroxyalkanoates from mixed microbial cultures: Impact on polymer quality and recovery." *Bioresource Technology* 189:195-202. doi: 10.1016/j.biortech.2015.03.062.

Sanchez-Garcia, M. D., E. Gimenez, and J. M. Lagaron. 2007. "Novel PET nanocomposites of interest in food packaging applications and comparative barrier performance with biopolyester nanocomposites." *Journal of Plastic Film and Sheeting* 23 (2):133-148. doi: 10.1177/8756087907083590.

Sanchez-Garcia, M. D., E. Gimenez, and J. M. Lagaron. 2008. "Morphology and barrier properties of solvent cast composites of thermoplastic biopolymers and purified cellulose fibers." *Carbohydrate Polymers* 71 (2):235-244. doi: 10.1016/j.carbpol.2007.05.041.

Savenkova, L., Z. Gercberga, V. Nikolaeva, A. Dzene, I. Bibers, and M. Kalnin. 2000. "Mechanical properties and biodegradation characteristics of PHB-based films." *Process Biochemistry* 35 (6):573-579. doi: 10.1016/S0032-9592(99)00107-7.

Serafim, L. S., P. C. Lemos, M. G. E. Albuquerque, and M. A. M. Reis. 2008. "Strategies for PHA production by mixed cultures and renewable waste materials." *Applied Microbiology and Biotechnology* 81 (4):615-628. doi: 10.1007/s00253-008-1757-y.

Serafim, L. S., P. C. Lemos, R. Oliveira, and M. A. M. Reis. 2004. "Optimization of polyhydroxybutyrate production by mixed cultures submitted to aerobic dynamic feeding conditions." *Biotechnology and Bioengineering* 87 (2):145-160. doi: 10.1002/bit.20085.

Sreekumar, S., P. Lemke, B. M. Moerschbacher, S. Torres-Giner, and J. M. Lagaron. 2017. "Preparation and optimization of submicron chitosan capsules by water-based electrospraying for food and bioactive packaging applications." *Food Additives and Contaminants - Part A Chemistry, Analysis, Control, Exposure and Risk Assessment* 34 (10):1795-1806. doi: 10.1080/19440049.2017.1347284.

Torres-Giner, S. 2011. "Electrospun nanofibers for food packaging applications." In *Multifunctional and Nanoreinforced Polymers for Food Packaging*, 108-125.

Torres-Giner, S., E. Gimenez, and J. M. Lagaron. 2008. "Characterization of the morphology and thermal properties of Zein Prolamine nanostructures obtained by electrospinning." *Food Hydrocolloids* 22 (4):601-614. doi: 10.1016/j.foodhyd.2007.02.005.

Torres-Giner, S., J. V. Gimeno-Alcañiz, M. J. Ocio, and J. M. Lagaron. 2011. "Optimization of electrospun polylactide-based ultrathin fibers for osteoconductive bone scaffolds." *Journal of Applied Polymer Science* 122 (2):914-925. doi: 10.1002/app.34208.

Torres-Giner, S., A. Martinez-Abad, and J. M. Lagaron. 2014. "Zein-based ultrathin fibers containing ceramic nanofillers obtained by electrospinning. II. Mechanical properties, gas barrier, and sustained release capacity of biocide thymol in multilayer polylactide films." *Journal of Applied Polymer Science* 131 (18):9270-9276. doi: 10.1002/app.40768.

Torres-Giner, S., N. Montanes, T. Boronat, L. Quiles-Carrillo, and R. Balart. 2016. "Melt grafting of sepiolite nanoclay onto poly(3-hydroxybutyrate-co-4-hydroxybutyrate) by reactive extrusion with multi-functional epoxy-based styrene-acrylic oligomer." *European Polymer Journal* 84:693-707. doi: 10.1016/j.eurpolymj.2016.09.057.

Torres-Giner, S., R. Pérez-Masiá, and J. M. Lagaron. 2016. "A review on electrospun polymer nanostructures as advanced bioactive platforms." *Polymer Engineering and Science* 56 (5):500-527. doi: 10.1002/pen.24274.

Torres-Giner, S., S. Wilkanowicz, B. Melendez-Rodriguez, and J. M. Lagaron. 2017. "Nanoencapsulation of Aloe vera in Synthetic and Naturally Occurring Polymers by Electrohydrodynamic Processing of Interest in Food Technology and Bioactive Packaging." *Journal of Agricultural and Food Chemistry* 65 (22):4439-4448. doi: 10.1021/acs.jafc.7b01393.

Villano, M., F. Valentino, A. Barbetta, L. Martino, M. Scandola, and M. Majone. 2014. "Polyhydroxyalkanoates production with mixed microbial cultures: From culture selection to polymer recovery in a high-rate continuous process." *New Biotechnology* 31 (4):289-296. doi: 10.1016/j.nbt.2013.08.001.

Zhang, K., M. Misra, and A. K. Mohanty. 2014. "Toughened sustainable green composites from poly(3-hydroxybutyrate-co-3-hydroxyvalerate) based ternary blends and miscanthus biofiber." *ACS Sustainable Chemistry and Engineering* 2 (10):2345-2354. doi: 10.1021/sc500353v.

Chapter II

Valorization of Municipal Biowaste into Electrospun Poly(3-hydroxybutyrate-co-3-hydroxyvalerate) Biopapers for Food Packaging Applications

Applied Bio Materials 2020, 3, 9, 6110-6123

Beatriz Meléndez-Rodríguez[1], Sergio Torres-Giner[1], Laura Lorini[2], Francesco Valentino[2], Chris Sammon[3], Luis Cabedo[4], and José María Lagarón[1]

[1] Novel Materials and Nanotechnology Group, Institute of Agrochemistry and Food Technology (IATA), Spanish Council for Scientific Research (CSIC), Paterna, Spain

[2] Department of Chemistry, "La Sapienza" University of Rome, Rome, Italy

[3] Materials and Engineering Research Institute, Sheffield Hallam University, Sheffield, United Kingdom

[4] Polymers and Advanced Materials Group (PIMA), Universitat Jaume I (UJI), Castellón, Spain

Abstract

The present study reports on the production and characterization of a new biopackaging material made of poly(3-hydroxybutyrate-*co*-3-hydroxyvalerate) (PHBV) derived from municipal biowaste (MBW) and produced by the mixed bacterial culture technology. After purification and extraction, the MBW-derived PHBV was processed by electrospinning to yield defect-free ultrathin fibers, which were thermally post-treated. Annealing at 130 °C, well below the biopolymer's melting temperature (T_m), successfully yielded a continuous film resulting from coalescence of the electrospun fibrillar morphology, the so-called biopaper, exhibiting enhanced optical and color properties compared to traditional melt compounding routes. The crystallinity and crystalline morphology were comprehensively studied as a function of temperature by attenuated total reflectance-Fourier transform infrared (ATR-FTIR) spectroscopy and combined time-resolved synchrotron small- and wide-angle X-ray scattering (SAXS and WAXS) experiments, which clearly indicated that the molecular order within the copolyester was improved up to a maximum at 130 °C, and then it decreased at the biopolymer's T_m. It was hypothesized that by annealing at the temperature at which the thermally induced molecular order is maximized, the fibers generated sufficient mobility to align alongside, hence reducing surface energy and porosity. The data suggest that this material shows a good balance between enhanced mechanical and improved barrier properties to vapors and gases in comparison to traditional paper and other currently used petroleum-derived polymers, thus presenting significant potential to be part of innovative food biopackaging designs for the protection and preservation of foods in a circular bioeconomy scenario.

Keywords: PHBV; electrospinning; biopapers; waste valorization; food packaging; circular bioeconomy

1. Introduction

The potential of polyhydroxyalkanoates (PHAs) as biobased and biodegradable replacements for conventional bulk commodity plastic packaging while promoting sustainable development has long been recognized (Koller 2014). These biopolymers are mainly produced by the action of bacteria, both Gram-positive (G+) and Gram-negative (G−) (Rehm 2003), during the fermentation of sugar or lipids under famine conditions (Saharan, Grewal, and Kumar 2014). However, there is also an increasing number of archaea that are being used to produce PHAs (Koller et al. 2017). The most studied PHA is poly(3-hydroxybutyrate) (PHB). The homopolyester shows thermal and mechanical properties similar to those of petrochemical polyolefins such as low-density polyethylene (LDPE) and polypropylene (PP) (Kourmentza and Kornaros 2016, Torres-Giner, Montanes, et al. 2018). However, its low ductility and toughness as well as its narrow processing window limit the use of PHB for packaging. For this reason, poly(3-hydroxybutyrate-*co*-3-hydroxyvalerate) (PHBV), that is, its copolymers with 3-hydroxyvalerate (3HV), shows reduced crystallinity and decreased stiffness, having also a lower melting temperature (T_m), which makes it a more interesting candidate in the areas of biodegradable packaging (Sängerlaub et al. 2019).

Current manufacturing processes of PHAs by bacterial fermentation involve fermentation, isolation, and purification from the fermentation broth (Acevedo et al. 2018, Fabra, Lopez-Rubio, and Lagaron 2014). Much effort and improvements are currently being made to reduce fermentation and downstream processing costs (Laycock et al. 2013), which are on the order of up to 15 times higher than for conventional polyolefins (Choi and Lee 1997). In this regard, the synthesis of PHAs produced by mixed microbial cultures (MMCs) using biowaste as feedstock, such as industrial waste and food processing by-products, can make its industrial production more competitive (Reis et al. 2011). In fact, pure culture systems based on refined feedstock and sterile cultivation conditions contribute the most to the PHA production cost (Fernández-Dacosta et al. 2015). Furthermore, the valorization of by-products and wastes is environmentally attractive in a more sustainable circular bioeconomy scenario (Gurieff and Lant 2007). In this regard, different organic wastes have been used as substrates to produce PHAs, for instance molasses (Albuquerque, Torres, and Reis 2010), olive and palm oil mill effluent (Dionisi et al. 2005, Hassan et al. 1997), fermented fruit waste (Melendez-Rodriguez et al. 2018), and cheese whey (CW) (Colombo et al. 2016).

Municipal waste, wastewaters, and the organic fraction of municipal solid waste (OFMSW) also show great potential as the feeding solution for PHA production. However, to date, few studies have shown the use of OFMSW for the production of these biopolymers (Morgan-Sagastume et al. 2015). Along with the production of biogas, the most common processes applied for biological sludge disposal, to stabilize organic matter and valorize different substrates into added-value marketable products, are composting and anaerobic digestion (Mata-Alvarez et al. 2014). Other research works have demonstrated that the use of OFMSW during the accumulation step led to improved PHA productivity (Korkakaki et al. 2016). Another study demonstrated that the PHA accumulation fed with fermentation volatile fatty acids (VFAs) that were obtained from food wastes and excess sludge was higher than the one produced with analytically pure VFAs (Zhang, Wu, and Chen 2014). PHA production was also reported utilizing MMC indigenous to an activated sludge process on carbon present in municipal wastewaters (Coats et al. 2007). Therefore, the integration of the so-called MMC–PHA production in this kind of

infrastructure using activated sludge as an inoculum can make this technology more economically and environmentally sustainable.

Electrospinning is an innovative processing technology that allows the formation of continuous polymer fibers, with diameters ranging from several nanometers to a few microns, by virtue of high voltage (Doshi and Reneker 1995). Both the solution properties, such as surface tension, viscosity, and conductivity, and the processing conditions, such as flow rate, voltage, and injector-to-collector distance, are known to impact size, size distribution, and morphology of the resultant fiber mats. The formation of fiber-based continuous films of reduced porosity, called biopapers, can be achieved by annealing the electrospun mats and the resultant coalescence and rearrangement of the nanofibers in the material to reduce surface tension (Cherpinski et al. 2017, Melendez-Rodriguez et al. 2018). The term biopaper refers to electrospun fiber-based material concepts made of biopolymers that, unlike conventional paper made of cellulose that involves severe chemical processes and contains petrochemical additives and/or hydrophobizing coatings, are fully functional in terms of physicochemical properties, biobased, and biodegradable. The term biopaper has also been coined in connection to biomaterials that serve as flat scaffolds and contain electrospun biopolymers, in which cells are printed onto each sheet in a two-dimensional (2D) pattern, and then the biopapers are stacked to generate a three-dimensional (3D) structure (Pal, Banthia, and Majumdar 2009). Biopapers make the use of electrospun PHA a very interesting alternative in the packaging industry since continuous and handable films can be obtained with minimal thermal exposure that can exhibit improved optical and mechanical strength as well as flexibility with excellent water resistance and gas and vapor barrier properties (Cherpinski, Torres-Giner, Cabedo, et al. 2018). Moreover, electrospinning allows for the incorporation of functional additives into the biopolymers and, thus, the formation of coatings or interlayers of interest in active and bioactive packaging (Alp-Erbay et al. 2019, Cherpinski, Gozutok, et al. 2018, Hu et al. 2018, Lasprilla-Botero et al. 2018, Quiles-Carrillo et al. 2019a, Spagnol et al. 2018).

The objective of this study was to valorize, for the first time, typical municipal biowaste streams into biopapers of PHBV produced by thermal post-treatment of electrospun mats and then asses the resulting morphology, crystallinity, and crystalline morphology as a function of temperature and their final physicochemical properties relevant for food biopackaging applications.

2. Experimental Section

2.1. Materials

The municipal biowaste (MBW) PHBV was produced at the pilot platform in the Treviso Municipal Wastewater Treatment Plant (Treviso, Italy), from a feedstock composed of a mixture of liquid slurry resulting from squeezing OFMSW and biological sludge from the treatment of urban wastewater. The commercial PHBV used for comparison was ENMAT Y1000P, which was produced by Tianan Biologic Materials (Ningbo, China) and supplied by Ocenic Resins S.L. (Valencia, Spain). According to the manufacturer, the 3HV fraction in the commercial copolyester is 2–3 mol %.

2,2,2-Trifluoroethanol (TFE), ≥ 99 % purity, 1-butanol, reagent grade with 99.5 % purity, methanol, sulfuric acid (H_2SO_4), benzoic acid, and d-limonene, 98 % purity, were all purchased from Sigma-Aldrich S.A. (Madrid, Spain). Chloroform, stabilized with ethanol and 99.8 % purity, was obtained from Panreac S.A. (Barcelona, Spain).

2.2. Production

The PHBV production consisted of three process steps using the fermented mixture of OFMSW and biological sludge. In the first stage, the precursors for PHA biosynthesis, that is, VFAs, were produced in an anaerobic fermentation reactor of 380 L. Then, biomass cultivation was carried out in a second aerobic reactor of 100 L, referred to as the sequencing batch reactor (SBR). Finally, for achieving PHA accumulation within the cellular cytoplasm, a third fed-batch aerobic reactor of 70–90 L was used. At the end of the accumulation step, the PHA concentration reached up to a value of 2.0–2.5 g/L, corresponding to a maximum PHA content of 50–60 % of cell dry weight, that is, the mass ratio of PHA vs volatile solids. This PHA-rich raw biomass was collected following a protocol addressed to the long-term PHA conservation inside the cells before the extraction/purification steps. In this protocol, once each accumulation was completed, the PHA-rich biomass was left to settle under gravity and, thereafter, the thickened slurry was centrifuged for 15 min at 4500 rpm in a Heraeus Megafuge 40 Centrifuge with a Swinging Bucket Rotor (maximum radius: 195 mm; minimum radius: 83 mm) from Thermo Fisher Scientific (Waltham, MA). Finally, the wet pellet was pretreated for 15 min at 145 °C and then dried at 60 °C overnight. A more detailed description of the production process can be found in the research study of Valentino et al. (Valentino et al. 2019).

2.3. Extraction and Purification

The unpurified PHBV was extracted using the chloroform-based extraction method reported previously (Fiorese et al. 2009). This purification method involves a solvent, which requires to be evaporated. While at the lab scale this possesses no relevant issues, evaporation methods of organic solvents are hardly applicable at an industrial scale, specially under sustainable manufacturing practices. In this regard, the consumption of large amounts of organic solvents can be avoided by “antisolvents”, that is, solvents in which the respective PHA is nonsoluble and precipitates (Madkour et al. 2013). To do this, the PHA solution must be mixed with a large volume of the nonsolvent, yielding a mixture of at least two different solvents in which PHA precipitates (Griffin 1994). Thereafter, the precipitated PHA can be separated from the solvent mixture by centrifugation or filtration and, at the large scale, the organic solvent could be recovered by separation techniques and reused for subsequent extraction processes. Furthermore, if water is used as the antisolvent, the sustainability of the process is improved (Li et al. 2015).

In this case, the MBW-derived PHBV was dissolved at 5 wt % in chloroform and the mixture was stirred at 50 °C for 24 h to degrade the non-PHA cellular material. Next, the solution was transferred to centrifugation tubes in which distilled water was added at 50 wt %. After manual shaking of the tubes, these were centrifuged for 5 min at 4000 rpm in an Avanti J-26S XP Centrifuge with a JLA-16.250 Rotor (maximum radius: 134 mm; average radius: 90 mm; minimum radius: 46 mm) from Beckman Coulter, Inc. (Brea, CA). Finally, the PHBV suspension

was recovered as sediment in the tubes with a pipette and transferred to beakers, leaving them in the extractor hood until the solvent was completely evaporated.

2.4. 3HV Content Determination

A powder sample of 3.5 mg was suspended in 2 ml of acidified methanol solution (3 % v/v H_2SO_4), containing benzoic acid at 0.005 % w/v as the internal standard, and 1 ml of chloroform in a screw-capped tube. Acid-catalyzed methanolysis occurred, and the 3-hydroxyacyl methyl esters of PHA were quantified by gas chromatography in a GC-FID PerkinElmer 8410 from PerkinElmer, Inc. (Waltham, MA). The relative abundance of 3-hydroxybutyrate (3HB) and 3HV monomers was determined using as a reference standard of the commercial PHBV copolymer with a known 3HV content of 5 wt % (Sigma-Aldrich S.r.l., Milan, Italy). The resultant molar fraction of 3HV in the copolyester was approximately 10 wt %.

2.5. Characterization of Solutions

The powder resulting from the purification process was dissolved at 15 wt % in a mixture of chloroform and butanol 75:25 (w/w) under magnetic stirring for 24 h at 50 °C. A solution of commercial PHBV was also prepared by dissolving the biopolymer at 10 wt % in neat TFE. Prior to electrospinning, the viscosity, conductivity, and surface tension of the PHBV solutions were characterized in the same conditions as reported earlier (Torres-Giner et al. 2017). To this end, a rotational viscometer Visco BasicPlus L from Fungilab S.A. (San Feliu de Llobregat, Spain) equipped with a low-viscosity adapter (LCP), a conductivity meter XS Con6 from Lab-box (Barcelona, Spain), and an EasyDyne K20 tensiometer from Krüss GmbH (Hamburg, Germany) were respectively used. All of the measurements were taken at room temperature in triplicate.

2.6. Electrospinning Process

The PHBV solutions were electrospun using a Fluidnatek LE-10 lab equipment manufactured by Bioinicia S.L. (Valencia, Spain), which is equipped with a horizontally scanning single needle injector. The conditions for processing the MBW-derived PHBV were optimal at a flow rate of 6 ml/h, 22 kV of voltage, and 25 cm of needle-to-collector distance. In the case of the commercial PHBV, electrospinning was carried out using previously optimized conditions, that is, 6 ml/h, 20 kV, and 15 cm (Melendez-Rodriguez, Figueroa-Lopez, et al. 2019). All of the PHBV solutions were electrospun for 1.3 h at 25 °C and 40 % relative humidity (RH), and the manufactured mats were stored in a desiccator at room temperature and at 0 % RH in the dark for, at least, a week prior to being annealed.

2.7. Preparation of Biopapers

The resultant fiber mats of PHBV were thermally post-treated in a 4122-model press from Carver, Inc. (Wabash, IN). Annealing was performed across the temperature range from 80 to 150 °C, for 5 s and without applying pressure. The electrospun mats of commercial PHBV were annealed at

155 °C, also for 5 s, also without applying pressure (Melendez-Rodriguez, Figueroa-Lopez, et al. 2019). An average thickness of approximately 30 μm was attained for all of the thermally postprocessed samples. The samples were stored in a desiccator at 0 % RH for 2 weeks before subsequent characterization.

2.8. Characterization

2.8.1. Microscopy

The morphology of the samples was determined by scanning electron microscopy (SEM) using an S-4800 model from Hitachi (Tokyo, Japan) and applying an accelerating voltage of 10 kV. For cross-section observation, the materials were cryo-fractured by immersion in liquid nitrogen. Prior to observation, the samples were fixed to beveled holders by conductive double-sided adhesive tape and a mixture of gold–palladium was sputtered on their surface under vacuum. Dimensions were estimated using a minimum of 20 SEM micrographs in their original magnification with Aperture software from Apple (Cupertino, CA).

2.8.2. Transparency

The light transmission of biopapers was determined using 50 mm × 30 mm specimens in an ultraviolet–visible (UV–vis) spectrophotometer VIS3000 (Dinko Instruments, Barcelona, Spain). The absorption of light was quantified at wavelengths in the 200–700 nm range. Equations 1 (Shiku et al. 2004) and 2 (Kanatt et al. 2012) were followed to determine the values of transparency (T) and opacity (O), respectively:

$$T = \frac{A_{600}}{L} \quad (1)$$

$$O = A_{500} \times L \quad (2)$$

in which A_{600} and A_{500} correspond to the absorbance values at 600 and 500 nm, respectively, whereas L represents the film thickness (mm).

2.8.3. Color

The color of the biopapers was estimated using a chroma meter CR-400 (Konica Minolta, Tokyo, Japan). Equation 3 (Arfat et al. 2017) was used to determine the color difference (ΔE^*) between the test sample and the control sample of commercial PHBV:

$$\Delta E^* = [(\Delta L^*)^2 + (\Delta a^*)^2 + (\Delta b^*)^2]^{0.5} \quad (3)$$

in which ΔL^* represents the difference in terms of lightness from black to white, whereas Δa^* and Δb^* correspond to the differences in color, from green to red and blue to yellow, respectively. Color changes were assessed using a previous grading (Agüero et al. 2019).

2.8.4. Thermal Analysis

The main thermal parameters of the samples were determined by differential scanning calorimetry (DSC) with a DSC-7 tool from PerkinElmer, Inc. (Waltham, MA), equipped with the Intracooler 2 cooling accessory. Thermal runs consisted of a first heating step from −30 to 180 °C, a cooling step to −30 °C, and a second heating step to 200 °C. The runs were set to 10 °C/min using a sample amount of ∼3 mg and aluminum pans. The thermograms were corrected with an empty pan, and the equipment was calibrated with indium.

Thermogravimetric analysis (TGA) was carried out in a TG-STDA thermobalance TGA/STDA851e/LF/1600 from Mettler-Toledo, LLC (Columbus, OH). The heating program consisted of a ramp from 50 to 900 °C at 10 °C/min under a 50 ml/min nitrogen flow rate using a sample amount of around 15 mg. All of the thermal tests were carried out in triplicate.

2.8.5. ATR-FTIR Spectroscopy

Variable-temperature Fourier transform infrared (FTIR) spectroscopy was performed using a Nicolet Nexus FTIR instrument (Thermo Fisher Scientific, Wilmington, DE) coupled to a variable-temperature single reflection diamond attenuated total reflectance (ATR) sampling accessory (Specac Ltd., Orpington, U.K.). Spectra were collected by averaging 64 scans at 4 cm^{-1} resolution using the blank ATR crystal at the same temperature as the background. The intensity of the infrared spectrum depends on a number of factors including path length and the molar extinction coefficient of the analyte. When using the ATR geometry, the path length can be considered to be constant as long as the contact between the sample and the ATR crystal is consistent. To ensure that any peak intensity changes in the data represented changes in the morphology of the samples, the samples were clamped directly onto the ATR crystal using a calibrated torque wrench (Specac Ltd., Orpington, U.K.) set at 80 cNm, which applies a load of ∼350 N via the sample accessory anvil. Reproducibility values of the sample contact and the resulting spectra intensity were validated prior to conducting the variable-temperature infrared measurements. Spectra were collected at 10 °C intervals from 30 to 100 °C and, thereafter, at 5 °C intervals up to 190 °C. To ensure validity of the selected temperature, spectra were not collected until the digital reading on the temperature controller had fully stabilized.

2.8.6. Time-Resolved Synchrotron Experiments

Simultaneous small-angle X-ray scattering (SAXS) and wide-angle X-ray scattering (WAXS) experiments as a function of temperature were carried out on beamline BL11—noncrystalline diffraction (NCD) (WAXS/SAXS station) located at the ALBA synchrotron facilities (Barcelona, Spain). The SAXS and WAXS q-axis calibrations were obtained by measuring silver behenate ($AgC_{22}H_{43}O_2$) and chromium(III) oxide (Cr_2O_3) standards, respectively. Scattering patterns were collected using the combination of two detectors, that is, a photon counting detector Pilatus 1M detector from Dectris AG (Baden, Switzerland) and a CDD WAXS LX255-HS detector from Rayonix, L.L.C. (Evanston, IL), operating simultaneously in SAXS and WAXS positions, respectively. The wavelength of the incident wave (λ) was 1 Å. The distances between the sample and the SAXS and WAXS detectors were set at 6.6328 and 0.120762 m, respectively, allowing a q-range between 0.025 and 0.22 $Å^{-1}$ for SAXS and a q-range between 0.5 and 8.4 $Å^{-1}$ for

WAXS. The beamline delivered a photon flux onto the sample of >1.5×10^{12} ph/s at 12.4 keV for a beam current of 150 mA with a bandpass ($\Delta E/E$) of 2.7×10^{-4} at 10.0 keV and a beam size at sample position of 349 μm × 379 μm. For the in situ thermal experiments, electrospun fiber mats, with a thickness of 100 μm, were placed on a "film type" THMS600 hot stage from Linkam Scientific Instruments Ltd (Epstom, U.K.). To analyze the evolution of the sample when exposed to thermal treatments, the samples were subjected to isotherms at 100 and 130 °C for up to 2 min and to thermal ramps from 0 to 180 °C at 10 °C/min.

2.8.7. Tensile Tests

The mechanical properties of the biopapers were determined in tensile conditions according to ASTM D638 using an Instron 4400 machine from Instron (Norwood, MA). Tensile tests were carried out in sextuple using 115 mm × 16 mm stamped dog-bone specimens at a cross-head speed of 10 mm/min at room temperature. The equipment was set with a load cell of 1 kN, and the specimens were preconditioned for 24 h prior to testing.

2.8.8. Permeability

The water vapor permeability (WVP) and d-limonene permeability (LP) of the biopapers were determined following the standardized gravimetric method ASTM E96-95. To do this, Payne permeability cups of 3.5 cm from Elcometer Sprl (Hermallesous-Argenteau, Belgium) were used. Both tests were performed at 25 °C in triplicate, and further details can be found elsewhere (Melendez-Rodriguez, Torres-Giner, et al. 2019).

The oxygen permeability was determined in duplicate at 60 % RH and 25 °C using an oxygen permeation analyzer M8001 (Systech Illinois, Thame, U.K.) with temperature and relative humidity control. The tested area was 5 cm^2.

2.8.9. Statistical Analysis

Analysis of variance (ANOVA) was performed using the software packaging STATGRAPHICS Centurion XVI v 16.1.03 from StatPoint Technologies, Inc. (Warrenton, VA). To evaluate the differences among the samples, Fisher's least significant difference (LSD) was set at the 95 % confidence level ($p < 0.05$).

3. Results and Discussion

3.1. Solution Properties and Morphology

The properties of the MBW-derived PHBV solution were measured and are reported in **Table 1** to evaluate its electrospinnability. One can observe that the MBW-derived PHBV solution presented a viscosity of 229.8 cP, which was significantly lower than that attained for the PHBV

commercial benchmark (~689 cP), even though the concentration of the commercial biopolymer in the solution was lower. This can be related to the different solvents used for the solution as well as the higher 3HV content and potentially lower molecular weight (M_W) of the MBW-derived PHBV. In this regard, not only can the feedstock used to feed the microorganisms affect the M_W of the resultant PHA but also the chemical digestion methods that were applied to disrupt the cell wall and then release PHAs (Kunasundari and Sudesh 2011). In any case, the attained value of viscosity is appropriate for electrospinning since it was similar to that reported for solutions containing 2 wt % PHBV obtained from fruit pulp biowaste purified using chloroform, that is, 296.8 cP (Melendez-Rodriguez et al. 2018). In the case of surface tension and conductivity, the MBW-derived PHBV solution presented values of 26.2 mN/m and 0.14 μS/cm, respectively. The surface tension was very similar for both PHBV solutions and also comparable to other PHAs derived from biowaste, which were reported in the 20.5–21.9 mN/m range, but the conductivity was lower, that is, 1.3–3.7 μS/cm range (Melendez-Rodriguez et al. 2018). The latter value can be ascribed to the low amount of remaining conductive impurities, and it represents a positive indicator for electrospinning since polymer solutions with high conductivities usually show lower processability (Torres-Giner et al. 2017).

Table 1. Properties of commercial and municipal biowaste (MBW)-derived poly(3-hydroxybutyrate-*co*-3-hydroxyvalerate) (PHBV) solutions.

Sample	Concentration (wt %)	Viscosity (cP)	Surface tension (mN/m)	Conductivity (μS/cm)
Commercial PHBV	10	688.8 ± 2.3[a]	21.9 ± 0.1[a]	3.74 ± 0.02[a]
MBW-derived PHBV	15	229.8 ± 1.5[a]	26.2 ± 0.3[a]	0.14 ± 0.01[a]

[a] Different letters in the same column mean a significant difference among the samples ($p < 0.05$).

Figure 1 shows the mats obtained after the electrospinning process of the MBW-derived PHBV solutions, before and after annealing, both the cryo-fracture surfaces and the top views. One can observe in the figure at room temperature, which corresponds to the electrospun mat without thermal post-treatment, that electrospinning yielded a mat composed of nonwoven ultrathin fibers. For instance, the electrospinning of the PHBV solution yielded homogenous and bead-free fibers having a mean diameter of 1.12 ± 0.12 μm. It can also be noticed that the application of annealing temperatures of 80, 110, and 125 °C resulted in a rearrangement of the fine fibers, but the material still maintained a high porosity level. At 130 °C, interestingly, the electrospun PHBV mat turned into a continuous film with a very low porosity due to the fiber coalescence process. This phenomenon is due to the compact packing rearrangement of the electrospun fibers to reduce their surface energy at temperatures below the biopolymer's T_m (Cherpinski et al. 2017). **Figure 2** displays, as an example, a zoomed top view of the biopaper annealed at 130 °C, which proved that the material is constituted by aligned side-by-side fibers of approximately 1.2–2 μm with minimal porosity.

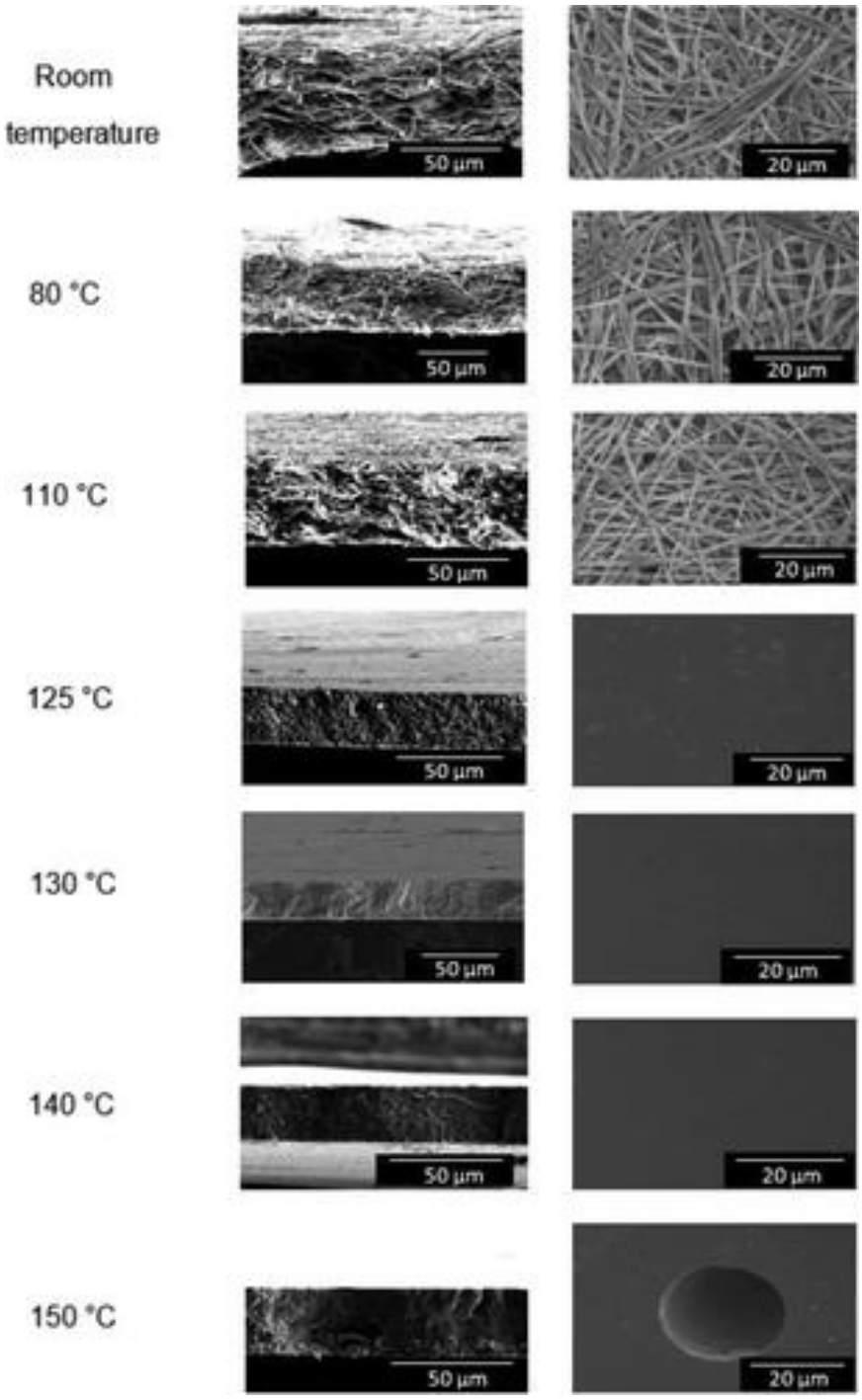

Figure 1. SEM images of the cross section (left) and top view (right) of the electrospun MBW-derived PHBV mats without thermal post-treatment and annealed at 80, 110, 125, 130, 140, and 150 °C for 5 s. Scale markers are of 50 and 20 µm, respectively.

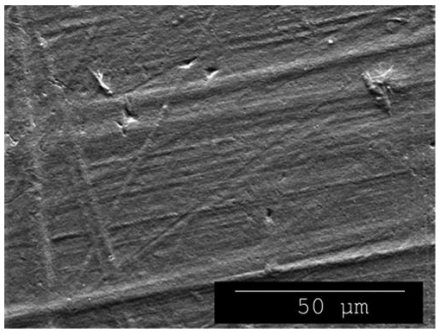

Figure 2. SEM image of the top view of the electrospun MBW-derived PHBV mat annealed at 130 °C for 5 s. Scale marker is of 50 µm.

Figure 1 also shows that at higher temperatures, that is, at 150 °C, some large voided areas were formed, which could be the result of thermal deterioration and release of volatile components. A similar film morphology evolution was recently observed for electrospun fiber mats of fruit-residue-derived PHBV (Melendez-Rodriguez et al. 2018). Based on the morphology observations, the electrospun mats postprocessed at 130 °C were selected for further characterization.

3.2. Optical Properties

Figure 3 displays the background transparency pictures of resulting annealed electrospun mats of MBW-derived and commercial PHBV. It can be observed that both biopapers show certain transparency and lack of color, suggesting that the PHBVs presented low crystallinity and were not thermally abused, respectively. Electrospinning is known to result in low-crystallinity materials due to the very rapid solidification process of the polymer jet. In the case of the MBW-derived PHBV, the samples showed even higher transparency associated with the higher 3HV content, which is known to yield materials with lower melting point, crystallinity, and density.

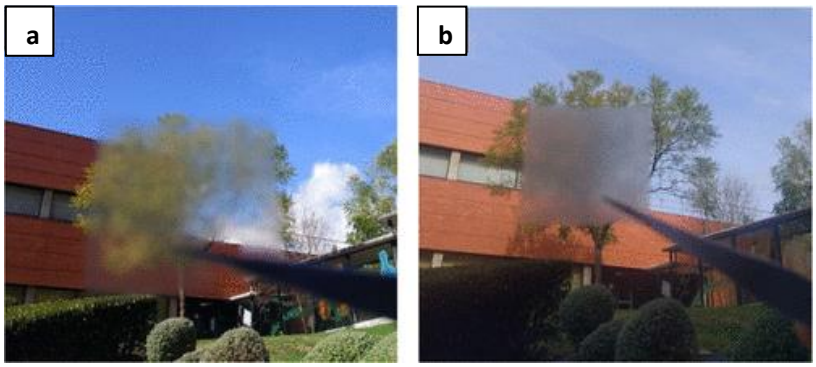

Figure 3. Background transparency pictures of the electrospun PHBV biopapers: (a) derived from MBW and (b) commercial grade.

To quantify the color properties of the electrospun biopaper of PHBV, the lightness and color parameters were determined by the values of L^* and a^* b^* coordinates, respectively. One can observe in **Table 2** that the MBW-derived PHBV biopaper showed a value of L^* of 89.39, while the values of a^* and b^* were −0.2 and 2.13, indicating that it was relatively luminous and only slightly yellow. These values were very similar to those obtained for the electrospun films of PHBV derived from fruit pulp biowastes, though the present samples showed slightly higher values of a^* and b^* (Figueroa-Lopez et al. 2019). Interestingly, the electrospun biopapers were brighter than PHB/PHBV blend films obtained by melt processing routes, which showed a value of L^* of 86.40 (Melendez-Rodriguez, Torres-Giner, et al. 2019). In terms of color difference, the electrospun biopaper made of MBW-derived PHBV showed a color difference of 1.03, which is nearly unnoticeable ($\Delta E^* < 1$) and it can be noticed only by an experienced observer ($\Delta E^* \geq 1$ and < 2). Regarding transparency and opacity, one can also observe that the MBW-derived PHBV biopaper presented a higher value of T and lower value of O than the biopaper made of commercial PHBV, which means that the biopaper obtained from MBW was more transparent and developed a less grayish color than the commercial one. This optical property can be regarded as an advantage for food packaging because transparency is associated with conventional plastics used in packaging and is better accepted by users. In this regard, Jung et al. (Jung et al. 2020) induced a color change from yellowish to bluish in PHB films to make them more commercially attractive.

Table 2. Optical properties of the electrospun PHBV biopapers.

Film	a^*	b^*	L^*	ΔE^*	T	O
Commercial PHBV	0.35 ± 0.03[a]	1.29 ± 0.01[a]	89.14 ± 0.02[a]	-	9.20 ± 0.08[a]	0.07 ± 0.02[a]
MBW-derived PHBV	–0.20 ± 0.02[a]	2.13 ± 0.03[a]	89.39 ± 0.03[a]	1.03 ± 0.02	2.56 ± 0.02[a]	0.010 ± 0.001[a]

[a] Different letters in the same column mean significant difference among the samples ($p < 0.05$).

3.3. Thermal Properties

Thermal characterization was measured on the selected MBW material annealed at 130 °C, since the full physicochemical characterization of the electrospun commercial PHBV material was published elsewhere (Melendez-Rodriguez, Figueroa-Lopez, et al. 2019). The DSC data for the other samples processed at the different temperatures are gathered in **Table S1**, which is included in the Supporting Information. The DSC curves, corresponding to the heating and cooling steps, of the MBW-derived PHBV biopaper, are presented in **Figure 4**. **Table 3** summarizes the main thermal values obtained from the DSC curves for the MBW-derived PHBV, and the values of the commercial PHBV were also included for comparison purposes. During the first heating, the sample showed a broad single melting endotherm at 154 °C with a shoulder at lower temperatures and with ΔH_m of nearly 58 J/g. In the cooling step, one can notice that the biopolymer crystallized from the melt in a broad range, showing a dominant peak corresponding to the crystallization temperature from the melt (T_c) at 60.3 °C and an enthalpy of crystallization (ΔH_c) of 38.1 J/g. Moreover, during the second heating step, the MBW-derived PHBV material further cold-crystallized and it showed a cold crystallization temperature (T_{cc}) at approximately 45 °C with an enthalpy of cold crystallization (ΔH_{cc}) of 9.8 J/g. The glass-transition temperature (T_g) of the

biopolymer was noticeable at −5 °C during the second heating. Moreover, the sample showed two endothermic melting peaks. The first one was observed at 132.4 °C, followed by a more intense second one at 149.4 °C, with a total enthalpy of melting (ΔH_m) of 60.5 J/g. A similar thermal behavior was observed previously for PHBV obtained from pulp fruit biowaste having a higher 3HV content, that is, approximately 20 mol % (Melendez-Rodriguez et al. 2018). Cold crystallization was unnoticeable in the complex melting endotherms, but this process cannot be ruled out. The presence of multiple melting peaks in a relatively low thermal range is linked to a dynamic crystal reorganization upon heating, where imperfect crystals develop thicker lamellar thicknesses during heating and thereafter melt at higher temperatures. This phenomenon, supported here by the below synchrotron and ATR-FTIR experiments, was previously observed and discussed by, among others, Zhang et al. (Zhang, Misra, and Mohanty 2014) in PHA copolyesters. The commercial biopaper, however, showed a single melting endotherm in the 170–172 °C range, both in the first heating and in the second one, with a T_c value at approximately 117 °C (Melendez-Rodriguez, Figueroa-Lopez, et al. 2019). These differences among both PHBV samples can be mainly ascribed to the different 3HV contents. In comparison with other PHBV films with different 3HV contents, Sanchez-Garcia et al. (Sanchez-Garcia, Gimenez, and Lagaron 2008) showed that copolyesters with 12 mol % 3HV exhibited double melting with peaks centered at approximately 145 and 157 °C. Elsewhere, Castro-Mayorga et al. (Castro Mayorga et al. 2018) showed that PHBV blends with contents of 3 and 18 mol % 3HVs also presented double-melting peaks with T_m values of 169.6 and 173.2 °C. In the case of the homopolyester, PHB showed only one melting peak at 169.4 °C (Cherpinski et al. 2017). Due to their higher 3HV contents, the T_m values of the MBW-derived PHBV were lower than the PHB ones and slightly higher than those obtained for PHBV derived from fruit pulp biowaste with 20 mol % 3HV, with a single melting peak at 139 °C (Melendez-Rodriguez et al. 2018). In the above works by the authors, the inherently complex thermal behavior generated during the dynamic DSC runs is highlighted as well as the difficulties in establishing reliable crystallinity data. It should be noted that many of these copolymers recently synthesized have never been studied in sufficient detail to determine, for instance, the enthalpy of melting for an infinity crystal (ΔH_m^0), required for crystallinity determination.

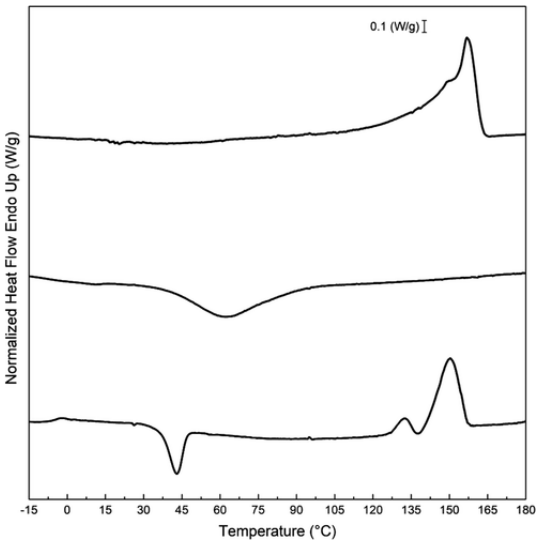

Figure 4. DSC curves taken, from top to bottom, during the first heating, cooling, and second heating of the electrospun biopaper of PHBV derived from MBW.

Table 3. Thermal properties of the electrospun PHBV biopapers obtained by DSC and TGA.

Biopaper	DSC									TGA			
	First heating		Cooling		Second heating								
	T_m (°C)	ΔH_m (J/g)	T_c (°C)	ΔH_c (J/g)	T_g (°C)	T_{cc} (°C)	ΔH_{cc} (J/g)	T_m (°C)	ΔH_m (J/g)	$T_{5\%}$ (°C)	T_{deg} (°C)	Mass loss at T_{deg} (%)	Residual mass (%)
Commercial PHBV*	171.5 ± 0.4[a]	75.2 ± 0.6[a]	116.8 ± 0.5[a]	85.6 ± 0.2[a]	2.6 ± 0.4[a]	-	-	170.4 ± 0.2[a]	83.2 ± 3.0[a]	259.9 ± 1.2[a]	277.3 ± 0.6[a]	62.0 ± 0.8[a]	2.0 ± 0.2[a]
MBW-derived PHBV	153.9 ± 0.1[b]	57.4 ± 5.4[b]	60.3 ± 1.9[b]	38.1 ± 5.5[b]	–5.0 ± 1.2[b]	44.7 ± 0.3[b]	9.8 ± 4.1[b]	132.4 ± 0.7[b] // 149.4 ± 0.3[c]	60.5 ± 0.6[b]	204.7 ± 2.0[b]	239.9 ± 0.8[b]	94.8 ± 1.7[b]	0.2 ± 0.1[b]

* Data reported in a previous study (Melendez-Rodriguez, Figueroa-Lopez, et al. 2019).

[a-c] Different letters in the same column mean significant difference among the samples ($p < 0.05$).

In **Table 3**, the thermal stability values of the MBW-derived PHBV and commercial biopapers obtained from TGA were also included. It can be observed that the copolyester presented a temperature at 5 % weight loss ($T_{5\%}$), considered as the onset-degradation temperature (T_{onset}), of ∼205 °C. Its thermal degradation temperature (T_{deg}) occurred at ∼240 °C, associating a mass loss of nearly 95 %, whereas the amount of residual mass was 0.2 %. Previously prepared films of PHBV with a 3HV content of 18 mol % were also thermally stable up to 249.8 °C (Castro-Mayorga, Fabra, and Lagaron 2016). However, other studies reported that PHBV with different 3HV contents showed higher thermal stability. For instance, PHBV with 20 mol % 3HV showed $T_{5\%}$ and T_{deg} values of approximately 267 and 290 °C, respectively, (Melendez-Rodriguez et al. 2018) while commercial PHBV with a 3HV content of 3 mol % showed $T_{5\%}$ and T_{deg} values of approximately 260 and 277 °C, respectively (Melendez-Rodriguez, Figueroa-Lopez, et al. 2019). This observation points out that thermal stability was not only dependent on the 3HV content but also related to other factors such as M_W, purity, or the presence of additives. Finally, it is also worthy to mention that a residue of 0.2 % was attained at 800 °C, which indicates that the extraction and purification process successfully removed any potential inorganic residues from the feedstock.

3.4. Crystalline Morphology

Figure 5 shows the evolution of the ATR-FTIR spectra of the electrospun fibers up 200 °C to determine the changes with heating of the molecular order of the MBW-derived PHBV. Moreover, in **Figure 6**, the evolution of the ratio of the absorbance of the bands 1230/1453 and the 1720 cm^{-1} full width at half-height-maximum (FWHH) for the MBW-derived PHBV fibers obtained by electrospinning are represented as a function of temperature. These two spectral features are related to the molecular order (crystallinity) in the biopolymer (Cherpinski et al. 2017). In particular, for PHA copolyesters, the stretching vibration of the carbonyl group ν(C═O) corresponds to the strongest peak observed at 1720 cm^{-1}. Furthermore, the complex and multiple peaks that were visible from 1000 to 880 cm^{-1} are known to arise from the stretching bands of the carbon–carbon single bond ν(C–C) (Torres-Giner et al. 2016). Finally, the band centered at ∼1080 cm^{-1} was related to ester bonds in the biopolymer, whereas the band at ∼1020 cm^{-}

[1] corresponding to C–O and C–O–C has been ascribed to stretching vibrations of ester groups in biopolyesters (Torres-Giner et al. 2011). Thus, both higher 1230/1453 bands ratios and lower 1720 cm^{-1} band widths were correlated previously with higher crystallinity in the biopolymer (Cherpinski et al. 2017).

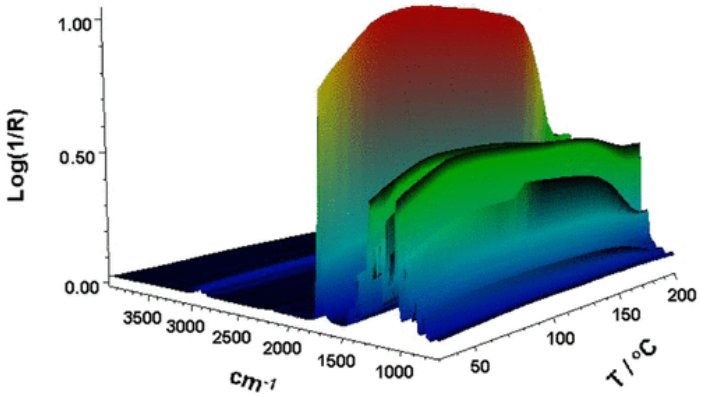

Figure 5. ATR-FTIR spectra taken across temperature of the electrospun MBW-derived PHBV fibers.

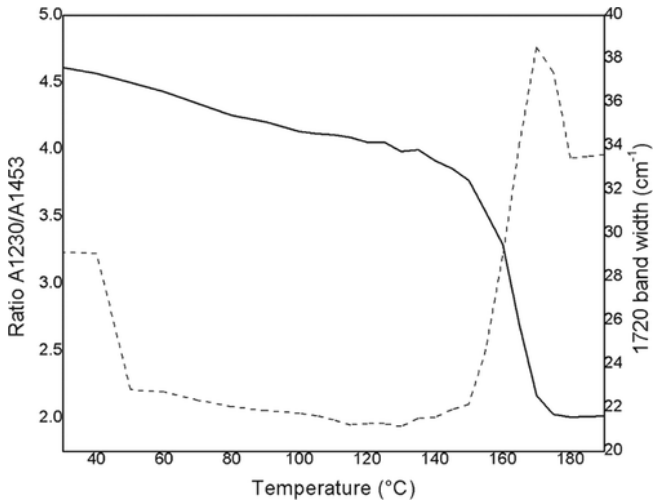

Figure 6. Evolution as a function of temperature of the ratio of the absorbance of the bands 1230/1453 (continuous line) and the 1720 cm^{-1} band full width at half-height-maximum (dashed line) for the electrospun MBW-derived PHBV fibers.

In the ATR-FTIR spectra, it was observed that with increasing temperature the electrospun material exhibited a continuous rise in intensity of the carbonyl band, seen at 1720 cm^{-1}, among

other peaks, up to approximately 130 °C. The band intensity started to decrease at temperatures higher than 130 °C. Moreover, the peak concomitantly increased its width and shifted toward higher wavenumbers. From this, one can infer that the molecular order initially increased with temperature up to about 130 °C, and after 140 °C, it sharply decreased prior to melting. This annealing phenomenon was however not picked up by the 1230/1453 band ratio, which decreased monotonically with increasing temperature, being more pronounced in the vicinity of melting, after 140 °C. These results, but specifically the ∼1720 cm^{-1} band evolution, do shed some light on the process of fiber coalescence observed by SEM, suggesting that this process takes place below the biopolymer melting point and is connected with a sufficiently thermally induced improvement in the molecular order and the presumed mobility of the fibers during that process to reduce surface tension.

The crystallinity and phase morphology of the electrospun MBW-derived PHBV fibers were further assessed by simultaneous time-resolved SAXS and WAXD experiments as a function of temperature using synchrotron radiation. These X-ray diffraction techniques are very useful to assess crystallinity, crystalline morphology, and the phase structure at the mesoscale in semicrystalline biopolymers (Riekel et al. 2003). **Figure 7** displays the simultaneous SAXS and WAXD diffractograms of the electrospun fibers in both isotherm conditions at 100 and 130 °C and for a thermal ramp from 0 to 180 °C at 10 °C/min (analogous to the DSC conditions). In the case of the isotherm at 130 °C, which intends to follow in situ the phase morphology alterations occurring in the sample during the annealing process, the SAXS diffractograms indicate that the peak associated with the long period (Sato et al. 2012) becomes better resolved after a few seconds at this temperature, again supporting the FTIR observations of the improved molecular order and phase structure regularity, developing during the annealing process. During the thermal ramp to melting, the SAXS peak became stronger with increasing temperature with the maximum at approximately 130 °C and after the peak begins to shift toward lower q values, implying an increase in the long period associated with longer repeat units prior to melting. **Figure 7** also shows the WAXD diffractogram evolution over time, exhibiting the most characteristic peaks of the PHB crystal at 2θ 8.8 and 11°, which correspond to the (020) and (110) diffractions, respectively, that arise from the lattice planes of the orthorhombic unit cells (Sato et al. 2012). The WASX diffractograms also exhibited four minor reflections at approximately 13.5, 16, 17.1, and 22°, which originate from the (021), (111), (121), and (040) lattice planes (Panaitescu et al. 2017, Vahabi et al. 2019). According to the literature, the PHB crystal lattice is representative of PHBV copolyesters based on up to 37 mol % 3HV (Škrbić and Divjaković 1996). **Figure 8** zooms the evolution of the peak corresponding to the (110) plane for the isotherms and for the heating ramp. In the case of the isotherms, it can be clearly observed that the crystalline peak increases in relative intensity with time, especially at 130 °C, suggesting again that the crystallinity and crystalline morphology improved during the first 20 s of the isothermal treatment.

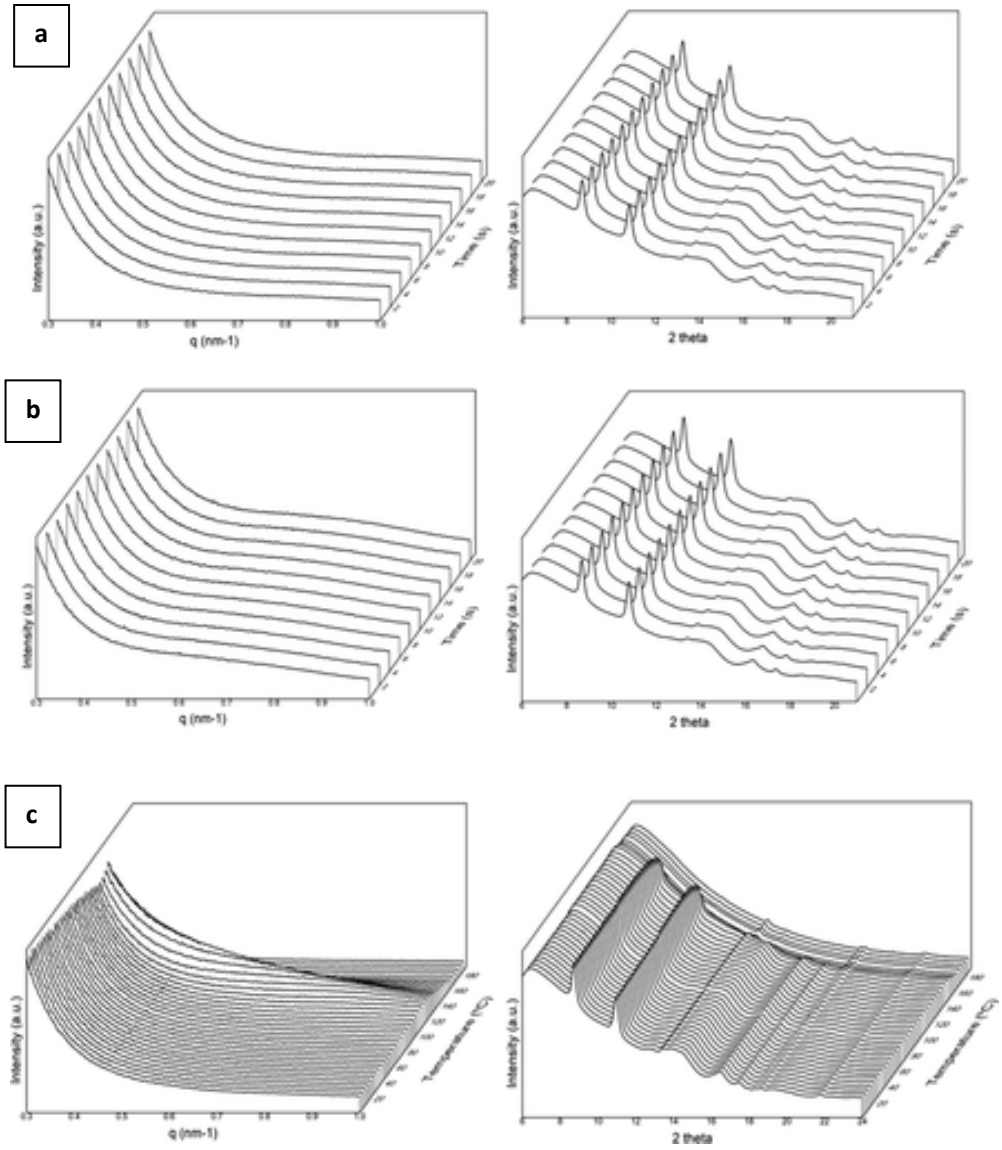

Figure 7. SAXS (left) and WAXS (right) pattern evolution of the electrospun MBW-derived PHBV fibers at (a) 100 °C for 20 s; (b) 130 °C for 20 s; and (c) during a thermal ramp from 0 up to 180 °C at 10 °C/min.

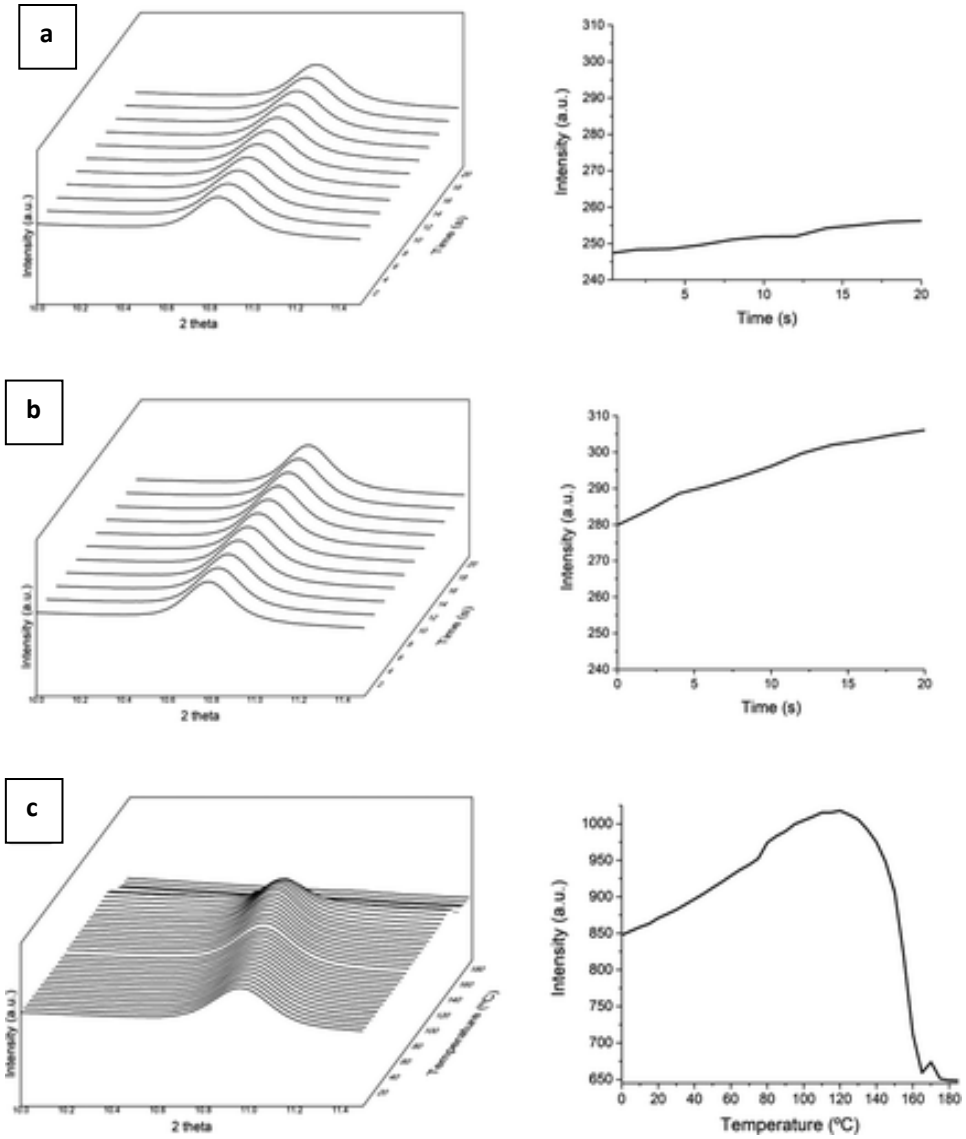

Figure 8. WAXS patterns zoomed around the 2θ 11° peak of the electrospun MBW-derived PHBV fibers for the two isotherms (a, b) and heating ramp (c) in **Figure 7**. The right plots quantify the evolution in relative intensity of the 2θ 11° peak seen in the left diffractograms.

From the heating ramp in **Figure 7** and **8**, it was also observed that the WAXD patterns, in good agreement with the SAXS pattern behavior, underwent a relative intensity increase, suggesting a clear improvement in phase morphology and crystallinity with increasing temperature up to 130 °C, followed by a sharp decrease associated with melting beyond 150 °C, which again correlates very well with the changes observed from FTIR spectroscopy in **Figure 6**.

3.5. Mechanical Performance

Figure 9 displays the stress vs strain curve of the MBW-derived PHBV biopaper. From this curve, the main mechanical properties were obtained and are summarized in **Table 4**. This table indicates that the biopaper presents characteristic properties of a rigid and brittle material, in good resemblance with some of the best commercial papers (Harini and Sukumar 2019, Tanpichai et al. 2020). In particular, the mean values of elastic modulus (E) and tensile strength at yield (σ_y) were 1583 and 13.6 MPa, respectively, whereas the elongation at break (ε_b) and toughness (T) values were below 3 % and 0.5 mJ/m^3, respectively. For the commercial PHBV biopaper, the values obtained were in the same range as the MBW-derived PHBV biopaper, which presented values of 1252 and 18.1 MPa for E and σ_y, respectively, whereas ε_b was 2.4 % and T was 0.3 mJ/m^3 (Melendez-Rodriguez, Figueroa-Lopez, et al. 2019). In comparison with other electrospun PHA films, the mechanical properties of the here-obtained MBW-derived PHBV are closer than those found by Cherpinski et al. (Cherpinski, Torres-Giner, Vartiainen, et al. 2018) who reported E and σ_y values in the range of 1000–2000 and 14–28 MPa, respectively, and an ε_b value of approximately 3 % for PHB and PHBV films prepared by electrospinning. Moreover, our recent studies also showed similar mechanical values for electrospun films of PHBV derived from fruit pulp biowaste in which the mean values of E, σ_y, and ε_b were 1200 MPa, 18 MPa, and 2.5 %, respectively (Melendez-Rodriguez et al. 2018). Furthermore, when compared with PHBV films prepared by compression molding, the here-developed biopapers showed higher ductility and toughness and slightly lower mechanical strength (Shibata et al. 2004, Torres-Giner, Hilliou, et al. 2018). These differences have been ascribed to both the inherently lower crystallinity generated by the electrospinning process and the particular biopaper morphology being constituted by an assembly of nonmolten ultrathin fibers (Cherpinski et al. 2017). In this regard, Alp-Erbay et al. (Alp-Erbay et al. 2019) also indicated that the interactions between the coalesced electrospun fibers (e.g., point bonding, slip of fibers over one another, alignment, among other phenomena) were responsible for the somewhat higher mechanical flexibility attained in the annealed electrospun materials.

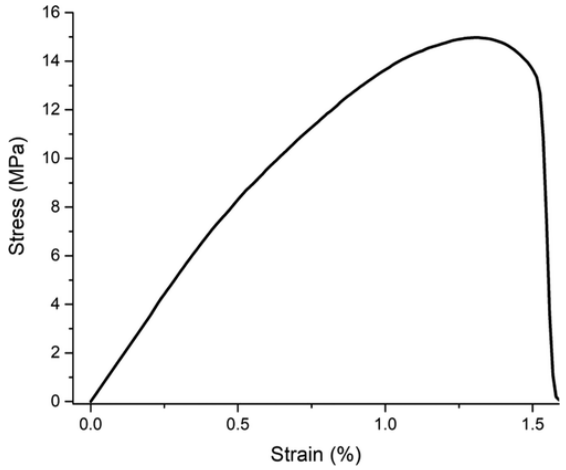

Figure 9. Typical tensile stress–strain curve of the electrospun MBW-derived PHBV biopaper.

Table 4. Mechanical properties of the electrospun PHBV biopapers.

Biopaper	E (MPa)	σ_y (MPa)	ε_b (%)	T (mJ/m^3)
Commercial PHBV*	1252 ± 79[a]	18.1 ± 2.1[a]	2.4 ± 0.3[a]	0.3 ± 0.1[a]
MBW-derived PHBV	1583 ± 249[a]	13.6 ± 3.3[a]	1.3 ± 0.4[b]	0.10 ± 0.01[a]

* Data reported in a previous study (Melendez-Rodriguez, Figueroa-Lopez, et al. 2019).

[a-b] Different letters in the same column mean significant difference among the samples ($p < 0.05$).

In a sustainable packaging context application, the mechanical properties of the MBW-derived PHBV biopaper are similar in terms of mechanical strength but somewhat less ductile than thermo-compressed films of polylactide (PLA), which showed E, σ_y, and ε_b values of 822.5 MPa, 39.6 MPa, and 5.5 %, respectively (Quiles-Carrillo et al. 2019b). In comparison with currently used petroleum-derived polymers, PET films show values of E, maximum tensile strength (σ_{max}), and ε_b in the ranges of 1000–1100 MPa, 50–60 MPa, and 50–90 %, respectively (Thomas and Visakh 2011). In the case of LDPE, its films are remarkably more flexible and ductile (Ali Dadfar et al. 2011). Therefore, the MBW-derived PHBV biopaper showed high rigidity and mechanical strength but a somewhat brittle behavior that is further supported by the lack of yielding in the tensile stress vs strain curve. However, if a comparison is drawn with conventional papers, these materials show lower resistance but somewhat higher ductility and flexibility, having E, σ_y, and ε_b values in the ranges of 500–700 MPa, 60–70 MPa, and 10–12 %, respectively (Harini and Sukumar 2019, Tanpichai et al. 2020).

3.6. Barrier Properties

The WVP, LP, and OP values of the electrospun MBW-derived PHBV biopaper are shown in **Table 5**. It can be observed that the here-produced biopaper presented a WVP value of 3.99×10^{-14} $kg \cdot m \cdot m^{-2} \cdot Pa^{-1} \cdot s^{-1}$, while its LP was 2.09×10^{-14} $kg \cdot m \cdot m^{-2} \cdot Pa^{-1} \cdot s^{-1}$. These values are clearly superior to uncoated conventional papers (Hu et al. 2018) and quite similar to but slightly lower than those obtained for the commercial PHBV biopaper, which showed WVP and LP values of 5.34×10^{-14} and 2.68×10^{-14} $kg \cdot m \cdot m^{-2} \cdot Pa^{-1} \cdot s^{-1}$, respectively (Melendez-Rodriguez, Figueroa-Lopez, et al. 2019). In comparison with other PHA films reported in the literature, the values obtained herein are higher than those reported for electrospun PHB films, that is, 5.22×10^{-15} and 3.20×10^{-15} $kg \cdot m \cdot m^{-2} \cdot Pa^{-1} \cdot s^{-1}$ for WVP and LP, respectively (Cherpinski et al. 2017). This barrier reduction is related to the lower crystallinity content developed in the copolyester, indicating as expected that the barrier properties decrease on increasing the 3HV content (Sanchez-Garcia, Gimenez, and Lagaron 2008). When compared with other PHBV films, the permeability of the here-prepared biopaper is in the same range. Thus, for PHBV with 3 mol % 3HV, the values obtained were 5.3×10^{-14} and 2.7×10^{-14} $kg \cdot m \cdot m^{-2} \cdot Pa^{-1} \cdot s^{-1}$ for WVP and LP, respectively (Melendez-Rodriguez, Torres-Giner, et al. 2019). For PHBV with a higher 3HV content, that is, 20 mol % 3HV, the values were in the range of $(1–3) \times 10^{-14}$ $kg \cdot m \cdot m^{-2} \cdot Pa^{-1} \cdot s^{-1}$ for WVP and $(0.3–3.5) \times 10^{-14}$ $kg \cdot m \cdot m^{-2} \cdot Pa^{-1} \cdot s^{-1}$ for LP (Melendez-Rodriguez et al. 2018). In relation to PHA films prepared by other techniques, solvent-cast PHBV films showed a slightly

higher barrier to limonene and water vapors. In particular, the WVP was 1.27×10^{-14} kg·m·m^{-2}·Pa^{-1}·s^{-1} and the LP was 1.99×10^{-13} kg·m·m^{-2}·Pa^{-1}·s^{-1} for films made of PHBV containing 3 mol % 3HV (Sanchez-Garcia, Gimenez, and Lagaron 2008). Similarly, compression-molded PHB films showed a WVP of 1.7×10^{-15} kg·m·m^{-2}·Pa^{-1}·s^{-1} and an LP value of 8.8×10^{-15} kg·m·m^{-2}·Pa^{-1}·s^{-1} (Sanchez-Garcia, Gimenez, and Lagaron 2007). The slightly lower barrier performance attained for the electrospun biopaper is ascribed to the particular fiber alignment, still leaving some porosity due to its fibrillar nature.

Table 5. Permeability of the electrospun PHBV biopapers.

Biopaper	WVP × 10^{14} (kg·m·m^{-2}·Pa^{-1}·s^{-1})	LP × 10^{14} (kg·m·m^{-2}·Pa^{-1}·s^{-1})	OP × 10^{20} (m^3·m·m^{-2}·Pa^{-1}·s^{-1})
Commercial PHBV*	5.34 ± 1.79[a]	2.68 ± 1.82[a]	3.74 ± 0.6[a]
MBW-derived PHBV	3.99 ± 1.32[a]	2.09 ± 0.30[a]	2.88 ± 0.36[a]

* Barrier data reported in a previous study (Melendez-Rodriguez, Figueroa-Lopez, et al. 2019).

[a] Different letters in the same column mean significant difference among the samples ($p < 0.05$).

The electrospun MBW-derived PHBV biopapers also presented good barrier properties to oxygen. In particular, the OP value was 2.88×10^{-20} m^3·m·m^{-2}·Pa^{-1}·s^{-1}, which is in the range of other electrospun PHA films, such as PHBV with 3 mol % 3HV (3.74×10^{-20} m^3·m·m^{-2}·Pa^{-1}·s^{-1}) (Melendez-Rodriguez, Figueroa-Lopez, et al. 2019), PHBV with 20 mol % 3HV (1.25×10^{-19} m^3·m·m^{-2}·Pa^{-1}·s^{-1}) (Melendez-Rodriguez et al. 2018), and PHB (1.20×10^{-18} m^3·m·m^{-2}·Pa^{-1}·s^{-1}) (Cherpinski, Torres-Giner, Vartiainen, et al. 2018). Since oxygen is more sensitive to the material free volume, morphological differences, and defects than vapors of higher M_W, the measured value indicates that the here-attained electrospun biopaper of PHBV derived from MBW presents a good uniformity and reduced porosity. In the context of packaging applications, the OP value obtained here is lower than in PET films (1.35×10^{-19} m^3·m·m^{-2}·Pa^{-1}·s^{-1}) but is considerably lower in comparison with that of LDPE films (2.15×10^{-17} m^3·m·m^{-2}·Pa^{-1}·s^{-1}). On the other hand, the permeability to oxygen is higher than that of a high-barrier ethylene–vinyl alcohol copolymer (EVOH) (7.7×10^{-20} m^3·m·m^{-2}·Pa^{-1}·s^{-1}) (Lagarón 2011).

4. Conclusions

In the present study, a PHBV material derived from municipal biowaste was developed, purified, ran by electrospinning, and postprocessed by a mild thermal treatment at 130 °C for 5 s, to obtain a fiber-based continuous film: the so-called biopaper. The resultant fiber-based film exhibited higher transparency and a less grayish color than a commercial PHBV. The thermal properties exhibited a multiple melting endotherm with the maximum of melting at approximately 155 °C. The material remained stable up to ∼205 °C, and the maximum of degradation occurred at approximately 240 °C. Interestingly, molecular order, crystallinity, and phase morphology at the

mesoscale were assessed by ATR-FTIR spectroscopy and time-resolved simultaneous WAXS and SAXS experiments using synchrotron radiation as a function of temperature and were found to correlate very well with each other. The results indicated that by heating the electrospun fibers up until 130 °C, the phase morphology and crystallinity are improved; beyond this temperature, the crystallinity begins to deteriorate until complete melting occurs. This improvement in phase morphology upon heating, resulting from thermally activated molecular chain rearrangements, allows the fibers to coalesce to reduce surface tension and hence to reduce structural porosity. In terms of mechanical properties, the biopaper was found to exhibit higher mechanical strength but somewhat lower ductility than commercial papers. However, the biopapers showed higher ductility and toughness than similar PHBV films prepared by melt compounding routes. These differences were ascribed to the particular morphology of the electrospun biopaper, having ill-defined crystallinity and being composed of aligned side-by-side fibers. Finally, in terms of barrier properties, the biopaper is clearly superior to traditional cellulose papers and showed similar values to other electrospun PHA films being slightly more permeable than their compression-molded counterpart films. In any case, the film showed high barrier to water vapor and oxygen and, hence, great interest in food packaging applications.

From the evidence presented, it can be concluded that the use of MBW is of significant interest to develop more sustainable packaging materials from both an environmental and an economic point of view, in full alignment with circular bioeconomy strategies, since the production of PHAs by these mixed microbial cultures can successfully minimize the costs associated with the fermentation and downstream processes. Furthermore, the combination of electrospinning and a mild annealing postprocessing below the biopolymer's T_m is able to yield unique biomaterials with balanced properties.

5. Supporting Information

Table S1. Thermal properties of the electrospun biopapers of MBW derived PHBV annealed at different temperatures and obtained from the first heating, subsequent cooling, and second heating runs by DSC.

Biopaper	DSC							
	First heating		Cooling		Second heating			
	T_m (°C)	ΔH_m (J/g)	T_c (°C)	ΔH_c (J/g)	T_{cc} (°C)	ΔH_{cc} (J/g)	T_m (°C)	ΔH_m (J/g)
As obtained	155.4 ± 1.5^{a,b}	57.6 ± 2.2^{a,c}	68.1 ± 4.1^{a}	43.9 ± 8.2^{a}	44.9 ± 0.7^{a}	4.6 ± 0.4^{a}	136.0 ± 2.8^{a} // 152.4 ± 2.5^{a}	56.7 ± 1.6^{a}
80 ºC	156.9 ± 1.9^{a}	61.7 ± 4.2^{a,b}	60.1 ± 2.1^{b}	42.3 ± 1.7^{a}	37.9 ± 1.3^{b}	3.7 ± 0.6^{a}	135.8 ± 4.4^{a,b} // 151.7 ± 2.3^{a}	62.9 ± 4.2^{b}
110 ºC	156.5 ± 2.6^{a}	62.2 ± 0.9^{b}	59.8 ± 2.5^{b}	37.5 ± 3.5^{a}	44.8 ± 0.6^{a}	9.5 ± 2.6^{b}	132.1 ± 0.5^{b} // 149.7 ± 0.6^{a}	63.6 ± 1.0^{b}
125 ºC	153.6 ± 0.7^{b}	56.2 ± 4.3^{a,c}	59.8 ± 1.7^{b}	38.5 ± 2.6^{a}	45.4 ± 1.1^{a}	5.1 ± 2.4^{a,b}	131.8 ± 0.7^{b} // 149.3 ± 1.1^{a}	62.2 ± 3.3^{b}
130 ºC	153.9 ± 0.1^{b}	57.4 ± 5.4^{a,b,c}	60.3 ± 1.9^{b}	38.1 ± 5.5^{a}	44.7 ± 0.3^{a}	9.8 ± 4.1^{b}	132.4 ± 0.7^{a,b} // 149.4 ± 0.3^{a}	60.5 ± 0.6^{b}
140 ºC	155.1 ± 0.2^{a,b}	58.1 ± 1.6^{a}	58.6 ± 1.5^{b}	39.6 ± 2.2^{a}	43.7 ± 1.3^{a}	6.4 ± 2.1^{a,b}	132.3 ± 1.2^{a,b} // 149.8 ± 0.8^{a}	59.6 ± 0.9^{b}
150 ºC	155.1 ± 0.8^{a,b}	53.6 ± 2.3^{c}	58.1 ± 0.3^{b}	40.4 ± 1.5^{a}	41.3 ± 4.8^{a,b}	9.6 ± 2.9^{b}	132.9 ± 0.1^{b} // 149.9 ± 0.4^{a}	60.3 ± 3.4^{a,b}

$^{a-c}$ Different letters in the same column indicate a significant difference among the samples ($p < 0.05$).

6. References

Acevedo, F., P. Villegas, V. Urtuvia, J. Hermosilla, R. Navia, and M. Seeger. 2018. "Bacterial polyhydroxybutyrate for electrospun fiber production." *International Journal of Biological Macromolecules* 106:692-697. doi: 10.1016/j.ijbiomac.2017.08.066.

Agüero, A., M. C. Morcillo, L. Quiles-Carrillo, R. Balart, T. Boronat, D. Lascano, S. Torres-Giner, and O. Fenollar. 2019. "Study of the influence of the reprocessing cycles on the final properties of polylactide pieces obtained by injection molding." *Polymers* 11 (12). doi: 10.3390/polym11121908.

Albuquerque, M. G. E., C. A. V. Torres, and M. A. M. Reis. 2010. "Polyhydroxyalkanoate (PHA) production by a mixed microbial culture using sugar molasses: Effect of the influent substrate concentration on culture selection." *Water Research* 44 (11):3419-3433. doi: 10.1016/j.watres.2010.03.021.

Ali Dadfar, S. M., I. Alemzadeh, S. M. Reza Dadfar, and M. Vosoughi. 2011. "Studies on the oxygen barrier and mechanical properties of low density polyethylene/organoclay nanocomposite films in the presence of ethylene vinyl acetate copolymer as a new type

of compatibilizer." *Materials and Design* 32 (4):1806-1813. doi: 10.1016/j.matdes.2010.12.028.

Alp-Erbay, E., K. J. Figueroa-Lopez, J. M. Lagaron, E. Çağlak, and S. Torres-Giner. 2019. "The impact of electrospun films of poly(ε-caprolactone) filled with nanostructured zeolite and silica microparticles on in vitro histamine formation by Staphylococcus aureus and Salmonella Paratyphi A." *Food Packaging and Shelf Life* 22. doi: 10.1016/j.fpsl.2019.100414.

Arfat, Y. A., J. Ahmed, N. Hiremath, R. Auras, and A. Joseph. 2017. "Thermo-mechanical, rheological, structural and antimicrobial properties of bionanocomposite films based on fish skin gelatin and silver-copper nanoparticles." *Food Hydrocolloids* 62:191-202. doi: 10.1016/j.foodhyd.2016.08.009.

Castro-Mayorga, J. L., M. J. Fabra, and J. M. Lagaron. 2016. "Stabilized nanosilver based antimicrobial poly(3-hydroxybutyrate-co-3-hydroxyvalerate) nanocomposites of interest in active food packaging." *Innovative Food Science and Emerging Technologies* 33:524-533. doi: 10.1016/j.ifset.2015.10.019.

Castro Mayorga, J. L., M. J. Fabra Rovira, L. Cabedo Mas, G. Sánchez Moragas, and J. M. Lagarón Cabello. 2018. "Antimicrobial nanocomposites and electrospun coatings based on poly(3-hydroxybutyrate-co-3-hydroxyvalerate) and copper oxide nanoparticles for active packaging and coating applications." *Journal of Applied Polymer Science* 135 (2). doi: 10.1002/app.45673.

Cherpinski, A., M. Gozutok, H. T. Sasmazel, S. Torres-Giner, and J. M. Lagaron. 2018. "Electrospun oxygen scavenging films of poly(3-hydroxybutyrate) containing palladium nanoparticles for active packaging applications." *Nanomaterials* 8 (7). doi: 10.3390/nano8070469.

Cherpinski, A., S. Torres-Giner, L. Cabedo, and J. M. Lagaron. 2017. "Post-processing optimization of electrospun submicron poly(3-hydroxybutyrate) fibers to obtain continuous films of interest in food packaging applications." *Food Additives and Contaminants - Part A Chemistry, Analysis, Control, Exposure and Risk Assessment* 34 (10):1817-1830. doi: 10.1080/19440049.2017.1355115.

Cherpinski, A., S. Torres-Giner, L. Cabedo, J. A. Méndez, and J. M. Lagaron. 2018. "Multilayer structures based on annealed electrospun biopolymer coatings of interest in water and aroma barrier fiber-based food packaging applications." *Journal of Applied Polymer Science* 135 (24). doi: 10.1002/app.45501.

Cherpinski, A., S. Torres-Giner, J. Vartiainen, M. S. Peresin, P. Lahtinen, and J. M. Lagaron. 2018. "Improving the water resistance of nanocellulose-based films with polyhydroxyalkanoates processed by the electrospinning coating technique." *Cellulose* 25 (2):1291-1307. doi: 10.1007/s10570-018-1648-z.

Choi, J. I., and S. Y. Lee. 1997. "Process analysis and economic evaluation for poly(3-hydroxybutyrate) production by fermentation." *Bioprocess Engineering* 17 (6):335-342. doi: 10.1007/s004490050394.

Coats, E. R., F. J. Loge, M. P. Wolcott, K. Englund, and A. G. McDonald. 2007. "Synthesis of polyhydroxyalkanoates in municipal wastewater treatment." *Water Environment Research* 79 (12):2396-2403. doi: 10.2175/106143007X183907.

Colombo, B., T. P. Sciarria, M. Reis, B. Scaglia, and F. Adani. 2016. "Polyhydroxyalkanoates (PHAs) production from fermented cheese whey by using a mixed microbial culture." *Bioresource Technology* 218:692-699. doi: 10.1016/j.biortech.2016.07.024.

Dionisi, D., G. Carucci, M. Petrangeli Papini, C. Riccardi, M. Majone, and F. Carrasco. 2005. "Olive oil mill effluents as a feedstock for production of biodegradable polymers." *Water Research* 39 (10):2076-2084. doi: 10.1016/j.watres.2005.03.011.

Doshi, J., and D. H. Reneker. 1995. "Electrospinning process and applications of electrospun fibers." *Journal of Electrostatics* 35 (2-3):151-160. doi: 10.1016/0304-3886(95)00041-8.

Fabra, M. J., A. Lopez-Rubio, and J. M. Lagaron. 2014. "Nanostructured interlayers of zein to improve the barrier properties of high barrier polyhydroxyalkanoates and other polyesters." *Journal of Food Engineering* 127:1-9. doi: 10.1016/j.jfoodeng.2013.11.022.

Fernández-Dacosta, C., J. A. Posada, R. Kleerebezem, M. C. Cuellar, and A. Ramirez. 2015. "Microbial community-based polyhydroxyalkanoates (PHAs) production from wastewater: Techno-economic analysis and ex-ante environmental assessment." *Bioresource Technology* 185:368-377. doi: 10.1016/j.biortech.2015.03.025.

Figueroa-Lopez, K. J., A. A. Vicente, M. A. M. Reis, S. Torres-Giner, and J. M. Lagaron. 2019. "Antimicrobial and antioxidant performance of various essential oils and natural extracts and their incorporation into biowaste derived poly(3-hydroxybutyrate-co-3-hydroxyvalerate) layers made from electrospun ultrathin fibers." *Nanomaterials* 9 (2). doi: 10.3390/nano9020144.

Fiorese, M. L., F. Freitas, J. Pais, A. M. Ramos, G. M. F. De Aragão, and M. A. M. Reis. 2009. "Recovery of polyhydroxybutyrate (PHB) from Cupriavidus necator biomass by solvent extraction with 1,2-propylene carbonate." *Engineering in Life Sciences* 9 (6):454-461. doi: 10.1002/elsc.200900034.

Griffin, G. J. L. 1994. Chemistry and technology of biodegradable polymers. edited by G. J. L. Griffin. London.: Blackie Academic & Professional

Gurieff, N., and P. Lant. 2007. "Comparative life cycle assessment and financial analysis of mixed culture polyhydroxyalkanoate production." *Bioresource Technology* 98 (17):3393-3403. doi: 10.1016/j.biortech.2006.10.046.

Harini, K., and M. Sukumar. 2019. "Development of cellulose-based migratory and nonmigratory active packaging films." *Carbohydrate Polymers* 204:202-213. doi: 10.1016/j.carbpol.2018.10.018.

Hassan, M. A., Y. Shirai, N. Kusubayashi, M. I. A. Karim, K. Nakanishi, and K. Hashimoto. 1997. "The production of polyhydroxyalkanoate from anaerobically treated palm oil mill effluent by Rhodobacter sphaeroides." *Journal of Fermentation and Bioengineering* 83 (5):485-488. doi: 10.1016/S0922-338X(97)83007-3.

Hu, M., C. Li, X. Li, M. Zhou, J. Sun, F. Sheng, S. Shi, and L. Lu. 2018. "Zinc oxide/silver bimetallic nanoencapsulated in PVP/PCL nanofibres for improved antibacterial activity." *Artificial Cells, Nanomedicine and Biotechnology* 46 (6):1248-1257. doi: 10.1080/21691401.2017.1366339.

Jung, H. R., T. R. Choi, Y. H. Han, Y. L. Park, J. Y. Park, H. S. Song, S. Y. Yang, S. K. Bhatia, R. Gurav, H. Park, S. Namgung, K. Y. Choi, and Y. H. Yang. 2020. "Production of blue-colored polyhydroxybutyrate (PHB) by one-pot production and coextraction of indigo and PHB from recombinant Escherichia coli." *Dyes and Pigments* 173. doi: 10.1016/j.dyepig.2019.107889.

Kanatt, S. R., M. S. Rao, S. P. Chawla, and A. Sharma. 2012. "Active chitosan-polyvinyl alcohol films with natural extracts." *Food Hydrocolloids* 29 (2):290-297. doi: 10.1016/j.foodhyd.2012.03.005.

Koller, M. 2014. "Poly(hydroxyalkanoates) for food packaging: Application and attempts towards implementation." *Applied Food Biotechnology* 1 (1):3-15. doi: 10.22037/afb.v1i1.7127.

Koller, M., L. Maršálek, M. M. de Sousa Dias, and G. Braunegg. 2017. "Producing microbial polyhydroxyalkanoate (PHA) biopolyesters in a sustainable manner." *New Biotechnology* 37:24-38. doi: 10.1016/j.nbt.2016.05.001.

Korkakaki, E., M. Mulders, A. Veeken, R. Rozendal, M. C. M. van Loosdrecht, and R. Kleerebezem. 2016. "PHA production from the organic fraction of municipal solid waste (OFMSW): Overcoming the inhibitory matrix." *Water Research* 96:74-83. doi: 10.1016/j.watres.2016.03.033.

Kourmentza, C., and M. Kornaros. 2016. "Biotransformation of volatile fatty acids to polyhydroxyalkanoates by employing mixed microbial consortia: The effect of pH and carbon source." *Bioresource Technology* 222:388-398. doi: 10.1016/j.biortech.2016.10.014.

Kunasundari, B., and K. Sudesh. 2011. "Isolation and recovery of microbial polyhydroxyalkanoates." *Express Polymer Letters* 5 (7):620-634. doi: 10.3144/expresspolymlett.2011.60.

Lagarón, J. M. 2011. "Multifunctional and nanoreinforced polymers for food packaging." In *Multifunctional and Nanoreinforced Polymers for Food Packaging*, 1-28.

Lasprilla-Botero, J., S. Torres-Giner, M. Pardo-Figuerez, M. álvarez-Láinez, and J. M. Lagaron. 2018. "Superhydrophobic bilayer coating based on annealed electrospun ultrathin poly(ε-caprolactone) fibers and electrosprayed nanostructured silica microparticles for easy emptying packaging applications." *Coatings* 8 (5). doi: 10.3390/coatings8050173.

Laycock, B., P. Halley, S. Pratt, A. Werker, and P. Lant. 2013. "The chemomechanical properties of microbial polyhydroxyalkanoates." *Progress in Polymer Science* 38 (3-4):536-583. doi: 10.1016/j.progpolymsci.2012.06.003.

Li, L., W. Huang, B. Wang, W. Wei, Q. Gu, and P. Chen. 2015. "Properties and structure of polylactide/poly (3-hydroxybutyrate-co-3-hydroxyvalerate) (PLA/PHBV) blend fibers." *Polymer* 68:183-194. doi: 10.1016/j.polymer.2015.05.024.

Madkour, M. H., D. Heinrich, M. A. Alghamdi, I. I. Shabbaj, and A. Steinbüchel. 2013. "PHA recovery from biomass." *Biomacromolecules* 14 (9):2963-2972. doi: 10.1021/bm4010244.

Mata-Alvarez, J., J. Dosta, M. S. Romero-Güiza, X. Fonoll, M. Peces, and S. Astals. 2014. "A critical review on anaerobic co-digestion achievements between 2010 and 2013." *Renewable and Sustainable Energy Reviews* 36:412-427. doi: 10.1016/j.rser.2014.04.039.

Melendez-Rodriguez, B., J. L. Castro-Mayorga, M. A. M. Reis, C. Sammon, L. Cabedo, S. Torres-Giner, and J. M. Lagaron. 2018. "Preparation and Characterization of Electrospun Food Biopackaging Films of Poly(3-hydroxybutyrate-co-3-hydroxyvalerate) Derived From Fruit Pulp Biowaste." *Frontiers in Sustainable Food Systems* 2. doi: 10.3389/fsufs.2018.00038.

Melendez-Rodriguez, B., K. J. Figueroa-Lopez, A. Bernardos, R. Martínez-Máñez, L. Cabedo, S. Torres-Giner, and J. M. Lagaron. 2019. "Electrospun antimicrobial films of poly(3-hydroxybutyrate-co-3-hydroxyvalerate) containing eugenol essential oil encapsulated in mesoporous silica nanoparticles." *Nanomaterials* 9 (2). doi: 10.3390/nano9020227.

Melendez-Rodriguez, B., S. Torres-Giner, A. Aldureid, L. Cabedo, and J. M. Lagaron. 2019. "Reactive melt mixing of poly(3-hydroxybutyrate)/rice husk flour composites with purified biosustainably produced poly(3-hydroxybutyrate-co-3-hydroxyvalerate)." *Materials* 12 (13). doi: 10.3390/ma12132152.

Morgan-Sagastume, F., M. Hjort, D. Cirne, F. Gérardin, S. Lacroix, G. Gaval, L. Karabegovic, T. Alexandersson, P. Johansson, A. Karlsson, S. Bengtsson, M. V. Arcos-Hernández, P. Magnusson, and A. Werker. 2015. "Integrated production of polyhydroxyalkanoates (PHAs) with municipal wastewater and sludge treatment at pilot scale." *Bioresource Technology* 181:78-89. doi: 10.1016/j.biortech.2015.01.046.

Pal, Kunal, Ajit Banthia, and Dipak K. Majumdar. 2009. "Polymeric Hydrogels: Characterization and Biomedical Applications." *Designed Monomers & Polymers,VSP, an imprint of Brill* 12:197-220. doi: 10.1163/156855509X436030.

Panaitescu, D. M., C. A. Nicolae, A. N. Frone, I. Chiulan, P. O. Stanescu, C. Draghici, M. Iorga, and M. Mihailescu. 2017. "Plasticized poly(3-hydroxybutyrate) with improved melt processing and balanced properties." *Journal of Applied Polymer Science* 134 (19). doi: 10.1002/app.44810.

Quiles-Carrillo, L., N. Montanes, J. M. Lagaron, R. Balart, and S. Torres-Giner. 2019a. "Bioactive multilayer polylactide films with controlled release capacity of gallic acid accomplished by incorporating electrospun nanostructured coatings and interlayers." *Applied Sciences (Switzerland)* 9 (3). doi: 10.3390/app9030533.

Quiles-Carrillo, L., N. Montanes, J. M. Lagaron, R. Balart, and S. Torres-Giner. 2019b. "In Situ Compatibilization of Biopolymer Ternary Blends by Reactive Extrusion with Low-Functionality Epoxy-Based Styrene–Acrylic Oligomer." *Journal of Polymers and the Environment* 27 (1):84-96. doi: 10.1007/s10924-018-1324-2.

Rehm, B. H. A. 2003. "Polyester synthases: Natural catalysts for plastics." *Biochemical Journal* 376 (1):15-33. doi: 10.1042/BJ20031254.

Reis, M., M. Albuquerque, M. Villano, and M. Majone. 2011. "Mixed Culture Processes for Polyhydroxyalkanoate Production from Agro-Industrial Surplus/Wastes as Feedstocks." In *Comprehensive Biotechnology, Second Edition*, 669-683.

Riekel, C., M. C. G. Gutiérrez, A. Gourrier, and S. Roth. 2003. "Recent synchrotron radiation microdiffraction experiments on polymer and biopolymer fibers." *Analytical and Bioanalytical Chemistry* 376 (5):594-601. doi: 10.1007/s00216-003-1976-0.

Saharan, B. S., A. Grewal, and P. Kumar. 2014. "Biotechnological production of polyhydroxyalkanoates: a review on trends and latest developments." *Chin. J. Biol.* 2014:1-18.

Sanchez-Garcia, M. D., E. Gimenez, and J. M. Lagaron. 2007. "Novel PET nanocomposites of interest in food packaging applications and comparative barrier performance with biopolyester nanocomposites." *Journal of Plastic Film and Sheeting* 23 (2):133-148. doi: 10.1177/8756087907083590.

Sanchez-Garcia, M. D., E. Gimenez, and J. M. Lagaron. 2008. "Morphology and barrier properties of solvent cast composites of thermoplastic biopolymers and purified cellulose fibers." *Carbohydrate Polymers* 71 (2):235-244. doi: 10.1016/j.carbpol.2007.05.041.

Sängerlaub, S., M. Brüggemann, N. Rodler, V. Jost, and K. D. Bauer. 2019. "Extrusion coating of paper with poly(3-hydroxybutyrate-co-3-hydroxyvalerate) (PHBV)-Packaging related functional properties." *Coatings* 9 (7). doi: 10.3390/coatings9070457.

Sato, H., N. Suttiwijitpukdee, T. Hashimoto, and Y. Ozaki. 2012. "Simultaneous synchrotron SAXS/WAXD study of composition fluctuations, cold-crystallization, and melting in biodegradable polymer blends of cellulose acetate butyrate and poly(3-hydroxybutyrate)." *Macromolecules* 45 (6):2783-2795. doi: 10.1021/ma202606y.

Shibata, M., S. Oyamada, S. I. Kobayashi, and D. Yaginuma. 2004. "Mechanical properties and biodegradability of green composites based on biodegradable polyesters and lyocell fabric." *Journal of Applied Polymer Science* 92 (6):3857-3863. doi: 10.1002/app.20405.

Shiku, Y., P. Y. Hamaguchi, S. Benjakul, W. Visessanguan, and M. Tanaka. 2004. "Effect of surimi quality on properties of edible films based on Alaska pollack." *Food Chemistry* 86 (4):493-499. doi: 10.1016/j.foodchem.2003.09.022.

Škrbić, Ž, and V. Divjaković. 1996. "Temperature influence on changes of parameters of the unit cell of biopolymer PHB." *Polymer* 37 (3):505-507. doi: 10.1016/0032-3861(96)82922-3.

Spagnol, C., E. H. Fragal, A. G. B. Pereira, C. V. Nakamura, E. C. Muniz, H. D. M. Follmann, R. Silva, and A. F. Rubira. 2018. "Cellulose nanowhiskers decorated with silver nanoparticles as an additive to antibacterial polymers membranes fabricated by electrospinning." *Journal of Colloid and Interface Science* 531:705-715. doi: 10.1016/j.jcis.2018.07.096.

Tanpichai, S., S. Witayakran, J. Wootthikanokkhan, Y. Srimarut, W. Woraprayote, and Y. Malila. 2020. "Mechanical and antibacterial properties of the chitosan coated cellulose paper for packaging applications: Effects of molecular weight types and concentrations of chitosan." *International Journal of Biological Macromolecules* 155:1510-1519. doi: 10.1016/j.ijbiomac.2019.11.128.

Thomas, S., and P. M. Visakh. 2011. "Engineering and Specialty Thermoplastics: Polyethers and Polyesters: State-of-the-art, New Challenges and Opportunities." In *Handbook of Engineering and Speciality Thermoplastics: Polyethers and Polyesters*, 1-14.

Torres-Giner, S., J. V. Gimeno-Alcañiz, M. J. Ocio, and J. M. Lagaron. 2011. "Optimization of electrospun polylactide-based ultrathin fibers for osteoconductive bone scaffolds." *Journal of Applied Polymer Science* 122 (2):914-925. doi: 10.1002/app.34208.

Torres-Giner, S., L. Hilliou, B. Melendez-Rodriguez, K. J. Figueroa-Lopez, D. Madalena, L. Cabedo, J. A. Covas, A. A. Vicente, and J. M. Lagaron. 2018. "Melt processability, characterization, and antibacterial activity of compression-molded green composite sheets made of poly(3-hydroxybutyrate-co-3-hydroxyvalerate) reinforced with coconut fibers impregnated with oregano essential oil." *Food Packaging and Shelf Life* 17:39-49. doi: 10.1016/j.fpsl.2018.05.002.

Torres-Giner, S., N. Montanes, T. Boronat, L. Quiles-Carrillo, and R. Balart. 2016. "Melt grafting of sepiolite nanoclay onto poly(3-hydroxybutyrate-co-4-hydroxybutyrate) by reactive extrusion with multi-functional epoxy-based styrene-acrylic oligomer." *European Polymer Journal* 84:693-707. doi: 10.1016/j.eurpolymj.2016.09.057.

Torres-Giner, S., N. Montanes, V. Fombuena, T. Boronat, and L. Sanchez-Nacher. 2018. "Preparation and characterization of compression-molded green composite sheets made of poly(3-hydroxybutyrate) reinforced with long pita fibers." *Advances in Polymer Technology* 37 (5):1305-1315. doi: 10.1002/adv.21789.

Torres-Giner, S., S. Wilkanowicz, B. Melendez-Rodriguez, and J. M. Lagaron. 2017. "Nanoencapsulation of Aloe vera in Synthetic and Naturally Occurring Polymers by Electrohydrodynamic Processing of Interest in Food Technology and Bioactive Packaging." *Journal of Agricultural and Food Chemistry* 65 (22):4439-4448. doi: 10.1021/acs.jafc.7b01393.

Vahabi, H., L. Michely, G. Moradkhani, V. Akbari, M. Cochez, C. Vagner, E. Renard, M. R. Saeb, and V. Langlois. 2019. "Thermal stability and flammability behavior of poly(3-hydroxybutyrate) (PHB) based composites." *Materials* 12 (14). doi: 10.3390/ma12142239.

Valentino, F., G. Moretto, L. Lorini, D. Bolzonella, P. Pavan, and M. Majone. 2019. "Pilot-Scale Polyhydroxyalkanoate Production from Combined Treatment of Organic Fraction of Municipal Solid Waste and Sewage Sludge." *Industrial and Engineering Chemistry Research* 58 (27):12149-12158. doi: 10.1021/acs.iecr.9b01831.

Zhang, K., M. Misra, and A. K. Mohanty. 2014. "Toughened sustainable green composites from poly(3-hydroxybutyrate-co-3-hydroxyvalerate) based ternary blends and miscanthus biofiber." *ACS Sustainable Chemistry and Engineering* 2 (10):2345-2354. doi: 10.1021/sc500353v.

Zhang, M., H. Wu, and H. Chen. 2014. "Coupling of polyhydroxyalkanoate production with volatile fatty acid from food wastes and excess sludge." *Process Safety and Environmental Protection* 92 (2):171-178. doi: 10.1016/j.psep.2012.12.002.

Chapter III

Development and Characterization of Electrospun Biopapers of Poly(3-hydroxybutyrate-*co*-3-hydroxyvalerate) Derived from Cheese Whey with Varying 3-Hydroxyvalerate Contents

Biomacromolecules 2021, 22, 7, 2935-2953

Beatriz Meléndez-Rodríguez[1], Maria A. M. Reis[2], Monica Carvalheira[2], Chris Sammon[3], Luis Cabedo[4], Sergio Torres-Giner[1], and José María Lagarón[1]

[1] Novel Materials and Nanotechnology Group, Institute of Agrochemistry and Food Technology (IATA), Spanish Council for Scientific Research (CSIC), Paterna, Spain

[2] UCIBIO-REQUIMTE, Chemistry Department, Faculty of Sciences and Technology, Universidade NOVA de Lisboa, Caparica, Portugal

[3] Materials and Engineering Research Institute, Sheffield Hallam University, Sheffield, United Kingdom

[4] Polymers and Advanced Materials Group, Universitat Jaume I (UJI), Castellón, Spain

Abstract

In the present study, three different newly developed copolymers of poly(3-hydroxybutyrate-*co*-3-hydroxyvalerate) (PHBV) with 20, 40, and 60 mol % contents in 3-hydroxyvalerate (3HV) were produced by the biotechnological process of mixed microbial cultures (MMCs) using cheese whey (CW), a by-product from the dairy industry, as feedstock. The CW-derived PHBV copolyesters were first purified and then processed by solution electrospinning, yielding fibers of approximately 2 μm in cross-section in all cases. The resultant electrospun PHBV mats were, thereafter, post-processed by annealing at different temperatures, below their maximum of melting, selected according to their 3HV content in order to obtain continuous films based on coalesced fibers, so-called biopapers. The resultant PHBV films were characterized in terms of their morphology, crystallinity, and mechanical and barrier properties to assess their potential application in food packaging. The CW-derived PHBV biopapers showed high contact transparency but a slightly yellow color. The fibers of the 20 mol % 3HV copolymer were seen to contain mostly poly(3-hydroxybutyrate) (PHB) crystals, the fibers of the 40 mol % 3HV copolymer a mixture of PHB and poly(3-hydroxyvalerate) (PHV) crystals and lowest crystallinity, and the fibers of the 60 mol % 3HV sample were mostly made of PHV crystals. To understand the interfiber coalesce process undergone by the materials during annealing, the crystalline morphology was also assessed by variable-temperature both combined small-angle and wide-angle X-ray scattering synchrotron and Fourier transform infrared experiments. From these experiments and, different from previously reported biopapers with lower 3HV contents, all samples were inferred to have a surface energy reduction mechanism for interfiber coalescence during annealing, which is thought to be activated by a temperature-induced decrease in molecular order. Due to their reduced crystallinity and molecular order, the CW-derived PHBV biopapers, especially the 40 mol % 3HV sample, were found to be more ductile and tougher. In terms of barrier properties, the three copolymers performed similarly to water and limonene, but to oxygen, the 40 mol % sample showed the highest relative permeability. Overall, the materials developed, which are compatible with the Circular Bioeconomy organic recycling strategy, can have an excellent potential as barrier interlayers or coatings of application interest in food packaging.

Keywords: PHBV; cheese whey; electrospinning; food packaging; Circular Bioeconomy

1. Introduction

Nowadays, the use of alternative materials to Conventional plastics is increasingly important due to the environmental issues associated to the extensive use of single-use plastics. Thus, from political institutions, such as the European Union (EU), different strategies that have been developed focused on a better design of plastic products, the increase in recycling rates, and the promotion of Circular Economy processes (EuropeanCommission 2020). For this reason, polyhydroxyalkanoates (PHAs), microbial biopolyesters produced during fermentation of lipids or sugar in famine conditions for energy and intracellular carbon storage compounds (Poli et al. 2011), are currently seen as a proper green alternative to petroleum-derived polymers due to their renewable origin and biodegradability (Li et al. 2019). Within PHAs, the most studied biopolyester is poly(3-hydroxybutyrate) (PHB). This homopolymer shows similar characteristics in terms of thermal and mechanical properties that most common polyolefins, such as polyethylene (PE) and polypropylene (PP) (Gutiérrez, Galván, and Álzate 2017). However, due to its high crystallinity and macromolecular organization, it results in a stiff and brittle material that it is unsuitable for use in packaging applications (Hablot et al. 2008). The poly(3-hydroxybutyrate-*co*-3- hydroxyvalerate) (PHBV) copolyester with high contents in 3-hydroxyvalerate (3HV), that is higher than 8 mol %, shows considerably lower crystallinity and broader thermal processing (Anderson and Dawes 1990). As a result, the melting temperature (T_m) of the PHB homopolyester significantly decreases with the 3HV content (Holmes 1988). For instance, Scandola et al. (Scandola et al. 1992) reported a decrease in T_m from 176 to 83 °C when the 3HV content increased from 0 to 55 mol %. From a mechanical point of view, PHBV is also more flexible, ductile, and tough (Jiang and Zhang 2013). In particular, it was reported that an increase in 3HV from 0 to 28 mol % improved the elongation at break and impact strength of PHB (Savenkova et al. 2000). Moreover, 15 mol % 3HV in PHBV increased the melt flow rate (MFR) of PHB by nearly 150 % (Gatenholm, Kubát, and Mathiasson 1992).

Nevertheless, commercial PHBV is currently limited to 3HV contents of 2 mol %, which shows relatively similar properties to other commercial PHB grades, so new materials of non-GMO origin with a better balance in properties, derived from wastes to reduce costs and valorize, among others, industrial/agricultural by-products, alternative processing strategies to minimize thermal exposure, etc., are being investigated for food packaging applications (Abdalkarim et al. 2020, Li et al. 2021). Thus, it is known that the industrial application of PHAs is yet restricted due to their high cost of production caused by the use of specific substrates and bacterial strains in sterilized operating conditions (Van Wegen, Ling, and Middelberg 1998). For these reasons, the utilization of food processing by-products or wastes from water treatment systems as carbon sources for PHA production with high comonomer contents is seen as a very promising alternative (Reis et al. 2003). Thus, different organic wastes from both citric and dairy industries (Carvalheira et al. 2018, Domingos et al. 2018, Melendez-Rodriguez et al. 2018, Oliveira et al. 2018), oils and biodiesel (Martla, Umsakul, and Sudesh 2018, Talan et al. 2020), and even sludge from treatment plants (Melendez-Rodriguez et al. 2020, Moretto et al. 2020, Tu et al. 2019) have been explored for the production of PHAs. In this context, the use of mixed microbial cultures (MMCs) particularly represents an affordable approach to reduce costs since sterile conditions and specific feedstock are not necessary (Reis et al. 2011). In this case, the culture selection is made by selective pressure using feast and famine regimes to select the optimal PHA-storing organisms (Van Loosdrecht, Pot, and Heijnen 1997). This strategy has been largely studied, showing an

efficient enrichment of this kind of organisms in the reactor (Albuquerque, Torres, and Reis 2010, Duque et al. 2014, Johnson et al. 2009).

Among the explored food processing by-products, cheese whey (CW) is a promising carbon source that is increasingly being seen as a value-added product rather than a waste. CW is the largest residue in the dairy industry, where over 160 million tons per year are produced (Guimarães, Teixeira, and Domingues 2010). Cheese production generates three main types of effluent, namely, CW that results from cheese production, second cheese whey (SCW) that is obtained from cottage cheese production, and cheese whey wastewater (CWW) derived from washing water of industrial processing equipment. The latter also contains CW and SCW. Traditional practices of CW disposal by the dairy industry include spraying onto fields or discharge into rivers, lakes, or oceans, with a negative environmental impact (Kosikowski 1979), as well as into the municipal sewage system that causes a high chemical oxygen demand (COD) and a high biological oxygen demand (BOD) due to its high lactose content (Smithers 2008). In some cases, it is also used in animal feeding or protein supplements (González Siso 1996). All these approaches in relation to the waste management of CW have not solved yet its environmental problems. Thus, its valorization is still critical for many dairy industries. According to this, the use of CW as feedstock in MMC reactors can represent a good strategy both to lower process costs and reduce its environmental impact. In this regard, Colombo et al. (Colombo et al. 2016) reported the PHA production by the fermentation of CW from MMC and showed the possibility of obtaining different PHA compositions by modifying the organic acid composition of the fermented CW. Similar results were obtained by Duque et al. (Duque et al. 2014), who produced PHA using CW and sugar cane molasses (SCM) as MMC feedstocks in a bioreactor.

In the field of PHAs, the electrospinning technology is a novel strategy to prepare materials of interest in food packaging applications. This technology allows us to create polymer nanofibers with diameters ranging from some nanometers to a few micrometers. This process is based on the application of electrostatic forces to polymer solutions through the action of a high-voltage electric field (Doshi and Reneker 1995), where the fibers formation is affected by both the solution properties and process conditions (Torres-Giner, Gimenez, and Lagaron 2008). The high surface-to-volume ratios of the fibers, the controllable pore sizes, and the possibility to nanoencapsulate different substances make electrospinning very promising for the formation of active and bioactive materials with also improved performance (Torres-Giner, Pérez-Masiá, and Lagaron 2016). More recently, it has been described that the electrospun fiber mats can be transformed into continuous films by the application of a thermal posttreatment below the biopolymer's T_m, also referred as annealing (Cherpinski et al. 2017). Since the fiber-based morphology is preserved in the resultant electrospun film, the annealed mats of naturally derived polymers are also called "biopapers" (Cherpinski et al. 2017). These have the advantage of being made purely of non-cellulosic biofibers that do not undergo aggressive chemical treatments, as is the case of the traditional paper (Figueroa-Lopez, Torres-Giner, et al. 2020). Thus, biopapers show better optical and barrier properties and higher ductility and toughness than traditional paper packaging and similar barrier performance compared to films of same materials obtained by conventional melt processing or solvent casting (Figueroa-Lopez, Cabedo, et al. 2020). The generation of new MMC-derived PHAs, with targeted increased HV contents, is known to yield more ductile materials, which, for the time being, still contain a number of cellular impurities. Finding minimally processed or purified new polymers that can undergo minimal thermal exposure during processing has been our target lately. Biopapers of MMC PHAs are one feasible

solution that we have putting forward since recently (Melendez-Rodriguez et al. 2020). In the latter work, a PHBV biopaper with a 10 mol % HV content derived from municipal waste was developed, where the mechanism of interfiber coalescence was found to be the classic heat-induced molecular order improvement.

In this context, the main objective of this research study was to obtain and characterize biopapers of newly developed PHBV copolymers derived from CW with different 3HV contents. The structure-properties-processing relationships of the materials were investigated for the first time by different techniques to assess their potential to constitute interlayers or coatings for food packaging applications. From a fundamental view point, the target of this study was set to understand the particular mechanisms triggering the required process of interfiber coalescence, leading to continuous films. From a technological view point, the objective was to offer property balanced, more sustainable, and cost affordable options to commercial PHAs films processed by conventional melt compounding strategies and also to traditional papers.

2. Experimental

2.1. Materials

PHBV copolyesters were produced at Universidade NOVA (Lisbon, Portugal) using MMCs fed with CW derived from wastes of the dairy Portuguese company (Lactogal Produtos Alimentares S.A.). The commercial PHBV (PHBV2), used for comparison, was ENMAT Y1000P, which was produced by Tianan Biologic Materials (Ningbo, China) and delivered in the form of pellets. According to the manufacturer, the 3HV fraction in the commercial copolyester is 2 mol %. 2,2,2-Trifluoroethanol (TFE), ≥ 99 % purity, sulfuric acid (H_2SO_4), with 95−97 % purity, D-limonene, with 98% purity, and 1-butanol, reagent grade with 99.5 % purity, were obtained from Sigma Aldrich S.A. (Madrid, Spain). Chloroform, stabilized with ethanol and 99.8 % purity, was purchased from Panreac S.A. (Barcelona, Spain). Valeric acid was obtained from Alfa Aesar by Thermo Fisher Scientific (Massachusetts, USA).

2.2. Production of PHBV

The PHBV production was performed at pilot-plant scale in three stages: (1) Acidogenic fermentation, (2) selection of the PHBV accumulating MMC, and (3) PHBV production. In the acidogenic fermentation, the organic matter present in the CW was biologically converted to organic acids and ethanol, which were the precursors for the PHBV biosynthesis. This stage was carried out in a 100 L up flow anaerobic sludge blanket reactor (UASB), inoculated with anaerobic granular sludge and operated at suitable operational conditions (pH controlled at 4−5 and temperature at 30 °C) in order to produce a fermented CW with the approximate 3HB/3HV monomer precursor ratio of approximately 80/20 wt %. The selection of the PHBV accumulating MMC was carried out in a sequencing batch reactor (SBR) inoculated with aerobic sludge from a municipal wastewater treatment plant, fed with the fermented waste produce in the UASB, and

operated under feast and famine regime. Finally, the PHBV production was carried out in a fed-batch reactor using the selected PHBV accumulating MMC (stage 2) and the fermented waste (stage 1). For the PHBV production, the fed-batch reactor was inoculated with sludge harvested from the SBR and fed in a pulse-wise manner with the fermented waste, controlled by the dissolved oxygen (DO) response. Whenever necessary, for the production of PHBV with 3HV contents of 40 and 60 mol %, the fermented CW was supplemented with the additional 3HV precursor valeric acid. After reaching the maximum PHBV content, the biological activity was stopped by quenching to pH 2−3 using sulfuric acid. The PHBV-enriched biomass was then subjected to the biopolymer extraction and purification steps.

The molar ratios of the resultant PHBV were determined by gas chromatography (GC) using the method described by Lanham et al. (Lanham et al. 2013) in a Bruker 430-GC gas chromatograph equipped with a flame ionization detector (FID) and a BR-SWax column (60 m, 0.53 mm internal diameter, 1 mm film thickness, Bruker, Torrance, CA, USA). The resultant contents of 3HV in the copolymers were approximately 20, 40, and 60 mol %. Molecular weights (M_{Ws}) of the PHBV copolyesters were 5.51×10^5, 4.83×10^5, and 5.46×10^5 g/mol, respectively, showing dispersity ($D = M_w/M_n$) values of 1.77, 3.46, and 2.92, being all determined by size exclusion chromatography (SEC) using a Waters apparatus as described by Pereira et al. (Pereira et al. 2019).

2.3. Extraction of PHBV

The unpurified PHBV materials were processed following the previously reported chloroform-based extraction method (Fiorese et al. 2009). For this, each unpurified PHBV was dissolved in chloroform at 5 wt %. The mixture was then stirred for 24 h at 50 °C to degrade the non-PHA cellular material. Later, the solution was transferred to centrifugation tubes in which distilled water was added at 50 wt %. After shaking the tubes manually, these were centrifuged for 5 min at 4000 rpm in an Avanti J-26S XP Centrifuge with a JLA-16.250 Rotor (maximum radius: 134 mm; average radius: 90 mm; minimum radius: 46 mm, Beckman Coulter, CA, USA). Afterward, the PHBV suspension was recovered from the bottom of the tubes with a pipette and transferred to beakers, leaving them in the extractor hood until the solvent was completely evaporated.

2.4. PHBV Solutions

The extracted PHBV powders were dissolved in a chloroform/butanol (75:25 wt/wt) mixture at 2 wt % under magnetic stirring for 24 h at 50 °C. The viscosity, surface tension, and conductivity were measured for all the prepared PHBV solutions prior to electrospinning. The apparent viscosity (η_a) was determined at 100 s^{-1} using a rotational viscosity meter Visco BasicPlus L from Fungilab S.A. (San Feliu de Llobregat, Spain) equipped with a low-viscosity adapter (LCP). The surface tension was measured following the Wilhemy plate method using an EasyDyne K20 tensiometer from Krüss GmbH (Hamburg, Germany). The conductivity was evaluated using a conductivity meter XS Con6 from Lab-box (Barcelona, Spain). All measurements were carried out at room temperature in triplicate. The commercial PHBV2 solution sample was prepared by dissolving the biopolymer at 10 wt % in TFE. The characterization of this solution, processing conditions, and characterization data were reported earlier (Melendez-Rodriguez et al. 2020).

2.5. Electrospinning Process

All the PHBV solutions were processed by electrospinning using a dual polarization Fluidnatek LE-10 lab tool manufactured by Bioinicia S.L. (Valencia, Spain). The equipment was operated with a motorized single needle injector, scanning horizontally toward a metallic fixed collector at room conditions, that is, 25 °C and 40 % relative humidity (RH). Optimal conditions were found at a flow rate of 4 ml/h, 10 kV of voltage, and 18 cm of needle-to-collector distance. Fiber deposition was carried out for 4 h for each PHBV. In the case of the commercial PHBV2 sample, electrospinning was carried out as previously reported, that is, 6 ml/h, 20 kV, and 15 cm (Melendez-Rodriguez et al. 2020). The resultant electrospun fiber mats were left to cure, stored in a desiccator at 0 % RH, for at least 1 week before further handling.

2.6. Biopapers Preparation

The resultant electrospun PHBV mats were subjected to annealing in a 4122-model press from Carver, Inc. (Wabash, IN, USA). The selected applied temperatures were optimized according to the 3HV content of the PHBV material and their melting profiles. Thus, the annealing temperature was at 120, 60, and 70 °C for 20, 40, and 60 mol %, respectively. Samples were thermally post-treated for 10 s, without pressure, and the resultant biopapers showed a thickness of nearly 60 μm. The targeted annealing temperature is the minimum temperature required for the fiber mats to yield interfiber cohesion and material continuity, thus ensuring minimal thermal exposure to the biopolymers that result in enhanced optical properties and mechanical and barrier performance.

2.7. Characterization of PHBV Films

2.7.1. Microscopy

The morphologies of the top views and cross-sections of the electrospun PHBV fibers and resultant biopapers were observed by scanning electron microscopy (SEM) using an S-4800 device from Hitachi (Tokyo, Japan). For the cross-section observations, the films were cryofractured by immersion in liquid nitrogen. The samples were fixed to beveled holders using conductive double-sided adhesive tape and sputtered with a mixture of gold-palladium under vacuum prior to observation. An accelerating voltage of 10 kV was used. The average fiber diameters were determined with the ImageJ software v 1.41 using a minimum of 20 SEM micrographs.

2.7.2. Transparency

The light transmission of the biopapers was determined in specimens of 50 mm × 30 mm by quantifying the absorption of light at wavelengths between 200 and 700 nm in an ultraviolet-visible (UV-Vis) spectrophotometer VIS3000 from Dinko Instruments (Barcelona, Spain). The transparency (T) and opacity (O) were respectively calculated using eqs 1 (Shiku et al. 2004) and 2 (Kanatt et al. 2012):

$$T = \frac{A_{600}}{L} \quad (1)$$

$$O = A_{500} \times L \quad (2)$$

where A_{500} and A_{600} are the absorbance values at 500 and 600 nm, respectively, and L is the film thickness (mm).

2.7.3. Color Measurements

The color of the electrospun PHBV biopapers was determined using a chroma meter CR-400 (Konica Minolta, Tokyo, Japan). The color difference (ΔE^*) was calculated, as defined by the Commission Internationale de l'Eclairage (CIE), using eq 3 (Arfat et al. 2017):

$$\Delta E^* = [(\Delta L^*)^2 + (\Delta a^*)^2 + (\Delta b^*)^2]^{0.5} \quad (3)$$

where ΔL^*, Δa^*, and Δb^* correspond to the differences in terms of lightness from black to white, color from green to red, and color from blue to yellow, respectively, between the test sample and a control sample of commercial PHBV biopaper (Melendez-Rodriguez et al. 2020). Color change was evaluated using the following assessment: Unnoticeable ($\Delta E^* < 1$), only an experienced observer can notice the difference ($\Delta E^* \geq 1$ and $\Delta E^* < 2$), an unexperienced observer notices the difference ($\Delta E^* \geq 2$ and $\Delta E^* < 3.5$), clear noticeable difference ($\Delta E^* \geq 3.5$ and $\Delta E^* < 5$), and the observer notices different colors ($\Delta E^* \geq 5$) (Mokrzycki and Tatol 2011).

2.7.4. Thermal Analysis

Thermal transitions of the electrospun PHBV biopapers were studied by differential scanning calorimetry (DSC) on a DSC-7 analyzer from PerkinElmer, Inc. (Waltham, MA, USA), equipped with a cooling accessory Intracooler 2 also from PerkinElmer, Inc. A three-step program under a nitrogen atmosphere, with a flow rate of 20 ml/min, was applied. A first heating step from -30 to 180 °C was followed by a cooling step to -30 °C, and a second heating run back to 180 °C, with 60 s isothermals between runs. The heating and cooling rates were set as 10 °C/min. The typical sample weight was approximately 3 mg, while an empty aluminum pan was used as a reference and calibration was performed using an indium sample. All tests were carried out in triplicate. Tm, enthalpy of melting (ΔH_m), cold crystallization temperature (T_{cc}), and enthalpy of the cold crystallization (ΔH_{cc}) were obtained from the heating scans, while the crystallization temperature from the melt (T_c) and enthalpy of crystallization (ΔH_c) were determined from the cooling scan.

Thermogravimetric analysis (TGA) was performed in a TG-STDA model TGA/STDA851e/LF/1600 thermobalance from Mettler-Toledo, LLC (Columbus, OH, USA). The samples, with a weight of about 15 mg, were heated from 50 to 900 °C, at a heating rate of 10 °C/min under a nitrogen flow rate of 50 ml/min.

2.7.5. ATR-FTIR Spectroscopy

Fourier transform infrared (FTIR) spectra were collected coupling the attenuated total reflection (ATR) accessory Golden Gate of Specac, Ltd. (Orpington, UK) to the Tensor 37 FTIR equipment (Bruker, Germany). Single spectra were collected in the wavelength range from 4000 to 600 cm^{-1} by averaging 20 scans at a resolution of 4 cm^{-1}. Variable-temperature FTIR was performed on a Nicolet Nexus FTIR instrument from Thermo Fisher Scientific Inc. (Wilmington, DE, USA) coupled to a variable-temperature single reflection diamond ATR sampling accessory of Specac Ltd. (Orpington, UK). Spectra were collected by averaging 64 scans at a 4 cm^{-1} resolution using the blank ATR crystal at the same temperature as the background. The electrospun mats were clamped directly onto the ATR crystal using a calibrated torque wrench from Specac Ltd. set at 80 cNm, which applies a load of 350 N via the sample accessory anvil. Further details about the equipment and the procedure can be found elsewhere (Melendez-Rodriguez et al. 2020). FTIR spectra were collected differently according to the type of PHBV. For the PHBV with 20 and 40 mol % 3HV, spectra were taken at 10 °C intervals from 30 to 100 °C, thereafter at 5 °C intervals up to 160 °C, and then again at 10 °C intervals until 180 °C. For the PHBV sample with 60 mol % 3HV, spectra were collected at 10 °C intervals from 30 to 60 °C, thereafter at 5 °C intervals up to 90 °C, and then again at 10 °C intervals until 160 °C.

2.7.6. Time-Resolved Synchrotron X-ray Scattering

Time-resolved simultaneous small-angle and wide-angle X-ray scattering (SAXS and WAXS) experiments as a function of temperature were carried out at the beam line BL11−Non-crystalline diffraction (NCD) (WAXS/ SAXS station) located at the ALBA synchrotron facilities (Barcelona, Spain). Scattering patterns were collected using the combination of two detectors, that is, a photon counting detector Pilatus 1M detector from Dectris AG (Baden, Switzerland) and a CDD WAXS LX255-HS detector from Rayonix, L.L.C. (Evanston, IL, USA), operating simultaneously in SAXS and WAXS positions, respectively. The wavelength of the incident radiation (λ) was 1 Å. For the in situ thermal experiments, the electrospun mats, with a thickness of 100 μm, were placed on a hot stage “film type” THMS600 from Linkam Scientific Instruments Ltd. (Epstom, UK). Further details regarding the facilities, setup, and measurements can be found in our previous study (Melendez-Rodriguez et al. 2020). The above experiments were carried out temperature wise in the electrospun mats of PHBVs with 20 and 40 mol % 3HV, by subjecting them to thermal ramps ranging from 0 to 180 °C at 10 °C/min.

2.7.7. WAXD

Wide-angle X-ray diffraction (WAXD) experiments were performed at room temperature in the electrospun mats of the three copolymers using a Bruker AXS D4 ENDEAVOR diffractometer (Billerica, MA, USA). The samples were scanned in the reflection mode using incident Cu K-alpha radiation (k = 1.54 Å), while the generator was set up at 40 kV and 40 mA. The data were collected over the (2θ) range of 2−40°.

2.7.8. Mechanical Tests

Tensile tests of the electrospun PHBV biopapers were performed according to ASTM standard method D638 using an Instron 4400 universal testing machine from Instron (Norwood, MA, USA) equipped with a 1 kN load cell. Tests were performed with 115 mm × 16 mm stamped dumbbell-shaped specimens using a cross-head speed of 10 $mm.min^{-1}$. Samples were conditioned to the test conditions, that is, 40 % RH and 25 °C, for 24 h prior to tensile assay. A minimum of six specimens were tested for each sample.

2.7.9. Permeability Tests

The water vapor permeability (WVP) of the electrospun PHBV biopapers was determined using the gravimetric method ASTM E96-95 in triplicate. The control samples were cups with aluminum films to estimate solvent loss through the sealing. For this, 5 ml of distilled water was placed inside a Payne permeability cup (diameter of 3.5 cm) from Elcometer Sprl (Hermallesous-Argenteau, Belgium). The film was not in direct contact with water but exposed to 100 % RH on one side and secured with silicon rings. They were placed within a desiccator, sealed with dried silica gel, at 0 % RH cabinet at 25 °C. The cups were weighted periodically using an analytical balance (± 0.0001 g). WVP was calculated from the regression analysis of weight loss data vs time, and the weight loss was calculated as the total loss minus the loss through the sealing. The permeability was obtained by multiplying the permeance by the film thickness.

For limonene permeability (LP), the procedure was similar to that described above for WVP with the difference that 5 ml of $_D$-limonene was placed inside the Payne permeability cups and these were placed under controlled room conditions of 25 °C and 40 % RH.

The oxygen permeability coefficient was derived from the oxygen transmission rate (OTR) measurements that were recorded using an Oxygen Permeation Analyzer M8001 from Systech Illinois (Thame, UK) at 60 % RH and 25 °C, in duplicate. The humidity equilibrated samples were purged with nitrogen, before exposure to an oxygen flow of 10 $ml \cdot min^{-1}$. The exposure area during the test was 5 cm^2 for each sample. In order to obtain the oxygen permeability (OP), film thickness and gas partial pressure were considered.

2.8. Statistical Analysis

The optical, thermal, mechanical, and barrier properties were evaluated through analysis of variance (ANOVA) using STATGRAPHICS Centurion XVI v 16.1.03 from StatPoint Technologies, Inc. (Warrenton, VA, USA). Fisher's least significant difference (LSD) was used at the 95 % confidence level ($p < 0.05$). Mean values and standard deviations (SD) were reported.

3. Results and Discussion

The electrospun PHBV mats of fibers and/or their resulting biopapers were characterized in terms of morphology, molecular order, optical, thermal, mechanical, and barrier performance.

3.1. Solution Properties and Morphology

The PHBV solutions were fine tuned for the three different copolymers and were characterized prior to be processed by electrospinning. The selection of solvents and conditions were based on our previous experience in other PHA materials (Melendez-Rodriguez et al. 2018, Melendez-Rodriguez et al. 2020). **Table 1** shows the viscosity, surface tension, and conductivity of the three optimal biopolymer solutions. One can observe that, for all the PHBV solutions, surface tension, conductivity, and viscosity were very similar, showing values in the range of nearly 22−23 mN/m, 0.06−0.13 μS/cm, and 157−216 cP, respectively. In this regard, it is well known that solution properties can strongly affect the electrospinning process (Li and Xia 2004). In particular, a medium-to-high viscosity values are habitually needed to produce fibers that, in the case of PHAs, are typically below 690 cP (Figueroa-Lopez et al. 2019, Melendez-Rodriguez et al. 2020). Conductivity is usually low in PHAs, which is in principle good for electrospinning without spraying, and surface tension is usually in the range of 21−26 mN/m (Figueroa-Lopez et al. 2019, Melendez-Rodriguez et al. 2018).

Table 1. Solution properties of the cheese whey (CW)-derived poly(3-hydroxybutyrate-*co*-3-hydroxyvalerate) (PHBV) with 3-hydroxyvalerate (3HV) contents of 20 mol % (PHBVCW20), 40 mol % (PHBVCW40), and 60 mol % (PHBVCW60).

Solution	3HV content (mol%)	Solids content (wt%)	Viscosity (cP)	Surface tension (mN/m)	Conductivity (μS/cm)	Fiber diameter (μm)
PHBVCW20	20	2	216.2 ± 2.4[a]	22.1 ± 0.1[a]	0.13 ± 0.03[a]	2.2 ± 0.2[a]
PHBVCW40	40		156.8 ± 1.3[b]	22.9 ± 0.3[b]	0.06 ± 0.01[b]	2.2 ± 0.1[a]
PHBVCW60	60		171.3 ± 1.1[c]	21.9 ± 0.1[a]	0.09 ± 0.01[a]	2.1 ± 0.2[a]

[a–c] Different letters in the same column indicate a significant difference among the samples ($p < 0.05$).

Figure 1 shows the morphology of fiber mats obtained by electrospinning and also the cryo-fracture surfaces and top views of their biopapers after annealing. It can be observed that the electrospinning of the PBHV solutions yielded similar mats composed of non-woven fibers with, in all cases, a mean fiber diameter of approximately 2.2 μm and showing no significant differences. Furthermore, by comparison of the top views of the electrospun mats before and after annealing, respectively, shown in the left and right images of **Figure 1**, one can observe that the thermal post-treatment led to continuous films made of fibers, the so-called biopapers, whose morphology is more suitable for food packaging applications. Since the here-prepared PHBV were expected to show different melting profiles due to variations in their 3HV content, the annealing temperatures were optimized for each electrospun mat. Optimization meant the lowest annealing temperatures required for efficient interfiber coalescence. These were found to be at

120, 60, and 70 °C, for the electrospun mats of PHBV with 20, 40, and 60 mol % 3HV, respectively. As it can be observed in the SEM micrographs, shown in the middle images of **Figure 1**, annealing at these temperatures, below the maximum T_m, successfully produced a compact packing rearrangement of the electrospun fibers in the mat. This process has been reported to occur due to fibers coalescence, which results in a densification of the electrospun mats (Figueroa-Lopez, Torres-Giner, et al. 2020, Melendez-Rodriguez et al. 2018). It is also remarkable to see that similar morphologies were attained in the different samples due to the right optimization and selection of the minimum annealing temperature needed for the process to occur. The main advantage of this innovative film preparation method to obtain interlayer self-adhering films without the need for tie layers is the very mild thermal processing undergone by the materials, which is expected to lead to higher transparency and better flexibility of these with a good control for the deposition of thin layers (Cherpinski et al. 2018, Melendez-Rodriguez et al. 2018).

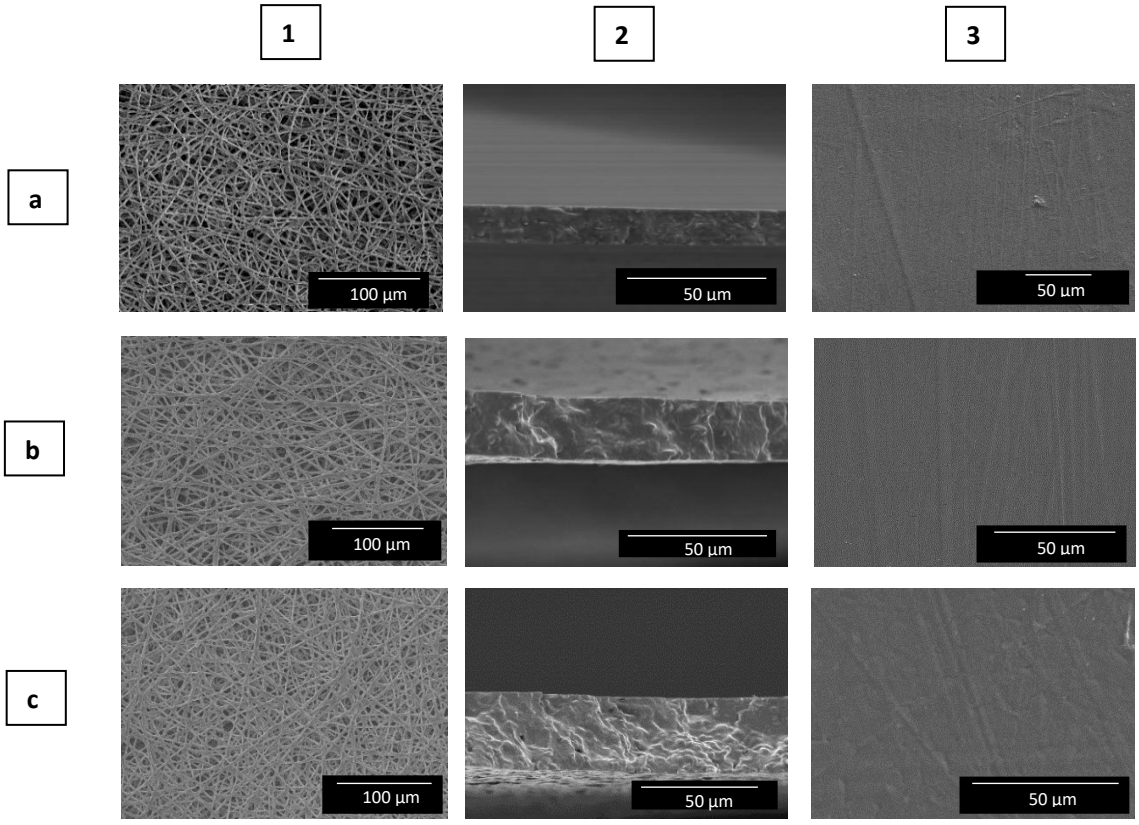

Figure 1. Scanning electron microscopy (SEM) images of the electrospun fibers in the top view (1) and their biopapers in cross-section (2) and top view (3) of the cheese whey (CW)-derived poly(3-hydroxybutyrate-*co*-3-hydroxyvalerate) (PHBV) with varying 3-hydroxyvalerate (3HV) contents: (a) 20 mol %, (b) 40 mol %, and (c) 60 mol %. Images were taken at 400× and 1000×, and the scale markers are 100 and 50 µm, respectively.

3.2. Optical Properties

Figure 2 displays the pictures of the resulting electrospun biopapers prepared with the three different types of PHBV. It can be seen that these annealed electrospun samples showed high contact transparency with a slight yellowish tone. Similar visual appearance with also high transparency has been previously reported for similar electrospun biopapers after annealing (Melendez-Rodriguez et al. 2018, Melendez-Rodriguez et al. 2020). The here-observed color development could be ascribed to potential Maillard reactions that could be generated during the annealing step due to the presence of impurities, which are due to remnant cellular debris, mainly proteins, endotoxins, or lipids (Pagliano et al. 2021). In this sense, purity achieved with chloroform extraction has been reported to be over 90 %, mainly depending on the strains used and the initial PHA content (Martínez-Sanz et al. 2014).

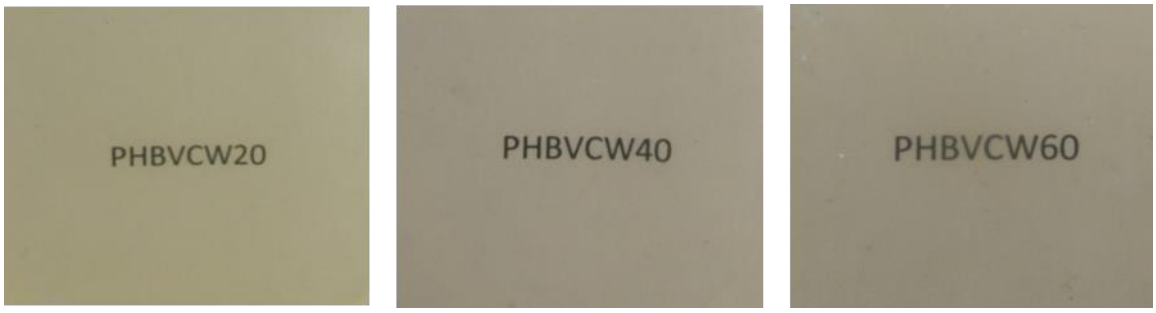

Figure 2. Background transparency pictures of the electrospun biopapers of cheese whey (CW)-derived poly(3-hydroxybutyrate-*co*-3-hydroxyvalerate) (PHBV) with 3-hydroxyvalerate (3HV) contents of 20 mol % (PHBVCW20), 40 mol % (PHBVCW40), and 60 mol % (PHBVCW60).

To quantify the optical properties of the PHBV biopapers, the values of L^* to show lightness, color coordinates (a^* and b^*), color difference as ΔE^* as well as the T and O values were determined and reported in **Table 2**. For L^*, all films showed similar values of approximately 88. With respect to a^* (green to red), the three materials presented negatives values, indicating that the films were slightly green. The positive values of the color coordinate b^* (blue to yellow) confirmed the development of some yellowish tones in the biopaper samples, more notably for the biopaper of PHBV with 20 mol % 3HV, with a value of 10.46. This observation could be related to the higher temperature thermal step applied during annealing. In the table, it is also reported, for comparison purposes, the color coordinates of an electrospun biopaper of commercial PHBV containing 2 mol % 3HV obtained previously in our lab in similar conditions (Melendez-Rodriguez et al. 2020). From this, it can be observed that the commercial PHBV film was slightly redder and less yellow that those prepared with the food waste-derived PHBV. The highest color difference was measured in the film of PHBV with 20 mol % that showed a value of 9.60, which means that an observer can easily notice different colors ($\Delta E^* \geq 5$). For the biopapers prepared using PHBV with 40 and 60 mol % 3HV, a similar value of ΔE^* was obtained. In particular, the values were 4.72 and 4.96, respectively, indicating that a clear difference is seen between these electrospun biopapers and the commercial PHBV biopaper ($\Delta E^* \geq 3.5$ and $\Delta E^* < 5$). Moreover, it can also be observed that the CW-derived PHBV biopapers presented higher

transparency than the biopaper made from the commercial copolyester. Particularly, the T values were reduced from 9.2, for the commercial PHBV biopaper, down to a value of 1.80 in the case of the biopaper of PHBV with 20 mol % 3HV, whereas the other two biopapers showed values in the 4.8-4.9 range. The higher transparency of the here-prepared electrospun films, when compared to the commercial low 3HV content biopapers, can be ascribed to the expected lower material density phases at the mesoscale, that is, lower crystallinity and crystallite lateral packing density.

Table 2. Optical properties of the electrospun biopapers of commercial and cheese whey (CW) derived poly(3-hydroxybutyrate-*co*-3-hydroxyvalerate) (PHBV) with 3-hydroxyvalerate (3HV) contents of 20 mol % (PHBVCW20), 40 mol % (PHBVCW40), and 60 mol % (PHBVCW60).

Biopaper	a^*	b^*	L^*	ΔE^*	T
Commercial PHBV2*	0.35 ± 0.03^a	1.29 ± 0.01^a	89.14 ± 0.02^a	-	9.20 ± 0.08^a
PHBVCW20	-2.31 ± 0.04^b	10.46 ± 0.02^b	88.19 ± 0.05^b	9.60 ± 0.03^a	1.80 ± 0.03^b
PHBVCW40	-0.85 ± 0.01^c	5.80 ± 0.02^c	88.43 ± 0.04^c	4.72 ± 0.02^b	4.84 ± 0.02^c
PHBVCW60	-0.47 ± 0.02^d	5.99 ± 0.02^d	87.80 ± 0.03^d	4.96 ± 0.02^c	4.89 ± 0.03^c

[a]Data reported in a previous study (Melendez-Rodriguez et al. 2020). [a−d] Different letters in the same column indicate a significant difference among the samples ($p < 0.05$).

a^*: red/green coordinates (+a red, −a green); b^*: yellow/blue coordinates (+b yellow, −b blue); L^*: luminosity (+L luminous, −L dark); ΔE^*: color differences; T: transparency.

3.3. Thermal Properties

Table 3 displays the thermal transitions obtained by DSC for the electrospun fiber mats of the three PHBV copolyesters with varying 3HV contents to estimate the crystallinity and ascertain the effect of annealing on the fibers. Hence, it is the first thermal run on the fibers that is relevant for the main purpose of this study. **Figure 3** gathers the DSC thermograms of the samples taken during the first and second heating and cooling runs. In the first heating run, it can be observed that the fiber samples presented a rather weak and complex melting behavior, with broad endothermic features and curved baselines. The PHBV copolyester with 20 mol % 3HV showed a T_m at 154.2 °C, the sample with 40 mol % 3HV showed two less defined peaks at 67.7 °C and at 139.3 °C, and the sample at 60 mol % a T_m at 80.6 °C. In terms of melting enthalpies and, in spite of the complex endothermic behaviour seen, an attempt was done to estimate them, which suggested that the electrospun fiber mat sample with 60 mol % has lower values. In any case, the curved baseline, associated to the sample moving during the run, and the various and broad endothermic signals, seem very complex to determine this parameter with any certainty.

Table 3. Thermal properties of the electrospun fiber mats of commercial poly(3-hydroxybutyrate) (PHB), commercial PHBV2 with 2 mol % 3-hydroxyvalerate (3HV) content, and cheese whey (CW) derived poly(3-hydroxybutyrate-*co*-3-hydroxyvalerate) (PHBV) with 3HV contents of 20 mol % (PHBVCW20), 40 mol % (PHBVCW40), and 60 mol % (PHBVCW60) in terms of: melting temperature (T_m), enthalpy of melting (ΔH_m), crystallization temperature (T_c), enthalpy of crystallization (ΔH_c), cold crystallization temperature (T_{cc}), and cold crystallization enthalpy (ΔH_{cc}).

Biopaper	First heating endotherm		Cooling exotherm		Second heating endotherm			
	T_m (°C)	ΔH_m (J/g)	T_c (°C)	ΔH_c (J/g)	T_{cc} (°C)	ΔH_{cc} (J/g)	T_m (°C)	ΔH_m (J/g)
Commercial PHB*	169.1 ± 0.9[a]	64.1 ± 1.1[a]	110.2 ± 0.9[a]	59.3 ± 2.0[a]	-	-	-	-
Commercial PHBV2	170.0 ± 0.8[a]	79.4 ± 1.5[b]	115.5 ± 0.4[b]	85.1 ± 1.7[b]	-	-	170.7 ± 0.6[a]	89.7 ± 1.0[a]
PHBVCW20	154.2 ± 0.5[b]	71.2 ± 0.3[c]	82.3 ± 1.2[c]	33.1 ± 1.4[c]	69.3 ± 0.2	20.3 ± 0.7	128.0 ± 0.5[b] // 153.8 ± 1.1[c]	49.8 ± 1.5[b]
PHBVCW40	67.7 ± 0.3[c] // 139.3 ± 0.4[d]	67.1 ± 0.8[d]	81.2 ± 0.7[c] // 41.2 ± 0.4[d]	7.2 ± 0.7[d]	-	-	152.6 ± 1.3[c]	6.3 ± 0.3[c]
PHBVCW60	80.6 ± 0.2[e]	39.9 ± 0.6[e]	41.4 ± 0.6[d]	3.6 ± 0.3[e]	-	-	131.0 ± 0.4[d]	1.2 ± 0.1[d]

*Data reported in previous study (Cherpinski et al. 2018).

[a–e] Different letters in the same column indicate a significant difference among the samples ($p < 0.05$). Dashes mean not measured for the case of PHB or thermal transition not unambiguously detected for the rest of samples.

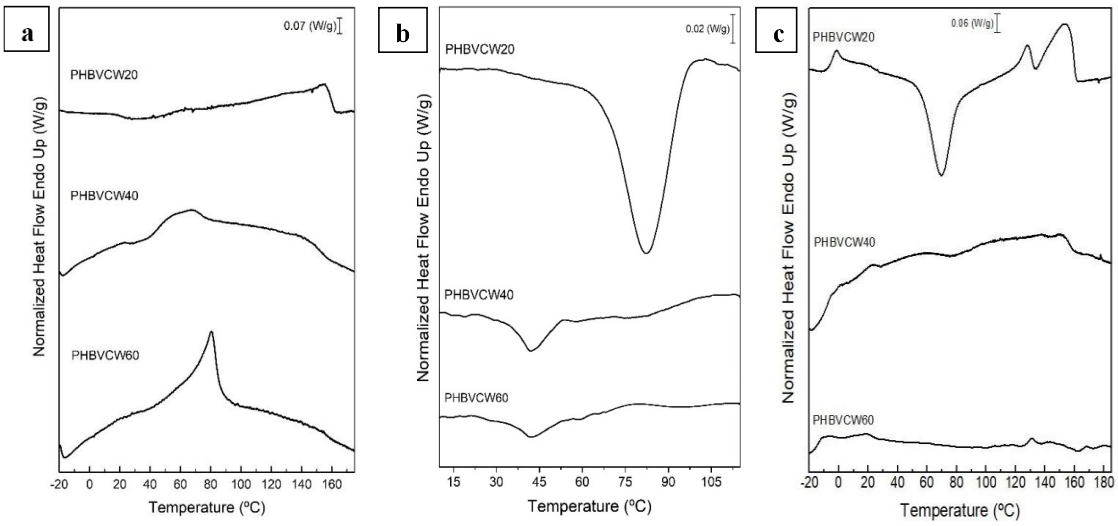

Figure 3. Differential scanning calorimetry (DSC) curves during (a) first heating, (b) cooling, and (c) second heating of the electrospun fiber mats of cheese whey (CW) derived poly(3-hydroxybutyrate-*co*-3-hydroxyvalerate) (PHBV) with 3-hydroxyvalerate (3HV) contents of 20 mol % (PHBVCW20), 40 mol % (PHBVCW40), and 60 mol % (PHBVCW60).

The subsequent cooling and second thermal runs are more related to the inherent crystalline morphology of the materials used. In relation to the cooling step, it can be observed that the PHBV samples with 40 and 60 mol % 3HV contents showed comparatively weaker crystallization events. Thus, the PHBV copolyester with 20 mol % 3HV presented a more intense and sharper peak at 82.3 °C, the PHBV with 40 mol % 3HV showed two weak crystallization events at 81.2 and 41.2 °C, and finally the PHBV sample with 60 mol % one broad and weak peak at 41.4 °C. These observations indicate that increasing the HV content impairs the crystallization process, which then require higher undercooling to peak. Accordingly, the crystallization enthalpies were clearly smaller for the 40 and 60 mol % HV samples. In all cases, as expected, the CW-derived PHBV copolyesters showed significantly lower T_c and crystallization enthalpies than those of the commercial PHBV and PHB (Cherpinski et al. 2018). Although it has been reported that crystallization properties can depend on the heating temperature attained during the first thermal run before crystallization (Di Lorenzo et al. 2009), our previous work (Martínez-Abad et al. 2016) indicated that, for the PHBV2 sample, heating to 200 °C before the cooling run, instead of to 180 °C, did not result in significant changes in T_c and ΔH_c, i.e., 118 °C and 89 J/g, respectively.

The second thermal run tells something about the inherent crystallinity of the biopolyesters once the thermal history of the fibers has been erased. In general, this second run also showed very complex and/or weak endothermic curves. From this, the PHBV copolyester with 20 mol % 3HV showed a cold crystallization peak and two broad endothermic features, being relatively close to one another, the first one centered at 128 °C and the second one at 154 °C. The 40 and 60 mol % 3HV CW-derived PHBV copolyesters presented what appears to be a very weak and rather broad endothermic peaks, with maxima at approximately 153 and 131 °C, respectively. This was expected in light of the very small crystallization enthalpy obtained for these two materials. The thermal data for the second heating run of the commercial PHB was not reported in the reference, whereas that of the PHBV2 showed a single melting peak at ca. 171 °C. Moreover, the PHBV copolyester with 20 mol % 3HV exhibited a very clear cold crystallization peak at ca. 69 °C. From the attempted estimation of the enthalpies of melting, and if we subtract the cold crystallization enthalpy for the case of the 20 mol % 3HV sample, all the CW-derived PHBV copolyesters, especially the 40 and 60 mol % 3HV samples, are expected to exhibit lower crystallinity compared to the PHBV2, and since melting occurred at lower temperatures and in a wider thermal range, a very ill-defined crystalline morphology is inferred.

Regarding the optimal annealing temperatures selected, it seems clear that, due to the complex and broad thermal behaviour of these materials during the first thermal run, the temperatures selected are well within the range in which endothermal events are taking place in the DSC runs, hence guaranteeing enough molecular mobility for the interfiber coalescence process to occur. It is worth noting that the microstructure of the copolyesters used herein was studied together with other PHA materials by nuclear magnetic resonance (NMR) spectroscopy in a previous study (Cheng et al. 2020). It was found out that the 20 mol % sample showed roughly random sequence distributions (indicating approximately equal reactivities for 3HB and 3HV), while the 40 and 60 mol % samples suggested blocky structures due to potential blending of different PHA molecules. The properties of crystallizable random copolymers have been long studied but have been recently reviewed (Pérez-Camargo et al. 2018). In particular, three different cases were reported: (a) total comonomer exclusion from the crystals, which occurs when the chemical repeat units are very different and the crystal lattice of each one of the components cannot tolerate the presence of the other; (b) total comonomer inclusion or isomorphic behavior, case that is obtained when the components can co-crystallize in the entire compositional range (as their chemical structures are

very similar), forming a single crystal structure with different crystalline density; (c) an intermediate and more complex case, where a balance between comonomer inclusion and exclusion occurs, leading to isodimorphic copolymers. The DSC melting behavior observed in these materials is far from pristine, but it may support a pseudo-eutectic point at a composition of 40 mol % 3HV since two melting and crystallization peaks are seen, reflecting the coexistence of two crystalline morphologies (see FTIR and X-ray data later). In this case, to the left of the pseudo-eutectic point, only the PHB-rich phase crystallizes while, to the right, only PHV-rich crystals are formed.

In this context, two crystalline forms have been reported in PHBV copolyesters according to Kunioka et al. (Kunioka, Tamaki, and Doi 1989) These authors studied the crystallinity and thermal properties of PHBV copolyesters from 0 to 95 mol % 3HV, reporting that the PHB crystal lattice is found in bacterial copolyesters with compositions up to 37 mol % 3HV, whereas the poly(3-hydroxyvalerate) (PHV) crystal lattice is formed for compositions from 53 mol % 3HV. Therefore, the transformation from the PHB to PHV crystal lattice seems to occur at approximately 40 mol % 3HV and compositions around this molar ratio are expected to show both crystal lattices. Similar results were reported by Škrbić and Divjaković (Škrbić and Divjaković 1996), who indicated that the PHB crystal lattice is representative of PHBV copolyesters based on up to 37 mol % 3HV. According to all of the above, the presence of a broad melting event peaking at a high temperature, which is the case of the commercial PHB (Cherpinski et al. 2018) and the here-developed CW-derived PHBV with 20 mol % 3HV, could be then assigned to some classical crystal reorganization process upon heating, by which ill-defined crystals of PHB ordered during the endothermic ramp into spherulites with thicker lamellar thicknesses and then melt at higher temperatures (Zhang, Misra, and Mohanty 2014). For the PHBV copolyester with 40 mol % 3HV, the composition at which two crystal lattices coexistence is expected to take place, the lower temperature endothermic event can be ascribed to the melting of the PHV crystals, whereas the peak at higher temperatures can be related to the melting of PHB crystals (Chan et al. 2019). On the other hand, in the case of the PHBV copolyester with 60 mol % 3HV, the single melting event at a lower temperature are due to PHV crystals.

Figure 4 plots the evolution with the 3HV content of the most intense melting peak of the here-developed PHBV obtained by MMCs using CW as the carbon substrate, compared with other PHBV obtained using pure cultures. From the figure, it can be seen that the T_m values, related to crystal size and perfection, showed a non-linear trend, exhibiting a decrease in the melting event with the increase in the 3HV content. As discussed above, this phenomenon is due to the disturbance of the crystallization process caused by the presence of the 3HV comonomer side chains (Bluhm et al. 1986). Savenkova et al. (Savenkova et al. 2000) reported a linear decrease in T_m with increasing 3HV content in the copolymers from 0 to 20 mol %, with a sharper slope above 13 mol %, presenting values from 180 to 123 °C. The authors of this study highlighted that due to the lower melting point and enthalpies of melting of the copolyesters, their processing window can be increased and also their flexibility and transparency, which would help reduce the technical issues faced during the processing and use of the homopolymer PHB. With respect to the samples with higher 3HV contents, the T_m values showed a minimum for the 40 mol % 3HV, followed by an increase for the 60 mol % 3HV. This phenomenon, already detected and discussed above, has been consistently observed and referred as a pseudo-eutectic point, and it has been attributed to the disturbance of crystal packing by the inclusion of 3HV units in the PHB lattice

(Bluhm et al. 1986, Laycock et al. 2014). This minimum in melting point at the pseudo-eutectic point is also linked to a decrease in the overall crystallinity of the sample (Laycock et al. 2014).

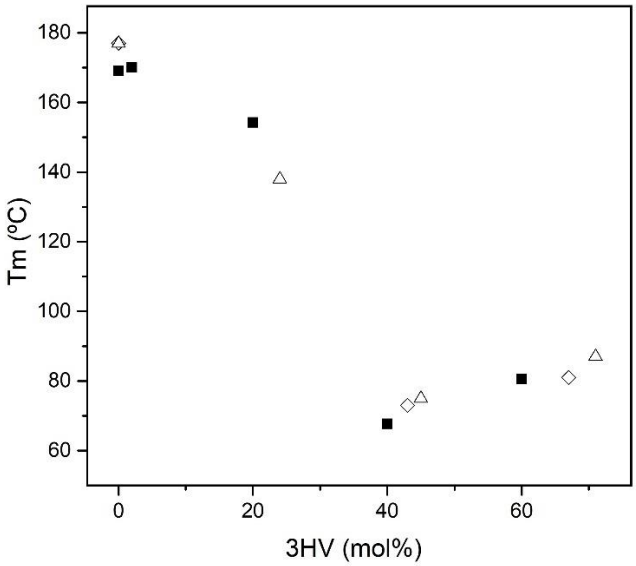

Figure 4. Melting temperature (T_m) as a function of the 3-hydroxyvalerate (3HV) content from mixed microbial cultures (MMCs): ■ electrospun fiber mats of commercial poly(3-hydroxybutyrate-*co*-3-hydroxyvalerate) (PHBV) and cheese whey (CW) derived PHBV. Data for the poly(3-hydroxybutyrate) (PHB) electrospun fiber mats (Cherpinski et al. 2018) and for the PHB and PHBV samples obtained from pure cultures of ◊ *Burkholderia cepacian* (Mitomo et al. 1999) and Δ *Ralstonia eutropha* (Kunioka and Doi 1990) were gathered from previous studies.

It can also be observed that, in comparison with other PHA materials obtained using pure cultures of *Burkholderia cepacian* (Mitomo et al. 1999) and *Ralstonia eutropha* (Kunioka and Doi 1990), the evolution of the T_m values with the 3HV content showed a similar trend, even though a previous study pointed out that PHA obtained from MMCs tended to show lower thermal transition values than those produced by pure cultures (Serafim et al. 2008).

Figure 5 shows the TGA curves of the electrospun PHBV fiber mats to ascertain their thermal stability. **Table 4** gathers the values of the onset degradation temperature (T_{onset}), measured at the temperature corresponding to a mass loss of 5 %, and degradation temperature (T_{deg}) obtained from the TGA curves. It can be observed that variations in the thermal stability of the PHBV copolymers were low but still significant. In particular, T_{onset} ranged between 207 and 228 °C, while T_{deg} occurred between 244 and 261 °C. In all cases, the thermal stability was lower than that of commercial PHBV2. The lower thermal stability as well as differences in the thermal stability within the CW-derived PHBV copolyesters can be ascribed to the presence of residual cations or impurities from the biological source used in the production process of the microbial copolyester (Chan et al. 2019). These values are, however, in agreement with those reported by other previous studies that showed that the thermal decomposition of the microbial copolyester occurred in a single and sharp degradation step from approximately 270 to 280 °C (Singh et al.

2008, Verhoogt et al. 1996). One can also see that a low-intense shoulder was formed at approximately 350 °C, which is due to residual carbonaceous material with higher thermal stability that has also been observed in some previous studies (Muniyasamy et al. 2019, Singh et al. 2021). This mass loss may be related to the thermal degradation of proteins or other impurities as well as degradation products such as crotonic acid (CA) and oligomers with new crotonyl chain ends (Xiang et al. 2016). In this regard, it has been reported that thermal degradation of PHBV is caused by chain scission, via random process, and hydrolysis, resulting in a reduction of the biopolymer's M_W and formation of CA (Bugnicourt et al. 2014, Modi, Koelling, and Vodovotz 2011). Finally, the amount of residual mass was very similar for all the CW-derived PHBV copolyesters, between 0.2 and 0.7 %.

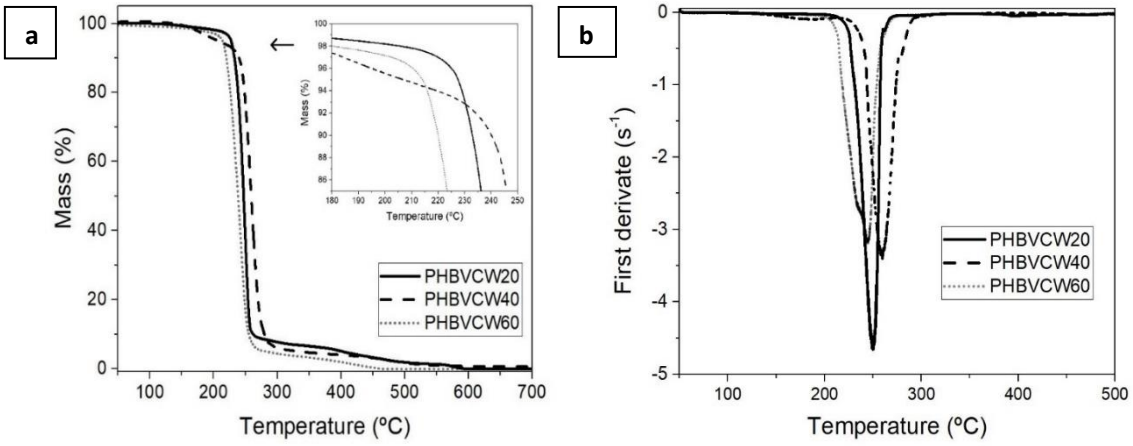

Figure 5. (a) Thermogravimetric analysis (TGA) and (b) first derivative (DTG) curves of the electrospun fiber mats of cheese whey (CW) derived poly(3-hydroxybutyrate-*co*-3-hydroxyvalerate) (PHBV) with 3-hydroxyvalerate (3HV) contents of 20 mol % (PHBVCW20), 40 mol % (PHBVCW40), and 60 mol % (PHBVCW60).

Table 4. Thermal properties of the electrospun fiber mats of commercial poly(3-hydroxybutyrate-*co*-3-hydroxyvalerate) (PHBV) and cheese whey (CW) derived PHBV with 3-hydroxyvalerate (3HV) contents of 20 mol % (PHBVCW20), 40 mol % (PHBVCW40), and 60 mol % (PHBVCW60) in terms of onset degradation temperature (T_{onset}), degradation temperature (T_{deg}), mass loss at T_{deg}, and residual mass at 800 °C.

Biopaper	$T_{5\%}$ (°C)	T_{deg} (°C)	Mass loss at T_{deg} (%)	Residual mass (%)
Commercial PHBV2	271.0 ± 1.4^{a}	296.5 ± 1.2^{a}	80.8 ± 0.7^{a}	1.6 ± 0.2^{a}
PHBVCW20	227.5 ± 0.8^{b}	249.8 ± 0.7^{b}	61.4 ± 1.1^{b}	$0.4 \pm 0.1^{b,c}$
PHBVCW40	206.8 ± 1.1^{c}	260.8 ± 0.5^{c}	55.6 ± 1.3^{c}	0.7 ± 0.2^{b}
PHBVCW60	214.1 ± 0.9^{d}	244.1 ± 0.4^{d}	67.4 ± 1.8^{d}	0.2 ± 0.1^{c}

[a–d] Different letters in the same column indicate a significant difference among the samples ($p < 0.05$).

3.4. Crystalline Morphology Evolution with Temperature

Figure 6 shows the ATR-FTIR spectra of the electrospun CW-derived PHBV fibers. In the FTIR spectra of the PHBV copolyesters taken at room temperature, shown in **Figure 6a**, the strongest peak observed at nearly 1720 cm^{-1} is assigned to the conformationally sensitive stretching vibration of the carbonyl group (C=O) (Guo et al. 2010). **Figure 6b** shows the spectral zoom of this band normalized in intensity. From this figure, it can be seen that there is a clear broadening toward higher wavenumbers of the band for the samples with 40 and 60 % 3HV content, ascribed to reduced molecular order compared to the 20 mol % 3HV sample, due to an increased multiplicity of coexisting molecular conformations along the polymer backbone. The complex and multiple peaks in the region from 1000 to 880 cm^{-1} arise from the stretching vibrational modes of the C−C bond (Torres-Giner et al. 2016). The band placed at 1080 cm^{-1} is assigned to the ester bonds of PHBV, whereas the stretching vibrations of ester groups corresponding to C−O and C−O−C can be seen at 1020 cm^{-1} (Torres-Giner et al. 2011). The bands from 1226 to 1276 cm^{-1} are linked to single C−O−C stretching vibration, the peaks at 1175 cm^{-1} are assigned to asymmetric stretching of C−O−C, and the peak at 1379 cm^{-1} is associated to the symmetric wagging of the methyl groups (Cherpinski et al. 2017). **Figure 6c** zooms the main spectral differences among the PHBV materials in the 1100−1350 cm^{-1} range, after normalization to the intensity of the 1720 cm^{-1} band. The observed changes in the bands linked to the single −C−O−C stretching vibration of PHBV are thought to result from the different composition and molecular order along the polymer backbone. In particular, the peak centered at ca. 1260 cm^{-1} was seen to rise with increasing 3HV content, whereas the intensity of the band at ca. 1276 cm^{-1} was reduced, and the one at ca. 1227 cm^{-1} vanished. Furthermore, the band at 1175 cm^{-1} that is assigned to asymmetric stretching of C−O−C was seen to increase the intensity and broaden for the samples with 40 and 60 mol %. The highest intensity rise for the latter band was seen for the 40 mol % 3HV sample. Overall, it could be interpreted that the fiber mats with a higher segmental molecular order along the polymer backbone corresponded to the 20 mol % 3HV sample, then the 60 mol %, and the least ordered but more similar to the latter is the 40 mol % sample. As discussed above, vibrational spectroscopy is sensitive to molecular conformational order along the polymer backbone, necessarily within crystals but not only, since the technique is in general not sensitive to the lateral order required to yield crystals.

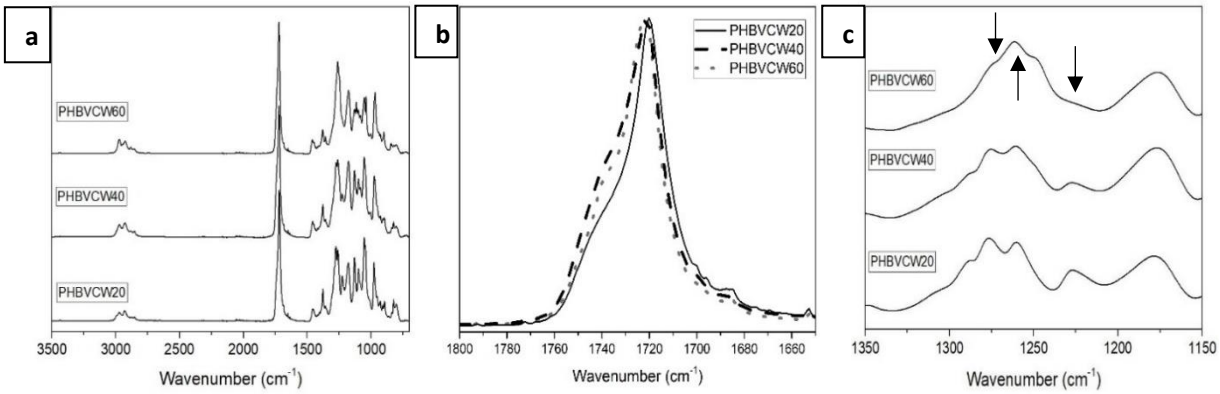

Figure 6. (a) ATR-FTIR spectra of the electrospun fibers of cheese whey (CW) derived poly(3-hydroxybutyrate-*co*-3-hydroxyvalerate) (PHBV) with 3-hydroxyvalerate (3HV) contents of 20 mol %, 40 mol % and 60 mol %. (b) ATR-FTIR spectra zoomed around the band at 1720 cm^{-1}. (c) ATR-FTIR spectra zoomed in the wavenumber range 1150−1350 cm^{-1}.

Figure 7 shows the evolution of the carbonyl band envelop at 1720 cm^{-1} during heating to ascertain the changes in molecular conformation along the biopolymer backbone unleashed by thermal activation. The analysis of the 1720 cm^{-1} sharp band has been used before to follow alterations in molecular order in PHAs (Melendez-Rodriguez et al. 2018, Melendez-Rodriguez et al. 2020). In the case of the CW-derived PHBV copolyester with 20 mol % 3HV, it can be seen that the electrospun fibers presented a continuous increase in the intensity of the carbonyl band at 1720 cm^{-1} until about 70 °C, suggesting classic thermally induced crystallinity development (Melendez-Rodriguez et al. 2020). This was followed by a continuous intensity drop until complete disappearance, associated to a progressive decreased in molecular order, ascribed first to the melting of small/defective crystals and, later, to the most robust crystallinity. The band decrease is accompanied by further broadening of the higher wavenumber broad contribution associated to disordered chain segments. Interestingly, upon melting, this broad band envelop, associated to a multiplicity of "gauge" molecular conformations, appears to show two components, suggesting that there is a bimodal distribution of disordered molecules in the material. The selected annealing temperature at 120 °C falls then within the regime where the material progressively decreases molecular order. The FTIR data suggest for this copolyester the existence or coexistence of two competing mechanisms during the thermal run, whereby initial heating perfects the molecular order of very ill-defined crystals, giving rise to the overall molecular order, and subsequent heating melts away, even before the T_m, some of the crystallinity. For the CW-derived copolyester with 40 mol %, it can be observed that the intensity of this band increased molecular order initially until nearly 50 °C, then, as per the previous samples, it began to progressively decrease intensity until it disappeared, leaving again a broad feature with two apparent components. In the case of the electrospun fibers of PHBV with 60 mol %, the band progressively increased intensity up to approximately 50 °C and, then, it decreased in a similar fashion as for the other two samples but disappearing at a lower temperature. The observations suggest that, for all the samples, there is an initial temperature regime, which is clearly milder for the 40 mol % 3HV sample, in which thermally activated molecular order seems to dominate at the molecular level. The described behavior depicts a very complex and dynamic crystalline phase structure development for the electrospun fibers of these copolymers, as earlier suggested by DSC analysis. In any case, it appears that the mechanism of interfiber coalescence during the selected annealing temperatures seems to be more largely dominated in these samples by molecular disorder, associated to early melting of some of the defective crystallinity. This is in contrast to a previous work carried out in a municipal waste-derived PHBV with 10 mol % 3HV material, where the mechanism of interfiber coalescence was clearly related to thermally induced molecular order (Melendez-Rodriguez et al. 2020).

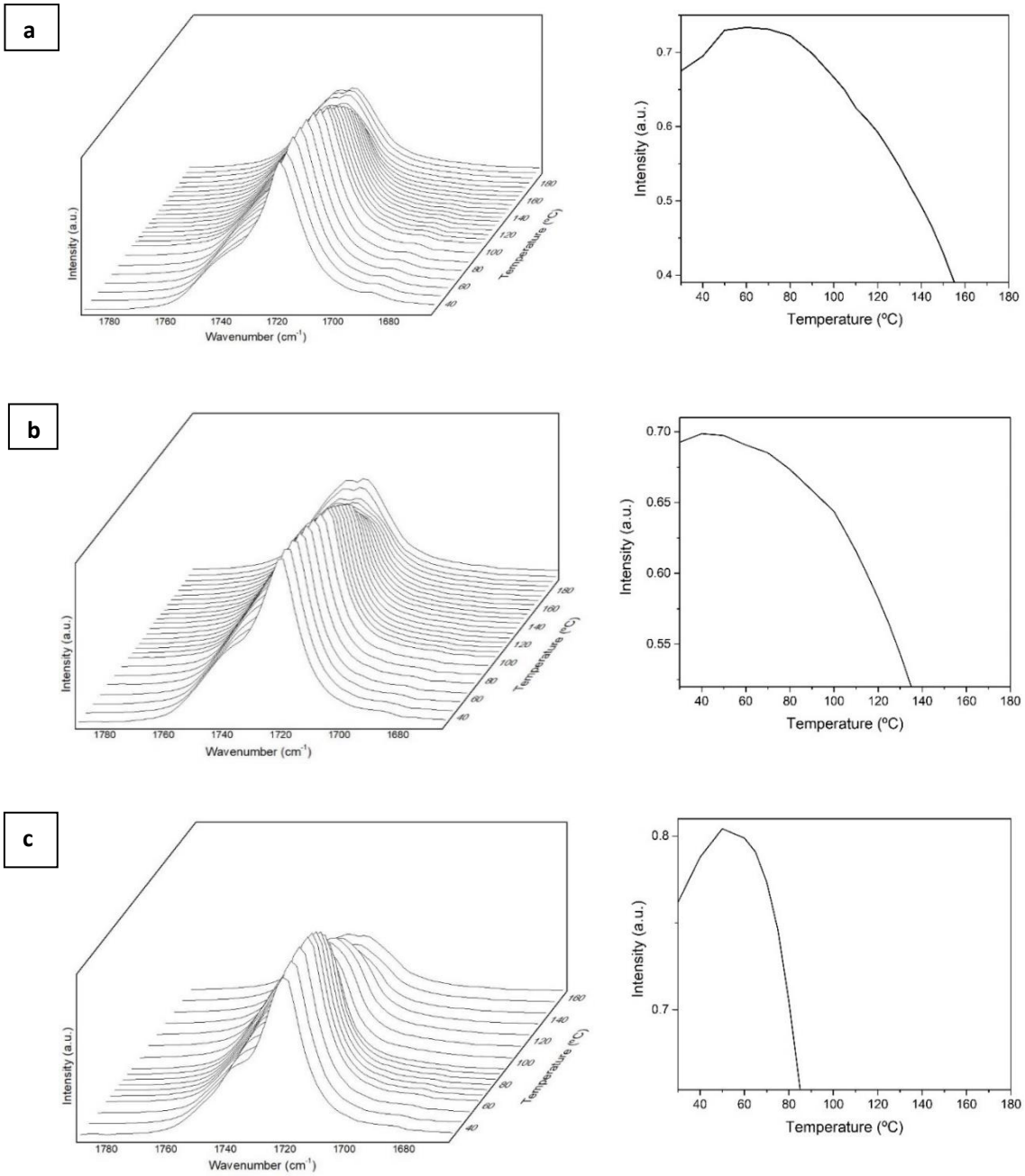

Figure 7. ATR-FTIR spectra taken during heating and zoomed in the C=O stretching vibrational range (left) and evolution with temperature of the intensity of the sharp peak at approximately 1720 cm^{-1} (right) of the electrospun fibers of cheese whey (CW) derived poly(3-hydroxybutyrate-*co*-3-hydroxyvalerate) (PHBV) with 3-hydroxyvalerate (3HV) contents of: (a) 20 mol %; (b) 40 mol %; and (c) 60 mol %.

In addition to the FTIR spectroscopy measurements, conventional room temperature WAXS experiments for the three samples and simultaneous time-resolved SAXS and WAXS experiments as a function of temperature using synchrotron radiation for the 20 and 40 mol % 3HV samples were also carried out in order to further ascertain the crystallinity and phase morphology of the electrospun CW-derived PHBV fibers. **Figure 8** shows the conventional room temperature

WAXS diffractograms of the fiber mats of the tree samples in the 2θ range from 5 to 32°. PHBV copolymers are known to present, as discussed above, isodimorphism, in which the crystalline structure is that of the pure PHB homopolymer for low 3HV contents and that of the pure PHV for high 3HV contents (Bluhm et al. 1986). With respect to the crystalline systems of the materials, both PHB and PHV crystalline lattices are orthorhombic with a space group $P2_12_12_1$ (D^2_4) (Marchessault et al. 1984, Yokouchi et al. 1973). The diffractogram of the copolymer sample with 20 mol % 3HV showed a clear PHB-like lattice where the most representative peaks are labeled in **Figure 8**. The peak at 13.5° 2θ corresponds to the (020) diffraction, the peak at 17° 2θ to the (110) diffraction, and the one at 25° 2θ to the (121) diffraction. On the other hand, the diffractogram of the PHBVCW60 exhibited a PHV-like pattern with major characteristic diffraction peaks (110), (020), and (111) at 13, 18, and 20° 2θ, respectively.

With respect to the sample containing 40 mol % HV, the diffractogram clearly shows the co-existence of mixed crystalline structures, where both PHB- and PHV-lattice crystals are present.

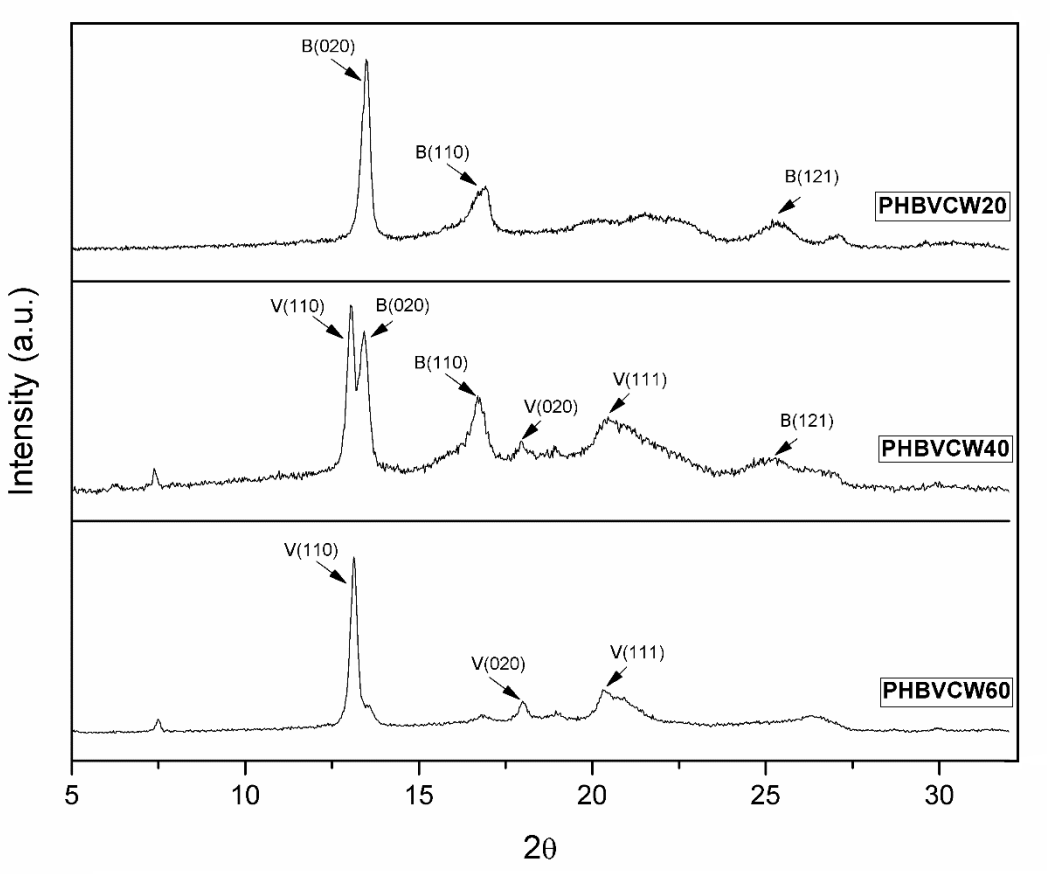

Figure 8. Wide angle X-ray diffraction (WAXD) patterns of the electrospun fibers of cheese whey (CW) derived poly(3-hydroxybutyrate-*co*-3-hydroxyvalerate) (PHBV) with 3-hydroxyvalerate (3HV) contents of 20 mol % (PHBVCW20), 40 mol % (PHBVCW40), and 60 mol % (PHBVCW60). The indexed diffraction peaks are labeled B(*h k l*) or V(*h k l*) for the poly(3-hydroxybutyrate (PHB) and poly(3-hydroxyvalerate) (PHV) lattices, respectively.

Unit cell parameters for both crystal lattices were estimated in the three CW PHBV samples from the above-mentioned three characteristic peaks using the quadratic form for their rhombic cell, and the results are gathered in **Table 5**. From this, it can be seen that, for the PHB lattice, *a* and *b* unit cell parameters increased slightly, whereas *c* decreased also slightly with increasing 3HV content. On the other hand, for the PHV lattice, *a* and *b* parameters were seen to decrease compared to the literature value for the pure PBV homopolymer crystal, whereas *c* is seen to increase. However, from 60 to 40 mol % in 3HV content, *a* and *b* were seen to increase slightly and *c* to decrease. It has been reported that the reduction in lattice parameters with reducing 3HV content in the PHV crystal was smaller than the increase in lattice parameters with increasing 3HV content in the PHB crystal (Scandola et al. 1992), but in the results presented here, there appears to be even an increase. **Table 5** also gathers the degree of crystallinity as obtained from the diffractograms in **Figure 8**. From this, a higher degree of crystallinity was seen for the PHB homopolymer and the lowest for the pseudo-eutectic composition. This does actually agree with results reported by Wang et al. (Wang et al. 2001), who also discussed the existence of a pseudo-eutectic point in a similar composition regime and exhibiting the lowest crystallinity. The FTIR experiments also suggested this sample as the one with the lowest molecular order, however very close to the 60 mol % 3HV content sample.

Table 5. Unit cell parameters *a*, *b*, and *c* of the poly(3-hydroxybutyrate (PHB)-type and poly(3-hydroxyvalerate) (PHV)-type crystalline lattices and percentage of crystallinity of the electrospun fibers of cheese whey (CW) derived poly(3-hydroxybutyrate-*co*-3-hydroxyvalerate) (PHBV) with 3-hydroxyvalerate (3HV) contents of 20 mol % (PHBVCW20), 40 mol % (PHBVCW40), and 60 mol % (PHBVCW60).

	PHB-like lattice (Å)			**PHV-like lattice (Å)**			**Crystallinity**
	a	*b*	*c*	*a*	*b*	*c*	%
PHB*	5.73	13.15	5.96	-	-	-	73
PHBVCW20	5.75	13.14	5.94	-	-	-	45
PHBVCW40	5.78	13.18	5.90	9.35	9.86	5.61	37
PHBVCW60	-	-	-	9.25	9.85	5.72	47
PHV*	-	-	-	9.52	10.08	5.56	-

*Taken from Reference 8 (Scandola et al. 1992).

Synchrotron radiation is also suitable to assess crystallinity, crystalline morphology, and the phase structure at the mesoscale in semicrystalline polymers (Riekel et al. 2003). **Figure 9** displays the simultaneous SAXS and WAXS diffractograms of the electrospun fibers of PHBV with 20 mol % 3HV during the heating ramp from 0 to 180 °C. The SAXS results indicated that, with increasing temperature, the SAXS peak increased intensity and shifted toward lower angles, as is typically the case in semicrystalline polymers, suggesting that the repeat unit increased before melting. **Figure 9** does also plot the evolution with temperature of the WAXD patterns, in which the most characteristic peaks of the PHB crystal were seen at 2θ values of 8.8 and 11°. These peaks correspond to the (020) and (110) diffractions, respectively, which arise from the lattice planes of the orthorhombic unit cells of the PHB crystals (Sato et al. 2012). In addition to these peaks, three minor reflections were also displayed at values of 2θ of approximately 13.5, 16, and

17.1°, which originate from the (021), (111), and (121) lattice planes, respectively (Panaitescu et al. 2017, Vahabi et al. 2019).

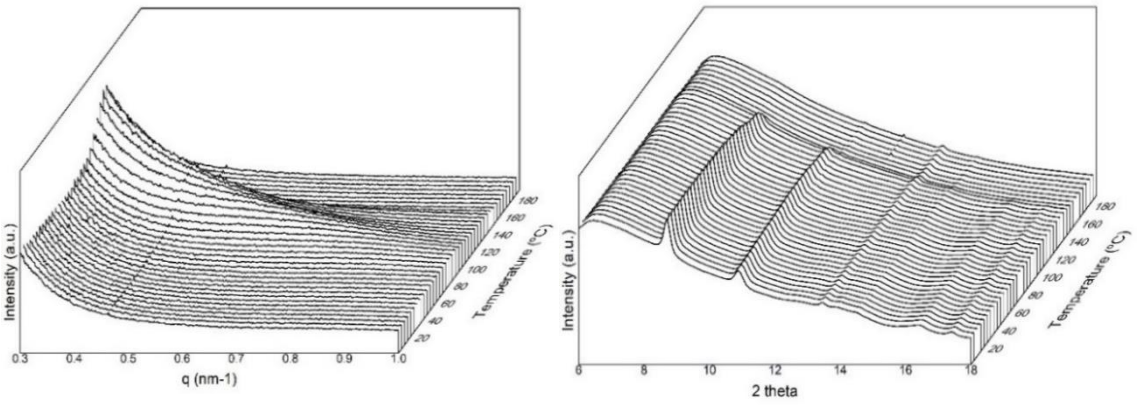

Figure 9. Small angle X-ray scattering (SAXS) (left) and wide-angle X-ray scattering (WAXS) (right) patterns evolution of the electrospun cheese whey (CW) derived poly(3-hydroxybutyrate-*co*-3-hydroxyvalerate) (PHBV) fibers with 20 mol % 3-hydroxyvalerate (3HV) taken during the heating ramp from 0 to 180 °C.

Figure 10 presents a close up of the evolution of the (110) plane peak during the heating ramp from 0 to 180 °C. From this figure, and just paying attention to the diffraction peak intensity, it can be observed that the peak increased up to about 60 °C, then it began to decrease slightly until around 100 °C, only to decrease more pronouncedly until approximately 140 °C, beyond which it suffered from a sharp intensity drop associated with complete melting. These observations are in good agreement with the above temperature evolving FTIR experiments. The down slope with increasing sample temperature, ascribed to molecular disorder, seems to be more abrupt and continuous in the FTIR data, perhaps suggesting that there is order at the molecular scale that disappears at a faster pace than the crystallinity. This is the main difference between the two techniques. Whereas the FTIR data is sensitive to ordered chain segments along the polymer backbone, not necessarily inside crystals or with lateral order, WAXS is sensitive to molecular lateral order, that is, to crystallinity. Thus, for this material, the mechanism of interfiber coalescence is confirmed to be dominated by the overall molecular disorder and early melting of some ill-defined crystals, effects that appeared sufficiently intense at the selected annealing temperature of 120 °C as stated before.

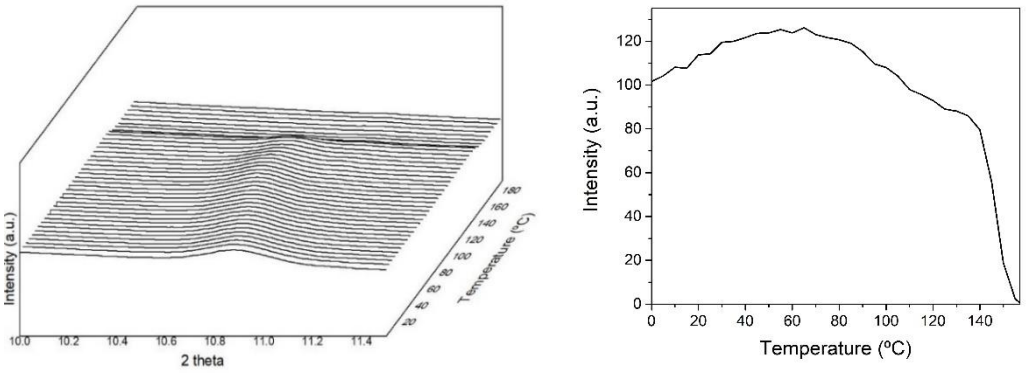

Figure 10. Wide angle X-ray scattering (WAXS) patterns zoomed around the 2θ 11° peak of the electrospun cheese whey (CW) derived poly(3-hydroxybutyrate-*co*-3-hydroxyvalerate) (PHBV) fibers mat with 20 mol % 3-hydroxyvalerate (3HV) for the heating ramp shown in **Figure 9**. The right plots quantify the evolution in relative intensity of the 2θ 11° peak seen in the left diffractogram.

Similarly, **Figure 11** plots the SAXS and WAXD diffractograms of the electrospun fibers for the PHBV copolyester with 40 mol % 3HV during the heating ramp from 0 to 180 °C. For this electrospun fibers mat, it can be seen an intensity increase in the SAXS patterns and a concomitant shift toward lower scattering angles, in the ranges above 50 and 130 °C, due to the long period increases associated with longer repeat units created before melting of the PHV and PHB crystals, respectively. In the WAXS diffractograms shown in **Figure 11**, one can observe that the strong peak centered at 2θ 8.3° as well as the low-intensity peaks at 2θ values of nearly 12 and 13°, increased intensity and then dropped drastically until they vanished at around 75 °C. These peaks have been ascribed to the (110), (002), and (211) lattice planes of the PHV crystals (Kunioka, Tamaki, and Doi 1989, Mitomo, Morishita, and Doi 1993). On the other hand, the peaks at 2θ values of 8.6 and 11°, corresponding to the (020) and (110) diffraction planes of the PHB crystal, were seen to disappear at around 160 °C.

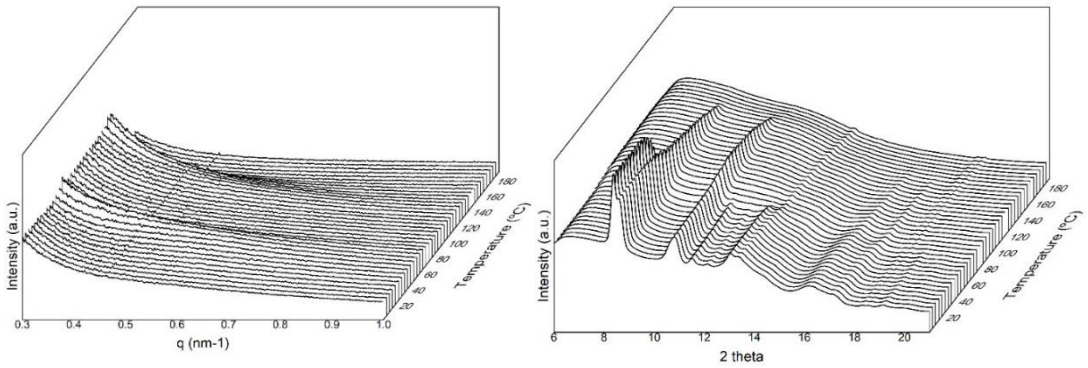

Figure 11. Small angle X-ray scattering (SAXS) (left) and wide-angle X-ray scattering (WAXS) (right) patterns evolution of the electrospun cheese whey (CW) derived poly(3-hydroxybutyrate-*co*-3-hydroxyvalerate) (PHBV) fibers mat with 40 mol % 3-hydroxyvalerate (3HV) taken during the heating ramp from 0 to 180 °C.

The evolution in intensity with temperature of the peaks centered at 2θ 8.3 and 8.6° peaks, ascribed to the (110) and (020) planes for PHV and PHB crystals, respectively, and at 2θ 11° peak of the (110) plane for PHB crystals, is presented in **Figure 12**. From this figure, it can be seen that the peak corresponding to the PHV crystals increased intensity until approximately 50 °C, then it sharply decreased to vanish at around 70 °C. On the other hand, the peak of the PHB crystals at approximately 8.6° decreased intensity with an initial very swallow slope, then at a faster slope until 80 °C, then faster until around 120 °C, and finally even more so until complete disappearance by melting. **Figure 12** also shows the evolution of the (110) plane of the PHB crystals, which are in better agreement with the FTIR data. This diffraction peak showed an initial increase in intensity until around 70 °C, then it began to drop intensity progressively until its full disappearance by melting. The reason why the peak (020) of the PHB crystals does not show an initial increase as does the (110) peak, but rather a very shallow decrease, is probably related to the fact that that the intensity of these two close planes will be influencing each other as one crystalline phase melts earlier, dragging the overall intensity of the two peaks envelop. The selected annealing temperature for this material is then in the regime in which the PHV crystals are melting entirely, while simultaneously the PHB crystals are being perfected. These two effects can be nicely discriminated in the synchrotron experiments but are averaged in the FTIR assays, hence the shallower initial intensity rise for the 1720 cm^{-1} band of this material in **Figure 7**.

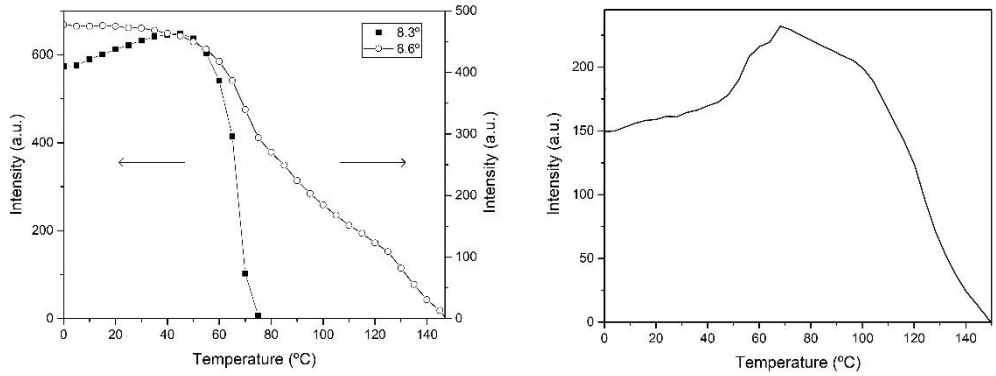

Figure 12. Evolution in intensity of the 2θ 8.3 and 8.6° peaks (left) and 2θ 11° peak (right) of the electrospun cheese whey (CW) derived poly(3-hydroxybutyrate-*co*-3-hydroxyvalerate) (PHBV) fibers with 40 mol % 3-hydroxyvalerate (3HV) for the heating ramp of the wide-angle X-ray scattering (WAXS) patterns shown in **Figure 11**.

3.5. Mechanical Properties

The most representative tensile stress−strain curves obtained at room temperature for the PHBV biopapers are gathered in **Figure 13**. **Table 6** displays the values of elastic modulus (E), tensile strength at yield (σ_y), elongation at break (ε_b), and toughness (T) obtained from the tensile curves. In general, the electrospun CW-derived PHBV biopapers presented a relative low E, in the range of 700−400 MPa, decreasing in general with increasing 3HV content, the exception being the 40 mol % sample. The three CW-derived PHBV biopapers showed lower E values than the counterpart biopaper prepared with commercial PHBV2 due to the lower 3HV content of the

latter, that is, 1252 MPa (Melendez-Rodriguez et al. 2019). Similar values of σy were observed for the electrospun biopapers of PHBV copolyesters with 20 and 40 mol % 3HV, showing values of 12.4 and 12.2 MPa, respectively, whereas the sample of PHBV copolyester with 60 mol % 3HV showed a lower value of 8.4 MPa, being all mechanically less resistant than the commercial PHBV2 biopaper. In particular, the electrospun biopapers of PHBV with 40 and 60 mol % content yielded a ε_b value of 18.3 % and 14.3 %, respectively, which is nearly 8 and 6 times higher than that of the commercial PHBV2 biopaper. The electrospun CW-derived PHBV biopapers were also tougher than the commercial PHBV2 biopaper due to the fact that these samples were significantly more flexible, and thus, they absorb more energy before fracture. Interestingly, the highest ductility and toughness were found for the electrospun biopaper of PHBV copolyester with 40 mol % 3HV, most likely due to the fact that it shows the lowest molecular order and crystallinity, as discussed above.

Table 6. Mechanical properties of the electrospun biopapers of commercial and cheese whey (CW) derived poly(3-hydroxybutyrate-*co*-3-hydroxyvalerate) (PHBV) with 3-hydroxyvalerate (3HV) contents of 20 mol % (PHBVCW20), 40 mol % (PHBVCW40), and 60 mol % (PHBVCW60) in terms of tensile modulus (E), tensile strength at yield (σ_y), elongation at break (ε_b), and toughness (T).

Biopaper	E (MPa)	σ_y (MPa)	ε_b (%)	T (mJ/m^3)
Commercial PHBV2*	1252 ± 79^a	18.1 ± 2.1^a	2.4 ± 0.3^a	0.3 ± 0.1^a
PHBVCW20	714 ± 92^b	12.4 ± 0.9^b	10.5 ± 2.1^b	0.8 ± 0.1^b
PHBVCW40	728 ± 83^b	12.2 ± 1.2^b	18.3 ± 2.7^c	1.6 ± 0.3^c
PHBVCW60	402 ± 97^c	8.4 ± 1.8^c	14.3 ± 4.0^{b,c}	0.9 ± 0.2^b

*Data reported in a previous study (Melendez-Rodriguez et al. 2019).

$^{a\text{-}c}$ Different letters in the same column indicate a significant difference among the samples ($p < 0.05$).

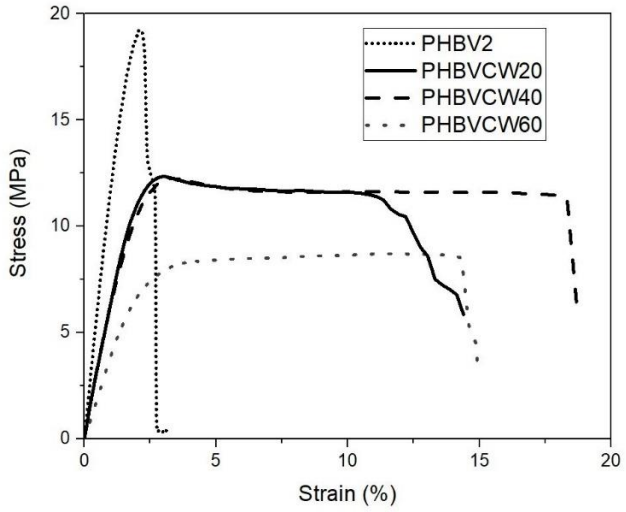

Figure 13. Tensile stress–strain curves of the electrospun biopapers of cheese whey (CW) derived poly(3-hydroxybutyrate-*co*-3-hydroxyvalerate) (PHBV) with 3-hydroxyvalerate (3HV) contents of 20 mol % (PHBVCW20), 40 mol % (PHBVCW40), and 60 mol % (PHBVCW60) and commercial PHBV2 (Melendez-Rodriguez et al. 2019).

The improvement in mechanical ductility with the 3HV content increase was expected, and it has been previously reported (Bohlmann 2005, Luzier 1992). The main factor contributing to this mechanical ductility enhancement is the known reduced crystallinity of PHBV copolyesters with high 3HV contents. Previously developed electrospun biopapers of PHBV copolyesters derived from different biowastes showed a similar trend in the mechanical response. For instance, a biopaper of PHBV with 20 mol % 3HV derived from juice fruit by-products showed values of E, σ_y, and ε_b, and T of 434 MPa, 7.1 MPa, 2.9 %, and 0.4 mJ/m^3 (Melendez-Rodriguez et al. 2018). In another work, biopapers of PHBV with 10 mol % 3HV obtained from municipal biowaste (MBW) feedstocks showed values of 1583 MPa, 13.6 MPa, 1.3 %, and 0.1 mJ/m^3, respectively (Melendez-Rodriguez et al. 2020). Differences in the mechanical properties among the biopapers of PHBV copolyesters with different 3HV contents can also be related to differences in the macro- and mesoscale morphologies of the films prepared by electrospinning and subsequent annealing (Alp-Erbay et al. 2019). A similar trend can also be observed when compared with PHBV films prepared by other techniques. For instance, Chan et al. (Chan et al. 2019) showed that cast-extruded films of PHBV copolyester with 24 mol % 3HV presented higher ductility but lower mechanical strength when compared to PHBV copolyester with 1 mol % 3HV. Furthermore, the tensile strength decreased further when the 3HV content increased to 63 mol %, showing a similar value of E but lower ε_b when compared to that of PHBV 24 mol % 3HV. Therefore, by right selection of the 3HV content, the PHBV copolymers can target the properties of conventional plastics such as PP (low 3HV content) or low-density polyethylene (LDPE, high 3HV content) in terms of mechanical performance (Modi, Koelling, and Vodovotz 2011).

3.6. Barrier Properties

The WVP, LP, and OP values of the electrospun PHBV biopapers are gathered in the bar graphs of **Figure 14**. In the case of WVP, the electrospun CW-derived PHBV biopapers presented a WVP in the range of (0.7–0.8) × 10^{-14} kg·m·m^{-2}·Pa^{-1}·s^{-1}, showing no significant differences among the PHBV copolyesters. It is very interesting to observe that the permeability to water, which is mostly driven by diffusion in PHAs since they are hydrophobic (Razumovskii et al. 1994), was lower than that of its commercial counterpart with the lowest HV content sample. The water uptake of PHA is known to be very low, i.e., around or below 0.6 % (Gallardo-Cervantes et al. 2021), albeit the determination of the water solubility for the materials was attempted from the quasi-isostatic permeation curves measured, using the time lag method (Gavara et al. 1996), the materials showed no lag, passing all the samples by the origin, hence confirming that there would be hardly no detectable differences in solubility among the samples, and that the permeability is driven by diffusivity across the free volume left by the post-processing step. The barrier properties to water vapor of the materials prepared in this study are similar to those reported for biopapers of the homopolymer PHB, which reported values of WPV of 0.5 × 10^{-14} kg·m·m^{-2}·Pa^{-1}·s^{-1} (Cherpinski et al. 2017). The latter study by Cherpinski et al. (Cherpinski et al. 2017) showed that, depending on the annealing conditions and the interfiber coalescence morphology attained, very different barrier results can be obtained. In the case of PHBV derived from fruit pulp biowaste and with 20 mol % 3HV, its annealed electrospun film showed WVP values, depending on the purification methodology, ranging from (0.5 to 3.3) × 10^{-14} kg·m·m^{-2}·Pa^{-1}·s^{-1} (Melendez-Rodriguez et al. 2018). Therefore, the different barrier values measured across different biopapers are thus related to the material, the purification procedure, and more importantly to a more or less efficient interfiber packing during the post-processing step.

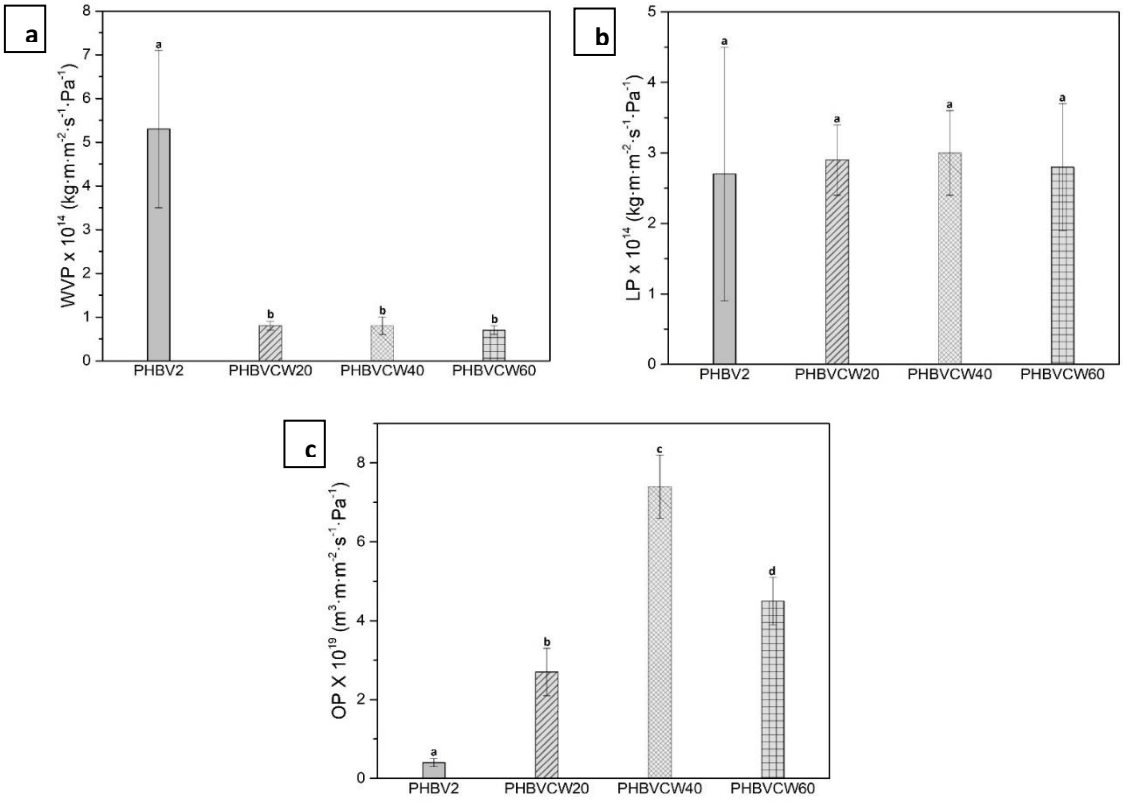

Figure 14. Permeabilities to (a) water vapor (WVP), (b) D-limonene (LP), and (c) oxygen (OP) for the electrospun biopapers of cheese whey (CW) derived poly(3-hydroxybutyrate-*co*-3-hydroxyvalerate) (PHBV) with 3-hydroxyvalerate (3HV) contents of 20 mol % (PHBVCW20), 40 mol % (PHBVCW40), and 60 mol % (PHBVCW60) and commercial PHBV2 (Melendez-Rodriguez et al. 2020).

In regard to LP, which is usually used as a standard system to test aroma barrier, it is known, as opposed to moisture, to be a strong plasticizer for PHA materials, hence solubility-driven (Sanchez-Garcia, Gimenez, and Lagaron 2007). All the CW-derived PHBV biopapers, including the commercial sample, showed again very similar values of LP, around 3.0×10^{-14} $kg \cdot m \cdot m^{-2} \cdot Pa^{-1} \cdot s^{-1}$, which can be ascribed to a strong limonene sorption-driven permeability mechanism for the copolyesters. Lower permeability should perhaps have been expected for the commercial PHBV biopaper, but since this sample may have comparatively lower interfiber packing efficiency, as suggested also by the water permeability results, the potential higher barrier effect could have been diminished.

The case of oxygen is also different since this is a very small non-condensable non-interactive gas molecule and the morphology at the mesoscale and below is expected to play a more relevant role. Hence, it can be observed that the highest barrier effect was attained for the commercial PHBV2 biopaper since this is the most crystalline and molecular ordered material. The second lowest OP value was observed for the electrospun biopaper of PHBV copolyester with 20 mol % 3HV, having a value at 2.7×10^{-19} $m^3 \cdot m \cdot m^{-2} \cdot Pa^{-1} \cdot s^{-1}$, while the biopapers of PHBV copolyesters with 40 and 60 mol % 3HV presented values of 7.4×10^{-19} $m^3 \cdot m \cdot m^{-2} \cdot Pa^{-1} \cdot s^{-1}$ and 4.5×10^{-19} $m^3 \cdot m \cdot m^{-2} \cdot Pa^{-1} \cdot s^{-1}$, respectively. Thus, the biopaper with the highest flexibility and lowest WAXS crystallinity and molecular order, that is, the 40 mol % 3HV sample, also showed the highest

permeability, suggesting highest free volume and hence lowest tortuosity. Again, interfiber packing differences after annealing may also have an effect on reducing potential bigger differences among the samples in comparison with the commercial PHBV.

Overall, the WVP, LP, and OP values of the here-prepared electrospun PHBV biopapers are within the range of those reported for cast-extruded films of commercial PHBV with 2 mol % 3HV, which showed values of 0.18×10^{-14} kg·m·m^{-2}·Pa^{-1}·s^{-1}, 1.03×10^{-14} kg·m·m^{-2}·Pa^{-1}·s^{-1}, and 2.10×10^{-19} m^3·m·m^{-2}·Pa^{-1}·s^{-1}, respectively (Quiles-Carrillo et al. 2019).

4. Conclusions

Three PHBV copolyesters with different 3HV contents, that is, 20, 40, and 60 mol %, were successfully produced at a pilot plant scale using the technology of MMCs fed with CW, a by-product of the dairy industry. The food waste-derived PHBV copolyesters were purified and processed by electrospinning to produce mats of fibers sizing 2 μm in cross-section. The resultant electrospun mats were, thereafter, thermally post-treated below their melting point to form continuous films composed of coalesced fibers, so-called biopapers, selecting different temperatures depending on their 3HV content, namely, 120, 60, and 70 °C for the 20, 40, and 60 mol %, respectively. The biopapers showed high transparency but a slight yellow color. The crystalline morphology and content were assessed by WAXS, yielding the lowest crystallinity for the pseudo-eutectic composition at the 40 mol % 3HV content sample. Variable-temperature experiments by both ATR-FTIR spectroscopy and combined WAXS and SAXS synchrotron experiments suggested, as the interfiber coalescence mechanism for the three materials, a temperature-induced molecular disorder. The CW-derived PHBV materials remained stable up to values in the 207−228 °C range, whereas the maximum of degradation occurred in the range of 244−261 °C. In terms of mechanical performance, the ductility and toughness of the biopapers increased significantly with the 3HV content. In particular, the ε_b value of the electrospun biopapers of PHBV increased from 2.4 %, for the commercial PHBV, up to 18.3 %, in the case of the PHBV copolyester with 40 mol %. In addition, the here-produced CW-derived PHBV biopapers showed good barrier properties to water and limonene vapors and oxygen, in the range found for cast-extruded films of commercial PHBV with very low 3HV content. Overall, the materials developed herein exhibit great value to constitute potential cost-effective Circular Bioeconomy biowaste-derived food biopackaging constituents in the form of interlayers or coatings.

5. References

Abdalkarim, S. Y. H., Y. Wang, H. Y. Yu, Z. Ouyang, R. A. M. Asad, M. Mu, Y. Lu, J. Yao, and L. Zhang. 2020. "Supermagnetic cellulose nanocrystal hybrids reinforced PHBV nanocomposites with high sensitivity to intelligently detect water vapor." *Industrial Crops and Products* 154. doi: 10.1016/j.indcrop.2020.112704.

Albuquerque, M. G. E., C. A. V. Torres, and M. A. M. Reis. 2010. "Polyhydroxyalkanoate (PHA) production by a mixed microbial culture using sugar molasses: Effect of the influent substrate concentration on culture selection." *Water Research* 44 (11):3419-3433. doi: 10.1016/j.watres.2010.03.021.

Alp-Erbay, Esen, Kelly J. Figueroa-Lopez, José M. Lagaron, Emre Çağlak, and Sergio Torres-Giner. 2019. "The impact of electrospun films of poly(ε-caprolactone) filled with nanostructured zeolite and silica microparticles on in vitro histamine formation by Staphylococcus aureus and Salmonella Paratyphi A." *Food Packaging and Shelf Life* 22:100414. doi: https://doi.org/10.1016/j.fpsl.2019.100414.

Anderson, A. J., and E. A. Dawes. 1990. "Occurrence, metabolism, metabolic role, and industrial uses of bacterial polyhydroxyalkanoates." *Microbiological Reviews* 54 (4):450-472+iii. doi: 10.1128/mmbr.54.4.450-472.1990.

Arfat, Y. A., J. Ahmed, N. Hiremath, R. Auras, and A. Joseph. 2017. "Thermo-mechanical, rheological, structural and antimicrobial properties of bionanocomposite films based on fish skin gelatin and silver-copper nanoparticles." *Food Hydrocolloids* 62:191-202. doi: 10.1016/j.foodhyd.2016.08.009.

Bluhm, T. L., G. K. Hamer, R. H. Marchessault, C. A. Fyfe, and R. P. Veregin. 1986. "Isodimorphism in Bacterial Poly(β-hydroxybutyrate-co-β-hydroxyvalerate)." *Macromolecules* 19 (11):2871-2876. doi: 10.1021/ma00165a035.

Bohlmann, G.M. 2005. "General characteristics, processability, industrial applications and marke evolution of biodegradable polymers." In *Handbook of Biodegradable Polymers*, 183−217. C. Bastioli

Bugnicourt, E., P. Cinelli, A. Lazzeri, and V. Alvarez. 2014. "Polyhydroxyalkanoate (PHA): Review of synthesis, characteristics, processing and potential applications in packaging." *Express Polymer Letters* 8 (11):791-808. doi: 10.3144/expresspolymlett.2014.82.

Carvalheira, M., J. Cassidy, J. M. Ribeiro, B. A. Oliveira, E. B. Freitas, C. Roca, G. Carvalho, A. Oehmen, and M. A. M. Reis. 2018. "Performance of a two-stage anaerobic digestion system treating fruit pulp waste: The impact of substrate shift and operational conditions." *Waste Management* 78:434-445. doi: 10.1016/j.wasman.2018.06.013.

Chan, C. M., L. J. Vandi, S. Pratt, P. Halley, Y. Ma, G. Q. Chen, D. Richardson, A. Werker, and B. Laycock. 2019. "Understanding the effect of copolymer content on the processability and mechanical properties of polyhydroxyalkanoate (PHA)/wood composites." *Composites Part A: Applied Science and Manufacturing* 124. doi: 10.1016/j.compositesa.2019.05.005.

Cheng, H. N., A. Biswas, K. Vermillion, B. Melendez-Rodriguez, and J. M. Lagaron. 2020. "NMR analysis and triad sequence distributions of poly(3-hydroxybutyrate-co-3-hydroxyvalerate)." *Polymer Testing* 90. doi: 10.1016/j.polymertesting.2020.106754.

Cherpinski, A., M. Gozutok, H. T. Sasmazel, S. Torres-Giner, and J. M. Lagaron. 2018. "Electrospun oxygen scavenging films of poly(3-hydroxybutyrate) containing palladium nanoparticles for active packaging applications." *Nanomaterials* 8 (7). doi: 10.3390/nano8070469.

Cherpinski, A., S. Torres-Giner, L. Cabedo, and J. M. Lagaron. 2017. "Post-processing optimization of electrospun submicron poly(3-hydroxybutyrate) fibers to obtain continuous films of interest in food packaging applications." *Food Additives and Contaminants - Part A Chemistry, Analysis, Control, Exposure and Risk Assessment* 34 (10):1817-1830. doi: 10.1080/19440049.2017.1355115.

Colombo, B., T. P. Sciarria, M. Reis, B. Scaglia, and F. Adani. 2016. "Polyhydroxyalkanoates (PHAs) production from fermented cheese whey by using a mixed microbial culture." *Bioresource Technology* 218:692-699. doi: 10.1016/j.biortech.2016.07.024.

Di Lorenzo, M. L., P. Sajkiewicz, A. Gradys, and P. L. Pietra. 2009. "Optimization of melting conditions for the analysis of crystallization kinetics of poly(3-hydroxybutyrate)." *E-Polymers*:1-12. doi: 10.1515/epoly.2009.9.1.313.

Domingos, J. M. B., S. Puccio, G. A. Martinez, N. Amaral, M. A. M. Reis, S. Bandini, F. Fava, and L. Bertin. 2018. "Cheese whey integrated valorisation: Production, concentration and exploitation of carboxylic acids for the production of polyhydroxyalkanoates by a fed-

batch culture." *Chemical Engineering Journal* 336:47-53. doi: 10.1016/j.cej.2017.11.024.

Doshi, J., and D. H. Reneker. 1995. "Electrospinning process and applications of electrospun fibers." *Journal of Electrostatics* 35 (2-3):151-160. doi: 10.1016/0304-3886(95)00041-8.

Duque, A. F., C. S. S. Oliveira, I. T. D. Carmo, A. R. Gouveia, F. Pardelha, A. M. Ramos, and M. A. M. Reis. 2014. "Response of a three-stage process for PHA production by mixed microbial cultures to feedstock shift: Impact on polymer composition." *New Biotechnology* 31 (4):276-288. doi: 10.1016/j.nbt.2013.10.010.

EuropeanCommission. 2020. "Single-use plastics." accessed 2020. https://ec.europa.eu/environment/waste/plastic_waste.htm.

Figueroa-Lopez, K. J., L. Cabedo, J. M. Lagaron, and S. Torres-Giner. 2020. "Development of Electrospun Poly(3-hydroxybutyrate-co-3-hydroxyvalerate) Monolayers Containing Eugenol and Their Application in Multilayer Antimicrobial Food Packaging." *Frontiers in Nutrition* 7. doi: 10.3389/fnut.2020.00140.

Figueroa-Lopez, K. J., S. Torres-Giner, D. Enescu, L. Cabedo, M. A. Cerqueira, L. M. Pastrana, and J. M. Lagaron. 2020. "Electrospun active biopapers of food waste derived poly(3-hydroxybutyrate-co-3-hydroxyvalerate) with short-term and long-term antimicrobial performance." *Nanomaterials* 10 (3). doi: 10.3390/nano10030506.

Figueroa-Lopez, K. J., A. A. Vicente, M. A. M. Reis, S. Torres-Giner, and J. M. Lagaron. 2019. "Antimicrobial and antioxidant performance of various essential oils and natural extracts and their incorporation into biowaste derived poly(3-hydroxybutyrate-co-3-hydroxyvalerate) layers made from electrospun ultrathin fibers." *Nanomaterials* 9 (2). doi: 10.3390/nano9020144.

Fiorese, M. L., F. Freitas, J. Pais, A. M. Ramos, G. M. F. De Aragão, and M. A. M. Reis. 2009. "Recovery of polyhydroxybutyrate (PHB) from Cupriavidus necator biomass by solvent extraction with 1,2-propylene carbonate." *Engineering in Life Sciences* 9 (6):454-461. doi: 10.1002/elsc.200900034.

Gallardo-Cervantes, Miguel, Yolanda González-García, Aida Alejandra Pérez-Fonseca, Martín Esteban González-López, Ricardo Manríquez-González, Denis Rodrigue, and Jorge Ramón Robledo-Ortíz. 2021. "Biodegradability and improved mechanical performance of polyhydroxyalkanoates/agave fiber biocomposites compatibilized by different strategies." *Journal of Applied Polymer Science* 138 (15):50182. doi: https://doi.org/10.1002/app.50182.

Gatenholm, P., J. Kubát, and A. Mathiasson. 1992. "Biodegradable natural composites. I. Processing and properties." *Journal of Applied Polymer Science* 45 (9):1667-1677. doi: 10.1002/app.1992.070450918.

Gavara, Rafael, Ramón Catalá, Pilar M. Hernández-Muñoz, and Rubén J. Hernández. 1996. "Evaluation of Permeability Through Permeation Experiments: Isostatic and Quasi-isostatic Methods Compared." *Packaging Technology and Science* 9 (4):215-224. doi: https://doi.org/10.1002/(SICI)1099-1522(199607)9:4<215::AID-PTS366>3.0.CO;2-U.

González Siso, M. I. 1996. "The biotechnological utilization of cheese whey: A review." *Bioresource Technology* 57 (1):1-11. doi: 10.1016/0960-8524(96)00036-3.

Guimarães, P. M. R., J. A. Teixeira, and L. Domingues. 2010. "Fermentation of lactose to bio-ethanol by yeasts as part of integrated solutions for the valorisation of cheese whey." *Biotechnology Advances* 28 (3):375-384. doi: 10.1016/j.biotechadv.2010.02.002.

Guo, L., H. Sato, T. Hashimoto, and Y. Ozaki. 2010. "FTIR study on hydrogen-bonding interactions in biodegradable polymer blends of poly(3-hydroxybutyrate) and poly(4-vinylphenol)." *Macromolecules* 43 (8):3897-3902. doi: 10.1021/ma100307m.

Gutiérrez, C. D. B., A. S. C. Galván, and C. A. C. Álzate. 2017. "The potential production of polyhydroxybutyrate (PHB) from renewable feedstocks." In *Biopolymers: Structure, Performance and Applications*, 195-220.

Hablot, E., P. Bordes, E. Pollet, and L. Avérous. 2008. "Thermal and thermo-mechanical degradation of poly(3-hydroxybutyrate)-based multiphase systems." *Polymer Degradation and Stability* 93 (2):413-421. doi: 10.1016/j.polymdegradstab.2007.11.018.

Holmes, P. A. 1988. "Biologically produced (R)-3-hydroxyalkanoate polymers and copolymers." *Developments in Crystalline Polymers* 2:1-65.

Jiang, L., and J. Zhang. 2013. "Biodegradable Polymers and Polymer Blends." In *Handbook of Biopolymers and Biodegradable Plastics: Properties, Processing and Applications*, 109-128.

Johnson, K., Y. Jiang, R. Kleerebezem, G. Muyzer, and M. C. M. Van Loosdrecht. 2009. "Enrichment of a mixed bacterial culture with a high polyhydroxyalkanoate storage capacity." *Biomacromolecules* 10 (4):670-676. doi: 10.1021/bm8013796.

Kanatt, S. R., M. S. Rao, S. P. Chawla, and A. Sharma. 2012. "Active chitosan-polyvinyl alcohol films with natural extracts." *Food Hydrocolloids* 29 (2):290-297. doi: 10.1016/j.foodhyd.2012.03.005.

Kosikowski, F. V. 1979. "Whey Utilization and Whey Products." *Journal of Dairy Science* 62 (7):1149-1160. doi: 10.3168/jds.S0022-0302(79)83389-5.

Kunioka, M., and Y. Doi. 1990. "Thermal Degradation of Microbial Copolyesters: Poly(3-hydroxybutyrate-co-3-hydroxyvalerate) and Poly(3-hydroxybutyrate-co-4-hydroxybutyrate)." *Macromolecules* 23 (7):1933-1936. doi: 10.1021/ma00209a009.

Kunioka, M., A. Tamaki, and Y. Doi. 1989. "Crystalline and Thermal Properties of Bacterial Copolyesters: Poly(3-hydroxybutyrate-co-3-hydroxyvalerate) and Poly(3-hydroxybutyrate-co-4-hydroxybutyrate)." *Macromolecules* 22 (2):694-697. doi: 10.1021/ma00192a031.

Lanham, A. B., A. R. Ricardo, M. G. E. Albuquerque, F. Pardelha, M. Carvalheira, M. Coma, J. Fradinho, G. Carvalho, A. Oehmen, and M. A. M. Reis. 2013. "Determination of the extraction kinetics for the quantification of polyhydroxyalkanoate monomers in mixed microbial systems." *Process Biochemistry* 48 (11):1626-1634. doi: 10.1016/j.procbio.2013.07.023.

Laycock, B., P. Halley, S. Pratt, A. Werker, and P. Lant. 2014. "The chemomechanical properties of microbial polyhydroxyalkanoates." *Progress in Polymer Science* 39 (2):397-442. doi: 10.1016/j.progpolymsci.2013.06.008.

Li, D., and Y. Xia. 2004. "Electrospinning of nanofibers: Reinventing the wheel?" *Advanced Materials* 16 (14):1151-1170. doi: 10.1002/adma.200400719.

Li, F., H. Y. Yu, Y. Li, S. Y. Hussain Abdalkarim, J. Zhu, and Y. Zhou. 2021. "“Soft-rigid” synergistic reinforcement of PHBV composites with functionalized cellulose nanocrystals and amorphous recycled polycarbonate." *Composites Part B: Engineering* 206. doi: 10.1016/j.compositesb.2020.108542.

Li, F., H. Y. Yu, Y. Y. Wang, Y. Zhou, H. Zhang, J. M. Yao, S. Y. H. Abdalkarim, and K. C. Tam. 2019. "Natural Biodegradable Poly(3-hydroxybutyrate- co-3-hydroxyvalerate) Nanocomposites with Multifunctional Cellulose Nanocrystals/Graphene Oxide Hybrids for High-Performance Food Packaging." *Journal of Agricultural and Food Chemistry* 67 (39):10954-10967. doi: 10.1021/acs.jafc.9b03110.

Luzier, W D. 1992. "Materials derived from biomass/biodegradable materials." *Proceedings of the National Academy of Sciences* 89 (3):839-842. doi: 10.1073/pnas.89.3.839.

Marchessault, R. H., H. Morikawa, J. F. Revol, and T. L. Bluhm. 1984. "Physical Properties of a Naturally Occurring Polyester: Poly(β-Hydroxyvalerate)/Poly(β-Hydroxybutyrate)." *Macromolecules* 17 (9):1882-1884. doi: 10.1021/ma00139a047.

Martínez-Abad, A., J. González-Ausejo, J. M. Lagarón, and L. Cabedo. 2016. "Biodegradable poly(3-hydroxybutyrate-co-3-hydroxyvalerate)/thermoplastic polyurethane blends with improved mechanical and barrier performance." *Polymer Degradation and Stability* 132:52-61. doi: 10.1016/j.polymdegradstab.2016.03.039.

Martínez-Sanz, M., M. Villano, C. Oliveira, M. G. E. Albuquerque, M. Majone, M. Reis, A. Lopez-Rubio, and J. M. Lagaron. 2014. "Characterization of polyhydroxyalkanoates synthesized from microbial mixed cultures and of their nanobiocomposites with bacterial cellulose nanowhiskers." *New Biotechnology* 31 (4):364-376. doi: 10.1016/j.nbt.2013.06.003.

Martla, M., K. Umsakul, and K. Sudesh. 2018. "Production and recovery of poly(3-hydroxybutyrate-co-3-hydroxyvalerate) from biodiesel liquid waste (BLW)." *Journal of Basic Microbiology* 58 (11):977-986. doi: 10.1002/jobm.201800279.

Melendez-Rodriguez, B., J. L. Castro-Mayorga, M. A. M. Reis, C. Sammon, L. Cabedo, S. Torres-Giner, and J. M. Lagaron. 2018. "Preparation and Characterization of Electrospun Food Biopackaging Films of Poly(3-hydroxybutyrate-co-3-hydroxyvalerate) Derived From Fruit Pulp Biowaste." *Frontiers in Sustainable Food Systems* 2. doi: 10.3389/fsufs.2018.00038.

Melendez-Rodriguez, B., S. Torres-Giner, L. Lorini, F. Valentino, C. Sammon, L. Cabedo, and J. M. Lagaron. 2020. "Valorization of Municipal Biowaste into Electrospun Poly(3-hydroxybutyrate- co-3-hydroxyvalerate) Biopapers for Food Packaging Applications." *ACS Applied Bio Materials* 3 (9):6110-6123. doi: 10.1021/acsabm.0c00698.

Melendez-Rodriguez, Beatriz, Kelly J. Figueroa-Lopez, Andrea Bernardos, Ramón Martínez-Máñez, Luis Cabedo, Sergio Torres-Giner, and Jose M. Lagaron. 2019. "Electrospun Antimicrobial Films of Poly(3-hydroxybutyrate-co-3-hydroxyvalerate) Containing Eugenol Essential Oil Encapsulated in Mesoporous Silica Nanoparticles." *Nanomaterials* 9 (2):227.

Mitomo, H., T. Takahashi, H. Ito, and T. Saito. 1999. "Biosynthesis and characterization of poly(3-hydroxybutyrate-co-3- hydroxyvalerate) produced by Burkholderia cepacia D1." *International Journal of Biological Macromolecules* 24 (4):311-318. doi: 10.1016/S0141-8130(98)00064-6.

Mitomo, Hiroshi, Norio Morishita, and Yoshiharu Doi. 1993. "Composition range of crystal phase transition of isodimorphism in poly(3-hydroxybutyrate-co-3-hydroxyvalerate)." *Macromolecules* 26 (21):5809-5811. doi: 10.1021/ma00073a041.

Modi, S., K. Koelling, and Y. Vodovotz. 2011. "Assessment of PHB with varying hydroxyvalerate content for potential packaging applications." *European Polymer Journal* 47 (2):179-186. doi: 10.1016/j.eurpolymj.2010.11.010.

Mokrzycki, W. S., and M. Tatol. 2011. "Colour difference δE - A survey." *Machine Graphics and Vision* 20 (4):383-411.

Moretto, G., I. Russo, D. Bolzonella, P. Pavan, M. Majone, and F. Valentino. 2020. "An urban biorefinery for food waste and biological sludge conversion into polyhydroxyalkanoates and biogas." *Water Research* 170. doi: 10.1016/j.watres.2019.115371.

Muniyasamy, S., O. Ofosu, B. Thulasinathan, A. S. Thondi Rajan, S. M. Ramu, S. Soorangkattan, J. B. Muthuramalingam, and A. Alagarsamy. 2019. "Thermal-chemical and biodegradation behaviour of alginic acid treated flax fibres/ poly(hydroxybutyrate-co-valerate) PHBV green composites in compost medium." *Biocatalysis and Agricultural Biotechnology* 22. doi: 10.1016/j.bcab.2019.101394.

Oliveira, C. S. S., M. O. D. Silva, C. E. Silva, G. Carvalho, and M. A. M. Reis. 2018. "Assessment of protein-rich cheese whey waste stream as a nutrients source for low-cost mixed microbial PHA production." *Applied Sciences (Switzerland)* 8 (10). doi: 10.3390/app8101817.

Pagliano, G., P. Galletti, C. Samorì, A. Zaghini, and C. Torri. 2021. "Recovery of Polyhydroxyalkanoates From Single and Mixed Microbial Cultures: A Review." *Frontiers in Bioengineering and Biotechnology* 9. doi: 10.3389/fbioe.2021.624021.

Panaitescu, Denis Mihaela, Cristian Andi Nicolae, Adriana Nicoleta Frone, Ioana Chiulan, Paul Octavian Stanescu, Constantin Draghici, Michaela Iorga, and Mona Mihailescu. 2017. "Plasticized poly(3-hydroxybutyrate) with improved melt processing and balanced properties." *Journal of Applied Polymer Science* 134 (19). doi: https://doi.org/10.1002/app.44810.

Pereira, J. R., D. Araújo, A. C. Marques, L. A. Neves, C. Grandfils, C. Sevrin, V. D. Alves, E. Fortunato, M. A. M. Reis, and F. Freitas. 2019. "Demonstration of the adhesive properties of the medium-chain-length polyhydroxyalkanoate produced by Pseudomonas chlororaphis subsp. aurantiaca from glycerol." *International Journal of Biological Macromolecules* 122:1144-1151. doi: 10.1016/j.ijbiomac.2018.09.064.

Pérez-Camargo, R. A., I. Arandia, M. Safari, D. Cavallo, N. Lotti, M. Soccio, and A. J. Müller. 2018. "Crystallization of isodimorphic aliphatic random copolyesters: Pseudo-eutectic behavior and double-crystalline materials." *European Polymer Journal* 101:233-247. doi: 10.1016/j.eurpolymj.2018.02.037.

Poli, A., P. Di Donato, G. R. Abbamondi, and B. Nicolaus. 2011. "Synthesis, production, and biotechnological applications of exopolysaccharides and polyhydroxyalkanoates by Archaea." *Archaea* 2011. doi: 10.1155/2011/693253.

Quiles-Carrillo, L., N. Montanes, J. M. Lagaron, R. Balart, and S. Torres-Giner. 2019. "In Situ Compatibilization of Biopolymer Ternary Blends by Reactive Extrusion with Low-Functionality Epoxy-Based Styrene–Acrylic Oligomer." *Journal of Polymers and the Environment* 27 (1):84-96. doi: 10.1007/s10924-018-1324-2.

Razumovskii, L. P., A. L. Iordanskii, G. E. Zaikov, E. D. Zagreba, and I. C. McNeill. 1994. "Sorption and diffusion of water and organic solvents in poly(β-hydroxybutyrate) films." *Polymer Degradation and Stability* 44 (2):171-175. doi: https://doi.org/10.1016/0141-3910(94)90161-9.

Reis, M. A. M., L. S. Serafim, P. C. Lemos, A. M. Ramos, F. R. Aguiar, and M. C. M. Van Loosdrecht. 2003. "Production of polyhydroxyalkanoates by mixed microbial cultures." *Bioprocess and Biosystems Engineering* 25 (6):377-385. doi: 10.1007/s00449-003-0322-4.

Reis, M., M. Albuquerque, M. Villano, and M. Majone. 2011. "Mixed Culture Processes for Polyhydroxyalkanoate Production from Agro-Industrial Surplus/Wastes as Feedstocks." In *Comprehensive Biotechnology, Second Edition*, 669-683.

Riekel, C., M. C. G. Gutiérrez, A. Gourrier, and S. Roth. 2003. "Recent synchrotron radiation microdiffraction experiments on polymer and biopolymer fibers." *Analytical and Bioanalytical Chemistry* 376 (5):594-601. doi: 10.1007/s00216-003-1976-0.

Sanchez-Garcia, M. D., E. Gimenez, and J. M. Lagaron. 2007. "Novel PET Nanocomposites of Interest in Food Packaging Applications and Comparative Barrier Performance With Biopolyester Nanocomposites." *Journal of Plastic Film & Sheeting* 23 (2):133-148. doi: 10.1177/8756087907083590.

Sato, H., N. Suttiwijitpukdee, T. Hashimoto, and Y. Ozaki. 2012. "Simultaneous synchrotron SAXS/WAXD study of composition fluctuations, cold-crystallization, and melting in biodegradable polymer blends of cellulose acetate butyrate and poly(3-hydroxybutyrate)." *Macromolecules* 45 (6):2783-2795. doi: 10.1021/ma202606y.

Savenkova, L., Z. Gercberga, I. Bibers, and M. Kalnin. 2000. "Effect of 3-hydroxy valerate content on some physical and mechanical properties of polyhydroxyalkanoates produced by Azotobacter chroococcum." *Process Biochemistry* 36 (5):445-450. doi: 10.1016/S0032-9592(00)00235-1.

Scandola, M., G. Ceccorulli, M. Pizzoli, and M. Gazzano. 1992. "Study of the Crystal Phase and Crystallization Rate of Bacterial Poly(3-hydroxybutyrate-co-3-hydroxyvalerate)." *Macromolecules* 25 (5):1405-1410. doi: 10.1021/ma00031a008.

Serafim, L. S., P. C. Lemos, C. Torres, M. A. M. Reis, and A. M. Ramos. 2008. "The influence of process parameters on the characteristics of polyhydroxyalkanoates produced by mixed cultures." *Macromolecular Bioscience* 8 (4):355-366. doi: 10.1002/mabi.200700200.

Shiku, Y., P. Y. Hamaguchi, S. Benjakul, W. Visessanguan, and M. Tanaka. 2004. "Effect of surimi quality on properties of edible films based on Alaska pollack." *Food Chemistry* 86 (4):493-499. doi: 10.1016/j.foodchem.2003.09.022.

Singh, S., A. K. Mohanty, T. Sugie, Y. Takai, and H. Hamada. 2008. "Renewable resource based biocomposites from natural fiber and polyhydroxybutyrate-co-valerate (PHBV) bioplastic." *Composites Part A: Applied Science and Manufacturing* 39 (5):875-886. doi: 10.1016/j.compositesa.2008.01.004.

Singh, S., B. Sithole, P. Lekha, K. Permaul, and R. Govinden. 2021. "Optimization of cultivation medium and cyclic fed-batch fermentation strategy for enhanced polyhydroxyalkanoate production by Bacillus thuringiensis using a glucose-rich hydrolyzate." *Bioresources and Bioprocessing* 8 (1). doi: 10.1186/s40643-021-00361-x.

Škrbić, Ž, and V. Divjaković. 1996. "Temperature influence on changes of parameters of the unit cell of biopolymer PHB." *Polymer* 37 (3):505-507. doi: 10.1016/0032-3861(96)82922-3.

Smithers, G. W. 2008. "Whey and whey proteins-From 'gutter-to-gold'." *International Dairy Journal* 18 (7):695-704. doi: 10.1016/j.idairyj.2008.03.008.

Talan, A., R. Kaur, R. D. Tyagi, and P. Drogui. 2020. "Bioconversion of oily waste to polyhydroxyalkanoates: Sustainable technology with circular bioeconomy approach and multidimensional impacts." *Bioresource Technology Reports* 11. doi: 10.1016/j.biteb.2020.100496.

Torres-Giner, S., E. Gimenez, and J. M. Lagaron. 2008. "Characterization of the morphology and thermal properties of Zein Prolamine nanostructures obtained by electrospinning." *Food Hydrocolloids* 22 (4):601-614. doi: 10.1016/j.foodhyd.2007.02.005.

Torres-Giner, S., J. V. Gimeno-Alcañiz, M. J. Ocio, and J. M. Lagaron. 2011. "Optimization of electrospun polylactide-based ultrathin fibers for osteoconductive bone scaffolds." *Journal of Applied Polymer Science* 122 (2):914-925. doi: 10.1002/app.34208.

Torres-Giner, S., N. Montanes, T. Boronat, L. Quiles-Carrillo, and R. Balart. 2016. "Melt grafting of sepiolite nanoclay onto poly(3-hydroxybutyrate-co-4-hydroxybutyrate) by reactive extrusion with multi-functional epoxy-based styrene-acrylic oligomer." *European Polymer Journal* 84:693-707. doi: 10.1016/j.eurpolymj.2016.09.057.

Torres-Giner, S., R. Pérez-Masiá, and J. M. Lagaron. 2016. "A review on electrospun polymer nanostructures as advanced bioactive platforms." *Polymer Engineering and Science* 56 (5):500-527. doi: 10.1002/pen.24274.

Tu, W., D. Zhang, H. Wang, and Z. Lin. 2019. "Polyhydroxyalkanoates (PHA) production from fermented thermal-hydrolyzed sludge by PHA-storing denitrifiers integrating PHA accumulation with nitrate removal." *Bioresource Technology* 292. doi: 10.1016/j.biortech.2019.121895.

Vahabi, Henri, Laurent Michely, Ghane Moradkhani, Vahideh Akbari, Marianne Cochez, Christelle Vagner, Estelle Renard, Mohammad Reza Saeb, and Valérie Langlois. 2019. "Thermal Stability and Flammability Behavior of Poly(3-hydroxybutyrate) (PHB) Based Composites." *Materials* 12 (14):2239.

Van Loosdrecht, M. C. M., M. A. Pot, and J. J. Heijnen. 1997. Importance of bacterial storage polymers in bioprocesses. In *Water Science and Technology*.

Van Wegen, R. J., Y. Ling, and A. P. J. Middelberg. 1998. "Industrial production of polyhydroxyalkanoates using escherichia coli: An economic analysis." *Chemical Engineering Research and Design* 76 (3):417-426. doi: 10.1205/026387698524848.

Verhoogt, H., B. A. Ramsay, B. D. Favis, and J. A. Ramsay. 1996. "The influence of thermal history on the properties of poly(3-hydroxybutyrate-co-12%-3-hydroxyvalerate)." *Journal of Applied Polymer Science* 61 (1):87-96. doi: 10.1002/(SICI)1097-4628(19960705)61:1<87::AID-APP10>3.0.CO;2-X.

Wang, Y., S. Yamada, N. Asakawa, T. Yamane, N. Yoshie, and Y. Inoue. 2001. "Comonomer compositional distribution and thermal and morphological characteristics of bacterial poly(3-hydroxybutyrate-co-3-hydroxyvalerate)s with high 3-hydroxyvalerate content." *Biomacromolecules* 2 (4):1315-1323. doi: 10.1021/bm010128o.

Xiang, H., X. Wen, X. Miu, Y. Li, Z. Zhou, and M. Zhu. 2016. "Thermal depolymerization mechanisms of poly(3-hydroxybutyrate-co-3-hydroxyvalerate)." *Progress in Natural Science: Materials International* 26 (1):58-64. doi: 10.1016/j.pnsc.2016.01.007.

Yokouchi, M., Y. Chatani, H. Tadokoro, K. Teranishi, and H. Tani. 1973. "Structural studies of polyesters: 5. Molecular and crystal structures of optically active and racemic poly (β-hydroxybutyrate)." *Polymer* 14 (6):267-272. doi: 10.1016/0032-3861(73)90087-6.

Zhang, K., M. Misra, and A. K. Mohanty. 2014. "Toughened sustainable green composites from poly(3-hydroxybutyrate-co-3-hydroxyvalerate) based ternary blends and miscanthus biofiber." *ACS Sustainable Chemistry and Engineering* 2 (10):2345-2354. doi: 10.1021/sc500353v.

Chapter IV

Electrospun Antimicrobial Films of Poly(3-hydroxybutyrate-*co*-3-hydroxyvalerate) Containing Eugenol Essential Oil Encapsulated in Mesoporous Silica Nanoparticles

Nanomaterials 2019, 9(2), 227

Beatriz Meléndez-Rodríguez[1], Kelly J. Figueroa-López[1], Andrea Bernardos[2,3,4,5], Ramón Martínez-Máñez[2,3,4,5], Luis Cabedo[6], Sergio Torres-Giner[1], and José María Lagarón[1]

[1] Novel Materials and Nanotechnology Group, Institute of Agrochemistry and Food Technology (IATA), Spanish Council for Scientific Research (CSIC), Paterna, Spain

[2] Instituto Interuniversitario de Investigación de Reconocimiento Molecular y Desarrollo Tecnológico (IDM), Universitat Politècnica de València (UPV), Universitat de València (UV), Valencia, Spain

[3] CIBER de Bioingeniería, Biomateriales y Nanomedicina (CIBER-BBN), Valencia, Spain

[4] Unidad Mixta de Investigación en Nanomedicina y Sensores, Universitat Politècnica de València (UPV), Instituto de Investigación Sanitaria La Fe, Valencia, Spain

[5] Unidad Mixta UPV-CIPF de Investigación en Mecanismos de Enfermedades y Nanomedicina, Universitat Politècnica de València (UPV), Centro de Investigación Príncipe Felipe, Valencia, Spain

[6] Polymers and Advanced Materials Group (PIMA), Universitat Jaume I (UJI), Castellón, Spain

Abstract

The main goal of this study was to develop poly(3-hydroxybutyrate-*co*-3-hydroxyvalerate) (PHBV) films with long-term antimicrobial capacity of interest in food packaging applications. To this end, eugenol was first highly efficiently encapsulated at 50 wt % in the pores of mesoporous silica nanoparticles by vapor adsorption. The eugenol-containing nanoparticles were then loaded in the 2.5–20 wt % range into PHBV by electrospinning and the resultant electrospun composite fibers were annealed at 155 °C to produce continuous films. The characterization showed that the PHBV films filled with mesoporous silica nanoparticles containing eugenol present sufficient thermal resistance and enhanced mechanical strength and barrier performance to water vapor and limonene. The antimicrobial activity of the films was also evaluated against foodborne bacteria for 15 days in open vs. closed conditions in order to simulate real packaging conditions. The electrospun PHBV films with loadings above 10 wt % of mesoporous silica nanoparticles containing eugenol successfully inhibited the bacterial growth, whereas the active films stored in hermetically closed systems increased their antimicrobial activity after 15 days due to the volatile portion accumulated in the system's headspace and the sustained release capacity of the films. The resultant biopolymer films are, therefore, potential candidates to be applied in active food packaging applications to provide shelf life extension and food safety.

Keywords*:* PHBV; MCM-41; eugenol; antimicrobial properties; active packaging

1. Introduction

Polyhydroxyalkanoates (PHAs) currently represent one of the most important alternative to petroleum-based materials in the frame of the Circular Economy (Torres-Giner, Montanes, et al. 2018). PHAs, which are synthesized by a wide range of microorganisms as carbon storage material, are thermoplastic materials, biodegradable, and present similar physical properties to other plastics, e.g., polypropylene (PP) and polystyrene (PS), such as high mechanical strength and water resistance (Reddy et al. 2003). PHAs have been prompted as potential packaging applications due to their biocompatibility and physical properties (Keshavarz and Roy 2010). However, the PHA production currently associates a high cost due to the carbon sources of the raw materials, i.e., low yield and productivity, and the down-stream process (Lee 1996). The synthesis of PHA through fermentation from industrial by-products and waste, particularly the use of mixed microbial cultures, is nowadays seen as an option to reduce the production costs (Choi and Lee 1997).

Among PHAs, the most widely studied and easiest-to-produce member of this family is poly(3-hydroxybutyrate) (PHB). This isotactic homopolyester presents a relatively high melting temperature (T_m) and good stiffness due to its high crystallinity (>50 %). However, the use of PHB has been limited due to several drawbacks, particularly its poor impact-strength resistance and low thermal stability. To overcome these shortcomings, the use of its copolymers, such as those made with 3-hydroxyvalerate (3HV) or 4-hydroxybutyrate (4HB) to produce poly(3-hydroxybutyrate-*co*-3-hydroxyvalerate) (PHBV) and poly(3-hydroxybutyrate-*co*-4-hydroxybutyrate) (P(3HB-*co*-4HB)), can improve these limitations and widen its processing window (Díez-Pascual and Díez-Vicente 2014, Torres-Giner, Montanes, Boronat, et al. 2016). In particular, PHBV is a potential candidate to be applied for packaging of films, blow-molded bottles, paper coatings, etc. (Khosravi-Darani and Bucci 2015). To this end, different studies have explored the use of PHBV due to its potential as a sustainable packaging material (Keskin et al. 2017, Kulkarni et al. 2011). For instance, PHBVs have been applied in the form of films, fibers, and foams for everyday articles such as shampoo bottles and plastic beverage bottles due to its renewability, biodegradability, and high water vapor barrier (Philip, Keshavarz, and Roy 2007). In addition, the incorporation of antimicrobial and/or antioxidant substances into a PHA-based packaging material can result in high interest to improve both protection and shelf life of foodstuffs during the storage period (Requena, Vargas, and Chiralt 2017, Robertson 1993, Torres-Giner, Hilliou, et al. 2018).

Electrospinning is an innovative technology to generate ultrathin fibrous mats made of a wide range of polymer and biopolymer materials with fiber diameters ranging from several nanometers to a few microns (Li and Xia 2004). Electrospun ultrathin fibers have prompted their use in a wide range of industrial sectors, including packaging applications (Torres-Giner 2011a, Torres-Giner, Busolo, et al. 2018). This technique is highly suitable for the encapsulation and/or sustained delivery of active and bioactive substances at the nanoscale level due to both the high surface-to-volume ratios of the electrospun fibers and the high porosity of their mats (Torres-Giner, Pérez-Masiá, and Lagaron 2016, Torres-Giner, Wilkanowicz, et al. 2017). In particular, electrospinning is interesting for the development of antimicrobial materials by either the use of inherently antimicrobial polymers or the nanoencapsulation of biocide substances (Torres-Giner 2011b). As a result, within the frame of active packaging, different recent studies have reported the encapsulation of metal nanoparticles (MNPs) in electrospun matrices. For instance, poly(vinyl

alcohol) (PVOH) and poly(N-isopropylacrylamide) (PNIPAAm) membranes containing silver nanoparticles (AgNPs) immobilized onto cellulose nanowhiskers (CNWs) presented antimicrobial activity against several Gram-negative (G-) and Gram-positive (G+) bacteria (Spagnol et al. 2018). In another study, polyvinylpyrrolidone (PVP)/poly(ε-caprolactone) (PCL) nanofibers functionalized with zinc oxide nanoparticles (ZnONPs) and AgNPs, also prepared by electrospinning, showed a high antibacterial activity against *Staphylococcus aureus* (*S. aureus*) and *Escherichia coli* (*E. coli*) (Hu et al. 2018). Similarly, electrospun chitosan/poly(ethylene oxide) (PEO) membranes containing AgNPs presented antimicrobial effect against *E. coli* (An et al. 2009). Recently developed electrospun PHA materials containing AgNPs (Castro-Mayorga, Fabra, Cabedo, et al. 2017) and copper oxide nanoparticles (CuONPs) (Castro Mayorga et al. 2018) have been also able to considerably reduce bacterial growth at very low contents. These novel NPs-containing electrospun materials offer significant potential as new antimicrobial coatings or interlayers, that is, internal layers in a multilayer system, for application in the design of active food packaging structures.

Natural antimicrobials, such as essential oils (EOs), are currently regarded as an alternative to synthetic preservatives of food because they are considered as Generally Recognized As Safe (GRAS) substances, being acceptable to consumers (Burt 2004) and having the capacity to exert a multitude of biological effects (Lang and Buchbauer 2012). For instance, eugenol, which has potential antimicrobial and antioxidant actions, has been effectively applied against foodborne pathogens (da Silva et al. 2018, Wieczyńska and Cavoski 2018). However, EOs are frequently unstable and can be easily degraded in stressful situations such as in the presence of oxygen, temperature and light, so that they can lose their antimicrobial activity (Majeed et al. 2015). To avoid this issue, encapsulation is considered a good way to protect and preserve the effectiveness of active and bioactive substances (Kailasapathy 2009). In this sense, silica mesoporous supports (SMPSs) (Kresge et al. 1992) show a great deal of potential for the storage and release of active substances (He et al. 2014, Vallet-Regi et al. 2001). In particular, the typical sizes of SMPSs range from microns to nanometers, presenting tailor-made pores of around 2–10 nm (Muñoz et al. 2003). The particular morphology of SMPSs renders a very large specific surface area, up to 1200 m^2/g and, then, an enhanced loading capacity for the encapsulation and release of natural antimicrobials (Bernardos et al. 2015). Within SMPSs, Mobil Composition of Matter (MCM), including both MCM-41 and MCM-48, are among of the most popular mesoporous molecular sieves in which their pore diameter can be nicely controlled by adjusting their synthesis conditions and/or by employing surfactants with different chain lengths in their preparation (Fan et al. 2003). Silica mesoporous materials are thus able to encapsulate organic molecules, forming host–guest complexes with volatile molecules (e.g., EOs) to efficiently control their volatility and reactivity. So far, many studies have employed MCM to encapsulate active substances with positive results in different applications, for instance, caprylic acid against foodborne pathogens (Ruiz-Rico et al. 2015), EOs as antifungal (Bernardos et al. 2015, Janatova et al. 2015, Ribes et al. 2017) and antimicrobial systems (Ruiz-Rico et al. 2017), and poplar-type propolis in drug delivery platforms (Popova et al. 2018). In particular, the antimicrobial and antifungal effect of the EOs-functionalized supports improved compared to the free compounds due to the EOs encapsulated inside MCM released in a controlled manner (Janatova et al. 2015, Ribes et al. 2017, Ruiz-Rico et al. 2017). These previous results suggest that the immobilization of EOs onto silica supports can represent a novel strategy to develop a new generation of long-term antimicrobial systems that may not only enhance the antimicrobial activity of EOs, but also mask their characteristic odor/taste for food-related applications.

In this study, it is initially reported the preparation of nanometric MCM-41 particles loaded with eugenol, a phenylpropene and an allyl chain-substituted guaiacol that is primarily extracted from cinnamon, bay leaf, nutmeg, basil, and clove (Chatterjee and Bhattacharjee 2013). The resultant MCM-41 particles containing eugenol were thereafter incorporated, for the first time, into PHBV by electrospinning. The generated electrospun composite fibers were thermally post-treated to produce films that were characterized in terms of their morphology, thermal, mechanical, and barrier properties. Finally, the antimicrobial performance against foodborne bacteria was also determined. In a packaging context, the active tests were carried out as a function of time in open vs. close conditions in order to simulate potential real conditions.

2. Materials and Methods

2.1. Materials

Commercial PHBV was ENMAT^{TM} Y1000P, produced by Tianan Biologic Materials (Ningbo, China) and delivered in the form of pellets by NaturePlast (Ifs, France). According to the manufacturer, this biopolymer resin presents a density of 1.23 g/cm³ and a melt flow index (MFI) of 5–10 g/10 min (190 °C, 2.16 kg). The 3HV fraction in the copolyester is 2–3 mol %.

Eugenol, with 99 % purity, tetraethyl orthosilicate (TEOS), n-cetyltrimethylammonium bromide (CTAB), sodium hydroxide (NaOH), 2,2,2-trifluoroethanol (TFE), ≥ 99 % purity, and D-limonene, with 98 % purity, were all purchased from Sigma Aldrich S.A. (Madrid, Spain).

2.2. Synthesis and Complexation of MCM-41

2.2.1. Synthesis of MCM-41

The MCM-41 type mesoporous particles were synthesized using the following procedure (Climent et al. 2009): 2 g of CTAB, 5.48 mmol, was first dissolved in 960 ml of deionized water. Then, 7.00 ml of NaOH, 2 M, was added to the CTAB solution, followed by adjusting the solution temperature to 95 °C. Later, 10 ml of TEOS, $5.14 \cdot 10^{-2}$ mol, was added dropwise to the surfactant solution. The mixture was allowed to stir for 3 h to produce a white precipitate. The solid product was centrifuged and washed several times with deionized water and ethanol and, thereafter, dried at 60 °C to obtain solid MCM particles. Lastly, to prepare the final porous material, i.e., the MCM-41 type particles, the as-synthetized MCM particles were calcined at 550 °C using air atmosphere for 5 h so that their template phase was removed.

2.2.2. Eugenol Complexation on MCM-41

Silica loading with eugenol was achieved via vapor adsorption by mixing 100 mg of eugenol with 100 mg of the MCM-41 type particles in a tightly closed vial (Bernardos et al. 2015). The mixture

was incubated in an oven at 40 °C for 24 h while being continuously shaken. The amount of eugenol loaded in the MCM-41 type support was determined by monitoring the sample weight increase before and after the loading process. Approximately 500 mg/g of the final weight corresponded to eugenol.

2.3. Electrospinning Process

Prior to electrospinning, different PHBV solutions were prepared by dissolving the biopolymer at 10 wt % in TFE. Then, the MCM-41 type particles, with and without eugenol, were added to the PHBV solutions at 2.5, 5, 7.5, 10, 15, and 20 wt %. A neat PHBV solution without MCM-41 type particles was also prepared as a control sample. All PHBV solutions were processed by electrospinning using a high-throughput Fluidnatek® LE-500 pilot-plant device with temperature and relative humidity (RH) control manufactured by Bioinicia S.L. (Valencia, Spain). The equipment was operated in the lab mode using a motorized single needle injector, scanning vertically towards a metallic fixed collector. The conditions were set at a flow-rate of 6 ml/h, 20 kV of voltage, and 15 cm of needle-to-collector distance. Each solution was electrospun for 2 h at 25 °C and 40 % RH. The collected mats were stored in darkness at room temperature in a desiccator at 0 % RH for one week before physical characterization.

2.4. Film Preparation

The resultant electrospun PHBV fibers mats were subjected to annealing in a 4122-model press from Carver, Inc. (Wabash, IN, USA) at 155 °C, for 5 s, without pressure. These conditions were selected based on our previous work (Cherpinski, Torres-Giner, et al. 2018). The thermally post-processed samples had an average thickness of approximately 60 µm.

2.5. Characterization

2.5.1. Electron Microscopy

The morphologies of the MCM-41 type particles as well as the electrospun PHBV fibers and films were observed by scanning electron microscopy (SEM) using an S-4800 device from Hitachi (Tokyo, Japan). The samples were fixed to beveled holders using conductive double-sided adhesive tape and sputtered with a mixture of gold-palladium under vacuum prior to observation. An accelerating voltage of 10 kV was used. For the cross-section observations, the films were previously cryo-fractured by immersion in liquid nitrogen.

Detailed morphology of the MCM-41 particles and their distribution in the PHBV fibers was further studied by transmission electron microscopy (TEM) using a JEOL 1010 from JEOL USA, Inc. (Peabody, MA, USA) using an accelerating voltage of 100 kV. The estimation of the dimensions was performed by means of the Aperture software from Apple (Cupertino, CA, USA) using a minimum of 20 SEM or TEM micrographs in their original magnification.

2.5.2. Thermal Analysis

Thermal transitions were studied by differential scanning calorimetry (DSC) on a DSC-7 analyzer from PerkinElmer, Inc. (Waltham, MA, USA), equipped with a cooling accessory Intracooler 2 also from PerkinElmer, Inc. A heating program was applied from −30 °C to 190 °C, followed by a cooling program to −30 °C. The heating and cooling rates were both set at 10 °C/min under nitrogen atmosphere with a flow-rate of 20 ml/min. The typical sample weight was ~3 mg while an empty aluminum pan was used as reference. Calibration was performed using an indium sample. All tests were carried out, at least, in duplicate.

Thermogravimetric analysis (TGA) was performed in a TG-STDA model TGA/STDA851e/LF/1600 thermobalance from Mettler-Toledo, LLC (Columbus, OH, USA). The samples, with a weight of about 15 mg, were heated from 50 °C to 800 °C at a heating rate of 10 °C/min under a nitrogen atmosphere with a flow-rate of 50 ml/min.

2.5.3. Mechanical Tests

Tensile tests of the PHBV films were performed according to ASTM standard method D638 using an Instron 4400 universal testing machine, equipped with a 1-kN load cell, from Instron (Norwood, MA, USA). The tests were performed, at room conditions, with 115 × 16 mm^2 stamped dumb-bell shaped specimens using a cross-head speed of 10 mm/min. Samples were conditioned for 24 h prior to tensile assay. A minimum of six specimens was measured for each sample and the average values with standard deviation (SD) were reported.

2.5.4. Permeability Tests

The water vapor permeability (WVP) of the film samples was determined using the gravimetric method ASTM E96-95 in triplicate. For this, 5 ml of distilled water was placed inside a Payne permeability cup (diameter of 3.5 cm) from Elcometer Sprl (Hermallesous-Argenteau, Belgium). The films were not in direct contact with water but exposed to 100 % RH on one side and secured with silicon rings. The samples were placed within a desiccator, filled with dried silica gel, at 0 % RH and 25 °C. The control samples were cups with aluminum films to estimate the solvent loss through the sealing and samples placed in cups but without permeant to compensate for mass losses due to eugenol release. The cups were weighted periodically using an analytical balance (±0.0001 g). WVP was calculated from the regression analysis of weight loss data vs. time and the weight loss was compensated by the marginal losses through the sealing and eugenol release. The permeability was obtained by multiplying the permeance by the film thickness.

Similar as described above for WVP, limonene permeability (LP) was measured placing 5 ml of $_D$-limonene inside the Payne permeability cups. The cups containing the films were placed at the controlled room conditions of 25 °C and 40 % RH. The samples were measured in triplicate and the limonene vapor permeation rate (LPRT) values were estimated from the steady-state permeation slopes and the weight loss was compensated by the comparatively marginal loss through the sealing and by the fluctuations in mass of the films due to eugenol evaporation and potential water sorption. LP was calculated taking into account the average film thickness in each case.

2.6. Antimicrobial Assays

The antibacterial activity of the neat eugenol, the eugenol-containing MCM-41 particles, and the electrospun films with MCM-41 with eugenol was evaluated against *S. aureus* CECT240 (ATCC 6538P) and *E. coli* CECT434 (ATCC 25922). These strains were obtained from the Spanish Type Culture Collection (CECT, Valencia, Spain) and stored in phosphate buffered saline (PBS) with 10 wt % tryptic soy broth (TSB, Conda Laboratories, Madrid, Spain) and 10 wt % glycerol at −80 °C. Previous to each study, a loopful of each bacteria was transferred to 10 ml of TSB and incubated at 37 °C for 24 h. A 100-µl aliquot from the culture was again transferred to TSB and grown at 37 °C to the mid-exponential phase of growth. An approximate count of 5×10^5 colony-forming units (CFU)/ml of a culture resulted in an absorbance value of 0.20, as determined by optical density at 600 nm (UV 4000 spectrophotometer, Dinko Instruments, Barcelona, Spain).

The minimum inhibitory concentration (MIC) and minimum bactericide concentration (MBC) of eugenol against the selected foodborne bacteria was tested following the plate micro-dilution protocol, as described in the Methods for Dilution Antimicrobial. Susceptibility Tests for Bacteria That Grow Aerobically; Approved Standard Tenth. Edition (M07-A10) by the Clinical and Laboratory Standards Institute (CLSI). For this, a 96-well plate with an alpha numeric coordination system (columns 12 and rows A-H) were used, where 10 µl of the tested samples were introduced in the wells with 90 µl of the bacteria medium. In the wells corresponding to A, B, C, E, F, and G columns different concentrations of eugenol, that is, 0.312, 0.625, 1.25, 2.5, 5, 10, 20, 40, 80, 160 µl/ml, were tested, in triplicate, from rows 1 to 10. Columns D and H were used as control of eugenol in TSB without bacteria. Row 11 was taken as positive control, that is, only TSB, and row 12 was used as negative control, that is, *S. aureus* and *E. coli* in TSB. The plates were incubated at 37 °C for 24 h. Thereafter, 10 µl of resazurin, a metabolic indicator, was added to each well and incubated again at 37 °C for 2 h. Upon obtaining the resazurin change, the wells were read through color difference. The MIC value was determined as the lowest concentration of eugenol presenting growth inhibition.

The antimicrobial performance of the films was evaluated by using a modification of the Japanese Industrial Standard JIS Z2801 (ISO 22196:2007). A microorganism suspension of *S. aureus* and *E. coli* was applied onto the test films of PHBV/MCM-41 with eugenol and also PHBV/MCM-41, as negative control without eugenol, both sizing 2×2 cm^2. After incubation for 24 h at 24 °C and at a RH of at least 95 %, bacteria were recovered with PBS, 10-fold serially diluted and incubated at 37 °C for 24 h in order to quantify the number of viable bacteria by conventional plate count. The antimicrobial activity was evaluated from 1 (initial day), 8, and 15 days. The antibacterial activity was taken as the test surface reduction (R) using the equation 1:

$$R = [log(B/A) - log(C/A)] = log(B/C) \quad (1)$$

where A is the mean of bacterial counts of the control sample immediately after inoculation, B is the mean of bacterial counts of the control sample after 24 h, and C is the mean of bacterial counts of the test sample after 24 h. Antimicrobial activity was evaluated with the following assessment: Nonsignificant ($R < 0.5$), slight ($R \geq 0.5$ and <1), significant ($R \geq 1$ and <3), and strong ($R \geq 3$) (Torres-Giner, Torres, et al. 2017).

3. Results

3.1. Morphology

Figure 1 shows the morphology of the here-obtained MCM-41 powder. Figure 1a,b present the SEM images of the MCM-41 powders with and without eugenol, respectively. One can observe that the silica particles presented a spherical shape with a mean size of around 100 nm, where the incorporation of eugenol slightly reduced their particle size. Therefore, the incorporation of eugenol did not alter the morphology of the mesoporous MCM-41 type nanoparticles. TEM was carried out in order to further ascertain the morphology of the MCM-41 particles. Figure 1c confirmed the spherical shape of the MCM-41 particle without eugenol, showing that their mean size was 96.1 ± 3.8 nm. A similar morphology can be observed in Figure 1d for the MCM-41 powder with eugenol, having a mean diameter of 88.6 ± 2.1 nm. Similar results were reported by Ribes et al. (Ribes et al. 2017) in which the immobilization of eugenol and thymol on the surface of MCM-41 did not affect the integrity of the mesoporous silica particles. Also, Ruiz-Rico et al. (Ruiz-Rico et al. 2017) observed that the appearance of fumed silica, amorphous silica, and MCM-41 particles did not change after functionalization with thymol. Indeed, MCM-41 has been widely used as a model material in the context of porosity characterization owing to its peculiar features, such as high surface area, large pore volume, low toxicity, high chemical and thermal stability, and versatile chemical modifiable surface. It has been reported that the pore structure is organized in the form of hexagonal arrays of uniform tubular channels of controlled width (Alfredsson et al. 1994, Beck et al. 1992). As a result, mesoporous silica nanoparticles are excellent candidates for reference adsorbents for standardizing adsorption measurements and methods for characterization of porous solids due to their regular pore structure, high stability, and also convenient method of synthesis (Ravikovitch et al. 1995, Sayed et al. 2018).

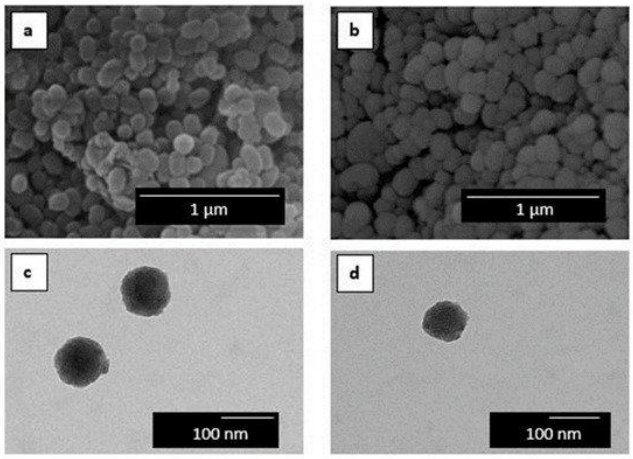

Figure 1. Scanning electron microscopy (SEM) images of: (a) Mobil Composition of Matter (MCM-41); (b) MCM-41 with eugenol. Scale markers of 1 µm. Transmission electron microscopy (TEM) images of: (c) MCM-41 and (d) MCM-41 with eugenol. Scale markers of 100 nm.

Figure 2 shows the resultant electrospun mats obtained from the neat PHBV solution and the different solutions of PHBV/MCM-41 with eugenol. One can observe that, in all cases, the electrospinning process generated a mat composed of non-woven fibers with a similar morphology. **Table 1** summarizes the mean diameters of the electrospun fibers. The neat PHBV fibers without MCM-41, processed in the same conditions, presented a mean diameter of 0.89 ± 0.30 µm. It can be observed that the mean diameters of the electrospun fibers varied in the 0.6–0.7 µm range when the silica particles were incorporated. However, one can observe that the electrospun fibers with the highest particle contents, that is, 15 and 20 wt % MCM-41, presented certain cross-linking or fibers coalescence. This can be related to difficulties encountered during the fiber formation more likely due to a phenomenon of particle aggregation in the electrospinning process. Indeed, it is known that high nano-sized filler contents habitually lead to the formation of beaded regions in the electrospun fibers (Torres-Giner and Lagaron 2010, Torres-Giner, Martinez-Abad, and Lagaron 2014).

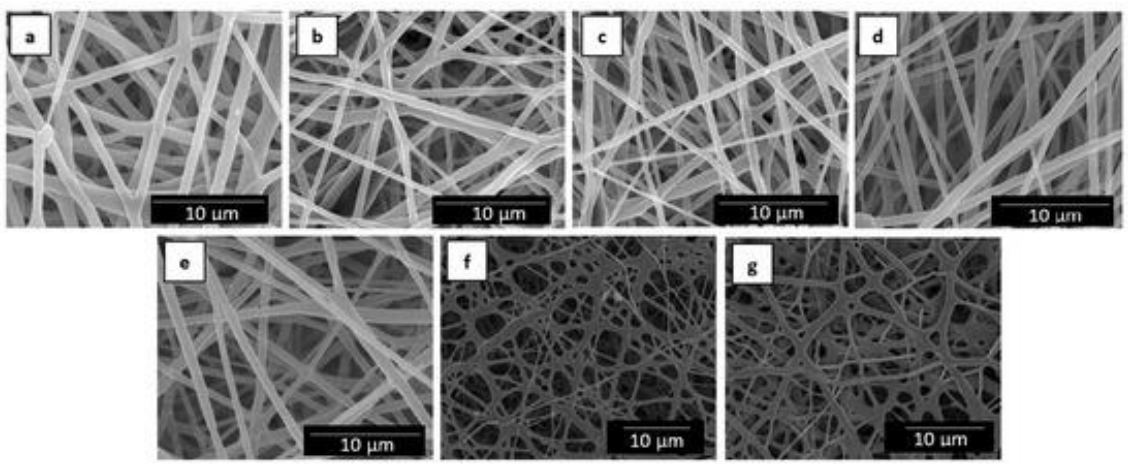

Figure 2. Scanning electron microscopy (SEM) images of the electrospun fibers of poly(3-hydroxybutyrate-*co*-3-hydroxyvalerate) (PHBV)/Mobil Composition of Matter (MCM)-41 with eugenol: (a) Neat PHBV; (b) 2.5 wt % MCM-41 + eugenol; (c) 5 wt % MCM-41 + eugenol; (d) 7.5 wt % MCM-41 + eugenol; (e) 10 wt % MCM-41 + eugenol; (f) 15 wt % MCM-41 + eugenol; (g) 20 wt % MCM-41 + eugenol. Scale markers of 10 µm.

Table 1. Mean diameters of the electrospun fibers of poly(3-hydroxybutyrate-*co*-3-hydroxyvalerate) (PHBV)/Mobil Composition of Matter (MCM)-41 with eugenol.

Fibers	Diameter (µm)
PHBV	0.89 ± 0.30
PHBV/2.5 wt % MCM-41 + eugenol	0.65 ± 0.19
PHBV/5 wt % MCM-41 + eugenol	0.66 ± 0.16
PHBV/7.5 wt % MCM-41 + eugenol	0.63 ± 0.18
PHBV/10 wt % MCM-41 + eugenol	0.64 ± 0.19
PHBV/15 wt % MCM-41 + eugenol	0.65 ± 0.19
PHBV/20 wt % MCM-41 + eugenol	0.67 ± 0.24

TEM was also performed in order to evaluate the distribution of the MCM-41 particles inside the electrospun fibers. The detailed morphologies of the electrospun mats of PHBV/MCM-41 with eugenol, at different particle contents, are shown in **Figure 3**. One can observe that at low contents, that is, from 2.5 wt % to 7.5 wt % MCM-41 with eugenol, the functionalized silica nanoparticles were relatively well distributed inside the electrospun fibers. However, for higher filler contents, the MCM-41 particles were mainly agglomerated in certain regions of the fibers. This fact supports the above-described morphology during the SEM analysis by which the silica nanoparticles interconnected the fibers in the electrospun mats. A similar morphology was recently reported, for instance, by Cherpinski et al. (Cherpinski, Gozutok, et al. 2018) in PHB fibers containing palladium nanoparticles (PdNPs).

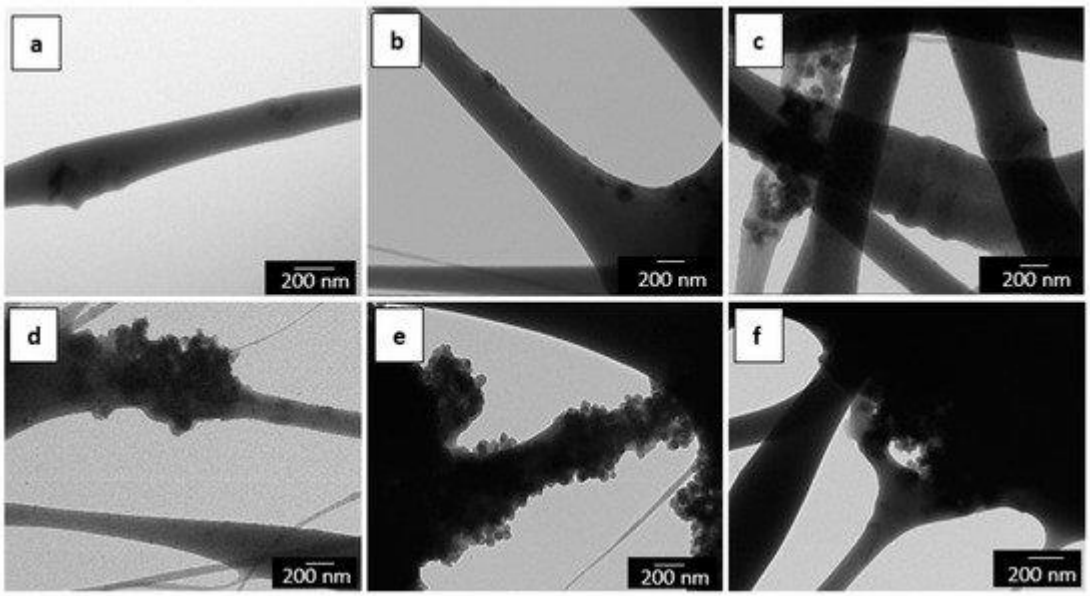

Figure 3. Transmission electron microscopy (TEM) images of the electrospun fibers of poly(3-hydroxybutyrate-*co*-3-hydroxyvalerate) (PHBV)/Mobil Composition of Matter (MCM)-41 with eugenol: (a) 2.5 wt % MCM-41 + eugenol; (b) 5 wt % MCM-41 + eugenol; (c) 7.5 wt % MCM-41 + eugenol; (d) 10 wt % MCM-41 + eugenol; (e) 15 wt % MCM-41 + eugenol; (f) 20 wt % MCM-41 + eugenol. Scale markers of 200 nm.

The morphology of the electrospun materials was also analyzed by SEM in order to ascertain the effect of the film-forming process on the PHBV fibers. **Figure 4** shows the SEM images at both the cross-section and surface of the electrospun PHBV materials containing different amounts of MCM-41 with eugenol. The surface cryo-fractures of the electrospun materials, shown in the left column, revealed the formation of a continuous film with much reduced porosity. This process has been ascribed to a process of fibers coalescence that occurs during annealing, that is, at a temperature below the polymer's T_m (Cherpinski et al. 2017). In the case of the electrospun films having the highest particle contents, that is, 15 and 20 wt % MCM-41 with eugenol, the films presented a higher porosity and also certain plastic deformation. This observation can be related to the above-described fiber morphology and, more importantly, to the presence of high loadings of eugenol that could plasticize the PHBV matrix and/or migrate during the annealing process. In the top view of the electrospun films, shown in the right column, one can clearly observe that the

film sample containing 20 wt % MCM-41 presented higher porosity on its surface. This morphology confirms that contents above 15 wt % MCM-41 with eugenol are not optimal to be processed by electrospinning and thermally post-treatment at 160 °C. Similar findings were concluded when electrospun mats of PHBV with ~20 mol % HV were post-treated at higher temperatures than optimal, resulting in an increased porosity due to partial polymer melting and/or degradation (Melendez-Rodriguez et al. 2018).

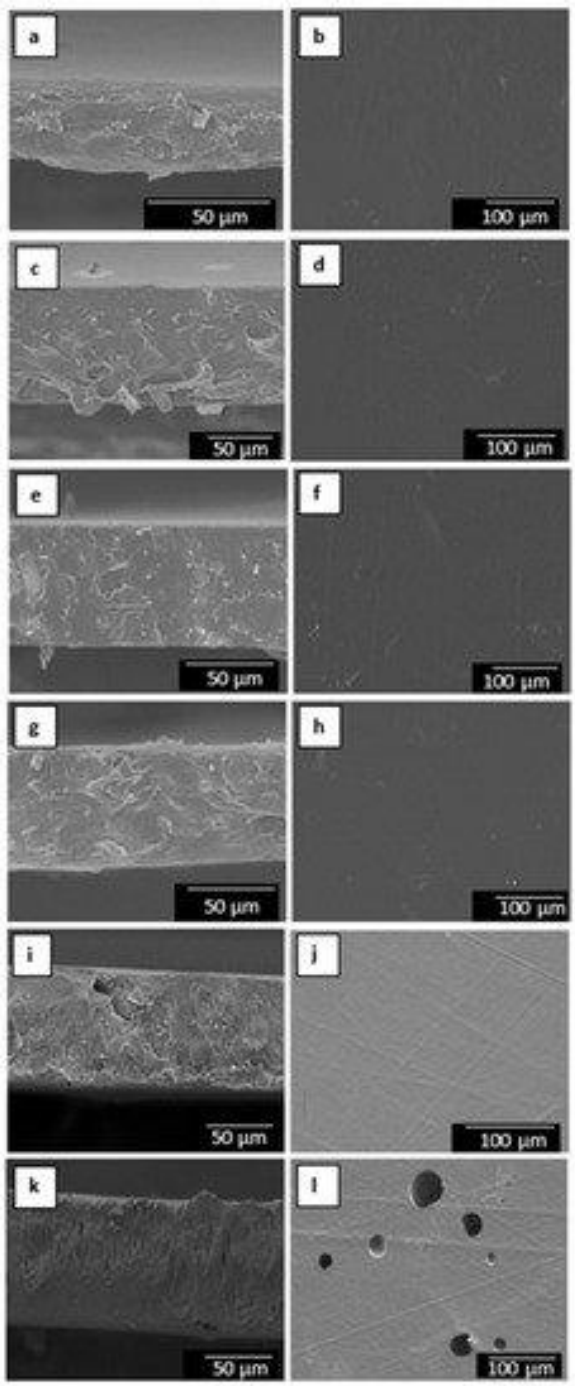

Figure 4. Scanning electron microscopy (SEM) images of the films cross-section (left) and top view (right) of poly(3-hydroxybutyrate-*co*-3-hydroxyvalerate) (PHBV)/Mobil Composition of Matter (MCM)-41 with eugenol: (a,b) 2.5 wt % MCM-41 + eugenol; (c,d) 5 wt % MCM-41 + eugenol; (e,f) 7.5 wt % MCM-41 + eugenol; (g,h) 10 wt % MCM-41 + eugenol; (k,j) 15 wt % MCM-41 + eugenol; (k,l) 20 wt % MCM-41 + eugenol. Scale markers of 50 µm and 100 µm.

Figure 5 shows the visual aspect of the resulting annealed electrospun PHBV films containing MCM-41 with eugenol. Although the contact transparency of the films was similar in all the samples, the films with the highest particle contents, that is, 15 and 20 wt % MCM-41 with eugenol, developed a yellow color. A similar yellowing and, in some cases, browning was previously observed by Muratore et al. (Muratore, Martini, and Barbosa 2018) after the incorporation of eugenol into commercial paper prepared by grafting of this EO onto cellulose at 120–180 °C. This effect was ascribed to the intrinsic eugenol color, which is a pale-yellow oily liquid, as well as secondary reactions and/or by-products due to thermal oxidation and chain scission of the substrate favored by high temperatures and prolonged time. Therefore, the incorporation of up to 10 wt % MCM-41 with eugenol successfully allows the production of contact transparent films of PHBV.

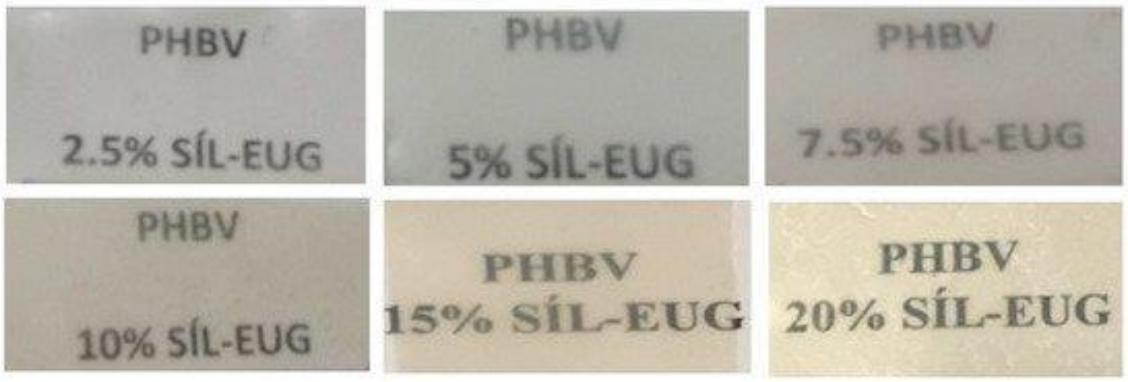

Figure 5. Visual aspect of the electrospun films of poly(3-hydroxybutyrate-*co*-3-hydroxyvalerate) (PHBV)/Mobil Composition of Matter (MCM)-41 with eugenol.

3.2. Thermal Properties

Table 2 displays the main thermal transitions, obtained by DSC during the heating and cooling steps, of the annealed electrospun neat PHBV film and the films containing MCM-41 without and with eugenol. It can be observed that the neat PHBV film presented a glass transition temperature (T_g) of 2.6 ± 0.4, while the addition of MCM-41 without eugenol had a negligible effect on T_g. Interestingly, after the incorporation of MCM-41 with eugenol, the T_g values were reduced to 1.8–0.6 °C in the PHBV film samples. Reductions of T_g are habitually associated to a plasticization process by low-molecular weight (M_W) molecules with high chemical affinity to the polymer matrix by which the free volume of the polymer is enlarged since they increase the distance between the polymer chains and then favor segmental motion (Torres-Giner, Montanes, Fenollar, et al. 2016). Some previous studies have already reported the plasticizing effect of eugenol on different polymer matrices. For instance, Fernandes Nassar et al. (Fernandes Nassar et al. 2018) reported a reduction in T_g when eugenol was incorporated into soy protein isolate (SPI) films, ascribing this effect to the plasticizing role that the aroma compound played in the protein matrix. Also, Narayanan et al. (Narayanan et al. 2013) observed a reduction in T_g from 4 °C, for the neat PHB film, to −14 °C, for PHB films containing up to 200 μg/g of eugenol.

Table 2. Thermal properties in terms of glass transition temperature (T_g), crystallization temperature (T_c), melting temperature (T_m), and normalized enthalpy of melting (ΔH_m) for the electrospun films of poly(3-hydroxybutyrate-*co*-3-hydroxyvalerate) (PHBV) and PHBV/Mobil Composition of Matter (MCM)-41 without and with eugenol.

Film	T_g (°C)	T_c (°C)	T_m (°C)	ΔH_m (J/g)
PHBV	2.6 ± 0.4	116.8 ± 0.5	170.4 ± 0.2	83.2 ± 3.0
PHBV/2.5 wt % MCM-41	2.6 ± 0.2	117.8 ± 0.6	169.9 ± 0.1	85.7 ± 0.5
PHBV/5 wt % MCM-41	2.3 ± 0.5	118.1 ± 0.4	170.1 ± 0.6	86.2 ± 4.0
PHBV/7.5 wt % MCM-41	2.4 ± 0.4	118.2 ± 0.2	171.7 ± 2.1	87.4 ± 7.3
PHBV/10 wt % MCM-41	2.3 ± 0.3	118.9 ± 0.1	170.2 ± 0.6	89.7 ± 6.3
PHBV/15 wt % MCM-41	2.2 ± 0.2	120.5 ± 0.3	170.1 ± 1.0	100.6 ± 7.4
PHBV/20 wt % MCM-41	2.5 ± 0.1	116.9 ± 0.1	169.0 ± 0.1	67.9 ± 5.9
PHBV/2.5 wt % MCM-41 + eugenol	1.8 ± 0.6	116.7 ± 0.1	169.0 ± 1.6	77.4 ± 3.4
PHBV/5 wt % MCM-41 + eugenol	1.4 ± 0.8	116.4 ± 0.6	167.4 ± 0.3	74.9 ± 6.2
PHBV/7.5 wt % MCM-41 + eugenol	1.5 ± 0.3	118.5 ± 0.3	168.8 ± 3.6	72.3 ± 6.9
PHBV/10 wt % MCM-41 + eugenol	1.3 ± 0.4	114.9 ± 0.7	165.4 ± 0.4	66.8 ± 4.8
PHBV/15 wt % MCM-41 + eugenol	0.9 ± 0.5	113.9 ± 0.2	163.4 ± 0.3	50.3 ± 4.5
PHBV/20 wt % MCM-41 + eugenol	0.6 ± 0.2	113.8 ± 0.6	160.5 ± 1.5/168.6 ± 0.1	47.4 ± 2.1

Whereas cold crystallization phenomenon was not observed in any of the PHBV films during heating, all the samples crystallized from the melt during cooling. In particular, the neat PHBV film showed a crystallization temperature (T_c) of 116.8 ± 0.5 °C. The presence of MCM-41 without eugenol increased the crystallization temperature of PHBV, up to reaching a maximum value of 120.5 °C for the film filled at 15 wt %. This result suggests that the nanoparticles provided a nucleating effect on the PHBV molecules, except for the film filled with 20 wt % MCM-41, possibly due to nanoparticles agglomeration as previously described during the morphological analysis. On the contrary, one can observe that the T_c values of the film samples containing MCM-41 with eugenol decreased as the filler content increased. Then, the T_c value was reduced up to a value of 113.8 ± 0.6 °C for the film filled with 20 wt % MCM-41 with eugenol. This restrained crystallization of PHBV can be ascribed to the above-described plasticizing effect of eugenol, which impair the packing of the polymer chains to form crystals.

During heating, the neat PHBV film melted in a single peak at 170.4 ± 0.2 °C while all the PHBV films containing MCM-41 without eugenol presented similar T_m values in the 169–171 °C range. However, the T_m values progressively reduced in the PHBV films containing MCM-41 with eugenol was as the filler content increased. Up to contents of 15 wt % MCM-41 with eugenol, the PHBV films presented a single melting peak in the 163–171 °C range, whereas the film filled with 20 wt % MCM-41 with eugenol showed two endothermic peaks, starting melting at 160.5 ± 1.5 °C. Therefore, the MCM-41 particles when loaded with eugenol were able to impair and induce some defects in the PHBV crystals, particularly at the highest tested contents. It is also worthy to note that the presence of MCM-41 without eugenol, up to fillings of 15 wt %, increased the values of enthalpy of melting (ΔH_m), confirming the formation of more perfect PHBV crystals

with thicker lamellae by a nucleation phenomenon. As opposite, all the PHBV films with MCM-41 with eugenol presented lower values of ΔH_m, being this reduction significantly noticeable for the films filled with contents above 15 wt %. Therefore, the presence of MCM-41 with eugenol impaired the crystallization of PHBV due to the above-described reduction of the biopolymer segments packing. It has been similarly reported that the addition of mesoporous silica nanoparticles has a slight influence on T_g or T_m in polymer nanocomposites (Ju, Kim, and Kang 2018, Loganathan et al. 2018), therefore supporting that the here-observed suppressed effect on the melt behavior is ascribed to eugenol. In this sense, Garrido-Miranda et al. (Garrido-Miranda et al. 2018) showed that the T_m value of PHB/thermoplastic starch (TPS)/organically modified montmorillonite (OMMT) nanocomposites was reduced by approximately 4 °C when 3 wt % eugenol was incorporated, concluding that eugenol induces the formation of less perfect crystals. Woranuch et al. (Woranuch and Yoksan 2013) also observed a ΔH_m reduction when eugenol-loaded chitosan nanoparticles were incorporated into thermoplastic flour (TPF) made of cassava, rice, and waxy rice through an extrusion process. The reduction observed was related to a plasticization by eugenol.

Figure 6 depicts the TGA curves of MCM-41 and MCM-41 with eugenol powders, the eugenol-free oil, and the electrospun films made of neat PHBV and PHBV/MCM-41 without and with eugenol. **Table 3** gathers the main relevant thermal parameters obtained from the TGA curves. As one can observe in the graph, the neat MCM-41 particles presented a mass loss of ~5 % at a temperature close to 100 °C, which can be ascribed to residual humidity on the surface and/or in the pores of the nanoparticles. In addition, the neat MCM-41 particles provided a residual mass of 95.0 ± 2.3 % measured at 800 °C. On the contrary, the eugenol free oil had a relatively low thermal stability, showing full decomposition at approximately 200 °C. Moreover, comparison of the TGA curves of the MCM-41 nanoparticles with and without eugenol corroborated that the eugenol loading was 49.5 ± 1.2 %. This loading capacity of MCM-41 was higher than other encapsulation techniques reported for polyphenols (Fang and Bhandari 2010).

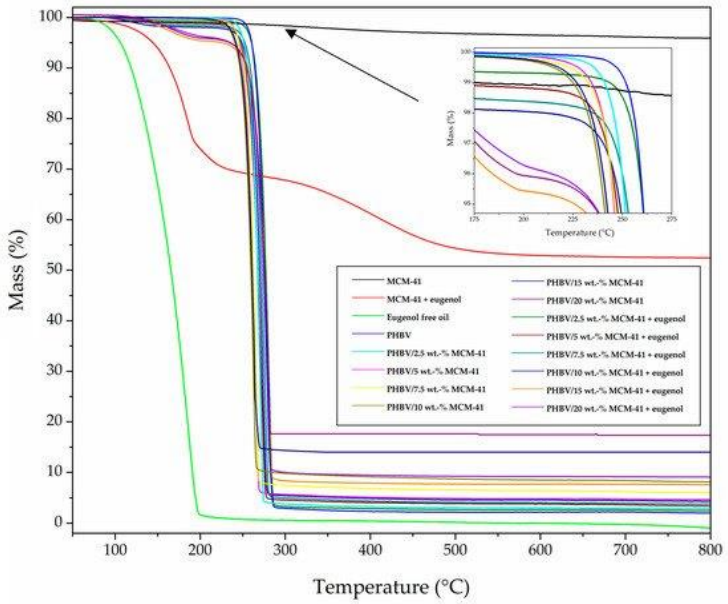

Figure 6. Thermogravimetric analysis (TGA) curves for Mobil Composition of Matter (MCM)-41, eugenol, MCM-41 with eugenol, poly(3-hydroxybutyrate-*co*-3-hydroxyvalerate) (PHBV), and PHBV/Mobil Composition of Matter (MCM)-41 without and with eugenol.

Table 3. Thermal properties in terms of mass loss was 5 % ($T_{5\%}$), degradation temperature (T_{deg}), mass loss at T_{deg}, and a residual mass at 800 °C for Mobil Composition of Matter (MCM)-41, MCM-41 with eugenol, eugenol free oil, and electrospun films of poly(3-hydroxybutyrate-*co*-3-hydroxyvalerate) (PHBV) and PHBV/MCM-41 without and with eugenol.

Sample	$T_{5\%}$ (°C)	T_{deg} (°C)	Mass loss (%)	Residual mass (%)
MCM-41 powder	-	-	-	95.0 ± 2.3
MCM-41 with eugenol powder	143.7 ± 2.4	178.3 ± 0.7	16.3 ± 0.5	52.4 ± 1.9
Eugenol free oil	105.9 ± 3.2	185.5 ± 0.6	80.6 ± 1.1	0.9 ± 0.1
PHBV	259.9 ± 1.2	277.3 ± 0.6	62.0 ± 0.8	2.0 ± 0.2
PHBV/2.5 wt % MCM-41	250.8 ± 2.3	270.9 ± 0.2	74.4 ± 1.2	3.3 ± 0.4
PHBV/5 wt % MCM-41	245.3 ± 2.7	265.4 ± 1.0	72.1 ± 0.6	5.4 ± 0.8
PHBV/7.5 wt % MCM-41	245.3 ± 2.2	265.4 ± 0.8	70.3 ± 0.3	8.0 ± 0.4
PHBV/10 wt % MCM-41	240.7 ± 1.8	262.7 ± 0.5	70.8 ± 0.2	9.1 ± 1.0
PHBV/15 wt % MCM-41	230.0 ± 2.0	262.0 ± 0.2	70.2 ± 0.7	14.6 ± 0.9
PHBV/20 wt % MCM-41	215.2 ± 1.7	256.4 ± 0.6	80.5 ± 0.9	17.2 ± 0.2
PHBV/2.5 wt % MCM-41 + eugenol	259.8 ± 2.6	281.0 ± 2.5	71.3 ± 0.3	2.5 ± 0.4
PHBV/5 wt % MCM-41 + eugenol	251.7 ± 1.4	276.4 ± 1.6	71.4 ± 0.3	3.4 ± 0.7
PHBV/7.5 wt % MCM-41 + eugenol	248.0 ± 2.7	273.7 ± 0.9	72.8 ± 0.4	3.8 ± 0.8
PHBV/10 wt % MCM-41 + eugenol	247.1 ± 3.2	271.8 ± 0.7	73.9 ± 0.7	4.3 ± 1.0
PHBV/15 wt % MCM-41 + eugenol	215.2 ± 7.3	261.0 ± 4.2	74.6 ± 1.4	7.5 ± 3.6
PHBV/20 wt % MCM-41 + eugenol	205.1 ± 5.1	259.2 ± 4.4	75.6 ± 1.2	9.1 ± 3.7

In relation to the neat PHBV film, a low-intense first weight loss process (<1 %) was observed at 100 °C due to absorbed moisture and/or volatiles leaving the samples. Trapped solvent losses were discarded by Fourier transform infrared (FTIR) spectroscopy and TGA of the neat PHBV fibers (results not shown). One can also observe that the biopolymer presented the onset of degradation, measured at the temperature at which the mass loss was 5 % ($T_{5\%}$), at 259.9 ± 1.2 °C. The degradation temperature (T_{deg}) occurred at 277.3 ± 0.6 °C, degrading in a single step and producing a residual mass of 2.0 ± 0.2 % at 800 °C. In addition, the weight loss process corresponding to thermal decomposition reaction of the biopolymer chain occurred sharply, approximately from 225 °C to 275 °C. The thermal degradation onset was shifted to lower temperatures when both the MCM-41 without and with eugenol, in all the composition range, was incorporated. This result suggests that the nanoparticles catalyzed thermal degradation. Interestingly, the $T_{5\%}$ and T_{deg} values were slightly improved at the lowest content of MCM-41 with eugenol, which can be related to the above-described nucleating effect and restricted mobility of the biopolymer chains by the presence of MCM-41 and eugenol. However, the thermal stability was reduced at the higher filler contents, that is, 15 wt % and 20 wt % MCM-41 with eugenol, due to the high content of both MCM-41 and eugenol. Furthermore, the residual weight at 800 °C of the PHBV/MCM-41 with eugenol films increased due to the presence of the mesoporous silica nanoparticles. In any case, the incorporation of up to 10 wt % of MCM-41 with eugenol had a relatively low influence on the thermal stability of the PHBV films, which can be considered a positive result since they encapsulate an active component with low thermal stability. In this sense, Requena et al. (Requena et al. 2016) reported that the incorporation of carvacrol and

eugenol enhanced the thermal sensitivity of PHBV, decreasing the onset temperature, whereas the incorporation of whole essential oils (oregano and clove) slightly promoted its thermal stability. The latter effect was suggested to occur due to a strong bonding of the eugenol with the polymer network.

3.3. Mechanical Properties

Since the resultant electrospun films may be subjected to various kinds of stress during use, the determination of the mechanical properties involves not only scientific but also technological and practical aspects. **Table 4** displays the values of elastic modulus (E), tensile strength at yield (σ_y), elongation at break (ε_b), and toughness (T) of the electrospun films made of PHBV and PHBV/MCM-41 with eugenol calculated from their strain–stress curves. In general, all the electrospun films presented characteristics of a brittle material associated to the inherent low ductility of PHBV, showing ε_b and T values below 3 % and 0.5 mJ/m^3, respectively. The film specimens also presented a relative high mechanical strength. In particular, the mean values of E were comprised in the of 1250–2000 MPa range while σ_y varied from approximately 18 to 30 MPa. The here-obtained mechanical properties of the PHBV films are similar to those recently reported in our group by Cherpinski et al. (Cherpinski et al. 2017) for PHB films also prepared by electrospinning and thereafter thermally post-treated, having a E value of 1104 MPa and ε_b and T values of 2.9 % and 0.3 mJ/m^3, respectively.

Table 4. Mechanical properties in terms of elastic modulus (E), tensile strength at yield (σ_y), elongation at break (ε_b), and toughness (T) for the electrospun films of poly(3-hydroxybutyrate-*co*-3-hydroxyvalerate) (PHBV) and PHBV/Mobil Composition of Matter (MCM)-41 with eugenol.

Film	E (MPa)	σ_y (MPa)	ε_b (%)	T (mJ/m^3)
PHBV	1252 ± 79	18.1 ± 2.1	2.4 ± 0.3	0.3 ± 0.1
PHBV/2.5 wt % MCM-41 + eugenol	1735 ± 60	27.0 ± 2.4	2.4 ± 0.1	0.4 ± 0.1
PHBV/5 wt % MCM-41 + eugenol	1976 ± 162	25.1 ± 7.8	1.7 ± 0.4	0.2 ± 0.1
PHBV/7.5 wt % MCM-41 + eugenol	2000 ± 365	27.7 ± 5.4	2.2 ± 0.2	0.4 ± 0.1
PHBV/10 wt % MCM-41 + eugenol	1802 ± 288	21.7 ± 5.8	1.8 ± 0.2	0.2 ± 0.1
PHBV/15 wt % MCM-41 + eugenol	1702 ± 140	29.4 ± 3.4	2.0 ± 0.3	0.3 ± 0.1
PHBV/20 wt % MCM-41 + eugenol	1462 ± 358	25.1 ± 5.4	2.1 ± 0.5	0.3 ± 0.2

It can be observed that the incorporation of MCM-41 with eugenol increased the mechanical strength of the PHBV films while the ductility was slightly reduced. This effect can be related to the reinforcing effect of MCM-41 as a filler in the PHBV matrix, while the smaller impact in ductility may be accounted for the plasticizing effect that the released eugenol may have in the polymer matrix. This mechanical enhancement of E and σ_y indicates a good transfer of mechanical energy from the hard filler, that is, MCM-41, as well as the interaction between the biopolymer matrix and the silica nanoparticles. Considering both the low concentration of MCM-41 and the presence of eugenol, which acts as plasticizer, the mechanical reinforcement of the

filler is thought to dominate the enhancement in E and σ_y. However, a comparative reduction, change in trend, in mechanical strength was observed when the content of the antimicrobial filler exceeded 10 wt %. This effect may be ascribed to a balance between filler agglomeration and stronger plasticizing effect of the released eugenol. High tensile strengths are generally necessary for food packaging films in order to withstand the normal stress encountered during their application, subsequent shipping, and handling (Rivero, García, and Pinotti 2009). Similarly, Voon et al. (Voon et al. 2012) reported that the addition of 3 wt % of mesoporous silica nanoparticles to bovine gelatin films improved their mechanical resistant properties, that is, σ_y, while it reduced ε_b. Others studies have also demonstrated that the incorporation of mesoporous silica nanoparticles can remarkably enhance the mechanical strength in PVOH-based materials due to the intermolecular interactions between the fillers and the polymer when prepared by in situ radical copolymerization (Jia et al. 2007, Tang et al. 2008). As compared to commercial biopolymers for packaging applications, the here-developed electrospun films of PHBV/MCM-41 with eugenol are slightly less deformable but more elastic than thermo-compressed PHBV films, stiffer but less ductile than rigid polylactide (PLA) films, and mechanically stronger but considerably more brittle than flexible poly(butylene adipate-*co*-terephthalate) (PBAT) (Quiles-Carrillo et al. 2019).

3.4. Barrier properties

Table 5 gathers the WVP and LP values of the electrospun PHBV/MCM-41 with eugenol films. It can be observed that the incorporation of low contents of MCM-41 with eugenol, that is, 2.5 and 5 wt %, induced an increase in the WVP values of the electrospun PHBV films while the water vapor barrier properties were improved for contents higher than 7.5 wt %. A similar effect was observed in the case of LP. The resultant increase in permeability observed at low filler loadings can be related to the plasticizing effect of eugenol on the PHBV matrix outweighing the barrier effect of the MCM-41 filler, as above discussed during the thermal analysis, with a subsequent increase in the matrix free volume. At higher contents, however, the barrier improvements can be ascribed to the presence of large quantities of mesoporous silica nanoparticles. Then, MCM-41 successfully acted as barrier elements forcing the permeant molecules to travel through a longer path to permeate across according to the early theory suggested by Nielsen (Nielsen 1967). It is also worthy to mention the change in the barrier trend observed for the film samples containing the highest filler contents, that is, 20 wt % MCM-41 with eugenol. This permeability change in trend can also be ascribed to the above-mentioned higher filler agglomeration resulting in a somewhat increased porosity as observed in the morphological analysis, leading to preferential paths for diffusion.

Table 5. Permeability values in terms of water vapor permeability (WVP) and $_{D}$-limonene permeability (LP) for the electrospun films of poly(3-hydroxybutyrate-*co*-3-hydroxyvalerate) (PHBV) and PHBV/Mobil Composition of Matter (MCM)-41 with eugenol.

Sample	WVP x 10^{14} ($kg \cdot m \cdot m^{-2} \cdot Pa^{-1} \cdot s^{-1}$)	LP x 10^{14} ($kg \cdot m \cdot m^{-2} \cdot Pa^{-1} \cdot s^{-1}$)
PHBV	5.34 ± 1.79	2.68 ± 1.82
PHBV/2.5 wt % MCM-41 + eugenol	8.68 ± 3.57	3.41 ± 0.97
PHBV/5 wt % MCM-41 + eugenol	8.84 ± 4.36	3.49 ± 1.17
PHBV/7.5 wt % MCM-41 + eugenol	4.25 ± 4.04	3.51 ± 0.54
PHBV/10 wt % MCM-41 + eugenol	2.99 ± 0.95	2.32 ± 0.68
PHBV/15 wt % MCM-41 + eugenol	0.25 ± 0.19	0.38 ± 0.20
PHBV/20 wt % MCM-41 + eugenol	4.08 ± 1.98	4.66 ± 2.91

The here-prepared electrospun films of PHBV/MCM-41 with eugenol showed higher WVP values than PHBV films with 12 mol % HV prepared by solvent casting, that is, 1.27×10^{-14} $kg \cdot m \cdot m^{-2} \cdot Pa^{-1} \cdot s^{-1}$ (Sanchez-Garcia, Gimenez, and Lagaron 2008) or PHB films obtained by compression-molded, that is, 1.7×10^{-15} $kg \cdot m \cdot m^{-2} \cdot Pa^{-1} \cdot s^{-1}$ (Sanchez-Garcia, Gimenez, and Lagaron 2007), which can be related to the higher mol % HV fraction in the here-used copolyester. Therefore, it can be considered that intermediate contents of MCM-41 with eugenol inside the fibers promoted lower free volume available for diffusion. Similar results were reported for instance by Hashemi Tabatabaei et al. (Hashemi Tabatabaei et al. 2018), who showed that the incorporation of 5 wt % mesoporous silica microparticles decreased the WVP value from 8.9 $g \cdot m \cdot m^{-2} \cdot Pa^{-1} \cdot s^{-1}$ to 1.6×10^{-11} $g \cdot m \cdot m^{-2} \cdot Pa^{-1} \cdot s^{-1}$ in gelatin/k-carrageenan films. Also, Hassannia-Kolaee et al. (Hassannia-Kolaee et al. 2016) reported a reduction of up to approximately 33 % in WVP for whey protein isolate (WPI)/pullulan (PUL) films containing 1, 3, and 5 wt % mesoporous silica nanoparticles prepared by a casting method. The barrier improvement achieved was attributed to the formation of hydrogen bonds between the polymer hydroxyl groups and the oxygen atoms of silica and also to the good dispersion of the nanoparticles in the polymer matrix. In relation to eugenol, some studies have also demonstrated that the direct incorporation of EOs, among them eugenol, in polymer films do not induce significant change in WVP, concluding that water permeability basically depends on the hydrophilic–hydrophobic ratio of the film constituents (Aguirre, Borneo, and Leon 2013, Tongnuanchan, Benjakul, and Prodpran 2012). Other studies have reported that the addition of EOs can negatively increase the water permeability depending on the nature of the polymer matrix and the type and concentration of EO (Atarés et al. 2010). However, this impairment may be attributed to the difficulties encountered to integrate the hydrophobic EO in hydrophilic networks that might cause matrix disruptions and create void spaces at the polymer–oil interface (Atarés and Chiralt 2016). However, in the current study, the expected plasticizing effect of the hydrophobic eugenol within the PHBV matrix is seen detrimental for the barrier performance at lower silica loadings.

3.5. Antimicrobial activity

S. aureus and *E. coli* are common microorganisms associated with food-related diseases. Therefore, the incorporation of active substances in the design of packaging materials can be an important technology not only to avoid food waste but also to enhance food safety (Torres-Giner, Gil, et al. 2018). For the pure eugenol in its original liquid form, the MIC and BIC values for *S. aureus* were 1.25 µl/ml and 2.5 µl/ml, respectively, and for *E. coli* these values were 2.5 µl/ml and 5 µl/ml, respectively. The MCM-41 particles with eugenol presented a MIC value against *S. aureus* and *E. coli* of 10 µg/ml and 20 µg/ml, respectively, while the BIC values were 40 µg/ml for both bacteria. The higher value observed for *E. coli* can be ascribed to the greater bacterial resistance of G- bacteria than G+ ones (Exner et al. 2017), thus a higher dose of the antimicrobial was needed to obtain the same efficacy.

The antimicrobial activity of the film samples was evaluated using the JIS Z2801. The reduction values in the open system against *S. aureus* and *E. coli* are gathered in **Table 6** and **Table 7**, respectively. **Table 8** and **Table 9** includes the values against *S. aureus* and *E. coli*, respectively, in the closed system. As expected, it can be observed that both the unfilled PHBV film and the different PHBV films containing MCM-41 without eugenol showed no inhibition effect on the bacterial growth ($R \leq 1$). In contrast, the incorporation of MCM-41 with eugenol into the PHVB film exhibited significant antibacterial activity against both bacteria. In the open system, at the initial day, that is, for the tests carried out the same day of the film production, the bacterial reduction on the film surface gradually increased with the content of MCM-41 with eugenol. As it can be seen in **Table 6** for *S. aureus*, at the lowest contents, that is, 2.5 and 5 wt % MCM-41 with eugenol, the films presented a slight antibacterial activity ($R \geq 1$ and < 2). For the highest tested contents, that is, 7.5 and 10 wt % MCM-41 with eugenol, the films generated a significant surface reduction ($R \geq 1$ and < 3). Although none of the films produced a strong reduction ($R \geq 3$), materials with values of surface reduction in the 1–2 range are usually considered as bacteriostatic (Castro-Mayorga, Fabra, Pourrahimi, et al. 2017). Therefore, electrospun PHBV films with 10 wt % MCM-41 with eugenol were able to provide a bacteriostatic effect against *S. aureus*. As also shown in the table, after 15 days, the films still kept a significant antibacterial activity. In particular, the films with 7.5 and 10 wt % MCM-41 with eugenol still presented significant values of reduction ($R \geq 1$ and < 3) while these presented slight values ($R \geq 0.5$ and < 1) for loadings of 2.5 and 5 wt %. This suggests that, although part of eugenol was released from the films, MCM-41 was still able to retain over time a significant amount of EO. Regarding *E. coli*, shown in **Table 7**, the required concentration of MCM-41 with eugenol to generate an antimicrobial effect in the open system was 15 wt %. At this content, the films presented a significant value of reduction, that is, R values of 1.30 and 1.40 at days 0 and 15, respectively. This supports the above-described higher antimicrobial resistance of *E. coli*, as a G- bacterium, which would need more exposure time to the active oil to render a similar antimicrobial activity.

Table 6. Antibacterial activity against *Staphylococcus aureus* (*S. aureus*) in the open system for the electrospun films of poly(3-hydroxybutyrate-*co*-3-hydroxyvalerate) (PHBV) and PHBV/Mobil Composition of Matter (MCM)-41 with eugenol.

Films	Initial		After 15 days	
	Bacterial counts [log (CFU/ml)]	R	Bacterial counts [log (CFU/ml)]	R
Control day 0	5.75 ± 0.09	-	5.75 ± 0.09	-
Control 24 h	5.67 ± 0.07	-	5.68 ± 0.03	-
PHBV	5.39 ± 0.56	0.28 ± 0.52	5.29 ± 0.41	0.38 ± 0.38
PHBV/2.5 wt % MCM-41	4.86 ± 0.54	0.81 ± 0.58	5.06 ± 0.48	0.61 ± 0.46
PHBV/2.5 wt % MCM-41 + eugenol	4.33 ± 0.35	1.04 ± 0.39	4.75 ± 0.09	0.92 ± 0.12
PHBV/5 wt % MCM-41	5.47 ± 0.58	0.20 ± 0.65	5.51 ± 0.09	0.16 ± 0.06
PHBV/5 wt % MCM-41 + eugenol	4.60 ± 0.23	1.07 ± 0.23	4.69 ± 0.14	0.99 ± 0.14
PHBV/7.5 wt % MCM-41	5.77 ± 0.07	0.10 ± 0.01	5.44 ± 0.55	0.24 ± 0.57
PHBV/7.5 wt % MCM-41 + eugenol	4.55 ± 0.06	1.12 ± 0.11	4.55 ± 0.12	1.12 ± 0.15
PHBV/10 wt % MCM-41	5.98 ± 0.57	0.31 ± 0.06	4.70 ± 0.06	0.97 ± 0.09
PHBV/10 wt % MCM-41 + eugenol	4.43 ± 0.24	1.23 ± 0.20	4.55 ± 0.07	1.24 ± 0.10

Table 7. Antibacterial activity against *Escherichia coli* (*E. coli*) in the open system for the electrospun films of poly(3-hydroxybutyrate-*co*-3-hydroxyvalerate) (PHBV) and PHBV/Mobil Composition of Matter (MCM)-41 with eugenol.

Films	Initial		After 15 days	
	Bacterial counts [log (CFU/ml)]	R	Bacterial counts [log (CFU/ml)]	R
Control day 0	5.76 ± 0.01	-	5.71 ± 0.02	-
Control 24 h	6.81 ± 0.01	-	6.80 ± 0.02	-
PHBV	5.99 ± 0.07	0.82 ± 0.01	6.08 ± 0.03	0.72 ± 0.05
PHBV/15 wt % MCM-41	6.41 ± 0.01	0.40 ± 0.03	6.15 ± 0.04	0.65 ± 0.06
PHBV/15 wt % MCM-41 + eugenol	5.51 ± 0.02	1.30 ± 0.02	5.40 ± 0.01	1.40 ± 0.06

Table 8. Antibacterial activity against *Staphylococcus aureus* (*S. aureus*) in the closed system for the electrospun films of poly(3-hydroxybutyrate-*co*-3-hydroxyvalerate) (PHBV) and PHBV/Mobil Composition of Matter (MCM)-41 with eugenol.

Films	Initial		After 15 days	
	Bacterial counts [log (CFU/ml)]	R	Bacterial counts [log (CFU/ml)]	R
Control day 0	5.61 ± 0.03	-	5.65 ± 0.01	-
Control 24 h	6.82 ± 0.06	-	6.85 ± 0.01	-
PHBV	6.23 ± 0.08	0.59 ± 0.01	6.11 ± 0.03	0.74 ± 0.05
PHBV/10 wt % MCM-41	6.30 ± 0.01	0.52 ± 0.03	6.09 ± 0.04	0.76 ± 0.06
PHBV/10 wt % MCM-41 + eugenol	5.47 ± 0.01	1.35 ± 0.15	5.21 ± 0.01	1.64 ± 0.09

Table 9. Antibacterial activity against *Escherichia coli* (*E. coli*) in the closed system for the electrospun films of poly(3-hydroxybutyrate-*co*-3-hydroxyvalerate) (PHBV) and PHBV/Mobil Composition of Matter (MCM)-41 with eugenol.

Films	Initial		After 15 days	
	Bacterial counts [log (CFU/ml)]	R	Bacterial counts [log (CFU/ml)]	R
Control day 0	5.68 ± 0.03	-	5.66 ± 0.06	-
Control 24 h	6.83 ± 0.01	-	6.60 ± 0.01	-
PHBV	6.10 ± 0.01	0.73 ± 0.01	6.11 ± 0.03	0.49 ± 0.04
PHBV/15 wt % MCM-41	6.24 ± 0.01	0.59 ± 0.03	6.26 ± 0.06	0.34 ± 0.01
PHBV/15 wt % MCM-41 + eugenol	5.49 ± 0.03	1.34 ± 0.03	5.02 ± 0.07	1.58 ± 0.01

The tested closed system was aimed to better represent the real conditions in a packaging material. In the case of *S. aureus*, which is shown in **Table 8**, the film with 10 wt % MCM-41 with eugenol was selected since this sample showed a high R value at a relatively low content of filler. One can observe that the antimicrobial activity was higher than that observed in the open system, showing R values of 1.35 and 1.64 for day 0 and 15, respectively. This confirms the high volatility of eugenol, which remained enclosed and still active in the system in comparison to the open one. In **Table 9**, for *E. coli*, the R values were 1.34 and 1.58 for day 0 and 15, respectively, in the closed system. Therefore, the here-achieved antimicrobial effect was somehow higher in the closed system than in the open one. This result has been recently ascribed to the volatile portion of active components accumulated in the system's headspace, which successfully contributed to decrease bacterial growth (Figueroa-Lopez et al. 2019). In any case, the differences in bacterial reduction in both tested packaging conditions, that is, the open and closed systems, for each type of bacteria was relatively low. This observation can be related to the use of MCM-41 that successfully performed as vehicles to control the release of eugenol and to render high antimicrobial activity.

Similar to this study, other authors have previously reported the antibacterial activity of eugenol in different biopolymer articles. For instance, PCL/gelatin electrospun membranes loaded with active peptide containing 30 wt % of eugenol successfully inhibited the growth of *E. coli* and *S. aureus* with inhibition rates of 71.6 % and 78.6 %, respectively (Li et al. 2018). In another study, compression-molded PHBV bilayer films were sprayed with four active components, among them eugenol, resulting in antimicrobial systems against G- and G+ bacteria such as *E. coli* and *Listeria innocua* (*L. innocua*) (Requena et al. 2016). In this previous research, the added active agents were more effective against G- than G+, which in agreement with the present results. The benefit of loading antimicrobial agents in MCM-41 has been also studied elsewhere, both against bacteria and fungi. For instance, Park et al. (Park, Barton, and Pendleton 2011) loaded allyl isothiocyanate, a natural antimicrobial, in MCM-41 as a novel controlled release vector against selected foodborne pathogenic microorganisms. In other studies, other volatile EOs were immobilized on the surface of mesoporous silica materials acting as antifungal agents and showing improved antimicrobial activity than the free compounds (Janatova et al. 2015, Ribes et al. 2017).

4. Conclusions

EOs are well known for their antimicrobial properties, being suitable as food preservatives. However, to ensure their long-term effect, which is controlled by their volatility, it may be necessary to encapsulate them in, for instance, porous materials. The present study evaluated the complexation of eugenol EO on MCM-41 to be thereafter incorporated into PHBV biopolymers by electrospinning. The resultant electrospun mats were annealed below the biopolymer melting point to generate continuous films. The thermal analysis performed on the films showed that the incorporation of MCM-41 with eugenol induced certain plasticization on PHBV as well as a reduction in crystallinity. Interestingly, the incorporation of MCM-41 with eugenol up to 10 wt % had a relatively low influence on the thermal stability of the PHBV films. During the mechanical analysis, it was observed that the mechanical strength of the PHBV films was increased while the ductility was only slightly reduced after the incorporation of MCM-41 with eugenol. The barrier properties were also enhanced due to the presence of the eugenol-containing nanofillers and were optimal around contents of 15 wt %. Finally, the antimicrobial activity against *S. aureus* and *E. coli* was studied in both an open and closed system to better represent the real conditions in packaging applications. The electrospun biopolymer films showed antibacterial activity after 15 days, being higher (as expected) in the ones that were studied in the closed system, which was ascribed to the accumulation of eugenol in the system's headspace. For all this, the films developed can be regarded as a sustainable material to be used in the form of interlayers or coatings for active food packaging applications.

5. References

Aguirre, A., R. Borneo, and A. E. Leon. 2013. "Antimicrobial, mechanical and barrier properties of triticale protein films incorporated with oregano essential oil." *Food Bioscience* 1:2-9. doi: 10.1016/j.fbio.2012.12.001.

Alfredsson, V., M. Keung, A. Monnier, G. D. Stucky, K. K. Unger, and F. Schüth. 1994. "High-resolution transmission electron microscopy of mesoporous MCM-41 type materials." *Journal of the Chemical Society, Chemical Communications* (8):921-922. doi: 10.1039/C39940000921.

An, J., H. Zhang, J. Zhang, Y. Zhao, and X. Yuan. 2009. "Preparation and antibacterial activity of electrospun chitosan/ poly(ethylene oxide) membranes containing silver nanoparticles." *Colloid and Polymer Science* 287 (12):1425-1434. doi: 10.1007/s00396-009-2108-y.

Atarés, L., and A. Chiralt. 2016. "Essential oils as additives in biodegradable films and coatings for active food packaging." *Trends in Food Science and Technology* 48:51-62. doi: 10.1016/j.tifs.2015.12.001.

Atarés, L., C. De Jesús, P. Talens, and A. Chiralt. 2010. "Characterization of SPI-based edible films incorporated with cinnamon or ginger essential oils." *Journal of Food Engineering* 99 (3):384-391. doi: 10.1016/j.jfoodeng.2010.03.004.

Beck, J. S., J. C. Vartuli, W. J. Roth, M. E. Leonowicz, C. T. Kresge, K. D. Schmitt, C. T. W. Chu, D. H. Olson, E. W. Sheppard, S. B. McCullen, J. B. Higgins, and J. L. Schlenker. 1992. "A New Family of Mesoporous Molecular Sieves Prepared with Liquid Crystal Templates." *Journal of the American Chemical Society* 114 (27):10834-10843. doi: 10.1021/ja00053a020.

Bernardos, A., T. Marina, P. Žáček, E. Pérez-Esteve, R. Martínez-Mañez, M. Lhotka, L. Kouřimská, J. Pulkrábek, and P. Klouček. 2015. "Antifungal effect of essential oil components against Aspergillus niger when loaded into silica mesoporous supports." *Journal of the Science of Food and Agriculture* 95 (14):2824-2831. doi: 10.1002/jsfa.7022.

Burt, S. 2004. "Essential oils: Their antibacterial properties and potential applications in foods - A review." *International Journal of Food Microbiology* 94 (3):223-253. doi: 10.1016/j.ijfoodmicro.2004.03.022.

Castro-Mayorga, J. L., M. J. Fabra, L. Cabedo, and J. M. Lagaron. 2017. "On the use of the electrospinning coating technique to produce antimicrobial polyhydroxyalkanoate materials containing in situ-stabilized silver nanoparticles." *Nanomaterials* 7 (1). doi: 10.3390/nano7010004.

Castro-Mayorga, J. L., M. J. Fabra, A. M. Pourrahimi, R. T. Olsson, and J. M. Lagaron. 2017. "The impact of zinc oxide particle morphology as an antimicrobial and when incorporated in poly(3-hydroxybutyrate-co-3-hydroxyvalerate) films for food packaging and food contact surfaces applications." *Food and Bioproducts Processing* 101:32-44. doi: https://doi.org/10.1016/j.fbp.2016.10.007.

Castro Mayorga, J. L., M. J. Fabra Rovira, L. Cabedo Mas, G. Sánchez Moragas, and J. M. Lagarón Cabello. 2018. "Antimicrobial nanocomposites and electrospun coatings based on poly(3-hydroxybutyrate-co-3-hydroxyvalerate) and copper oxide nanoparticles for active packaging and coating applications." *Journal of Applied Polymer Science* 135 (2). doi: 10.1002/app.45673.

Chatterjee, D., and P. Bhattacharjee. 2013. "Comparative evaluation of the antioxidant efficacy of encapsulated and un-encapsulated eugenol-rich clove extracts in soybean oil: Shelf-life and frying stability of soybean oil." *Journal of Food Engineering* 117 (4):545-550. doi: 10.1016/j.jfoodeng.2012.11.016.

Cherpinski, A., M. Gozutok, H. T. Sasmazel, S. Torres-Giner, and J. M. Lagaron. 2018. "Electrospun oxygen scavenging films of poly(3-hydroxybutyrate) containing palladium

nanoparticles for active packaging applications." *Nanomaterials* 8 (7). doi: 10.3390/nano8070469.

Cherpinski, A., S. Torres-Giner, L. Cabedo, and J. M. Lagaron. 2017. "Post-processing optimization of electrospun submicron poly(3-hydroxybutyrate) fibers to obtain continuous films of interest in food packaging applications." *Food Additives and Contaminants - Part A Chemistry, Analysis, Control, Exposure and Risk Assessment* 34 (10):1817-1830. doi: 10.1080/19440049.2017.1355115.

Cherpinski, A., S. Torres-Giner, J. Vartiainen, M. S. Peresin, P. Lahtinen, and J. M. Lagaron. 2018. "Improving the water resistance of nanocellulose-based films with polyhydroxyalkanoates processed by the electrospinning coating technique." *Cellulose* 25 (2):1291-1307. doi: 10.1007/s10570-018-1648-z.

Choi, J. I., and S. Y. Lee. 1997. "Process analysis and economic evaluation for poly(3-hydroxybutyrate) production by fermentation." *Bioprocess Engineering* 17 (6):335-342. doi: 10.1007/s004490050394.

Climent, E., P. Calero, M. D. Marcos, R. Martínez-Máñez, F. Sancenón, and J. Soto. 2009. "Selective chromofluorogenic sensing of heparin by using functionalised silica nanoparticles containing binding sites and a signalling reporter." *Chemistry - A European Journal* 15 (8):1816-1820. doi: 10.1002/chem.200802074.

da Silva, F. F. M., F. J. Q. Monte, T. L. G. de Lemos, P. G. G. do Nascimento, A. K. de Medeiros Costa, and L. M. M. de Paiva. 2018. "Eugenol derivatives: synthesis, characterization, and evaluation of antibacterial and antioxidant activities." *Chemistry Central Journal* 12 (1). doi: 10.1186/s13065-018-0407-4.

Díez-Pascual, A. M., and A. L. Díez-Vicente. 2014. "ZnO-reinforced poly(3-hydroxybutyrate-co-3-hydroxyvalerate) bionanocomposites with antimicrobial function for food packaging." *ACS Applied Materials and Interfaces* 6 (12):9822-9834. doi: 10.1021/am502261e.

Exner, Martin, Sanjay Bhattacharya, Bärbel Christiansen, Jürgen Gebel, Peter Goroncy-Bermes, Philippe Hartemann, Peter Heeg, Carola Ilschner, Axel Kramer, Elaine Larson, Wolfgang Merkens, Martin Mielke, Peter Oltmanns, Birgit Ross, Manfred Rotter, Ricarda Schmithausen, Hans-Günther Sonntag, and Matthias Trautmann. 2017. "Antibiotic resistance: What is so special about multidrug-resistant Gram-negative bacteria?" *GMS Hygiene and Infection Control* 12. doi: 10.3205/dgkh000290.

Fan, J., C. Yu, F. Gao, J. Lei, B. Tian, L. Wang, Q. Luo, B. Tu, W. Zhou, and D. Zhao. 2003. "Cubic mesoporous silica with large controllable entrance sizes and advanced adsorption properties." *Angewandte Chemie - International Edition* 42 (27):3146-3150. doi: 10.1002/anie.200351027.

Fang, Z., and B. Bhandari. 2010. "Encapsulation of polyphenols - A review." *Trends in Food Science and Technology* 21 (10):510-523. doi: 10.1016/j.tifs.2010.08.003.

Fernandes Nassar, S., C. Dombre, E. Gastaldi, F. Touchaleaume, and P. Chalier. 2018. "Soy protein isolate nanocomposite film enriched with eugenol, an antimicrobial agent: Interactions and properties." *Journal of Applied Polymer Science* 135 (10). doi: 10.1002/app.45941.

Figueroa-Lopez, Kelly J., António A. Vicente, Maria A.M. Reis, Sergio Torres-Giner, and Jose M. Lagaron. 2019. "Antimicrobial and Antioxidant Performance of Various Essential Oils and Natural Extracts and Their Incorporation into Biowaste Derived Poly(3-hydroxybutyrate-co-3-hydroxyvalerate) Layers Made from Electrospun Ultrathin Fibers." *Nanomaterials* 9 (2):144.

Garrido-Miranda, K. A., B. L. Rivas, M. A. Pérez-Rivera, E. A. Sanfuentes, and C. Peña-Farfal. 2018. "Antioxidant and antifungal effects of eugenol incorporated in bionanocomposites of poly(3-hydroxybutyrate)-thermoplastic starch." *LWT* 98:260-267. doi: 10.1016/j.lwt.2018.08.046.

Hashemi Tabatabaei, R., S. M. Jafari, H. Mirzaei, A. Mohammadi Nafchi, and D. Dehnad. 2018. "Preparation and characterization of nano-SiO2 reinforced gelatin-k-carrageenan biocomposites." *International Journal of Biological Macromolecules* 111:1091-1099. doi: 10.1016/j.ijbiomac.2018.01.116.

Hassannia-Kolaee, M., F. Khodaiyan, R. Pourahmad, and I. Shahabi-Ghahfarrokhi. 2016. "Development of ecofriendly bionanocomposite: Whey protein isolate/pullulan films with nano-SiO2." *International Journal of Biological Macromolecules* 86:139-144. doi: 10.1016/j.ijbiomac.2016.01.032.

He, D., X. He, K. Wang, Z. Zou, X. Yang, and X. Li. 2014. "Remote-controlled drug release from graphene oxide-capped mesoporous silica to cancer cells by photoinduced pH-jump activation." *Langmuir* 30 (24):7182-7189. doi: 10.1021/la501075c.

Hu, M., C. Li, X. Li, M. Zhou, J. Sun, F. Sheng, S. Shi, and L. Lu. 2018. "Zinc oxide/silver bimetallic nanoencapsulated in PVP/PCL nanofibres for improved antibacterial activity." *Artificial Cells, Nanomedicine and Biotechnology* 46 (6):1248-1257. doi: 10.1080/21691401.2017.1366339.

Janatova, A., A. Bernardos, J. Smid, A. Frankova, M. Lhotka, L. Kourimská, J. Pulkrabek, and P. Kloucek. 2015. "Long-term antifungal activity of volatile essential oil components released from mesoporous silica materials." *Industrial Crops and Products* 67:216-220. doi: 10.1016/j.indcrop.2015.01.019.

Jia, X., Y. Li, Q. Cheng, S. Zhang, and B. Zhang. 2007. "Preparation and properties of poly(vinyl alcohol)/silica nanocomposites derived from copolymerization of vinyl silica nanoparticles and vinyl acetate." *European Polymer Journal* 43 (4):1123-1131. doi: 10.1016/j.eurpolymj.2007.01.019.

Ju, C., T. Kim, and H. Kang. 2018. "Renewable, eugenol-modified polystyrene layer for liquid crystal orientation." *Polymers* 10 (2). doi: 10.3390/polym10020201.

Kailasapathy, K. 2009. "Encapsulation technologies for functional foods and nutraceutical product development." *CAB Reviews: Perspectives in Agriculture, Veterinary Science, Nutrition and Natural Resources* 4:1-19. doi: 10.1079/PAVSNNR20094033.

Keshavarz, T., and I. Roy. 2010. "Polyhydroxyalkanoates: bioplastics with a green agenda." *Current Opinion in Microbiology* 13 (3):321-326. doi: 10.1016/j.mib.2010.02.006.

Keskin, G., G. Klzll, M. Bechelany, C. Pochat-Bohatier, and M. Öner. 2017. "Potential of polyhydroxyalkanoate (PHA) polymers family as substitutes of petroleum based polymers for packaging applications and solutions brought by their composites to form barrier materials." *Pure and Applied Chemistry* 89 (12):1841-1848. doi: 10.1515/pac-2017-0401.

Khosravi-Darani, K., and D. Z. Bucci. 2015. "Application of poly(hydroxyalkanoate) in food packaging: Improvements by nanotechnology." *Chemical and Biochemical Engineering Quarterly* 29 (2):275-285. doi: 10.15255/CABEQ.2014.2260.

Kresge, C. T., M. E. Leonowicz, W. J. Roth, J. C. Vartuli, and J. S. Beck. 1992. "Ordered mesoporous molecular sieves synthesized by a liquid-crystal template mechanism." *Nature* 359 (6397):710-712. doi: 10.1038/359710a0.

Kulkarni, S. O., P. P. Kanekar, J. P. Jog, P. A. Patil, S. S. Nilegaonkar, S. S. Sarnaik, and P. R. Kshirsagar. 2011. "Characterisation of copolymer, poly (hydroxybutyrate-co-hydroxyvalerate) (PHB-co-PHV) produced by Halomonas campisalis (MCM B-1027), its biodegradability and potential application." *Bioresource Technology* 102 (11):6625-6628. doi: 10.1016/j.biortech.2011.03.054.

Lang, G., and G. Buchbauer. 2012. "A review on recent research results (2008-2010) on essential oils as antimicrobials and antifungals. A review." *Flavour and Fragrance Journal* 27 (1):13-39. doi: 10.1002/ffj.2082.

Lee, S. Y. 1996. "Plastic bacteria? Progress and prospects for polyhydroxyalkanoate production in bacteria." *Trends in Biotechnology* 14 (11):431-438. doi: 10.1016/0167-7799(96)10061-5.

Li, D., and Y. Xia. 2004. "Electrospinning of nanofibers: Reinventing the wheel?" *Advanced Materials* 16 (14):1151-1170. doi: 10.1002/adma.200400719.

Li, Zhenguang, Peiqiong Zhou, Fang Zhou, Yunhui Zhao, Lixia Ren, and Xiaoyan Yuan. 2018. "Antimicrobial eugenol-loaded electrospun membranes of poly(ε-caprolactone)/gelatin incorporated with REDV for vascular graft applications." *Colloids and Surfaces B: Biointerfaces* 162:335-344. doi: https://doi.org/10.1016/j.colsurfb.2017.12.004.

Loganathan, S., J. Jacob, R. B. Valapa, and S. Thomas. 2018. "Influence of linear and branched amine functionalization in mesoporous silica on the thermal, mechanical and barrier properties of sustainable poly(lactic acid) biocomposite films." *Polymer* 148:149-157. doi: 10.1016/j.polymer.2018.06.035.

Majeed, H., Y. Y. Bian, B. Ali, A. Jamil, U. Majeed, Q. F. Khan, K. J. Iqbal, C. F. Shoemaker, and Z. Fang. 2015. "Essential oil encapsulations: Uses, procedures, and trends." *RSC Adv.* 5 (72):58449-58463.

Melendez-Rodriguez, B., J. L. Castro-Mayorga, M. A. M. Reis, C. Sammon, L. Cabedo, S. Torres-Giner, and J. M. Lagaron. 2018. "Preparation and Characterization of Electrospun Food Biopackaging Films of Poly(3-hydroxybutyrate-co-3-hydroxyvalerate) Derived From Fruit Pulp Biowaste." *Frontiers in Sustainable Food Systems* 2. doi: 10.3389/fsufs.2018.00038.

Muñoz, B., A. Rámila, J. Pérez-Pariente, I. Díaz, and M. Vallet-Regí. 2003. "MCM-41 organic modification as drug delivery rate regulator." *Chemistry of Materials* 15 (2):500-503. doi: 10.1021/cm021217q.

Muratore, F., R. E. Martini, and S. E. Barbosa. 2018. "Bioactive paper by eugenol grafting onto cellulose. Effect of reaction variables." *Food Packaging and Shelf Life* 15:159-168. doi: 10.1016/j.fpsl.2017.12.010.

Narayanan, A., Neera, Mallesha, and K. V. Ramana. 2013. "Synergized antimicrobial activity of eugenol incorporated polyhydroxybutyrate films against food spoilage microorganisms in conjunction with pediocin." *Applied Biochemistry and Biotechnology* 170 (6):1379-1388. doi: 10.1007/s12010-013-0267-2.

Nielsen, L. E. 1967. "Models for the Permeability of Filled Polymer Systems." *Journal of Macromolecular Science: Part A - Chemistry* 1 (5):929-942. doi: 10.1080/10601326708053745.

Park, Sun-Young, Mary Barton, and Phillip Pendleton. 2011. "Mesoporous silica as a natural antimicrobial carrier." *Colloids and Surfaces A: Physicochemical and Engineering Aspects* 385 (1):256-261. doi: https://doi.org/10.1016/j.colsurfa.2011.06.021.

Philip, S., T. Keshavarz, and I. Roy. 2007. "Polyhydroxyalkanoates: Biodegradable polymers with a range of applications." *Journal of Chemical Technology and Biotechnology* 82 (3):233-247. doi: 10.1002/jctb.1667.

Popova, M., H. Lazarova, B. Trusheva, M. Popova, V. Bankova, J. Mihály, H. Najdenski, I. Tsvetkova, and Á Szegedi. 2018. "Nanostructured silver silica materials as potential propolis carriers." *Microporous and Mesoporous Materials* 263:28-33. doi: 10.1016/j.micromeso.2017.11.043.

Quiles-Carrillo, L., N. Montanes, J. M. Lagaron, R. Balart, and S. Torres-Giner. 2019. "In Situ Compatibilization of Biopolymer Ternary Blends by Reactive Extrusion with Low-Functionality Epoxy-Based Styrene–Acrylic Oligomer." *Journal of Polymers and the Environment* 27 (1):84-96. doi: 10.1007/s10924-018-1324-2.

Ravikovitch, P. I., S. C. O'Domhnaill, A. V. Neimark, F. Schiith, and K. K. Unger. 1995. "Capillary Hysteresis in Nanopores: Theoretical and Experimental Studies of Nitrogen Adsorption on MCM-41." *Langmuir* 11 (12):4765-4772. doi: 10.1021/la00012a030.

Reddy, C. S. K., R. Ghai, Rashmi, and V. C. Kalia. 2003. "Polyhydroxyalkanoates: An overview." *Bioresource Technology* 87 (2):137-146. doi: 10.1016/S0960-8524(02)00212-2.

Requena, R., A. Jiménez, M. Vargas, and A. Chiralt. 2016. "Poly[(3-hydroxybutyrate)-co-(3-hydroxyvalerate)] active bilayer films obtained by compression moulding and applying essential oils at the interface." *Polymer International* 65 (8):883-891. doi: 10.1002/pi.5091.

Requena, R., M. Vargas, and A. Chiralt. 2017. "Release kinetics of carvacrol and eugenol from poly(hydroxybutyrate-co-hydroxyvalerate) (PHBV) films for food packaging applications." *European Polymer Journal* 92:185-193. doi: 10.1016/j.eurpolymj.2017.05.008.

Ribes, S., M. Ruiz-Rico, É Pérez-Esteve, A. Fuentes, P. Talens, R. Martínez-Máñez, and J. M. Barat. 2017. "Eugenol and thymol immobilised on mesoporous silica-based material as

an innovative antifungal system: Application in strawberry jam." *Food Control* 81:181-188. doi: 10.1016/j.foodcont.2017.06.006.

Rivero, S., M. A. García, and A. Pinotti. 2009. "Composite and bi-layer films based on gelatin and chitosan." *Journal of Food Engineering* 90 (4):531-539. doi: 10.1016/j.jfoodeng.2008.07.021.

Robertson, G. L. 1993. *Food Packaging: Principles and Practice*.

Ruiz-Rico, M., C. Fuentes, T. Pérez-Esteve, A. I. Jiménez-Belenguer, A. Quiles, M. D. Marcos, R. Martínez-Máñez, and J. M. Barat. 2015. "Bactericidal activity of caprylic acid entrapped in mesoporous silica nanoparticles." *Food Control* 56:77-85. doi: 10.1016/j.foodcont.2015.03.016.

Ruiz-Rico, M., É Pérez-Esteve, A. Bernardos, F. Sancenón, R. Martínez-Máñez, M. D. Marcos, and J. M. Barat. 2017. "Enhanced antimicrobial activity of essential oil components immobilized on silica particles." *Food Chemistry* 233:228-236. doi: 10.1016/j.foodchem.2017.04.118.

Sanchez-Garcia, M. D., E. Gimenez, and J. M. Lagaron. 2007. "Novel PET nanocomposites of interest in food packaging applications and comparative barrier performance with biopolyester nanocomposites." *Journal of Plastic Film and Sheeting* 23 (2):133-148. doi: 10.1177/8756087907083590.

Sanchez-Garcia, M. D., E. Gimenez, and J. M. Lagaron. 2008. "Morphology and barrier properties of solvent cast composites of thermoplastic biopolymers and purified cellulose fibers." *Carbohydrate Polymers* 71 (2):235-244. doi: 10.1016/j.carbpol.2007.05.041.

Sayed, E., C. Karavasili, K. Ruparelia, R. Haj-Ahmad, G. Charalambopoulou, T. Steriotis, D. Giasafaki, P. Cox, N. Singh, L. P. N. Giassafaki, A. Mpenekou, C. K. Markopoulou, I. S. Vizirianakis, M. W. Chang, D. G. Fatouros, and Z. Ahmad. 2018. "Electrosprayed mesoporous particles for improved aqueous solubility of a poorly water soluble anticancer agent: in vitro and ex vivo evaluation." *Journal of Controlled Release* 278:142-155. doi: 10.1016/j.jconrel.2018.03.031.

Spagnol, C., E. H. Fragal, A. G. B. Pereira, C. V. Nakamura, E. C. Muniz, H. D. M. Follmann, R. Silva, and A. F. Rubira. 2018. "Cellulose nanowhiskers decorated with silver nanoparticles as an additive to antibacterial polymers membranes fabricated by electrospinning." *Journal of Colloid and Interface Science* 531:705-715. doi: 10.1016/j.jcis.2018.07.096.

Tang, S., P. Zou, H. Xiong, and H. Tang. 2008. "Effect of nano-SiO2 on the performance of starch/polyvinyl alcohol blend films." *Carbohydrate Polymers* 72 (3):521-526. doi: 10.1016/j.carbpol.2007.09.019.

Tongnuanchan, P., S. Benjakul, and T. Prodpran. 2012. "Properties and antioxidant activity of fish skin gelatin film incorporated with citrus essential oils." *Food Chemistry* 134 (3):1571-1579. doi: 10.1016/j.foodchem.2012.03.094.

Torres-Giner, S. 2011a. "Electrospun nanofibers for food packaging applications." In *Multifunctional and Nanoreinforced Polymers for Food Packaging*, 108-125.

Torres-Giner, S. 2011b. "Novel Antimicrobials Obtained by Electrospinning Methods." In *Antimicrobial Polymers*, 261-285.

Torres-Giner, S., M. Busolo, A. Cherpinski, and J. M. Lagaron. 2018. CHAPTER 10: Electrospinning in the Packaging Industry. In *RSC Soft Matter*.

Torres-Giner, S., L. Gil, L. Pascual-Ramírez, and J. A. Garde-Belza. 2018. "Packaging: Food waste reduction." *Encyclopedia of Polymer Applications* 3:1990-2009.

Torres-Giner, S., L. Hilliou, B. Melendez-Rodriguez, K. J. Figueroa-Lopez, D. Madalena, L. Cabedo, J. A. Covas, A. A. Vicente, and J. M. Lagaron. 2018. "Melt processability, characterization, and antibacterial activity of compression-molded green composite sheets made of poly(3-hydroxybutyrate-co-3-hydroxyvalerate) reinforced with coconut fibers impregnated with oregano essential oil." *Food Packaging and Shelf Life* 17:39-49. doi: 10.1016/j.fpsl.2018.05.002.

Torres-Giner, S., and J. M. Lagaron. 2010. "Zein-based ultrathin fibers containing ceramic nanofillers obtained by electrospinning. I. morphology and thermal properties." *Journal of Applied Polymer Science* 118 (2):778-789. doi: 10.1002/app.32180.

Torres-Giner, S., A. Martinez-Abad, and J. M. Lagaron. 2014. "Zein-based ultrathin fibers containing ceramic nanofillers obtained by electrospinning. II. Mechanical properties, gas barrier, and sustained release capacity of biocide thymol in multilayer polylactide films." *Journal of Applied Polymer Science* 131 (18):9270-9276. doi: 10.1002/app.40768.

Torres-Giner, S., N. Montanes, T. Boronat, L. Quiles-Carrillo, and R. Balart. 2016. "Melt grafting of sepiolite nanoclay onto poly(3-hydroxybutyrate-co-4-hydroxybutyrate) by reactive extrusion with multi-functional epoxy-based styrene-acrylic oligomer." *European Polymer Journal* 84:693-707. doi: 10.1016/j.eurpolymj.2016.09.057.

Torres-Giner, S., N. Montanes, O. Fenollar, D. García-Sanoguera, and R. Balart. 2016. "Development and optimization of renewable vinyl plastisol/wood flour composites exposed to ultraviolet radiation." *Materials and Design* 108:648-658. doi: 10.1016/j.matdes.2016.07.037.

Torres-Giner, S., N. Montanes, V. Fombuena, T. Boronat, and L. Sanchez-Nacher. 2018. "Preparation and characterization of compression-molded green composite sheets made of poly(3-hydroxybutyrate) reinforced with long pita fibers." *Advances in Polymer Technology* 37 (5):1305-1315. doi: 10.1002/adv.21789.

Torres-Giner, S., R. Pérez-Masiá, and J. M. Lagaron. 2016. "A review on electrospun polymer nanostructures as advanced bioactive platforms." *Polymer Engineering and Science* 56 (5):500-527. doi: 10.1002/pen.24274.

Torres-Giner, S., A. Torres, M. Ferrándiz, V. Fombuena, and R. Balart. 2017. "Antimicrobial activity of metal cation-exchanged zeolites and their evaluation on injection-molded pieces of bio-based high-density polyethylene." *Journal of Food Safety* 37 (4). doi: 10.1111/jfs.12348.

Torres-Giner, S., S. Wilkanowicz, B. Melendez-Rodriguez, and J. M. Lagaron. 2017. "Nanoencapsulation of Aloe vera in Synthetic and Naturally Occurring Polymers by Electrohydrodynamic Processing of Interest in Food Technology and Bioactive Packaging." *Journal of Agricultural and Food Chemistry* 65 (22):4439-4448. doi: 10.1021/acs.jafc.7b01393.

Vallet-Regi, M., A. Rámila, R. P. Del Real, and J. Pérez-Pariente. 2001. "A new property of MCM-41: Drug delivery system." *Chemistry of Materials* 13 (2):308-311. doi: 10.1021/cm0011559.

Voon, H. C., R. Bhat, A. M. Easa, M. T. Liong, and A. A. Karim. 2012. "Effect of Addition of Halloysite Nanoclay and SiO 2 Nanoparticles on Barrier and Mechanical Properties of Bovine Gelatin Films." *Food and Bioprocess Technology* 5 (5):1766-1774. doi: 10.1007/s11947-010-0461-y.

Wieczyńska, J., and I. Cavoski. 2018. "Antimicrobial, antioxidant and sensory features of eugenol, carvacrol and trans-anethole in active packaging for organic ready-to-eat iceberg lettuce." *Food Chemistry* 259:251-260. doi: 10.1016/j.foodchem.2018.03.137.

Woranuch, S., and R. Yoksan. 2013. "Eugenol-loaded chitosan nanoparticles: II. Application in bio-based plastics for active packaging." *Carbohydrate Polymers* 96 (2):586-592. doi: 10.1016/j.carbpol.2012.09.099.

Chapter V

Development and Characterization of Electrospun Fiber-Based Poly(ethylene-co-vinyl Alcohol) Films of Application Interest as High-Gas-Barrier Interlayers in Food Packaging

Polymers 2021, 13(13), 2061

Beatriz Meléndez-Rodríguez[1], Sergio Torres-Giner[1,†], Lorenzo Zavagna[1,‡], Chris Sammon[2], Luis Cabedo[3], Cristina Prieto[1], and José María Lagarón[1]

[1] Novel Materials and Nanotechnology Group, Institute of Agrochemistry and Food Technology (IATA), Spanish Council for Scientific Research (CSIC), Paterna, Spain

[2] Materials and Engineering Research Institute, Sheffield Hallam University, Sheffield, UK

[3] Polymers and Advanced Materials Group (PIMA), School of Technology and Experimental Sciences, Universitat Jaume I (UJI), Castellón, Spain

[†] This author is currently with the Research Institute of Food Engineering for Development (IIAD), Universitat Politècnica de València (UPV), Valencia, Spain.

[‡] This author is on leave from the Interuniversity National Consortium of Materials Science and Technology (INSTM), Florence, Italy.

Abstract

In the present study, poly(ethylene-co-vinyl alcohol) with 44 mol % ethylene content ($EVOH_{44}$) was managed to be processed, for the first time, by electrospinning assisted by the coaxial technology of solvent jacket. In addition to this, different suspensions of cellulose nanocrystals (CNCs), with contents ranging from 0.1 to 1.0 wt %, were also electrospun to obtain hybrid bio-/non-bio nanocomposites. The resultant fiber mats were thereafter optimally annealed to promote interfiber coalescence at 145 °C, below the $EVOH_{44}$ melting point, leading to continuous transparent fiber-based films. The morphological analysis revealed the successful distribution of CNCs into $EVOH_{44}$ up to contents of 0.5 wt %. The incorporation of CNCs into the ethylene-vinyl alcohol copolymer caused a decrease in the crystallization and melting temperatures (T_c and T_m) of about 12 and 7 °C, respectively, and also crystallinity. However, the incorporation of CNCs led to enhanced thermal stability of the copolymer matrix for a nanofiller content of 1.0 wt %. Furthermore, the incorporation of 0.1 and 0.5 wt % CNCs produced increases in the tensile modulus (E) of ca. 38 % and 28 %, respectively, but also yielded a reduction in the elongation at break and toughness. The oxygen barrier of the hybrid nanocomposite fiber-based films decreased with increasing the CNCs content, but they were seen to remain high barrier, especially in the low relative humidity (RH) regime, i.e., at 20 % RH, showing permeability values lower than 0.6×10^{-20} $m^3 \cdot m \cdot m^{-2} \cdot Pa^{-1} \cdot s^{-1}$. In general terms, an optimal balance in physical properties was found for the hybrid copolymer composite with a CNC loading of 0.1 wt %. On the overall, the present study demonstrates the potential of annealed electrospun fiber-based high-barrier polymers, with or without CNCs, to develop novel barrier interlayers to be used as food packaging constituents.

Keywords: EVOH; cellulose nanocrystals; electrospinning; high barrier; food packaging

1. Introduction

Polymers have been replacing the materials traditionally used in packaging, such as metal, glass, or cardboard, because they are more flexible, lighter, and habitually more cost-effective (Torres-Giner, Gil, et al. 2018). However, polymer-based materials present certain disadvantages, such as higher permeability and sorption to gases like oxygen or carbon dioxide, moisture, and organic vapors. In addition, polymer films must also present transparency, high mechanical and chemical resistance as well as be food contact approved (Sidwell 1992). In this sense, the thermoplastic poly(ethylene-*co*-vinyl alcohol) (EVOH), also habitually termed ethylene vinyl alcohol copolymers, are one of the most used polymer materials in high-barrier packaging films. EVOH is produced by the hydrolysis of ethylene vinyl acetate copolymer (EVA), where the acetate groups are transformed in alcohol ones (Marie et al. 2001). In food packaging, EVOH is habitually placed in the form of thin inner layers, typically well below 10 μm, being protected from moisture by external layers of such as polypropylene (PP), polyethylene terephthalate (PET) or low- and high-density polyethylene (LDPE and HDPE) in multilayer structures (Mokwena et al. 2009). The characteristics that make it suitable for this purpose are its flexibility, transparency, thermal resistance, and high-oxygen-barrier property based on its high degree of crystallinity (Katayama 2005, Luzi, Torre, and Puglia 2020, Yokoyama et al. 2009). Moreover, EVOH films are highly transparent and hydrophilic, yet water-insoluble, and can be recycled in the polyolefin regrinding process with existing infrastructure (Gavara et al. 2016). Interestingly, the EVOH copolymers, including that with 44 mol % ethylene content ($EVOH_{44}$), with high vinyl-alcohol contents, have been proven to be able to degrade under certain environmental conditions and biological media (Arboleda E, Mejía G, and López O 2004, Erlandsson, Karlsson, and Albertsson 1997, Mejía G, López O, and Sierra 2001, Tomita, Kojoh, and Suzuki 1997).

The ethylene molar fraction present in the copolymer highly changes the properties of EVOH due to alterations in its molecular structure. In particular, when the ethylene content is below 42 mol %, EVOH crystals are small, dense, and in monoclinic crystal structure. However, for ethylene contents from 42 to 80 mol %, its crystals are larger, less dense, and in hexagonal crystal structure (Cerrada et al. 1998). The crystallinity structure highly affects both the gas barrier and melting temperature (T_m), being higher for the materials with lower ethylene contents, but these copolymers are also highly plasticized by moisture (Mokwena and Tang 2012). For instance, when the ethylene content in EVOH is increased, the oxygen transmission rate (OTR) increases exponentially (Ito et al. 2001).

In addition to multilayers, nanofillers can be employed with EVOH in order to improve their thermal, mechanical, and barrier properties. In this respect, cellulose nanomaterials have been regarded as great candidates since they are low-cost, renewable, and environmentally friendly (Tajeddin 2014). Indeed, cellulose is the most abundant natural polysaccharide with an annual production around 75–100 billion tons (De Souza Lima and Borsali 2004), and it is formed of repeating rings of β-1,4-linked D-glucopyranose united by strong intermolecular hydrogen bonds (García et al. 2016). It is part of the structure of plants and algae, bacteria and fungi, and tunicate (Raquez et al. 2013). There are two main types of nanocelluloses, that is, mechanically sheared cellulose nanofibers (CNFs), also termed micro-fibrillated cellulose (MFC), with amorphous and crystalline parts, and hydrolytically extracted cellulose nanocrystals (CNCs) made of high-purity single crystals (Fortunati et al. 2012, Henriksson et al. 2007). Another type of nanocellulose derives from bacterial cellulose (BC), whose morphology can be engineered by controlling the biosynthesis pathway (Gatenholm and Klemm 2010). Among nanocellulose materials, CNC is

one of the most promising nanofillers to reinforce the mechanical and barrier properties of polymers due to their high crystallinity and strong network (Mariano, El Kissi, and Dufresne 2014). Several studies have already reported the reinforcement achieved when CNCs have been incorporated to a polymer matrix (Ashori et al. 2019, Voronova et al. 2015). For instance, a polyvinyl alcohol (PVA)/chitosan nanocomposite film reinforced with CNCs, prepared using the solvent casting and evaporation technique, showed an increase of 130 % in tensile strength (Perumal et al. 2018). In other study, a PET/CNCs film improved the water vapor transmission rate of PET from 37 to 10 $g \cdot m^{-2} \cdot day^{-1}$ (Lei et al. 2018). Furthermore, CNCs can serve as vehicles to develop active polymeric materials with, for instance, antimicrobial and antioxidant properties (He et al. 2021, Pal et al. 2019), ultraviolet light (UV) blocking (Yang et al. 2018), heavy metal absorbers (Yu et al. 2013), etc. Nanohybrids made from CNCs/metal nanoparticles (MNPs) have also gained interest due to their combined properties. Thus, oxygen scavenging nanocomposites were obtained with the incorporation of CNCs and palladium nanoparticles (PdNPs) into EVOH films (Cherpinski et al. 2019). CNCs acted as a support for the dispersion of the PdNPs in the polymer matrix, while the PdNPs acted as oxygen scavengers. Similarly, alginate bionanocomposite films with CNCs and silver nanoparticles (AgNPs) showed improved water and UV barrier of interest in food packaging (Yadav, Liu, and Chiu 2019).

However, there are some drawbacks to consider when CNCs was used as blending element to reinforce or make more sustainable polymer matrices. In particular, CNCs tend to form aggregates in the polymer matrix causing an overall reduction of the physical properties of the nanocomposites. This agglomeration is produced by the hydrophilic nature of cellulose, which is prone to form strong intermolecular hydrogen bonds and, in the case of CNCs, this effect is increased due to its large surface area and high surface energy (Miao and Hamad 2013). As a result, CNCs are prepared in the form of water suspensions, which however tend to re-agglomerate during the drying process. For instance, in spray drying, CNCs agglomeration is caused by capillary, hydrogen-bonding, and van der Waals forces. Alternatively, ice crystal growth plays a key role in CNCs agglomeration during freeze drying. Agglomeration of CNCs unsuccessfully affects the mechanical and barrier advantages of the polymer nanocomposites. The minimum degree of the CNCs dispersion is also so-called percolation threshold, where a three-dimensional network is obtained from a specific concentration of nanoparticles (Venkatraman et al. 2019). This percolation threshold depends on the aspect ratio and the orientation and distribution of the CNCs (Favier et al. 1997). Moreover, the method used to form the nanocomposites also influences on the dispersion of CNCs (Oksman et al. 2016).

Therefore, novel strategies have been explored to reduce the aggregations of CNCs prior or during their incorporation into the polymer matrices. For example, unlike spray and freeze drying, less agglomeration was reported to occur in the spray-freeze drying technique, in which the dispersed state of CNCs in water can be “frozen” in (Khoshkava and Kamal 2014a). Moreover, the use of mechanical energy can be applied to separate the nanoparticles, such as high shear mixing or ultrasonication, as well as the change in the surface energy of the particles by surfactants/compatibilizers (Cao et al. 2016, Gupta et al. 2017). Traditional melt-processing methods such as extrusion (González et al. 2020), compounding (Arias et al. 2015), and injection molding (Zhang et al. 2014) have also been used to incorporate CNCs into polymer matrices. However, the use of high temperatures during these processes could also cause the degradation of the CNCs (Oksman et al. 2006). In addition, it has been found that these methods produce more particle aggregation and mechanical degradation due to the high shear attained during processing (Sapkota et al. 2015). Thus, solution processing methods such as solution casting (Roohani et al.

2008), solution precipitation (Li, Sun, et al. 2020), or electrospinning (Fabra et al. 2016, Martínez-Sanz, Lopez-Rubio, and Lagaron 2014, Martínez-Sanz et al. 2016, Martínez-Sanz et al. 2012, Sanders et al. 2019) have been explored. In some cases, different methods can be combined to attain higher CNCs dispersion (Orr and Shofner 2017).

In this regard, electrospinning is a promising technology for dispersing CNCs in polymer matrices since it works with polymer solutions and can incorporate the fillers into submicron fibers (Mehrasa et al. 2016, Zhang et al. 2009). Moreover, the electrospun mats can be, thereafter, post-treated at temperatures below the T_m of the polymer, forming fiber-based continuous films with eliminated porosity. These materials are also called "biopapers" when made of biopolymers (Melendez-Rodriguez et al. 2018, Melendez-Rodriguez et al. 2020) due to their biofiber-based morphology and improved properties compared to traditional cellulosic papers. Thus, these materials can be produced after using minimal thermal exposure and they show good optical as well as mechanical and barrier properties, potentially offering high value in food packaging applications (Echegoyen et al. 2017). Moreover, electrospinning is suitable for the incorporation of nanofillers and/or functional additives within the polymer fibers, for instance volatile or thermolabile substances such as essential oils (Figueroa-Lopez et al. 2020, Torres-Giner, Pérez-Masiá, and Lagaron 2016). In addition, the resultant electrospun layers can be used as coatings or interlayers (Figueroa-Lopez et al. 2020) to improve the mechanical and barrier properties of multilayer systems. A few previous studies have reported the electrospinning of polymers containing CNCs. For example, Redondo et al. (Redondo et al. 2020) incorporated CNCs into polyurethane (PU) fibers and reported an improvement in the mechanical properties of the nanocomposite fiber mats. In another work, PVA mats prepared by electrospinning were mixed with CNC solutions to form aerogels that were subsequently hot-pressed to form nanocomposites. Authors showed good CNCs dispersion with increased mechanical properties (Pirani, Abushammala, and Hashaikeh 2013). In the case of the ethylene vinyl alcohol copolymer with 27 mol % ethylene content ($EVOH_{27}$), Martinez et al. (Martínez-Sanz et al. 2011) developed fibers reinforced with bacterial cellulose nanowhiskers (BCNWs) by electrospinning with a more uniform morphology than the neat EVOH27 fibers. However, none of the previous studies reported the production of post-processed continuous films or their properties.

The current study was aimed at obtaining for the first time (i) a new high-barrier electrospun material made of $EVOH_{44}$ copolymer and (ii) hybrid nanocomposites made of two high-barrier materials, one of which, incorporating CNCs in powder form, can impart a stiffer and more sustainable bio-based character to $EVOH_{44}$. The reason to select $EVOH_{44}$ within the EVOH family is that this polymer shows lower Tm and, hence, lower postprocessing temperatures than other EVOH family copolymers with higher vinyl-alcohol contents by which it could be more compatible with the processing temperatures of more conventional or biodegradable polymers to form multilayers. However, the processability of this copolymer by the electrohydrodynamic technique used was proven to be very difficult, so the study had to resource to the coaxial technology of solvent jacket. The study also characterized physical properties such as optical, thermal, mechanical, and barrier properties, relevant for multilayer food packaging applications of the annealed electrospun continuous films produced.

2. Experimental

2.1. Materials

The ethylene vinyl alcohol copolymer grade (Soarnol AT4403) containing 44 mol % of ethylene, that is, $EVOH_{44}$, was supplied in pellets by The Nippon Synthetic Chemical Industry Co., Ltd. (NIPPON GOHSEI, Osaka, Japan). It has a density of 1.14 g/m^3, melt flow rate (MFR) of 3.5 g/10 min (210 °C, 2.16 kg), and a volatile content < 0.3 %. The CNCs were provided by CelluForce NCC® (Montreal, QC, Canada). It is a 100 % cellulose sulphate sodium salt, which was obtained from wood pulp. The nanofiller was supplied as a spray-dried solid white powder with a bulk density of 0.7 g/cm^3. 2-propanol (99.5 %, for analysis) was purchased by ACROS ORGANICS (Thermo Fisher Scientific,Waltham, MA, USA).

2.2. Preparation of Solutions

The $EVOH_{44}$ solutions for electrospinning were prepared in concentration of 6 % (wt/vol) in a 70/30 vol/vol mixture of 2-propanol/water. The mixture was continuously stirred and heated in a thermal bath at approximately 80–90 °C on an AGIMATIC-N magnetic stirrer from JP Selecta (Barcelona, Spain). Complete dissolution of the polymer was achieved after around 2–3 h and the solutions were cooled down at room temperature prior to electrospinning. Since precipitation of the polymer always occurs after 3–4 h at room temperature (Kenawy et al. 2003), the precipitated mixture was heated again to 60 °C for 30–45 min when needed. Solutions containing 0.1, 0.5, and 1.0 % (wt/wt) of CNCs were prepared following a similar procedure previously described (Martínez-Sanz et al. 2012). Briefly, the CNC powder was first immersed in water and homogenized at 15000 rpm for 3 min with a T25 digital Ultraturrax from IKA® (Staufen, Germany). Thereafter, the resultant dispersion was added to the polymer solution according to the compositions described above.

2.3. Characterization of the Solutions

All the prepared $EVOH_{44}$ solutions, prior to electrospinning, were characterized in terms of viscosity, surface tension, and conductivity. A rotational viscosity meter Visco BasicPlus L (Fungilab S.A., San Feliu de Llobregat, Spain) with a low-viscosity adapter (LCP) was used to measure the apparent viscosity (ηa), which was performed at 100 s^{-1}. The Wilhemy plate method was followed to determine the surface tension with an Easy-Dyne K20 tensiometer (Krüss GmbH, Hamburg, Germany). Finally, a conductivity meter XS Con6 (Lab-box, Barcelona, Spain) was employed to evaluate the solution conductivity. Three replicates were carried out for each measurement.

2.4. Electrospinning Process

The electrospinning setup used consisted of an Fluidnatek® LE-10 commercial lab equipment manufactured by Bioinicia S.L. (Valencia, Spain). The equipment was operated at environmental conditions of 25 °C and 40 % relative humidity (RH) with a motorized single needle injector, scanning horizontally towards a metallic fixed collector to obtain homogeneous depositions.

High-content vinyl-alcohol EVOH copolymers have been reported to be relatively easy to electrospin, but the one selected in this work (with 44 mol % ethylene) proved difficult to process due to very fast drying at the tip of the nozzle. To prevent needle clogging, a coaxial setup was used where pure 2-propanol was fluxed through the exterior needle to create a solvent jacket around the tip, as previously reported by Yu et al. (Yu et al. 2014). In this setup, the sheath fluid flow-rate and the polymer solutions flowrates were found optimal at 250 µl/h and 6 ml/h, respectively. A voltage of 24 kV and a distance between the tip and collector of 21 cm were set.

2.5. Film Preparation

The obtained EVOH mats were then converted into continuous fiber-based films by annealing below the polymer melting point in a 4122-model press from Carver, Inc. (Wabash, IN, USA). This post-processing was performed across the temperature range from 110 to 155 °C, for 15 s. The average thickness of all the attained films was approximately 30 µm and they were stored in a desiccator at 0 % RH before characterization.

2.6. Characterization of the Films

2.6.1. Electron Microscopy

For the observation of the CNCs as well as fiber and film morphologies, an S-4800 scanning electron microscopy (SEM) instrument from Hitachi (Tokyo, Japan) was used. Prior to this, both the electrospun $EVOH_{44}$ fibers and their resultant films were fixed to beveled holders using conductive double-sided adhesive tape and sputtered with a mixture of gold-palladium under vacuum. For the cross-section observations, the films were cryofractured by immersion in liquid nitrogen. In all cases, an accelerating voltage of 10 kV was used. The estimation of the dimensions was performed by means of the Aperture software from Apple (Cupertino, CA, USA) using a minimum of 20 SEM micrographs in their original magnification.

Transmission electron microscopy (TEM) was also performed to further study the distribution of CNCs in the $EVOH_{44}$ fibers using a JEOL 1010 from JEOL USA, Inc. (Peabody, MA, USA) with an accelerating voltage of 100 kV.

2.6.2. Transparency

The light transmission of the films was determined using 50 mm × 30 mm specimens in an ultraviolet-visible (UV-vis) spectrophotometer VIS3000 (Dinko Instruments, Barcelona, Spain). The absorption of light was quantified at wavelengths in the 200–700 nm range. Equation (1) (Shiku et al. 2004) and Equation (2) (Kanatt et al. 2012) were followed to determine the values of transparency (T) and opacity (O), respectively:

$$T = \frac{A_{600}}{L} \quad (1)$$

$$O = A_{500} \times L \quad (2)$$

in which A_{600} and A_{500} correspond to the absorbance values at 600 and 500 nm, respectively, whereas L represents the film thickness (mm).

2.6.3. Color

The color of the films was estimated using a Chroma Meter CR-400 (Konica Minolta, Tokyo, Japan) with the D65 illuminant. The color difference (ΔE^*) between the samples with CNCs and the neat $EVOH_{44}$ was determined by the Equation (3) (Arfat et al. 2017):

$$\Delta E^* = [(\Delta L^*)^2 + (\Delta a^*)^2 + (\Delta b^*)^2]^{0.5} \quad (3)$$

in which ΔL^* represents the difference in terms of lightness from black to white, whereas Δa^* and Δb^* correspond to the differences in color, from green to red and blue to yellow, respectively. Color changes were assessed using a previous grading: Unnoticeable ($\Delta E^* < 1$), only an experienced observer can notice the difference ($\Delta E^* \geq 1$ and < 2), an unexperienced observer notices the difference ($\Delta E^* \geq 2$ and < 3.5), clear noticeable difference ($\Delta E^* \geq 3.5$ and < 5), and the observer notices different colors ($\Delta E^* \geq 5$) (Agüero et al. 2019).

2.6.4. Thermal Analysis

Thermal transitions were studied using differential scanning calorimetry (DSC) on a DSC-7 analyzer from PerkinElmer, Inc. (Waltham, MA, USA), equipped with a cooling accessory Intracooler 2 also from PerkinElmer, Inc. A two-step program, with heating and cooling rates of 10 °C/min and a nitrogen atmosphere with a flow-rate of 20 ml/min, was applied. It consisted of a first heating step from -30 to 180 °C, followed by one minute isotherm at 180 °C and a cooling run back to -30 °C. All tests were carried out in triplicate and sample weights were of ca. 3 mg. An empty aluminum pan was used as reference. Calibration was performed using an indium sample and the thermograms were corrected with those of an empty pan. The glass transition temperature (T_g), T_m, and enthalpy of melting (ΔH_m) were obtained from the heating scans, while the crystallization temperature from the melt (T_c) and enthalpy of crystallization (ΔH_c) were determined from the cooling scans. The enthalpies were normalized to the actual polymer content in the composites. The $EVOH_{44}$ crystallinity content (χ_c) was estimated according to Equation (4) (Luzi, Torre, and Puglia 2020):

$$\chi_c\ (\%) = \frac{1}{(1 - m_f)}\left[\frac{\Delta H_m - \Delta H_{cc}}{\Delta H_{m_0}}\right] \times 100 \quad (1)$$

where ΔH_m is the enthalpy for melting, ΔH_{m0} is melting enthalpy for a 100 % crystalline EVOH sample and (1 - m_f) is the weight fraction of $EVOH_{44}$ in the sample. The ΔHm_0 value of $EVOH_{44}$ was calculated following Equation (5) (Faisant et al. 1998):

$$\Delta H_{m_0} = \alpha \Delta H_{m_0}^{PVA} + \beta \Delta H_{m_0}^{PE} \quad (2)$$

where ΔH_{m0}^{PVA} is enthalpy of melting for a 100 % crystalline poly(vinyl alcohol) (PVOH), taken as 169.2 J g^{-1}, and ΔH_{m0}^{PE} is enthalpy of melting for a 100 % crystalline of polyethylene (PE), taken as 290.0 J g^{-1}, whereas α and β correspond to the weight fractions of vinyl alcohol (α = 0.56) and ethylene (β = 0.44) in $EVOH_{44}$.

Thermogravimetric analysis (TGA) was performed in a TG-STDA model TGA/STDA851e/LF/1600 thermobalance from Mettler-Toledo, LLC (Columbus, OH, USA), under a nitrogen flow-rate of 50 ml/min. The samples, with a weight of about 15 mg, were heated from 50 to 900 °C at a heating rate of 10 °C/min. The onset degradation temperature, measured at the temperature corresponding to a 5 % weight loss ($T_{5\%}$) and the thermal degradation temperature (T_{deg}) were determined.

2.6.5. ATR-FTIR Spectroscopy

Fourier transform infrared spectroscopy (FTIR) single spectra were collected in the 600–4000 cm^{-1} wavelength range using the Tensor 37 FTIR equipment (Bruker, Germany) coupled to the attenuated total reflection (ATR) accessory Golden Gate (Specac, Ltd., Orpington, UK). Spectra were taken by averaging 20 scans at a resolution of 4 cm^{-1}.

A Nicolet Nexus FTIR instrument (Thermo Fisher Scientific, Wilmington, DE, USA) coupled to a variable-temperature single reflection diamond ATR sampling accessory (Specac Ltd., Orpington, UK) was used to collect spectra as a function of temperature. Spectra were collected using the blank ATR crystal at the same temperature as the background by averaging 64 scans at 4 cm^{-1} resolution. The samples were clamped directly onto the ATR crystal using a calibrated torque wrench (Specac Ltd.) set at 80 cNm, which applies a load of 350 N via the sample accessory anvil, to ensure that any peak intensity changes in the data represented changes to the morphology of the samples. Prior to conducting the variable temperature infrared measurements, reproducibility of the sample contact and resulting spectra intensity were validated. Spectra were collected from 30 to 130 °C at 10 °C intervals and, thereafter, up to 200 °C at 5 °C intervals. Spectra were not collected until the digital reading on the temperature controller had fully stabilized to ensure the validity of the selected temperature.

2.6.6. Mechanical Tests

The ASTM standard method D638 was followed to determine the mechanical properties of the films using an Instron 4400 universal testing machine from Instron (Norwood, MA, USA) equipped with a 1-kN load cell. Tensile tests of the films were performed with 115 × 16 mm^2 stamped dumb-bell shaped specimens using a cross-head speed of 10 mm/min at room conditions. The samples were, prior to tensile assay, conditioned at 40 % RH and 25 °C for 24 h. At least six specimens were measured for each sample.

2.6.7. Permeability Tests

The water vapor permeability (WVP) of the films was determined following the standardized gravimetric method ASTM E96-95. Payne permeability cups of 3.5 cm of diameter from Elcometer Sprl (Hermallesous-Argenteau, Belgium) were used with 5 ml of distilled water. The testing was done at 25 °C on films exposed to 100 % RH placed within a desiccator containing dried silica gel that generated 0 % RH. Cups with aluminum films were used as control samples to estimate solvent loss through the sealing. The cups were weighted daily using an analytical balance (±0.0001 g). WVP was calculated from the regression analysis of weight loss data vs. time and the weight loss was calculated as the total loss minus the loss through the sealing. The permeability was obtained by multiplying the permeance by the film thickness.

The oxygen permeability (OP) was determined in duplicate at 0, 20 % and 80 % RH and 25 °C, using an Oxygen Permeation Analyzer M8001 (Systech Illinois, Thame, UK) with temperature and RH control, purged with nitrogen before exposure to an oxygen flow of 10 ml/min. The tested area was 5 cm^2.

2.7. Statistical Analysis

The software packaging STATGRAPHICS Centurion XVI v 16.1.03 (StatPoint Technologies, Inc.,Warrenton, VA, USA) was used to evaluate the differences among the samples by analysis of variance (ANOVA). Fisher's least significant difference (LSD) was set at the 95 % confidence level ($p < 0.05$).

3. Results and Discussion

3.1. Solution Properties and Morphology

The properties of the $EVOH_{44}$ solution and its suspensions with CNCs were characterized to assess their processability by electrospinning. **Table 1** summarizes the values obtained for each solution. The pure $EVOH_{44}$ solution presented a viscosity of 71.9 cP, a surface tension of 23.8 mN/m, and a conductivity of 11.63 µS/cm. When CNCs was added to the solutions, their properties varied slightly, though the differences were still significant. Thus, for contents of 0.1, 0.5, and 1.0 wt % of CNCs in the $EVOH_{44}$ solutions, the values for viscosity, surface tension, and conductivity were in the range of 74–80 cP, 24–25 mN/m, and 11.8–12.1 µS/cm. The slight increase in viscosity can be related to the presence of the nanofiller in the suspensions, which could stablish secondary bonding interactions with the $EVOH_{44}$ molecules via the hydroxyl groups. Similarly, the slight increase in surface tension and conductivity may be related to the higher polarity of the nanocellulose particles. Changes in the electrospun morphologies of EVOH due to variations in solution properties have been previously studied (Torres-Giner, Echegoyen, et al. 2018). In particular, a decrease in the diameter of EVOH fibers was reported when the solution conductivity decreased.

Table 1. Properties of the poly(ethylene-*co*-vinyl alcohol) with 44 mol % of ethylene ($EVOH_{44}$) solution and suspensions, with cellulose nanocrystals (CNCs), and mean diameter of their corresponding electrospun fibers and beaded regions.

Sample	Viscosity (cP)	Surface tension (mN/m)	Conductivity (µS/cm)	Mean Fiber Diameter (nm)	Mean Diameter of Beaded Regions (µm)
$EVOH_{44}$	71.9 ± 1.2^{a}	23.8 ± 0.1^{a}	11.63 ± 0.03^{a}	410.0 ± 128.0^{a}	1.1 ± 0.2^{a}
$EVOH_{44}$ + 0.1 wt % CNCs	74.3 ± 0.8^{b}	$24.1 \pm 0.4^{a,b}$	$11.80 \pm 0.02^{a,b}$	410.4 ± 99.4^{a}	$1.3 \pm 0.3^{a,b}$
$EVOH_{44}$ + 0.5 wt % CNCs	77.4 ± 1.1^{c}	$24.3 \pm 0.7^{a,b}$	$12.00 \pm 0.05^{b,c}$	501.7 ± 79.6^{a}	$1.5 \pm 0.2^{a,b}$
$EVOH_{44}$ + 1 wt % CNCs	80.1 ± 0.7^{d}	24.9 ± 0.5^{b}	12.10 ± 0.03^{c}	592.4 ± 102.9^{a}	1.8 ± 0.1^{b}

[a–d] Different letters in the same column mean significant difference among the samples ($p < 0.05$).

The morphology of the as-received CNC powder was observed by SEM. **Figure 1** shows the SEM micrographs of the CNCs at both low and high magnification, that is, 400× (**Figure 1a**) and 3000× (**Figure 1b**), respectively. It can be observed that CNCs were mainly in the form of shrunken particles with a wide particle size distribution (**Figure 1c**). This particular type of morphology is known to occur during spray-drying due to the rapid evaporation of the solvent and the formation of an external crust during the first stages of drying, which collapses when the solvent present in the inner parts of the droplet evaporates and leads to a partial shrinkage of the particle (Rojas-Lema et al. 2020). It can also be observed that particle sizes varied from large particles of nearly 20 µm down to nanoparticles below 100 nm. A similar morphology, showing the co-presence of nanoparticles and large particles as a result of agglomeration has been previously reported for CNCs processed by spray-drying (Abdallah and Kamal 2018, Beck, Bouchard, and Berry 2012, Di Giorgio et al. 2020). Agglomeration is produced during the drying process when the capillary, van der Waals, and hydrogen bonding forces overcome the electrostatic repulsion force produced by the negative charge on the surface of the CNCs (Khoshkava and Kamal 2014b). The resulting powdered product obtained by the spray-drying technique, thus, consists of compact particles typically in the micro-size range.

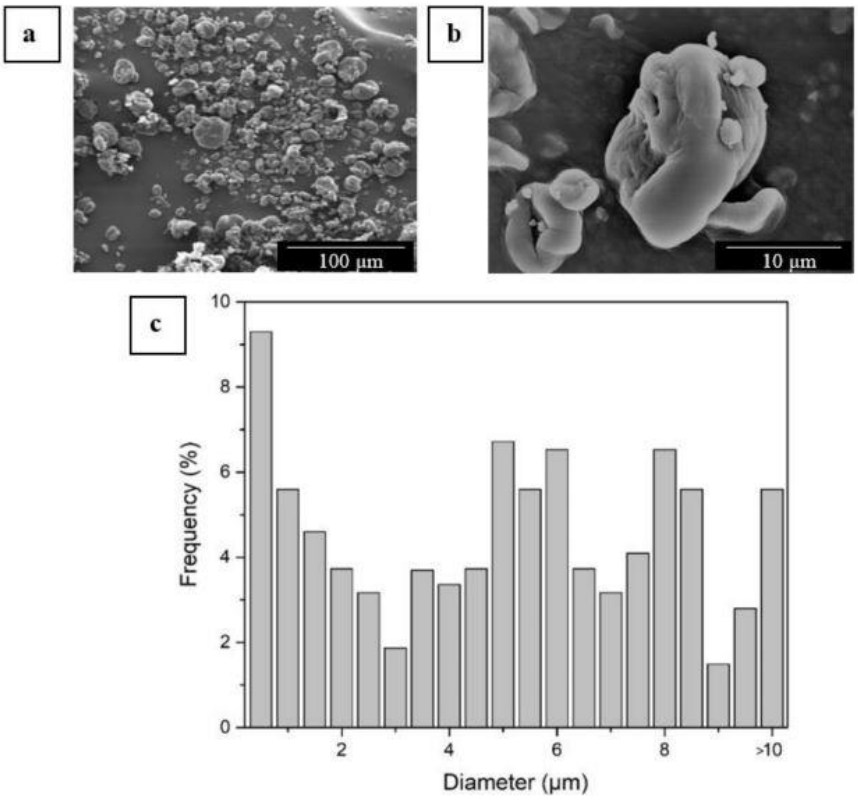

Figure 1. Scanning electron microscopy (SEM) images of the as-received cellulose nanocrystals (CNCs) in powder form taken at low (a) and high (b) magnification, showing scale markers of 100 and 10 µm, respectively; (c) diameter histogram.

The SEM images of the electrospun mats of the $EVOH_{44}$ fibers, prior to the thermal post-treatment, are gathered in **Figure 2**. As it can be seen from these micrographs, all the mats, even those of neat $EVOH_{44}$, presented some beads along the fiber axis. The beaded fiber morphology observed herein is similar to those observed in previous works reporting the preparation of electrospun fibers of EVOH with different contents of ethylene (Martínez-Sanz, Lopez-Rubio, and Lagaron 2013a, Martínez-Sanz et al. 2011). The presence of beads in the fibers are habitually associated to a non-optimal concentration of the polymer and/or of the operating parameters (Torres-Giner, Gimenez, and Lagaron 2008). However, the concentration and parameters used resulted in successful electrospinning for this material. The mean diameters of the beaded regions increased with the CNCs content, in a range from 1.1 to 1.8 µm. As shown in previous **Table 1**, the mean diameter of the neat $EVOH_{44}$ fibers obtained by electrospinning, included in **Figure 2a**, were around 410 nm. The incorporation of CNCs resulted in an increase in the diameter of the $EVOH_{44}$ fibers for contents above 0.5 wt %. Thus, the samples with a 0.1 wt % CNCs (see **Figure 2b**) exhibited fibers with similar size as the pure $EVOH_{44}$, that is, 410 nm, but with more beaded regions. In the case of the samples with 0.5 and 1.0 wt % of CNCs, gathered respectively in **Figure 2c,d**, the fibers showed mean diameters of approximately 502 and 592 nm. This effect can be ascribed to the slight viscosity increase described above. This result differs from previous studies in which the presence of CNCs reduced fiber diameter due to an increase in conductivity as CNCs is negatively charged (Peresin et al. 2010, Rojas, Montero, and Habibi 2009). Moreover, the bigger beaded areas in the fibers could be generated to accommodate CNCs agglomerates.

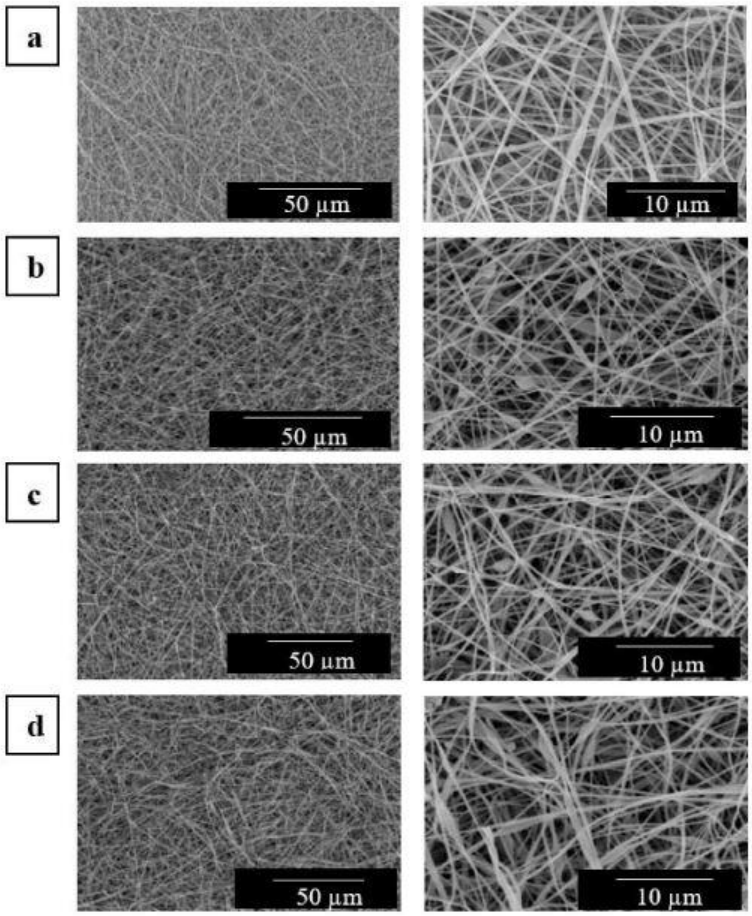

Figure 2. Scanning electron microscopy (SEM) images of the electrospun mats of poly(ethylene-*co*-vinyl alcohol) with 44 mol % of ethylene ($EVOH_{44}$), pure (a) and with cellulose nanocrystals (CNCs): (b) 0.1 wt %; (c) 0.5 wt %; (d) 1.0 wt %. Left images were taken 800× at with scale markers of 50 µm, while right images were taken at 3000× with scale markers of 10 µm.

As a result of potential agglomeration of CNCs in the electrospun $EVOH_{44}$ fiber beaded regions, the fibers were also observed by TEM. **Figure 3** displays the TEM micrographs of the electrospun fibers, in which it can be discerned that the CNCs distribution was highly dependent on the added content. For electrospun fibers with a content of 0.1 wt %, shown in **Figure 3a**, the incorporated CNCs were relatively well distributed along the fiber axis since agglomerates are hard to spot. **Figure 3b** reveals that the electrospun $EVOH_{44}$ fibers with 0.5 wt % also showed a good distribution of CNCs. However, agglomeration was very noticeable in **Figure 3c**, in which it can be observed that CNCs at 1.0 wt % were mainly located in the beaded regions. Similar results have been observed previously for BCNWs incorporated into polyethylene oxide (PEO) fibers by electrospinning (Park et al. 2007).

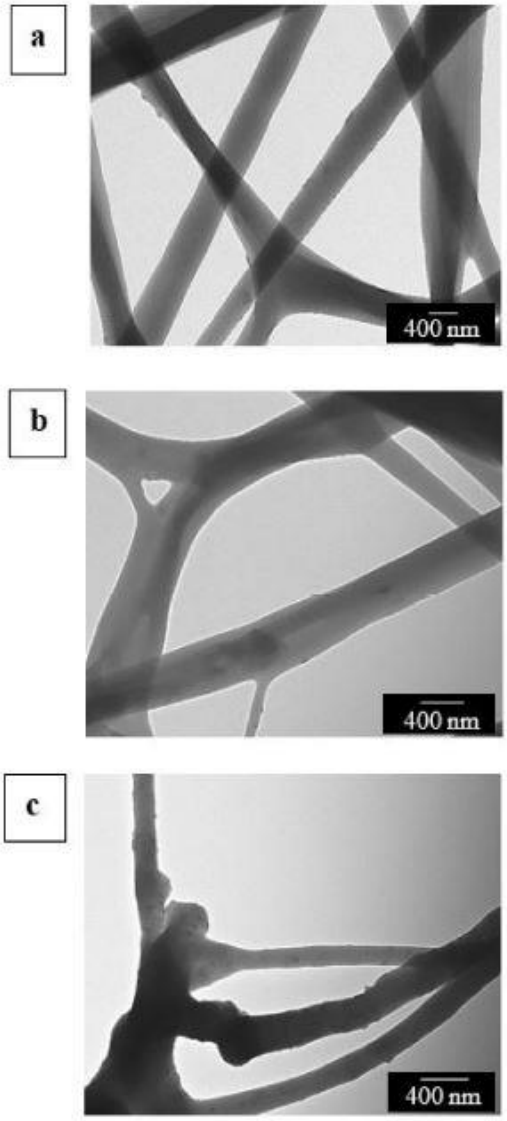

Figure 3. Transmission electron microscopy (TEM) images of the electrospun fibers of poly(ethylene-*co*-vinyl alcohol) with 44 mol % of ethylene ($EVOH_{44}$) with cellulose nanocrystals (CNCs): (a) 0.1 wt %; (b) 0.5 wt %; (c) 1.0 wt %. Images taken at 10000× with scale markers of 400 nm.

3.2. Thermal Properties of the Electrospun Fibers

The DSC curves for the different electrospun $EVOH_{44}$ fiber mats of the various materials, corresponding to the first heating and cooling steps, are gathered in **Figure 4**.

Table 2 displays the main thermal values obtained from the DSC curves. Regarding the neat $EVOH_{44}$, one can observe in **Figure 4a** that, during the first heating, it showed a T_g at approximately 41 °C. The low-intensity endothermic peak observed in the glass transition region is often connected with endothermic relaxation phenomena occurring at the transient state from glassy to rubbery for the amorphous phase. Then, the $EVOH_{44}$ copolymer melted at nearly 164 °C with a ΔH_m of 60.1 J/g, resulting in a crystallinity degree of 27.0 %. In relation to the $EVOH_{44}$

composites, the T_g values increased in temperature, ranging between 41.7–44.0 °C, suggesting a filler-induced "rigidization" of the amorphous phase. This effect was seen maximum for the sample with the highest dispersed amount of CNCs, that is, 1 wt %. The fibers of the nanocomposites also exhibited a somewhat broader melting endothermic events towards lower temperatures than the pristine polymer. Thus, the melting points and enthalpies were seen to decrease with increasing filler content, suggesting a crystallinity distortion induced by the filler. More specifically, the T_m of $EVOH_{44}$ was reduced by 7.1 °C in the nanocomposite with 1 wt % CNCs, and the crystallinity decreased to 23.4 %, 24.1 %, and 22.8 % for the 0.1, 0.5, and 1.0 wt % CNC content, respectively. In this regard, it is interesting to mention that Martínez-Sanz et al. (Martínez-Sanz et al. 2012) also reported a decrease in T_m by adding BCNWs to electrospun $EVOH_{29}$ fibers. Alterations in crystallinity have been linked to a covalent or hydrogen bonding between the EVOH hydroxyl groups (OH) and low-molecular weight (M_W) additives in the amorphous phase (Vannini et al. 2016).

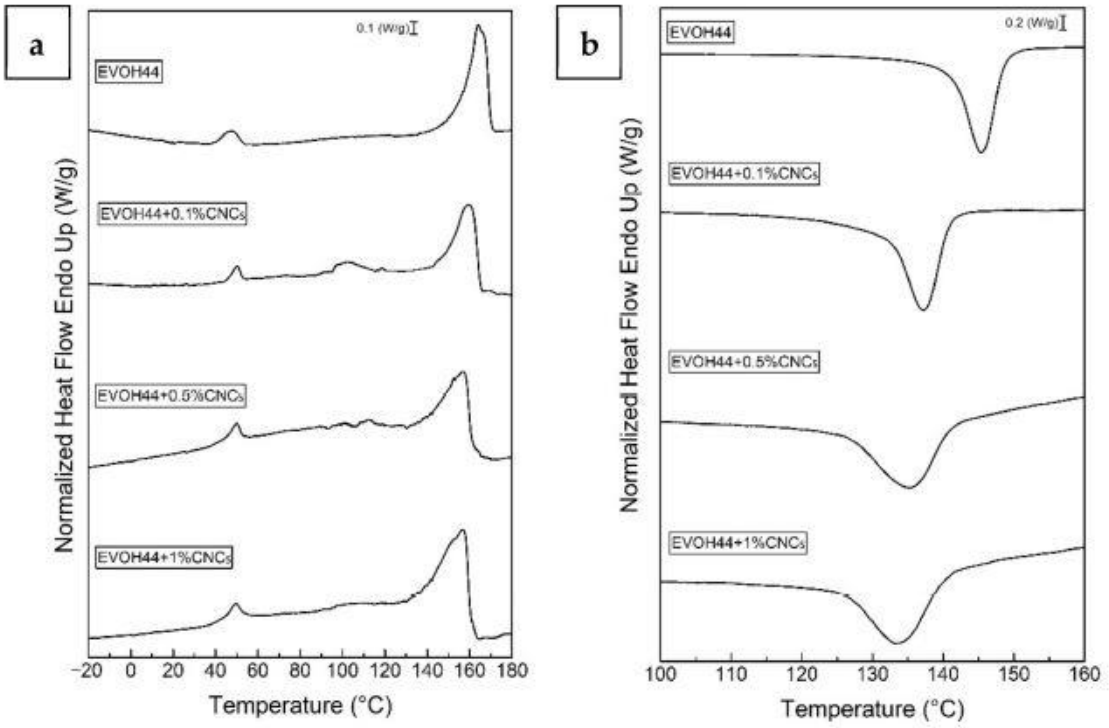

Figure 4. Differential scanning calorimetry (DSC) curves during first heating (a) and cooling (b) of the electrospun fibers of poly(ethylene-*co*-vinyl alcohol) with 44 mol % of ethylene ($EVOH_{44}$) with and without cellulose nanocrystals (CNCs).

Figure 4b also shows that in agreement with the melting data, the neat $EVOH_{44}$ showed during crystallization a T_c value centered at 145.4 °C and a ΔH_c value of 61.8 J/g, that decreased and broadened with increasing the filler content. In particular, the lowest T_c value was observed for the nanocomposite sample with 1 wt % CNCs, with a reduction of 12.2 °C. Thus, the presence of CNCs impedes the proper lateral order of the copolymer chains, requiring higher undercoolings to crystallize, and doing so to a lesser extent than in the unfilled material.

Table 2. Thermal properties of the electrospun poly(ethylene-*co*-vinyl alcohol) with 44 mol % of ethylene ($EVOH_{44}$) fibers with and without cellulose nanocrystals (CNCs) in terms of: glass transition temperature (T_g), melting temperature (T_m), enthalpy of melting (ΔH_m) and crystallinity (% X_c), crystallization temperature (T_c) and enthalpy of crystallization (ΔH_c).

Sample	First Heating			Cooling	
	T_g (°C)	T_m (°C)	ΔH_m (J/g) (%X_c)	T_c (°C)	ΔH_c (J/g)
$EVOH_{44}$	40.6 ± 0.3[a]	163.9 ± 1.2[a]	60.1 ± 2.1[a] (27.0)	145.4 ± 0.8[a]	61.8 ± 2.1[a]
$EVOH_{44}$ + 0.1 wt % CNCs	44.0 ± 0.5[b]	160.1 ± 2.2[b]	52.0 ± 1.0[b] (23.4)	137.2 ± 0.3[b]	50.1 ± 1.1[b]
$EVOH_{44}$ + 0.5 wt % CNCs	42.5 ± 0.7[c]	157.2 ± 1.4[b]	53.4 ± 2.4[b] (24.1)	135.3 ± 1.0[c]	44.2 ± 1.5[c]
$EVOH_{44}$ + 1.0 wt % CNCs	41.7 ± 0.2[c]	156.8 ± 1.6[b]	50.1 ± 1.1[b] (22.8)	133.2 ± 0.5[d]	38.5 ± 1.4[d]

[a–d] Different letters in the same column mean significant difference among the samples ($p < 0.05$).

The results obtained for the here-prepared electrospun $EVOH_{44}$ fibers agree reasonably well with those reported in the literature for materials produced by other techniques. For instance, $EVOH_{44}$ films obtained by extrusion showed T_m values around 160 °C and 162 °C, during the first and second heating, respectively (López-de-Dicastillo et al. 2010). In another study, $EVOH_{44}$ films prepared by solvent casting presented a T_c of 140 °C and T_m values of 163 °C and 165 °C, during the first and second heating, respectively (Fernández et al. 2008). Moreover, in the latter study, MFC was added to solvent-cast $EVOH_{44}$ films, reporting also lower T_c and T_m values compared to the pristine copolymer.

3.3. Film Forming by Interfiber Coalescence Induced by Annealing

In order to induce fiber mat densification, different annealing temperatures below the copolymer melting point were screened to ascertain the most optimal thermal treatment that can lead to continuous fiber-based films better suited for their use in packaging. The morphology evolution of the electrospun materials obtained at different annealing temperatures is shown in **Figure 5** from top views (**Figure 5a**) and cryo-fracture surfaces (**Figure 5b**). From this figure, it can be seen that at temperatures below 145 °C, the electrospun materials still showed some level of porosity and non-homogeneous surface. At 145 °C and 150 °C, a compact interfiber coalescence of the $EVOH_{44}$ fibers occurred, causing a material densification and alignment side by side of the fibers. At 155 °C, the continuous structure was lost due to the appearance of holes caused by partial melting of the copolymer. As a result, 145 °C was selected as the minimum annealing temperature, below the melting point of $EVOH_{44}$, to thermally process the material to turn it into a continuous film.

Similarly, the electrospun mats of $EVOH_{44}$ with the different CNCs contents were also annealed at 145 °C and, thereafter, observed by SEM. The resulting morphology in both top view and cross-

section of the materials, are presented in **Figure 6**. As it can be seen, homogeneous fiber-based films were obtained in all cases.

Furthermore, the distribution of the CNCs in the electrospun biopapers of $EVOH_{44}$ was also analyzed by TEM. In **Figure 7**, it can be seen that, as was previously observed in the electrospun fibers, the CNC distribution was better at both 0.1 wt % (**Figure 7a**) and 0.5 wt % loadings (**Figure 7b**), whereas more nanocrystal aggregates were easily found at the highest content, that is, at 1.0 wt % (**Figure 7c**). These results suggest that the CNCs distribution achieved in the $EVOH_{44}$ fibers during electrospinning was seemingly preserved in the films.

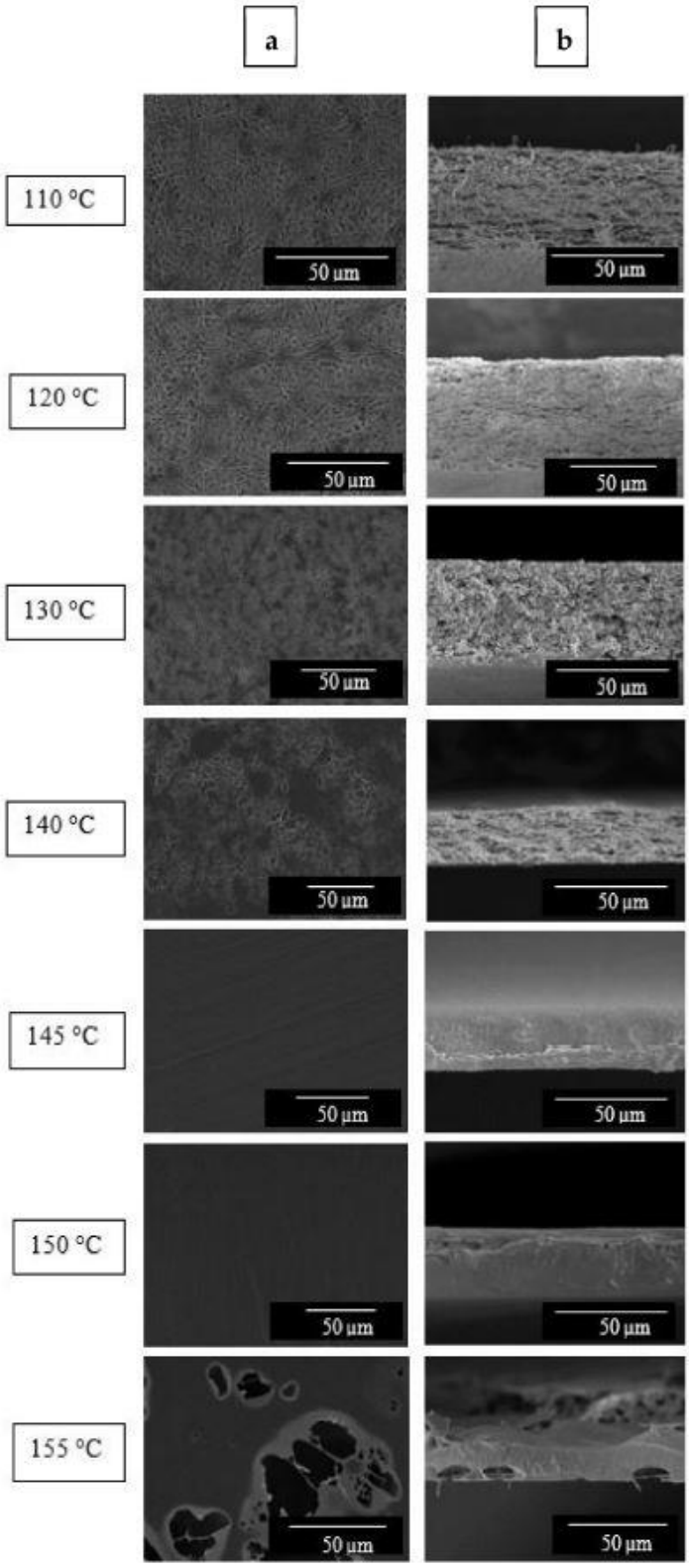

Figure 5. Scanning electron microscopy (SEM) images at the top view (a) and cross-section (b) of the electrospun mats of poly(ethylene-*co*-vinyl alcohol) with 44 mol % of ethylene ($EVOH_{44}$) annealed at: 110, 120, 130, 140, 145, 150, and 155 °C for 15 s. Images were taken at 1100× with scale markers of 50 µm.

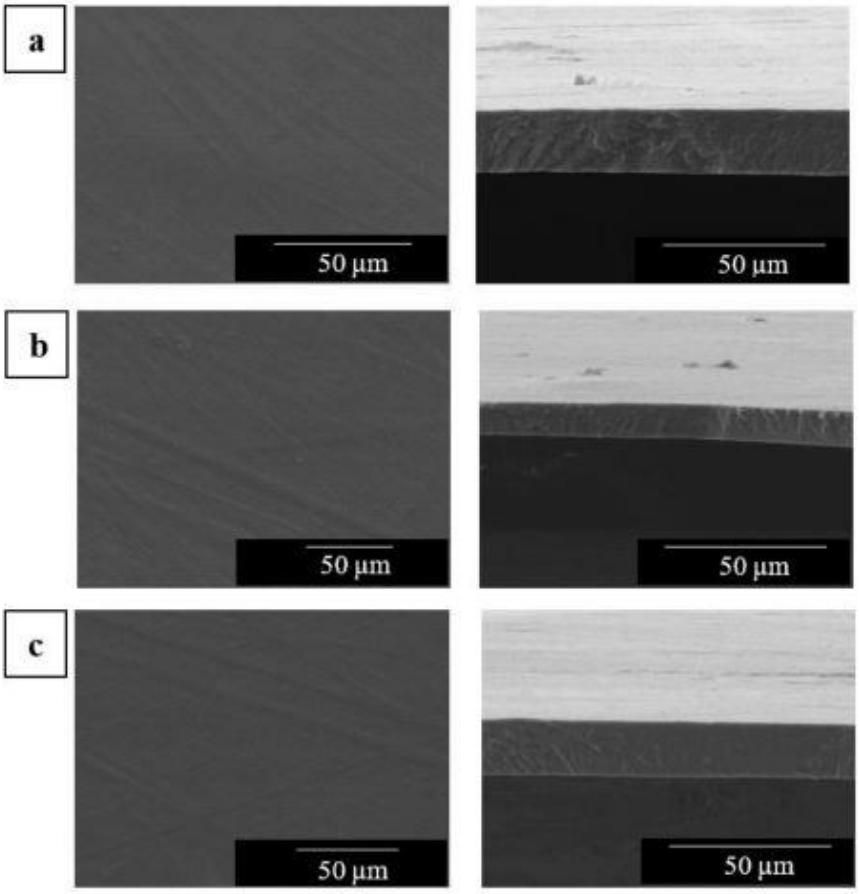

Figure 6. Scanning electron microscopy (SEM) images in top view (left) and cross-section (right) of the electrospun mats of poly(ethylene-*co*-vinyl alcohol) with 44 mol % of ethylene ($EVOH_{44}$) with cellulose nanocrystals (CNCs): (a) 0.1 wt %; (b) 0.5 wt %; (c) 1.0 wt %. The electrospun mats were thermally post-treated at 145 °C for 15 s. Images were taken at 1100× with scale markers are of 50 µm.

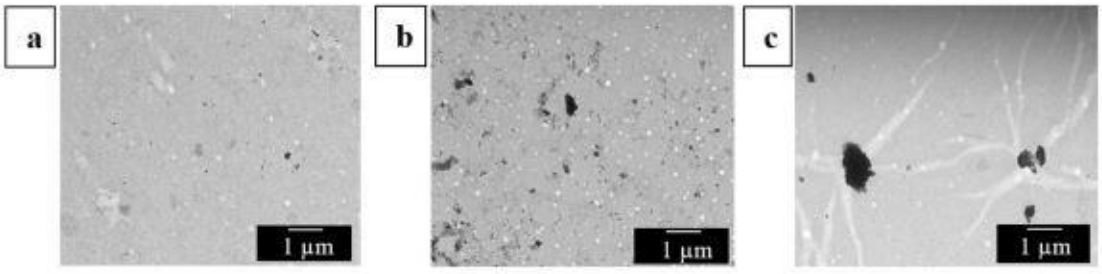

Figure 7. Transmission electron microscopy (TEM) images of the annealed electrospun films of poly(ethylene-co-vinyl alcohol) with 44 mol % of ethylene ($EVOH_{44}$) with cellulose nanocrystals (CNCs): (a) 0.1 wt %; (b) 0.5 wt %; (c) 1.0 wt %. Images were taken at 3000× with scale markers of 1 µm.

3.4. Variable-Temperature FTIR Spectroscopy

An insight into the spectral changes associated to the molecular order of the electrospun $EVOH_{44}$ fibers was carried out by ATR-FTIR during heating from 30 to 200 °C, as it can be seen in **Figure 8**.

One characteristic feature of the EVOH spectra is the peak centered at approximately 3330 cm^{-1}, which corresponds to the stretching band of the O-H oscillators (Lasagabaster et al. 2006). The breadth and position of this band indicates the presence of strong hydrogen bonding within the copolymer, the broadness is due to intra- and intermolecular hydrogen-bonded OH dimer and multimers, with varying strengths and geometries (Cava, Sammon, and Lagaron 2006, Coleman et al. 1993). In addition, the $EVOH_{44}$ spectra showed bands at nearly 2933 and 2852 cm^{-1} corresponding to the C-H antisymmetric and symmetric stretching vibrations, respectively. The features at approximately 1437 and 1456 cm^{-1} are attributed to OH deformation, the band at 1374 cm^{-1} is likely arising from OH deformation, and CH_2 wagging and the band at 842 cm^{-1} is assigned to skeletal vibrations and CH_2 rocking (Lagaron et al. 2003, Nir, Narkis, and Siegmann 1998).

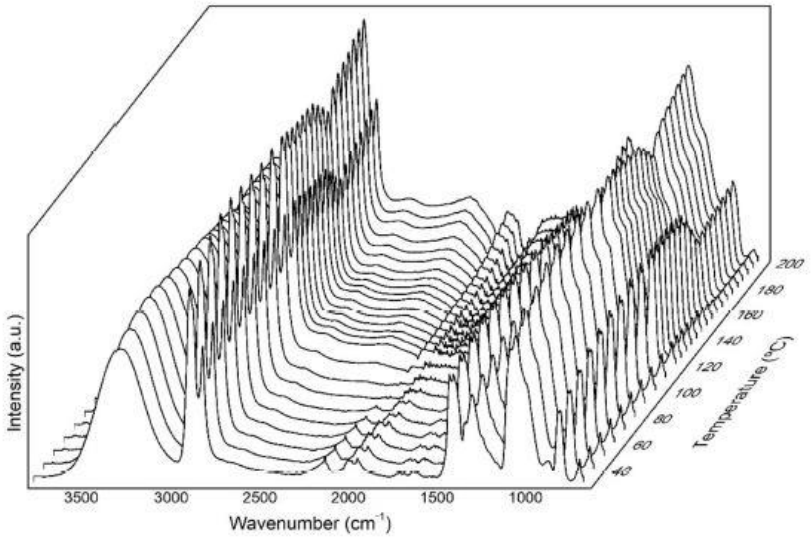

Figure 8. Fourier transform infrared spectroscopy (FTIR) spectra taken during heating of the electrospun fibers of poly(ethylene-*co*-vinyl alcohol) with 44 mol % of ethylene ($EVOH_{44}$).

Many FTIR bands in polymers are conformationally sensitive, being the sharper peaks associated to ordered chain segments along the backbone, arising mostly from within crystals. When the relative intensity of conformationally sensitive bands rises upon heating, they typically sharpen, shifting in position and become narrower (Melendez-Rodriguez et al. 2020). From **Figure 8**, a progressive increase in the intensity of many bands was initially observed, associated to classical crystal perfecting, followed by a leveling-off of these and a subsequent decrease up to around 160 °C. The steeper final drop in intensity observed is ascribed to the decrease in molecular order preceding to the melting of the sample. Therefore, at the selected annealing temperature of 145 °C, many of the bands in the spectra are in the regime in which they begin to decrease intensity, suggesting that the molecular order has started to decreased. Therefore, at this temperature,

enough thermally-induced molecular motions are enabled for the interfiber coalescence process to occur, being able to reduce the high surface energy of the fibers.

3.5. Optical Properties of the Annealed Electrospun Films

The contact transparency pictures of the films are gathered in **Figure 9**. From this figure, it can be seen that, regardless of the CNCs content, all the $EVOH_{44}$ film samples presented high contact transparency. Similar good optical properties have been reported earlier for electrospun fibers subjected to interfiber coalescence by annealing (Martínez-Sanz, Lopez-Rubio, and Lagaron 2013a, Torres-Giner, Echegoyen, et al. 2018). **Table 3** shows that the color parameters changed slightly between the different samples, in most cases being not significant, showing values ranging between 2.79–2.84, -4.69–(-5.10), and 90.84–91.28, for the a^*, b^*, and L^*, respectively. This implies that all the films were luminous with a slight tendency towards red and blue colors. In terms of color difference, the film samples with CNCs showed a ΔE^* value < 1, which indicates that the color change with respect to the neat $EVOH_{44}$ film was unnoticeable. On the other hand, regarding transparency, it was observed that the T and O values decreased with increasing CNCs content. Thus, the neat $EVOH_{44}$ film and the composite film with 0.1 wt % CNCs showed T values of 7.9 and 7.7, respectively. However, $EVOH_{44}$ with 0.5 and 1.0 wt % CNCs presented T values of 4.6 and 3.6, respectively. In terms of opacity, the O values slightly decreased from 0.004 to 0.002. Since the color variations were minimal and the nanocomposite films preserved most of the high transparency of the $EVOH_{44}$ film, it is inferred again the good distribution of the dispersed nanofillers across the copolymer matrix. Similar results were reported by Martinez-Sanz, after the incorporation of BCNWs into an $EVOH_{29}$ matrix by electrospinning before melt-mixing. In the previous work, it was already demonstrated that this methodology can be an efficient process to disperse BCNWs, since the resultant nanocomposites exhibited higher transparency than the ones developed by direct melt-mixing (Martínez-Sanz et al. 2012).

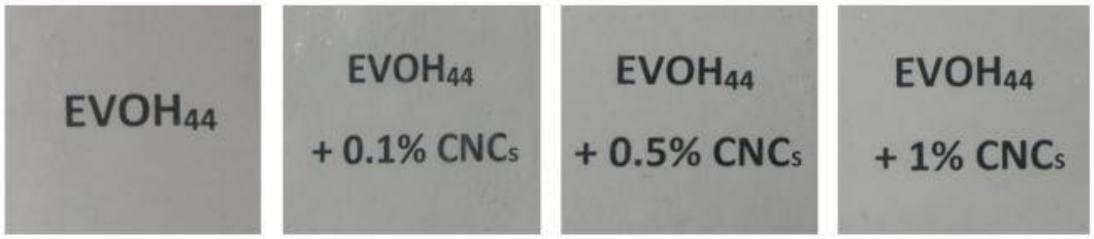

Figure 9. Contact transparency pictures of the annealed electrospun films of poly(ethylene-*co*-vinyl alcohol) with 44 mol % of ethylene ($EVOH_{44}$) with and without cellulose nanocrystals (CNCs).

Table 3. Optical and color properties of the annealed electrospun films of poly(ethylene-*co*-vinyl alcohol) with 44 mol % of ethylene ($EVOH_{44}$) with and without cellulose nanocrystals (CNCs).

Film	a^*	b^*	L^*	ΔE^*	T	O
$EVOH_{44}$	2.81 ± 0.02^a	-4.94 ± 0.04^a	91.04 ± 0.05^a	-	7.87 ± 0.04^a	0.004 ± 0.001^a
$EVOH_{44}$ + 0.1 wt % CNCs	2.79 ± 0.03^a	-4.69 ± 0.03^b	91.28 ± 0.03^b	0.35 ± 0.03^a	7.70 ± 0.03^a	0.003 ± 0.002^a
$EVOH_{44}$ + 0.5 wt % CNCs	2.81 ± 0.01^a	$-5.02 \pm 0.05^{a,c}$	90.92 ± 0.04^a	0.14 ± 0.04^b	4.64 ± 0.02^b	0.002 ± 0.001^a
$EVOH_{44}$ + 1.0 wt % CNCs	2.84 ± 0.02^a	-5.10 ± 0.04^c	90.84 ± 0.04^a	$0.26 \pm 0.03^{a,b}$	3.61 ± 0.03^c	0.002 ± 0.001^a

a^*: red/green coordinates (+a red, -a green); b^*: yellow/blue coordinates (+b yellow, -b blue); L^*: Luminosity (+L luminous, -L dark); ΔE^*: color differences; T: transparency; O: opacity.

$^{a–c}$ Different letters in the same column mean significant difference among the samples ($p < 0.05$).

3.6. Thermal Stability of the Annealed Electrospun Films

Figure 10 shows the TGA curves of the CNC powder and electrospun $EVOH_{44}$ films, whereas **Table 4** gathers the main TGA parameters. The CNCs presented a $T_{5\%}$ at 215.6 °C and a T_{deg} at 288.9 °C with a mass loss of 41.3 % and a residual mass of 5.8 %. These results are consistent with the existing literature for CNCs. For example, Mano et al. (Mano et al. 2017) showed that the main thermal degradation of CNCs occurred at about 277 °C. Similar results were reported by Cheng et al. (Cheng et al. 2015), where CNCs presented a T_{deg} close to 300 °C.

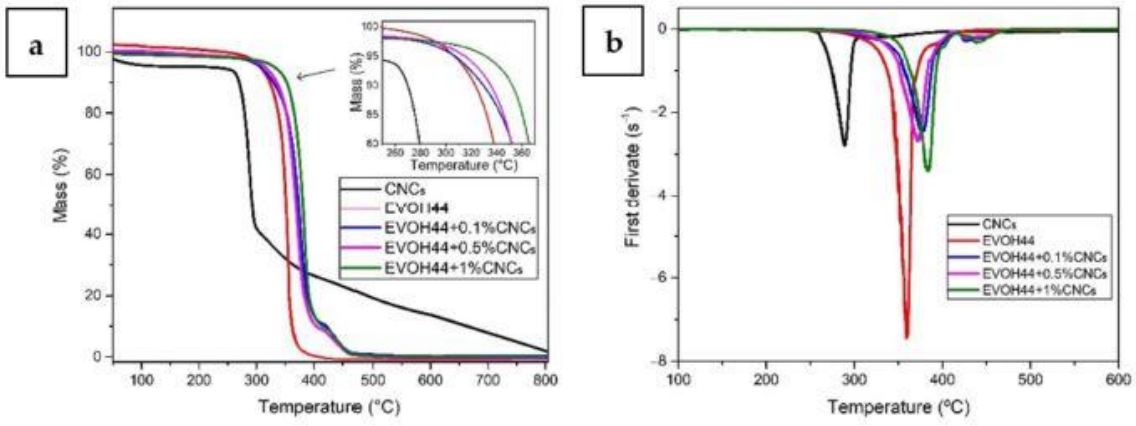

Figure 10. (a) Thermogravimetric (TGA) and (b) first derivative (DTG) curves of the cellulose nanocrystals (CNCs) and of the annealed electrospun films of poly(ethylene-*co*-vinyl alcohol) with 44 mol % of ethylene ($EVOH_{44}$) with and without CNCs.

Table 4. Thermogravimetric analysis (TGA) main parameters of the annealed electrospun films of poly(ethylene-*co*-vinyl alcohol) with 44 mol % of ethylene ($EVOH_{44}$) with and without cellulose nanocrystals (CNCs) in terms of: onset temperature of degradation ($T_{5\%}$), degradation temperature (T_{deg}), mass loss at T_{deg}, and residual mass at 800 °C.

Sample	$T_{5\%}$ (°C)	T_{deg} (°C)	Mass Loss at T_{deg} (%)	Residual Mass (%)
CNCs	215.6 ± 0.4^{a}	288.9 ± 0.5^{a}	41.3 ± 0.2^{a}	5.8 ± 0.8^{a}
$EVOH_{44}$	306.8 ± 0.9^{b}	359.7 ± 0.7^{b}	48.5 ± 0.3^{b}	0.1 ± 0.1^{b}
$EVOH_{44}$ + 0.1 wt % CNCs	306.9 ± 0.7^{b}	377.4 ± 1.4^{c}	60.0 ± 0.5^{c}	0.1 ± 0.1^{b}
$EVOH_{44}$ + 0.5 wt % CNCs	314.9 ± 1.5^{c}	372.6 ± 1.1^{d}	59.6 ± 0.8^{c}	0.1 ± 0.1^{b}
$EVOH_{44}$ + 1.0 wt % CNCs	331.2 ± 0.3^{d}	383.6 ± 1.4^{e}	59.7 ± 0.4^{c}	0.1 ± 0.1^{b}

[a–d] Different letters in the same column mean significant difference among the samples ($p < 0.05$).

In **Figure 10** and **Table 4** it can be seen that the electrospun neat $EVOH_{44}$ film showed a $T_{5\%}$ and a T_{deg} at 306.8 °C and 359.7 °C, respectively, with a mass loss of 48.5 % and a residual mass of 0.1 %. These results are consistent with other values reported in the literature. For instance, a bar-coated film of poly(ethylene-*co*-vinyl alcohol) with 32 mol % of ethylene ($EVOH_{32}$) film showed a T_{deg} at 349.1 °C (Kim, Kwon, and Seo 2014). In another study, a solvent-casted $EVOH_{32}$ film presented a $T_{5\%}$ and a T_{deg} at 270.5 °C and 381.0 °C, respectively, and a residual mass of 2.2% (Cherpinski et al. 2019). The addition of CNCs improved the thermal stability of $EVOH_{44}$ since a clear increase in both $T_{5\%}$ and a T_{deg} was observed, particularly for contents above 0.5 wt %. Thus, the $T_{5\%}$ increased to 314.9 °C and 331.2 °C, for the $EVOH_{44}$ films with a 0.5 wt % and 1 wt % CNCs, respectively. The T_{deg} values also increased, being located at 377.4, 372.6, and 383.6 °C, for the film samples with 0.1, 0.5, and 1.0 wt % CNCs, respectively. Finally, all the nanocomposite films presented a mass loss at T_{deg} of approximately 60 % and a residual mass of 0.1 %. Therefore, CNCs successfully delayed the thermal degradation of $EVOH_{44}$. Furthermore, the nanofillers also benefited from $EVOH_{44}$ since they seemed to be better stabilized in the copolymer matrix. This phenomenon has been previously reported by Orr et al. (Orr, Sonekan, and Shofner 2020), who prepared and characterized $EVOH_{48}$ films with CNCs by the solution casting method. Also, Noorani et al. (Noorani, Simonsen, and Atre 2007) reported an increase in thermal stability when CNCs was added to a polysulfone resin by a solvent exchange process, indicating not only good CNCs dispersion, but also a good interfacial interaction with the polymer matrix.

3.7. ATR-FTIR Spectroscopy of the Annealed Electrospun Films

Figure 11 displays the FTIR spectra of the CNCs powder and of the various electrospun $EVOH_{44}$ mats loaded with CNCs. For the CNCs powder, the strong and broad absorption peak at 3326 cm^{-1} was ascribed to the -OH stretching vibration of the sample with a contribution from any sorbed water (Singh et al. 2017). Assignments can also be made for the peak at 2900 cm^{-1} (CH stretching vibrations), 1054, and 898 cm^{-1} (C-O stretching) (Flauzino Neto et al. 2013, Yan et al. 2019, Zaman et al. 2012). The band at 1640 cm^{-1} was also associated with the sorbed water (Flauzino

Neto et al. 2013). Furthermore, the peaks at 1612 and 1429 cm^{-1} were assigned to asymmetric and symmetric stretching vibrations of -COOH (Islam and Karim 2010). Finally, the 667 cm^{-1} peak was attributed to the C–OH out-of-plane bending mode (Cha, He, and Ni 2012). There was no indication of remaining lignin in the CNCs since the lignin contribution has characteristic peaks around 1500 cm^{-1} (Sun et al. 2005).

Upon the addition of CNCs to the pure $EVOH_{44}$, there was no evidence of any new peaks or changes in the position of the characteristic $EVOH_{44}$ peaks. This result suggests that, for the loadings used, there was no detectable interaction that could be picked up by the technique between $EVOH_{44}$ and CNCs, which are both known to be strongly self-associated polymers. These finding are in accordance with those reported elsewhere in the literature for other similar systems. For example, in an $EVOH_{32}$ film with BCNWs, the cellulose characteristic bands were not observed up to concentrations of 3 wt % BCNWs (Martínez-Sanz, Lopez-Rubio, and Lagaron 2013a). In another study, an $EVOH_{32}$ film with 1.0 wt % CNCs was also no loaded enough to show unambiguous changes in the spectra (Cherpinski et al. 2019).

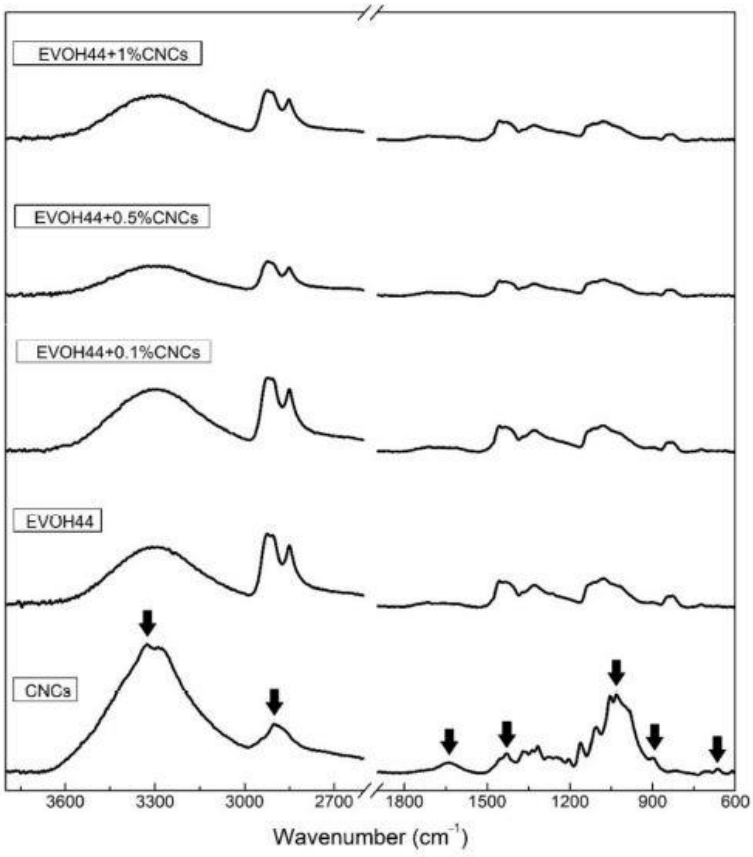

Figure 11. Fourier transform infrared spectroscopy (FTIR) spectra of the cellulose nanocrystals (CNCs) powder and of the annealed electrospun films of poly(ethylene-*co*-vinyl alcohol) with 44 mol % of ethylene ($EVOH_{44}$) with and without CNCs. The arrows refer to the bands discussed in the text.

3.8. Mechanical Properties of the Annealed Electrospun Films

Table 5 gathers the values of the elastic modulus (E), tensile strength at yield (σ_y), elongation at break (ε_b), and toughness (T) of the electrospun $EVOH_{44}$ films calculated from their strain-stress curves obtained at room temperature and shown in **Figure 12**. The neat $EVOH_{44}$ film showed values of E of 4699 MPa, σ_y of 38.7 MPa, ε_b of 10.4 %, and T of 3.2 mJ/m^3. When CNCs were incorporated into $EVOH_{44}$, the E values increased for contents of 0.1 and 0.5 wt %, by 37.75 % and 28.15 %, respectively, while σ_y was kept in the 30–40 MPa range, hence resulting in more rigid films. However, the mechanical strength decreased at the CNCs loading of 1.0 wt %, showing values of E and σ_y of 4135 and 25.2 MPa, respectively. Moreover, the ductility of the electrospun $EVOH_{44}$ films decreased significantly for all the CNCs contents, showing values of ε_b and T in the ranges of 0.7–1.6 % and a T of 0.2–0.3 mJ/m^3.

Table 5. Mechanical properties of the annealed electrospun films of poly(ethylene-*co*-vinyl alcohol) with 44 mol % of ethylene ($EVOH_{44}$) with and without cellulose nanocrystals (CNCs) in terms of: tensile modulus (E), tensile strength at yield (σ_y), elongation at break (ε_b), and toughness (T).

Film	E (MPa)	σ_y (MPa)	ε_b (%)	T (mJ/m^3)
$EVOH_{44}$	4699 ± 350^a	38.7 ± 5.2^a	10.4 ± 3.6^a	3.2 ± 1.4^a
$EVOH_{44}$ + 0.1 wt % CNCs	6473 ± 257^b	39.2± 8.6^{a,b}	0.8 ± 0.5^b	0.2 ± 0.1^b
$EVOH_{44}$ + 0.5 wt % CNCs	6022 ± 584^b	30.2 ± 8.3^{a,b}	0.7 ± 0.2^b	0.2 ± 0.1^b
$EVOH_{44}$ + 1.0 wt % CNCs	4135 ± 399^a	25.2 ± 7.7^b	1.6 ± 0.7^b	0.3 ± 0.1^b

$^{a-b}$ Different letters in the same column mean significant difference among the samples ($p < 0.05$).

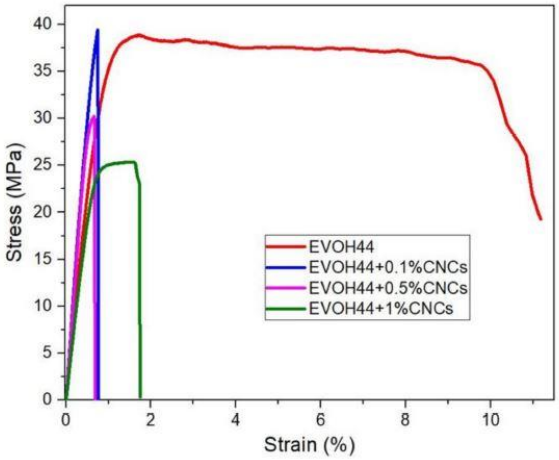

Figure 12. Tensile stress–strain curves of the annealed electrospun films of poly(ethylene-*co*-vinyl alcohol) with 44 mol % of ethylene ($EVOH_{44}$) with and without cellulose nanocrystals (CNCs).

Previous works dealing with polymer nanocomposites based on CNCs have reported a similar mechanical behavior. For instance, $EVOH_{32}$/cellulose nanowhisker (CNW) nanocomposites prepared by melt compounding showed an increase in tensile modulus and tensile strength but accompanied with a decrease in ductility when increasing the nanofiller content, producing stronger but more brittle materials (Martínez-Sanz, Lopez-Rubio, and Lagaron 2013b). Also, polylactide acid (PLA) nanocomposite fibers containing 1–3 wt % BCNWs prepared by electrospinning and, then, melt-mixed with PLA pellets by melt compounding showed a percentage increase in Young's modulus and tensile strength of about 15 %, but a decrease in ε_b of 10 % (Martínez-Sanz, Lopez-Rubio, and Lagaron 2012). In another study, PLA/MFC nanocomposites prepared by solvent mixing and, then, hot-pressed into sheets, also presented an increase in both tensile modulus and tensile strength, but a decrease in strain at break (Suryanegara, Nakagaito, and Yano 2009). Similarly, functionalized cellulose nanocrystal methyl ester (CNC-me) incorporated into PHBV films prepared by solution casting showed an increase in Young's modulus and tensile strength of 250 % and 147 %, respectively, when increasing the CNCs content, while ε_b considerably decreased (Yu, Yan, and Yao 2014). A similar effect was observed for PVOH films reinforced with CNCs also prepared by solvent casting (Ogunsona and Mekonnen 2020, Yang et al. 2020). Different factors have been hypothesized to influence the mechanical properties of polymers reinforced with CNCs. Thus, in addition to potential interactions between the polymer matrix and cellulosic nanofillers in the amorphous phase, the dispersion and distribution of the CNCs in the matrix has a significant effect (Yu, Yan, and Yao 2014). In particular, it has been described that an increase in mechanical strength is due to a good stress transfer across the interphase due to the interfacial bond that occurs between the CNCs and the polymer matrix (McCrum N. G., Buckley C. P., and B. 1988, Razi, Portier, and Raman 1999). Moreover, achieving the percolation threshold is critical for obtaining an enhanced mechanical performance. This consists on the formation of a 3-dimensional (3D) nanocrystal network via hydrogen bonding forces that connect the fillers throughout the polymer matrix. This phenomenon can be affected by different parameters, such as particle interactions, orientation, or aspect ratio (Azizi Samir, Alloin, and Dufresne 2005). With CNCs, it has been described that a good dispersion of the nanocrystals, without agglomerations, can favor the elimination of the defects or stress concentrators (Cao et al. 2016). Therefore, even though, the FTIR analysis did not resolve any potential hydrogen bonding interactions between the components, it is clear that the electrospun $EVOH_{44}$ films having 0.1 wt % CNCs, with best reported filler distribution, showed an optimal balance in mechanical properties. On the contrary, the sample with 1.0 wt % CNCs, which showed more agglomerations, presented a reduction in the reinforcement of the copolymer matrix.

3.9. Barrier Properties of the Annealed Electrospun Films

The WVP and OP values of the annealed electrospun $EVOH_{44}$ films, with and without CNCs, are shown in **Table 6**. The neat $EVOH_{44}$ film showed the highest barrier performance, that is, the lowest permeabilities. Thus, for WVP, $EVOH_{44}$ film showed a value of 1.6×10^{-14} $kg \cdot m \cdot m^{-2} \cdot Pa^{-1} \cdot s^{-1}$. OP was measured at different % RH, namely 0 %, 20 %, and 80 %, in order to assess the effect of humidity on the oxygen permeability. From **Figure 13**, which plots the evolution of the oxygen barrier as function of % RH, it can be observed that the $EVOH_{44}$ film presented good oxygen barrier at low humidity, showing values of 1.1×10^{-20} and 0.1×10^{-20} $m^3 \cdot m \cdot m^{-2} \cdot Pa^{-1} \cdot s^{-1}$ for 0 % and 20 % RH, respectively. However, at the highest humidity, that is, 80 %, the barrier decreased to 4.7×10^{-20} $m^3 \cdot m \cdot m^{-2} \cdot Pa^{-1} \cdot s^{-1}$. In hydrophilic polymers, which is

the case of the EVOH copolymers, it has been reported an increase in the permeability to oxygen gas due to water-induced plasticization at high humidity (Zhang, Lim, and Tung 2001). In this plasticization regime, sorbed water molecules intercept the strong polymer interchain self-association, leading to water molecules clustering, and hence to an increase in free volume that allow the gas molecules to diffuse through (Lagaron et al. 2003). It is also known that at lower humidity, the sorbed water is not able to break the strong interchain hydrogen bonding, hence the water molecules block the existing free volume instead, thus reducing the available sites for diffusion (Zhang, Lim, and Tung 2001).

Table 6. Values of water vapor permeability (WVP), and oxygen permeability (OP) of the annealed electrospun films of poly(ethylene-*co*-vinyl alcohol) with 44 mol % of ethylene ($EVOH_{44}$) with and without cellulose nanocrystals (CNCs).

Film	WVP × 10^{14} ($kg \cdot m \cdot m^{-2} \cdot Pa^{-1} \cdot s^{-1}$)	OP × 10^{20} ($m^3 \cdot m \cdot m^{-2} \cdot Pa^{-1} \cdot s^{-1}$)		
		0% RH	20% RH	80% RH
$EVOH_{44}$	1.6 ± 0.4^{a}	1.1 ± 0.2^{a}	0.10 ± 0.04^{a}	4.7 ± 0.3^{a}
$EVOH_{44}$ + 0.1 wt % CNCs	3.7 ± 0.3^{b}	1.4 ± 0.1^{a}	0.38 ± 0.01^{b}	8.3 ± 0.2^{b}
$EVOH_{44}$ + 0.5 wt % CNCs	$4.1 \pm 0.9^{b,c}$	2.7 ± 0.2^{b}	$0.53 \pm 0.03^{b,c}$	8.8 ± 0.2^{b}
$EVOH_{44}$ + 1.0 wt % CNCs	4.5 ± 0.1^{c}	2.3 ± 0.4^{b}	0.61 ± 0.01^{c}	8.7 ± 0.2^{b}

[a–c] Different letters in the same column mean significant difference among the samples ($p < 0.05$).

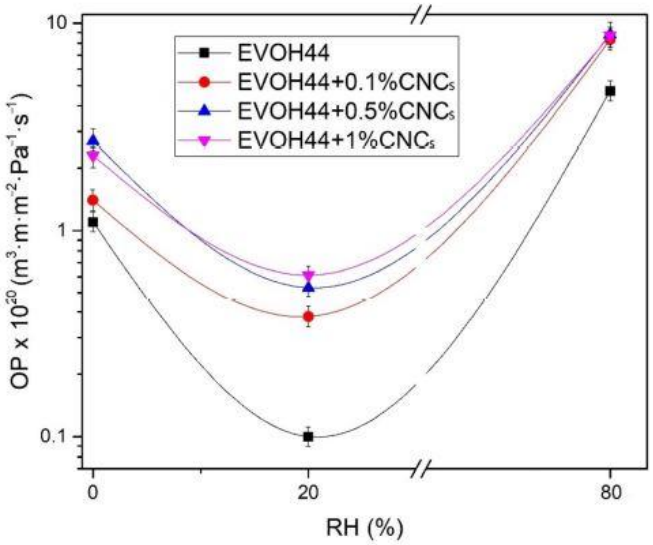

Figure 13. Evolution of oxygen permeability (OP) in log scale as a function of the percentage of relative humidity (% RH) of the annealed electrospun films of poly(ethylene-*co*-vinyl alcohol) with 44 mol % of ethylene ($EVOH_{44}$) with and without cellulose nanocrystals (CNCs).

Compared to other $EVOH_{44}$ films studied in the literature, the values reported herein for the $EVOH_{44}$ films are within the same order of magnitude. For instance, $EVOH_{44}$ films prepared by extrusion showed a WVP of 0.25×10^{-14} $kg \cdot m \cdot m^{-2} \cdot Pa^{-1} \cdot s^{-1}$ (Martínez-Sanz, Lopez-Rubio, and Lagaron 2012), whereas for others prepared by solvent casting it was 0.11×10^{-14} $kg \cdot m \cdot m^{-2} \cdot Pa^{-1} \cdot s^{-1}$ (Fernández et al. 2008). In terms of oxygen barrier, an OP value of 0.77×10^{-21} $m^3 \cdot m \cdot m^{-2} \cdot Pa^{-1} \cdot s^{-1}$ was reported for $EVOH_{32}$ in dry conditions, while a value of 9.1×10^{-20} $m^3 \cdot m \cdot m^{-2} \cdot Pa^{-1} \cdot s^{-1}$ was obtained in wet conditions (Lagaron, Catalá, and Gavara 2004). The OP of a solvent-cast $EVOH_{44}$ film was studied at different % RH, resulting in values of 0.42×10^{-20} $m^3 \cdot m \cdot m^{-2} \cdot Pa^{-1} \cdot s^{-1}$ at 65 % RH and 0.26×10^{-20} $m^3 \cdot m \cdot m^{-2} \cdot Pa^{-1} \cdot s^{-1}$ at 0% RH (Maes et al. 2018). Also, the OP of a melt-extruded $EVOH_{44}$ film was measured at different % RH, with values of 9×10^{-20} $m^3 \cdot m \cdot m^{-2} \cdot Pa^{-1} \cdot s^{-1}$ at 50 % RH and 9×10^{-19} $m^3 \cdot m \cdot m^{-2} \cdot Pa^{-1} \cdot s^{-1}$ at 90 % RH. These results indicate that the barrier properties of the annealed electrospun fiber-based $EVOH_{44}$ films obtained are somewhat lower, but within the same order of magnitude, than films of this copolymer processed by other techniques.

When CNCs were incorporated into the electrospun $EVOH_{44}$ fibers, an increase in permeability was observed in the resulting films. In general terms, the films with different CNCs contents showed minor differences between them, in most cases being not significant, though there was a tendency for the barrier properties to decrease with increasing the nanofiller content. Finally, the OP values were also determined at the three % RH tested, exhibiting a similar trend as for the case of the $EVOH_{44}$ film. Therefore, the best barrier performance for oxygen was also found at 20 % RH. However, the effect of the CNCs loading at this % RH was also the most significant, which points out that the hydrophilic and rigid nature of the CNCs and the lower crystallinity of the copolymer matrix, increased the free volume, thus facilitating gas diffusion.

Although, in general nanocelluloses, when used as fillers, have been reported to improve the gas barrier properties of polymers (Karkhanis et al. 2018, Li, Shi, et al. 2020), the fact that the polymer used in this study is already a very high-gas-barrier material explains the reduction observed (Chowdhury et al. 2019). Syverud et al. (Syverud and Stenius 2008) reported OP values of 4.3–5.8×10^{-20} $m^3 \cdot m \cdot m^{-2} \cdot Pa^{-1} \cdot s^{-1}$ for MFC films, whereas Nair et al. (Nair et al. 2014) reported OP values of 6.9×10^{-21} and $0.1–1.2 \times 10^{-21}$ $m^3 \cdot m \cdot m^{-2} \cdot Pa^{-1} \cdot s^{-1}$ for CNCs and EVOH films, respectively. In addition, it should be noted that the introduction of the CNCs in the experiments reported here was found to lead to a lower crystallinity for the copolymer, factor that is known to reduce permeability by increasing free volume and reducing tortuosity (Belbekhouche et al. 2011, Guinault et al. 2010). Similar observations have been previously reported after addition of MFC to EVOH, which led to a decrease in WVP due to changes in morphology and crystallinity (Fernández et al. 2008). The same observation was also found by Petersson et al. (Petersson and Oksman 2006), who showed a reduction in OP when microcrystalline cellulose (MCC) was added to PLA due to a decrease in the degree of crystallinity.

4. Conclusions

The present study demonstrated the potential of the electrospinning process to obtain a new high-gas-barrier transparent fiber-based $EVOH_{44}$ film. This material shows barrier properties somewhat lower than those of the same copolymer processed by other conventional processing technologies. The incorporation of CNCs increased the thermal and mechanical resistance of the fiber-based $EVOH_{44}$ film, unfortunately for contents not exciding of 0.5 wt %, and exhibiting optimal balanced properties at 0.1 wt %. In this case, hybrid bio-/non-bio nanocomposites can be obtained with enhanced rigidity but reduced flexibility and slightly lower barrier properties. Still these hybrid nanocomposites offer the advantage of remaining in the high-barrier regime. The lower annealing temperature required for the $EVOH_{44}$ copolymer and its nanocomposites with CNCs, enable them to be used as barrier interlayers, compatible with many more polymers and biopolymers than their higher vinyl-alcohol content homologous copolymers. Future work will deal with the application of these novel barrier materials as very thin interlayers in compostable multilayer systems, to ascertain the overall barrier reinforcement and physicochemical properties, and also, their biodegradability under industrial and home composting conditions.

5. References

Abdallah, W., and M. R. Kamal. 2018. "Influence of process variables on physical characteristics of spray freeze dried cellulose nanocrystals." *Cellulose* 25 (10):5711-5730. doi: 10.1007/s10570-018-1975-0.

Agüero, A., M. C. Morcillo, L. Quiles-Carrillo, R. Balart, T. Boronat, D. Lascano, S. Torres-Giner, and O. Fenollar. 2019. "Study of the influence of the reprocessing cycles on the final properties of polylactide pieces obtained by injection molding." *Polymers* 11 (12). doi: 10.3390/polym11121908.

Arboleda E, C., A. I. Mejía G, and B. L. López O. 2004. "Poly (vinylalcohol-co-ethylene) biodegradation on semi solid fermentation by Phanerochaete chrysosporium." *Acta Farmaceutica Bonaerense* 23 (2):123-128.

Arfat, Y. A., J. Ahmed, N. Hiremath, R. Auras, and A. Joseph. 2017. "Thermo-mechanical, rheological, structural and antimicrobial properties of bionanocomposite films based on fish skin gelatin and silver-copper nanoparticles." *Food Hydrocolloids* 62:191-202. doi: 10.1016/j.foodhyd.2016.08.009.

Arias, A., M. C. Heuzey, M. A. Huneault, G. Ausias, and A. Bendahou. 2015. "Enhanced dispersion of cellulose nanocrystals in melt-processed polylactide-based nanocomposites." *Cellulose* 22 (1):483-498. doi: 10.1007/s10570-014-0476-z.

Ashori, A., M. Jonoobi, N. Ayrilmis, A. Shahreki, and M. A. Fashapoyeh. 2019. "Preparation and characterization of polyhydroxybutyrate-co-valerate (PHBV) as green composites using nano reinforcements." *International Journal of Biological Macromolecules* 136:1119-1124. doi: 10.1016/j.ijbiomac.2019.06.181.

Azizi Samir, My Ahmed Said, Fannie Alloin, and Alain Dufresne. 2005. "Review of Recent Research into Cellulosic Whiskers, Their Properties and Their Application in Nanocomposite Field." *Biomacromolecules* 6 (2):612-626. doi: 10.1021/bm0493685.

Beck, S., J. Bouchard, and R. Berry. 2012. "Dispersibility in water of dried nanocrystalline cellulose." *Biomacromolecules* 13 (5):1486-1494. doi: 10.1021/bm300191k.

Belbekhouche, Sabrina, Julien Bras, Gilberto Siqueira, Corinne Chappey, Laurent Lebrun, Bertine Khelifi, Stéphane Marais, and Alain Dufresne. 2011. "Water sorption behavior and gas barrier properties of cellulose whiskers and microfibrils films." *Carbohydrate Polymers* 83 (4):1740-1748. doi: https://doi.org/10.1016/j.carbpol.2010.10.036.

Cao, Y., P. Zavattieri, J. Youngblood, R. Moon, and J. Weiss. 2016. "The relationship between cellulose nanocrystal dispersion and strength." *Construction and Building Materials* 119:71-79. doi: 10.1016/j.conbuildmat.2016.03.077.

Cava, D., C. Sammon, and J. M. Lagaron. 2006. "Water Diffusion and Sorption-Induced Swelling as a Function of Temperature and Ethylene Content in Ethylene-Vinyl Alcohol Copolymers as Determined by Attenuated Total Reflection Fourier Transform Infrared Spectroscopy." *Applied Spectroscopy* 60 (12):1392-1398. doi: 10.1366/000370206779321382.

Cerrada, M. L., E. Pérez, J. M. Pereña, and R. Benavente. 1998. "Wide-angle X-ray diffraction study of the phase behavior of vinyl alcohol-ethylene copolymers." *Macromolecules* 31 (8):2559-2564. doi: 10.1021/ma9705127.

Cha, Ruitao, Zhibin He, and Yonghao Ni. 2012. "Preparation and characterization of thermal/pH-sensitive hydrogel from carboxylated nanocrystalline cellulose." *Carbohydrate Polymers* 88 (2):713-718. doi: https://doi.org/10.1016/j.carbpol.2012.01.026.

Cheng, Dong, Yangbing Wen, Lijuan Wang, Xingye An, Xuhai Zhu, and Yonghao Ni. 2015. "Adsorption of polyethylene glycol (PEG) onto cellulose nano-crystals to improve its dispersity." *Carbohydrate Polymers* 123:157-163. doi: https://doi.org/10.1016/j.carbpol.2015.01.035.

Cherpinski, A., A. Biswas, J. M. Lagaron, A. Dufresne, S. Kim, M. Buttrum, E. Espinosa, and H. N. Cheng. 2019. "Preparation and evaluation of oxygen scavenging nanocomposite films incorporating cellulose nanocrystals and Pd nanoparticles in poly(ethylene-co-vinyl alcohol)." *Cellulose* 26 (12):7237-7251. doi: 10.1007/s10570-019-02613-8.

Chowdhury, Reaz A., Md Nuruddin, Caitlyn Clarkson, Francisco Montes, John Howarter, and Jeffrey P. Youngblood. 2019. "Cellulose Nanocrystal (CNC) Coatings with Controlled Anisotropy as High-Performance Gas Barrier Films." *ACS Applied Materials & Interfaces* 11 (1):1376-1383. doi: 10.1021/acsami.8b16897.

Coleman, M. M., X. Yang, H. Zhang, and P. C. Painter. 1993. "Ethylene-co-vinyl alcohol blends." *Journal of Macromolecular Science, Part B* 32 (3):295-326. doi: 10.1080/00222349308215486.

De Souza Lima, M. M., and R. Borsali. 2004. "Rodlike cellulose microcrystals: Structure, properties, and applications." *Macromolecular Rapid Communications* 25 (7):771-787. doi: 10.1002/marc.200300268.

Di Giorgio, L., L. Martín, P. R. Salgado, and A. N. Mauri. 2020. "Synthesis and conservation of cellulose nanocrystals." *Carbohydrate Polymers* 238. doi: 10.1016/j.carbpol.2020.116187.

Echegoyen, Y., M. J. Fabra, J. L. Castro-Mayorga, A. Cherpinski, and J. M. Lagaron. 2017. "High throughput electro-hydrodynamic processing in food encapsulation and food packaging applications: Viewpoint." *Trends in Food Science and Technology* 60:71-79. doi: 10.1016/j.tifs.2016.10.019.

Erlandsson, B., S. Karlsson, and A. C. Albertsson. 1997. "Biodegradation of C-14 labeled poly(ethylene-CO-vinyl alcohol)." Polymeric Materials Science and Engineering, Proceedings of the ACS Division of Polymeric Materials Science and Engineering.

Fabra, M. J., A. López-Rubio, J. Ambrosio-Martín, and J. M. Lagaron. 2016. "Improving the barrier properties of thermoplastic corn starch-based films containing bacterial cellulose nanowhiskers by means of PHA electrospun coatings of interest in food packaging." *Food Hydrocolloids* 61:261-268. doi: 10.1016/j.foodhyd.2016.05.025.

Faisant, J. B., A. Aït-Kadi, M. Bousmina, and L. Deschênes. 1998. "Morphology, thermomechanical and barrier properties of polypropylene-ethylene vinyl alcohol blends." *Polymer* 39 (3):533-545. doi: 10.1016/S0032-3861(97)00313-3.

Favier, V., G. R. Canova, S. C. Shrivastava, and J. Y. Cavaillé. 1997. "Mechanical percolation in cellulose whisker nanocomposites." *Polymer Engineering and Science* 37 (10):1732-1739. doi: 10.1002/pen.11821.

Fernández, Avelina, M. Dolores Sánchez, Mikael Ankerfors, and Jose M. Lagaron. 2008. "Effects of ionizing radiation in ethylene-vinyl alcohol copolymers and in composites containing microfibrillated cellulose." *Journal of Applied Polymer Science* 109 (1):126-134. doi: https://doi.org/10.1002/app.27709.

Figueroa-Lopez, K. J., L. Cabedo, J. M. Lagaron, and S. Torres-Giner. 2020. "Development of Electrospun Poly(3-hydroxybutyrate-co-3-hydroxyvalerate) Monolayers Containing Eugenol and Their Application in Multilayer Antimicrobial Food Packaging." *Frontiers in Nutrition* 7. doi: 10.3389/fnut.2020.00140.

Flauzino Neto, Wilson Pires, Hudson Alves Silvério, Noélio Oliveira Dantas, and Daniel Pasquini. 2013. "Extraction and characterization of cellulose nanocrystals from agro-industrial residue – Soy hulls." *Industrial Crops and Products* 42:480-488. doi: https://doi.org/10.1016/j.indcrop.2012.06.041.

Fortunati, E., I. Armentano, Q. Zhou, A. Iannoni, E. Saino, L. Visai, L. A. Berglund, and J. M. Kenny. 2012. "Multifunctional bionanocomposite films of poly(lactic acid), cellulose nanocrystals and silver nanoparticles." *Carbohydrate Polymers* 87 (2):1596-1605. doi: 10.1016/j.carbpol.2011.09.066.

García, A., A. Gandini, J. Labidi, N. Belgacem, and J. Bras. 2016. "Industrial and crop wastes: A new source for nanocellulose biorefinery." *Industrial Crops and Products* 93:26-38. doi: 10.1016/j.indcrop.2016.06.004.

Gatenholm, P., and D. Klemm. 2010. "Bacterial nanocellulose as a renewable material for biomedical applications." *MRS Bulletin* 35 (3):208-213. doi: 10.1557/mrs2010.653.

Gavara, R., R. Catalá, G. López Carballo, J. P. Cerisuelo, I. Dominguez, V. Muriel-Galet, and P. Hernandez-Muñoz. 2016. "Use of EVOH for food packaging applications." *Use of EVOH for Food Packaging Applications*:1-6.

González, K., L. Iturriaga, A. González, A. Eceiza, and N. Gabilondo. 2020. "Improving mechanical and barrier properties of thermoplastic starch and polysaccharide nanocrystals nanocomposites." *European Polymer Journal* 123. doi: 10.1016/j.eurpolymj.2019.109415.

Guinault, A., C. Sollogoub, S. Domenek, A. Grandmontagne, and V. Ducruet. 2010. "Influence of crystallinity on gas barrier and mechanical properties of pla food packaging films." *International Journal of Material Forming* 3 (1):603-606. doi: 10.1007/s12289-010-0842-9.

Gupta, A., W. Simmons, G. T. Schueneman, D. Hylton, and E. A. Mintz. 2017. "Rheological and thermo-mechanical properties of poly(lactic acid)/lignin-coated cellulose nanocrystal composites." *ACS Sustainable Chemistry and Engineering* 5 (2):1711-1720. doi: 10.1021/acssuschemeng.6b02458.

He, Y., H. Li, X. Fei, and L. Peng. 2021. "Carboxymethyl cellulose/cellulose nanocrystals immobilized silver nanoparticles as an effective coating to improve barrier and antibacterial properties of paper for food packaging applications." *Carbohydrate Polymers* 252. doi: 10.1016/j.carbpol.2020.117156.

Henriksson, M., G. Henriksson, L. A. Berglund, and T. Lindström. 2007. "An environmentally friendly method for enzyme-assisted preparation of microfibrillated cellulose (MFC) nanofibers." *European Polymer Journal* 43 (8):3434-3441. doi: 10.1016/j.eurpolymj.2007.05.038.

Islam, Md Shahidul, and Mohammad Rezaul Karim. 2010. "Fabrication and characterization of poly(vinyl alcohol)/alginate blend nanofibers by electrospinning method." *Colloids and Surfaces A: Physicochemical and Engineering Aspects* 366 (1):135-140. doi: https://doi.org/10.1016/j.colsurfa.2010.05.038.

Ito, K., Y. Saito, T. Yamamoto, Y. Ujihira, and K. Nomura. 2001. "Correlation study between oxygen permeability and free volume of ethylene-vinyl alcohol copolymer through positronium lifetime measurement [1]." *Macromolecules* 34 (18):6153-6155. doi: 10.1021/ma001813a.

Kanatt, S. R., M. S. Rao, S. P. Chawla, and A. Sharma. 2012. "Active chitosan-polyvinyl alcohol films with natural extracts." *Food Hydrocolloids* 29 (2):290-297. doi: 10.1016/j.foodhyd.2012.03.005.

Karkhanis, Sonal S., Nicole M. Stark, Ronald C. Sabo, and Laurent M. Matuana. 2018. "Water vapor and oxygen barrier properties of extrusion-blown poly(lactic acid)/cellulose nanocrystals nanocomposite films." *Composites Part A: Applied Science and Manufacturing* 114:204-211. doi: https://doi.org/10.1016/j.compositesa.2018.08.025.

Katayama, T. 2005. "New development of ethylene-vinyl alcohol copolymer fiber." *Kinoshi Kenkyu Kaishi/Annals of the High Performance Paper Society, Japan* (44):43-48.

Kenawy, E. R., J. M. Layman, J. R. Watkins, G. L. Bowlin, J. A. Matthews, D. G. Simpson, and G. E. Wnek. 2003. "Electrospinning of poly(ethylene-co-vinyl alcohol) fibers." *Biomaterials* 24 (6):907-913. doi: 10.1016/S0142-9612(02)00422-2.

Khoshkava, V., and M. R. Kamal. 2014a. "Effect of cellulose nanocrystals (CNC) particle morphology on dispersion and rheological and mechanical properties of polypropylene/CNC nanocomposites." *ACS Applied Materials and Interfaces* 6 (11):8146-8157. doi: 10.1021/am500577e.

Khoshkava, V., and M. R. Kamal. 2014b. "Effect of drying conditions on cellulose nanocrystal (CNC) agglomerate porosity and dispersibility in polymer nanocomposites." *Powder Technology* 261:288-298. doi: 10.1016/j.powtec.2014.04.016.

Kim, Dowan, Hyok Kwon, and Jongchul Seo. 2014. "EVOH nanocomposite films with enhanced barrier properties under high humidity conditions." *Polymer Composites* 35 (4):644-654. doi: https://doi.org/10.1002/pc.22707.

Lagaron, J. M., R. Catalá, and R. Gavara. 2004. "Structural characteristics defining high barrier properties in polymeric materials." *Materials Science and Technology* 20 (1):1-7. doi: 10.1179/026708304225010442.

Lagaron, Jose M., Enrique Gimenez, Ramon Catala, and Rafael Gavara. 2003. "Mechanisms of Moisture Sorption in Barrier Polymers Used in Food Packaging: Amorphous Polyamide vs. High-Barrier Ethylene-Vinyl Alcohol Copolymer Studied by Vibrational Spectroscopy." *Macromolecular Chemistry and Physics* 204 (4):704-713. doi: https://doi.org/10.1002/macp.200390039.

Lasagabaster, Aurora, María José Abad, Luis Barral, and Ana Ares. 2006. "FTIR study on the nature of water sorbed in polypropylene (PP)/ethylene alcohol vinyl (EVOH) films." *European Polymer Journal* 42 (11):3121-3132. doi: https://doi.org/10.1016/j.eurpolymj.2006.03.029.

Lei, W., C. Fang, X. Zhou, Q. Yin, S. Pan, R. Yang, D. Liu, and Y. Ouyang. 2018. "Cellulose nanocrystals obtained from office waste paper and their potential application in PET packing materials." *Carbohydrate Polymers* 181:376-385. doi: 10.1016/j.carbpol.2017.10.059.

Li, C., C. Sun, C. Wang, H. Tan, Y. Xie, and Y. Zhang. 2020. "Cellulose nanocrystal reinforced poly(lactic acid) nanocomposites prepared by a solution precipitation approach." *Cellulose* 27 (13):7489-7502. doi: 10.1007/s10570-020-03294-4.

Li, Hui, Hongbo Shi, Yunqing He, Xiang Fei, and Lincai Peng. 2020. "Preparation and characterization of carboxymethyl cellulose-based composite films reinforced by cellulose nanocrystals derived from pea hull waste for food packaging applications." *International Journal of Biological Macromolecules* 164:4104-4112. doi: https://doi.org/10.1016/j.ijbiomac.2020.09.010.

López-de-Dicastillo, Carol, Miriam Gallur, Ramón Catalá, Rafael Gavara, and Pilar Hernandez-Muñoz. 2010. "Immobilization of β-cyclodextrin in ethylene-vinyl alcohol copolymer for active food packaging applications." *Journal of Membrane Science* 353 (1):184-191. doi: https://doi.org/10.1016/j.memsci.2010.02.049.

Luzi, F., L. Torre, and D. Puglia. 2020. "Antioxidant Packaging Films Based on Ethylene Vinyl Alcohol Copolymer (EVOH) and Caffeic Acid." *Molecules* 25 (17). doi: 10.3390/molecules25173953.

Maes, Caroline, Wout Luyten, Geert Herremans, Roos Peeters, Robert Carleer, and Mieke Buntinx. 2018. "Recent Updates on the Barrier Properties of Ethylene Vinyl Alcohol

Copolymer (EVOH): A Review." *Polymer Reviews* 58 (2):209-246. doi: 10.1080/15583724.2017.1394323.

Mano, Valdir, Stefano Chimenti, Giacomo Ruggeri, Fabiano Vargas Pereira, and Everton Luiz de Paula. 2017. "P(CL-b-LLA) diblock copolymers grafting onto cellulosic nanocrystals." *Polymer Bulletin* 74 (9):3673-3688. doi: 10.1007/s00289-017-1919-0.

Mariano, M., N. El Kissi, and A. Dufresne. 2014. "Cellulose nanocrystals and related nanocomposites: Review of some properties and challenges." *Journal of Polymer Science, Part B: Polymer Physics* 52 (12):791-806. doi: 10.1002/polb.23490.

Marie, E., Y. Chevalier, N. Issartel, F. Eydoux, L. Germanaud, and P. Flores. 2001. "The controlled solvolysis of ethylene-vinyl acetate copolymers." *Macromolecules* 34 (17):5838-5847. doi: 10.1021/ma0102666.

Martínez-Sanz, M., A. Lopez-Rubio, and J. M. Lagaron. 2013a. "Nanocomposites of ethylene vinyl alcohol copolymer with thermally resistant cellulose nanowhiskers by melt compounding (I): Morphology and thermal properties." *Journal of Applied Polymer Science* 128 (5):2666-2678. doi: 10.1002/app.38433.

Martínez-Sanz, M., A. Lopez-Rubio, and J. M. Lagaron. 2014. "Dispersing Bacterial Cellulose Nanowhiskers in Polylactides via Electrohydrodynamic Processing." *Journal of Polymers and the Environment* 22 (1):27-40. doi: 10.1007/s10924-013-0619-6.

Martínez-Sanz, M., A. Lopez-Rubio, M. Villano, C. S. S. Oliveira, M. Majone, M. Reis, and J. M. Lagarón. 2016. "Production of bacterial nanobiocomposites of polyhydroxyalkanoates derived from waste and bacterial nanocellulose by the electrospinning enabling melt compounding method." *Journal of Applied Polymer Science* 133 (2). doi: 10.1002/app.42486.

Martínez-Sanz, M., R. T. Olsson, A. Lopez-Rubio, and J. M. Lagaron. 2011. "Development of electrospun EVOH fibres reinforced with bacterial cellulose nanowhiskers. Part I: Characterization and method optimization." *Cellulose* 18 (2):335-347. doi: 10.1007/s10570-010-9471-1.

Martínez-Sanz, M., R. T. Olsson, A. Lopez-Rubio, and J. M. Lagaron. 2012. "Development of bacterial cellulose nanowhiskers reinforced EVOH composites by electrospinning." *Journal of Applied Polymer Science* 124 (2):1398-1408. doi: 10.1002/app.35052.

Martínez-Sanz, Marta, Amparo Lopez-Rubio, and Jose M. Lagaron. 2012. "Optimization of the Dispersion of Unmodified Bacterial Cellulose Nanowhiskers into Polylactide via Melt Compounding to Significantly Enhance Barrier and Mechanical Properties." *Biomacromolecules* 13 (11):3887-3899. doi: 10.1021/bm301430j.

Martínez-Sanz, Marta, Amparo Lopez-Rubio, and Jose M. Lagaron. 2013b. "Nanocomposites of ethylene vinyl alcohol copolymer with thermally resistant cellulose nanowhiskers by melt compounding (II): Water barrier and mechanical properties." *Journal of Applied Polymer Science* 128 (3):2197-2207. doi: https://doi.org/10.1002/app.38432.

McCrum N. G., Buckley C. P., and Bucknall C. B. 1988. *Principles of polymer engineering*. Oxford, UK: Oxford University Press.

Mehrasa, M., M. A. Asadollahi, B. Nasri-Nasrabadi, K. Ghaedi, H. Salehi, A. Dolatshahi-Pirouz, and A. Arpanaei. 2016. "Incorporation of mesoporous silica nanoparticles into random electrospun PLGA and PLGA/gelatin nanofibrous scaffolds enhances mechanical and cell proliferation properties." *Materials Science and Engineering C* 66:25-32. doi: 10.1016/j.msec.2016.04.031.

Mejía G, A. I., B. L. López O, and L. Sierra. 2001. "Biodegradation of poly(vinylalcohol-co-ethylene) with the fungus phanerochaete chrysosporium." *Materials Research Innovations* 4 (2-3):148-154. doi: 10.1007/s100190000085.

Melendez-Rodriguez, B., J. L. Castro-Mayorga, M. A. M. Reis, C. Sammon, L. Cabedo, S. Torres-Giner, and J. M. Lagaron. 2018. "Preparation and Characterization of Electrospun Food Biopackaging Films of Poly(3-hydroxybutyrate-co-3-hydroxyvalerate) Derived From Fruit Pulp Biowaste." *Frontiers in Sustainable Food Systems* 2. doi: 10.3389/fsufs.2018.00038.

Melendez-Rodriguez, B., S. Torres-Giner, L. Lorini, F. Valentino, C. Sammon, L. Cabedo, and J. M. Lagaron. 2020. "Valorization of Municipal Biowaste into Electrospun Poly(3-

hydroxybutyrate- co-3-hydroxyvalerate) Biopapers for Food Packaging Applications." *ACS Applied Bio Materials* 3 (9):6110-6123. doi: 10.1021/acsabm.0c00698.

Miao, C., and W. Y. Hamad. 2013. "Cellulose reinforced polymer composites and nanocomposites: A critical review." *Cellulose* 20 (5):2221-2262. doi: 10.1007/s10570-013-0007-3.

Mokwena, K. K., and J. Tang. 2012. "Ethylene Vinyl Alcohol: A Review of Barrier Properties for Packaging Shelf Stable Foods." *Critical Reviews in Food Science and Nutrition* 52 (7):640-650. doi: 10.1080/10408398.2010.504903.

Mokwena, K. K., J. Tang, C. P. Dunne, T. C. S. Yang, and E. Chow. 2009. "Oxygen transmission of multilayer EVOH films after microwave sterilization." *Journal of Food Engineering* 92 (3):291-296. doi: 10.1016/j.jfoodeng.2008.11.011.

Nair, Sandeep S., J. Y. Zhu, Yulin Deng, and Arthur J. Ragauskas. 2014. "High performance green barriers based on nanocellulose." *Sustainable Chemical Processes* 2 (1):23. doi: 10.1186/s40508-014-0023-0.

Nir, Y., M. Narkis, and A. Siegmann. 1998. "Morphology and infrared spectroscopy of strongly interacting polymer blends: EVOH/copolyamide-6/6.9." *Journal of Macromolecular Science, Part B* 37 (6):863-882. doi: 10.1080/00222349808212422.

Noorani, Sweda, John Simonsen, and Sundar Atre. 2007. "Nano-enabled microtechnology: polysulfone nanocomposites incorporating cellulose nanocrystals." *Cellulose* 14 (6):577-584. doi: 10.1007/s10570-007-9119-y.

Ogunsona, Emmanuel O., and Tizazu H. Mekonnen. 2020. "Multilayer assemblies of cellulose nanocrystal – polyvinyl alcohol films featuring excellent physical integrity and multi-functional properties." *Journal of Colloid and Interface Science* 580:56-67. doi: https://doi.org/10.1016/j.jcis.2020.07.012.

Oksman, K., Y. Aitomäki, A. P. Mathew, G. Siqueira, Q. Zhou, S. Butylina, S. Tanpichai, X. Zhou, and S. Hooshmand. 2016. "Review of the recent developments in cellulose nanocomposite processing." *Composites Part A: Applied Science and Manufacturing* 83:2-18. doi: 10.1016/j.compositesa.2015.10.041.

Oksman, K., A. P. Mathew, D. Bondeson, and I. Kvien. 2006. "Manufacturing process of cellulose whiskers/polylactic acid nanocomposites." *Composites Science and Technology* 66 (15):2776-2784. doi: 10.1016/j.compscitech.2006.03.002.

Orr, M. P., and M. L. Shofner. 2017. "Processing strategies for cellulose nanocrystal/polyethylene-co-vinyl alcohol composites." *Polymer* 126:211-223. doi: 10.1016/j.polymer.2017.08.043.

Orr, Matthew P., Amidat Sonekan, and Meisha L. Shofner. 2020. "Effect of processing method on cellulose nanocrystal/polyethylene-co-vinyl alcohol composites." *Polymer Engineering & Science* 60 (12):2979-2990. doi: https://doi.org/10.1002/pen.25527.

Pal, N., S. Banerjee, P. Roy, and K. Pal. 2019. "Reduced graphene oxide and PEG-grafted TEMPO-oxidized cellulose nanocrystal reinforced poly-lactic acid nanocomposite film for biomedical application." *Materials Science and Engineering C* 104. doi: 10.1016/j.msec.2019.109956.

Park, Won-Il, Minsung Kang, Hun-Sik Kim, and Hyoung-Joon Jin. 2007. "Electrospinning of Poly(ethylene oxide) with Bacterial Cellulose Whiskers." *Macromolecular Symposia* 249-250 (1):289-294. doi: https://doi.org/10.1002/masy.200750347.

Peresin, M. S., Y. Habibi, J. O. Zoppe, J. J. Pawlak, and O. J. Rojas. 2010. "Nanofiber composites of polyvinyl alcohol and cellulose nanocrystals: Manufacture and characterization." *Biomacromolecules* 11 (3):674-681. doi: 10.1021/bm901254n.

Perumal, A. B., P. S. Sellamuthu, R. B. Nambiar, and E. R. Sadiku. 2018. "Development of polyvinyl alcohol/chitosan bio-nanocomposite films reinforced with cellulose nanocrystals isolated from rice straw." *Applied Surface Science* 449:591-602. doi: 10.1016/j.apsusc.2018.01.022.

Petersson, L., and K. Oksman. 2006. "Biopolymer based nanocomposites: Comparing layered silicates and microcrystalline cellulose as nanoreinforcement." *Composites Science and Technology* 66 (13):2187-2196. doi: https://doi.org/10.1016/j.compscitech.2005.12.010.

Pirani, S., H. M. N. Abushammala, and R. Hashaikeh. 2013. "Preparation and characterization of electrospun PLA/nanocrystalline cellulose-based composites." *Journal of Applied Polymer Science* 130 (5):3345-3354. doi: 10.1002/app.39576.

Raquez, J. M., Y. Habibi, M. Murariu, and P. Dubois. 2013. "Polylactide (PLA)-based nanocomposites." *Progress in Polymer Science* 38 (10-11):1504-1542. doi: 10.1016/j.progpolymsci.2013.05.014.

Razi, P. S., R. Portier, and A. Raman. 1999. "Studies on Polymer-Wood Interface Bonding: Effect of Coupling Agents and Surface Modification." *Journal of Composite Materials* 33 (12):1064-1079. doi: 10.1177/002199839903301201.

Redondo, A., D. Jang, L. T. J. Korley, I. Gunkel, and U. Steiner. 2020. "Electrospinning of cellulose nanocrystal-reinforced polyurethane fibrous mats." *Polymers* 12 (5). doi: 10.3390/POLYM12051021.

Rojas-Lema, S., J. Terol, E. Fages, R. Balart, L. Quiles-Carrillo, C. Prieto, and S. Torres-Giner. 2020. "Microencapsulation of copper(ii) sulfate in ionically cross-linked chitosan by spray drying for the development of irreversible moisture indicators in paper packaging." *Polymers* 12 (9). doi: 10.3390/POLYM12092039.

Rojas, O. J., G. A. Montero, and Y. Habibi. 2009. "Electrospun nanocomposites from polystyrene loaded with cellulose nanowhiskers." *Journal of Applied Polymer Science* 113 (2):927-935. doi: 10.1002/app.30011.

Roohani, M., Y. Habibi, N. M. Belgacem, G. Ebrahim, A. N. Karimi, and A. Dufresne. 2008. "Cellulose whiskers reinforced polyvinyl alcohol copolymers nanocomposites." *European Polymer Journal* 44 (8):2489-2498. doi: 10.1016/j.eurpolymj.2008.05.024.

Sanders, J. E., Y. Han, T. S. Rushing, and D. J. Gardner. 2019. "Electrospinning of cellulose nanocrystal-filled poly (Vinyl alcohol) solutions: Material property assessment." *Nanomaterials* 9 (5). doi: 10.3390/nano9050805.

Sapkota, J., S. Kumar, C. Weder, and E. J. Foster. 2015. "Influence of processing conditions on properties of poly (Vinyl acetate)/cellulose nanocrystal nanocomposites." *Macromolecular Materials and Engineering* 300 (5):562-571. doi: 10.1002/mame.201400313.

Shiku, Y., P. Y. Hamaguchi, S. Benjakul, W. Visessanguan, and M. Tanaka. 2004. "Effect of surimi quality on properties of edible films based on Alaska pollack." *Food Chemistry* 86 (4):493-499. doi: 10.1016/j.foodchem.2003.09.022.

Sidwell, J. A. 1992. *Food Contact Polymeric Materials*.

Singh, Suman, Kirtiraj K. Gaikwad, Su-Il Park, and Youn Suk Lee. 2017. "Microwave-assisted step reduced extraction of seaweed (Gelidiella aceroso) cellulose nanocrystals." *International Journal of Biological Macromolecules* 99:506-510. doi: https://doi.org/10.1016/j.ijbiomac.2017.03.004.

Sun, X. F., F. Xu, R. C. Sun, P. Fowler, and M. S. Baird. 2005. "Characteristics of degraded cellulose obtained from steam-exploded wheat straw." *Carbohydrate Research* 340 (1):97-106. doi: https://doi.org/10.1016/j.carres.2004.10.022.

Suryanegara, Lisman, Antonio Norio Nakagaito, and Hiroyuki Yano. 2009. "The effect of crystallization of PLA on the thermal and mechanical properties of microfibrillated cellulose-reinforced PLA composites." *Composites Science and Technology* 69 (7):1187-1192. doi: https://doi.org/10.1016/j.compscitech.2009.02.022.

Syverud, Kristin, and Per Stenius. 2008. "Strength and barrier properties of MFC films." *Cellulose* 16 (1):75. doi: 10.1007/s10570-008-9244-2.

Tajeddin, B. 2014. "Cellulose-Based Polymers for Packaging Applications." In *Lignocellulosic Polymer Composites: Processing, Characterization, and Properties*, 477-498.

Tomita, K., K. Kojoh, and A. Suzuki. 1997. "Isolation of thermophiles assimilating poly(ethylene-co vinyl alcohol)." *Journal of Fermentation and Bioengineering* 84 (5):400-402. doi: 10.1016/S0922-338X(97)81998-8.

Torres-Giner, S., Y. Echegoyen, R. Teruel-Juanes, J. D. Badia, A. Ribes-Greus, and J. M. Lagaron. 2018. "Electrospun Poly(ethylene-co-vinyl alcohol)/Graphene Nanoplatelets Composites of Interest in Intelligent Food Packaging Applications." *Nanomaterials* 8 (10). doi: 10.3390/nano8100745.

Torres-Giner, S., L. Gil, L. Pascual-Ramírez, and J. A. Garde-Belza. 2018. "Packaging: Food waste reduction." *Encyclopedia of Polymer Applications* 3:1990-2009.

Torres-Giner, S., E. Gimenez, and J. M. Lagaron. 2008. "Characterization of the morphology and thermal properties of Zein Prolamine nanostructures obtained by electrospinning." *Food Hydrocolloids* 22 (4):601-614. doi: 10.1016/j.foodhyd.2007.02.005.

Torres-Giner, S., R. Pérez-Masiá, and J. M. Lagaron. 2016. "A review on electrospun polymer nanostructures as advanced bioactive platforms." *Polymer Engineering and Science* 56 (5):500-527. doi: 10.1002/pen.24274.

Vannini, Micaela, Paola Marchese, Annamaria Celli, and Cesare Lorenzetti. 2016. "Strategy To Modify the Crystallization Behavior of EVOH32 through Interactions with Low-Molecular-Weight Molecules." *Industrial & Engineering Chemistry Research* 55 (12):3517-3524. doi: 10.1021/acs.iecr.5b04191.

Venkatraman, P., A. M. Gohn, A. M. Rhoades, and E. J. Foster. 2019. "Developing high performance PA 11/cellulose nanocomposites for industrial-scale melt processing." *Composites Part B: Engineering* 174. doi: 10.1016/j.compositesb.2019.106988.

Voronova, M. I., O. V. Surov, S. S. Guseinov, V. P. Barannikov, and A. G. Zakharov. 2015. "Thermal stability of polyvinyl alcohol/nanocrystalline cellulose composites." *Carbohydrate Polymers* 130:440-447. doi: 10.1016/j.carbpol.2015.05.032.

Yadav, M., Y. K. Liu, and F. C. Chiu. 2019. "Fabrication of cellulose nanocrystal/silver/alginate bionanocomposite films with enhanced mechanical and barrier properties for food packaging application." *Nanomaterials* 9 (11). doi: 10.3390/nano9111523.

Yan, Huiqiong, Xiuqiong Chen, Meixi Feng, Zaifeng Shi, Wei Zhang, Yue Wang, Chaoran Ke, and Qiang Lin. 2019. "Entrapment of bacterial cellulose nanocrystals stabilized Pickering emulsions droplets in alginate beads for hydrophobic drug delivery." *Colloids and Surfaces B: Biointerfaces* 177:112-120. doi: https://doi.org/10.1016/j.colsurfb.2019.01.057.

Yang, W., G. Qi, J. M. Kenny, D. Puglia, and P. Ma. 2020. "Effect of Cellulose Nanocrystals and Lignin Nanoparticles on Mechanical, Antioxidant and Water Vapour Barrier Properties of Glutaraldehyde Crosslinked PVA Films." *Polymers (Basel)* 12 (6). doi: 10.3390/polym12061364.

Yang, X., Y. Zhao, H. Mussana, M. Tessema, and L. Liu. 2018. "Characteristics of cotton fabric modified with chitosan (CS)/cellulose nanocrystal (CNC) nanocomposites." *Materials Letters* 211:300-303. doi: 10.1016/j.matlet.2017.09.075.

Yokoyama, Y., H. Kimata, S. Mitarai, S. Hirano, and T. Shirakawa. 2009. "Ethylene vinyl alcohol (EVOH) fiber compared to cotton underwear in the treatment of childhood atopic dermatitis: A double-blind randomized study." *Indian Pediatrics* 46 (7):611-614.

Yu, D. G., Y. Xu, Z. Li, L. P. Du, B. G. Zhao, and X. Wang. 2014. "Coaxial electrospinning with mixed solvents: From flat to round eudragit l100 nanofibers for better colon-targeted sustained drug release profiles." *Journal of Nanomaterials* 2014. doi: 10.1155/2014/967295.

Yu, Houyong, Chenfeng Yan, and Juming Yao. 2014. "Fully biodegradable food packaging materials based on functionalized cellulose nanocrystals/poly(3-hydroxybutyrate-co-3-hydroxyvalerate) nanocomposites." *RSC Advances* 4 (104):59792-59802. doi: 10.1039/C4RA12691B.

Yu, X., S. Tong, M. Ge, L. Wu, J. Zuo, C. Cao, and W. Song. 2013. "Adsorption of heavy metal ions from aqueous solution by carboxylated cellulose nanocrystals." *Journal of Environmental Sciences (China)* 25 (5):933-943. doi: 10.1016/S1001-0742(12)60145-4.

Zaman, Masuduz, Huining Xiao, Felipe Chibante, and Yonghao Ni. 2012. "Synthesis and characterization of cationically modified nanocrystalline cellulose." *Carbohydrate Polymers* 89 (1):163-170. doi: https://doi.org/10.1016/j.carbpol.2012.02.066.

Zhang, D., A. B. Karki, D. Rutman, D. P. Young, A. Wang, D. Cocke, T. H. Ho, and Z. Guo. 2009. "Electrospun polyacrylonitrile nanocomposite fibers reinforced with Fe3O4 nanoparticles: Fabrication and property analysis." *Polymer* 50 (17):4189-4198. doi: 10.1016/j.polymer.2009.06.062.

Zhang, W., X. He, C. Li, X. Zhang, C. Lu, X. Zhang, and Y. Deng. 2014. "High performance poly (vinyl alcohol)/cellulose nanocrystals nanocomposites manufactured by injection molding." *Cellulose* 21 (1):485-494. doi: 10.1007/s10570-013-0141-y.

Zhang, Zhongbin, Loong-Tak Lim, and Marvin A. Tung. 2001. "Limonene transport and mechanical properties of EVOH and nylon 6,6 films as influenced by RH." *Journal of Applied Polymer Science* 79 (11):1949-1957. doi: https://doi.org/10.1002/1097-4628(20010314)79:11<1949::AID-APP1002>3.0.CO;2-F.

Block II: Development of PHA-based structural layers by melt compounding

Chapter VI

Reactive Melt Mixing of Poly(3-Hydroxybutyrate)/Rice Husk Flour Composites with Purified Biosustainably Produced Poly(3-Hydroxybutyrate-co-3-Hydroxyvalerate)

Materials 2019, 12(13), 2152

Beatriz Meléndez-Rodríguez[1], Sergio Torres-Giner[1], Abdulaziz Aldureid[2], Luis Cabedo[2], and José María Lagarón[1]

[1] Novel Materials and Nanotechnology Group, Institute of Agrochemistry and Food Technology (IATA), Spanish Council for Scientific Research (CSIC), Paterna, Spain

[2] Polymers and Advanced Materials Group (PIMA), Universitat Jaume I (UJI), Castellón, Spain

Abstract

Novel green composites based on commercial poly(3-hydroxybutyrate) (PHB) filled with 10 wt % rice husk flour (RHF) were melt-compounded in a mini-mixer unit using triglycidyl isocyanurate (TGIC) as compatibilizer and dicumyl peroxide (DCP) as initiator. Purified poly(3-hydroxybutyrate-*co*-3-hydroxyvalerate) (PHBV) produced by mixed bacterial cultures derived from fruit pulp waste was then incorporated into the green composite in contents in the 5–50 wt % range. Films for testing were obtained thereafter by thermo-compression and characterized. Results showed that the incorporation of up to 20 wt % of biowaste derived PHBV yielded green composite films with a high contact transparency, relatively low crystallinity, high thermal stability, improved mechanical ductility, and medium barrier performance to water vapor and aroma. This study puts forth the potential use of purified biosustainably produced PHBV as a cost-effective additive to develop more affordable and waste valorized food packaging articles.

Keywords: PHB; PHBV; rice husk; green composites; biosustainability; waste valorization

1. Introduction

The current concern to reduce the use of petroleum-derived materials has led to the search for natural and biodegradable polymers. Polyhydroxyalkanoates (PHAs) is a family of linear polyesters produced in nature by the action of bacteria during fermentation of sugar or lipids in famine conditions (Rehm 2003). PHAs represent a good alternative to conventional polymers in the frame of the circular economy since they are fully bio-based and biodegradable (Alaerts, Augustinus, and Van Acker 2018). Among the different commercially available PHAs, the most widely studied is poly(3-hydroxybutyrate) (PHB). This isotactic homopolyester presents a relatively high melting temperature (T_m) and good stiffness and strength due to its high crystallinity (>50 %). As a result, PHB articles present similar performance or even greater than some commodities plastics such as polypropylene (PP) and barrier properties close to those of polyethylene terephthalate (PET) (Smith 2005). PHB undergoes rapid and complete disintegration within a maximum period of 6 months through the action of enzymes and/or chemical deterioration associated with living microorganisms. Moreover, PHB is biodegradable not only in composting conditions but also in other environments such as marine water (Cava et al. 2006).

However, the use of PHB for packaging applications is limited due to its excessive brittleness and narrow processing temperature window (Reis et al. 2008). To overcome these limitations, its copolymer with 3-hydroxyvalerate (HV), that is, poly(3-hydroxybutyrate-*co*-3-hydroxyvalerate) (PHBV), can result advantageous since it shows higher ductility as well as reduced crystallinity and lower T_m (Nduko, Matsumoto, and Taguchi 2012). PHBV articles have been proposed to be applied in the areas of food and cosmetic packaging such as shampoo bottles, plastic beverage bottles, milk cartons, cosmetic containers, among others, due to its renewability, biodegradability, and high water vapor barrier (Keshavarz and Roy 2010, Philip, Keshavarz, and Roy 2007). However, obtaining PHAs habitually requires large investments due to both the high cost of the carbon source and the lack of efficient cultivation techniques (Blunt, Levin, and Cicek 2018). Indeed, the current production cost of PHAs is estimated to be up to 15-fold higher than conventional polyolefins (Kourmentza et al. 2017). Therefore, great efforts in their industrial production are currently focused on reducing the manufacturing cost to make it more competitive (Jacquel et al. 2007). In this sense, biowaste derived PHAs are both economically and environmentally attractive, in particular, those that use food waste as the raw material source. For instance, fermented cheese whey (CW), which is mostly not fully valorized at present, can be used as the feeding solution for PHA production (Domingos et al. 2018). Nowadays, most significant research efforts are targeted to optimize the extraction methods, especially in mixed cultures, and also to reduce the amounts of chemicals used to make the process environmentally friendly (Samorì et al. 2015).

Despite of the extraordinary suitability of PHAs as candidates for sustainable food packaging applications, they are still not cost-effective due to the fermentation and downstream processes during bioreactor production (Lee 1996). In this context, a possible strategy to reduce price is the use of agro-food waste derived fillers, which also allows a more sustainable packaging concept since they valorize residues obtained from the agricultural and food industries, and thus reduce the overall impact of the industrial production cycle (Torres-Giner, Montanes, et al. 2018). The combination of a bio-based and biodegradable polymer with natural fillers is habitually termed "green composite", which means that the whole material is obtained from renewable resources and it is also biodegradable (Zini and Scandola 2011). Over the past few years, the use of natural

fillers to develop polymer composites has significantly increased because of their significant processing advantages, biodegradability, low cost, non-abrasive, low relative density, high specific strength, and renewable nature (Nabi Saheb and Jog 1999). Moreover, these natural fillers represent an environmentally friendly solution since they decrease polluting emissions and energy requirements for processing as well as enhance energy recovery and end-of-life biodegradability (Abdul Khalil, Bhat, and Ireana Yusra 2012, Joshi et al. 2004, La Mantia and Morreale 2011). In this context, different green composites have been obtained using lignocellulosic fillers derived from food, agricultural, industrial, and marine resources such as rice husk (Ndazi and Karlsson 2011, Yussuf, Massoumi, and Hassan 2010), almond husk (Liminana et al. 2018, Quiles-Carrillo, Montanes, Garcia-Garcia, et al. 2018, Quiles-Carrillo, Montanes, Sammon, et al. 2018), walnut shell (Montava-Jordà, Quiles-Carrillo, et al. 2019), peanut shell (Garcia-Garcia et al. 2016), coconut fibers (Torres-Giner, Hilliou, et al. 2018), orange peel (Quiles-Carrillo, Montanes, Lagaron, et al. 2018), recycled cotton (Montava-Jordà, Torres-Giner, et al. 2019), *Posidonia oceanica* seaweed (Ferrero et al. 2015), etc.

Rice (*Oryza sativa* L.) is an important crop cultivated mostly in China, India, and Indonesia (Aprianti et al. 2015). The annual world rice production is approximately 600 million tons, of which 20% is currently wasted as rice husk (Adam, Appaturi, and Iqbal 2012). Most of this by-product is used as a bedding material for animals, burned, or landfilled, causing several environmental and health problems. Rice husk is a relatively hard material since it is typically composed of 20 wt % ash, 38 wt % cellulose, 22 wt % lignin, 18 wt % pentose, and 2 wt % of other organic components (Adam, Kandasamy, and Balakrishnan 2006). Therefore, rice husk has been used to reinforce several thermoplastics such as high-density polyethylene (HDPE) (Panthapulakkal, Law, and Sain 2005, Zhao et al. 2009), PP (Nascimento et al. 2010), PP and HDPE (Kim et al. 2004), polylactide (PLA) (Battegazzore et al. 2014), and also recently PHB (Bertini et al. 2012, Boitt et al. 2014, Moura et al. 2018, Sánchez-Safont et al. 2018). However, the inherently poor interfacial adhesion between the lignocellulosic fillers and polymers generally yields a composite with low dispersion and a high content of particle aggregates (Borah and Kim 2016). This effect is related to the low chemical affinity between lignocellulosic fillers with most polymer and biopolymer matrices, which compromises the strength and also increases moisture absorption of the green composites (Rowell, Young, and Rowell 1997). To improve the interfacial adhesion between both composite components, compatibilizers or coupling agents are generally added or the filler surfaces are chemically pretreated (Lu, Wu, and McNabb Jr 2000). Moreover, in the case of reactive compatibilizers, chemical bonds between the fillers and polymer matrix are formed and the overall performance of the composite can be remarkably improved (George, Sreekala, and Thomas 2001). For instance, the maleic anhydride (MA) grafting of PHBV matrix prior to extrusion has successfully increased the hydrophilicity of the biopolyester matrix making it more compatible with lignocellulosic fillers (Chan et al. 2018).

In this context, triglycidyl isocyanurate (TGIC) and dicumyl peroxide (DCP) can be effectively combined to compatibilize polymer composites. On the one hand, TGIC is a three-functional epoxy compound that plays a hinge-like role between lignocellulosic fillers and polyester matrices. The hydroxyl (–OH) groups of cellulose present on the fillers' surface and the ones from the end groups of the biopolyester molecular chains, namely hydroxyl or carboxyl, can readily react with the epoxy groups of TGIC during melt blending (Hao and Wu 2018). Also, TGIC has been reported to provide a chain-extension effect on the processability of PET, increasing its molecular weight (M_W) and potentially avoiding chain scission by hydrolysis (Dhavalikar and Xanthos 2003). On the other hand, DCP has been used as a free-radical grafting initiator in

different polymer systems. In this sense, peroxides can form covalent carbon–carbon cross-links between the biopolymer chain segments, promoting the compatibilization of immiscible components in binary polymer blends (Quiles-Carrillo et al. 2019) and also in polymer composites (Wei, McDonald, and Stark 2015). In the latter case, the addition of DCP to the composite mixture during melt mixing can give rise to both cross-linking of the polymer chains and grafting of natural fillers onto the polymer chains. Interestingly, due to the presence of three reactive –OH groups on each cellulose unit, the grafting of the cellulosic fillers onto the polymer chains dominates over the cross-linking of polymers because of the higher free radical reactivity of the –OH groups of cellulose (Ahmad and Luyt 2012). Based on this phenomenon, different studies have for instance reported that DCP improved the mechanical properties of low-density polyethylene (LDPE)/wood fiber composites via peroxide-initiated cross-linking process (Gu, Sain, and Kokta 2015, Joseph, Thomas, and Pavithran 1996, Mokoena, Djoković, and Luyt 2004, Nogellova, Kokta, and Chodák 1998).

The objective of this study is to develop highly sustainable materials with enhanced performance based on commercial PHB and rice husk fillers containing different amounts of purified PHBV that was produced by mixed bacterial cultures derived from wastes of the food industry. The green composites were prepared by melt compounding in a laboratory melt-mixer and shaped into films by thermo-compression. The resultant green composite films were characterized in terms of their morphology and optical characteristics as well as thermal, mechanical, and barrier properties in order to ascertain their potential in food packaging applications.

2. Materials and Methods

2.1. Materials

Commercial PHB homopolyester was supplied as P226F in the form of pellets by Biomer (Krailling, Germany). According to the manufacturer, this biopolymer resin presents a density of 1.25 g/cm³ and a melt flow index (MFI) of 10 g/10 min (5 kg, 180 °C). Biowaste derived PHBV copolyester was produced at pilot-plant scale at Universidade NOVA (Lisbon, Portugal) using mixed microbial cultures fed with fermented fruit pulps supplied by SumolCompal S.A. (Carnaxide, Portugal) as an industrial residue of the juice industry. The molar fraction of HV in the copolymer was ~20 mol %. The PHBV was purified with chloroform (Sigma-Aldrich S.A., Madrid, Spain) to produce a solid powder. Further details about the biopolymer and its purification route can be found elsewhere (Melendez-Rodriguez et al. 2018).

Rice husk was kindly provided by Herba Ingredients (Valencia, Spain). It was delivered in the form of flakes as a by-product of the rice industry. $_D$-limonene, with 98 % purity, TGIC (reference 379506), with a M_W of 297.26 g/mol, and DCP (reference 329541), with a M_W of 270.37 g/mol and 98 % assay, were all purchased from Sigma-Aldrich S.A. (Madrid, Spain).

2.2. Preparation of RHF

The procedure to obtain rice husk flour (RHF) consisted on a mechanical grinding following to sieving to ensure a low particle size. For this, the native rice husk was ground in a mechanical knife mill (Thermomix TM21, Vorwerk, Madrid, Spain) and then sieved in a 140-μm mesh (TED-0300, Filtra Vibración S.L., Badalona, Spain). The resultant powder was dried at 100 °C in oven (T3060, Heraeus Instruments, Hanau, Germany) for 24 h. **Figure 1** shows the as-received flakes of rice husk (Figure 1a) and the resultant RHF (Figure 1b).

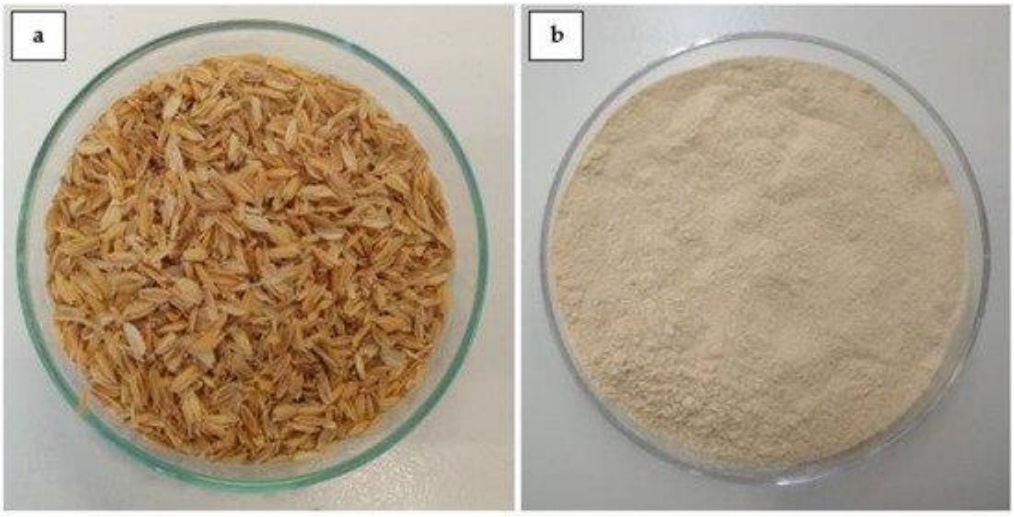

Figure 1. (a) As-received flakes of rice husk; (b) rice husk flour (RHF).

2.3. Melt Mixing

Prior to processing, both PHA resins were dried at 60 °C for 24 h in an oven (Digitheat, JP selecta S.A., Barcelona, Spain) to remove any residual moisture. Then, different amounts of purified PHBV, from 5 wt % to 50 wt %, were manually pre-mixed with commercial PHB in a zipper bag. A fixed content of RHF was added at 10 wt % to the mixture whereas the reactive compatibilizers, that is, TGIC and DCP, were incorporated at 1 part per hundred resin (phr) and 0.25 phr of PHB/PHBV/RHF composite, respectively. A PHB/RHF composite without PHBV and a PHB/PHBV blend without RHF were also prepared as control materials. **Table 1** summarizes the different formulations prepared.

Table 1. Set of formulations prepared according to the weight content (wt %) of poly(3-hydroxybutyrate) (PHB), poly(3-hydroxybutyrate-*co*-3-hydroxyvalerate) (PHBV), and rice husk flour (RHF) in which triglycidyl isocyanurate (TGIC) and dicumyl peroxide (DCP) were added as parts per hundred resin (phr) of PHB/PHBV/RHF composite.

Sample	PHB (wt %)	PHBV (wt %)	RHF (wt %)	TGIC (phr)	DCP (phr)
PHB/RHF	90	0	10	1	0.25
PHB/PHBV	90	10	0	1	0.25
PHB/PHBV5/RHF	85	5	10	1	0.25
PHB/PHBV10/RHF	80	10	10	1	0.25
PHB/PHBV20/RHF	70	20	10	1	0.25
PHB/PHBV30/RHF	60	30	10	1	0.25
PHB/PHBV50/RHF	40	50	10	1	0.25

To prepare the samples, a total amount of 12 g of material was melt-compounded in a 16 cm^3 Brabender Plastograph Original E mini-mixer from Brabender GmbH & Co. KG (Duisburg, Germany). First the biopolymers and, then, the RHF powder were fed to the internal mixing chamber at a rotating speed of 60 rpm for 1 min. After this, TGIC and DCP were added and the whole composition was melt-mixed at 100 rpm for another 3 min. The processing temperature was set at 180 °C. Once the mixing process was completed, each batch was withdrawn from the mini-mixer and cooled in air to room temperature. The resultant doughs were stored in dissectors containing silica gel at 0 % relative humidity (RH) and 25 °C for at least 48 h for conditioning.

The different doughs were, thereafter, thermo-compressed into films using a hot-plate hydraulic press (Carver 4122, Wabash, IN, USA). The samples were first placed in the plates at 180 °C for 1 min, without pressure, to remove any residual moisture and then hot-pressed at 4–5 bars for 3 min. Flat films with a total thickness of ~100 μm were obtained and stored in a desiccator at 25 °C and 0 % RH for 15 days before characterization.

2.4. Characterization

2.4.1. Morphology

The morphologies of the RHF particles and the film cross-sections were observed by scanning electron microscopy (SEM) using an S-4800 device from Hitachi (Tokyo, Japan). For the cross-section observations, the films were cryo-fractured by immersion in liquid nitrogen. The samples were previously fixed to beveled holders using conductive double-sided adhesive tape and sputtered with a mixture of gold-palladium under vacuum. An accelerating voltage of 10 kV and a working distance of 15 mm were selected during SEM analysis. The estimation of the dimensions was performed by means of the ImageJ software v 1.41 (NIH, Bethesda, MD, USA) using a minimum of 20 SEM micrographs.

The particle size distribution was determined by dynamic light scattering (DLS) using a laser diffraction analyzer Mastersizer 2000 from Malvern Panalytical Ltd. (Malvern, UK). According to the manufacturer, the error for the equipment of median diameter (D_{50}) is 3 %. Measurements were taken under stirring to avoid settling of large particles.

2.4.2. Transparency

The light transmission of the films was determined in specimens of 50 × 30 mm^2 by quantifying the absorption of light at wavelengths between 200 nm and 700 nm in an ultraviolet–visible (UV–vis) spectrophotometer VIS3000 from Dinko Instruments (Barcelona, Spain). The transparency (T) and opacity (O) were calculated using Equation (1) (Figueroa-Lopez, Andrade-Mahecha, and Torres-Vargas 2018) and Equation (2) (Kanatt et al. 2012), respectively:

$$T = \frac{A_{600}}{L} \quad (1)$$

$$O = A_{500} \times L \quad (2)$$

where A_{500} and A_{600} are the absorbance values at 500 nm and 600 nm, respectively, and L is the film thickness (mm).

2.4.3. Color Measurements

The color of the films was determined using a chroma meter CR-400 (Konica Minolta, Tokyo, Japan). The color difference (ΔE^*) was calculated using the following Equation (3) (Figueroa-Lopez, Andrade-Mahecha, and Torres-Vargas 2018), as defined by the Commission Internationale de l'Eclairage (CIE):

$$\Delta E^* = [(\Delta L^*)^2 + (\Delta a^*)^2 + (\Delta b^*)^2]^{0.5} \quad (3)$$

where ΔL^*, Δa^*, and Δb^* correspond to the differences in terms of lightness from black to white, from green to red, and from blue to yellow, respectively, between the film samples and the control film of PHB/PHBV.

2.4.4. Thermal Analysis

Thermal transitions were studied by differential scanning calorimetry (DSC) on a DSC-7 analyzer equipped with the cooling accessory Intracooler 2 from PerkinElmer, Inc. (Waltham, MA, USA). A two-step program under nitrogen atmosphere and with a flow rate of 20 ml/min was applied: first heating from −30 °C to 190 °C followed by cooling to −30 °C. The heating and cooling rates were both set at 10 °C/min and the typical sample weight was ~3 mg. An empty aluminum pan was used as reference whereas calibration was performed using an indium sample. The values of T_m and enthalpy of melting (ΔH_m) were obtained from the heating scan, while the crystallization temperature from the melt (T_c) and enthalpy of crystallization (ΔH_c) were determined from the cooling scan. All DSC measurements were performed in triplicate.

Thermogravimetric analysis (TGA) was performed in a TG-STDA model TGA/STDA851e/LF/1600 thermobalance from Mettler-Toledo, LLC (Columbus, OH, USA). The samples, with a weight of ~15 mg, were heated from 50 °C to 800 °C at a heating rate of 10 °C/min under a flow rate of 50 ml/min of nitrogen (N_2). All TGA measurements were also done in triplicate.

2.4.5. Mechanical Tests

Tensile tests were performed on stamped dumbbell-shaped film samples sizing 115 × 16 mm^2 using an Instron 4400 universal testing machine, equipped with a 1-kN load cell, from Instron (Norwood, MA, USA) according to the ASTM standard method D638. The tests were done using a cross-head speed of 10 mm/min. Samples were conditioned for 24 h prior to analysis and the tests were performed at room conditions, that is, 40 % RH and 25 °C. A minimum of six specimens were tested for each sample.

2.4.6. Permeability Tests

The gravimetric method ASTM E96-95 was used to determinate the water vapor permeability (WVP) of the films. To this end, Payne permeability cups (diameter of 3.5 cm) from Elcometer Sprl (Hermallesous-Argenteau, Belgium) were filled with 5 ml of distilled water. The films were not in direct contact with water but exposed to 100 % RH on one side and secured with silicon rings. They were placed within a desiccator and sealed with dried silica gel at 0 % RH and 25 °C. The control samples consisted of cups with aluminum films to estimate solvent loss through the sealing. The cups were weighted periodically using an analytical balance (±0.0001 g). WVP was calculated from the regression analysis of weight loss data vs. time, whereas the weight loss was calculated as the total loss minus the loss through the sealing. The permeability was obtained by multiplying the permeance by the film thickness. All WVP measurements were performed in triplicate.

The limonene permeability (LP), similar as described above for WVP, was measured placing 5 ml of $_D$-limonene inside the Payne permeability cups. The cups containing the films were placed at controlled room conditions of 40 % RH and 25 °C. The limonene vapor permeation rate (LPRT) values were estimated from the steady-state permeation slopes and the weight loss was calculated as the total cell loss minus the loss through the sealing. LP was calculated taking into account the average film thickness in each case. LP measurements were performed in triplicate.

2.5. Statistical Analysis

The optical, thermal, mechanical, and barrier properties were evaluated through analysis of variance (ANOVA) using STATGRAPHICS Centurion XVI v 16.1.03 from StatPoint Technologies, Inc. (Warrenton, VA, USA). Fisher's least significant difference (LSD) was used at the 95 % confidence level ($p < 0.05$). Mean values and standard deviations were also reported.

3. Results

3.1. Morphology of RHF Particles

The morphology of the RHF powder was observed by SEM for determining the particle size and shape. In the low-magnification SEM image, shown in Figure 2a, one can see that the particles were not uniform in morphology and their dimension varied broadly. In particular, small particles slightly below 10 µm, in the form of rod-like particles or rectangular junks, coexisted with short fibers, having lengths above 100 µm. The magnified SEM image, included in Figure 2b, illustrates that the outer surface of rice husk was relatively smooth but its inner part was densely covered with orderly bulges. In this regard, it has been reported that the globular structure of rice husk is responsible for its high absorption capacity (Scaglioni and Badiale-Furlong 2016), which can also positively contribute to favoring mechanical interactions with the biopolymer matrix. Similar morphologies were reported for instance by Schneider et al. (Schneider et al. 2019), in which the RHF particles also presented a heterogeneous morphology, namely larger particles of different textures, some smoother, others rough, with also grooves along the structure. The histogram of particle size of RHF is shown in Figure 2c, where one can see that the average fiber length was ~190 µm whereas the diameter corresponding to 90 % cumulative (D_{90}) was ~320 µm.

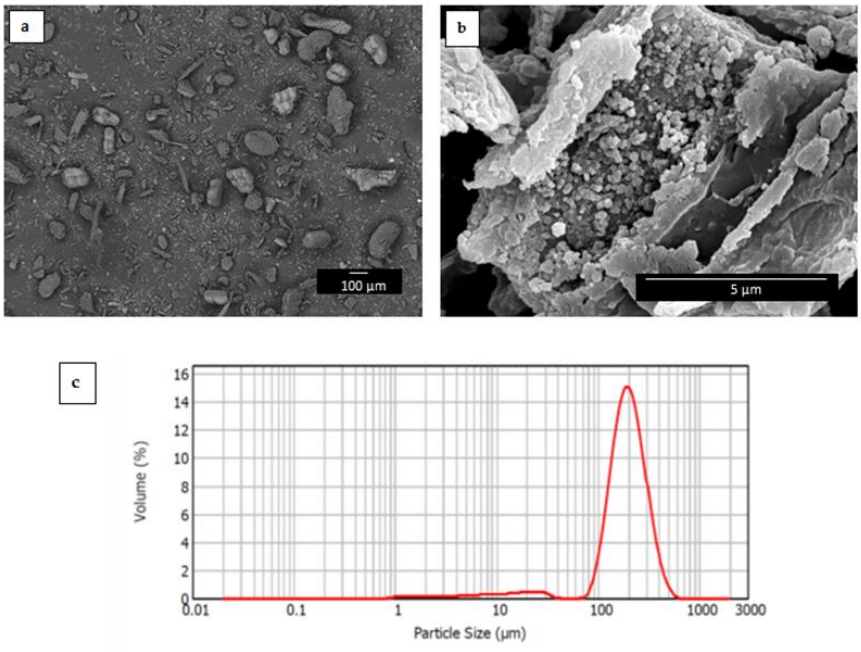

Figure 2. Scanning electron microscopy (SEM) images of rice husk flour (RHF) taken at (a) 50x with scale marker of 100 µm and (b) 10,000x with scale marker of 5 µm; (c) particle size histogram of RHF.

3.2. Morphology of PHB/PHBV/RHF Films

The morphology of the film cross-sections was observed by SEM and the images are gathered in **Figure 3**. One can observe that all films presented a smooth and featureless fracture surface without much deformation, corresponding to a typical brittle fracture behavior. The presence of the RHF particles can be observed in the cross-sections of all the composite film samples, that is, Figure 3a,c–g, whereas the surface of the PHB/PHBV film in Figure 3b suggests that the matrix was monophasic. Interestingly, the images taken at higher magnifications revealed that RHF fillers were tightly bonded to the polymer as inferred from the absence of gap between the particles and the biopolymer matrix. Moreover, no evidence of filler pull-out or void formation was noticed. At the same time, a rough surface attributed to the matrix deformation can be observed in the fillers surrounding. Additionally, RHF aggregates were not observed but individual particles appeared regularly distributed along the biopolymer matrix indicating that an effective mixing was attained.

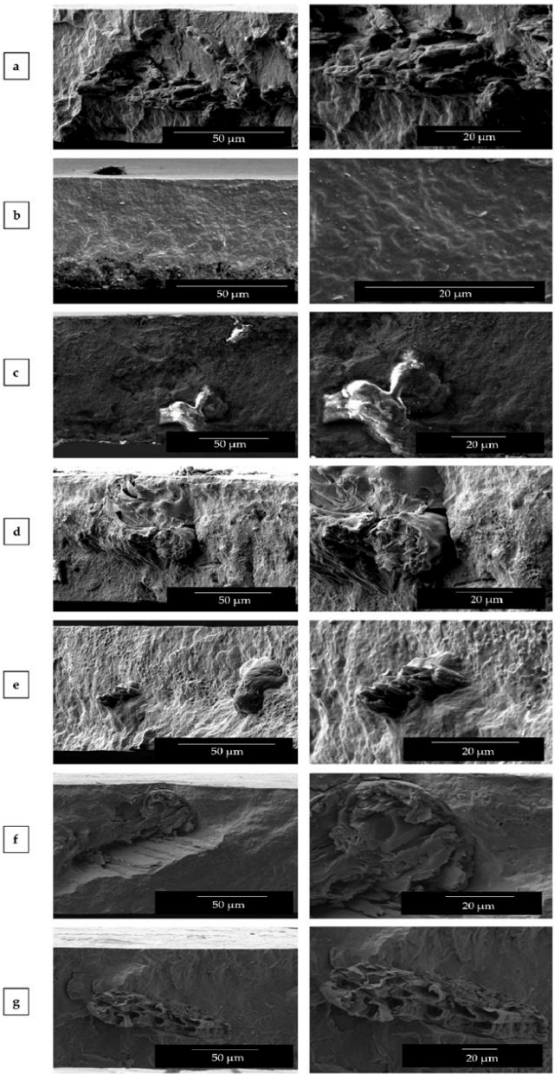

Figure 3. Scanning electron microscopy (SEM) images of the cross-sections of the thermo-compressed films made of poly(3-hydroxybutyrate) (PHB), poly(3-hydroxybutyrate-*co*-3-hydroxyvalerate) (PHBV), and rice husk flour (RHF): (a) PHB/RHF; (b) PHB/PHBV; (c) PHB/PHBV5/RHF; (d) PHB/PHBV10/RHF; (e) PHB/PHBV20/RHF; (f) PHB/PHBV30/RHF; (g) PHB/PHBV50/RHF. Images were taken at 1000x with scale markers of 50 µm (left column) and at 2500x with scale markers of 20 µm (right column).

The above observation suggests that a high interfacial adhesion was achieved in the composites due to the combined use of TGIC and DCP during melt processing. Similar morphologies were also described, for instance, by Rosa et al. (Rosa et al. 2009) for PP/RHF composites when MA-modified polypropylene (MAPP) was added as coupling agent. The presence of MAPP successfully reduced the voids sizes and turned the surface more homogeneous, confirming its effect on promoting adhesion in the interfacial region. In relation to TGIC, Hao and Wu (Hao and Wu 2018) recently showed that the addition during melt blending of the isocyanurate additive improved the interfacial adhesion of PLA/sisal fibers (SF) composites. The compatibilization achieved in the green composite was ascribed to the reaction of the –OH groups present at end groups of the biopolyester molecular chains and on the cellulose surface with the epoxy functional groups of TGIC. In the first reaction, ester bonds are known to be formed with the PHA chains by glycidyl esterification of carboxylic acid end groups, which precedes hydroxyl end group etherification (Torres-Giner et al. 2016). The second reaction generates C–O–C bonds with subsequent hydroxyl side-group formation on the cellulose surface (Quiles-Carrillo, Montanes, Lagaron, et al. 2018). This reactive compatibilization habitually leads to green composites with enhanced performance properties (Formela et al. 2018). For DCP, Wei et al. (Wei, McDonald, and Stark 2015, Wei, Stark, and McDonald 2015) recently described the coupling mechanism of cellulose to PHB and PHBV. Briefly, when the peroxide is exposed to heat during extrusion it decomposes into strong free radicals, which tend to abstract hydrogens (H') from the biopolymer and cellulose molecular chains and initiate the grafting process between the two phases in the composites. The authors postulated that the grafted copolymers formed on the interfaces of cellulose and PHA coupled the hydrophilic filler to the hydrophobic biopolymer matrix. Therefore, grafting of RHF onto the PHB/PHBV matrix was successfully achieved by the formation of low concentrations of DCP derived radicals at high temperature during extrusion that initiated both the formation both H abstraction and triggered the reaction of the epoxy groups of TGIC with the OH groups of both cellulose and the terminal groups of the biopolyester chains. In relation to the addition of the biowaste derived PHBV, a good mixture between the two PHAs was attained since it was not possible perceive the presence of two phases in the biopolymer matrix, even at the highest PHBV content, that is, 50 wt %. In the film surfaces one can still observe the presence of some remaining impurities, which may be ascribed to organic remnants of small amounts of cell debris or fatty acids from the bioproduction process of PHBV. A similar morphology was recently reported by Martinez-Abad et al. (Martínez-Abad et al. 2016) for PHB/unpurified PHBV blends, who also observed a good degree of interaction between the commercial homopolyester and the biosustainably produced copolyester.

3.3. Optical Properties of PHB/PHBV/RHF Films

The visual aspect of the films is displayed in **Figure 4** to ascertain their optical properties. Simple naked eye examination of the films indicates that all the samples were slightly opaque but also showed high contact transparency. Additionally, the composite films developed a yellow-to-brown color due to the intrinsic natural color of the RHF powder, which one can observe in previous Figure 1b.

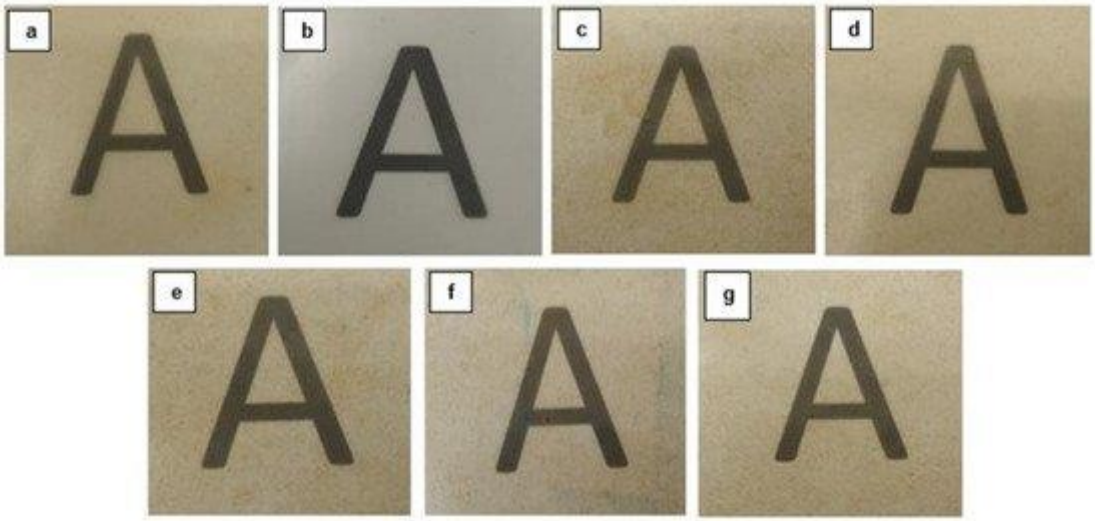

Figure 4. Visual aspect of the thermo-compressed films made of poly(3-hydroxybutyrate) (PHB), poly(3-hydroxybutyrate-*co*-3-hydroxyvalerate) (PHBV), and rice husk flour (RHF): (a) PHB/RHF; (b) PHB/PHBV; (c) PHB/PHBV5/RHF; (d) PHB/PHBV10/RHF; (e) PHB/PHBV20/RHF; (f) PHB/PHBV30/RHF; (g) PHB/PHBV50/RHF.

To quantify the color change resulted from the addition of PHBV in PHB/RHF, the color coordinates (a^*, b^*, L^*) and the values of ΔE^*, T, and O were determined and reported in **Table 2**. One can observe that the a^* b^* coordinates of the PHB/RHF film confirmed the above observed yellow-to-brown color of the sample whereas the PHB/PHBV film presented a natural color. The incorporation of PHBV into the green composite films resulted in a slightly increased the value of a^* and, most notably, of b^*, confirming the development of a brown tonality. Moreover, the composite films became darker since the L^* values were also reduced. In any case, the color differences in the composite films containing different amounts of PHBV were relatively low, that is, ΔE^* values remained below 6. One can also observe that the composite films also presented slightly lower transparency and higher opacity with the increasing PHBV contents, having values of T and O around 10–15 % and 5 % higher, respectively. This haze increase is typically observed in polymer blends due to differences in the refractive index of light diffraction of each polymer (Maruhashi and Iida 2001). Although the brownish color of the film samples may seem a disadvantage for food packaging, it also offers the capacity to partially block the transmission of ultraviolet and visible (UV–vis) light. This can be a desirable attribute since the films can provide more protection to foodstuff from light, especially UV radiation, which can cause lipid oxidation in the food products (Figueroa-Lopez et al. 2019, Kanatt et al. 2012).

Table 2. Optical properties of the thermo-compressed films made of poly(3-hydroxybutyrate) (PHB), poly(3-hydroxybutyrate-*co*-3-hydroxyvalerate) (PHBV), and rice husk flour (RHF).

Film	a^*	b^*	L^*	ΔE^*	T	O
PHB/RHF	-0.04 ± 0.01^{a}	11.82 ± 0.03^{a}	80.20 ± 0.02^{a}	-	9.08 ± 0.07^{a}	0.107 ± 0.03^{a}
PHB/PHBV	-0.25 ± 0.03^{b}	1.94 ± 0.02^{b}	86.40 ± 0.04^{b}	-	8.48 ± 0.03^{b}	0.099 ± 0.02^{a}
PHB/PHBV5/RHF	0.44 ± 0.05^{c}	14.60 ± 0.02^{c}	78.05 ± 0.03^{c}	3.55 ± 0.05^{a}	9.06 ± 0.05^{a}	0.111 ± 0.03^{a}
PHB/PHBV10/RHF	0.52 ± 0.04^{c}	14.84 ± 0.07^{c}	77.62 ± 0.03^{d}	4.01 ± 0.06^{b}	9.91 ± 0.04^{c}	0.116 ± 0.05^{a}
PHB/PHBV20/RHF	0.56 ± 0.05^{c}	15.28 ± 0.06^{d}	77.56 ± 0.05^{d}	4.39 ± 0.04^{c}	10.05 ± 0.03^{d}	0.116 ± 0.02^{a}
PHB/PHBV30/RHF	0.70 ± 0.07^{d}	15.36 ± 0.05^{d}	77.29 ± 0.06^{e}	4.64 ± 0.03^{d}	10.18 ± 0.08^{e}	0.117 ± 0.04^{a}
PHB/PHBV50/RHF	1.12 ± 0.08^{e}	16.17 ± 0.03^{e}	76.36 ± 0.04^{f}	5.92 ± 0.06^{e}	10.17 ± 0.05^{e}	0.113 ± 0.04^{a}

a^*: red/green coordinates (+a red, −a green); b^*: yellow/blue coordinates (+b yellow, −b blue); L^*: Luminosity (+L luminous, −L dark); ΔE^*: color differences; T: transparency; O: opacity.

$^{a–f}$ Different letters in the same column indicate a significant difference among the samples ($p < 0.05$).

3.4. Crystallinity of PHB/PHBV/RHF Films

Figure 5 displays the DSC thermograms of the film samples obtained during the heating (Figure 5a) and cooling (Figure 5b) scans. **Table 3** displays the main thermal transitions obtained from the DSC curves. One can observe that melting in the PHB/RHF film took place in two peaks, which were noted as T_{m1} and T_{m2}, whereas the unfilled PHB/PHBV film melted in a single peak. The double-melting peak phenomenon can be ascribed to the formation of crystalline structures with dissimilar lamellae thicknesses or the presence of crystallite blocks with different degrees of perfection (Montava-Jordà, Torres-Giner, et al. 2019). The first peak originates from the melting of the PHB fraction that crystallized previously during the film formation, while in the second peak contributes the melting of the recrystallized PHB fraction during heating. In this context, other works have reported that melt-extruded films of neat PHB melt in 170–175 °C range (de Matos Costa et al. 2019, Ollier et al. 2018). Then, one can consider that the presence of the RHF fillers restricted the chain-folding process of PHB during crystallization.

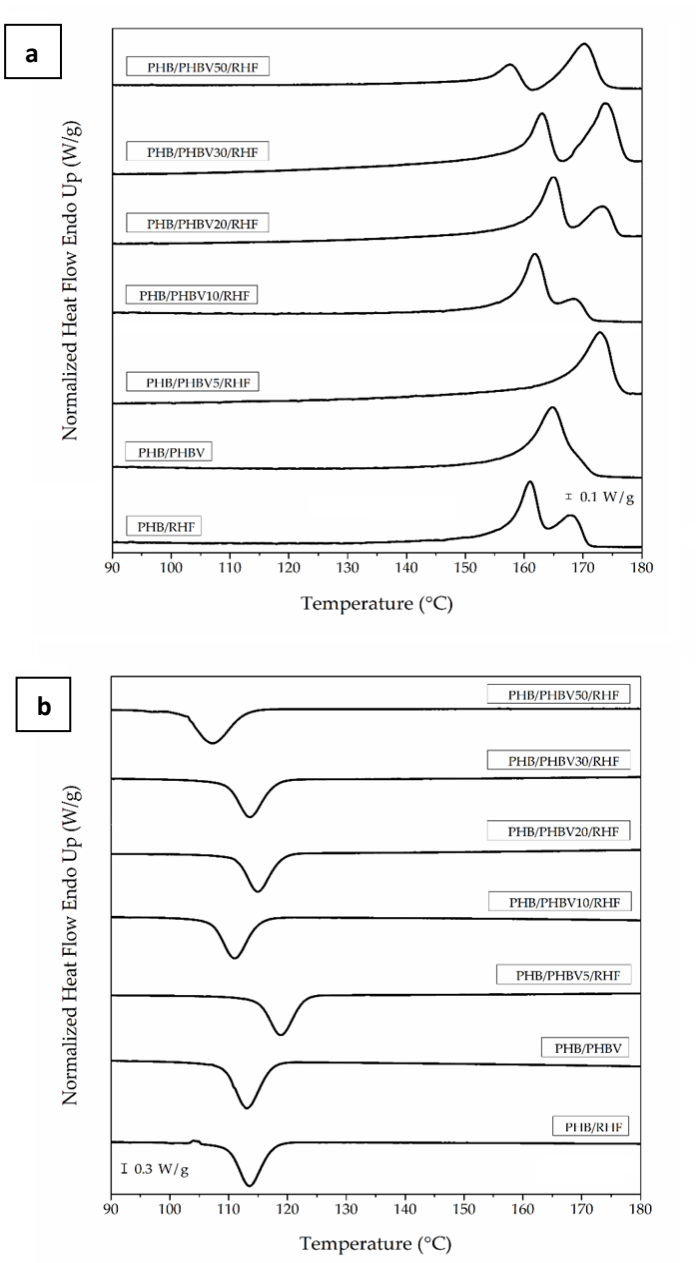

Figure 5. Differential scanning calorimetry (DSC) curves during (a) heating and (b) cooling of the thermo-compressed films made of poly(3-hydroxybutyrate) (PHB), poly(3-hydroxybutyrate-*co*-3-hydroxyvalerate) (PHBV), and rice husk flour (RHF).

Table 3. Main thermal parameters of the thermo-compressed films made of poly(3-hydroxybutyrate) (PHB), poly(3-hydroxybutyrate-*co*-3-hydroxyvalerate) (PHBV), and rice husk flour (RHF) in terms of: crystallization temperature (T_c), normalized enthalpy of crystallization (ΔH_c), melting temperature (T_m), and normalized melting enthalpy (ΔH_m).

Film	T_c (°C)	ΔH_c (J/g)	Tm_1 (°C)	Tm_2 (°C)	ΔH_m (J/g)
PHB/RHF	113.1 ± 0.6[a]	70.2 ± 0.2[a]	160.5 ± 0.8[a]	167.2 ± 0.9[a]	71.8 ± 2.3[a]
PHB/PHBV	113.3 ± 0.3[a]	73.3 ± 0.4[b]	165.1 ± 0.3[b]	-	76.9 ± 1.4[b]
PHB/PHBV5/RHF	118.9 ± 0.6[b]	59.8 ± 1.8[c]	171.9 ± 1.5[c]	-	63.7 ± 4.8[c]
PHB/PHBV10/RHF	110.9 ± 0.2[c]	60.1 ± 3.9[c]	162.6 ± 1.1[d]	168.3 ± 0.4[a]	63.4 ± 1.6[c]
PHB/PHBV20/RHF	115.4 ± 0.6[d]	78.0 ± 4.1[d]	166.0 ± 1.5[b]	173.3 ± 0.3[b]	61.4 ± 0.3[c]
PHB/PHBV30/RHF	113.2 ± 0.6[a]	72.7 ± 4.7[d]	162.6 ± 0.7[d]	173.9 ± 0.1[c]	59.4 ± 2.2[c]
PHB/PHBV50/RHF	107.7 ± 0.6[e]	64.8 ± 0.8[c]	158.4 ± 1.1[e]	171.0 ± 0.8[d]	53.8 ± 0.1[d]

[a–e] Different letters in the same column indicate a significant difference among the samples ($p < 0.05$).

Interestingly, the incorporation into PHB/RHF of low contents of PHBV, that is, 5 wt %, yielded the film sample with the highest melting peak, that is, ~172 °C, whereas it also suppressed the double-melting peak behavior. This observation points out that the co-addition of 5 wt % PHBV and 10 wt % RHF enhanced the crystallization of PHB molecules, which was further supported by the shift of T_c from 113.1 °C, for the PHB/RHF film, to 118.9 °C, for the PHB/PHBV5/RHF film. The addition of higher contents of PHBV, however, led to films with two melting peaks. The first melting peak can be related to the PHBV-rich fraction, which was seen in the 158–166 °C range, whereas the second one corresponds to PHB melting, observed in 168–174 °C range. This result points out that fully miscibility was only attained in the composite blends containing low amounts of PHBV, that is, 5–10 wt %. At higher PHBV contents, the composite films formed a two-phase system and the T_m values were also reduced. Thus, the films produced with PHBV contents higher than 10 wt % showed a two phase crystallization, having a liquid–liquid separation at temperatures higher than 165 °C. One assumes that in these samples, due to the fact that the HV content in PHBV was relatively high, that is, 20 mol %, phase segregation preceded co-crystallization. One can also observe that the melting enthalpy of the first peak decreased while that of the second peak increased with the increase of the PHBV content in the blend. This observation indicates that crystallization occurred mainly in the PHB-rich regions by which the HV units were partially included into the PHB lattice and also induced some defects in the biopolymer crystals (Yoshie, Asaka, and Inoue 2004). In this regards, different studies on the crystallization behavior of PHB/PHBV blends have indicated that their degree of miscibility decreases gradually as the HV in the copolyester increases. For instance, blends of PHB with PHBV were fully miscible over up to approximately 60 wt % of copolyester with a HV content of 18.4 mol % (Organ 1994). On the contrary, blends consisting of PHB and PHBV of high contents of HV, that is, 76 mol %, showed no depression of the melting point of each PHA, indicating total immiscibility (Kumagai and Doi 1992). In another work, Saito et al. (Saito, Inoue, and Yoshie 2001) studied the competition between co-crystallization and phase segregation in

blends of PHB and PHBV with different HV contents. The authors observed almost perfect co-crystallization in blends based on PHB and PHBV with 9 mol % HV, whereas HV contents >15 mol % induced phase segregation, that is, increased the percentage of PHBV that segregates from the growth front of crystals prior to co-crystallization.

3.5. Thermal Stability of PHB/PHBV/RHF Films

TGA curves are plotted in **Figure 6** and the most relevant properties obtained from the curves are listed in **Table 4**. In relation to RHF, one can observe three main weight losses. The first one occurred around 100 °C, showing a mass loss of ~2 %, which corresponds to the moisture released from the lignocellulosic filler. Following the TGA curve of RHF, the second and main degradation peak started at approximately 180 °C and ended at 340 °C with an average mass loss of ~47 %. This weight loss includes the degradation of low-M_W components, mainly hemicellulose, followed by cellulose degradation. This zone represents the main devolatilization step of biomass pyrolysis and it is referred as the "active pyrolysis zone" since mass loss rate is high (Mansaray and Ghaly 1998). After this, RHF gradually degraded over a range of temperature from approximately 340 °C to 650 °C with a mass loss of ~16 %, which can be seen as a tailing in both TGA and DTG curves. This mass loss is related to the degradation of lignin and it is called "passive pyrolysis zone" since the percentage of mass loss is smaller and the mass loss rate is also much lower compared to that in the second zone (Mansaray and Ghaly 1998). Indeed, when the temperature reached 650 °C, the degradation rates were no longer significant as most volatiles were already pyrolyzed. The rest was converted into char and gases, resulting in a residual mass of nearly 33 %, which can be related to the high silicate content in rice husk (George, Sreekala, and Thomas 2001).

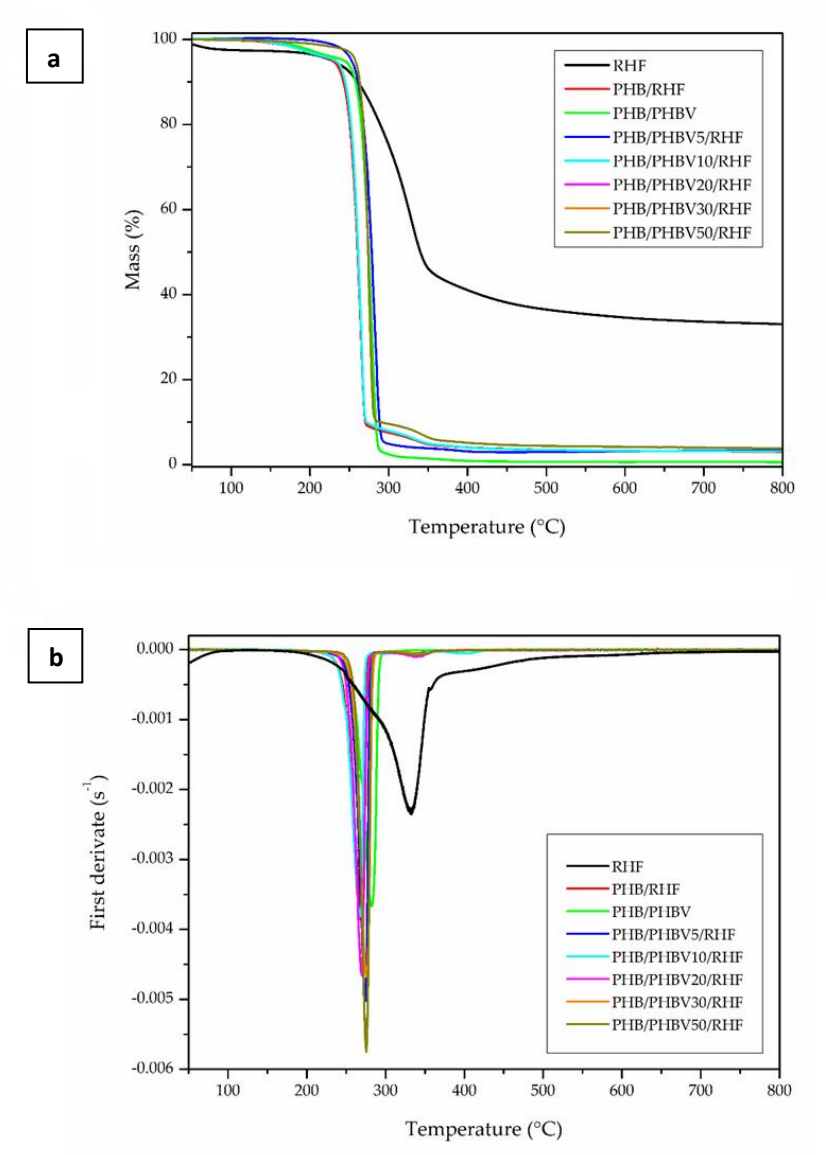

Figure 6. (a) Thermogravimetric analysis (TGA) and (b) first derivative (DTG) curves of the thermo-compressed films made of poly(3-hydroxybutyrate) (PHB), poly(3-hydroxybutyrate-*co*-3-hydroxyvalerate) (PHBV), and rice husk flour (RHF).

Table 4. Main thermal parameters of the thermo-compressed films made of poly(3-hydroxybutyrate) (PHB), poly(3-hydroxybutyrate-*co*-3-hydroxyvalerate) (PHBV), and rice husk flour (RHF) in terms of: onset temperature of degradation ($T_{5\%}$), degradation temperature (T_{deg}), mass loss at T_{deg}, and residual mass at 800 °C.

Film	$T_{5\%}$ (°C)	T_{deg} (°C)	Mass loss (%)	Residual mass (%)
RHF	228.9 ± 1.5[a]	335.2 ± 0.7[a]	28.5 ± 0.8[a]	33.1 ± 0.3[a]
PHB/RHF	242.5 ± 1.2[b]	270.0 ± 0.5[b]	67.4 ± 0.7[b]	3.1 ± 1.3[b]
PHB/PHBV	252.6 ± 1.9[c]	282.8 ± 0.4[c]	69.4 ± 1.5[b]	0.6 ± 0.1[c]
PHB/PHBV5/RHF	242.5 ± 1.5[b]	268.2 ± 0.5[d]	65.4 ± 0.3[c]	3.5 ± 0.2[b]
PHB/PHBV10/RHF	247.1 ± 1.3[d]	270.0 ± 0.5[b]	63.9 ± 0.4[d]	3.1 ± 0.8[b]
PHB/PHBV20/RHF	247.5 ± 1.4[d]	274.6 ± 0.6[e]	69.8 ± 1.2[b]	3.3 ± 0.9[b]
PHB/PHBV30/RHF	253.5 ± 1.7[c]	275.5 ± 0.6[e]	61.7 ± 0.2[e]	3.2 ± 0.2[b]
PHB/PHBV50/RHF	257.2 ± 1.6[e]	275.5 ± 0.6[e]	61.5 ± 0.3[e]	3.8 ± 0.4[b]

[a–e] Different letters in the same column indicate a significant difference among the samples ($p < 0.05$).

Thermal degradation of the unfilled PHB/PHBV film occurred through a single and sharp degradation step that ranged from about 250 °C to 290 °C. PHA degradation typically follows a random chain scission model of the ester linkage that involves a *cis*-elimination reaction of β-CH and a six-member ring transition to form crotonic acid and its oligomers (Bugnicourt et al. 2014). The presence of RHF reduced both the onset degradation temperature ($T_{5\%}$) and degradation temperature (T_{deg}) by approximately 10 °C and 15 °C, respectively, and also generated a low-intensity second mass centered around 330 °C. This reduction in thermal stability can be mainly ascribed to the lower degradation temperature of the lignocellulosic particles as well as to the presence of some remaining water. One can also observe that all composite films presented a similar thermal degradation profile though certain stability increase was attained for the highest PHBV contents. For instance, the $T_{5\%}$ value increased from 242.5 °C, for the PHB/RHF film, to 257.2 °C, for the PHB/PHBV50/RHF film. Similarly, the values of T_{deg} also increased from 270 °C, for the PHB/RHF film, to 275.5 °C, for the PHB/PHBV50/RHF film. The improvement achieved in the thermal stability can be ascribed to the high purity of the PHBV incorporated in the blend, based on the previous selection of the optimal purification route (Melendez-Rodriguez et al. 2018), which has also been reported to be more thermally stable than PHB (Li et al. 2003). Finally, the amount of residual mass was in the 3–4 % range, being mainly ascribed to the formed char from RHF.

3.6. Mechanical Properties of PHB/PHBV/RHF Films

Figure 7 shows the tensile stress–strain curves, obtained at room temperature, for the thermo-compressed films. The mechanical results, in terms of tensile modulus (E), tensile strength at yield (σ_y), elongation at break (ε_b), and toughness are summarized in **Table 5**. One can see that all the films were relatively stiff and also brittle due to the intrinsically high crystallinity of PHB, which is derived from secondary crystallization that occurs post-processing with age (Laycock et al. 2013). This mechanical brittleness habitually represents an obstacle to the practical applications of PHB, for instance in packaging. The presence of RHF further promoted rigidity and brittleness of PHB, showing E and ε_b values of 3025 MPa and 1.1 %, respectively. One can also observe that the unfilled PHB/PHBV film showed the lowest E value, that is, 1785 MPa, and also the highest values of ε_b and toughness, that is, 8.4 % and 1.9 mJ/m^3, respectively. Whereas the mechanical properties of the PHB/RHF and PHB/PHBV5/RHF films were relatively similar, the incorporation of 10 wt % PHBV into PHB/RHF successfully resulted in a film with very balanced performance in terms of mechanical strength and ductility. In particular, the PHB/PHBV10/RHF film showed moderate values of E and σ_y, that is, 2508 MPa and 30.4 MPa, respectively, and a 3-fold increase in ε_b and remarkable higher toughness in comparison to the PHB/RHF film. However, the films produced at higher PHBV contents, that is, 20–50 wt %, showed lower and relatively similar performance. These results indicate that PHBV can successfully produce a toughening effect on the PHB matrix at low or intermediate contents, which can be ascribed to the high solubility achieved in these films samples as described above during the crystallinity analysis. The resultant lower stiffness and higher flexibility of these PHBV-containing films can be attributed to the presence of dislocations, crystal strain, and smaller crystallites in the PHB/PHBV soluble regions due to the insertion of the HV units into the PHB lattice, which acted as defects in the HB crystals (Orts et al. 1990).

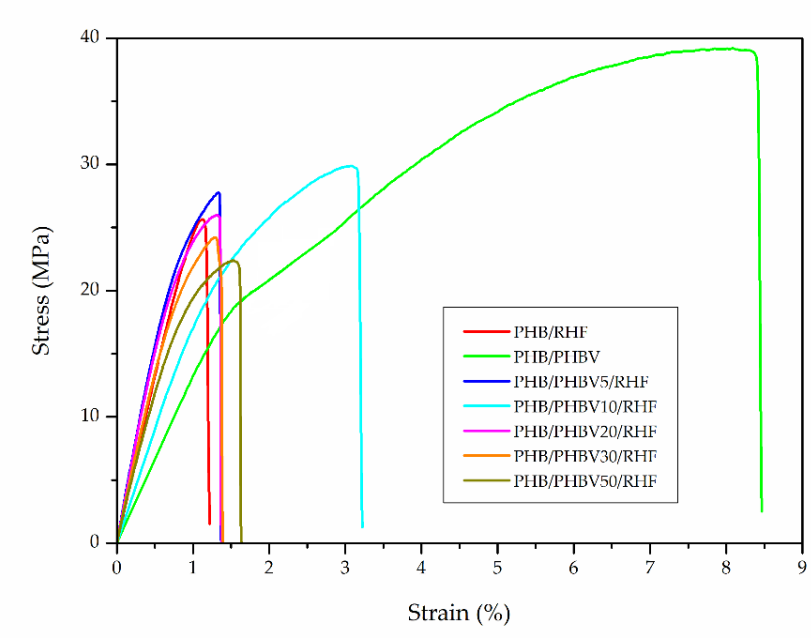

Figure 7. Tensile stress–strain curves of the thermo-compressed films made of poly(3-hydroxybutyrate) (PHB), poly(3-hydroxybutyrate-*co*-3-hydroxyvalerate) (PHBV), and rice husk flour (RHF).

Table 5. Mechanical properties of the thermo-compressed films made of poly(3-hydroxybutyrate) (PHB), poly(3-hydroxybutyrate-*co*-3-hydroxyvalerate) (PHBV), and rice husk flour (RHF) in terms of: tensile modulus (E), tensile strength at yield (σ_y), elongation at break (ε_b), and toughness.

Film	E (MPa)	σ_y (MPa)	ε_b (%)	Toughness (mJ/m^3)
PHB*	~2900[a]	~37[a]	~4[a]	-
PHB/RHF	3025 ± 101[b]	26.7 ± 2.7[b]	1.1 ± 0.1[b]	0.1 ± 0.1[a]
PHB/PHBV	1785 ± 129[c]	38.9 ± 2.0[a]	8.4 ± 1.1[c]	1.9 ± 0.3[b]
PHB/PHBV5/RHF	2985 ± 119[a,b]	27.2 ± 1.1[b]	1.4 ± 0.1[d]	0.3 ± 0.1[a]
PHB/PHBV10/RHF	2508 ± 207[d]	30.4 ± 2.7[b]	3.3 ± 1.3[a]	0.8 ± 0.3[c]
PHB/PHBV20/RHF	2830 ± 193[a,b,d]	26.5 ± 2.5[b]	1.2 ± 0.3[b,d]	0.1 ± 0.1[a]
PHB/PHBV30/RHF	2765 ± 201[a,b,d]	23.9 ± 0.7[b]	1.3 ± 0.2[b,d]	0.2 ± 0.1[a]
PHB/PHBV50/RHF	2649 ± 104[d]	19.5 ± 3.0[c]	1.3 ± 0.4[b,d]	0.2 ± 0.1[a]

*Average mechanical properties for compression-molded films of neat PHB (Laycock et al. 2013).

[a–d] Different letters in the same column indicate a significant difference among the samples ($p < 0.05$).

3.7. Barrier Performance of PHB/PHBV/RHF Films

Table 6 finally gathers the WVP and LP values of the PHB-based films. The barrier performance to water vapor is one of the main parameters of application interest in packaging, while d-limonene is a commonly used standard compound to test mass transport of aromas. The PHB/RHF film showed somewhat higher WVP values than compression-molded PHB films previously reported by our group, that is, $1.7–1.75 \times 10^{-15}$ $kg \cdot m \cdot m^{-2} \cdot s^{-1} \cdot Pa^{-1}$ (Cherpinski et al. 2017, Sanchez-Garcia, Gimenez, and Lagaron 2007). The lower water vapor barrier attained for the here-prepared green composite films can be related to the high tendency of the lignocellulosic fillers to adsorb water since transport of water vapor molecules is mainly a diffusivity-driven property in PHAs due to their intrinsically low hydrophilic character (Razumovskii et al. 1994). The incorporation of biowaste derived PHBV into PHB/RHF increased slightly the WVP values in the films. At low PHBV contents, however, the barrier performance of the composite films was relatively similar since the samples showed variations close to the detection limit of the technique, with deviations oscillating in the $6.0–7.5 \times 10^{-16}$ $kg \cdot m \cdot m^{-2} \cdot s^{-1} \cdot Pa^{-1}$ range. Only the films with the highest PHBV contents, that is, 30 wt % and 50 wt %, displayed a significant decrease in the water barrier properties, which was still within the same order of magnitude. The barrier drop observed can be attributed to the higher contribution of the biomass derived PHBV, which results in an overall decrease in molecular order and crystallinity, the presence of defects and discontinuities across the polymer morphology as well as certain plasticization induced by the remaining biomass impurities of PHBV with consequent increase in free volume (Martínez-Abad et al. 2016).

Table 6. Water vapor permeability (WVP) and $_D$-limonene permeability (LP) of the thermo-compressed films made of poly(3-hydroxybutyrate) (PHB), poly(3-hydroxybutyrate-*co*-3-hydroxyvalerate) (PHBV), and rice husk flour (RHF).

Film	WVP × 10^{15} (kg·m·m^{-2}·Pa^{-1}·s^{-1})	LP × 10^{15} (kg·m·m^{-2}·Pa^{-1}·s^{-1})
PHB*	1.75[a]	1.95[a]
PHB/RHF	4.52 ± 0.38[b]	2.58 ± 1.35[a]
PHB/PHBV	3.27 ± 0.15[c]	2.04 ± 0.19[a]
PHB/PHBV5/RHF	4.55 ± 0.75[b]	2.16 ± 0.54[a]
PHB/PHBV10/RHF	5.03 ± 0.64[b]	3.10 ± 0.65[a]
PHB/PHBV20/RHF	5.36 ± 0.69[b]	3.38 ± 0.63[a]
PHB/PHBV30/RHF	6.01 ± 0.60[b]	3.72 ± 0.32[a]
PHB/PHBV50/RHF	7.46 ± 0.90[b]	5.04 ± 1.50[a]

*Barrier data for compression-molded PHB films reported in literature (Cherpinski et al. 2017).

[a–c] Different letters in the same column indicate a significant difference among the samples ($p < 0.05$).

Similar to WVP, one can observe that the incorporation of PHBV tended to decrease the barrier properties to $_D$-limonene of the PHB/RHF composite films. This aroma compound, as opposed to moisture, is a strong plasticizing component for PHAs, thus, solubility plays a more important role in permeability than diffusion. The LP increase observed suggests that the presence of PHBV favored an increased sorption of $_D$-limonene in the film. Indeed, our previous studies dealing with PHA materials have shown that the LP value of films made of PHBV with 12 mol % HV is two order of magnitude higher, that is, 1.99×10^{-13} kg·m·m^{-2}·s^{-1}·Pa^{-1} (Sanchez-Garcia, Gimenez, and Lagaron 2008), than that of neat PHB films, that is, 1.95×10^{-15} kg·m·m^{-2}·s^{-1}·Pa^{-1} (Cherpinski et al. 2017). In any case, the present results indicate that the incorporation of up to 20 wt % PHBV does not significantly affect the barrier properties of the PHB-based films against water or aroma. In a more packaging oriented application context, the composite films containing low amounts of PHBV present WVP values in the same order of magnitude than those films of petroleum-based PET, that is, 2.30×10^{-15} kg·m·m^{-2}·s^{-1}·Pa^{-1} (Lagarón 2011), which is typically used in medium-barrier applications. In terms of d-limonene, the here-prepared PHB/PHBV/RHF films are two order of magnitude more barrier than compression-molded PET films, that is, 1.17×10^{-13} kg·m·m^{-2}·s^{-1}·Pa^{-1} (Sanchez-Garcia, Gimenez, and Lagaron 2007).

4. Discussion

Results showed an optimum morphology with a regular distribution of RHF, tightly bonded and with absence of gap along the PHB matrix due to the use of reactive compatibilizers. The biowaste derived PHBV also showed a good miscibility with the PHB/RHF composite system, in particular at the lowest contents, that is, 5–10 wt %. At higher concentrations, however, a two-phases system was attained, indicating that crystallization occurred mainly in the PHB-rich regions. The incorporation of PHBV also increased the thermal stability of PHB/RHF, increasing the processing window of the films. With respect to the mechanical properties, contents in the 5–10 wt % range of PHBV yielded films with a more balanced performance in terms of strength and ductility, counteracting the stiffness and fragility induced by RHF. Finally, although the incorporation of PHBV increased the permeability of the films, the water vapor barrier properties of the PHB/PHBV/RHF films still remained in values close to those of PET films, whereas they still presented a high barrier to aroma.

5. Conclusions

The use of natural fillers and biopolymers obtained from agro-food waste currently represents a sustainable alternative to petroleum-based materials. The green composite films prepared herein are potential candidates to be used in rigid packaging for low and medium barrier applications, being processable by current conventional machinery. The valorization of agro-food waste, as well as the relative preservation of physicochemical properties, supports the use of purified biosustainably produced PHBV in the food packaging industry to develop more cost-effective PHA-based articles.

6. References

Abdul Khalil, H. P. S., A. H. Bhat, and A. F. Ireana Yusra. 2012. "Green composites from sustainable cellulose nanofibrils: A review." *Carbohydrate Polymers* 87 (2):963-979. doi: 10.1016/j.carbpol.2011.08.078.

Adam, F., J. N. Appaturi, and A. Iqbal. 2012. "The utilization of rice husk silica as a catalyst: Review and recent progress." *Catalysis Today* 190 (1):2-14. doi: 10.1016/j.cattod.2012.04.056.

Adam, F., K. Kandasamy, and S. Balakrishnan. 2006. "Iron incorporated heterogeneous catalyst from rice husk ash." *Journal of Colloid and Interface Science* 304 (1):137-143. doi: 10.1016/j.jcis.2006.08.051.

Ahmad, E. E. M., and A. S. Luyt. 2012. "Effects of organic peroxide and polymer chain structure on mechanical and dynamic mechanical properties of sisal fiber reinforced polyethylene composites." *Journal of Applied Polymer Science* 125 (3):2216-2222. doi: 10.1002/app.36434.

Alaerts, L., M. Augustinus, and K. Van Acker. 2018. "Impact of bio-based plastics on current recycling of plastics." *Sustainability (Switzerland)* 10 (5). doi: 10.3390/su10051487.

Aprianti, E., P. Shafigh, S. Bahri, and J. N. Farahani. 2015. "Supplementary cementitious materials origin from agricultural wastes - A review." *Construction and Building Materials* 74:176-187. doi: 10.1016/j.conbuildmat.2014.10.010.

Battegazzore, D., S. Bocchini, J. Alongi, A. Frache, and F. Marino. 2014. "Cellulose extracted from rice husk as filler for poly(lactic acid): Preparation and characterization." *Cellulose* 21 (3):1813-1821. doi: 10.1007/s10570-014-0207-5.

Bertini, F., M. Canetti, A. Cacciamani, G. Elegir, M. Orlandi, and L. Zoia. 2012. "Effect of ligno-derivatives on thermal properties and degradation behavior of poly(3-hydroxybutyrate)-based biocomposites." *Polymer Degradation and Stability* 97 (10):1979-1987. doi: 10.1016/j.polymdegradstab.2012.03.009.

Blunt, W., D. B. Levin, and N. Cicek. 2018. "Bioreactor operating strategies for improved polyhydroxyalkanoate (PHA) productivity." *Polymers* 10 (11). doi: 10.3390/polym10111197.

Boitt, A. P. W., I. O. Barcellos, L. D. Alberti, and D. Z. Bucci. 2014. "Evaluation of the influence of the use of waste from the processing of rice in physicochemical properties and biodegradability of PHB in composites." *Polimeros* 24 (6):640-645. doi: 10.1590/0104-1428.1593.

Borah, J. S., and D. S. Kim. 2016. "Recent development in thermoplastic/wood composites and nanocomposites: A review." *Korean Journal of Chemical Engineering* 33 (11):3035-3049. doi: 10.1007/s11814-016-0183-6.

Bugnicourt, E., P. Cinelli, A. Lazzeri, and V. Alvarez. 2014. "Polyhydroxyalkanoate (PHA): Review of synthesis, characteristics, processing and potential applications in packaging." *Express Polymer Letters* 8 (11):791-808. doi: 10.3144/expresspolymlett.2014.82.

Cava, D., E. Giménez, R. Gavara, and J. M. Lagaron. 2006. "Comparative performance and barrier properties of biodegradable thermoplastics and nanobiocomposites versus PET for food packaging applications." *Journal of Plastic Film and Sheeting* 22 (4):265-274. doi: 10.1177/8756087906071354.

Chan, C. M., L. J. Vandi, S. Pratt, P. Halley, D. Richardson, A. Werker, and B. Laycock. 2018. "Mechanical properties of poly(3-hydroxybutyrate-co-3-hydroxyvalerate)/wood flour composites: Effect of interface modifiers." *Journal of Applied Polymer Science* 135 (43). doi: 10.1002/app.46828.

Cherpinski, Adriane, Sergio Torres-Giner, Luis Cabedo, and Jose M. Lagaron. 2017. "Post-processing optimization of electrospun submicron poly(3-hydroxybutyrate) fibers to obtain continuous films of interest in food packaging applications." *Food Additives & Contaminants: Part A* 34 (10):1817-1830. doi: 10.1080/19440049.2017.1355115.

de Matos Costa, A. R., R. M. Santos, E. N. Ito, L. H. de Carvalho, and E. L. Canedo. 2019. "Melt and cold crystallization in a poly(3-hydroxybutyrate) poly(butylene adipate-co-terephthalate) blend." *Journal of Thermal Analysis and Calorimetry* 137 (4):1341-1346. doi: 10.1007/s10973-019-08027-9.

Dhavalikar, R., and M. Xanthos. 2003. "Parameters affecting the chain extension and branching of PET in the melt state by polyepoxides." *Journal of Applied Polymer Science* 87 (4):643-652. doi: 10.1002/app.11425.

Domingos, J. M. B., S. Puccio, G. A. Martinez, N. Amaral, M. A. M. Reis, S. Bandini, F. Fava, and L. Bertin. 2018. "Cheese whey integrated valorisation: Production, concentration and exploitation of carboxylic acids for the production of polyhydroxyalkanoates by a fed-batch culture." *Chemical Engineering Journal* 336:47-53. doi: 10.1016/j.cej.2017.11.024.

Ferrero, B., V. Fombuena, O. Fenollar, T. Boronat, and R. Balart. 2015. "Development of natural fiber-reinforced plastics (NFRP) based on biobased polyethylene and waste fibers from Posidonia oceanica seaweed." *Polymer Composites* 36 (8):1378-1385. doi: 10.1002/pc.23042.

Figueroa-Lopez, K. J., M. M. Andrade-Mahecha, and O. L. Torres-Vargas. 2018. "Development of antimicrobial biocomposite films to preserve the quality of bread." *Molecules* 23 (1). doi: 10.3390/molecules23010212.

Figueroa-Lopez, K. J., A. A. Vicente, M. A. M. Reis, S. Torres-Giner, and J. M. Lagaron. 2019. "Antimicrobial and antioxidant performance of various essential oils and natural extracts and their incorporation into biowaste derived poly(3-hydroxybutyrate-co-3-hydroxyvalerate) layers made from electrospun ultrathin fibers." *Nanomaterials* 9 (2). doi: 10.3390/nano9020144.

Formela, K., Ł Zedler, A. Hejna, and A. Tercjak. 2018. "Reactive extrusion of bio-based polymer blends and composites–current trends and future developments." *Express Polymer Letters* 12 (1):24-57. doi: 10.3144/expresspolymlett.2018.4.

Garcia-Garcia, D., A. Carbonell-Verdu, A. Jordá-Vilaplana, R. Balart, and D. Garcia-Sanoguera. 2016. "Development and characterization of green composites from bio-based polyethylene and peanut shell." *Journal of Applied Polymer Science* 133 (37). doi: 10.1002/app.43940.

George, J., M. S. Sreekala, and S. Thomas. 2001. "A review on interface modification and characterization of natural fiber reinforced plastic composites." *Polymer Engineering and Science* 41 (9):1471-1485. doi: 10.1002/pen.10846.

Gu, R., M. Sain, and B. V. Kokta. 2015. "Evaluation of wood composite additives in the mechanical property changes of PE blends." *Polymer Composites* 36 (2):287-293. doi: 10.1002/pc.22942.

Hao, M., and H. Wu. 2018. "Effect of in situ reactive interfacial compatibilization on structure and properties of polylactide/sisal fiber biocomposites." *Polymer Composites* 39:E174-E187. doi: 10.1002/pc.24484.

Jacquel, N., C. W. Lo, H. S. Wu, Y. H. Wei, and S. S. Wang. 2007. "Solubility of polyhydroxyalkanoates by experiment and thermodynamic correlations." *AIChE Journal* 53 (10):2704-2714. doi: 10.1002/aic.11274.

Joseph, K., S. Thomas, and C. Pavithran. 1996. "Effect of chemical treatment on the tensile properties of short sisal fibre-reinforced polyethylene composites." *Polymer* 37 (23):5139-5149. doi: 10.1016/0032-3861(96)00144-9.

Joshi, S. V., L. T. Drzal, A. K. Mohanty, and S. Arora. 2004. "Are natural fiber composites environmentally superior to glass fiber reinforced composites?" *Composites Part A: Applied Science and Manufacturing* 35 (3):371-376. doi: 10.1016/j.compositesa.2003.09.016.

Kanatt, S. R., M. S. Rao, S. P. Chawla, and A. Sharma. 2012. "Active chitosan-polyvinyl alcohol films with natural extracts." *Food Hydrocolloids* 29 (2):290-297. doi: 10.1016/j.foodhyd.2012.03.005.

Keshavarz, T., and I. Roy. 2010. "Polyhydroxyalkanoates: bioplastics with a green agenda." *Current Opinion in Microbiology* 13 (3):321-326. doi: 10.1016/j.mib.2010.02.006.

Kim, H. S., H. S. Yang, H. J. Kim, and H. J. Park. 2004. "Thermogravimetric analysis of rice husk flour filled thermoplastic polymer composites." *Journal of Thermal Analysis and Calorimetry* 76 (2):395-404. doi: 10.1023/B:JTAN.0000028020.02657.9b.

Kourmentza, C., J. Plácido, N. Venetsaneas, A. Burniol-Figols, C. Varrone, H. N. Gavala, and M. A. M. Reis. 2017. "Recent advances and challenges towards sustainable polyhydroxyalkanoate (PHA) production." *Bioengineering* 4 (2). doi: 10.3390/bioengineering4020055.

Kumagai, Y., and Y. Doi. 1992. "Enzymatic degradation of poly(3-hydroxybutyrate)-based blends: poly(3-hydroxybutyrate)/poly(ethylene oxide) blend." *Polymer Degradation and Stability* 35 (1):87-93. doi: 10.1016/0141-3910(92)90139-V.

La Mantia, F. P., and M. Morreale. 2011. "Green composites: A brief review." *Composites Part A: Applied Science and Manufacturing* 42 (6):579-588. doi: 10.1016/j.compositesa.2011.01.017.

Lagarón, J. M. 2011. "Multifunctional and Nanoreinforced Polymers for Food Packaging." In.: Woodhead Publishing.

Laycock, B., P. Halley, S. Pratt, A. Werker, and P. Lant. 2013. "The chemomechanical properties of microbial polyhydroxyalkanoates." *Progress in Polymer Science* 38 (3-4):536-583. doi: 10.1016/j.progpolymsci.2012.06.003.

Lee, S. Y. 1996. "Plastic bacteria? Progress and prospects for polyhydroxyalkanoate production in bacteria." *Trends in Biotechnology* 14 (11):431-438. doi: 10.1016/0167-7799(96)10061-5.

Li, S. D., J. D. He, P. H. Yu, and M. K. Cheung. 2003. "Thermal degradation of poly(3-hydroxybutyrate) and poly(3-hydroxybutyrate-co-3-hydroxyvalerate) as studied by TG, TG-FTIR, and Py-GC/MS." *Journal of Applied Polymer Science* 89 (6):1530-1536. doi: 10.1002/app.12249.

Liminana, P., D. Garcia-Sanoguera, L. Quiles-Carrillo, R. Balart, and N. Montanes. 2018. "Development and characterization of environmentally friendly composites from poly(butylene succinate) (PBS) and almond shell flour with different compatibilizers." *Composites Part B: Engineering* 144:153-162. doi: 10.1016/j.compositesb.2018.02.031.

Lu, J. Z., Q. Wu, and H. S. McNabb Jr. 2000. "Chemical coupling in wood fiber and polymer composites: A review of coupling agents and treatments." *Wood and Fiber Science* 32 (1):88-104.

Mansaray, K. G., and A. E. Ghaly. 1998. "Thermogravimetric Analysis of Rice Husks in an Air Atmosphere." *Energy Sources* 20 (7):653-663. doi: 10.1080/00908319808970084.

Martínez-Abad, A., L. Cabedo, C. S. S. Oliveira, L. Hilliou, M. Reis, and J. M. Lagarón. 2016. "Characterization of polyhydroxyalkanoate blends incorporating unpurified biosustainably produced poly(3-hydroxybutyrate-co-3-hydroxyvalerate)." *Journal of Applied Polymer Science* 133 (2). doi: 10.1002/app.42633.

Maruhashi, Y., and S. Iida. 2001. "Transparency of polymer blends." *Polymer Engineering and Science* 41 (11):1987-1995. doi: 10.1002/pen.10895.

Melendez-Rodriguez, B., J. L. Castro-Mayorga, M. A. M. Reis, C. Sammon, L. Cabedo, S. Torres-Giner, and J. M. Lagaron. 2018. "Preparation and Characterization of Electrospun Food Biopackaging Films of Poly(3-hydroxybutyrate-co-3-hydroxyvalerate) Derived From Fruit Pulp Biowaste." *Frontiers in Sustainable Food Systems* 2. doi: 10.3389/fsufs.2018.00038.

Mokoena, M. A., V. Djoković, and A. S. Luyt. 2004. "Composites of linear low density polyethylene and short sisal fibres: The effects of peroxide treatment." *Journal of Materials Science* 39 (10):3403-3412. doi: 10.1023/B:JMSC.0000026943.47803.0b.

Montava-Jordà, S., L. Quiles-Carrillo, N. Richart, S. Torres-Giner, and N. Montanes. 2019. "Enhanced interfacial adhesion of polylactide/poly(ε-caprolactone)/walnut shell flour composites by reactive extrusion with maleinized linseed oil." *Polymers* 11 (5). doi: 10.3390/polym11050758.

Montava-Jordà, S., S. Torres-Giner, S. Ferrandiz-Bou, L. Quiles-Carrillo, and N. Montanes. 2019. "Development of sustainable and cost-competitive injection-molded pieces of partially bio-based polyethylene terephthalate through the valorization of cotton textile waste." *International Journal of Molecular Sciences* 20 (6). doi: 10.3390/ijms20061378.

Moura, A., C. Bolba, R. Demori, L. P. F. C. Lima, and R. M. C. Santana. 2018. "Effect of Rice Husk Treatment with Hot Water on Mechanical Performance in Poly(hydroxybutyrate)/Rice Husk Biocomposite." *Journal of Polymers and the Environment* 26 (6):2632-2639. doi: 10.1007/s10924-017-1156-5.

Nabi Saheb, D., and J. P. Jog. 1999. "Natural fiber polymer composites: A review." *Advances in Polymer Technology* 18 (4):351-363. doi: 10.1002/(SICI)1098-2329(199924)18:4<351::AID-ADV6>3.0.CO;2-X.

Nascimento, G. C., D. M. Cechinel, R. Piletti, E. Mendes, M. M. S. Paula, H. G. Riella, and M. A. Fiori. 2010. Effect of different concentrations and sizes of particles of rice husk ash - RHS in the mechanical properties of polypropylene. In *Materials Science Forum*.

Ndazi, B. S., and S. Karlsson. 2011. "Characterization of hydrolytic degradation of polylactic acid/rice hulls composites in water at different temperatures." *Express Polymer Letters* 5 (2):119-131. doi: 10.3144/expresspolymlett.2011.13.

Nduko, J. M., K. Matsumoto, and S. Taguchi. 2012. Biological lactate-polymers synthesized by one-pot microbial factory: Enzyme and metabolic engineering. In *ACS Symposium Series*.

Nogellova, Z., B. V. Kokta, and I. Chodák. 1998. "A composite LDPE/wood flour crosslinked by peroxide." *Journal of Macromolecular Science - Pure and Applied Chemistry* 35 (7-8):1069-1077. doi: 10.1080/10601329808002101.

Ollier, R. P., D. A. D'Amico, W. F. Schroeder, V. P. Cyras, and V. A. Alvarez. 2018. "Effect of clay treatment on the thermal degradation of PHB based nanocomposites." *Applied Clay Science* 163:146-152. doi: 10.1016/j.clay.2018.07.025.

Organ, S. J. 1994. "Phase separation in blends of poly(hydroxybutyrate) with poly(hydroxybutyrate-co-hydroxyvalerate): variation with blend components." *Polymer* 35 (1):86-92. doi: 10.1016/0032-3861(94)90054-X.

Orts, W. J., R. H. Marchessault, T. L. Bluhm, and G. K. Hamer. 1990. "Observation of strain-induced β form in poly (β-hydroxyalkanoates)." *Macromolecules* 23 (26):5368-5370. doi: 10.1021/ma00228a014.

Panthapulakkal, S., S. Law, and M. Sain. 2005. "Enhancement of processability of rice husk filled high-density polyethylene composite profiles." *Journal of Thermoplastic Composite Materials* 18 (5):445-458. doi: 10.1177/0892705705054398.

Philip, S., T. Keshavarz, and I. Roy. 2007. "Polyhydroxyalkanoates: Biodegradable polymers with a range of applications." *Journal of Chemical Technology and Biotechnology* 82 (3):233-247. doi: 10.1002/jctb.1667.

Quiles-Carrillo, L., N. Montanes, D. Garcia-Garcia, A. Carbonell-Verdu, R. Balart, and S. Torres-Giner. 2018. "Effect of different compatibilizers on injection-molded green composite pieces based on polylactide filled with almond shell flour." *Composites Part B: Engineering* 147:76-85. doi: 10.1016/j.compositesb.2018.04.017.

Quiles-Carrillo, L., N. Montanes, A. Jorda-Vilaplana, R. Balart, and S. Torres-Giner. 2019. "A comparative study on the effect of different reactive compatibilizers on injection-molded pieces of bio-based high-density polyethylene/polylactide blends." *Journal of Applied Polymer Science* 136 (16). doi: 10.1002/app.47396.

Quiles-Carrillo, L., N. Montanes, J. M. Lagaron, R. Balart, and S. Torres-Giner. 2018. "On the use of acrylated epoxidized soybean oil as a reactive compatibilizer in injection-molded compostable pieces consisting of polylactide filled with orange peel flour." *Polymer International* 67 (10):1341-1351. doi: 10.1002/pi.5588.

Quiles-Carrillo, L., N. Montanes, C. Sammon, R. Balart, and S. Torres-Giner. 2018. "Compatibilization of highly sustainable polylactide/almond shell flour composites by reactive extrusion with maleinized linseed oil." *Industrial Crops and Products* 111:878-888. doi: 10.1016/j.indcrop.2017.10.062.

Razumovskii, L. P., A. L. Iordanskii, G. E. Zaikov, E. D. Zagreba, and I. C. McNeill. 1994. "Sorption and diffusion of water and organic solvents in poly(β-hydroxybutyrate) films." *Polymer Degradation and Stability* 44 (2):171-175. doi: https://doi.org/10.1016/0141-3910(94)90161-9.

Rehm, B. H. A. 2003. "Polyester synthases: Natural catalysts for plastics." *Biochemical Journal* 376 (1):15-33. doi: 10.1042/BJ20031254.

Reis, K. C., J. Pereira, A. C. Smith, C. W. P. Carvalho, N. Wellner, and I. Yakimets. 2008. "Characterization of polyhydroxybutyrate-hydroxyvalerate (PHB-HV)/maize starch blend films." *Journal of Food Engineering* 89 (4):361-369. doi: 10.1016/j.jfoodeng.2008.04.022.

Rosa, S. M. L., E. F. Santos, C. A. Ferreira, and S. M. B. Nachtigalt. 2009. "Studies on the properties of rice-husk-filled-PP composites - Effect of maleated PP." *Materials Research* 12 (3):333-338. doi: 10.1590/S1516-14392009000300014.

Rowell, R. M., R. A. Young, and J. K. Rowell. 1997. *Paper and Composites from Agro-Based Resources*:351-375.

Saito, M., Y. Inoue, and N. Yoshie. 2001. "Cocrystallization and phase segregation of blends of poly (3-hydroxybutyrate) and poly(3-hydroxybutyrate-co-3-hydroxyvalerate)." *Polymer* 42 (13):5573-5580. doi: 10.1016/S0032-3861(01)00011-8.

Samorì, C., F. Abbondanzi, P. Galletti, L. Giorgini, L. Mazzocchetti, C. Torri, and E. Tagliavini. 2015. "Extraction of polyhydroxyalkanoates from mixed microbial cultures: Impact on

polymer quality and recovery." *Bioresource Technology* 189:195-202. doi: 10.1016/j.biortech.2015.03.062.

Sanchez-Garcia, M. D., E. Gimenez, and J. M. Lagaron. 2008. "Morphology and barrier properties of solvent cast composites of thermoplastic biopolymers and purified cellulose fibers." *Carbohydrate Polymers* 71 (2):235-244. doi: https://doi.org/10.1016/j.carbpol.2007.05.041.

Sanchez-Garcia, M.D., E. Gimenez, and J.M. Lagaron. 2007. "Novel PET Nanocomposites of Interest in Food Packaging Applications and Comparative Barrier Performance With Biopolyester Nanocomposites." *Journal of Plastic Film & Sheeting* 23 (2):133-148. doi: 10.1177/8756087907083590.

Sánchez-Safont, E. L., A. Aldureid, J. M. Lagarón, J. Gámez-Pérez, and L. Cabedo. 2018. "Biocomposites of different lignocellulosic wastes for sustainable food packaging applications." *Composites Part B: Engineering* 145:215-225. doi: 10.1016/j.compositesb.2018.03.037.

Scaglioni, P. T., and E. Badiale-Furlong. 2016. "Rice husk as an adsorbent: A new analytical approach to determine aflatoxins in milk." *Talanta* 152:423-431. doi: 10.1016/j.talanta.2016.02.042.

Schneider, L. T., G. Bonassa, H. J. Alves, T. R. W. Meier, E. P. Frigo, and J. G. Teleken. 2019. "Use of rice husk in waste cooking oil pretreatment." *Environmental Technology (United Kingdom)* 40 (5):594-604. doi: 10.1080/09593330.2017.1397772.

Smith, R. 2005. *Biodegradable polymers for industrial applications, Biodegradable Polymers for Industrial Applications*.

Torres-Giner, S., L. Hilliou, B. Melendez-Rodriguez, K. J. Figueroa-Lopez, D. Madalena, L. Cabedo, J. A. Covas, A. A. Vicente, and J. M. Lagaron. 2018. "Melt processability, characterization, and antibacterial activity of compression-molded green composite sheets made of poly(3-hydroxybutyrate-co-3-hydroxyvalerate) reinforced with coconut fibers impregnated with oregano essential oil." *Food Packaging and Shelf Life* 17:39-49. doi: 10.1016/j.fpsl.2018.05.002.

Torres-Giner, S., N. Montanes, T. Boronat, L. Quiles-Carrillo, and R. Balart. 2016. "Melt grafting of sepiolite nanoclay onto poly(3-hydroxybutyrate-co-4-hydroxybutyrate) by reactive extrusion with multi-functional epoxy-based styrene-acrylic oligomer." *European Polymer Journal* 84:693-707. doi: 10.1016/j.eurpolymj.2016.09.057.

Torres-Giner, S., N. Montanes, V. Fombuena, T. Boronat, and L. Sanchez-Nacher. 2018. "Preparation and characterization of compression-molded green composite sheets made of poly(3-hydroxybutyrate) reinforced with long pita fibers." *Advances in Polymer Technology* 37 (5):1305-1315. doi: 10.1002/adv.21789.

Wei, L., A. G. McDonald, and N. M. Stark. 2015. "Grafting of Bacterial Polyhydroxybutyrate (PHB) onto Cellulose via In Situ Reactive Extrusion with Dicumyl Peroxide." *Biomacromolecules* 16 (3):1040-1049. doi: 10.1021/acs.biomac.5b00049.

Wei, L., N. M. Stark, and A. G. McDonald. 2015. "Interfacial improvements in biocomposites based on poly(3-hydroxybutyrate) and poly(3-hydroxybutyrate-co-3-hydroxyvalerate) bioplastics reinforced and grafted with α-cellulose fibers." *Green Chemistry* 17 (10):4800-4814. doi: 10.1039/c5gc01568e.

Yoshie, N., A. Asaka, and Y. Inoue. 2004. "Cocrystallization and phase segregation in crystalline/crystalline polymer blends of bacterial copolyesters." *Macromolecules* 37 (10):3770-3779. doi: 10.1021/ma049858p.

Yussuf, A. A., I. Massoumi, and A. Hassan. 2010. "Comparison of polylactic Acid/Kenaf and polylactic Acid/Rise husk composites: The influence of the natural fibers on the mechanical, thermal and biodegradability properties." *Journal of Polymers and the Environment* 18 (3):422-429. doi: 10.1007/s10924-010-0185-0.

Zhao, Q., B. Zhang, H. Quan, R. C. M. Yam, R. K. K. Yuen, and R. K. Y. Li. 2009. "Flame retardancy of rice husk-filled high-density polyethylene ecocomposites." *Composites Science and Technology* 69 (15-16):2675-2681. doi: 10.1016/j.compscitech.2009.08.009.

Zini, E., and M. Scandola. 2011. "Green composites: An overview." *Polymer Composites* 32 (12):1905-1915. doi: 10.1002/pc.21224.

Chapter VII

Blends of Poly(3-Hydroxybutyrate-*co*-3-Hydroxyvalerate) with Fruit Pulp Biowaste Derived Poly(3-Hydroxybutyrate-*co*-3-Hydroxyvalerate-*co*-3-Hydroxyhexanoate) for Organic Recycling Food Packaging

Polymers 2021, 13(7), 1155

Beatriz Meléndez-Rodríguez[1], Sergio Torres-Giner[1†], Maria A. M. Reis[2], Fernando Silva[2], Mariana Matos[2], Luis Cabedo[3], and José María Lagarón[1]

[1] Novel Materials and Nanotechnology Group, Institute of Agrochemistry and Food Technology (IATA), Spanish Council for Scientific Research (CSIC), Paterna, Spain

[2] UCIBIO-REQUIMTE-Applied Molecular Biosciences Unit, Chemistry Department, Faculty of Sciences and Technology, New University of Lisbon, Lisbon, Portugal

[3] Polymers and Advanced Materials Group (PIMA), Universitat Jaume I (UJI), Castellón, Spain

[†] This author is currently with the Research Institute of Food Engineering for Development (IIAD), Universitat Politècnica de València (UPV), Valencia, Spain

Abstract

In the present study, a new poly(3-hydroxybutyrate-*co*-3-hydroxyvalerate-*co*-3-hydroxyhexanoate) [P(3HB-*co*-3HV-*co*-3HHx)] terpolyester with approximately 68 mol % of 3-hydroxybutyrate (3HB), 17 mol % of 3-hydroxyvalerate (3HV), and 15 mol % of 3-hydroxyhexanoate (3HHx) was obtained via the mixed microbial culture (MMC) technology using fruit pulps as feedstock, a processing by-product of the juice industry. After extraction and purification performed in a single step, the P(3HB-*co*-3HV-*co*-3HHx) powder was melt-mixed, for the first time, in contents of 10, 25, and 50 wt % with commercial poly(3-hydroxybutyrate-*co*-3-hydroxyvalerate) (PHBV). Thereafter, the resultant doughs were thermo-compressed to obtain highly miscible films with good optical properties, which can be of interest in rigid and semirigid organic recyclable food packaging applications. The results showed that the developed blends exhibited a progressively lower melting enthalpy with increasing the incorporation of P(3HB-*co*-3HV-*co*-3HHx), but retained the PHB crystalline morphology, albeit with an inferred lower crystalline density. Moreover, all the melt-mixed blends were thermally stable up to nearly 240 °C. As the content of terpolymer increased in the blends, the mechanical response of their films showed a brittle-to-ductile transition. On the other hand, the permeabilities to water vapor, oxygen, and, more notably, limonene were seen to increase. On the overall, this study demonstrates the value of using industrial biowaste derived P(3HB-*co*-3HV-*co*-3HHx) terpolyesters as potentially cost-effective and sustainable plasticizing additives to balance the physical properties of organic recyclable polyhydroxyalkanoate (PHA)-based food packaging materials.

Keywords: polyhydroxyalkanoates; waste valorization; food packaging; Circular Bioeconomy; organic recycling

1. Introduction

The massive use of synthetic plastics in recent decades has caused a deep damage to the environment. Polymers derived from fossil hydrocarbons are habitually non-biodegradable, making them difficult to eliminate and being accumulated in landfills or in natural environments (Barnes et al. 2009). This environmental issue becomes particularly relevant for packaging applications, in which the articles are generally discarded after a short and single use and, thus, a change in the strategies related to the type of material used is necessary (Alfei, Schito, and Zuccari 2021, Torres-Giner et al. 2021).

Polyhydroxyalkanoates (PHAs) are a family of linear polyesters produced in nature by the action of bacteria, both Gram-positives and Gram-negatives, during fermentation of sugar or lipids in famine conditions (Rehm 2003). PHAs are currently regarded as a good alternative to conventional petroleum-based polymers. These biopolyesters are biodegradable both in composting conditions and in natural environments, while they are fully bio-based. Therefore, PHAs can be integrated inside the so-called Circular Bioeconomy strategies that aim, by organic recycling, to bring the carbon back to the soil (Dobrucka 2019). The first identified and best-characterized PHA was poly(3-hydroxybutyrate) (PHB) (Winnacker 2019). However, PHB has poor physical properties in terms of brittleness and low processability due to its highly crystalline nature (Madison and Huisman 1999). The use of PHA copolymers can improve these properties and the most common one is poly(3-hydroxybutyrate-*co*-3-hydroxyvalerate) (PHBV). In particular, the percentage of 3-hydroxyvalerate (3HV) in the copolyester can modify the relevant properties of the polymer. For example, the degree of crystallinity of PHB can decrease up to approximately 40 % with increasing the 3HV content to 30 mol % that, in turns, reduces the melting temperature (T_m) and brittleness while improves the processing window (Mitomo, Barham, and Morimoto 1987). Similarly, the mechanical properties are enhanced in terms of ductility when the 3HV content increases (Chan et al. 2019). Thus, an increased in elongation at break (ε_b) from 5.6 %, for PHB, to 690 %, was reported for a film of PHBV with 20 mol % 3HV prepared by solvent casting (Savenkova et al. 2000). In another study, ε_b increased from 3 % to 44 % in solvent-casted PHBV films with a change in the 3HV content from 7 mol % to 40 mol % (Martínez-Sanz et al. 2014). Furthermore, the use of terpolymers has also been identified as an effective strategy to improve the material properties of PHB (Zhao and Chen 2007). In this regard, the poly(3-hydroxybutyrate-*co*-3-hydroxyvalerate-*co*-3-hydroxyhexanoate) [P(3HB-*co*-3HV-*co*-3HHx) or PHBVHHx] terpolyester is very promising. For instance, Zhao et al. (Zhao and Chen 2007) produced various P(3HB-*co*-3HV-*co*-3HHx) terpolymers with 3HV and 3-hydroxyhexanoate (3HHx) molar contents ranging between 2.3–7.1 mol % and 5.0–15.1 mol %, respectively. It was demonstrated that the P(3HB-*co*-3HV-*co*-3HHx) terpolymer shows higher thermal stability and ε_b compared to the PHB homopolymer and its PHBV copolymer with 5 mol % 3HV and also poly(3-hydroxybutyrate-*co*-3-hydroxyhexanoate) [P(3HB-*co*-3HHx)] with 12 mol % 3HHx. In particular, ε_b increased from 4.5 %, for PHB, to 481.1 % for P(3HB-*co*-3HV-*co*-3HHx) with 13.4 mol % 3HHx content. P(3HB-*co*-3HV-*co*-3HHx) also presented lower melting temperatures and enthalpies of fusion than the homopolymer, that is, 162 °C and 97 J/g, for PHB, and 104 °C and 20.8 J/g, for the terpolyester with 15.1 mol % 3HHx content, respectively. This fact is due to its lower crystallinity and the formation of crystals with lower degree of perfection. Moreover, Ye et al. (Ye et al. 2010) reported that P(3HB-*co*-3HV-*co*-3HHx) showed higher crystallization rate and degree of crystallinity than P(3HB-*co*-3HHx), and also an improvement of the ductile performance, which was explained by the simultaneous introduction of 3HV and 3HHx monomers. Thus, one can consider that all these changes in the material

properties would positively contribute to attain property-balanced materials, more suitable for use in food packaging. Furthermore, some studies have indicated that these terpolymers are biocompatible and non-cytotoxic (Ji, Li, and Chen 2008, Liang, Zhao, and Chen 2008).

Nevertheless, the synthesis of P(3HB-*co*-3HV-*co*-3HHx) has been scarcely reported in a few studies. Some bacterial strains have been used in the P(3HB-*co*-3HV-*co*-3HHx) production, such as *Rhodospirillum rubrum* and *Rhodococcus* sp. NCIMB 40,126 (Brandl et al. 1989, Haywood et al. 1991). Moreover, the use of recombinant strains modified through genetic engineering has been described to obtain a higher control of the resultant PHA, such as *Escherichia coli* (Park et al. 2001), *Cupriavidus necator* (Bhubalan et al. 2010), *Ralstonia eutropha* (Jung et al. 2019), among others (Reiser, Mitsky, and Gruys 2000, Zhang et al. 2009). However, the use of pure microbial cultures for PHA production requires pure substrates as the carbon resources and also sterile conditions, making this process expensive and not highly sustainable from an industrial upscaling point of view (Choi and Lee 1997). An alternative to reduce the market price while increasing sustainability would be through the use of mixed microbial cultures (MMCs) in combination with the use of industrial by-products of agro-food wastes such as feedstocks (Koller et al. 2005, RamKumar Pandian et al. 2010). In this regard, there are several organic wastes of industrial by-products that have been reported for the production of PHAs such as oil mill (Dionisi et al. 2005, Hassan et al. 1996), molasses (Tripathi et al. 2012), paper mill effluents (Bengtsson et al. 2008), dairy whey (Bosco and Chiampo 2010, Duque et al. 2014), fermented fruit (Arumugam et al. 2019, Khumwanich, Napathorn, and Suwannasilp 2014), and municipal solid waste (Papa et al. 2020). In this sense, the use of biowastes for PHA production has shown to increase the economic value of the final product, while it reduces the overall environmental impact of the biopolymer production (Babu, O'Connor, and Seeram 2013).

Blending by melt mixing with additives and fillers has also demonstrated to be a convenient approach to improve the properties of PHAs. Thus, it is common to use mixtures with different commercial biopolymers (Nishida et al. 2019, Zembouai, Bruzaud, Kaci, Benhamida, Corre, Grohens, and Lopez-Cuesta 2014), waste derived fillers (Sánchez-Safont et al. 2020, Torres-Tello et al. 2017) or a combination of both (Melendez-Rodriguez et al. 2019, Sarasini et al. 2018), which increase some of the final properties such as thermal, mechanical or barrier. These properties can be modified depending on the polymers and the ratios used in the blends (Furukawa et al. 2007). The techniques most commonly used to prepare the PHA blends are solvent solution (Choe et al. 1995, Peng et al. 2003) and melt mixing (Nerkar et al. 2014, Zembouai, Bruzaud, Kaci, Benhamida, Corre, Grohens, Taguet, et al. 2014). The latter technique shows certain advantages as it is a fast method, it is environmentally friendly as no solvents are required, and large mass production can be easily scaled up (Koyama et al. 2009, Verma and Goh 2018). In this context, the use of waste derived PHA in melt-mixed blends with commercial PHA has been previously assessed by our group. Thus, Martinez-Abad et al. (Martínez-Abad, Cabedo, et al. 2016) reported blends of commercial PHBV with unpurified PHBV obtained by MMCs from cheese whey (CW). The obtained blends showed good miscibility and their thermal, mechanical, and barrier properties were not substantially affected for loadings of up to 10 wt % of the food waste derived PHBV, whereas the sustainable profile of PHBV was improved. Also, blends of commercial PHB and purified PHBV obtained from fruit pulp waste filled with 10 wt % rice husk flour (RHF) also showed good miscibility, increased thermal stability, and slightly better mechanical properties in terms of strength and ductility (Melendez-Rodriguez et al. 2019).

In this study, a newly developed P(3HB-*co*-3HV-*co*-3HHx) produced by MMC using biomass derived from fruit pulp, an industrial by-product of the juice industry, was melt-mixed with

commercial PHBV at contents from 10 to 50 wt %. The neat PHAs and resultant PHBV/P(3HB-*co*-3HV-*co*-3HHx) blends were subsequently thermo-compressed to produce films that were characterized in terms of their morphology and optical characteristics as well as thermal, mechanical, and barrier properties to evaluate their potential in food packaging applications.

2. Materials and Methods

2.1. Materials

A commercial PHBV grade, ENMAT^{TM} Y1000P, was obtained in the form of pellets from Tianan Biologic Materials (Ningbo, China). According to the manufacturer, the 3HV fraction in the copolyester is 2 mol % and the weight-average molecular weight (M_W) is ~2.8×10^5 g/mol. P(3HB-*co*-3HV-*co*-3HHx) terpolyester was produced at pilot-plant scale at Universidade NOVA (Lisboa, Portugal) using the technology of MMC fed with fermented fruit pulp supplied by Sumol+Compal S.A. (Carnaxide, Portugal), as an industrial residue of the juice industry.

$_D$-limonene, with 98 % purity, was purchased from Sigma-Aldrich S.A. (Madrid, Spain). Chloroform, stabilized with ethanol and 99.8 % purity, and sodium hydroxide (NaOH) were obtained from Panreac S.A. (Barcelona, Spain). Methyl 3-hydroxyhexanoate and heptadecane were supplied by Sigma Aldrich Química S.A. (Sintra, Portugal).

2.2. Production of P(3HB-*co*-3HV-*co*-3HHx)

The experimental setup to produce a terpolymer of P(3HB-*co*-3HV-*co*-3HHx) consisted of 3-pilot scale bioreactors inoculated with biomass from wastewater treatment plants for the microorganism selection. A 60-L up-flow anaerobic sludge blanket (UASB) reactor fed with fruit pulp waste was used to produce the precursors for PHA. This reactor was operated at hydraulic retention time (HRT) of 1 day, a temperature of 30 °C, and the pH was kept at approximately 5.0. After filtration, the effluent rich in fermentation products (FP) was fed as carbon source to the subsequent steps of the process. A sequencing batch reactor (SBR) with a volume of 100 L was fed with the FP and operated under a feast and famine regime with the goal of producing a PHA-accumulating culture. The reactor operated in 12-h cycles consisting of 11 h of aeration and 1 h of settling. The HRT and sludge retention time were set to 1 day and 4 days, respectively. PHA accumulation was carried out in a 50-L aerobic fed-batch reactor inoculated with 25 L of biomass purged from the SBR at the end of famine phase. The reactor was fed with the FP-rich effluent from the UASB reactor in a pulse-wise mode controlled by the dissolved oxygen (DO) response.

A mass with a P(3HB-*co*-3HV-*co*-3HHx) content of approximately 41 wt % was attained at the end of the accumulation assay. The terpolymer showed the following composition: 68 mol % of 3-hydroxybutyrate (3HB), 17 mol % of 3HV, and 15 mol % of 3HHx. Results were obtained by gas chromatography (GC) according to the methodology described by Lanham et al. (Lanham et al. 2013). Samples were calibrated through standard curves with a solution made of a commercial copolymer of PHBV with 12 mol % 3HV content and methyl 3-hydroxyhexanoate and heptadecane as internal standard. The M_W of the P(3HB-*co*-3HV-*co*-3HHx) was 7.90×10^5 g/mol

and the PDI 1.62, which was measured by size exclusion chromatography (SEC) as described by Rebocho et al. (Rebocho et al. 2020).

Finally, the medium-containing PHA was lyophilized. For this, the liquid material was first neutralized with a 2M solution of NaOH and then centrifuged three consecutive times at 4000 rpm for 15 min. The resultant pellet was washed gently with distilled water. The obtained material was stored at −80 °C for at least 3 h and freeze-dried for a week to produce an unpurified biomass powder containing the P(3HB-*co*-3HV-*co*-3HHx).

2.3. Extraction and Purification of P(3HB-*co*-3HV-*co*-3HHx)

The unpurified biomass containing the P(3HB-*co*-3HV-*co*-3HHx) was processed following the previously reported chloroform-based extraction and purification one-step method (Fiorese et al. 2009). For this, the biomass was dissolved in chloroform at 5 wt % and the mixture was then stirred for 24 h at 50 °C to degrade the non-PHA cellular material. Later, the solution was transferred to centrifugation tubes in which distilled water was added at 50 wt %. After shaking the tubes manually, these were centrifuged for 5 min at 4000 rpm in an Avanti J-26S XP Centrifuge with a JLA-16.250 Rotor (maximum radius: 134 mm; average radius: 90 mm; minimum radius: 46 mm, Beckman Coulter, CA, USA). Afterwards, the P(3HB-*co*-3HV-*co*-3HHx) phase was recovered from the bottom of the tubes with a pipette and transferred to beakers, leaving them in the extractor hood until the solvent was completely evaporated.

2.4. Melt Mixing

Prior to processing, both PHA resins were vacuum-dried at 60 °C for 24 h in an oven (Digitheat, JP Selecta S.A., Barcelona, Spain) to remove any residual moisture. Then, different amounts of the purified P(3HB-*co*-3HV-*co*-3HHx) powder, from 10 to 50 wt %, were manually pre-mixed with the commercial PHBV pellets in a zipper bag. Neat PHBV and P(3HB-*co*-3HV-*co*-3HHx) formulations were also prepared under identical processing conditions as control materials. **Table 1** summarizes the different formulations prepared.

Table 1. Set of formulations prepared according to the weight content (wt %) of poly(3-hydroxybutyrate-*co*-3-hydroxyvalerate) (PHBV) and poly(3-hydroxybutyrate-*co*-3-hydroxyvalerate-*co*-3-hydroxyhexanoate) [P(3HB-*co*-3HV-*co*-3HHx)].

Sample	PHBV (wt %)	P(3HB-*co*-3HV-*co*-3HHx) (wt %)
PHBV	100	0
PHBV90/P(3HB-*co*-3HV-*co*-3HHx)10	90	10
PHBV75/P(3HB-*co*-3HV-*co*-3HHx)25	75	25
PHBV50/P(3HB-*co*-3HV-*co*-3HHx)50	50	50
P(3HB-*co*-3HV-*co*-3HHx)	0	100

To prepare each sample, a total amount of 12 g of material was melt-compounded in a 16-cm^3 Brabender Plastograph Original E internal mixer from Brabender GmbH & Co. KG (Duisburg, Germany). The mixture was fed to the internal mixing chamber at a rotating speed of 60 rpm for 1 min and, after this, it was melt-mixed at 100 rpm for another 3 min. The processing temperature was set at 180 °C. Once the mixing process was completed, each batch was withdrawn from the mini-mixer and allowed to cool at room temperature. The resultant doughs were stored in dissectors containing silica gel at 0 % relative humidity (RH) and 25 °C for, at least, 48 h for conditioning.

The different doughs were, thereafter, thermo-compressed into films using a hot-plate hydraulic press (Carver 4122, Wabash, IN, USA). The samples were first placed in the plates at 180 °C for 1 min, without pressure, to ensure thermal softening of the biopolymers and then hot-pressed at 4–5 bars for 3 min. In the case of the neat P(3HB-*co*-3HV-*co*-3HHx), the temperature was reduced to 155 °C since this was the lowest molding temperature in which, after the intensive melt-mixing step, the pure material did not show signs of degradation. Flat films of 10 cm × 10 cm with a total thickness of ca. 100 μm were obtained and stored in a desiccator at 25 °C and 0 % RH for 15 days prior to characterization.

2.5. Characterization

2.5.1. Scanning Electron Microscopy

The morphologies of the film cross-sections were observed by scanning electron microscopy (SEM) using an S-4800 device from Hitachi (Tokyo, Japan). For the cross-section observations, the films were cryo-fractured by immersion in liquid nitrogen. Sample observations were performed following the conditions reported previously (Melendez-Rodriguez et al. 2019). The estimation of the dimensions was performed by means of the ImageJ software v 1.41 (National Institutes of Health, Bethesda, Maryland, USA) using a minimum of 20 SEM micrographs.

2.5.2. Transparency

The light transmission of the films was determined in specimens of 50 mm × 30 mm by quantifying the absorption of light at wavelengths between 200 and 700 nm in an ultraviolet–visible (UV–Vis) spectrophotometer VIS3000 from Dinko Instruments (Barcelona, Spain). The transparency (T) and opacity (O) were calculated using Equation (1) (Shiku et al. 2004) and Equation (2) (Kanatt et al. 2012), respectively:

$$T = \frac{A_{600}}{L} \quad (1)$$

$$O = A_{500} \times L \quad (2)$$

where A_{500} and A_{600} are the absorbance values at 500 and 600 nm, respectively, and L is the film thickness (mm).

2.5.3. Color Measurements

The color of the films was determined using a chroma meter CR-400 (Konica Minolta, Tokyo, Japan). The color difference (ΔE^*) was calculated using the following Equation (3) (Arfat et al. 2017), as defined by the Commission Internationale de l'Eclairage (CIE):

$$\Delta E^* = [(\Delta L^*)^2 + (\Delta a^*)^2 + (\Delta b^*)^2]^{0.5} \quad (3)$$

where ΔL^*, Δa^*, and Δb^* correspond to the differences in terms of lightness from black to white, color from green to red, and color from blue to yellow, respectively, between the test samples and the control sample of commercial PHBV. Color change was evaluated using the following assessment (Mokrzycki and Tatol 2011): Unnoticeable ($\Delta E^* < 1$), only an experienced observer can notice the difference ($\Delta E^* \geq 1$ and < 2), an unexperienced observer notices the difference ($\Delta E^* \geq 2$ and < 3.5), clear noticeable difference ($\Delta E^* \geq 3.5$ and < 5), and the observer notices different colors ($\Delta E^* \geq 5$).

2.5.4. Thermal Analysis

Thermal transitions of the films were studied by differential scanning calorimetry (DSC) on a DSC 8000 device from PerkinElmer, Inc. (Waltham, MA, USA), equipped with the cooling accessory Intracooler 2 from PerkinElmer, Inc. A three-step program under nitrogen atmosphere and with a flow-rate of 20 ml/min was applied: First heating from −30 to 180 °C, followed by cooling to −30 °C, and completed by a second heating to 200 °C. The heating and cooling rates were both set at 10 °C/min and the typical sample weight was ~3 mg. An empty aluminum pan was used as reference, whereas calibration was performed using an indium sample. The glass transition temperature (T_g), cold crystallization temperature (T_{cc}), enthalpy of cold crystallization (ΔH_{cc}), T_m, and enthalpy of melting (ΔH_m) were obtained from the heating scans, while the crystallization temperature from the melt (T_c) and enthalpy of crystallization (ΔH_c) were determined from the cooling scan. All DSC measurements were performed in triplicate.

Thermogravimetric analysis (TGA) was performed in a TGA-550 device (TA Instruments, New Castle, DE, USA). Film samples, with a weight of ~15 mg, were heated from 50 to 800 °C at a heating rate of 10 °C/min under a flow-rate of 50 ml/min of nitrogen (N_2). All TGA measurements were done in triplicate.

2.5.5. WAXD Experiments

Wide angle X-ray diffraction (WAXD) measurements were performed using a Bruker AXS D4 ENDEAVOR diffractometer (Billerica, MA, USA). The samples were scanned, at room temperature, in the reflection mode using incident Cu K-alpha (α) radiation (k = 1.54 Å), while the generator was set up at 40 kV and 40 mA. The data were collected over the range of scattering angles (2θ) comprised in the 2–40° range.

2.5.6. Mechanical Tests

Tensile tests were performed according to the ASTM D638 standard, using dumbbell samples (Type IV) die-cut from the hot-pressed films. Tensile tests were conducted in a universal testing machine (Shimatzu AGS-X 500N) at room temperature with a cross-head speed of 10 mm/min. Samples were conditioned for 24 h prior to analysis and the tests were performed at room conditions, that is, 40 % RH and 25 °C. A minimum of six specimens were tested for each sample.

2.5.7. Permeability Tests

The water vapor permeability (WVP) and D-limonene permeability (LP) of the films were determined following the standardized gravimetric method ASTM E96-95. To do this, Payne permeability cups of 3.5 cm from Elcometer Sprl (Hermallesous-Argenteau, Belgium) were used. Both tests were performed at 25 °C in triplicate, and further details can be found elsewhere (Melendez-Rodriguez et al. 2019).

The oxygen permeability coefficient was derived from the oxygen transmission rate (OTR) measurements that were recorded at 60 % RH and 25 °C, in duplicate, using an Oxygen Permeation Analyzer M8001 (Systech Illinois, Thame, UK). The humidity equilibrated samples were purged with nitrogen, before exposure to an oxygen flow of 10 ml/min. The exposure area during the test was 5 cm^2 for each sample. In order to obtain the oxygen permeability (OP), film thickness and gas partial pressure were considered.

2.6. Statistical Analysis

The optical, thermal, mechanical, and barrier properties were evaluated through analysis of variance (ANOVA) using STATGRAPHICS Centurion XVI v 16.1.03 from StatPoint Technologies, Inc. (Warrenton, VA, USA). Fisher's least significant difference (LSD) was used at the 95 % confidence level ($p < 0.05$). Mean values and standard deviations were also reported.

3. Results and Discussion

3.1. Morphology

The morphology of the film cross-sections was observed by SEM and the images are gathered in **Figure 1**. It can be observed that all the films presented a smooth and featureless fracture surface, without significant plastic deformation, indicating a typical brittle fracture behavior. Moreover, both good mixture and compatibility between the two PHAs were expected to be attained since no indications of phase segregation were observed, even at the highest P(3HB-*co*-3HV-*co*-3HHx) content, that is, 50 wt %. However, the film fracture surfaces of the PHBV-based materials revealed the presence of some microparticles, which can be ascribed to nucleating agents added by the manufacturer, such as boron nitride (Ivorra-Martinez, Quiles-Carrillo, et al. 2020). In the case of the neat P(3HB-*co*-3HV-*co*-3HHx), one can observe the presence of some impurities in

the form of small lumps, which can be related to organic traces of cell debris or fatty acids derived from the bioproduction process of P(3HB-*co*-3HV-*co*-3HHx). Similar observations were previously reported in blends made of commercial PHB and food waste derived PHBV (Melendez-Rodriguez et al. 2019). Also, Martinez-Abad et al. (Martínez-Abad, Cabedo, et al. 2016) observed, for PHBV/unpurified PHBV blends, a good degree of interaction between the two PHAs with small amounts of impurities related to the biowaste polymer. Therefore, it can be concluded that both the commercial PHBV and the food waste derived P(3HB-*co*-3HV-*co*-3HHx) presented good miscibility since both biopolymers share a majority of 3HB content.

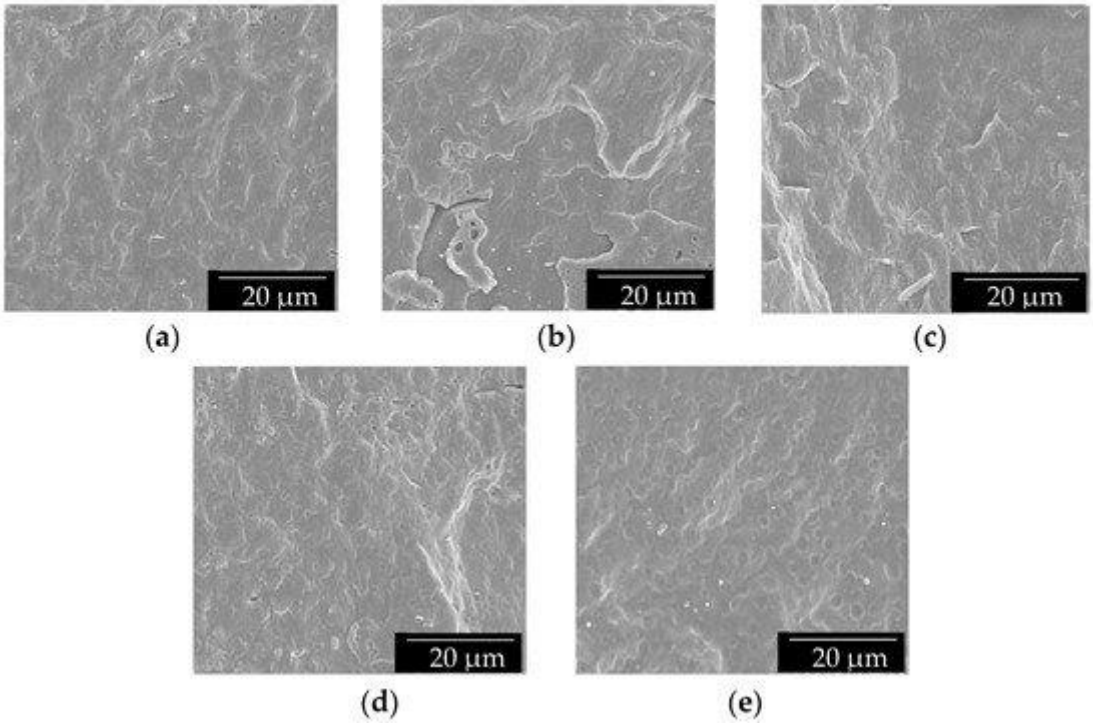

Figure 1. Scanning electron microscopy (SEM) images of the cross-sections of the thermo-compressed films made of poly(3-hydroxybutyrate-*co*-3-hydroxyvalerate) (PHBV) and poly(3-hydroxybutyrate-*co*-3-hydroxyvalerate-*co*-3-hydroxyhexanoate) [P(3HB-*co*-3HV-*co*-3HHx)]: (**a**) PHBV; (**b**) PHBV90/P(3HB-*co*-3HV-*co*-3HHx)10; (**c**) PHBV75/P(3HB-*co*-3HV-*co*-3HHx)25; (**d**) PHBV50/P(3HB-*co*-3HV-*co*-3HHx)50; (**e**) P(3HB-*co*-3HV-*co*-3HHx). Images were taken at 2000x with scale markers of 20 µm.

3.2. Optical Properties

Figure 2 displays the visual aspect of the films to assess their optical properties. Simple naked eye examination of this figure indicates that all the film samples were slightly opaque, but they also showed good contact transparency with a brownish yellow color. For the film samples with the highest concentrations in P(3HB-*co*-3HV-*co*-3HHx), that is, 50 wt % and, especially, for the neat terpolymer film, small brown lumps can be observed in the material. These structures can be related to small impurities of the fruit juice based on cellulose that remained after the purification process and could develop a somewhat darker color due to processing. This result points out that additional efforts in the development of alternative more efficient purification processes will be required in the future for the optimal performance of these biopolymers.

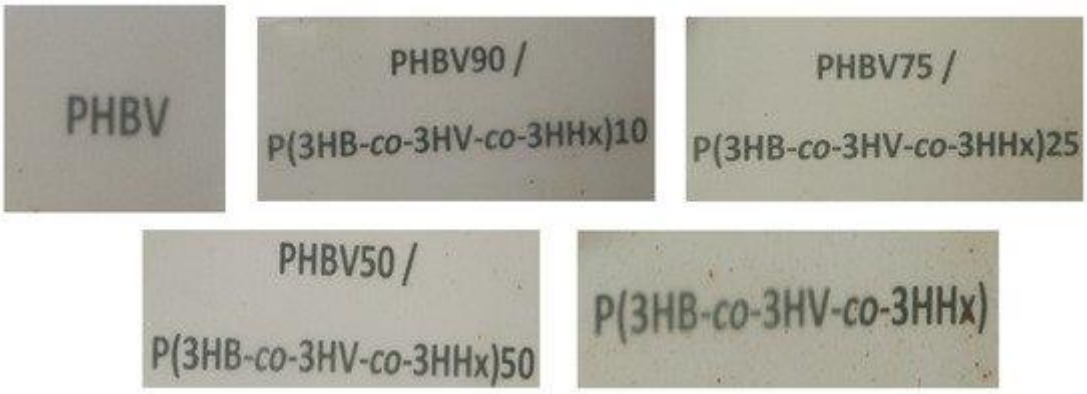

Figure 2. Contact transparency images of the thermo-compressed films of poly(3-hydroxybutyrate-*co*-3-hydroxyvalerate) (PHBV), poly(3-hydroxybutyrate-*co*-3-hydroxyvalerate-*co*-3-hydroxyhexanoate) [P(3HB-*co*-3HV-*co*-3HHx)], and their blends.

To quantify the color change resulting from the addition of P(3HB-*co*-3HV-*co*-3HHx) to PHBV, the color coordinates (a^*, b^*, L^*) and the values of ΔE^*, T, and O were determined and reported in **Table 2**. From this, it can be observed that all the film samples presented similar values for the a^*, b^* and L^* coordinates, with a tendency to green and yellow color, confirming the brownish color of the blends. The incorporation of P(3HB-*co*-3HV-*co*-3HHx) into the films slightly altered the color properties, being the differences still significant. However, the L^* values were not significantly different except for the neat P(3HB-*co*-3HV-*co*-3HHx) film, which was the darkest sample. In any case, the color differences in the composite films containing different amounts of P(3HB-*co*-3HV-*co*-3HHx) with respect to the neat PHBV were relatively low, that is, $\Delta E^* \geq 1$ and < 2, which means that only an experienced observer could notice the difference. As opposite, the neat P(3HB-*co*-3HV-*co*-3HHx) film presented a higher AE^* value, near to 5, hence, there was a clear noticeable difference with the control sample. It can also be noticed that all the blend films presented similar transparency and opacity that the neat PHBV, except the pure P(3HB-*co*-3HV-*co*-3HHx), which presented the highest transparency with a value of approximately 2.9. The latter value can be related to a lower degree of crystallinity, as it will be discussed below. Although light colors may seem an advantage for use in packaging, slightly brownish color in the films may act as an UV barrier to prevent light-induced lipids oxidation, which is also important in food applications (Gómez-Guillén et al. 2007).

Table 2. Color parameters (a^*, b^*, L^*, and ΔE^*) and transparency (T) and opacity (O) values of the thermo-compressed films of poly(3-hydroxybutyrate-*co*-3-hydroxyvalerate) (PHBV), poly(3-hydroxybutyrate-*co*-3-hydroxyvalerate-*co*-3-hydroxyhexanoate) [P(3HB-*co*-3HV-*co*-3HHx)], and their blends.

Film	a^*	b^*	L^*	ΔE^*	T	O
PHBV	$-0.46 \pm 0.07^{a,d}$	5.58 ± 0.20^{a}	88.25 ± 0.10^{a}	-	9.55 ± 0.35^{a}	0.11 ± 0.07^{a}
PHBV90/P(3HB-*co*-3HV-*co*-3HHx)10	$-0.56 \pm 0.03^{a,c}$	6.92 ± 0.30^{b}	87.52 ± 0.14^{a}	1.53 ± 0.18^{a}	8.10 ± 0.42^{b}	0.10 ± 0.03^{a}
PHBV75/P(3HB-*co*-3HV-*co*-3HHx)25	-0.19 ± 0.02^{b}	3.70 ± 0.09^{c}	88.59 ± 0.30^{a}	1.93 ± 0.11^{a}	$9.29 \pm 0.38^{a,c}$	0.11 ± 0.04^{a}
PHBV50/P(3HB-*co*-3HV-*co*-3HHx)50	-0.69 ± 0.04^{c}	4.72 ± 0.07^{d}	88.29 ± 0.22^{a}	0.89 ± 0.07^{c}	$8.64 \pm 0.33^{b,c}$	0.11 ± 0.04^{a}
P(3HB-*co*-3HV-*co*-3HHx)	-0.36 ± 0.02^{d}	7.84 ± 0.10^{e}	83.83 ± 0.52^{b}	4.97 ± 0.21^{d}	2.85 ± 0.19^{d}	0.15 ± 0.05^{a}

a^*: red/green coordinates (+a red, −a green); b^*: yellow/blue coordinates (+b yellow, −b blue); L^*: Luminosity (+L luminous, −L dark); ΔE*: color differences; T: transparency; O: opacity.

$^{a–e}$ Different letters in the same column indicate a significant difference among the samples ($p < 0.05$).

3.3. Thermal Properties

Figure 3 displays the DSC thermograms of the film samples obtained during the first heating, cooling, and second heating. The summary of the main thermal transitions obtained from the DSC curves are gathered in **Table S1**, which is available in the Supporting Information. One can observe that the film samples showed a glass transition region with T_g at approximately 1.7 and 0.2 °C for the neat PHBV and P(3HB-*co*-3HV-*co*-3HHx) films, respectively, whereas intermediate values in the range of 1.4–0.6 °C were attained for their blends, suggesting intercomponent miscibility. During the first heating, the neat PHBV presented an endothermic peak with two components, with maximum at 178 °C and a ΔH_m value of 74 J/g. The blends with different contents in P(3HB-*co*-3HV-*co*-3HHx) presented the maximum of melting in the range of 169–174 °C with ΔH_m values of 74 and 68 J/g for the film samples with 10 and 25 wt % of terpolymer, respectively, whereas the films with 50 wt % of terpolymer showed a value of 43 J/g. As it can also be observed in the DSC curves, the neat P(3HB-*co*-3HV-*co*-3HHx) presented a very complex melting behavior, exhibiting the highest endothermic peaks at 111 °C, ascribed to the lowest crystalline density fractions of the terpolymer (Doi, Kitamura, and Abe 1995, Ivorra-Martinez, Manuel-Mañogil, et al. 2020), and at 173 °C, for the most thermodynamically stable 3HB-rich fractions (Vahabi et al. 2019); and having a whole ΔH_m value of 33 J/g. Thus, in the blend samples, a drop in T_m and ΔH_m was generally observed when P(3HB-*co*-3HV-*co*-3HHx) was incorporated into PHBV.

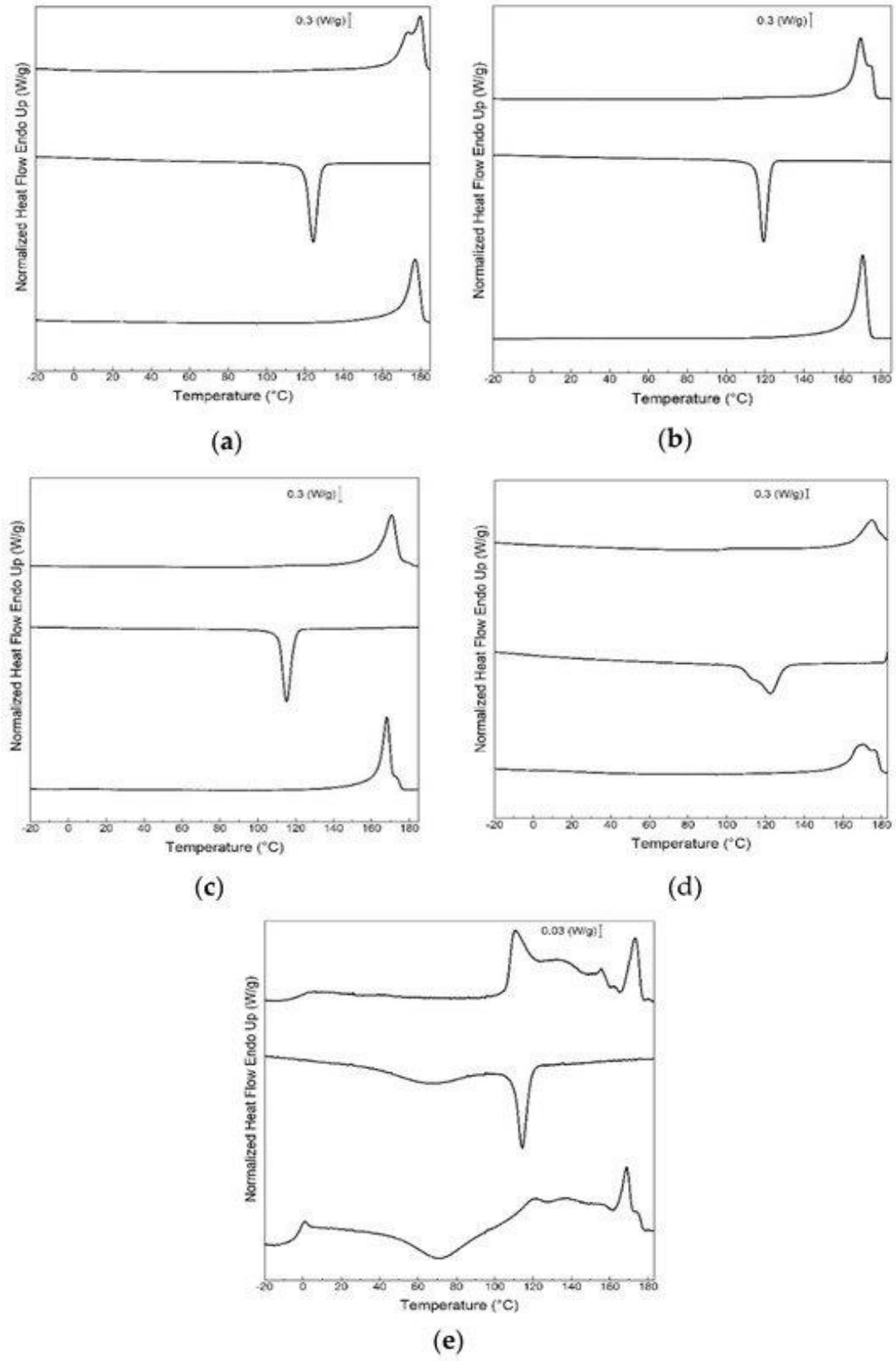

Figure 3. Differential scanning calorimetry (DSC) curves during first heating, cooling, and second heating of the thermo-compressed films of: (a) Neat poly(3-hydroxybutyrate-*co*-3-hydroxyvalerate) (PHBV); (b) PHBV90/P(3HB-*co*-3HV-*co*-3HHx)10; (c) PHBV75/P(3HB-*co*-3HV-*co*-3HHx)25; (d) PHBV50/P(3HB-*co*-3HV-*co*-3HHx)50; (e) neat poly(3-hydroxybutyrate-*co*-3-hydroxyvalerate-*co*-3-hydroxyhexanoate) [P(3HB-*co*-3HV-*co*-3HHx)].

Regarding the cooling step, the samples with terpolymer contents up to 25 wt % crystallized from the melt in a single peak. However, for higher contents and, especially for the pure terpolymer, multiple broader crystallization events were observed. The neat PHBV showed a T_c at 123 °C, while their blends with P(3HB-*co*-3HV-*co*-3HHx) exhibited less intense T_c peaks that also shifted to lower values, in the 115–119 °C range. In the case of the neat P(3HB-*co*-3HV-*co*-3HHx), this film sample showed two clear crystallization peaks. The first one, which is ascribed to the 3HB-rich crystalline fractions (Cai and Qiu 2009, Vandewijngaarden et al. 2016), appeared in the form of a sharp peak at 114 °C and the other, as a broader peak and at the lower temperature of 65 °C, being ascribed to other crystalline fractions within the terpolymer requiring higher undercooling to crystallize. Moreover, the neat P(3HB-*co*-3HV-*co*-3HHx) showed a clear exothermic cold crystallization event during the second heating step, with T_{cc} at approximately 72 °C. In the second heating run, the blend samples were seen to present a reduction in ΔH_m. In particular, whereas the neat PHBV showed a value of 85 J/g, the blends presented values of 76, 66, and 51 J/g for terpolymer contents of 10, 25 and 50 wt %, respectively. In the case of the neat P(3HB-*co*-3HV-*co*-3HHx), it showed the lowest ΔH_m, having a value of 24 J/g, which confirms the lowest and most ill-defined crystallinity for this sample. The reduction in crystallinity, inferred from the lower ΔH_m, in the terpolymer can be attributed to the other two terpolymer fractions impairing the crystallization of the 3HB fractions (Zhao and Chen 2007). Since both PHAs were highly miscible, this factor may add further disturbance to the molecular lateral order of the terpolymer. In this regard, Kai et al. (Kai, Ying, and Guo-Qiang 2003) reported a decrease in the crystallization degree and crystallization rate of PHB when P(3HB-*co*-3HHx) was introduced into the blends. Qu et al. (Qu et al. 2006) also showed a decrease in crystallinity with increasing 3HHx content in the P(3HB-*co*-3HHx) copolyester due to the diluting effect of the 3HHx component on the crystallinity of the 3HB parts. Furthermore, a decrease in crystallinity has been previously reported for other miscible polymer systems. For example, polylactide (PLA) melt-compounded with oligomer of lactic acid (OLA) also showed a reduction in the T_m values with respect to the neat PLA (Rojas-Lema et al. 2020). In particular, the oligomer impaired crystallization by inhibiting the correct packing of the PLA chains, although it also enhanced its mobility due to a plasticizing effect.

3.4. Crystallinity

The crystalline phase was also studied by WAXD experiments on the PHA films. The diffractograms, included in **Figure 4**, revealed two main peaks located at 13.6 and 17.0° 2θ, corresponding to the (020) and (110) lattice planes of the orthorhombic unit cell of PHB (Sato et al. 2012). These intense peaks were followed by three other minor reflections centered at approximately 22.6, 25.8, and 26.9° 2θ, which originate from (111), (121), and (040) lattice planes (Panaitescu et al. 2017, Vahabi et al. 2019). The diffraction peaks found here agree well with those reported in the literature, where the crystal lattice of PHBV with 3HV contents below 30 mol % corresponds to the unit cell of PHB (Škrbić and Divjaković 1996). In regard to the terpolymer, the same PHB orthorhombic lattice was seen to dominate the diffractogram. This is in agreement with other studies where P(3HB-*co*-3HHx) with less than 25 mol % of HHx was seen to present a dominant PHB lattice, with slightly different *d*-spacing in the peaks than those of the homopolymer (Sato et al. 2004, Xie, Noda, and Akpalu 2008). Therefore, all the blends presented a similar diffractogram with the characteristic peaks of the PHB lattice. However, by looking at the right diffractograms in **Figure 4**, the peaks associated to the (200) and (110) planes clearly shifted towards lower 2θ angles for terpolymer contents above 10 mol %. This finding

suggests that a significant lower crystalline density of PHB crystals was produced in the blends with increasing the terpolymer content in excess of 10 mol %. The strongest peak observed in the neat PHBV and PHBV-containing blends at 2θ around 27° is attributed to the boron nitride used as a nucleating agent in commercial formulations (Öner et al. 2018), which was not observed in the food waste derived P(3HB-*co*-3HV-*co*-3HHx). In any case, the lower relative intensity of the peaks with respect to the amorphous halo suggests a lower crystallinity in the terpolymer than in the neat PHBV, which agrees with the DSC measurements shown above. This trend was also visible for the blends, having more crystallinity those with higher PHBV contents and being especially noticeable for the one with 50 wt % loading of the terpolymer.

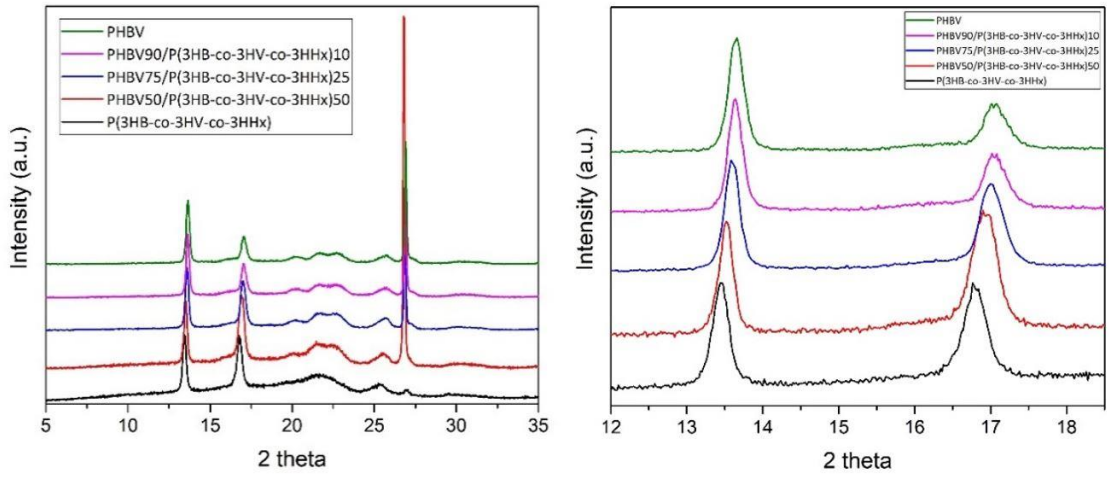

Figure 4. Wide angle X-ray diffraction (WAXD) patterns in the 2theta (2θ) ranges 5–35° (left) and 12–18.5° (right), from top to bottom, of the thermo-compressed films of: Neat poly(3-hydroxybutyrate-*co*-3-hydroxyvalerate) (PHBV); PHBV90/P(3HB-*co*-3HV-*co*-3HHx)10; PHBV75/P(3HB-*co*-3HV-*co*-3HHx)25; PHBV50/P(3HB-*co*-3HV-*co*-3HHx)50; and neat poly(3-hydroxybutyrate-*co*-3-hydroxyvalerate-*co*-3-hydroxyhexanoate) [P(3HB-*co*-3HV-*co*-3HHx)]. The data was normalized to the intensity of the (020) peak and shifted along the *Y*-axis for comparison purposes.

3.5. Thermal Stability

The thermal stability of the film samples was evaluated by TGA experiments. **Figure 5** shows the TGA curves of the different films and in **Table 3** are gathered the most relevant parameters obtained from the TGA curves. From Figure 5a, it can be observed that the thermal degradation of both neat materials took place in a single step according to a random chain scission mechanism. This process is known to lead to a reduction in M_W and formation of volatile acid products such as crotonic acid (Bhardwaj et al. 2006), showing degradation temperatures (T_{deg}) of 286 and 266 °C for neat PHBV and P(3HB-*co*-3HV-*co*-3HHx), respectively, in agreement with literature values (Ferreira, Zavaglia, and Duek 2001, Hu et al. 2009). In relation to the onset-degradation temperature (T_{onset}), defined as the temperature at 5 % weight loss, the terpolymer showed lower stability compared to PHBV, particularly a reduction from 243 to 235 °C (Zhao and Chen 2007). The blend films presented a T_{onset} in the range of 239–243 °C, decreasing with an increase of the

P(3HB-*co*-3HV-*co*-3HHx) content. As it can be seen in Figure 5b, their T_{deg} occurred in the range of 281–286 °C for the samples with lower P(3HB-*co*-3HV-*co*-3HHx) content, that is, 10 and 25 wt %, and approximately at 267 °C for the 50/50 blend. Thus, the thermal stability of the melt-mixed blends was slightly reduced with increasing the P(3HB-*co*-3HV-*co*-3HHx) content compared with PHBV, showing lower T_{onset} and T_{deg} values. This decrease in the thermal resistance can be attributed to the impurities that remained in the terpolyester and could not be removed during the purification process. In this sense, it has been reported that the presence of fermentation residues in PHA can accelerate its thermal degradation mechanisms (Hablot et al. 2008). Finally, the amount of residual mass was below 1 % for all the samples, showing the neat P(3HB-*co*-3HV-*co*-3HHx) the lowest value, that is, 0.2 %. This difference in the residual mass of the commercial polymer with respect to the terpolymer can be attributed to the presence of the inorganic nucleating agents, as previously observed by SEM and also confirmed by WAXD.

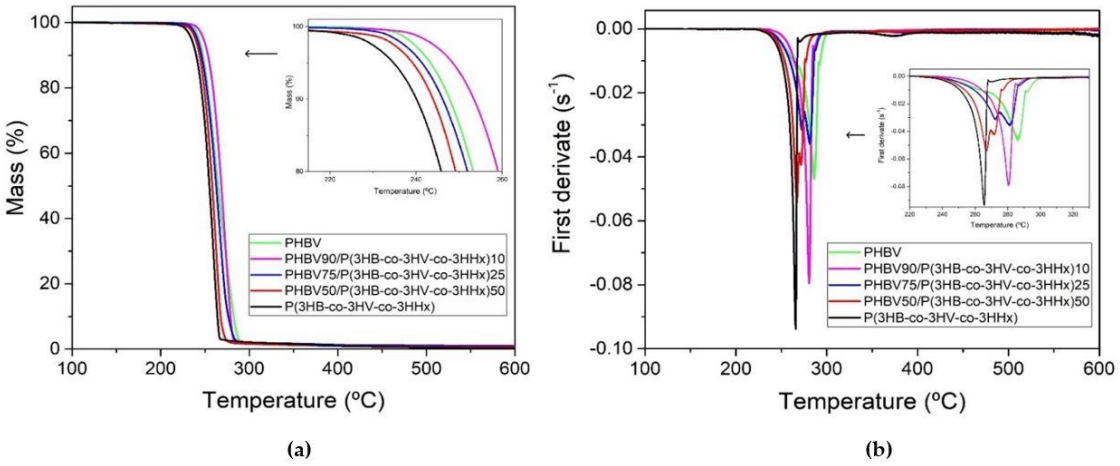

Figure 5. (a) Thermogravimetric analysis (TGA) and (b) first derivative (DTG) curves of the thermo-compressed films of poly(3-hydroxybutyrate-*co*-3-hydroxyvalerate) (PHBV), poly(3-hydroxybutyrate-*co*-3-hydroxyvalerate-*co*-3-hydroxyhexanoate) [P(3HB-*co*-3HV-*co*-3HHx)], and their blends.

Table 3. Main thermogravimetric analysis (TGA) parameters of the thermo-compressed films of poly(3-hydroxybutyrate-*co*-3-hydroxyvalerate) (PHBV), poly(3-hydroxybutyrate-*co*-3-hydroxyvalerate-*co*-3-hydroxyhexanoate) [P(3HB-*co*-3HV-*co*-3HHx)], and their blends in terms of: Onset temperature of degradation ($T_{5\%}$), degradation temperature (T_{deg}), mass loss at T_{deg}, and residual mass at 800 °C.

Film	$T_{5\%}$ (°C)	T_{deg} (°C)	Mass loss (%)	Residual mass (%)
PHBV	243.3 ± 1.2[a]	286.2 ± 0.9[a]	95.4 ± 0.8[a]	1.0 ± 0.2[a]
PHBV90/P(3HB-*co*-3HV-*co*-3HHx)10	242.5 ± 1.5[a]	280.5 ± 1.2[b]	94.6 ± 1.0[a]	0.8 ± 0.1[a]
PHBV75/P(3HB-*co*-3HV-*co*-3HHx)25	241.4 ± 1.8[a, b]	281.1 ± 1.3[b]	95.3 ± 0.9[a]	0.9 ± 0.2[a]
PHBV50/P(3HB-*co*-3HV-*co*-3HHx)50	239.2 ± 1.3[b]	267.1 ± 1.1[c]	88.3 ± 1.2[b]	0.7 ± 0.2[a]
P(3HB-*co*-3HV-*co*-3HHx)	234.8 ± 1.2[c]	265.5 ± 1.6[c]	94.5 ± 1.1[a]	0.2 ± 0.1[b]

[a-c] Different letters in the same column indicate a significant difference among the samples ($p < 0.05$).

3.6. Mechanical Properties

Figure 6 gathers the results of the tensile test results conducted on the thermo-compressed films of PHBV and P(3HB-*co*-3HV-*co*-3HHx). Figure 6a plots the main mechanical parameters obtained in the tests, while Figure 6b presents a representative stress–strain curve as obtained from the tensile tests for each of the compositions studied.

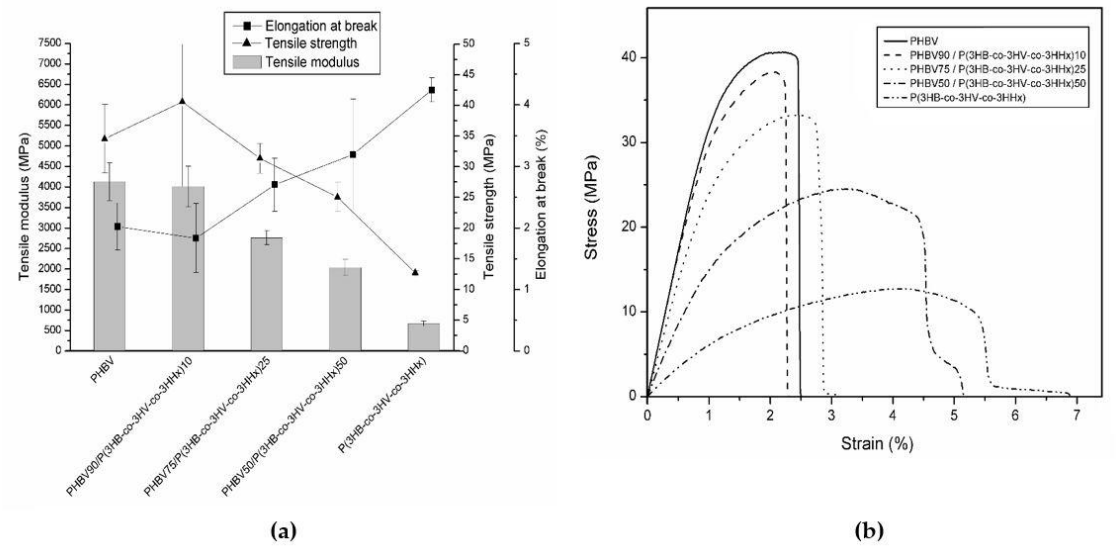

Figure 6. (a) Mechanical properties of the thermo-compressed films of poly(3-hydroxybutyrate-*co*-3-hydroxyvalerate) (PHBV), poly(3-hydroxybutyrate-*co*-3-hydroxyvalerate-*co*-3-hydroxyhexanoate) [P(3HB-*co*-3HV-*co*-3HHx)], and their blends in terms of: tensile modulus, tensile strength, and elongation at break. (b) Their corresponding tensile stress–strain curves.

From Figure 6a, it can be seen that PHBV was a stiff material, presenting an elastic modulus at room temperature above 4 GPa and a tensile strength of approximately 35 MPa. However, the neat PHBV also exhibited a brittle behavior with an elongation-at-break value of around 2 %, which occurred prior to yielding, as it can be observed in Figure 6b. The intrinsic brittleness of PHBV has been widely reported in the scientific literature and ascribed to its crystalline nature (Sanchez-Safont, Cabedo, and Gamez-Perez 2021). As oppose to this, P(3HB-*co*-3HV-*co*-3HHx) presented much lower elastic modulus and tensile strength than PHBV, while it also exhibited a lower brittle fracture after yielding with an elongation at break above 4 %. This behavior is in accordance with previous works (Zhao and Chen 2007). For instance, Bhubalan et al. (Bhubalan et al. 2010) reported that, due to interference with the crystallization process, the higher the 3HHx fraction in the terpolymer, the higher the increase in flexibility. As it can be seen in Figure 6a, the mechanical properties of the blend films were in between those of the neat PHAs. This result means that a good interaction between both materials was achieved (Martínez-Abad, González-Ausejo, et al. 2016). Thus, the tensile modulus of the blends ranged from almost 4 GPa, for the composition having a 10 wt % of terpolymer, to 2 GPa for the 50/50 blend. With respect to the tensile strength, a similar decreasing trend with the incorporation of the terpolymer was seen. Regarding ductility, an increase in the elongation at break with increasing terpolymer content was

observed. This change in the mechanical response, i.e., from a rigid but fragile to a more ductile behavior, of the PHBV after melt mixing with P(3HB-*co*-3HV-*co*-3HHx), can also be spotted in the stress–strain curves in Figure 6b. From this Figure 6b, the film sample containing 50 wt % of the terpolymer was seen to exhibit a post-yielding fracture.

3.7. Barrier Performance

Table 4 gathers the WVP, LP, and OP values of the thermo-compressed films based on PHBV and P(3HB-*co*-3HV-*co*-3HHx). The barrier properties to gases and vapors of packaging materials play a key role in food quality and shelf-life extension aspects. The neat PHBV film presented good barrier properties to both vapors and the gas with values of 1.2×10^{-15} kg·m·m^{-2}·Pa^{-1}·s^{-1}, 1.7×10^{-15} kg·m·m^{-2}·Pa^{-1}·s^{-1}, and 1.6×10^{-19} m^3·m·m^{-2}·Pa^{-1}·s^{-1} for WVP, LP, and OP, respectively. On the contrary and as expected, the barrier performance of the P(3HB-*co*-3HV-*co*-3HHx) film was significantly lower, especially to the aroma component, with values of 7.3×10^{-15} kg·m·m^{-2}·Pa^{-1}·s^{-1}, 18.4×10^{-15} kg·m·m^{-2}·Pa^{-1}·s^{-1}, and 5.2×10^{-19} m^3·m·m^{-2}·Pa^{-1}·s^{-1} for WVP, LP, and OP, respectively. In relation to the blends, it can be observed that these films presented a barrier performance in between the pristine polymers. In particular, the values of permeability ranged between $1.3–3.4 \times 10^{-15}$ kg·m·m^{-2}·Pa^{-1}·s^{-1}, $1.8–3.7 \times 10^{-15}$ kg·m·m^{-2}·Pa^{-1}·s^{-1}, and $2.7–3.6 \times 10^{-19}$ m^3·m·m^{-2}·Pa^{-1}·s^{-1}, respectively. In spite of the clear decrease in barrier properties, all the permeability values of the blend films were still within the same order of magnitude as the neat PHBV film.

Table 4. Water vapor permeability (WVP), D-limonene permeability (LP), and oxygen permeability (OP) of the thermo-compressed films of poly(3-hydroxybutyrate-*co*-3-hydroxyvalerate) (PHBV), poly(3-hydroxybutyrate-*co*-3-hydroxyvalerate-*co*-3-hydroxyhexanoate) [P(3HB-*co*-3HV-*co*-3HHx)], and their blends.

Film	WVP × 10^{15} (kg·m·m^{-2}·Pa^{-1}·s^{-1})	LP × 10^{15} (kg·m·m^{-2}·Pa^{-1}·s^{-1})	OP x 10^{19} (kg·m·m^{-2}·Pa^{-1}·s^{-1})
PHBV	1.19 ± 0.08^{a}	1.73 ± 0.22^{a}	1.60 ± 0.24^{a}
PHBV90/P(3HB-*co*-3HV-*co*-3HHx)10	1.27 ± 0.14^{a}	1.80 ± 0.15^{a}	2.69 ± 0.38^{b}
PHBV75/P(3HB-*co*-3HV-*co*-3HHx)25	2.42 ± 0.41^{b}	2.03 ± 0.21^{a}	3.34 ± 0.51^{b}
PHBV50/P(3HB-*co*-3HV-*co*-3HHx)50	3.39 ± 0.33^{c}	3.65 ± 0.44^{b}	$3.61 \pm 0.47^{b,c}$
P(3HB-*co*-3HV-*co*-3HHx)	7.29 ± 0.89^{d}	18.4 ± 6.9^{c}	5.16 ± 1.05^{c}

[a-d] Different letters in the same column indicate a significant difference among the samples ($p < 0.05$).

The barrier decrease is attributed to the above-described lower crystallinity of P(3HB-*co*-3HV-*co*-3HHx) and potentially also due to the biomass impurities remaining in the terpolymer and its blends. In particular, the higher crystallinity observed for PHBV can be responsible for the lower values of OP since oxygen is a non-interacting and non-condensable permeant which permeability is driven by diffusion. As a result, the higher the crystallinity, the higher the material density and the lower the fraction of the amorphous phase, resulting in lower free volume and higher tortuosity for the gas molecules to diffuse through. Limonene, which is known to be a strong plasticizer for

PHAs and highly sorbed into the amorphous regions of this biopolymer, showed values of nearly 13 wt% of uptake in solvent-cast films (Sanchez-Garcia, Gimenez, and Lagaron 2008). In comparison to PHB films also prepared by compression molding, similar WVP and LP values as the here-obtained PHBV film were reported, that is, 1.8 and 2.0 × 10^{-15} kg·m·m^{-2}·Pa^{-1}·s^{-1}, respectively (Cherpinski et al. 2017). In terms of OP, similar values were also obtained, that is, 2.2 × 10^{-19} m^3·m·m^{-2}·Pa^{-1}·s^{-1} (Sanchez-Garcia, Gimenez, and Lagaron 2007). For compression-molded PHBV films with 12 mol % 3HV, the values for WVP, LP, and OP were higher than the ones obtained here, that is, 6.9 × 10^{-15} kg·m·m^{-2}·Pa^{-1}·s^{-1}, 1.9 × 10^{-13} kg·m·m^{-2}·Pa^{-1}·s^{-1}, and 15.7 × 10^{-19} m^3·m·m^{-2}·Pa^{-1}·s^{-1}, respectively (Sanchez-Garcia, Gimenez, and Lagaron 2007).

Furthermore, barrier properties within the same order of magnitude as the ones measured in this study, were previously reported for other PHA blends. For example, Martinez-Abad (Martínez-Abad, Cabedo, et al. 2016) reported no significant changes in water and limonene permeabilities when blending commercial PHBV with unpurified food waste derived PHBV at contents up to 15 wt %, above which there was a slight decrease. More similar barrier results to the ones measured here were found when commercial PHB was blended with PHBV obtained using MMC, where a lower barrier performance was observed with respect to the neat homopolyester. Thus, the WPV and LP values increased from 1.8 and 1.9 × 10^{-15} kg·m·m^{-2}·Pa^{-1}·s^{-1}, for neat PHB, to 7.5 and 5.0 × 10^{-15} kg·m·m^{-2}·Pa^{-1}·s^{-1}, for the blend obtained with the highest food waste derived PHBV content, that is, 50 wt % (Melendez-Rodriguez et al. 2019). Finally, the barrier values obtained here are in the same range of those of polyethylene terephthalate (PET) films, with WVP and OP values of 2.3 × 10^{-15} kg·m·m^{-2}·Pa^{-1}·s^{-1} and 1.4 × 10^{-19} m^3·m·m^{-2}·Pa^{-1}·s^{-1}, respectively (Lagaron, Catalá, and Gavara 2004). As expected, the blends also presented higher barrier in terms of OP than low-density polyethylene (LDPE) films, with an OP value of 2.15 × 10^{-17} m^3·m·m^{-2}·Pa^{-1}·s^{-1}, but, of course, lower than the high-barrier ethylene–vinyl alcohol copolymer (EVOH), with OP at 0.77 × 10^{-21} m^3·m·m^{-2}·Pa^{-1}·s^{-1} (Lagaron, Catalá, and Gavara 2004). Moreover, the present PHA blends showed higher barrier properties than other biopolyesters. For example, PLA and PBAT films prepared by thermo-compression presented values of 12.3 and 33.1 × 10^{-15} kg·m·m^{-2}·Pa^{-1}·s^{-1}, for WVP, and 3.3 and 72.6 × 10^{-15} kg·m·m^{-2}·Pa^{-1}·s^{-1}, for LP, respectively (Quiles-Carrillo et al. 2019). Films of these two biopolymers showed also higher OP values, that is, 2.2 and 9.1 × 10^{-18} m^3·m·m^{-2}·Pa^{-1}·s^{-1}, respectively (Quiles-Carrillo et al. 2019).

4. Conclusions

A new PHA terpolymer, P(3HB-*co*-3HV-*co*-3HHx), was produced from MMCs fed with fruit pulp biowaste with a comonomer content of ca. 68 mol % 3HB, 17 mol % 3HV, and 15 mol % 3HHx. The terpolymer was extracted and purified using a previously developed one-step method and, thereafter, melt-mixed in contents of up to 50 wt % with commercial PHBV. The morphological analysis revealed good interpolymer miscibility and good optical properties, in spite of the presence of remnant impurities. From the DSC and WAXS results, the lateral molecular order and density were inferred to be reduced, but the crystalline morphology remained that of the PHB crystals across composition. The thermal stability of the blends was not substantially affected by the incorporation of the food waste derived terpolymer. On the other hand, the materials were seen to be more flexible than the neat rigid PHBV film as a result of the

plasticizing effect brought in by the terpolymer. The permeability to water and limonene vapors and oxygen gas was reduced in the blends, particularly for limonene, but remained within the same order of magnitude.

Therefore, this research study demonstrates further the potential of PHA blends that make use of potentially lower cost PHAs derived from Circular Bioeconomy strategies to constitute novel packaging materials, which will profit from the more sustainable organic recycling end-of-life scenario. In particular, the PHA blends prepared herein can be used, depending on composition, to constitute rigid or semirigid packaging articles, such as injection-molded and thermoformed monolayer articles, and also in disposables, such as plates and trays, which can be organic recycled in industrial and home composting or, even, that will be able to biodegrade in soil or marine environments. Future studies will focus on the development of novel polymers with further enhanced flexibility by increasing the comonomer content, and in alternative purification methodologies that can achieve higher purity using water-based systems.

5. Supporting Information

Table S1. DSC parameters of the thermo-compressed films made of poly(3-hydroxybutyrate-*co*-3-hydroxyvalerate) (PHBV) and poly(3-hydroxybutyrate-*co*-3-hydroxyvalerate-*co*-3-hydroxyhexanoate) [P(3HB-*co*-3HV-*co*-3HHx)] in terms of: glass transition temperature (T_g), melting temperature (T_m), enthalpy of melting (ΔH_m), crystallization temperature (T_c), enthalpy of crystallization (ΔH_c), cold crystallization temperature (T_{cc}), and enthalpy of the cold crystallization (ΔH_{cc}).

Film	First heating			Cooling				Second heating				
	T_g (°C)	T_m (°C)	ΔH_m (J/g)	T_{c1} (°C)	T_{c2} (°C)	ΔH_{c1} (J/g)	ΔH_{c2} (J/g)	T_g (°C)	T_{cc} (°C)	ΔH_{cc} (J/g)	T_m (°C)	ΔH_m (J/g)
PHBV	1.7 ± 0.2^{a}	177.6 ± 3.1^{a}	74.4 ± 8.0^{a}	-	122.7 ± 2.1^{a}	-	81.6 ± 1.7^{a}	1.6 ± 0.1^{a}	-	-	174.5 ± 3.7^{a}	85.2 ± 6.7^{a}
PHBV90/ P(3HB-*co*-3HV-*co*-3HHx)10	1.4 ± 0.3^{a}	169.3 ± 2.4^{b}	74.4 ± 9.4^{a}	-	119.2 ± 0.3^{b}	-	74.4 ± 3.6^{b}	1.2 ± 0.2^{a}	-	-	170.4 ± 0.1^{a}	76.4 ± 3.9^{a}
PHBV75/ P(3HB-*co*-3HV-*co*-3HHx)25	0.7 ± 0.2^{b}	170.6 ± 0.4^{b}	68.2 ± 6.2^{a}	-	115.1 ± 0.1^{c,d}	-	64.4 ± 2.7^{c}	0.6 ± 0.1^{b}	-	-	168.1 ± 0.1^{b}	65.5 ± 4.3^{b}
PHBV50/ P(3HB-*co*-3HV-*co*-3HHx)50	0.6 ± 0.1^{b}	174.4 ± 0.9^{a}	43.2 ± 5.4^{b}	-	118.9 ± 2.0^{b,d}	-	50.8 ± 2.3^{d}	0.5 ± 0.1^{b}	-	-	166.6 ± 3.3^{b}	50.5 ± 2.1^{c}
P(3HB-*co*-3HV-*co*-3HHx)	0.2 ± 0.1^{c}	110.5 ± 1.3^{c} // 173.3 ± 1.8^{a,b}	33.4 ± 0.2^{c}	65.2 ± 1.2	114.4 ± 3.3^{d}	2.8 ± 0.4	6.9 ± 2.5^{e}	0.6 ± 0.1^{b}	71.5 ± 3.2	15.1 ± 1.6	119.7 ± 0.8^{c} // 168.7 ± 1.4^{b}	24.4 ± 1.7^{d}

$^{a-d}$ Different letters in the same column indicate a significant difference among the samples ($p < 0.05$).

6. References

Alfei, S., A. M. Schito, and G. Zuccari. 2021. "Biodegradable and compostable shopping bags under investigation by ftir spectroscopy." *Applied Sciences (Switzerland)* 11 (2):1-18. doi: 10.3390/app11020621.

Arfat, Y. A., J. Ahmed, N. Hiremath, R. Auras, and A. Joseph. 2017. "Thermo-mechanical, rheological, structural and antimicrobial properties of bionanocomposite films based on fish skin gelatin and silver-copper nanoparticles." *Food Hydrocolloids* 62:191-202. doi: 10.1016/j.foodhyd.2016.08.009.

Arumugam, A., T. Anudakshaini, R. Shruthi, K. Jeyavishnu, S. S. Harini, and J. Sharad. 2019. "Low-cost production of PHA using cashew apple (Anacardium occidentale L.) juice as potential substrate: optimization and characterization." *Biomass Conversion and Biorefinery*:1-12.

Babu, R. P., K. O'Connor, and R. Seeram. 2013. "Current progress on bio-based polymers and their future trends." *Prog. Biomater.* 2 (8):1-16.

Barnes, D. K. A., F. Galgani, R. C. Thompson, and M. Barlaz. 2009. "Accumulation and fragmentation of plastic debris in global environments." *Philosophical Transactions of the Royal Society B: Biological Sciences* 364 (1526):1985-1998. doi: 10.1098/rstb.2008.0205.

Bengtsson, S., A. Werker, M. Christensson, and T. Welander. 2008. "Production of polyhydroxyalkanoates by activated sludge treating a paper mill wastewater." *Bioresource Technology* 99 (3):509-516. doi: 10.1016/j.biortech.2007.01.020.

Bhardwaj, R., A. K. Mohanty, L. T. Drzal, F. Pourboghrat, and M. Misra. 2006. "Renewable resource-based green composites from recycled cellulose fiber and poly(3-hydroxybutyrate-co-3-hydroxyvalerate) bioplastic." *Biomacromolecules* 7 (6):2044-2051. doi: 10.1021/bm050897y.

Bhubalan, K., D. N. Rathi, H. Abe, T. Iwata, and K. Sudesh. 2010. "Improved synthesis of P(3HB-co-3HV-co-3HHx) terpolymers by mutant Cupriavidus necator using the PHA synthase gene of Chromobacterium sp. USM2 with high affinity towards 3HV." *Polymer Degradation and Stability* 95 (8):1436-1442. doi: 10.1016/j.polymdegradstab.2009.12.018.

Bosco, F., and F. Chiampo. 2010. "Production of polyhydroxyalcanoates (PHAs) using milk whey and dairy wastewater activated sludge. Production of bioplastics using dairy residues." *Journal of Bioscience and Bioengineering* 109 (4):418-421. doi: 10.1016/j.jbiosc.2009.10.012.

Brandl, H., E. J. Knee Jr, R. C. Fuller, R. A. Gross, and R. W. Lenz. 1989. "Ability of the phototrophic bacterium Rhodospirillum rubrum to produce various poly (β-hydroxyalkanoates): Potential sources for biodegradable polyesters." *International Journal of Biological Macromolecules* 11 (1):49-55. doi: 10.1016/0141-8130(89)90040-8.

Cai, H., and Z. Qiu. 2009. "Effect of comonomer content on the crystallization kinetics and morphology of biodegradable poly(3-hydroxybutyrate-co-3-hydroxyhexanoate)." *Physical Chemistry Chemical Physics* 11 (41):9569-9577. doi: 10.1039/b907677h.

Chan, C. M., L. J. Vandi, S. Pratt, P. Halley, Y. Ma, G. Q. Chen, D. Richardson, A. Werker, and B. Laycock. 2019. "Understanding the effect of copolymer content on the processability and mechanical properties of polyhydroxyalkanoate (PHA)/wood composites."

Composites Part A: Applied Science and Manufacturing 124. doi: 10.1016/j.compositesa.2019.05.005.

Cherpinski, A., S. Torres-Giner, L. Cabedo, and J. M. Lagaron. 2017. "Post-processing optimization of electrospun submicron poly(3-hydroxybutyrate) fibers to obtain continuous films of interest in food packaging applications." *Food Additives and Contaminants - Part A Chemistry, Analysis, Control, Exposure and Risk Assessment* 34 (10):1817-1830. doi: 10.1080/19440049.2017.1355115.

Choe, S., Y. J. Cha, H. S. Lee, J. S. Yoon, and H. J. Choi. 1995. "Miscibility of poly(3-hydroxybutyrate-co-3-hydroxyvalerate) and poly(vinyl chloride) blends." *Polymer* 36 (26):4977-4982. doi: 10.1016/0032-3861(96)81624-7.

Choi, J. I., and S. Y. Lee. 1997. "Process analysis and economic evaluation for poly(3-hydroxybutyrate) production by fermentation." *Bioprocess Engineering* 17 (6):335-342. doi: 10.1007/s004490050394.

Dionisi, D., G. Carucci, M. Petrangeli Papini, C. Riccardi, M. Majone, and F. Carrasco. 2005. "Olive oil mill effluents as a feedstock for production of biodegradable polymers." *Water Research* 39 (10):2076-2084. doi: 10.1016/j.watres.2005.03.011.

Dobrucka, R. 2019. "Bioplastic packaging materials in circular economy." *Logforum* 15 (1):129-137. doi: 10.17270/J.LOG.2019.322.

Doi, Y., S. Kitamura, and H. Abe. 1995. "Microbial Synthesis and Characterization of Poly(3-hydroxybutyrate-co-3-hydroxyhexanoate)." *Macromolecules* 28 (14):4822-4828. doi: 10.1021/ma00118a007.

Duque, A. F., C. S. S. Oliveira, I. T. D. Carmo, A. R. Gouveia, F. Pardelha, A. M. Ramos, and M. A. M. Reis. 2014. "Response of a three-stage process for PHA production by mixed microbial cultures to feedstock shift: Impact on polymer composition." *New Biotechnology* 31 (4):276-288. doi: 10.1016/j.nbt.2013.10.010.

Ferreira, B. M. P., C. A. C. Zavaglia, and E. A. R. Duek. 2001. "Films of poly(L-lactic acid)/poly(hydroxybutyrate-co-hydroxyvalerate) blends: In vitro degradation." *Mater Res* 4 (1):34-42.

Fiorese, M. L., F. Freitas, J. Pais, A. M. Ramos, G. M. F. De Aragão, and M. A. M. Reis. 2009. "Recovery of polyhydroxybutyrate (PHB) from Cupriavidus necator biomass by solvent extraction with 1,2-propylene carbonate." *Engineering in Life Sciences* 9 (6):454-461. doi: 10.1002/elsc.200900034.

Furukawa, T., H. Sato, R. Murakami, J. Zhang, I. Noda, S. Ochiai, and Y. Ozaki. 2007. "Comparison of miscibility and structure of poly(3-hydroxybutyrate-co-3-hydroxyhexanoate)/poly(l-lactic acid) blends with those of poly(3-hydroxybutyrate)/poly(l-lactic acid) blends studied by wide angle X-ray diffraction, differential scanning calorimetry, and FTIR microspectroscopy." *Polymer* 48 (6):1749-1755. doi: 10.1016/j.polymer.2007.01.020.

Gómez-Guillén, M. C., M. Ihl, V. Bifani, A. Silva, and P. Montero. 2007. "Edible films made from tuna-fish gelatin with antioxidant extracts of two different murta ecotypes leaves (Ugni molinae Turcz)." *Food Hydrocolloids* 21 (7):1133-1143. doi: 10.1016/j.foodhyd.2006.08.006.

Hablot, E., P. Bordes, E. Pollet, and L. Avérous. 2008. "Thermal and thermo-mechanical degradation of poly(3-hydroxybutyrate)-based multiphase systems." *Polymer Degradation and Stability* 93 (2):413-421. doi: 10.1016/j.polymdegradstab.2007.11.018.

Hassan, M. A., Y. Shirai, N. Kusubayashi, M. I. A. Karim, K. Nakanishi, and K. Hashimoto. 1996. "Effect of organic acid profiles during anaerobic treatment of palm oil mill effluent

on the production of polyhydroxyalkanoates by Rhodobacter sphaeroides." *Journal of Fermentation and Bioengineering* 82 (2):151-156. doi: 10.1016/0922-338X(96)85038-0.

Haywood, G. W., A. J. Anderson, D. Roger Williams, E. A. Dawes, and D. F. Ewing. 1991. "Accumulation of a poly(hydroxyalkanoate) copolymer containing primarily 3-hydroxyvalerate from simple carbohydrate substrates by Rhodococcus sp. NCIMB 40126." *International Journal of Biological Macromolecules* 13 (2):83-88. doi: 10.1016/0141-8130(91)90053-W.

Hu, Y. J., X. Wei, W. Zhao, Y. S. Liu, and G. Q. Chen. 2009. "Biocompatibility of poly(3-hydroxybutyrate-co-3-hydroxyvalerate-co-3-hydroxyhexanoate) with bone marrow mesenchymal stem cells." *Acta Biomaterialia* 5 (4):1115-1125. doi: 10.1016/j.actbio.2008.09.021.

Ivorra-Martinez, J., J. Manuel-Mañogil, T. Boronat, L. Sanchez-Nacher, R. Balart, and L. Quiles-Carrillo. 2020. "Development and characterization of sustainable composites from bacterial polyester poly(3-hydroxybutyrate-co-3-hydroxyhexanoate) and almond shell flour by reactive extrusion with oligomers of lactic acid." *Polymers* 12 (5). doi: 10.3390/POLYM12051097.

Ivorra-Martinez, J., L. Quiles-Carrillo, T. Boronat, S. Torres-Giner, and J. A. Covas. 2020. "Assessment of the mechanical and thermal properties of injection-molded poly(3-hydroxybutyrate-co-3-hydroxyhexanoate)/hydroxyapatite nanoparticles parts for use in bone tissue engineering." *Polymers* 12 (6). doi: 10.3390/polym12061389.

Ji, Y., X. T. Li, and G. Q. Chen. 2008. "Interactions between a poly(3-hydroxybutyrate-co-3-hydroxyvalerate-co-3-hydroxyhexanoate) terpolyester and human keratinocytes." *Biomaterials* 29 (28):3807-3814. doi: 10.1016/j.biomaterials.2008.06.008.

Jung, H. R., J. M. Jeon, D. H. Yi, H. S. Song, S. Y. Yang, T. R. Choi, S. K. Bhatia, J. J. Yoon, Y. G. Kim, C. J. Brigham, and Y. H. Yang. 2019. "Poly(3-hydroxybutyrate-co-3-hydroxyvalerate-co-3-hydroxyhexanoate) terpolymer production from volatile fatty acids using engineered Ralstonia eutropha." *International Journal of Biological Macromolecules* 138:370-378. doi: 10.1016/j.ijbiomac.2019.07.091.

Kai, Z., D. Ying, and C. Guo-Qiang. 2003. "Effects of surface morphology on the biocompatibility of polyhydroxyalkanoates." *Biochemical Engineering Journal* 16 (2):115-123. doi: 10.1016/S1369-703X(03)00029-9.

Kanatt, S. R., M. S. Rao, S. P. Chawla, and A. Sharma. 2012. "Active chitosan-polyvinyl alcohol films with natural extracts." *Food Hydrocolloids* 29 (2):290-297. doi: 10.1016/j.foodhyd.2012.03.005.

Khumwanich, P., S. C. Napathorn, and B. B. Suwannasilp. 2014. "Polyhydroxyalkanoate production with a feast/famine feeding regime using sludge from wastewater treatment plants of the food and beverage industry." *Journal of Biobased Materials and Bioenergy* 8 (6):641-647. doi: 10.1166/jbmb.2014.1476.

Koller, M., R. Bona, G. Braunegg, C. Hermann, P. Horvat, M. Kroutil, J. Martinz, J. Neto, L. Pereira, and P. Varila. 2005. "Production of polyhydroxyalkanoates from agricultural waste and surplus materials." *Biomacromolecules* 6 (2):561-565. doi: 10.1021/bm049478b.

Koyama, T., S. Tanoue, Y. Iemoto, T. Maekawa, and T. Unryu. 2009. "Melt compounding of various polymers with organoclay by shear flow." *Polymer Composites* 30 (8):1065-1073. doi: 10.1002/pc.20657.

Lagaron, J. M., R. Catalá, and R. Gavara. 2004. "Structural characteristics defining high barrier properties in polymeric materials." *Materials Science and Technology* 20 (1):1-7. doi: 10.1179/026708304225010442.

Lanham, A. B., A. R. Ricardo, M. G. E. Albuquerque, F. Pardelha, M. Carvalheira, M. Coma, J. Fradinho, G. Carvalho, A. Oehmen, and M. A. M. Reis. 2013. "Determination of the extraction kinetics for the quantification of polyhydroxyalkanoate monomers in mixed microbial systems." *Process Biochemistry* 48 (11):1626-1634. doi: 10.1016/j.procbio.2013.07.023.

Liang, Y. S., W. Zhao, and G. Q. Chen. 2008. "Study on the biocompatibility of novel terpolyester poly(3-hydroxybutyrate- co-3-hydroxyvalerate-co-3-hydroxyhexanoate)." *Journal of Biomedical Materials Research - Part A* 87 (2):441-449. doi: 10.1002/jbm.a.31801.

Madison, L. L., and G. W. Huisman. 1999. "Metabolic engineering of poly(3-hydroxyalkanoates): From DNA to plastic." *Microbiology and Molecular Biology Reviews* 63 (1):21-53. doi: 10.1128/mmbr.63.1.21-53.1999.

Martínez-Abad, A., L. Cabedo, C. S. S. Oliveira, L. Hilliou, M. Reis, and J. M. Lagarón. 2016. "Characterization of polyhydroxyalkanoate blends incorporating unpurified biosustainably produced poly(3-hydroxybutyrate-co-3-hydroxyvalerate)." *Journal of Applied Polymer Science* 133 (2). doi: 10.1002/app.42633.

Martínez-Abad, A., J. González-Ausejo, J. M. Lagarón, and L. Cabedo. 2016. "Biodegradable poly(3-hydroxybutyrate-co-3-hydroxyvalerate)/thermoplastic polyurethane blends with improved mechanical and barrier performance." *Polymer Degradation and Stability* 132:52-61. doi: 10.1016/j.polymdegradstab.2016.03.039.

Martínez-Sanz, M., M. Villano, C. Oliveira, M. G. E. Albuquerque, M. Majone, M. Reis, A. Lopez-Rubio, and J. M. Lagaron. 2014. "Characterization of polyhydroxyalkanoates synthesized from microbial mixed cultures and of their nanobiocomposites with bacterial cellulose nanowhiskers." *New Biotechnology* 31 (4):364-376. doi: 10.1016/j.nbt.2013.06.003.

Melendez-Rodriguez, B., S. Torres-Giner, A. Aldureid, L. Cabedo, and J. M. Lagaron. 2019. "Reactive melt mixing of poly(3-hydroxybutyrate)/rice husk flour composites with purified biosustainably produced poly(3-hydroxybutyrate-co-3-hydroxyvalerate)." *Materials* 12 (13). doi: 10.3390/ma12132152.

Mitomo, H., P. J. Barham, and H. Morimoto. 1987. "Crystallization and morphology of poly(β-hydroxybutyrate) and its copolymer." *Polymer Journal* 19 (11):1241-1253. doi: 10.1295/polymj.19.1241.

Mokrzycki, W. S., and M. Tatol. 2011. "Colour difference δE - A survey." *Machine Graphics and Vision* 20 (4):383-411.

Nerkar, M., J. A. Ramsay, B. A. Ramsay, and M. Kontopoulou. 2014. "Melt Compounded Blends of Short and Medium Chain-Length Poly-3-hydroxyalkanoates." *Journal of Polymers and the Environment* 22 (2):236-243. doi: 10.1007/s10924-013-0635-6.

Nishida, M., T. Tanaka, Y. Hayakawa, T. Ogura, Y. Ito, and M. Nishida. 2019. "Multi-scale instrumental analyses of plasticized polyhydroxyalkanoates (PHA) blended with polycaprolactone (PCL) and the effects of crosslinkers and graft copolymers." *RSC Advances* 9 (3):1551-1561. doi: 10.1039/C8RA10045D.

Öner, M., G. Kızıl, G. Keskin, C. Pochat-Bohatier, and M. Bechelany. 2018. "The effect of boron nitride on the thermal and mechanical properties of poly(3-hydroxybutyrate-co-3-hydroxyvalerate)." *Nanomaterials* 8 (11). doi: 10.3390/nano8110940.

Panaitescu, D. M., C. A. Nicolae, A. N. Frone, I. Chiulan, P. O. Stanescu, C. Draghici, M. Iorga, and M. Mihailescu. 2017. "Plasticized poly(3-hydroxybutyrate) with improved melt processing and balanced properties." *Journal of Applied Polymer Science* 134 (19). doi: 10.1002/app.44810.

Papa, G., T. Pepè Sciarria, A. Carrara, B. Scaglia, G. D'Imporzano, and F. Adani. 2020. "Implementing polyhydroxyalkanoates production to anaerobic digestion of organic fraction of municipal solid waste to diversify products and increase total energy recovery." *Bioresource Technology* 318. doi: 10.1016/j.biortech.2020.124270.

Park, S. J., W. S. Ahn, P. R. Green, and S. Y. Lee. 2001. "Biosynthesis of poly(3-hydroxybutyrate-co-3-hydroxyvalerate-co-3-hydroxyhexanoate) by metabolically engineered Escherichia coli strains." *Biotechnology and Bioengineering* 74 (1):81-86. doi: 10.1002/bit.1097.

Peng, S., Y. An, C. Chen, B. Fei, Y. Zhuang, and L. Dong. 2003. "Miscibility and Crystallization Behavior of Poly(3-hydroxyvalerate-co-3-hydroxyvalerate)/ Poly(propylene carbonate) Blends." *Journal of Applied Polymer Science* 90 (14):4054-4060. doi: 10.1002/app.12970.

Qu, X. H., Q. Wu, J. Liang, B. Zou, and G. Q. Chen. 2006. "Effect of 3-hydroxyhexanoate content in poly(3-hydroxybutyrate-co-3- hydroxyhexanoate) on in vitro growth and differentiation of smooth muscle cells." *Biomaterials* 27 (15):2944-2950. doi: 10.1016/j.biomaterials.2006.01.013.

Quiles-Carrillo, L., N. Montanes, J. M. Lagaron, R. Balart, and S. Torres-Giner. 2019. "In Situ Compatibilization of Biopolymer Ternary Blends by Reactive Extrusion with Low-Functionality Epoxy-Based Styrene–Acrylic Oligomer." *Journal of Polymers and the Environment* 27 (1):84-96. doi: 10.1007/s10924-018-1324-2.

RamKumar Pandian, S., V. Deepak, K. Kalishwaralal, N. Rameshkumar, M. Jeyaraj, and S. Gurunathan. 2010. "Optimization and fed-batch production of PHB utilizing dairy waste and sea water as nutrient sources by Bacillus megaterium SRKP-3." *Bioresource Technology* 101 (2):705-711. doi: 10.1016/j.biortech.2009.08.040.

Rebocho, A. T., J. R. Pereira, L. A. Neves, V. D. Alves, C. Sevrin, C. Grandfils, F. Freitas, and M. A. M. Reis. 2020. "Preparation and characterization of films based on a natural p(3hb)/mcl-pha blend obtained through the co-culture of cupriavidus necator and pseudomonas citronellolis in apple pulp waste." *Bioengineering* 7 (2). doi: 10.3390/bioengineering7020034.

Rehm, B. H. A. 2003. "Polyester synthases: Natural catalysts for plastics." *Biochemical Journal* 376 (1):15-33. doi: 10.1042/BJ20031254.

Reiser, S. E., T. A. Mitsky, and K. J. Gruys. 2000. "Characterization and cloning of an (R)-specific trans-2,3-enoylacyl-CoA hydratase from Rhodospirillum rubrum and use of this enzyme for PHA production in Escherichia coli." *Applied Microbiology and Biotechnology* 53 (2):209-218. doi: 10.1007/s002530050010.

Rojas-Lema, S., L. Quiles-Carrillo, D. Garcia-Garcia, B. Melendez-Rodriguez, R. Balart, and S. Torres-Giner. 2020. "Tailoring the properties of thermo-compressed polylactide films for food packaging applications by individual and combined additions of lactic acid oligomer and halloysite nanotubes." *Molecules* 25 (8). doi: 10.3390/molecules25081976.

Sanchez-Garcia, M. D., E. Gimenez, and J. M. Lagaron. 2007. "Novel PET Nanocomposites of Interest in Food Packaging Applications and Comparative Barrier Performance With Biopolyester Nanocomposites." *Journal of Plastic Film & Sheeting* 23 (2):133-148. doi: 10.1177/8756087907083590.

Sanchez-Garcia, M. D., E. Gimenez, and J. M. Lagaron. 2008. "Morphology and barrier properties of solvent cast composites of thermoplastic biopolymers and purified cellulose fibers." *Carbohydrate Polymers* 71 (2):235-244. doi: 10.1016/j.carbpol.2007.05.041.

Sánchez-Safont, E. L., A. Aldureid, J. M. Lagarón, J. Gamez-Perez, and L. Cabedo. 2020. "Effect of the Purification Treatment on the Valorization of Natural Cellulosic Residues as Fillers

in PHB-Based Composites for Short Shelf Life Applications." *Waste Biomass Valorization* 1.

Sanchez-Safont, E. L., L. Cabedo, and J. Gamez-Perez. 2021. "Cellulose-Reinforced Biocomposites Based on PHB and PHBV for Food Packaging Applications." *Sustainable Food Packaging Technology*:225-261.

Sarasini, F., F. Luzi, F. Dominici, G. Maffei, A. Iannone, A. Zuorro, R. Lavecchia, L. Torre, A. Carbonell-Verdu, R. Balart, and D. Puglia. 2018. "Effect of different compatibilizers on sustainable composites based on a PHBV/PBAT matrix filled with coffee silverskin." *Polymers* 10 (11). doi: 10.3390/polym10111256.

Sato, H., M. Nakamura, A. Padermshoke, H. Yamaguchi, H. Terauchi, S. Ekgasit, I. Noda, and Y. Ozaki. 2004. "Thermal behavior and molecular interaction of poly(3-hydroxybutyrate-co-3- hydroxyhexanoate) studied by wide-angle X-ray diffraction." *Macromolecules* 37 (10):3763-3769. doi: 10.1021/ma049863t.

Sato, H., N. Suttiwijitpukdee, T. Hashimoto, and Y. Ozaki. 2012. "Simultaneous synchrotron SAXS/WAXD study of composition fluctuations, cold-crystallization, and melting in biodegradable polymer blends of cellulose acetate butyrate and poly(3-hydroxybutyrate)." *Macromolecules* 45 (6):2783-2795. doi: 10.1021/ma202606y.

Savenkova, L., Z. Gercberga, I. Bibers, and M. Kalnin. 2000. "Effect of 3-hydroxy valerate content on some physical and mechanical properties of polyhydroxyalkanoates produced by Azotobacter chroococcum." *Process Biochemistry* 36 (5):445-450. doi: 10.1016/S0032-9592(00)00235-1.

Shiku, Y., P. Y. Hamaguchi, S. Benjakul, W. Visessanguan, and M. Tanaka. 2004. "Effect of surimi quality on properties of edible films based on Alaska pollack." *Food Chemistry* 86 (4):493-499. doi: 10.1016/j.foodchem.2003.09.022.

Škrbić, Ž, and V. Divjaković. 1996. "Temperature influence on changes of parameters of the unit cell of biopolymer PHB." *Polymer* 37 (3):505-507. doi: 10.1016/0032-3861(96)82922-3.

Torres-Giner, S., K. J. Figueroa-Lopez, B. Melendez-Rodriguez, C. Prieto, M. Pardo-Figuerez, and J. M. Lagaron. 2021. "Emerging Trends in Biopolymers for Food Packaging." *Sustainable Food Packaging Technology*:1-33.

Torres-Tello, E. V., J. R. Robledo-Ortíz, Y. González-García, A. A. Pérez-Fonseca, C. F. Jasso-Gastinel, and E. Mendizábal. 2017. "Effect of agave fiber content in the thermal and mechanical properties of green composites based on polyhydroxybutyrate or poly(hydroxybutyrate-co-hydroxyvalerate)." *Industrial Crops and Products* 99:117-125. doi: 10.1016/j.indcrop.2017.01.035.

Tripathi, A. D., A. Yadav, A. Jha, and S. K. Srivastava. 2012. "Utilizing of Sugar Refinery Waste (Cane Molasses) for Production of Bio-Plastic Under Submerged Fermentation Process." *Journal of Polymers and the Environment* 20 (2):446-453. doi: 10.1007/s10924-011-0394-1.

Vahabi, H., L. Michely, G. Moradkhani, V. Akbari, M. Cochez, C. Vagner, E. Renard, M. R. Saeb, and V. Langlois. 2019. "Thermal stability and flammability behavior of poly(3-hydroxybutyrate) (PHB) based composites." *Materials* 12 (14). doi: 10.3390/ma12142239.

Vandewijngaarden, J., R. Wauters, M. Murariu, P. Dubois, R. Carleer, J. Yperman, J. D'Haen, B. Ruttens, S. Schreurs, N. Lepot, R. Peeters, and M. Buntinx. 2016. "Poly(3-hydroxybutyrate-co-3-hydroxyhexanoate)/Organomodified Montmorillonite Nanocomposites for Potential Food Packaging Applications." *Journal of Polymers and the Environment* 24 (2):104-118. doi: 10.1007/s10924-016-0751-1.

Verma, D., and K. L. Goh. 2018. "Functionalized Graphene-Based Nanocomposites for Energy Applications." In *Functionalized Graphene Nanocomposites and Their Derivatives: Synthesis, Processing and Applications*, 219-243.

Winnacker, M. 2019. "Polyhydroxyalkanoates: Recent Advances in Their Synthesis and Applications." *European Journal of Lipid Science and Technology* 121 (11). doi: 10.1002/ejlt.201900101.

Xie, Y., I. Noda, and Y. A. Akpalu. 2008. "Influence of cooling rate on the thermal behavior and solid-state morphologies of polyhydroxyalkanoates." *Journal of Applied Polymer Science* 109 (4):2259-2268. doi: 10.1002/app.28278.

Ye, H. M., Z. Wang, H. H. Wang, G. Q. Chen, and J. Xu. 2010. "Different thermal behaviors of microbial polyesters poly(3-hydroxybutyrate-co-3-hydroxyvalerate-co-3-hydroxyhexanoate) and poly(3-hydroxybutyrate-co-3-hydroxyhexanoate)." *Polymer* 51 (25):6037-6046. doi: 10.1016/j.polymer.2010.10.030.

Zembouai, I., S. Bruzaud, M. Kaci, A. Benhamida, Y. M. Corre, Y. Grohens, and J. M. Lopez-Cuesta. 2014. "Synergistic effect of Compatibilizer and cloisite 30B on the functional properties of poly(3-hydroxybutyrateco- 3-hydroxyvalerate)/Polylactide blends." *Polymer Engineering and Science* 54 (10):2239-2251. doi: 10.1002/pen.23776.

Zembouai, I., S. Bruzaud, M. Kaci, A. Benhamida, Y. M. Corre, Y. Grohens, A. Taguet, and J. M. Lopez-Cuesta. 2014. "Poly(3-Hydroxybutyrate-co-3-Hydroxyvalerate)/Polylactide Blends: Thermal Stability, Flammability and Thermo-Mechanical Behavior." *Journal of Polymers and the Environment* 22 (1):131-139. doi: 10.1007/s10924-013-0626-7.

Zhang, H. F., L. Ma, Z. H. Wang, and G. Q. Chen. 2009. "Biosynthesis and characterization of 3-hydroxyalkanoate terpolyesters with adjustable properties by Aeromonas hydrophila." *Biotechnology and Bioengineering* 104 (3):582-589. doi: 10.1002/bit.22409.

Zhao, W., and G. Q. Chen. 2007. "Production and characterization of terpolyester poly(3-hydroxybutyrate-co-3-hydroxyvalerate-co-3-hydroxyhexanoate) by recombinant Aeromonas hydrophila 4AK4 harboring genes phaAB." *Process Biochemistry* 42 (9):1342-1347. doi: 10.1016/j.procbio.2007.07.006.

Block III: Development of barrier multilayer systems based on PHA

Chapter VIII

Barrier Biopaper Multilayers Obtained by Impregnation of Electrospun Poly(3-hydroxybutyrate-*co*-3-hydroxyvalerate) with Protein and Polysaccharide Hydrocolloids

Carbohydrate Polymer Technologies and Applications 2021, 100150

Beatriz Meléndez-Rodríguez[1], Marie-Stella M'Bengue[1,†], Sergio Torres-Giner[1,‡], Luis Cabedo[2], Cristina Prieto[1], and José María Lagarón[1]

[1] Novel Materials and Nanotechnology Group, Institute of Agrochemistry and Food Technology (IATA), Spanish Council for Scientific Research (CSIC), Paterna, Spain

[2] Polymers and Advanced Materials Group (PIMA), School of Technology and Experimental Sciences, Universitat Jaume I (UJI), Castellón, Spain

[†] On leave from Grenoble INP – Pagora, UGA, International School of Paper, Print Media and Biomaterials, Saint-Martin d'Hères Cedex, France

[‡] This author is currently with the Research Institute of Food Engineering for Development (IIAD), Universitat Politècnica de València (UPV), Valencia, Spain

Abstract

Multilayer biopapers composed of two electrospun layers of poly(3-hydroxybutyrate-*co*-3-hydroxyvalerate) (PHBV) were impregnated, at the inner side of one of the layers, with cellulose nanocrystals (CNCs) and their composites with hydrocolloids, to develop high-barrier fully biobased structures. The study aimed for the first time at comparing the impregnation of electrospun fibers with several biopolymer solutions. Thus, neat CNCs, and CNCs mixed as a minor fraction, that is, 2 wt %, with gelatin (GE), agar (AG), xanthan gum (XG), and gum arabic (GA) were assessed in their potential to improve the barrier properties of PHBV. Glycerol plasticizer was added to the composite formulations. The impregnated electrospun multilayer mats were subsequently annealed, below the PHBV melting point, to yield continuous films by an interfiber coalescence process, so-called biopapers, and thereafter characterized to evaluate their potential for high barrier food packaging applications. The morphological characterization revealed good interlayer adhesion, more noticeably for those containing CNCs and their nanocomposites with AG and XG. From their mechanical response, it was inferred that the material behavior was governed mainly by the rigidity of the PHBV substrates, and this could not be significantly improved by impregnation with any of the various hydrocolloids. Whereas the water vapor barrier was not seen to improve in any of the samples, the barrier to the organic vapor limonene, used as a standard for aroma barrier, was however improved in the samples impregnated with AG and XG composites. Interestingly, the oxygen barrier properties were significantly improved but only by impregnation with pure CNCs. This study reports for the first time a scalable impregnation technology approach to produce fully biobased barrier multilayers.

Keywords: Nanocellulose; PHBV; additives; multilayers; gas barrier; food packaging

1. Introduction

In a context of global environmental problems, a change of perspective towards the use of petroleum derived materials has been gaining relevance in recent decades. The massive production of plastics, about 360 million tons per year, in combination to their non-biodegradable nature represent a serious end-of-life management problem (Geyer, Jambeck, and Law 2017). Every year, around eight billion kilograms of plastic waste reach the oceans from the coast, being 40 % of which single-use items (Commission 2018). Thus, the use of bio-based, biodegradable, and eco-friendly polymers as substitutes for traditional petrochemical ones is becoming increasingly important.

In this regard, cellulose is of great interest due to its biodegradability and abundancy (Huber et al. 2012). Cellulose is a polysaccharide composed of β-D-glucose subunits, which is found mainly in plant cell walls, but also in the tissues of algae and in the epidermal cell membrane of tunicates. Moreover, it can also be synthesized by bacteria (Zhao et al. 2017). Among the cellulose derivatives, cellulose nanomaterials (CNMs) have gained relevance based on their lack of toxicity and high-mechanical and -barrier properties (Mokhena and John 2020). In this regard, cellulose nanocrystals (CNCs) have received significant interest due to its high surface area and aspect ratio, exceptional optical transparency, unique morphology, and the possibilities for surface modification (Trache et al. 2020). As mentioned, CNCs present high-gas barrier by forming a dense hydrogen bonded self-associated network of crystals, leading to a reduced free volume, and hence preventing the passage of gas molecules. This makes CNCs very attractive for use in food packaging structures, where they could help extending food shelf-life by reducing oxygen permeation (Ahankari et al. 2021).

However, despite the previous advantages, CNCs possess some drawbacks for their use in food packaging applications, such as their moisture sensitivity and brittleness after dehydration (Aulin, Gällstedt, and Lindström 2010). Therefore, the use of plasticizers is considered as a good alternative to enhance CNCs processability. Thus, glycerol, which has shown to improve mechanical properties such as flexibility and elasticity of polymer films (Li et al. 2018, Tong, Xiao, and Lim 2013), has been used as a plasticizer for cellulose-based materials, decreasing their stiffness and increasing their elongation at break. For instance, Xiao et al. (Xiao et al. 2003) reported an increase in elongation at break, from 6.9 to 25.4 %, in regenerated cellulose films when glycerol was added. However, glycerol also decreases the barrier properties because it intercepts the hydrogen bonding between the nanocellulose chains, facilitating the permeability of the gas molecules (Hubbe et al. 2017). Thus, a balance must be found between good plasticizing efficiency and gas barrier properties.

One feasible strategy is to combine CNCs with other high-gas-barrier biopolymers, which include proteins, such as gelatin (GE), or polysaccharides, such as agar (AG), xanthan gum (XG), and gum arabic (GA). Among them, GE is a cost-effective water-soluble protein derived from collagen (Clarke et al. 2016, Nur Hanani, Roos, and Kerry 2012). It is abundant in nature and it can form films with nontoxic and biodegradable properties (Ge et al. 2021). Although it presents good barrier to oxygen, it has poor mechanical strength and low water barrier (Gómez-Guillén et al. 2009). For this reason, its use in combination with plasticizers or other hydrophobic biopolymers can provide stability, resistance, flexibility, and increased water barrier (Cao, Yang, and Fu 2009). CNCs have been also used along with GE as a reinforcement strategy. For example, Santos et al. (Santos et al. 2014) reported that GE/CNCs nanocomposites, plasticized with glycerol and sonicated, showed a better stiffness-to-ductility balance and a reduced water vapor

permeability for CNCs contents of up to 5 wt %. In another work, the incorporation of 0.5 wt % of CNCs into GE increased the tensile strength and Young's modulus of GE by 77 and 48 %, respectively (Leite et al. 2020). Alternatively, AG is a polysaccharide derived from red algae (Akshay Kumar et al. 2021). It has interesting properties, such as water solubility, biodegradability, and good strength (Kanmani and Rhim 2014, Rhim, Wang, and Hong 2013). Moreover, AG has been used along with CNCs in different composites to obtain enhanced mechanical and barrier properties. Hence, the AG/CNCs composite using glycerol as plasticizer resulted in more flexible films with 23 % less WVP (Reddy and Rhim 2014). A similar work based on AG/CNCs composite films presented analogous results with increased mechanical properties and reduced WVP (Atef, Rezaei, and Behrooz 2014). These results point out the good interaction between CNCs and AG. Furthermore, XG is an extracellular polysaccharide mainly produced by the Gram-negative bacterium *Xanthomonas campestris* (Jansson, Kenne, and Lindberg 1975). It has been distinguished for its non-toxicity, thermal stability and biocompatibility properties (Kumar, Rao, and Han 2018). XG can be soluble in both cold and hot water and its films present low water vapor permeability and great mechanical properties (Guo et al. 2014). Composites made of XG/chitosan (CS) blends reinforced with CNCs showed improved mechanical performance by increasing the CNCs content from 2 to 10 wt % (Madhusudana Rao, Kumar, and Han 2017). Finally, GA is an exudate from the stems and branches of *Acacia* species trees (Montenegro et al. 2012). It has been largely used in the food industry as stabilizer, emulsifier, flavoring agent and thickener, but also in the pharmaceutical, cosmetic, printing, and textile industries (Verbeken, Dierckx, and Dewettinck 2003). However, its use as coating or packaging film is limited due to its lack of strength, poor barrier properties, and high hydrophilicity (Aphibanthammakit et al. 2018). For this reason, the use of CNCs as a filler has been seen as a great reinforcement in composites. As an example, Kang et al. (Kang et al. 2021) reported an increase in tensile strength and elongation at break by incorporating 4 wt % CNCs into GA films as well as a 10.6 and 25.3 % decrease in water vapor and oxygen permeabilities, respectively.

As cited above, since CNCs are strongly plasticized by moisture sorption (Wang et al. 2018), it can only be used, as most oxygen-barrier polymers, protected between water-barrier layers. For this reason, the use of multilayer systems where a CNCs-based middle layer protected between hydrophobic polymers has been seen as a great alternative to overcome this problem (Fotie et al. 2020, Le Gars et al. 2020). Among the hydrophobic polymers available, biopolymers such as polyhydroxyalkanoates (PHAs) stand out for their biodegradability and compostability, whereas they can also be processed using conventional plastic machinery (Bhatia et al. 2021). The poly(3-hydroxybutyrate) (PHB) homopolymer and its poly(3-hydroxybutyrate-*co*-3-hydroxyvalerate) (PHBV) (Guk Choi et al. 2003), poly(3-hydroxybutyrate-*co*-4-hydroxybutyrate) [(P3HB-*co*-P4HB)] (Torres-Giner et al. 2016), poly(3-hydroxybutyrate-*co*-3-hydroxyhexanoate) [P(3HB-*co*-3HHx)] (Qiu, Han, and Chen 2006), or poly(3-hydroxybutyrate-*co*-3-hydroxyvalerate-*co*-3-hydroxyhexanoate) [P(3HB-*co*-3HV-*co*-3HHx)] (Zhang et al. 2009) copolymers, are the most studied PHAs since they have been used as substitutes for petrochemical polymers such as polypropylene (PP) and polyethylene (PE). In particular, PHBV has low crystallinity and moderate flexibility (Chen, Don, and Yen 2006, Zhao and Chen 2007), high moisture resistance, and medium-gas-barrier properties (Gallardo-Cervantes et al. 2021).

Electrospinning, is an emerging processing technology in which the use of an electric field allows the creation of polymer micro- and nanofibers (Doshi and Reneker 1995) and it is currently seen as a promising alternative to develop polymer layers after annealing. These layers are useful for

the packaging industry since they can improve the mechanical and barrier performance of some polymers (Torres-Giner 2011). Thus, a very short thermal post-treatment to the fibers, below their melting point, convert them into continuous films, so-called biopapers, by interfiber coalescence, exhibiting adhesive properties, improved transparency, flexibility, and barrier performance (Cherpinski, Torres-Giner, Cabedo, et al. 2018, Melendez-Rodriguez et al. 2020). For instance, electrospun PHB and PHBV coatings have already been reported to improve the moisture resistance of nanopapers based on cellulose nanofibrils (CNFs) and lignocellulose nanofibrils (LCNFs) when structured in a multilayer fashion (Cherpinski, Torres-Giner, Vartiainen, et al. 2018). In another study, coatings made of electrospun PHB/bacterial cellulose, which covered the inner layer of thermoplastic corn starch (TPCS)/bacterial cellulose composites, improved their water- and oxygen-barrier properties (Fabra et al. 2016). In addition, electrospun fibers can be functionalized with the use of additives with antimicrobial or antioxidant properties, which increases their application interest in active packaging applications (Figueroa-Lopez, Cabedo, et al. 2020, Figueroa-Lopez, Enescu, et al. 2020, Figueroa-Lopez, Torres-Giner, et al. 2020)

From all of the above and to the best of our knowledge, electrospun PHAs have only been used before to reduce the moisture sensitivity of previously formed nanopapers made of cellulose nanofibers (CNF). This study offers the opposite perspective, in which electrospun PHA biopapers were impregnated with CNCs and also with various hydrocolloids containing CNCs in order to improve the barrier properties, assessing whether these novel layered materials could offer advantages in biobased food packaging applications. To this end, CNCs were used alone and mixed as a minor component with a protein and various polysaccharides, adding glycerol as a plasticizer, and the mechanical and barrier properties of the resultant nanocomposite films were determined and compared to an equivalent multilayer film of neat PHBV. Therefore, the interest of the study mainly comes from the fact that, during optimal annealing post-processing, the electrospun fibers can successfully coalesce, resulting in denser thinner and continuous layers. Thus, it was uncertain if, by a simple and scalable impregnation process, an improvement in barrier properties of PHBV could be achieved.

2. Experimental

2.1. Materials

The commercial PHBV used was ENMAT Y1000P, supplied by Tianan Biologic Materials (Ningbo, China). The 3HV fraction is approximately 2 mol % and the molecular weight (M_W) is ~2.8×10^5 g/mol. CNCs were provided by CelluForce NCC® (Quebec, Canada) as pure cellulose sulfate sodium salt, which was obtained from wood pulp, and was received as a spray-dried solid white powder with a bulk density of 0.7 g/cm^3.

2,2,2-Trifluoroethanol (TFE), ≥ 99 % purity, $_D$-limonene, with 98 % purity, and GE type-B from bovine skin were obtained from Sigma Aldrich S.A. (Madrid, Spain). Glycerol, pharmaceutic grade, with a density of 1.26 g/cm^3, was purchased from Panreac S.A. (Barcelona, Spain). Potato dextrose AG was supplied by Scharlab S.L. (Barcelona, Spain), whereas XG and GA were obtained from Guinama S.L. (Valencia, Spain). The chemical structures of the hydrocolloids are shown in **Figure 1**.

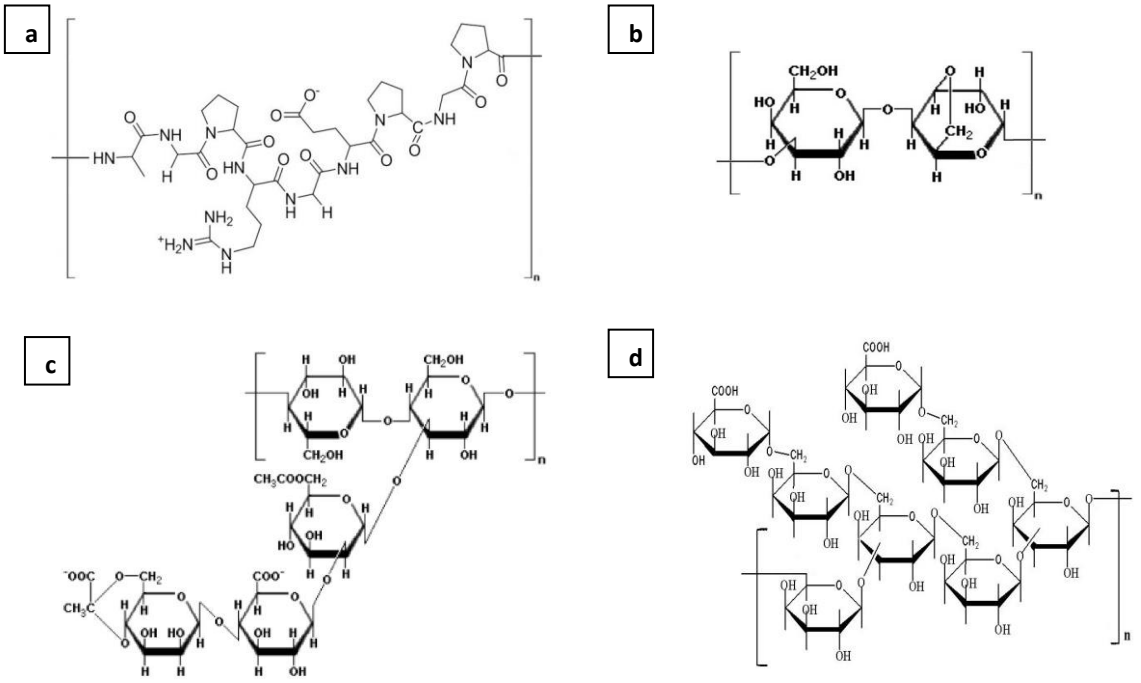

Figure 1. Scheme of the chemical structures of: (a) Gelatin (GE); (b) Agar (AG); (c) Xanthan gum (XG); (d) Gum arabic (GA).

2.2. Electrospinning process

The commercial PHBV pellets were dissolved at 10 wt % in TFE under magnetic stirring for 24 h at 50 °C. Later, the solution was electrospun using a Fluidnatek® LE-10 lab device manufactured by Bioinicia S.L. (Valencia, Spain). The equipment was operated with a single needle injector, with a diameter of 0.9 mm, scanning horizontally towards a metal plate collector at room temperature conditions, that is, 25 °C and 40 % relative humidity (RH). The optimal processing conditions were set at a flow-rate of 6 ml/h, 20 kV of voltage, and 20 cm needle-to-collector distance.

2.3. CNCs and CNC blends

The CNCs was prepared as a 2 % (w/v) aqueous solution. Briefly, the CNCs powder was first immersed in water and homogenized at 15000 rpm for 3 min with a T25 digital Ultra-turrax from IKA® (Staufen, Germany) and then magnetically stirred without temperature for at least 12 h. In addition, several nanocomposite solutions of the protein and three polysaccharides containing CNCs were also prepared as previously described by Reddy and Rhim (Reddy and Rhim 2014). To this end, water solutions with total solid contents of 2 % (w/v) were similarly prepared, where 98 % (w/w) correspond to the biopolymers, that is, GE, AG, XG, and GA, and 2 % (w/w) to CNCs. In these biopolymer solutions, 1 wt % of glycerol was added as a plasticizer, replacing the same quantity of water.

2.4. Solution properties

The viscosity, surface tension, and conductivity for all the solutions prepared above was measured. The apparent viscosity (ηa) was determined at 100 s^{-1} using a rotational viscosity meter Visco BasicPlus L from Fungilab S.A. (San Feliu de Llobregat, Spain) equipped with a low viscosity adapter (LCP). The surface tension was measured following the Wilhemy plate method using an EasyDyne K20 tensiometer from Krüss GmbH (Hamburg, Germany). The conductivity was evaluated using a conductivity meter XS Con6 from Lab-box (Barcelona, Spain). All measurements were carried out at room temperature in triplicate.

2.5. Preparation of the multilayers

The CNCs and the biocomposites with CNCs were impregnated onto the commercial electrospun PHBV fibers mat using the K Control Coater standard K101 model from RK PrintCoat Instruments Ltd (Litlington, UK). The roll number used was 8. The impregnation process was carried out two times. After the first application, the impregnation was dried in the oven at 90 °C for 10 min, and after the second impregnation, this was dried also at 90 °C but for 15 min. By drying at 90 °C, the electrospun nanofiber morphology of PHBV was not affected, in agreement with previous studies (Melendez-Rodriguez et al. 2018, Melendez-Rodriguez et al. 2020).

To generate the continuous multilayers, the electrospun PHBV substrates with no impregnation, and impregnated with CNCs and with CNCs and the hydrocolloids were sandwiched with similar non-impregnated layers of electrospun PHBV fibers and annealed at 160 °C for 2 s, without pressure, in a 4122-model press from Carver, Inc. (Wabash, IN, USA). Annealing of the PHBV at 160 °C, below the PHBV's melting point, is known from previous works to lead to continuous layers by a process of interfiber coalescence (Figueroa-Lopez, Cabedo, et al. 2020). The average thickness of the resultant multilayer biopapers was approximately 100 μm. The schemes of these assemblies are shown in **Figure 2**. The samples were stored in a desiccator at 0 % RH for at least 2 weeks before subsequent characterization.

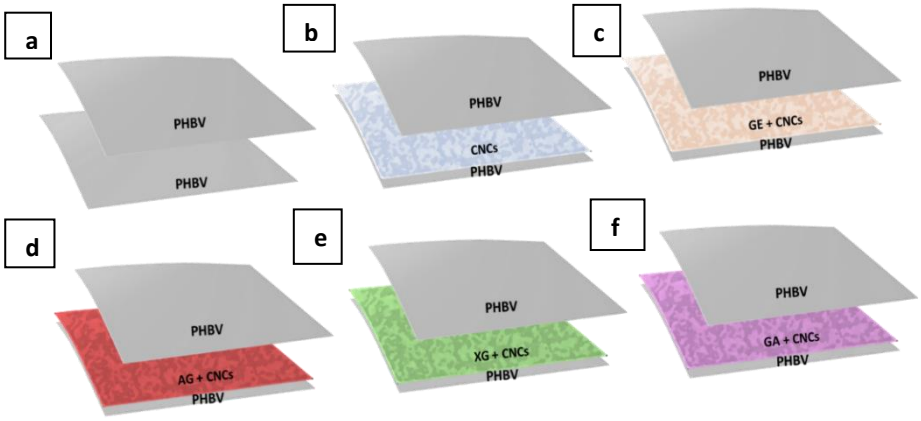

Figure 2. Scheme of the multilayer biopapers of: (a) neat poly(3-hydroxybutyrate-*co*-3-hydroxyvalerate (PHBV); (b) PHBV impregnated with cellulose nanocrystals (CNCs); (c) PHBV impregnated with CNCs and gelatin (GE); (d) PHBV impregnated with CNCs and agar (AG); (e) PHBV impregnated with CNCs and xanthan gum (XG); and (f) PHBV impregnated with CNCs and gum arabic (GA).

2.6. Characterization

2.6.1. Scanning electron microscopy

The surface morphology of the neat and impregnated PHBV fibers and the cross-sections of the multilayer biopapers were observed by scanning electron microscopy (SEM) using an S-4800 device from Hitachi (Tokyo, Japan). For cross-section observation, the multilayers were cryo-fractured by immersion in liquid nitrogen and, then, fixed to beveled holders using conductive double-sided adhesive tape and sputtered with a mixture of gold-palladium under vacuum prior to observation. An accelerating voltage of 10 kV was used and the estimation of the dimensions was performed by means of the Aperture software from Apple (Cupertino, CA, USA) using a minimum of 20 SEM micrographs in their original magnification.

2.6.2. Mechanical tests

Tensile tests on the multilayer biopapers were performed according to ASTM standard method D638 using a 4400 universal testing machine from Instron (Norwood, MA, USA) equipped with a 1-kN load cell. The tests were performed with 115 mm × 16 mm stamped dumb-bell shaped specimens. Samples were conditioned at 40 % RH and 25 °C for 24 h prior to tensile assay. A minimum of six specimens were measured for each sample, at room conditions, using a cross-head speed of 10 mm/min.

2.6.3. Barrier properties

The water vapor permeance (WVP) of the multilayer biopapers was determined using the gravimetric method ASTM E96–95 in triplicate. The control samples were cups with aluminum films to estimate solvent loss through the sealing. For this, 5 ml of distilled water was placed inside a Payne permeability cup (diameter of 3.5 cm) from Elcometer Sprl (Hermallesous-Argenteau, Belgium). The multilayers were not in direct contact with water but exposed to 100 % RH on one side and secured with silicon rings. They were placed within a desiccator, sealed with dried silica gel, at 0 % RH cabinet at 25 °C. WVP was calculated from the regression analysis of weight loss data vs. time, and the weight loss was calculated as the total loss minus the loss through the sealing.

For limonene permeance (LP), the procedure was similar to that described above for WVP with the difference that 5 ml of $_{D}$-limonene was placed inside the Payne permeability cups and these were placed under controlled room conditions of 25 °C and 40 % RH.

The oxygen permeance (OP) coefficient was derived from the oxygen transmission rate (OTR) measurements that were recorded using an Oxygen Permeation Analyzer M8001 from Systech Illinois (Thame, UK) at 20 % RH and 25 °C, in duplicate. The humidity equilibrated samples were purged with nitrogen, before exposure to an oxygen flow of 10 ml/min. The exposure area during the test was 5 cm^2 for each sample.

2.7. Statistical analysis

The mechanical and barrier properties were evaluated through analysis of variance (ANOVA) using STATGRAPHICS Centurion XVI v16.1.03 from StatPoint Technologies, Inc. (Warrenton, VA, USA). Fisher's least significant difference (LSD) was used at the 95 % confidence level ($p < 0.05$). Mean values and standard deviations were also reported.

3. Results and discussion

3.1. Solution properties and morphology

The solutions of pure CNCs and of their biocomposites with GE, AG, XG, and GA were characterized in terms of viscosity, surface tension, and conductivity, and the results are gathered in **Table 1**. From this table, it can be seen that the solutions gave quite different results depending on the biopolymers. The neat CNCs solution showed values of 15.1 cP, 49.9 mN/m, and 195.0 μS/cm, for viscosity, surface tension, and conductivity, respectively. Regarding the nanocomposites, XG presented the highest values in all the three properties, that is, 939.2 cP for viscosity, 76.1 mN/m for surface tension, and 1631.5 μS/cm for conductivity. The high viscosity value suggests that this polysaccharide potentially shows a higher M_W and also to the stronger interaction of the carboxyl groups (–COO–) and ether group (–C–O–C–), shown in previous **Figure 1**, with the terminal hydroxyl groups (OH–) of PHBV and cellulose. The blends with GE and GA showed certain similar values, ranging between 5.2–9.6 cP, 47.8–60.4 mN/m and 356.4–368.6 μS/cm for viscosity, surface tension, and conductivity, respectively, which, as suggested by their chemical structure, points to a moderate interaction with PHBV/CNCs composite. Finally, the biocomposite solution with AG presented values of 1.9 cP, 55.9 mN/m, and 1554.1 μS/cm, for viscosity, surface tension, and conductivity. The latter values can be ascribed to the lack of chemical interactions of this hydrocolloid with the biocomposite.

Table 1. Solution properties of the neat cellulose nanocrystals (CNCs) and modified CNCs with gelatin (GE), agar (AG), xanthan gum (XG), and gum arabic (GA).

Solution	Viscosity (cP)	Surface tension (mN/m)	Conductivity (μS/cm)
CNCs	15.1 ± 0.6^{a}	49.9 ± 0.1^{a}	195.0 ± 6.1^{a}
GE with CNCs	5.2 ± 1.5^{b}	47.8 ± 1.6^{a}	356.4 ± 28.8^{b}
AG with CNCs	1.9 ± 0.3^{c}	55.9 ± 0.5^{b}	1554.1 ± 33.8^{c}
XG with CNCs	939.2 ± 2.2^{d}	76.1 ± 0.1^{c}	1631.5 ± 21.9^{d}
GA with CNCs	9.6 ± 2.1^{e}	60.4 ± 0.7^{d}	368.6 ± 26.6^{b}

[a–e] Different letters in the same column indicate a significant difference among the samples ($p < 0.05$).

The morphologies of the PHBV electrospun surfaces impregnated with and without CNCs and with their biocomposites with the hydrocolloids, as well as the cross-section of the multilayers after the thermal post-treatment of annealing, were observed by SEM and the images are presented in **Figure 3**. In **Figure 3a** one can observe the top view of the neat electrospun PHBV mats obtained after electrospinning and the cryofracture surfaces of the PHBV multilayer obtained after annealing. The electrospun mat without thermal post-treatment showed the occurrence of ultrathin fibers with mean diameters of 0.92 ± 0.11 μm. After annealing, below the biopolyester melting point, a continuous biopaper with a homogeneous surface and no apparent porosity was formed by coalescence of interfibers in agreement with our previous study (Melendez-Rodriguez et al. 2018).

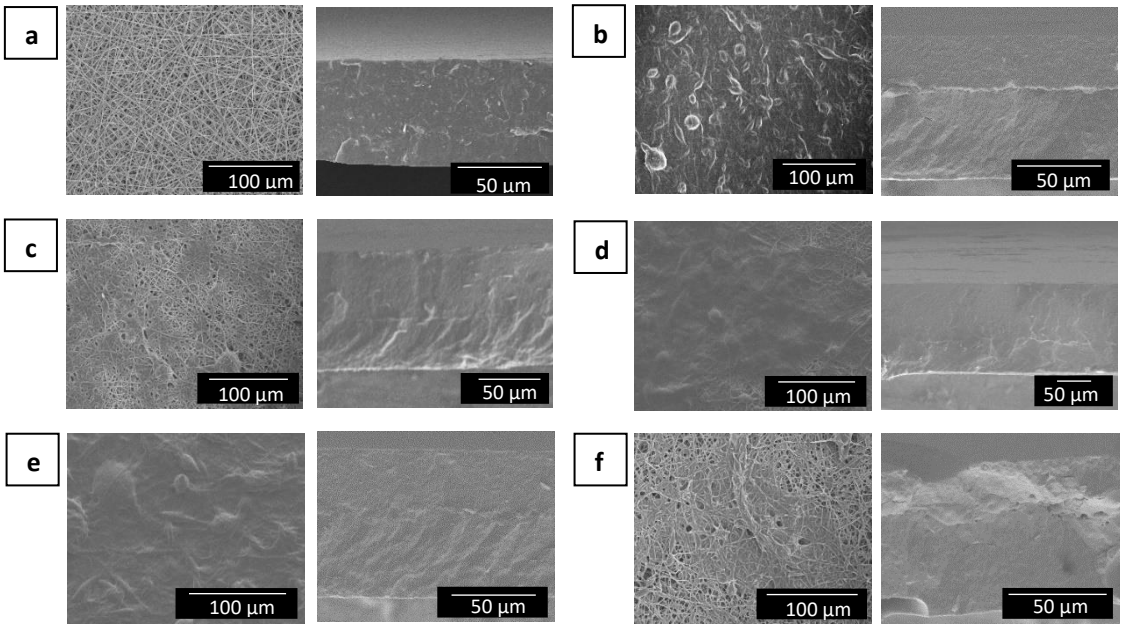

Figure 3. Scanning electron microscopy (SEM) images of the top view of the fiber mats (left) and cross-section of the multilayers after thermal post-treatment (right) of: (a) neat poly(3-hydroxybutyrate-*co*-3-hydroxyvalerate) (PHBV); (b) PHBV impregnated with cellulose nanocrystals (CNCs); (c) PHBV impregnated with gelatin (GE) and CNCs; (d) PHBV impregnated with agar (AG) and CNCs; (e) PHBV impregnated with xanthan gum (XG) and CNCs; and (f) PHBV impregnated with gum arabic (GA) and CNCs. The images were taken at 1000× and 400× with scale markers of 50 μm and 100 μm, respectively.

Figure 3b shows the surface of the electrospun PHBV mats after CNCs impregnation. The main characteristics of the CNCs solution used were a relatively low surface tension and conductivity and relatively high viscosity in comparison with the CNCs solutions containing the hydrocolloids. It has been reported that the viscosity of CNCs depends on factors such as particle concentration and aspect ratio, as well as particle size and surface area (Moberg et al. 2017, Qiao et al. 2016). From this figure, an efficient impregnation of the fibers was seen, since the porosity of the mat at the surface was very much reduced. The cross-section of the multilayer biopaper also showed a continuous non-porous morphology. Moreover, the presence of the CNCs, interphasing between the two electrospun layers, could be easily discerned. This irregular CNCs interphase could be

the result of the densification suffered by the fibers during the interfiber coalescence process. Other researchers have reported before the way the CNCs can suitably cover the surface of substrate fibers, such as paper or polyethersulfone (PES) membranes, transitioning this to a smoother morphology (Aguilar-Sanchez et al. 2021, Gicquel et al. 2017). The good impregnation properties of CNCs have been ascribed before to secondary forces via hydrogen bonding to itself, so-called self-association, and to the polymer matrix of PES membranes (Bai et al. 2020).

The impregnation of PHBV with the hydrocolloid/CNC composites showed a different behavior depending on the hydrocolloid used. For XG, and to a significant extent for AG, in **Figure 3d** and e it can be respectively observed that a somewhat better fiber impregnation was produced. These differences can be explained in terms of the solution viscosity values reported above. However, in all the cases, the cross-section of their multilayers showed a compact structure, with not so clear interphase between layers after annealing, when compared to the biopaper of CNCs without hydrocolloids. The GE and GA-containing nanocomposite biopapers, respectively shown in **Figure 3c** and **f**, indicated a less efficient impregnation of the fibers, leaving significant porosity. After annealing, they also presented homogeneous surfaces with no apparent interphase between layers. By looking at **Figure 3** and the values gathered in **Table 1**, it appears that the best impregnation, resulting in efficient coating of the interfibers porosity, was seen for the materials prepared with the PHBV solutions with the highest viscosity values, that is, CNCs and specially CNCs/XG. The rest of the solutions could perhaps diffuse more easily through the interfibers porosity. Penetration between the electrospun fibers depends on both the porosity of the substrate and the concentration and viscosity of the impregnation solution, as well as the impregnation process, making it difficult to predict the resulting final structure (Desmaisons et al. 2018, Lavoine et al. 2014).

3.2. Mechanical properties

The requirements of the multilayer materials used in packaging applications are mainly its mechanical resistance and flexibility as well as sealability. For this reason, the mechanical properties of the multilayers were assessed by tensile measurements. **Table 2** shows the results of the tensile test in terms of elastic modulus (E), tensile strength at yield (σ_y), and elongation at break (ε_b). The most representative tensile stress-strain curves obtained for each multilayer at room temperature are gathered in **Figure 4**. One can observe that all the multilayer materials exhibited a stiff and brittle behavior similar to the control multilayer of PHBV/PHBV. It can be seen that the multilayers of PHBV and with CNCs, that is, PHBV/CNCs/PHBV, performed almost equally in terms of E and ε_b with values around 3660 MPa and 1.3 %, respectively. Regarding tensile strength, the PHBV multilayer with CNCs showed slightly lower values, not statistically significant though, than the control PHBV multilayer. Thus, the PHBV multilayer exhibited values of 26.3 MPa, while with the incorporation of CNCs the values dropped to 24.2 MPa. These slight differences in σy when adding a layer of nanocellulose between two layers of electrospun PHBV have been previously reported and ascribed to layer delamination at high stress. Thus, Cherpinski et al. (Cherpinski, Torres-Giner, Vartiainen, et al. 2018) obtained values of 2014.9 MPa, 28.0 MPa, and 2.8 %, for E, σ_y, and ε_b, respectively, for an electrospun PHBV film monolayer, while for a multilayer made of PHBV/CNFs/ PHBV the values obtained were 2056.7 MPa, 21.0 MPa and 5.9 % for E, σ_y and ε_b, respectively.

Table 2. Mechanical properties in terms of elastic modulus (E), tensile strength at yield (σ_y), and elongation at break (ε_b) of the multilayers of poly(3-hydroxybutyrate-*co*-3-hydroxyvalerate) (PHBV) with and without interlayers of cellulose nanocrystals (CNCs) and modified CNCs with gelatin (GE), agar (AG), xanthan gum (XG), and gum arabic (GA).

Multilayer	E (MPa)	σ_y (MPa)	ε_b (%)
PHBV/PHBV	3676 ± 597[a]	26.3 ± 7.6[a]	1.2 ± 0.1[a]
PHBV/CNCs/PHBV	3636 ± 820[a]	24.2 ± 6.0[a]	1.3 ± 0.2[a]
PHBV/CNCs+GE/PHBV	3536 ± 508[a]	25.0 ± 3.0[a]	1.2 ± 0.1[a]
PHBV/CNCs+AG/PHBV	3591 ± 463[a]	27.8 ± 4.7[a]	1.1 ± 0.2[a]
PHBV/CNCs+XG/PHBV	2972 ± 822[a]	21.9 ± 6.8[a]	1.2 ± 0.1[a]
PHBV/CNCs+GA/PHBV	3397 ± 860[a]	24.4 ± 5.5[a]	1.3 ± 0.3[a]

[a] Different letter in the same column indicate a significant difference among the samples ($p < 0.05$).

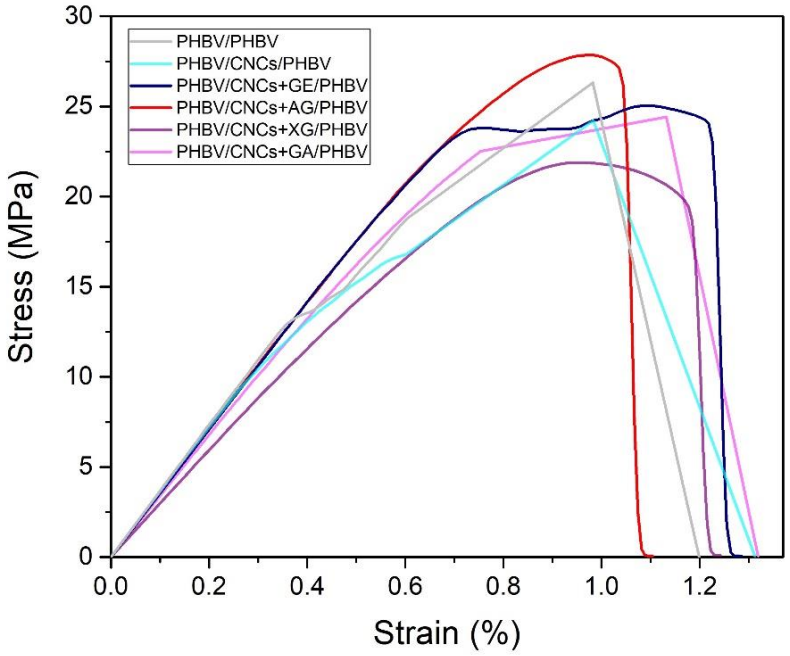

Figure 4. Typical tensile stress–strain curves of the multilayers composed of: poly(3-hydroxybutyrate-*co*-3-hydroxyvalerate) (PHBV); PHBV with cellulose nanocrystal (CNCs); PHBV with CNCs and gelatin (GE); PHBV with CNCs and agar (AG); PHBV with CNCs and xanthan gum (XG); and PHBV with CNCs and gum arabic (GA).

Concerning the composites based on PHBV with CNCs and hydrocolloids, it can be seen that all the multilayers presented a quite similar εb, ranging between 1.1–1.3 %, and in the same trend as the multilayer of neat PHBV and with only CNCs. Although the multilayers with different formulations presented lower performances in relation to E, the values were also in the same range as for the control sample and with CNCs, that is, 2972–3591 MPa. Similarly, the σ_y values remained close to those achieved by the multilayers of the PHBV control and with CNCs, ranging between 21.9–27.8 MPa. The effect of CNCs addition on the mechanical performance of polymer films has been previously studied (Fox et al. 2012, Peresin et al. 2010, Shojaeiarani and Bajwa 2018), reporting that the nanocrystals induced a stiffening effect for an optimum concentration. Thus, it has been previously reported that CNCs contents up to 7 wt %, around the percolation threshold, in a chitosan matrix showed an improvement of σ_y and a reduction of ε_b due to the good dispersion of the nanofiller (Pereda et al. 2014). However, when that optimal value was exceeded, the opposite effect occurred. This is due to agglomeration of the CNCs, which in turn leads to a reduction in their interaction with the matrix and, thus, decreases the reinforcement but increases the ductility of the films (Abdollahi et al. 2013). In the current study, it is worthy to note that CNCs were used as an impregnating material, not as an additive within the fibers. Therefore, since the comparative mass fraction of the CNCs nanofibers coating is very low, the mechanical performance of the materials is mainly dominated by the intrinsic mechanical behavior of the largest phase material in the multilayer, that is, the PHBV outer layers. In fact, it may be considered as a favorable result that the properties of the modified multilayers did not get worse than the control PHBV sample, suggesting a good adhesion among the layers.

3.3. Barrier properties

Since limonene is considered a standard system for testing aroma barrier in food packaging, and oxygen and moisture permeation can dramatically detriment food shelf-life, the permeance of the multilayers based on PHBV, CNCs, and CNCs with hydrocolloids to these vapors and gas were measured. The WVP, LP, and OP values are gathered in **Table 3**.

In terms of WVP, it can be seen that the PHBV/PHBV multilayer showed higher barrier than the multilayer of PHBV with pure CNCs, with values of 6.0 and 24.1 × 10^{-11} kg·m^{-2}·Pa^{-1}·s^{-1}, respectively. This result can be related to the fact that it has been reported before that CNCs do not confer significant water barrier performance, even as interlayers, since the nanomaterial is hydrophilic in nature (Figueroa-Lopez, Torres-Giner, et al. 2020). In the latter study, however, a slight improvement in water barrier was seen since the CNCs layer was applied as a coating sandwiched between continuous and smooth layers of PHBV produced by film blowing, being pre-activated to enhance adhesion with corona treatment and pre-coated with a primer and a wetting agent. Likewise, the multilayers of CNCs with AG and XG exhibited also poorer barrier to water, showing values of 19.8 and 10.3 × 10^{-11} kg·m^{-2}·Pa^{-1}·s^{-1}, respectively, probably due to their hydrophilic nature and higher porosity. Furthermore, the samples with GE and GA retained a similar WVP as the non-impregnated multilayer, with WVP values of 5.2 and 7.6 × 10^{-11} kg·m^{-2}·Pa^{-1}·s^{-1}, respectively.

Table 3. Thickness and permeance values in terms of water vapor permeance (WVP), D-limonene permeance (LP), and oxygen permeance (OP) of the multilayers of poly(3-hydroxybutyrate-*co*-3-hydroxyvalerate) (PHBV) with and without interlayers of cellulose nanocrystals (CNCs) and modified CNCs with gelatin (GE), agar (AG), xanthan gum (XG), and gum arabic (GA).

Multilayer	Thickness (mm)	Permeance		
		WVP x 10^{11} ($kg \cdot m^{-2} \cdot Pa^{-1} \cdot s^{-1}$)	LP x 10^{11} ($kg \cdot m^{-2} \cdot Pa^{-1} \cdot s^{-1}$)	OP x 10^{16} ($m^3 \cdot m^{-2} \cdot Pa^{-1} \cdot s^{-1}$)
PHBV/PHBV	0.097 ± 0.002	6.04 ± 2.53[a]	2.98 ± 0.30[a]	3.60 ± 0.60[a]
PHBV/CNCs/PHBV	0.100 ± 0.005	24.12± 5.94[b]	1.53 ± 0.49[b,d]	0.42 ± 0.17[b]
PHBV/CNCs+GE/PHBV	0.108 ± 0.007	5.18 ± 0.53[a]	2.61 ± 0.34[a]	23.08 ± 0.33[c]
PHBV/CNCs+AG/PHBV	0.106 ± 0.004	19.84 ± 5.97[b]	0.90 ± 0.21[b,c]	7.81 ± 1.10[d]
PHBV/CNCs+XG/PHBV	0.108 ± 0.003	10.30 ± 5.90[a,b]	0.50 ± 0.10[c]	2.57 ± 0.77[a]
PHBV/CNCs+GA/PHBV	0.109 ± 0.004	7.57 ± 1.86[a,b]	1.82 ± 0.14[d]	2.42 ± 1.10[a]

[a-d] Different letters in the same column indicate a significant difference among the samples ($p < 0.05$).

Regarding aroma barrier, the multilayer of PHBV with CNCs exhibited better barrier than the neat PHBV multilayer, showing values of 1.5 and 2.9 × 10^{-11} $kg \cdot m^{-2} \cdot Pa^{-1} \cdot s^{-1}$, respectively. This can be explained by the fact that limonene is a strong plasticizer for PHA materials, but this is not the same for hydrophilic materials, such as CNCs, that can offer a good barrier to the permeant (Sanchez-Garcia, Gimenez, and Lagaron 2007). It has been reported a limonene uptake of up to 13 wt % for a solvent-cast PHBV film (Sanchez-Garcia, Gimenez, and Lagaron 2008). The multilayers containing the CNCs interlayer with GE and GA showed somewhat improved barrier values, that is, 2.6 and 1.8 × 10^{-11} $kg \cdot m^{-2} \cdot Pa^{-1} \cdot s^{-1}$, respectively; whereas the samples with AG and XG, exhibited the best barrier to limonene vapor, with permeance reductions between 70 and 83 % compared to the control, that is, 0.9 and 0.5 × 10^{-11} $kg \cdot m^{-2} \cdot Pa^{-1} \cdot s^{-1}$, respectively. These two multilayer samples, specially the one containing XG, and also the one based on only CNCs, exhibited in previous **Figure 3** the best impregnation in terms of reduced porosity.

Regarding the permeance of the small non-condensable gas oxygen molecule, the sample with only CNCs showed clearly lower OP, with a reduction of 88 %, than the control PHBV bilayer sample. This OP reduction value is in good agreement with previous studies in which CNCs were used as a continuous interlayer coating. For instance, Le Gars et al. (Le Gars et al. 2020) reported a nearly 90 % permeation decrease in multilayers of polylactide (PLA) and CNCs (PLA/CNCs/PLA). In another study, Fotie et al. (Fotie et al. 2020) studied multilayers of polyethylene terephthalate (PET), PLA, oriented polypropylene (OPP), PP, and PE with 1 μm of a continuous CNCs interlayer applied by lamination, reporting in all cases an OP reduction between 90 and 100 %. It is, therefore, very interesting to see that CNCs can also achieve a very high-barrier effect, even when impregnated over electrospun mats, which upon annealing suffer a significant shrinkage during fiber coalescence. It is also inferred from the good oxygen barrier results that this interesting interfiber coalescence process, unique to electrospun biopapers, can reduce the free volume, creating a high-barrier continuous interphase. Concerning the multilayer of PHBV with CNCs and XG or GA, these samples showed a similar but slightly higher barrier performance as the control multilayer, with values of 2.6 and 2.4 × 10^{-16} $m^3 \cdot m^{-2} \cdot Pa^{-1} \cdot s^{-1}$, respectively. However, the samples with GE and AG showed the worst performance in barrier, with values of 23.1 and 7.8 × 10^{-16} $m^3 \cdot m^{-2} \cdot Pa^{-1} \cdot s^{-1}$, respectively. These last two samples exhibited

in **Figure 3** the least favorable impregnation morphology. Since no oxygen barrier, driven by diffusion, was seen even for the multilayers containing the most favorable polysaccharides in terms of interphase morphology, but they presented aroma barrier, driven by solubility, it is possible that these hydrocolloids are not able to stablish a continuous interphase between the layers, further supported by the morphology data in **Figure 3**.

4. Conclusions

In this study, various multilayered films composed of two electrospun PHBV fiber layers, one of which was impregnated with CNCs and hydrocolloids with CNCs, were prepared and characterized. To obtain the nanocomposites, the nanocellulose was mixed in a 2 % (w/w) with a protein, GE, and three polysaccharides, AG, XG, and GA, whereas glycerol was added in all the formulations as a plasticizer. The multilayers were post-processed by a mild thermal treatment at 160 °C for 2 s, to obtain a fiber-based continuous structure. The morphology, mechanical properties, assessed via tensile tests, and barrier properties, measured in terms of permeance to water and limonene vapors and oxygen gas, of the multilayers were reported. SEM images showed that the best impregnation of the PHBV fibers was achieved with CNCs and, to a lesser extent, with their biocomposites with AG and XG. After annealing below the PHBV's melting point, all the multilayers showed good interlayer adhesion, with the layers adhering properly and showing no voids or gaps. The impregnation with neat CNCs and CNCs with hydrocolloids did not affect the mechanical properties of pure PHBV, which were found to be governed by the mechanical response of the outer structural layers of PHBV, but their barrier properties to limonene were improved in all the cases, especially, with CNCs and their biocomposites with AG and XG. The oxygen permeance was seen to be largely improved only after impregnation with CNCs. The results showed, therefore, that the best impregnation material in terms of the properties analyzed, with the exception of the water permeance, corresponded to CNCs. Some of the hydrocolloid nanocomposites with the best impregnation morphology showed only improvements in aroma barrier.

5. References

Abdollahi, Mehdi, Mehdi Alboofetileh, Rabi Behrooz, Masoud Rezaei, and Reza Miraki. 2013. "Reducing water sensitivity of alginate bio-nanocomposite film using cellulose nanoparticles." *International Journal of Biological Macromolecules* 54:166-173. doi: https://doi.org/10.1016/j.ijbiomac.2012.12.016.

Aguilar-Sanchez, Andrea, Blanca Jalvo, Andreas Mautner, Samer Nameer, Tiina Pöhler, Tekla Tammelin, and Aji P. Mathew. 2021. "Waterborne nanocellulose coatings for improving the antifouling and antibacterial properties of polyethersulfone membranes." *Journal of Membrane Science* 620:118842. doi: https://doi.org/10.1016/j.memsci.2020.118842.

Ahankari, Sandeep S., Aditya R. Subhedar, Swarnim S. Bhadauria, and Alain Dufresne. 2021. "Nanocellulose in food packaging: A review." *Carbohydrate Polymers* 255:117479. doi: https://doi.org/10.1016/j.carbpol.2020.117479.

Akshay Kumar, K. P., Ehsan Nazarzadeh Zare, Rafael Torres-Mendieta, Stanisław Wacławek, Pooyan Makvandi, Miroslav Černík, Vinod V. T. Padil, and Rajender S. Varma. 2021. "Electrospun fibers based on botanical, seaweed, microbial, and animal sourced biomacromolecules and their multidimensional applications." *International Journal of Biological Macromolecules* 171:130-149. doi: https://doi.org/10.1016/j.ijbiomac.2020.12.205.

Aphibanthammakit, Chutima, Michaël Nigen, Sébastien Gaucel, Christian Sanchez, and Pascale Chalier. 2018. "Surface properties of Acacia senegal vs Acacia seyal films and impact on specific functionalities." *Food Hydrocolloids* 82:519-533. doi: https://doi.org/10.1016/j.foodhyd.2018.04.032.

Atef, Maryam, Masoud Rezaei, and Rabi Behrooz. 2014. "Preparation and characterization agar-based nanocomposite film reinforced by nanocrystalline cellulose." *International Journal of Biological Macromolecules* 70:537-544. doi: https://doi.org/10.1016/j.ijbiomac.2014.07.013.

Aulin, Christian, Mikael Gällstedt, and Tom Lindström. 2010. "Oxygen and oil barrier properties of microfibrillated cellulose films and coatings." *Cellulose* 17 (3):559-574. doi: 10.1007/s10570-009-9393-y.

Bai, Langming, Junwen Ding, Haorui Wang, Nanqi Ren, Guibai Li, and Heng Liang. 2020. "High-performance nanofiltration membranes with a sandwiched layer and a surface layer for desalination and environmental pollutant removal." *Science of The Total Environment* 743:140766. doi: https://doi.org/10.1016/j.scitotenv.2020.140766.

Bhatia, Shashi Kant, Sachin V. Otari, Jong-Min Jeon, Ranjit Gurav, Yong-Keun Choi, Ravi Kant Bhatia, Arivalagan Pugazhendhi, Vinod Kumar, J. Rajesh Banu, Jeong-Jun Yoon, Kwon-Young Choi, and Yung-Hun Yang. 2021. "Biowaste-to-bioplastic (polyhydroxyalkanoates): Conversion technologies, strategies, challenges, and perspective." *Bioresource Technology* 326:124733. doi: https://doi.org/10.1016/j.biortech.2021.124733.

Cao, Na, Xinmin Yang, and Yuhua Fu. 2009. "Effects of various plasticizers on mechanical and water vapor barrier properties of gelatin films." *Food Hydrocolloids* 23 (3):729-735. doi: https://doi.org/10.1016/j.foodhyd.2008.07.017.

Chen, C. Will, Trong-Ming Don, and Hsiao-Feng Yen. 2006. "Enzymatic extruded starch as a carbon source for the production of poly(3-hydroxybutyrate-co-3-hydroxyvalerate) by Haloferax mediterranei." *Process Biochemistry* 41 (11):2289-2296. doi: https://doi.org/10.1016/j.procbio.2006.05.026.

Cherpinski, Adriane, Sergio Torres-Giner, Luis Cabedo, Jose Alberto Méndez, and Jose M. Lagaron. 2018. "Multilayer structures based on annealed electrospun biopolymer coatings of interest in water and aroma barrier fiber-based food packaging applications." *Journal of Applied Polymer Science* 135 (24):45501. doi: https://doi.org/10.1002/app.45501.

Cherpinski, Adriane, Sergio Torres-Giner, Jari Vartiainen, Maria Soledad Peresin, Panu Lahtinen, and Jose M. Lagaron. 2018. "Improving the water resistance of nanocellulose-based films with polyhydroxyalkanoates processed by the electrospinning coating technique." *Cellulose* 25 (2):1291-1307. doi: 10.1007/s10570-018-1648-z.

Clarke, David, Stefano Molinaro, Andrey Tyuftin, Declan Bolton, S. Fanning, and Joe P. Kerry. 2016. "Incorporation of commercially-derived antimicrobials into gelatin-based films and

assessment of their antimicrobial activity and impact on physical film properties." *Food Control* 64:202-211. doi: https://doi.org/10.1016/j.foodcont.2015.12.037.

Commission, European. 2018. "Plastic Waste: a European strategy to protect the planet, defend our citizens and empower our industries."

Desmaisons, Johanna, Martine Rueff, Julien Bras, and Alain Dufresne. 2018. "Impregnation of paper with cellulose nanocrystal reinforced polyvinyl alcohol: synergistic effect of infrared drying and CNC content on crystallinity." *Soft Matter* 14 (46):9425-9435. doi: 10.1039/C8SM01484A.

Doshi, Jayesh, and Darrell H. Reneker. 1995. "Electrospinning process and applications of electrospun fibers." *Journal of Electrostatics* 35 (2):151-160. doi: https://doi.org/10.1016/0304-3886(95)00041-8.

Fabra, María José, Amparo López-Rubio, Jesús Ambrosio-Martín, and Jose M. Lagaron. 2016. "Improving the barrier properties of thermoplastic corn starch-based films containing bacterial cellulose nanowhiskers by means of PHA electrospun coatings of interest in food packaging." *Food Hydrocolloids* 61:261-268. doi: https://doi.org/10.1016/j.foodhyd.2016.05.025.

Figueroa-Lopez, K. J., D. Enescu, S. Torres-Giner, L. Cabedo, M. A. Cerqueira, L. Pastrana, P. Fuciños, and J. M. Lagaron. 2020. "Development of electrospun active films of poly(3-hydroxybutyrate-co-3-hydroxyvalerate) by the incorporation of cyclodextrin inclusion complexes containing oregano essential oil." *Food Hydrocolloids* 108:106013. doi: https://doi.org/10.1016/j.foodhyd.2020.106013.

Figueroa-Lopez, Kelly J., Luis Cabedo, Jose M. Lagaron, and Sergio Torres-Giner. 2020. "Development of Electrospun Poly(3-hydroxybutyrate-co-3-hydroxyvalerate) Monolayers Containing Eugenol and Their Application in Multilayer Antimicrobial Food Packaging." *Frontiers in Nutrition* 7 (140). doi: 10.3389/fnut.2020.00140.

Figueroa-Lopez, Kelly J., Sergio Torres-Giner, Inmaculada Angulo, Maria Pardo-Figuerez, Jose Manuel Escuin, Ana Isabel Bourbon, Luis Cabedo, Yuval Nevo, Miguel A. Cerqueira, and Jose M. Lagaron. 2020. "Development of Active Barrier Multilayer Films Based on Electrospun Antimicrobial Hot-Tack Food Waste Derived Poly(3-hydroxybutyrate-co-3-hydroxyvalerate) and Cellulose Nanocrystal Interlayers." *Nanomaterials* 10 (12):2356.

Fotie, Ghislain, Stefano Gazzotti, Marco Aldo Ortenzi, and Luciano Piergiovanni. 2020. "Implementation of High Gas Barrier Laminated Films Based on Cellulose Nanocrystals for Food Flexible Packaging." *Applied Sciences* 10 (9):3201.

Fox, Justin, Jeong J. Wie, Barnaby W. Greenland, Stefano Burattini, Wayne Hayes, Howard M. Colquhoun, Michael E. Mackay, and Stuart J. Rowan. 2012. "High-Strength, Healable, Supramolecular Polymer Nanocomposites." *Journal of the American Chemical Society* 134 (11):5362-5368. doi: 10.1021/ja300050x.

Gallardo-Cervantes, Miguel, Yolanda González-García, Aida Alejandra Pérez-Fonseca, Martín Esteban González-López, Ricardo Manríquez-González, Denis Rodrigue, and Jorge Ramón Robledo-Ortíz. 2021. "Biodegradability and improved mechanical performance of polyhydroxyalkanoates/agave fiber biocomposites compatibilized by different strategies." *Journal of Applied Polymer Science* 138 (15):50182. doi: https://doi.org/10.1002/app.50182.

Ge, Haiyan, Yan Wu, Lana L. Woshnak, and Susan Hazels Mitmesser. 2021. "Effects of hydrocolloids, acids and nutrients on gelatin network in gummies." *Food Hydrocolloids* 113:106549. doi: https://doi.org/10.1016/j.foodhyd.2020.106549.

Geyer, Roland, Jenna R. Jambeck, and Kara Lavender Law. 2017. "Production, use, and fate of all plastics ever made." *Science Advances* 3 (7):e1700782. doi: 10.1126/sciadv.1700782.

Gicquel, Erwan, Céline Martin, José Garrido Yanez, and Julien Bras. 2017. "Cellulose nanocrystals as new bio-based coating layer for improving fiber-based mechanical and barrier properties." *Journal of Materials Science* 52 (6):3048-3061. doi: 10.1007/s10853-016-0589-x.

Gómez-Guillén, M. C., M. Pérez-Mateos, J. Gómez-Estaca, E. López-Caballero, B. Giménez, and P. Montero. 2009. "Fish gelatin: a renewable material for developing active biodegradable films." *Trends in Food Science & Technology* 20 (1):3-16. doi: https://doi.org/10.1016/j.tifs.2008.10.002.

Guk Choi, Gang, Moo Woong Kim, Jeong-Yoon Kim, and Young Ha Rhee. 2003. "Production of poly(3-hydroxybutyrate-co-3-hydroxyvalerate) with high molar fractions of 3-hydroxyvalerate by a threonine-overproducing mutant of Alcaligenes sp. SH-69." *Biotechnology Letters* 25 (9):665-670. doi: 10.1023/A:1023437013044.

Guo, Jimin, Liming Ge, Xinying Li, Changdao Mu, and Defu Li. 2014. "Periodate oxidation of xanthan gum and its crosslinking effects on gelatin-based edible films." *Food Hydrocolloids* 39:243-250. doi: https://doi.org/10.1016/j.foodhyd.2014.01.026.

Hubbe, Martin A., Ana Ferrer, Preeti Tyagi, Yuanyuan Yin, Carlos Salas, Lokendra Pal, and Orlando J. Rojas. 2017. "Nanocellulose in Thin Films, Coatings, and Plies for Packaging Applications: A Review." *2017* 12 (1):91.

Huber, Tim, Jörg Müssig, Owen Curnow, Shusheng Pang, Simon Bickerton, and Mark P. Staiger. 2012. "A critical review of all-cellulose composites." *Journal of Materials Science* 47 (3):1171-1186. doi: 10.1007/s10853-011-5774-3.

Jansson, Per-erik, Lennart Kenne, and Bengt Lindberg. 1975. "Structure of the extracellular polysaccharide from xanthomonas campestris." *Carbohydrate Research* 45 (1):275-282. doi: https://doi.org/10.1016/S0008-6215(00)85885-1.

Kang, Shufang, Yaqing Xiao, Xinyu Guo, Aiyun Huang, and Huaide Xu. 2021. "Development of gum arabic-based nanocomposite films reinforced with cellulose nanocrystals for strawberry preservation." *Food Chemistry* 350:129199. doi: https://doi.org/10.1016/j.foodchem.2021.129199.

Kanmani, Paulraj, and Jong-Whan Rhim. 2014. "Antimicrobial and physical-mechanical properties of agar-based films incorporated with grapefruit seed extract." *Carbohydrate Polymers* 102:708-716. doi: https://doi.org/10.1016/j.carbpol.2013.10.099.

Kumar, Anuj, Kummara Madhusudana Rao, and Sung Soo Han. 2018. "Application of xanthan gum as polysaccharide in tissue engineering: A review." *Carbohydrate Polymers* 180:128-144. doi: https://doi.org/10.1016/j.carbpol.2017.10.009.

Lavoine, Nathalie, Isabelle Desloges, Bertine Khelifi, and Julien Bras. 2014. "Impact of different coating processes of microfibrillated cellulose on the mechanical and barrier properties of paper." *Journal of Materials Science* 49 (7):2879-2893. doi: 10.1007/s10853-013-7995-0.

Le Gars, Manon, Benjamin Dhuiège, Aurore Delvart, Mohamed N. Belgacem, Karim Missoum, and Julien Bras. 2020. "High-Barrier and Antioxidant Poly(lactic acid)/Nanocellulose Multilayered Materials for Packaging." *ACS Omega* 5 (36):22816-22826. doi: 10.1021/acsomega.0c01955.

Leite, Liliane S. F., Caio M. Ferreira, Ana C. Corrêa, Francys K. V. Moreira, and Luiz H. C. Mattoso. 2020. "Scaled-up production of gelatin-cellulose nanocrystal bionanocomposite films by continuous casting." *Carbohydrate Polymers* 238:116198. doi: https://doi.org/10.1016/j.carbpol.2020.116198.

Li, Xiufang, Huijie Zhang, Lei He, Zhen Chen, Ziqi Tan, Renchuan You, and Dong Wang. 2018. "Flexible nanofibers-reinforced silk fibroin films plasticized by glycerol." *Composites*

Part B: Engineering 152:305-310. doi: https://doi.org/10.1016/j.compositesb.2018.08.136.

Madhusudana Rao, Kummara, Anuj Kumar, and Sung Soo Han. 2017. "Polysaccharide based bionanocomposite hydrogels reinforced with cellulose nanocrystals: Drug release and biocompatibility analyses." *International Journal of Biological Macromolecules* 101:165-171. doi: https://doi.org/10.1016/j.ijbiomac.2017.03.080.

Melendez-Rodriguez, Beatriz, Jinneth L. Castro-Mayorga, Maria A. M. Reis, Chris Sammon, Luis Cabedo, Sergio Torres-Giner, and Jose M. Lagaron. 2018. "Preparation and Characterization of Electrospun Food Biopackaging Films of Poly(3-hydroxybutyrate-co-3-hydroxyvalerate) Derived From Fruit Pulp Biowaste." *Frontiers in Sustainable Food Systems* 2 (38). doi: 10.3389/fsufs.2018.00038.

Melendez-Rodriguez, Beatriz, Sergio Torres-Giner, Laura Lorini, Francesco Valentino, Chris Sammon, Luis Cabedo, and Jose Maria Lagaron. 2020. "Valorization of Municipal Biowaste into Electrospun Poly(3-hydroxybutyrate-co-3-hydroxyvalerate) Biopapers for Food Packaging Applications." *ACS Applied Bio Materials* 3 (9):6110-6123. doi: 10.1021/acsabm.0c00698.

Moberg, Tobias, Karin Sahlin, Kun Yao, Shiyu Geng, Gunnar Westman, Qi Zhou, Kristiina Oksman, and Mikael Rigdahl. 2017. "Rheological properties of nanocellulose suspensions: effects of fibril/particle dimensions and surface characteristics." *Cellulose* 24 (6):2499-2510. doi: 10.1007/s10570-017-1283-0.

Mokhena, T. C., and M. J. John. 2020. "Cellulose nanomaterials: new generation materials for solving global issues." *Cellulose* 27 (3):1149-1194. doi: 10.1007/s10570-019-02889-w.

Montenegro, Mariana, Laura Boiero, Lorena Valle, and Claudio Borsarelli. 2012. "Gum Arabic: More Than an Edible Emulsifier." In.

Nur Hanani, Z. A., Y. H. Roos, and Joe P. Kerry. 2012. "Use of beef, pork and fish gelatin sources in the manufacture of films and assessment of their composition and mechanical properties." *Food Hydrocolloids* 29 (1):144-151. doi: https://doi.org/10.1016/j.foodhyd.2012.01.015.

Pereda, Mariana, Alain Dufresne, Mirta I. Aranguren, and Norma E. Marcovich. 2014. "Polyelectrolyte films based on chitosan/olive oil and reinforced with cellulose nanocrystals." *Carbohydrate Polymers* 101:1018-1026. doi: https://doi.org/10.1016/j.carbpol.2013.10.046.

Peresin, Maria S., Youssef Habibi, Arja-Helena Vesterinen, Orlando J. Rojas, Joel J. Pawlak, and Jukka V. Seppälä. 2010. "Effect of Moisture on Electrospun Nanofiber Composites of Poly(vinyl alcohol) and Cellulose Nanocrystals." *Biomacromolecules* 11 (9):2471-2477. doi: 10.1021/bm1006689.

Qiao, Congde, Guangxin Chen, Jianlong Zhang, and Jinshui Yao. 2016. "Structure and rheological properties of cellulose nanocrystals suspension." *Food Hydrocolloids* 55:19-25. doi: https://doi.org/10.1016/j.foodhyd.2015.11.005.

Qiu, Yuan-Zheng, Jing Han, and Guo-Qiang Chen. 2006. "Metabolic engineering of Aeromonas hydrophila for the enhanced production of poly(3-hydroxybutyrate-co-3-hydroxyhexanoate)." *Applied Microbiology and Biotechnology* 69 (5):537-542. doi: 10.1007/s00253-005-0034-6.

Reddy, Jeevan Prasad, and Jong-Whan Rhim. 2014. "Characterization of bionanocomposite films prepared with agar and paper-mulberry pulp nanocellulose." *Carbohydrate Polymers* 110:480-488. doi: https://doi.org/10.1016/j.carbpol.2014.04.056.

Rhim, J. W., L. F. Wang, and S. I. Hong. 2013. "Preparation and characterization of agar/silver nanoparticles composite films with antimicrobial activity." *Food Hydrocolloids* 33 (2):327-335. doi: https://doi.org/10.1016/j.foodhyd.2013.04.002.

Sanchez-Garcia, M. D., E. Gimenez, and J. M. Lagaron. 2007. "Novel PET Nanocomposites of Interest in Food Packaging Applications and Comparative Barrier Performance With Biopolyester Nanocomposites." *Journal of Plastic Film & Sheeting* 23 (2):133-148. doi: 10.1177/8756087907083590.

Sanchez-Garcia, M. D., E. Gimenez, and J. M. Lagaron. 2008. "Morphology and barrier properties of solvent cast composites of thermoplastic biopolymers and purified cellulose fibers." *Carbohydrate Polymers* 71 (2):235-244. doi: https://doi.org/10.1016/j.carbpol.2007.05.041.

Santos, Talita M., Men de Sá M. Souza Filho, Carlos Alberto Caceres, Morsyleide F. Rosa, João Paulo S. Morais, Alaídes M. B. Pinto, and Henriette M. C. Azeredo. 2014. "Fish gelatin films as affected by cellulose whiskers and sonication." *Food Hydrocolloids* 41:113-118. doi: https://doi.org/10.1016/j.foodhyd.2014.04.001.

Shojaeiarani, Jamileh, and Dilpreet Bajwa. 2018. "Functionalized Cellulose Nanocrystals for Improving the Mechanical Properties of Poly(Lactic Acid)." ASME 2018 International Mechanical Engineering Congress and Exposition.

Tong, Qunyi, Qian Xiao, and Loong-Tak Lim. 2013. "Effects of glycerol, sorbitol, xylitol and fructose plasticisers on mechanical and moisture barrier properties of pullulan–alginate–carboxymethylcellulose blend films." *International Journal of Food Science & Technology* 48 (4):870-878. doi: https://doi.org/10.1111/ijfs.12039.

Torres-Giner, S. 2011. "5 - Electrospun nanofibers for food packaging applications." In *Multifunctional and Nanoreinforced Polymers for Food Packaging*, edited by José-María Lagarón, 108-125. Woodhead Publishing.

Torres-Giner, S., N. Montanes, T. Boronat, L. Quiles-Carrillo, and R. Balart. 2016. "Melt grafting of sepiolite nanoclay onto poly(3-hydroxybutyrate-co-4-hydroxybutyrate) by reactive extrusion with multi-functional epoxy-based styrene-acrylic oligomer." *European Polymer Journal* 84:693-707. doi: https://doi.org/10.1016/j.eurpolymj.2016.09.057.

Trache, Djalal, Ahmed Fouzi Tarchoun, Mehdi Derradji, Tuan Sherwyn Hamidon, Nanang Masruchin, Nicolas Brosse, and M. Hazwan Hussin. 2020. "Nanocellulose: From Fundamentals to Advanced Applications." *Frontiers in Chemistry* 8 (392). doi: 10.3389/fchem.2020.00392.

Verbeken, D., S. Dierckx, and K. Dewettinck. 2003. "Exudate gums: occurrence, production, and applications." *Applied Microbiology and Biotechnology* 63 (1):10-21. doi: 10.1007/s00253-003-1354-z.

Wang, Jinwu, Douglas J. Gardner, Nicole M. Stark, Douglas W. Bousfield, Mehdi Tajvidi, and Zhiyong Cai. 2018. "Moisture and Oxygen Barrier Properties of Cellulose Nanomaterial-Based Films." *ACS Sustainable Chemistry & Engineering* 6 (1):49-70. doi: 10.1021/acssuschemeng.7b03523.

Xiao, Chaobo, Zhenjun Zhang, Jinhua Zhang, Yongshang Lu, and Lina Zhang. 2003. "Properties of regenerated cellulose films plasticized with α-monoglycerides." *Journal of Applied Polymer Science* 89 (13):3500-3505. doi: https://doi.org/10.1002/app.12509.

Zhang, H. F., L. Ma, Z. H. Wang, and G. Q. Chen. 2009. "Biosynthesis and characterization of 3-hydroxyalkanoate terpolyesters with adjustable properties by Aeromonas hydrophila." *Biotechnol Bioeng* 104 (3):582-9. doi: 10.1002/bit.22409.

Zhao, Wei, and Guo-Qiang Chen. 2007. "Production and characterization of terpolyester poly(3-hydroxybutyrate-co-3-hydroxyvalerate-co-3-hydroxyhexanoate) by recombinant

Aeromonas hydrophila 4AK4 harboring genes phaAB." *Process Biochemistry* 42 (9):1342-1347. doi: https://doi.org/10.1016/j.procbio.2007.07.006.

Zhao, Yadong, Carl Moser, Mikael E. Lindström, Gunnar Henriksson, and Jiebing Li. 2017. "Cellulose Nanofibers from Softwood, Hardwood, and Tunicate: Preparation–Structure–Film Performance Interrelation." *ACS Applied Materials & Interfaces* 9 (15):13508-13519. doi: 10.1021/acsami.7b01738.

Chapter IX

High-Oxygen-Barrier Multilayer Films Based on Polyhydroxyalkanoates and Cellulose Nanocrystals

Nanomaterials 2021, 11(6), 1443

Beatriz Meléndez-Rodríguez[1], Sergio Torres-Giner[1,†], Inmaculada Angulo[2], María Pardo-Figuerez[1,3], Loïc Hilliou[4], José Manuel Escuin[5], Luis Cabedo[6], Yuval Nevo[7], Cristina Prieto[1], and José María Lagarón[1]

[1] Novel Materials and Nanotechnology Group, Institute of Agrochemistry and Food Technology (IATA), Spanish Council for Scientific Research (CSIC), Paterna, Spain

[2] Gaiker Technology Centre, Basque Research and Technology Alliance (BRTA). Parque Tecnológico de Bizkaia, edificio 202, Zamudio (Bizkaia), Spain

[3] Bioinicia R&D, Bioinicia S.L., Valencia, Spain

[4] IPC/I3N, Institute for Polymers and Composites, Department of Polymer Engineering, University of Minho, Braga, Portugal

[5] Tecnopackaging S.L., Poligono Industrial Empresarium, Zaragoza, Spain

[6] Polymers and Advanced Materials Group (PIMA), School of Technology and Experimental Sciences, Universitat Jaume I (UJI), Castellón, Spain

[7] Melodea Bio-Based Solutions, Faculty of Agriculture-Hebrew University, Rehovot, Israel

[†] Current address: Research Institute of Food Engineering for Development (IIAD), Universitat Politècnica de València (UPV), Valencia, Spain

Abstract

This study reports on the development and characterization of organic recyclable high-oxygen-barrier multilayer films based on different commercial polyhydroxyalkanoate (PHA) materials, including a blend with commercial poly(butylene adipate-*co*-terephthalate) (PBAT), which contained an inner layer of cellulose nanocrystals (CNCs) and an electrospun hot-tack adhesive layer of poly(3-hydroxybutyrate-*co*-3-hydroxyvalerate) (PHBV) derived from cheese whey (CW). As a result, the full multilayer structures were made from bio-based and/or compostable materials. A characterization of the produced films was carried out in terms of morphological, optical, mechanical, and barrier properties with respect to water vapor, limonene, and oxygen. Results indicate that the multilayer films exhibited a good interlayer adhesion and contact transparency. The stiffness of the multilayers was generally improved upon incorporation of the CNC interlayer, whereas the enhanced elasticity of the blend was reduced to some extent in the multilayer with CNCs, but this was still much higher than for the neat PHAs. In terms of barrier properties, it was found that 1 µm of the CNC interlayer was able to reduce the oxygen permeance between 71 % and 86 %, while retaining the moisture and aroma barrier of the control materials.

Keywords: PHBV; nanocellulose; multilayers; barrier films; packaging

1. Introduction

Packaging materials based on biopolymers that can biodegrade in both industrial and home compost conditions currently represent an alternative to solve the environmental issue of plastic accumulation (Babu, O'Connor, and Seeram 2013, Quiles-Carrillo et al. 2017). Polyhydroxyalkanoates (PHAs) are thermoplastic biopolyesters produced by various microorganisms, mainly bacteria, during fermentation of sugar or lipids under famine conditions as energy-reserve inclusions in the cytoplasm (Rehm 2003). The most widely studied PHA is poly(3-hydroxybutyrate) (PHB), whose thermal and mechanical characteristics are similar to polypropylene (PP) (Tian et al. 2021). However, PHB is brittle and presents a poor processing window due to its high crystallinity and low thermal stability. For these reasons, PHB is being progressively replaced by its poly(3-hydroxybutyrate-*co*-3-hydroxyvalerate) (PHBV) and poly(3-hydroxybutyrate-*co*-4-hydroxybutyrate) P(3HB-*co*-4HB) copolymers (Nduko, Matsumoto, and Taguchi 2012, Thellen, Cheney, and Ratto 2013). PHAs are not only bio-based but also industrially compostable and biodegradable in the environment (Thellen et al. 2008, Weng, Wang, and Wang 2011). Thus, PHAs show a great potential to replace conventional polyolefins for packaging applications (Raza, Abid, and Banat 2018).

Furthermore, PHA microbial polyesters show relatively high water vapor and moderate oxygen barrier properties (Rivera-Briso and Serrano-Aroca 2018). In this scenario, nanocellulose can play an important role in packaging applications as a novel and sustainable oxygen barrier material (Cherpinski et al. 2019, Martínez-Sanz, Lopez-Rubio, and Lagaron 2013, Vartiainen et al. 2014). On the one hand, cellulose is a naturally occurring polymer that is stored in plant cell walls, which can be isolated from various wooden and nonwooden sources by different chemical and mechanical treatments (Dufresne 2012). On the other hand, it is fully biodegradable in the environment (Leppänen et al. 2020, Zinge and Kandasubramanian 2020). For example, Qi et al. (Qi, Chang, and Zhang 2009) reported complete biodegradation of cellulose films in soil at about 30 °C within 1 month. Within the different kinds of celluloses, there are three main categories, namely, cellulose nanofibrils (CNFs), which contain amorphous and crystalline regions (Moon et al. 2011), cellulose nanocrystals (CNCs), and bacterial nanocellulose (BNC), with the latter still under development for large-scale industrial production (Kim et al. 2015, Velásquez-Riaño and Bojacá 2017). In the case of CNCs, these can be obtained by processing cellulose under carefully controlled acidic treatment conditions (Peng et al. 2011). These cellulosic particles show diameters in the 5–20 nm range, whereas lengths range from 100 to 400 nm. Furthermore, CNCs have high self-assembly properties, which allows the production of continuous materials such as high-quality self-supporting transparent films and coatings that are habitually termed “nanopapers” (Barhoum et al. 2017). These nanocellulose films exhibit very low gas permeability, which makes them perfect candidates for compostable high-gas-barrier packaging applications (Lavoine et al. 2012). However, nanopapers are also highly hydrophilic due to the presence of a large number of hydroxyl groups (–OH), which represents a disadvantage for their use in packaging in moist environments.

So far, some research studies have dealt with the improvement of the barrier properties of nanopapers in high-humidity conditions, for instance, by dispersing CNCs in hydrophobic polymer matrices (Karkhanis et al. 2018), by performing surface modifications on CNC films (Visanko et al. 2015), and by crosslinking treatments (Shimizu, Saito, and Isogai 2016). Another innovative strategy is the development of multilayer systems that can protect the CNC layers with hydrophobic polymers as outer layers, such as PP and polyethylene terephthalate (PET) (Kim,

Choi, and Jin 2020, Nuruddin et al. 2020). Multilayers are structures widely used in the food packaging industry that are created by assembling a different number of layers, typically between three and nine, where each layer provides a particular performance to the whole system. Typically, the outer layers, also called structural layers, provide food contact, printability, and mechanical and moisture resistance, whereas the intermediate layers provide the necessary barrier to gases and organic vapors to preserve food quality and safety (Fang et al. 2005). Therefore, the high performance of multilayer films makes them very suitable for use in the packaging industry, especially for extending goods shelf life (Benetto et al. 2015).

Today, there are different methods for the preparation of multilayers, for instance, layer-by-layer (LbL) assembly (Xiang et al. 2014), co-extrusion (Winotapun et al. 2019), co-injection stretch blow molding (Akkapeddi and Lynch 2013), lamination (Rhim 2013), metallization (Del Nobile et al. 1999), and coatings by plasma (Wang, Wang, et al. 2020) or solvent casting (Rhim et al. 2006). More recently, electrospinning has emerged as an innovative technique to generate polymer mats composed of fibers with diameters ranging from micro- to nanoscale via the action of high-electric fields, allowing the formation of coatings and monolayers of interest in the packaging industry (Echegoyen et al. 2017, Torres-Giner 2011, Torres-Giner et al. 2018). In this context, Figueroa-Lopez et al. (Figueroa-Lopez, Cabedo, et al. 2020) developed electrospun PHBV fibers containing eugenol as potential antimicrobial monolayers in multilayer structures for food packaging. Similarly, Cherpinski et al. (Cherpinski, Torres-Giner, Cabedo, et al. 2018) developed electrospun coatings of biopolyesters to improve the barrier properties and water resistance of paper packaging. Furthermore, electrospinning allows the incorporation of functional ingredients into the polymer fibers since it is carried out at room temperature, opening up novel opportunities in active and bioactive packaging (Torres-Giner, Pérez-Masiá, and Lagaron 2016). Additionally, the application on the electrospun fiber mats of a thermal post-treatment below the biopolymer's melting temperature (T_m), also called annealing, yields the formation of continuous films, so-called biopapers (Alp-Erbay et al. 2019, Melendez-Rodriguez et al. 2018, Melendez-Rodriguez et al. 2020). Electrospinning can favor the preservation of thermolabile and volatile substances in the film layers since the annealing process of the electrospun fibers is carried out at lower temperatures and shorter times in comparison with the melting routes (Alp-Erbay et al. 2019, Melendez-Rodriguez et al. 2019). Moreover, these annealed electrospun mats, so-called biopapers, can also originally perform as hot-tack (HT) interlayers via a mechanism of interfiber coalescence, adhering different film layers without the need for tie layers (Fabra, López-Rubio, and Lagaron 2014).

Previous studies in our laboratory developed multilayers for their use in both rigid and flexible packaging with antimicrobial and vapor barrier properties, in which electrospun PHA fibers with active substances and CNC coatings were used as intermediate layers to provide these properties (Figueroa-Lopez, Cabedo, et al. 2020, Figueroa-Lopez, Torres-Giner, et al. 2020). Following this concept, the present study focuses on the development of new multilayer designs for use as a high-oxygen-barrier film. To this end, a film prepared with three different types of PHA-based substrates, i.e., a commercial PHBV film, an extruded PHBV film, and a PHA-based blend film with poly(butylene adipate-*co*-terephthalate) (PBAT), was coated with a CNC layer. In parallel, another film was coated with electrospun industrial biowaste-derived PHA fibers, used as HT. Thereafter, the two coated layers were assembled together by lamination, and their morphological, optical, mechanical, and barrier properties were evaluated to assess the potential application of the resulting multilayer films in organic recyclable food packaging.

2. Materials and Methods

2.1. Materials

The CNC commercial aqueous solution was supplied by Melodea Ltd. (Rehovot, Israel) with a concentration of 2 wt %, yielding a pH of 4.5. The CNC suspension was stored at 4 °C as received to be used within a 1-month period. 1-Butanol, reagent grade with 99.5 % purity, and d-limonene, with 98 % purity, were both obtained from Sigma Aldrich S.A. (Madrid, Spain). Chloroform of 99.8 % purity was purchased from Panreac S.A. (Barcelona, Spain). The food contact primer, Loctite Liofol PR1550, was supplied by Henkel Ibérica S.A. (Barcelona, Spain).

A PHBV copolyester was obtained from fermented cheese whey (CW), a waste of the dairy industry. Further details about the material and its synthesis can be found elsewhere (Cruz et al. 2016). The PHBV copolymer was purified using the chloroform-based extraction method reported previously (Melendez-Rodriguez et al. 2018, Melendez-Rodriguez et al. 2019, Melendez-Rodriguez et al. 2020). The 3HV content of the copolymer was 20 mol % as determined by gas chromatography (GC) using the method described by Lanham et al. (Lanham et al. 2013) in a Bruker 430-GC gas chromatograph equipped with a flame ionization detector (FID) and a BR-SWax column (60 m, 0.53 mm internal diameter, 1 mm film thickness, Bruker, Torrance, CA, USA).

A commercial film of PHBV containing 8 mol % 3HV, so-called PHBV8, with a thickness of 25 µm, was purchased from Goodfellow Cambridge Limited (Huntindgon, UK) as grade BV301025.

The PHA blend compound containing 50 wt % PHB and 50 wt % PBAT was produced by Tecnopackaging (Zaragoza, Spain). For this, the PHB grade (Biomer® P309) was supplied by Biomer (Krailling, Germany). This grade has a melt flow index (MFI) of 10 g/10 min at 180 °C for a load of 2.16 kg. A film blowing grade of PBAT (Ecoflex® F blend C1200) was supplied by BASF (Ludwigshafen am Rhein, Germany). This grade has an MFI of 2.5–4 g/10 min at 190 °C for a load of 2.16 kg and was claimed to be fully compostable by the manufacturer. Film blowing of the blend was also performed by Tecnopackaging using film blowing extrusion equipment (LABTECH LF400 from Techlab Systems S.L., Lezo, Spain). The parameters used in the machine were as follows: max. bubble diameter of 350 mm, variable blowing speed, twin-screw extruder LE25-30/C, large 2.4 m high film tower, pneumatically operated film nip rolls, screw speed infinite variable from 0 to 300 rpm, and motorized adjustment of film tower height. The set parameters of the film blowing experiments were as follows: screw speed of 65 rpm, screw pressure of 196 bar, screw temperature profile of 170 °C/170 °C/168 °C/168 °C, superior roll speed of 1.8 m/min, collection roll speed of 2.7 m/min, and tower height of 1500 mm. The resulting blown film, so-called PHB Blend, had a thickness of around 60 µm and a film width of 250 mm.

A noncommercial PHBV film, so-called PHBV2, was obtained by delamination of a two-layer co-extruded film blowing film. The procedure reported earlier by Cunha et al. (Cunha et al. 2016) was followed to obtain the bilayer film made of $PHBV_{int}/PBAT_{out}$ (PBAT as external layer and PHBV as internal layer). The PHBV used was ENMAT Y1000P, produced by Tianan Biologic Materials (Ningbo, China), whereas the PBAT grade used was the same grade as described above. In the case of PHBV, the 3HV fraction was 2 mol % with a density of 1.25 g/cm^3 and a molecular weight (M_W) of 2.8×10^5 g/mol. The bilayer coextruded film was performed at the University of Minho (Portugal) in a laboratory blown film extrusion line (Periplast, Portugal), which was

configured with an extrusion/co-extrusion head and die for the production of bilayered films from combined grades. The set temperature profile in both extruders was 150 °C/155 °C/155 °C from hopper to screw tip, and the head and die were kept at 155 °C/155 °C/160 °C. The screw speed was set at 46 rpm, which corresponded to outputs of approximately 3 kg/h. All materials were dried for 24 h at 60 °C before processing. During co-extrusion, both fan speed and air ring aperture were kept constant (to maintain similar cooling conditions), while both the blow-up ratio (BUR) and the take-up ratio (TUR) were varied to produce films with thicknesses ranging roughly from 70 to 150 mm. Since the bilayer film showed easy delamination, the PHBV layer was separated from the PBAT layer, and the former was used as substrate in this study. The PHBV2 film had a thickness of ca. 70 μm.

2.2. Application of the CNCs

A layer of CNCs was applied using lab or pilot applicators (see below) on one side of the three film substrates, that is, PHBV8, PHBV2, and PHB Blend. Before applying CNCs, a corona treatment (100 watt·cm^2/min) was applied on the three substrates in order to make them more hydrophilic, decreasing the contact angles of the surfaces. A food contact primer layer containing a wetting agent to facilitate homogeneous coating was applied on the substrates prior to coating with CNCs since it was seen to improve the adhesion between the substrates and the CNC layer. The food contact primer and wetting agent were mixed in an IKA Eurostar 6000 mixer (IKA®-Werke GmbH & Co. KG, Staufen, Germany) at low speed (200 rpm) to avoid bubbles. During processing, it was observed that the primer allowed an increase in the stability of the layers at elevated temperatures. In addition, the CNC layer was easier to coat using the primer.

The multilayers of PHBV8 and PHBV2 were laminated at a lab scale, whereas the PHB Blend was laminated at a pilot scale. At a lab scale, the food contact primer was applied on the surface of the treated films by means of an automatic film applicator (Zehntner ACC378.100) with a profile rod coater of 6 μm wet thickness and dried in an oven at 90 °C for 1 min. On top of the primer, the CNC solution was coated using the same automatic film applicator (Zehntner ACC378.100) with a profile rod of 100 μm wet thickness and a speed of 5 mm/sec. The drying temperature in the oven was 90 °C for 15 min, and the final thickness of the CNC layer was ca. 1 μm. At a pilot scale, the primer was applied onto the PHB Blend by a meter bar head with a profile rod of 6 μm in a Rotary Koater (ROKO) Model 30-30-01 equipment (TMI Machine Testing Inc., New Castle, DE, USA) and dried at 50 °C. The CNC solution was applied on top of the primer with a profile rod of 50 μm. Drying was performed in continuous in the lamination equipment at 90 °C at 1 m/min to ensure complete drying of the CNC solution.

2.3. Electrospinning of Food Waste Derived PHBV

In order to improve the adhesion between the uncoated and the CNC-coated substrates, an electrospun fiber mat of the PHBV derived from industrial cheese whey was applied on the uncoated substrate. The electrospun fibers were used as HT due to the fact that the high roughness of the ultrathin fiber mat was found to facilitate film bonding upon annealing.

Prior to electrospinning, the purified PHBV powder was dissolved at 8 wt % in a mixture of chloroform and butanol 75:25 (w/w) under magnetic stirring for 24 h at 50 °C. This solvent

mixture is, to the best of our knowledge, the most optimal and sustainable organic solvent system able to successfully electrospin PHAs. The PHBV solution was processed by electrospinning using a high-throughput dual polarization Fluidnatek® LE-500 pilot-plant device containing a roll-to-roll system manufactured by Bioinicia S.L. (Valencia, Spain). The equipment was operated with a motorized multi-needle injector, scanning vertically toward the different substrate collectors (PHBV8, PHBV2, and PHB Blend) at 25 °C and 40 % RH. The conditions were optimized for the solution, being set at a flow rate of 45 ml/h, 22 kV of voltage, and 30 cm of needle-to-collector distance.

2.4. Lamination

Lamination of the coated layers was carried out using a Reliant Powerbond equipment (Reliant Machinery Ltd., Luton, UK), depositing the samples over the equipment conveyor belt that traveled through the oven at a speed of 5 m/min at 140 °C for 20 s. The resultant multilayer samples based on PHBV2 and PHB Blend had an average thickness in the 130–150 μm range, whereas that based on the PHBV8 presented a thickness of 50 μm. The final structures are depicted in **Figure 1**. Equivalent multilayers without CNCs were obtained, in the same conditions, as controls.

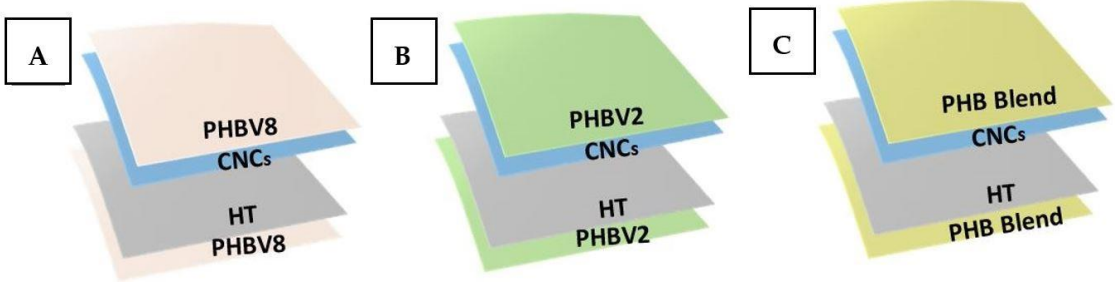

Figure 1. Schematics of the multilayer films of (A) poly(3-hydroxybutyrate-*co*-3-hydroxyvalerate) containing 8 mol % 3-hydroxyvalerate (PHBV8), (B) poly(3-hydroxybutyrate-*co*-3-hydroxyvalerate) with 2 mol % 3-hydroxyvalerate (PHBV2), and (C) poly(3-hydroxybutyrate) with poly(butylene adipate-*co*-terephthalate) blend (PHB Blend). The electrospun biowaste-derived poly(3-hydroxybutyrate-*co*-3-hydroxyvalerate) with 20 mol % 3-hydroxyvalerate mat was used as a hot-tack (HT) coating on one layer, while the cellulose nanocrystal (CNC) layer was added on the other one.

2.5. Characterization

2.5.1. Scanning Electron Microscopy

The cross-section of the three multilayers was observed by scanning electron microscopy (SEM) using an S-4800 device from Hitachi (Tokyo, Japan). The multilayers were cryo-fractured by immersion in liquid nitrogen and, then, fixed to beveled holders using conductive double-sided adhesive tape. The samples were sputtered with a mixture of gold/palladium under vacuum prior to observation. An accelerating voltage of 10 kV was used, and the estimation of the dimensions

was performed by means of the Aperture software from Apple (Cupertino, CA, USA) using a minimum of 20 SEM micrographs in their original magnification.

2.5.2. Transparency

The light transmission of the multilayers was determined in specimens of 50 mm × 30 mm by quantifying the absorption of light at wavelengths between 200 and 700 nm in an ultraviolet–visible (UV–Vis) spectrophotometer VIS3000 from Dinko Instruments (Barcelona, Spain). The transparency (T) and opacity (O) were calculated using Equations (1) (Shiku et al. 2004) and (2) (Kanatt et al. 2012), respectively.

$$T = \frac{A_{600}}{L} \quad (1)$$

$$O = A_{500} \times L \quad (2)$$

where A_{500} and A_{600} are the absorbance values at 500 and 600 nm, respectively, and L is the film thickness (mm).

2.5.3. Color Measurements

The multilayer color was determined using a chroma meter CR-400 (Konica Minolta, Tokyo, Japan). The color difference (ΔE^*) was calculated, as defined by the Commission Internationale de l'Eclairage (CIE), using Equation (3) (Arfat et al. 2017).

$$\Delta E^* = [(\Delta L^*)^2 + (\Delta a^*)^2 + (\Delta b^*)^2]^{0.5} \quad (3)$$

where ΔL^*, Δa^*, and Δb^* correspond to the differences in terms of lightness from black to white, color from green to red, and color from blue to yellow, respectively, between the test multilayers with CNCs and the control samples (without CNCs). Color change was evaluated using the following assessment: unnoticeable ($\Delta E^* < 1$), only an experienced observer can notice the difference ($\Delta E^* \geq 1$ and < 2), an unexperienced observer can notice the difference ($\Delta E^* \geq 2$ and < 3.5), clear noticeable difference ($\Delta E^* \geq 3.5$ and < 5), and the observer can notice different colors ($\Delta E^* \geq 5$) (Mokrzycki and Tatol 2011).

2.5.4. Mechanical Tests

Tensile tests of the multilayers were conducted in a universal testing machine Shimatzu AGS-X 500N (Shimatzu, Kyoto, Japan) at room temperature with a crosshead speed of 10 mm/min. Dumbbell samples according to ASTM D638 (Type IV) standard were die-cut from the multilayer assembly both in the machine direction (MD) and in the transversal direction (TD). Samples were conditioned to the test conditions at 40 % RH and 25 °C for 24 h prior to tensile assay. At least

six samples were tested for each material, and the average values of the mechanical parameters and standard deviations were reported.

2.5.5. Permeance Tests

The water vapor permeance (WVP) of the multilayers was determined using the gravimetric method ASTM E96-95 in triplicate. The control samples were cups with aluminum films to estimate solvent loss through the sealing. For this, 5 ml of distilled water was placed inside a Payne permeability cup (diameter of 3.5 cm) from Elcometer Sprl (Hermallesous-Argenteau, Belgium). The multilayers were not in direct contact with water but exposed to 100 % RH on one side and secured with silicon rings. They were placed within a desiccator, sealed with dried silica gel, at 0 % RH in a cabinet at 25 °C. WVP was calculated from the regression analysis of weight loss data vs. time, and the weight loss was calculated as the total loss minus the loss through the sealing.

For limonene permeance (LP), the procedure was similar to that described above for WVP with the difference that 5 ml of $_{D}$-limonene was placed inside the Payne permeability cups, which were placed under controlled room conditions of 25 °C and 40 % RH.

The oxygen permeance (OP) coefficient was derived from the oxygen transmission rate (OTR) measurements that were recorded using an Oxygen Permeation Analyzer M8001 from Systech Illinois (Thame, UK) at 20 % RH and 25 °C, in duplicate. The samples were purged with nitrogen, before exposure to an oxygen flow of 10 ml/min. The exposure area during the test was 5 cm^2 for each sample.

2.6. Statistical Analysis

The optical, mechanical, and barrier properties were evaluated through analysis of variance (ANOVA) using STATGRAPHICS Centurion XVI v 16.1.03 from StatPoint Technologies, Inc. (Warrenton, VA, USA). Fisher's least significant difference (LSD) was used at the 95 % confidence level (p <0.05).

3. Results and Discussion

3.1. Morphology of the Multilayers

The morphologies of the cross-sections of the three multilayers with and without CNCs analyzed by SEM are shown in **Figure 2**. The multilayers without CNCs, **Figure 2IA–C**, showed homogeneous surfaces without separation between the two layers. The HT could not be discerned in the SEM images, indicating good adhesion with the PHBV8, PHBV2, and PHB Blend layers, since all were based on PHA. When the CNCs were incorporated, this material was seen to form a continuous layer approximately of ca. 1 µm after cryofracture (see **Figure 2IIA–C**), thus supporting a good adhesion between the different layers.

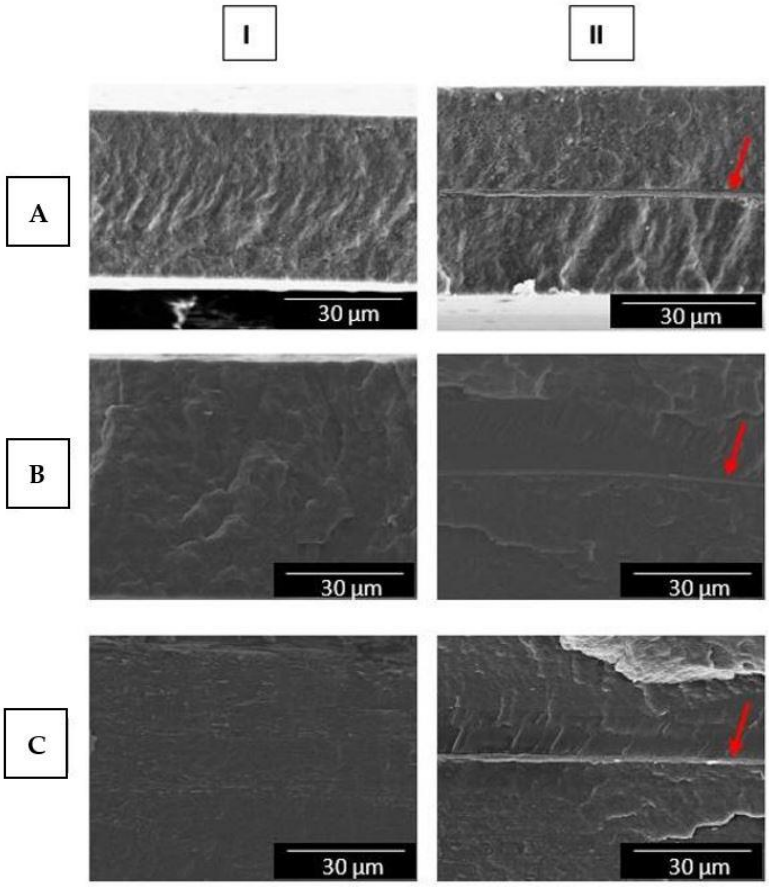

Figure 2. Scanning electron microscopy (SEM) micrographs of the cross-sections of the multilayer films of: (A) poly(3-hydroxybutyrate-*co*-3-hydroxyvalerate) containing 8 mol % 3-hydroxyvalerate (PHBV8), (B) poly(3-hydroxybutyrate-*co*-3-hydroxyvalerate) with 2 mol % 3-hydroxyvalerate (PHBV2), and (C) poly(3-hydroxybutyrate) with poly(butylene adipate-*co*-terephthalate) blend (PHB Blend), without (I) and with cellulose nanocrystals (CNCs) (II) coating. Images were taken at 1500× with scale markers of 30 µm. Red arrows indicate the CNC layer.

The display of the CNC layer when coated in a multilayer system was previously reported (Kwon et al. 2020, Ogunsona and Mekonnen 2020). The natural adhesive properties of electrospun polymers have also been reported when used as an interlayer in a multilayer system. Thus, previous works have shown the way in which annealed polymer fibers keep layers of different polymers together without the need for synthetic adhesives, maintaining the biodegradability and/or renewability of the final structure (Fabra, López-Rubio, and Lagaron 2014). In addition to this advantage, improvements in optical and barrier properties have been reported when intermediate layers of electrospun fibers are used, as this technique allows the thickness to be controlled as required (Busolo, Torres-Giner, and Laaron 2009, Fabra et al. 2013).

3.2. Optical Properties

The pictures of the resulting multilayers prepared with the three different substrates are displayed in **Figure 3**. All three substrates, regardless of whether the CNCs were present or not, showed a good contact transparency. More specifically, a slight yellowish tone was presented in the case of PHBV2 and PHB Blend substrates, whilst no color was observed in the PHBV8. These colors are intrinsic to the materials used, and the incorporation of CNCs and HT did not affect the final color of the multilayers, as both are colorless and the thickness used was likely not sufficient to have any influence on this.

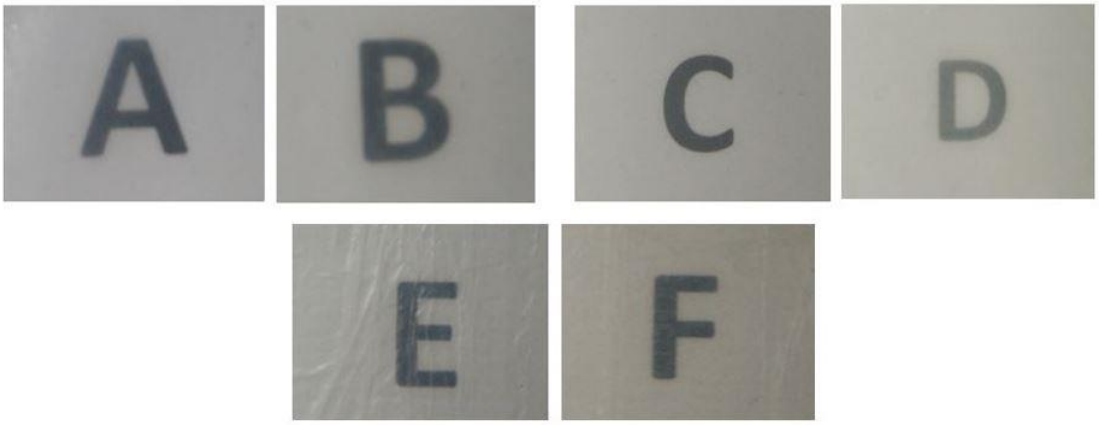

Figure 3. Contact transparency pictures of the multilayers made of (A) poly(3-hydroxybutyrate-*co*-3-hydroxyvalerate) containing 8 mol % 3-hydroxyvalerate (PHBV8) without cellulose nanocrystals (CNCs), (B) PHBV8 with CNCs, (C) PHBV with 2 mol % 3-hydroxyvalerate (PHBV2) without CNCs, (D) PHBV2 with CNCs, (E) poly(3-hydroxybutyrate) with poly(butylene adipate-*co*-terephthalate) blend (PHB Blend) without CNCs, and (F) PHB Blend with CNCs. Letters were placed underneath the films to assess their contact transparency.

The color parameters (a^*, b^*, L^*) and the transparency (T) and opacity (O) values are reported in **Table 1**. All substrates presented positive values in a^*, indicating that the multilayers tended to be red instead of green, while b^* varied from negative values toward a blue tonality. With respect to L^*, all the multilayers showed values around 90. The color differences between the multilayers when CNCs were added are also reported. While PHBV8 and PHB Blend presented differences that only an experienced observer would notice, PHBV2 showed clear noticeable differences, which could be ascribed to the fact that the film was more heterogeneous and, therefore, depending on the area chosen, its thickness could vary. Regarding the T value, the most transparent multilayers were PHB Blend, followed by PHBV8 and, finally, PHBV2. It should be noted that the addition of the CNC coating made all multilayers more transparent, meaning that the CNC coating resulted in a smoother surface of the substrate and, consequently, greater transparency. This homogeneity caused UV–Vis light to pass through the films without inducing light scattering. Lastly, all the multilayers showed similar low values of O, ranging between 0.02 and 0.2. Transparency is a key property in many types of food packaging, as visual inspection through the material is preferred by the consumers (Cozzolino et al. 2014). In this case, it can be

stated that all tested multilayers provided a good level of transparency, which could be of interest when transparent packaging is required.

Table 1. Optical properties of the multilayer films of poly(3-hydroxybutyrate-*co*-3-hydroxyvalerate) (PHBV) containing 8 mol % (PHBV8) and 2 mol % 3-hydroxyvalerate (PHBV2) and poly(3-hydroxybutyrate) with poly(butylene adipate-*co*-terephthalate) blend (PHB Blend), with and without cellulose nanocrystals (CNCs).

Sample	a^*	b^*	L^*	ΔE^*	T	O
PHBV8	2.05 ± 0.05^{a}	-3.07 ± 0.08^{a}	90.98 ± 0.02^{a}	-	11.51 ± 0.04^{a}	0.03 ± 0.01^{a}
PHBV8 with CNCs	2.41 ± 0.07^{a}	-3.89 ± 0.05^{b}	90.53 ± 0.02^{a}	1.00 ± 0.02^{a}	9.29 ± 0.03^{b}	0.02 ± 0.01^{a}
PHBV2	1.46 ± 0.07^{b}	0.28 ± 0.02^{c}	90.58 ± 0.03^{a}	-	14.39 ± 0.07^{c}	$0.07 \pm 0.02^{a,b}$
PHBV2 with CNCs	0.53 ± 0.02^{c}	4.17 ± 0.07^{d}	90.07 ± 0.05^{a}	4.03 ± 0.03^{b}	10.86 ± 0.05^{d}	0.18 ± 0.01^{b}
PHB Blend	1.43 ± 0.03^{b}	-0.64 ± 0.03^{e}	90.43 ± 0.04^{a}	-	4.70 ± 0.02^{e}	0.13 ± 0.03^{b}
PHB Blend with CNCs	1.35 ± 0.02^{b}	-0.28 ± 0.02^{f}	90.07 ± 0.03^{a}	0.52 ± 0.03^{c}	3.43 ± 0.03^{f}	0.13 ± 0.04^{b}

a^*: red/green coordinates (+a red, −a green); b^*: yellow/blue coordinates (+b yellow, −b blue); L^*: luminosity (+L luminous, −L dark); ΔE^*: color differences; T: transparency; O: opacity.

$^{a–f}$ Different letters in the same column indicate a significant difference among the samples ($p < 0.05$).

3.3. Mechanical Properties

The mechanical properties in both transversal direction (TD) and machine direction (MD) in terms of elastic modulus (E), tensile strength (σ_y), elongation at break (ε_b), and tensile toughness (T) of the multilayers were assessed, and the results are gathered in **Table 2**. The compositions with pure PHBV presented a stiff and brittle mechanical behavior, with elastic moduli above 2 GPa, elongation at break below 3 %, and very low tensile toughness for both materials, being more remarkable for the sample with lower HV content when compared to the PHBV8. This mechanical behavior is in good agreement with the brittle nature of PHB and PHBV with low HV content (Laycock et al. 2014). Blending the PHB with PBAT resulted in a toughening effect, as derived from the considerable increase in the elongation at break and tensile toughness compared to the PHBV materials. However, this toughening effect entailed a decrease in the elastic modulus.

Table 2. Mechanical properties in terms of elastic modulus (E), tensile strength at yield (σ_y), elongation at break (ε_b), and toughness (T) of the different multilayers of poly(3-hydroxybutyrate-*co*-3-hydroxyvalerate) (PHBV) containing 8 mol % (PHBV8) and 2 mol % 3-hydroxyvalerate (PHBV2) and poly(3-hydroxybutyrate) with poly(butylene adipate-*co*-terephthalate) blend (PHB Blend) with and without cellulose nanocrystals (CNCs) in the transversal direction (TD) and machine direction (MD).

Sample	MD				TD			
	E (MPa)	**σ_y (MPa)**	**ε_b (%)**	**T (mJ/m^3)**	**E (MPa)**	**σ_y (MPa)**	**ε_b (%)**	**T (mJ/m^3)**
PHBV8	3223 ± 436^{a}	24.5 ± 0.6^{a}	2.6 ± 0.2^{a}	0.45 ± 0.05^{a}	2713 ± 469^{a}	23.4 ± 1.6^{a}	2.3 ± 0.3^{a}	0.37 ± 0.08^{a}
PHBV8 with CNCs	2304 ± 568^{a,c}	22.4 ± 2.8^{a,d}	2.1 ± 0.1^{b}	0.33 ± 0.06^{a}	2413 ± 364^{a,d}	21.7 ± 1.3^{a}	1.9 ± 0.2^{a,c}	0.28 ± 0.06^{a}
PHBV2	4267 ± 229^{b}	39.0 ± 1.9^{b}	1.4 ± 0.1^{c}	0.33 ± 0.02^{a}	4580 ± 317^{b}	38.0 ± 0.5^{b}	1.3 ± 0.1^{b}	0.29 ± 0.03^{a}
PHBV2 with CNCs	4789 ± 209^{b}	44.9 ± 1.0^{c}	0.19 ± 0.01^{d}	0.59 ± 0.05^{a}	4515 ± 132^{b}	42.1 ± 2.2^{b}	1.5 ± 0.1^{b,c}	0.40 ± 0.01^{a}
PHB Blend	1773 ± 138^{c}	23.0 ± 0.1^{d}	59.1 ± 39.2^{e}	12.60 ± 3.10^{b}	1624 ± 82^{c}	20.8 ± 1.1^{a}	61.0 ± 32.8^{d}	12.40 ± 8.80^{b}
PHB Blend with CNCs	2087 ± 332^{c}	23.7 ± 2.7^{a,d}	36.1 ± 14.7^{e}	7.50 ± 1.60^{b}	1937 ± 183^{c,d}	20.9 ± 0.7^{a}	10.6 ± 6.0^{e}	1.84 ± 0.89^{c}

$^{a–e}$ Different letters in the same column indicate a significant difference among the samples ($p < 0.05$).

Generally speaking, it can be seen that the CNC coating did not significantly change the mechanical properties of the multilayers. However, a slight reinforcing effect could be inferred for some cases. For instance, the elastic moduli of PHBV2 in MD and PHB blend in both directions increased approximately 15 % with the addition of the CNCs. On the other hand, the sample PHBV8 presented a decrease when incorporating the CNC layer. This was probably due to a delamination of the multilayer assembly upon tensile testing. This mechanical behavior is consistent with the literature and previous works of the group (Wang, Chen, et al. 2020). Thus, Cherpinski et al. (Cherpinski, Torres-Giner, Vartiainen, et al. 2018) reported values of 2056.7 MPa, 21.0 MPa, and 5.9 %, for E, σ_y, and ε_b, respectively, for a multilayer of CNFs with double-sided PHBV coatings prepared by electrospinning, which were quite similar to the neat PHBV. Moreover, previous work in our lab also showed no difference in mechanical properties between multilayers with a CNC coating and those without the CNC layer (Figueroa-Lopez, Torres-Giner, et al. 2020).

3.4. Barrier Properties

The permeance to water vapor (WVP), limonene (LP), and oxygen (OP) was measured in order to assess which multilayer system presented better barrier properties and how the addition of a CNC coating could affect their barrier performance. **Table 3** shows the permeance values in terms of WVP, LP, and OP of the multilayers with and without CNCs. It can be seen that the PHB Blend showed the best barrier performance, showing values of 0.85×10^{-11} kg·m^{-2}·Pa^{-1}·s^{-1}, 1.10×10^{-11} kg·m^{-2}·Pa^{-1}·s^{-1}, and 3.90×10^{-16} m^3·m^{-2}·s^{-1}·Pa^{-1}, for WVP, LP, and OP, respectively. PHBV2 also showed good barrier properties, i.e., 0.90×10^{-11} kg·m^{-2}·Pa^{-1}·s^{-1}, 2.02×10^{-11} kg·m^{-2}·Pa^{-1}·s^{-1}, and 6.37×10^{-16} m^3·m^{-2}·s^{-1}·Pa^{-1}, for WVP, LP, and OP, respectively. Lastly, PHBV8 presented the lowest barrier properties, with values of 11.47 ×

10^{-11} kg·m^{-2}·Pa^{-1}·s^{-1}, 13.91 × 10^{-11} kg·m^{-2}·Pa^{-1}·s^{-1}, and 57.81 × 10^{-16} m^{3}·m^{-2}·s^{-1}·Pa^{-1}, for WVP, LP, and OP, respectively. The PHBV8 presented the lowest barrier performance due to its lowest thickness and because it contained a higher fraction of 3HV in the copolymer composition (Martínez-Sanz et al. 2016, Shogren 1997). In the case of the PHB Blend, the highest barrier values achieved were likely the result of a higher thickness, the presence of the PHB homopolymer (Sanchez Garcia and Lagaron 2012, Sanchez-Garcia, Gimenez, and Lagaron 2007), and perhaps a more favorable morphology of the film since this material was more flexible due to the elastomeric PBAT component.

Table 3. Average thickness and permeance values in terms of water vapor permeance (WVP), d-limonene permeance (LP), and oxygen permeance (OP) of the multilayers of poly(3-hydroxybutyrate-*co*-3-hydroxyvalerate) (PHBV) containing 8 mol % (PHBV8) and 2 mol % 3-hydroxyvalerate (PHBV2) and poly(3-hydroxybutyrate) with poly(butylene adipate-*co*-terephthalate) blend (PHB Blend), with and without cellulose nanocrystals (CNCs).

Sample	Thickness (mm)	Permeance		
		WVP × 10^{11} (kg·m^{-2}·Pa^{-1}·s^{-1})	**LP × 10^{11} (kg·m^{-2}·Pa^{-1}·s^{-1})**	**OP × 10^{16} (m^{3}·m^{-2}·Pa^{-1}·s^{-1})**
PHBV8	0.050 ± 0.002	11.47 ± 0.06^{a}	13.91 ± 0.50^{a}	57.81 ± 21.45^{a}
PHBV8 with CNCs	0.055 ± 0.001	10.95 ± 0.05^{a}	12.52 ± 0.33^{b}	14.63 ± 3.34^{b}
PHBV2	0.137 ± 0.006	0.90 ± 0.10^{b}	2.02 ± 0.23^{c}	6.37 ± 0.45^{c}
PHBV2 with CNCs	0.140 ± 0.007	0.86 ± 0.02^{b}	1.70 ± 0.22^{c}	0.88 ± 0.07^{d}
PHB Blend	0.150 ± 0.003	0.85 ± 0.03^{b}	1.10 ± 0.20^{d}	3.90 ± 0.91^{e}
PHB Blend with CNCs	0.160 ± 0.004	0.82 ± 0.04^{b}	0.79 ± 0.21^{d}	1.12 ± 0.61^{d}

$^{a–e}$ Different letters in the same column indicate a significant difference among the samples ($p < 0.05$).

The excellent oxygen barrier properties imparted by CNCs are well known. However, at the same time, it is known that, when CNC is exposed to high-humidity conditions, these excellent properties decrease dramatically due to its hydrophilic nature. For this reason, the application of a CNC interlayer between moisture barrier polymers is considered as the most adequate method to overcome the biopolymer moisture sensitivity (Aulin et al. 2013, Cherpinski, Torres-Giner, Vartiainen, et al. 2018, Hubbe et al. 2017). Furthermore, CNCs also provide flexibility and sealability to the final structure (Mascheroni et al. 2016, Rampazzo et al. 2017). When CNCs were added to the multilayers, a small or null barrier improvement was seen for water and limonene, yet an improvement was clearly observed for oxygen. The permeance to oxygen gas was seen to decrease between approximately 71 % and 86 % for the different materials, with PHBV2 being the material with the highest barrier improvement. Therefore, this study further confirms that a barrier improvement to oxygen is provided by CNCs, which is in agreement with the previous literature. Thus, Le Gars et al. (Le Gars et al. 2020) reported a decrease in OP of about 90 % in multilayers of polylactide (PLA) and CNCs (PLA/CNCs/PLA) compared to neat PLA. Similarly, Fotie et al. (Fotie et al. 2020) prepared multilayers of five different polymers, i.e., PET, PLA, oriented polypropylene (OPP), PP, and PE with a 1 µm CNC interlayer, and, in all cases, an OP reduction between 90 % and 100 % was achieved after lamination.

4. Conclusions

In this study, three different multilayer systems based on different commercial PHAs were assembled with a CNC interlayer and an HT layer made of PHBV fibers produced by electrospinning. The resultant structures were characterized in terms of morphological, optical, mechanical, and barrier properties. The SEM images showed good adhesion between the different layers, with no separation between them, along with a ca. 1 μm thick CNC coating. All the samples showed good contact transparency, and, while the substrates of PHBV2 and PHB Blend were slightly yellowish, the PHBV8 showed no color. In terms of mechanical properties, the PHB Blend exhibited, as expected, improved toughness and ductility compared to the other two multilayers, and, while these properties were reduced when CNCs were present in the structure, they were still much higher than for the pure commercial PHAs. All the multilayers showed improved barrier properties toward oxygen, while the water and limonene permeance remained largely unaffected.

The multilayer systems presented in this study, especially the so-called PHB Blend, exhibited the best balance in all the measured properties. Despite the fact that the film components are known to lead a compostable packaging, a complete biodegradation study is currently underway in the films and will be reported elsewhere. Furthermore, the use of bio-based compostable materials to generate such structures, especially in the case of the hot-tack derived from food by-products, has been shown to not only offer significant advantages in the design of oxygen-sensitive food packaging technologies, but also contribute to the compliance with current trends toward a Circular Bioeconomy future for the overall food chain.

5. References

Akkapeddi, K., and B. Lynch. 2013. "Compa tibilizer additives for improving the delamination resistance of PET/PA-MXD6 multilayer coinjection stretch blow molded bottles." Annual Technical Conference - ANTEC, Conference Proceedings.

Alp-Erbay, E., K. J. Figueroa-Lopez, J. M. Lagaron, E. Çağlak, and S. Torres-Giner. 2019. "The impact of electrospun films of poly(ε-caprolactone) filled with nanostructured zeolite and silica microparticles on in vitro histamine formation by Staphylococcus aureus and Salmonella Paratyphi A." *Food Packaging and Shelf Life* 22. doi: 10.1016/j.fpsl.2019.100414.

Arfat, Y. A., J. Ahmed, N. Hiremath, R. Auras, and A. Joseph. 2017. "Thermo-mechanical, rheological, structural and antimicrobial properties of bionanocomposite films based on fish skin gelatin and silver-copper nanoparticles." *Food Hydrocolloids* 62:191-202. doi: 10.1016/j.foodhyd.2016.08.009.

Aulin, C., E. Karabulut, A. Tran, L. Waìšgberg, and T. Lindström. 2013. "Transparent nanocellulosic multilayer thin films on polylactic acid with tunable gas barrier properties." *ACS Applied Materials and Interfaces* 5 (15):7352-7359. doi: 10.1021/am401700n.

Babu, R. P., K. O'Connor, and R. Seeram. 2013. "Current progress on bio-based polymers and their future trends." *Prog. Biomater.* 2 (8):1-16.

Barhoum, A., P. Samyn, T. Öhlund, and A. Dufresne. 2017. "Review of recent research on flexible multifunctional nanopapers." *Nanoscale* 9 (40):15181-15205. doi: 10.1039/c7nr04656a.

Benetto, E., C. Jury, E. Igos, J. Carton, P. Hild, C. Vergne, and J. Di Martino. 2015. "Using atmospheric plasma to design multilayer film from polylactic acid and thermoplastic starch: A screening life cycle assessment." *Journal of Cleaner Production* 87 (1):953-960. doi: 10.1016/j.jclepro.2014.10.056.

Busolo, M. A., S. Torres-Giner, and J. M. Laaron. 2009. "Enhancing the gas barrier properties of polylactic acid by means of electrospun ultrathin zein fibers." Annual Technical Conference - ANTEC, Conference Proceedings.

Cherpinski, A., A. Biswas, J. M. Lagaron, A. Dufresne, S. Kim, M. Buttrum, E. Espinosa, and H. N. Cheng. 2019. "Preparation and evaluation of oxygen scavenging nanocomposite films incorporating cellulose nanocrystals and Pd nanoparticles in poly(ethylene-co-vinyl alcohol)." *Cellulose* 26 (12):7237-7251. doi: 10.1007/s10570-019-02613-8.

Cherpinski, A., S. Torres-Giner, L. Cabedo, J. A. Méndez, and J. M. Lagaron. 2018. "Multilayer structures based on annealed electrospun biopolymer coatings of interest in water and aroma barrier fiber-based food packaging applications." *Journal of Applied Polymer Science* 135 (24). doi: 10.1002/app.45501.

Cherpinski, A., S. Torres-Giner, J. Vartiainen, M. S. Peresin, P. Lahtinen, and J. M. Lagaron. 2018. "Improving the water resistance of nanocellulose-based films with polyhydroxyalkanoates processed by the electrospinning coating technique." *Cellulose* 25 (2):1291-1307. doi: 10.1007/s10570-018-1648-z.

Cozzolino, C. A., G. Cerri, A. Brundu, and S. Farris. 2014. "Microfibrillated cellulose (MFC): pullulan bionanocomposite films." *Cellulose* 21 (6):4323-4335. doi: 10.1007/s10570-014-0433-x.

Cruz, M. V., F. Freitas, A. Paiva, F. Mano, M. Dionísio, A. M. Ramos, and M. A. M. Reis. 2016. "Valorization of fatty acids-containing wastes and byproducts into short- and medium-chain length polyhydroxyalkanoates." *New Biotechnology* 33 (1):206-215. doi: 10.1016/j.nbt.2015.05.005.

Cunha, M., B. Fernandes, J. A. Covas, A. A. Vicente, and L. Hilliou. 2016. "Film blowing of PHBV blends and PHBV-based multilayers for the production of biodegradable packages." *Journal of Applied Polymer Science* 133 (2). doi: 10.1002/app.42165.

Del Nobile, M. A., G. Mensitieri, A. Aldi, and L. Nicolais. 1999. "Transport mechanisms of gases through metallized films intended for food packaging applications." *Packaging Technology and Science* 12 (6):261-269. doi: 10.1002/(SICI)1099-1522(199911/12)12:6<261::AID-PTS483>3.0.CO;2-O.

Dufresne, A. 2012. *Nanocellulose: From nature to high performance tailored materials*, *Nanocellulose: From Nature to High Performance Tailored Materials*.

Echegoyen, Y., M. J. Fabra, J. L. Castro-Mayorga, A. Cherpinski, and J. M. Lagaron. 2017. "High throughput electro-hydrodynamic processing in food encapsulation and food packaging applications: Viewpoint." *Trends in Food Science and Technology* 60:71-79. doi: 10.1016/j.tifs.2016.10.019.

Fabra, M. J., M. A. Busolo, A. Lopez-Rubio, and J. M. Lagaron. 2013. "Nanostructured biolayers in food packaging." *Trends in Food Science and Technology* 31 (1):79-87. doi: 10.1016/j.tifs.2013.01.004.

Fabra, M. J., A. López-Rubio, and J. M. Lagaron. 2014. "On the use of different hydrocolloids as electrospun adhesive interlayers to enhance the barrier properties of polyhydroxyalkanoates of interest in fully renewable food packaging concepts." *Food Hydrocolloids* 39:77-84. doi: 10.1016/j.foodhyd.2013.12.023.

Fang, J. M., P. A. Fowler, C. Escrig, R. Gonzalez, J. A. Costa, and L. Chamudis. 2005. "Development of biodegradable laminate films derived from naturally occurring carbohydrate polymers." *Carbohydrate Polymers* 60 (1):39-42. doi: 10.1016/j.carbpol.2004.11.018.

Figueroa-Lopez, K. J., L. Cabedo, J. M. Lagaron, and S. Torres-Giner. 2020. "Development of Electrospun Poly(3-hydroxybutyrate-co-3-hydroxyvalerate) Monolayers Containing Eugenol and Their Application in Multilayer Antimicrobial Food Packaging." *Frontiers in Nutrition* 7. doi: 10.3389/fnut.2020.00140.

Figueroa-Lopez, K. J., S. Torres-Giner, I. Angulo, M. Pardo-Figuerez, J. M. Escuin, A. I. Bourbon, L. Cabedo, Y. Nevo, M. A. Cerqueira, and J. M. Lagaron. 2020. "Development of active barrier multilayer films based on electrospun antimicrobial hot-tack food waste derived poly(3-hydroxybutyrate-co-3-hydroxyvalerate) and cellulose nanocrystal interlayers." *Nanomaterials* 10 (12):1-24. doi: 10.3390/nano10122356.

Fotie, G., S. Gazzotti, M. A. Ortenzi, and L. Piergiovanni. 2020. "Implementation of high gas barrier laminated films based on cellulose nanocrystals for food flexible packaging." *Applied Sciences (Switzerland)* 10 (9). doi: 10.3390/app10093201.

Hubbe, M. A., A. Ferrer, P. Tyagi, Y. Yin, C. Salas, L. Pal, and O. J. Rojas. 2017. "Nanocellulose in thin films, coatings, and plies for packaging applications: A review." *BioResources* 12 (1):2143-2233. doi: 10.15376/biores.12.1.2143-2233.

Kanatt, S. R., M. S. Rao, S. P. Chawla, and A. Sharma. 2012. "Active chitosan-polyvinyl alcohol films with natural extracts." *Food Hydrocolloids* 29 (2):290-297. doi: 10.1016/j.foodhyd.2012.03.005.

Karkhanis, S. S., N. M. Stark, R. C. Sabo, and L. M. Matuana. 2018. "Performance of poly(lactic acid)/ cellulose nanocrystal composite blown films processed by two different compounding approaches." *Polymer Engineering and Science* 58 (11):1965-1974. doi: 10.1002/pen.24806.

Kim, J. K., B. Choi, and J. Jin. 2020. "Transparent, water-stable, cellulose nanofiber-based packaging film with a low oxygen permeability." *Carbohydrate Polymers* 249. doi: 10.1016/j.carbpol.2020.116823.

Kim, J., L. Zhai, S. Mun, H. U. Ko, and Y. M. Yun. 2015. "Cellulose nanocrystals, nanofibers, and their composites as renewable smart materials." Proceedings of SPIE - The International Society for Optical Engineering.

Kwon, G., K. Lee, D. Kim, Y. Jeon, U. J. Kim, and J. You. 2020. "Cellulose nanocrystal-coated TEMPO-oxidized cellulose nanofiber films for high performance all-cellulose nanocomposites." *Journal of Hazardous Materials* 398. doi: 10.1016/j.jhazmat.2020.123100.

Lanham, A. B., A. R. Ricardo, M. G. E. Albuquerque, F. Pardelha, M. Carvalheira, M. Coma, J. Fradinho, G. Carvalho, A. Oehmen, and M. A. M. Reis. 2013. "Determination of the extraction kinetics for the quantification of polyhydroxyalkanoate monomers in mixed microbial systems." *Process Biochemistry* 48 (11):1626-1634. doi: 10.1016/j.procbio.2013.07.023.

Lavoine, N., I. Desloges, A. Dufresne, and J. Bras. 2012. "Microfibrillated cellulose - Its barrier properties and applications in cellulosic materials: A review." *Carbohydrate Polymers* 90 (2):735-764. doi: 10.1016/j.carbpol.2012.05.026.

Laycock, B., P. Halley, S. Pratt, A. Werker, and P. Lant. 2014. "The chemomechanical properties of microbial polyhydroxyalkanoates." *Progress in Polymer Science* 39 (2):397-442. doi: 10.1016/j.progpolymsci.2013.06.008.

Le Gars, M., B. Dhuiège, A. Delvart, M. N. Belgacem, K. Missoum, and J. Bras. 2020. "High-barrier and antioxidant poly(lactic acid)/nanocellulose multilayered materials for packaging." *ACS Omega* 5 (36):22816-22826. doi: 10.1021/acsomega.0c01955.

Leppänen, I., M. Vikman, A. Harlin, and H. Orelma. 2020. "Enzymatic Degradation and Pilot-Scale Composting of Cellulose-Based Films with Different Chemical Structures." *Journal of Polymers and the Environment* 28 (2):458-470. doi: 10.1007/s10924-019-01621-w.

Martínez-Sanz, M., A. Lopez-Rubio, and J. M. Lagaron. 2013. "High-barrier coated bacterial cellulose nanowhiskers films with reduced moisture sensitivity." *Carbohydrate Polymers* 98 (1):1072-1082. doi: 10.1016/j.carbpol.2013.07.020.

Martínez-Sanz, M., A. Lopez-Rubio, M. Villano, C. S. S. Oliveira, M. Majone, M. Reis, and J. M. Lagarón. 2016. "Production of bacterial nanobiocomposites of polyhydroxyalkanoates derived from waste and bacterial nanocellulose by the electrospinning enabling melt compounding method." *Journal of Applied Polymer Science* 133 (2). doi: 10.1002/app.42486.

Mascheroni, E., R. Rampazzo, M. A. Ortenzi, G. Piva, S. Bonetti, and L. Piergiovanni. 2016. "Comparison of cellulose nanocrystals obtained by sulfuric acid hydrolysis and ammonium persulfate, to be used as coating on flexible food-packaging materials." *Cellulose* 23 (1):779-793. doi: 10.1007/s10570-015-0853-2.

Melendez-Rodriguez, B., J. L. Castro-Mayorga, M. A. M. Reis, C. Sammon, L. Cabedo, S. Torres-Giner, and J. M. Lagaron. 2018. "Preparation and Characterization of Electrospun Food Biopackaging Films of Poly(3-hydroxybutyrate-co-3-hydroxyvalerate) Derived From Fruit Pulp Biowaste." *Frontiers in Sustainable Food Systems* 2. doi: 10.3389/fsufs.2018.00038.

Melendez-Rodriguez, B., S. Torres-Giner, A. Aldureid, L. Cabedo, and J. M. Lagaron. 2019. "Reactive melt mixing of poly(3-hydroxybutyrate)/rice husk flour composites with purified biosustainably produced poly(3-hydroxybutyrate-co-3-hydroxyvalerate)." *Materials* 12 (13). doi: 10.3390/ma12132152.

Melendez-Rodriguez, B., S. Torres-Giner, L. Lorini, F. Valentino, C. Sammon, L. Cabedo, and J. M. Lagaron. 2020. "Valorization of Municipal Biowaste into Electrospun Poly(3-hydroxybutyrate- co-3-hydroxyvalerate) Biopapers for Food Packaging Applications." *ACS Applied Bio Materials* 3 (9):6110-6123. doi: 10.1021/acsabm.0c00698.

Mokrzycki, W. S., and M. Tatol. 2011. "Colour difference δE - A survey." *Machine Graphics and Vision* 20 (4):383-411.

Moon, R. J., A. Martini, J. Nairn, J. Simonsen, and J. Youngblood. 2011. "Cellulose nanomaterials review: Structure, properties and nanocomposites." *Chemical Society Reviews* 40 (7):3941-3994. doi: 10.1039/c0cs00108b.

Nduko, J. M., K. Matsumoto, and S. Taguchi. 2012. Biological lactate-polymers synthesized by one-pot microbial factory: Enzyme and metabolic engineering. In *ACS Symposium Series*.

Nuruddin, M., D. M. Korani, H. Jo, R. A. Chowdhury, F. J. Montes, J. A. Howarter, and J. P. Youngblood. 2020. "Gas and Water Vapor Barrier Performance of Cellulose Nanocrystal-Citric Acid-Coated Polypropylene for Flexible Packaging." *ACS Applied Polymer Materials* 2 (11):4405-4414. doi: 10.1021/acsapm.0c00483.

Ogunsona, E. O., and T. H. Mekonnen. 2020. "Multilayer assemblies of cellulose nanocrystal – Polyvinyl alcohol films with robust physical integrity and multi-functional properties." *Journal of Colloid and Interface Science* 580:56-67. doi: 10.1016/j.jcis.2020.07.012.

Peng, B. L., N. Dhar, H. L. Liu, and K. C. Tam. 2011. "Chemistry and applications of nanocrystalline cellulose and its derivatives: A nanotechnology perspective." *Canadian Journal of Chemical Engineering* 89 (5):1191-1206. doi: 10.1002/cjce.20554.

Qi, H., C. Chang, and L. Zhang. 2009. "Properties and applications of biodegradable transparent and photoluminescent cellulose films prepared via a green process." *Green Chemistry* 11 (2):177-18. doi: 10.1039/b814721c.

Quiles-Carrillo, L., N. Montanes, T. Boronat, R. Balart, and S. Torres-Giner. 2017. "Evaluation of the engineering performance of different bio-based aliphatic homopolyamide tubes prepared by profile extrusion." *Polymer Testing* 61:421-429. doi: 10.1016/j.polymertesting.2017.06.004.

Rampazzo, R., D. Alkan, S. Gazzotti, M. A. Ortenzi, G. Piva, and L. Piergiovanni. 2017. "Cellulose Nanocrystals from Lignocellulosic Raw Materials, for Oxygen Barrier Coatings on Food Packaging Films." *Packaging Technology and Science* 30 (10):645-661. doi: 10.1002/pts.2308.

Raza, Z. A., S. Abid, and I. M. Banat. 2018. "Polyhydroxyalkanoates: Characteristics, production, recent developments and applications." *International Biodeterioration and Biodegradation* 126:45-56. doi: 10.1016/j.ibiod.2017.10.001.

Rehm, B. H. A. 2003. "Polyester synthases: Natural catalysts for plastics." *Biochemical Journal* 376 (1):15-33. doi: 10.1042/BJ20031254.

Rhim, J. W. 2013. "Effect of PLA lamination on performance characteristics of agar/κ-carrageenan/clay bio-nanocomposite film." *Food Research International* 51 (2):714-722. doi: 10.1016/j.foodres.2013.01.050.

Rhim, J. W., K. A. Mohanty, S. P. Singh, and P. K. W. Ng. 2006. "Preparation and properties of biodegradable multilayer films based on soy protein isolate and poly(lactide)." *Industrial and Engineering Chemistry Research* 45 (9):3059-3066. doi: 10.1021/ie051207+.

Rivera-Briso, A. L., and Á Serrano-Aroca. 2018. "Poly(3-Hydroxybutyrate-co-3-Hydroxyvalerate): Enhancement strategies for advanced applications." *Polymers* 10 (7). doi: 10.3390/polym10070732.

Sanchez-Garcia, M. D., E. Gimenez, and J. M. Lagaron. 2007. "Novel PET nanocomposites of interest in food packaging applications and comparative barrier performance with biopolyester nanocomposites." *Journal of Plastic Film and Sheeting* 23 (2):133-148. doi: 10.1177/8756087907083590.

Sanchez Garcia, M. D., and J. M. Lagaron. 2012. "Nanocomposites for food and beverage packaging materials." In *Nanotechnology in the Food, Beverage and Nutraceutical Industries*, 335-361.

Shiku, Y., P. Y. Hamaguchi, S. Benjakul, W. Visessanguan, and M. Tanaka. 2004. "Effect of surimi quality on properties of edible films based on Alaska pollack." *Food Chemistry* 86 (4):493-499. doi: 10.1016/j.foodchem.2003.09.022.

Shimizu, M., T. Saito, and A. Isogai. 2016. "Water-resistant and high oxygen-barrier nanocellulose films with interfibrillar cross-linkages formed through multivalent metal ions." *Journal of Membrane Science* 500:1-7. doi: 10.1016/j.memsci.2015.11.002.

Shogren, R. 1997. "Water vapor permeability of biodegradable polymers." *Journal of Environmental Polymer Degradation* 5 (2):91-95. doi: 10.1007/BF02763592.

Thellen, C., S. Cheney, and J. A. Ratto. 2013. "Melt processing and characterization of polyvinyl alcohol and polyhydroxyalkanoate multilayer films." *Journal of Applied Polymer Science* 127 (3):2314-2324. doi: 10.1002/app.37850.

Thellen, C., M. Coyne, D. Froio, M. Auerbach, C. Wirsen, and J. A. Ratto. 2008. "A processing, characterization and marine biodegradation study of melt-extruded polyhydroxyalkanoate (PHA) films." *Journal of Polymers and the Environment* 16 (1):1-11. doi: 10.1007/s10924-008-0079-6.

Tian, J., R. Zhang, Y. Wu, and P. Xue. 2021. "Additive manufacturing of wood flour/polyhydroxyalkanoates (PHA) fully bio-based composites based on micro-screw extrusion system." *Materials and Design* 199. doi: 10.1016/j.matdes.2020.109418.

Torres-Giner, S. 2011. "Electrospun nanofibers for food packaging applications." In *Multifunctional and Nanoreinforced Polymers for Food Packaging*, 108-125.

Torres-Giner, S., M. Busolo, A. Cherpinski, and J. M. Lagaron. 2018. CHAPTER 10: Electrospinning in the Packaging Industry. In *RSC Soft Matter*.

Torres-Giner, S., R. Pérez-Masiá, and J. M. Lagaron. 2016. "A review on electrospun polymer nanostructures as advanced bioactive platforms." *Polymer Engineering and Science* 56 (5):500-527. doi: 10.1002/pen.24274.

Vartiainen, J., T. Kaijunen, H. Nykänen, T. Maim, and T. Tammelin. 2014. "Improving multilayer packaging performance with nanocellulose barrier layer." TAPPI PLACE Conference 2014.

Velásquez-Riaño, M., and V. Bojacá. 2017. "Production of bacterial cellulose from alternative low-cost substrates." *Cellulose* 24 (7):2677-2698. doi: 10.1007/s10570-017-1309-7.

Visanko, M., H. Liimatainen, J. A. Sirviö, K. S. Mikkonen, M. Tenkanen, R. Sliz, O. Hormi, and J. Niinimäki. 2015. "Butylamino-functionalized cellulose nanocrystal films: Barrier properties and mechanical strength." *RSC Advances* 5 (20):15140-15146. doi: 10.1039/c4ra15445b.

Wang, L., C. Chen, J. Wang, D. J. Gardner, and M. Tajvidi. 2020. "Cellulose nanofibrils versus cellulose nanocrystals: Comparison of performance in flexible multilayer films for packaging applications." *Food Packaging and Shelf Life* 23. doi: 10.1016/j.fpsl.2020.100464.

Wang, S., Y. Wang, Y. Zou, G. Chen, J. Ouyang, D. Jia, and Y. Zhou. 2020. "Scalable-Manufactured Superhydrophobic Multilayer Nanocomposite Coating with Mechanochemical Robustness and High-Temperature Endurance." *ACS Applied Materials and Interfaces* 12 (31):35502-35512. doi: 10.1021/acsami.0c10539.

Weng, Y. X., X. L. Wang, and Y. Z. Wang. 2011. "Biodegradation behavior of PHAs with different chemical structures under controlled composting conditions." *Polymer Testing* 30 (4):372-380. doi: 10.1016/j.polymertesting.2011.02.001.

Winotapun, C., S. Phattarateera, A. Aontee, N. Junsook, W. Daud, N. Kerddonfag, and W. Chinsirikul. 2019. "Development of multilayer films with improved aroma barrier properties for durian packaging application." *Packaging Technology and Science* 32 (8):405-418. doi: 10.1002/pts.2452.

Xiang, F., P. Tzeng, J. S. Sawyer, O. Regev, and J. C. Grunlan. 2014. "Improving the gas barrier property of clay-polymer multilayer thin films using shorter deposition times." *ACS Applied Materials and Interfaces* 6 (9):6040-6048. doi: 10.1021/am403445z.

Zinge, C., and B. Kandasubramanian. 2020. "Nanocellulose based biodegradable polymers." *European Polymer Journal* 133. doi: 10.1016/j.eurpolymj.2020.109758.

IV. GENERAL DISCUSSION

General discussion

The consumption of plastics has grown exponentially since its creation in the 1950s. Their longevity, practicality and safety have allowed them to be used in almost all fields of application (Hernández-López et al. 2019). However, despite these advantages, due to their excessive consumption and low recovery rate, as well as their non-biodegradability and low recyclability, they accumulate in the environment in inappropriate places where they are not properly treated, causing pollution and damage to ecosystems (Martínez-Camacho et al. 2013). Thus, the use of biopolymers, of renewable and biodegradable origin, has become relevant to minimise environmental problems. In this context, this PhD thesis has focused on the development and characterization of novel polyhydroxyalkanoates (PHAs) in order to obtain compostable materials to be used in food packaging applications. PHAs have emerged as promising candidates to replace petroleum-based plastics, as they possess similar physicochemical characteristics and can be processed in the same processing machines with the advantages that they can be synthesized by mixed microbial cultures (MMCs) using fermented agricultural and urban waste as substrates (Yadav et al. 2021). However, this has the disadvantage that the polymer has to be recovered and extracted from the cellular material in order to be processed.

Thus, in the first block of the PhD thesis, in Chapter I, different extraction routes of PHAs derived from industrial by-products for their use in electrospinning (Block I) and melt compounding (Block II) were studied. The biopolymer used was a poly(hydroxybutyrate-*co*-hydroxyvalerate) (PHBV) with a 3-hydroxyvalerate (3HV) content of 20 mol %, synthesized by MMCs through fruit pulp fermentation. This waste-derived PHBV was subjected to two extraction methods, with sodium hypochlorite (NaClO) and with chloroform, and the yield of the polymer as well as the properties of the material obtained were studied. In addition, a part of the sample was left unextracted for comparative purposes to determine whether it could be processed without this step. The samples that were not extracted, even after filtration and centrifugation, had many impurities belonging to the residual biomass. This made it impossible to process them by electrospinning, as it clogged the injector, so these samples were excluded from the study. Samples extracted in both chloroform and NaClO could be processed by electrospinning, although samples extracted with NaClO also had to be filtered and centrifuged to properly remove all impurities, which reduced their yield. The electrospun fibers from the samples extracted by both methods were subjected to thermal post-treatment at 125 °C, a temperature lower than the melting temperature (T_m) of the polymer, to form homogeneous biopapers without porosity. The biopapers were studied in terms of morphology, crystallinity, thermal, mechanical and barrier properties. The samples obtained by chloroform extraction showed higher yield and higher purity, as the biopapers were more transparent and had lower crystallinity, due to the presence of fewer nucleating impurities. Both electrospun films were highly hydrophobic, comparable to commercial PHAs and with good thermal degradation. In terms of mechanical properties, both materials showed brittle characteristics, typical of PHAs, although the sample extracted with NaClO showed more rigidity due to the presence of more impurities. Finally, the materials exhibited different barrier performances. The sample extracted with chloroform showed lower wettability, due to the presence of fewer impurities and therefore less free volume in the film, which in turn led to higher permeability and limonene uptake. With respect to oxygen, both presented similar values, although the one extracted with chloroform presented a higher barrier. Therefore, chloroform extraction was seen as a better method to extract waste-derived PHAs and

to form electrospun films with improved properties, so this route was chosen for all subsequent studies.

Based on these results, in the next chapters (Chapter II, III, and VII) PHAs from different by-products were studied. In Chapter II, PHBV derived from municipal biowaste (MBW), with 10 mol % 3HV content, was characterized. First, it was extracted with chloroform and then processed by electrospinning and thermally post-treated at 130 °C to form the biopaper. The films showed transparency and lack of color, suggesting that the samples had few impurities and low crystallinity, and an adequate choice of temperature that did not degrade the sample. Moreover, the electrospun fibers were studied in terms of their crystallinity and phase morphology by simultaneous time-resolved small-angle X-ray scattering (SAXS) and wide-angle X-ray scattering (WAXS) experiments using synchrotron radiation as a function of temperature, while their molecular order was assessed by attenuated total reflectance and Fourier transform infrared (ATR-FTIR) spectroscopy. Both studies correlated perfectly, showing that a thermal treatment up to 130 °C improved both crystallinity and phase morphology with an increase in molecular order allowing a coalescence of the fibers and the formation of homogeneous films with reduced porosity. However, at higher temperatures, melting of the polymer was observed with a consequent reduction in molecular order as well as in phase morphology and crystallinity. In this case, the mechanism of coalescence between fibers was associated with thermally induced molecular order. In terms of mechanical and barrier properties, the biopapers exhibited characteristics of a rigid and brittle material with a high barrier to vapors and gases (water, limonene and oxygen) in the same order of magnitude as commercial melt compounded PHAs.

Depending on the monomer content, PHAs are known to vary in their physical and thermal properties as well as in their mechanical and barrier performance, allowing their use in a wide range of applications (Muthuraj, Valerio, and Mekonnen 2021). In order to study these characteristics, in Chapter III, a cheese whey (CW)-derived PHBV with three different 3HV contents, i.e. 20, 40, and 60 mol %, was characterized. After being extracted with chloroform and processed by electrospinning, each material was annealed at a different temperature depending on its 3HV content. Thus, the selected temperatures were 120, 60, and 70 °C for the 20, 40, and 60 mol % 3HV contents, respectively. All three biopapers presented a high transparency with a slight yellowish color. However, other properties changed according to the 3HV content. In terms of thermal properties, the samples with 40 and 60 mol % 3HV showed weak and broad peaks in both melting and cooling endothermic curves while the sample with 20 mol % 3HV presented clearer and more prominent peaks. Furthermore, T_m decreased with increasing 3HV content up to around 40 mol %, from which it started to increase again. This is related to the crystal lattice of the PHBV copolyesters, which has been reported as poly(3-hydroxybutyrate) (PHB) in compositions up to 37 mol % of 3HV and poly(3-hydroxyvalerate) (PHV) crystal lattice from 53 mol % of 3HV. In intermediate compositions both crystal lattices coexist (Kunioka, Tamaki, and Doi 1989). For the samples studied here, their crystalline morphology and content were assessed by WAXS, showing that the sample with 20 mol % 3HV presented a PHB-rich phase, the sample with 60 mol % 3HV, a PHV-rich phase, and the sample with 40 mol % 3HV showed the coexistence of the two crystalline morphologies referred to as a pseudo-eutectic point and lowest crystallinity. By combined SAXS and WAXS and ATR-FTIR experiments at variable temperature it was deduced that the coalescence mechanism of the fibers was mainly attributed to molecular disorder, associated with the early melting of the defective crystallinity part during annealing, in contrast to what was observed in the previous chapter. Mechanical properties also varied as a function of 3HV content, with the materials becoming more ductile and tougher as the

content increased. With respect to barrier properties, all three materials showed similar performance with respect to water and limonene. For oxygen, the 40 mol % 3HV sample showed higher permeability, attributed to its higher flexibility and lower crystallinity and molecular order, resulting in materials with high free volume and lowest tortuosity.

One of the advantages of the electrospinning technique is the encapsulation of volatile active substances, such as essential oils (EOs), within the fibers. They provide the material with antimicrobial and antioxidant properties, which are of great importance when used in food packaging. For this reason, in Chapter IV, eugenol EO encapsulated in Mobil Composition of Matter (MCM-41), a type of mesoporous silica nanoparticles, was incorporated into a commercial PHBV solution in the range of 2.5-20 wt % to assess its antimicrobial capacity. After electrospinning, the fibers were annealed at 155 °C and the resulting biopapers were studied for their morphological, thermal, mechanical, barrier and antimicrobial properties. The nanoparticles were well distributed in the polymer matrix, except at the highest loading, i.e. 20 wt %, where some agglomeration was observed. The biopapers were transparent with a slight yellow color at higher particle contents, that is, 15 and 20 wt %. The incorporation of MCM-41 into the polymer matrix did not affect the thermal properties of PHBV, however, when loaded with eugenol, some plasticization occurred, which reduced the crystallinity of PHBV. The thermal stability of PHBV was not affected up to a content of 10 wt % of MCM-41 with eugenol. The mechanical properties of the PHBV were modified when the nanoparticles were added, specifically, there was an increase in strength due to the reinforcement caused by MCM-41 and a reduction in ductility due to the plasticizing effect of eugenol. However, there was a reduction in mechanical strength at higher loads due to the agglomeration effect of the nanoparticles and the increased plasticising effect of eugenol. The water vapor and limonene barrier properties improved as the nanoparticle content increased, with the most optimal at 15 wt % MCM-41 with eugenol. Finally, antimicrobial activity was observed after 15 days in both open and closed systems against *Staphylococcus aureus* (*S. aureus*) and *Escherichia coli* (*E. coli*), with significant antimicrobial activity ($R \geq 1$ and <3) for 10 and 15 wt % MCM-41 with eugenol contents, respectively. This confirmed that MCM-41 was able to perform a controlled release of eugenol that extended its antimicrobial activity. Furthermore, in the closed system, performed to simulate a real packaging, the antimicrobial effect was higher due to the accumulation of eugenol in the system´s headspace.

In addition to the antimicrobial capacity of the material, oxygen barrier is one of the most critical properties in food packaging applications. It is known that by limiting oxygen permeability, the shelf life of the product is prolonged, preventing spoilage both by the growth of microorganisms and by the oxidation of certain substances, such as lipids, which affect the color and flavor of the packaged food (Zabihzadeh Khajavi et al. 2020). On this basis, in Chapter V, a poly(ethylene-*co*-vinyl alcohol) (EVOH) copolymers, known for its high oxygen barrier, was processed for the first time by electrospinning. The EVOH used had an ethylene content of 44 mol %, which conferred particular characteristics compared to other EVOH with different monomer contents. In addition, cellulose nanocrystals (CNCs), which also have an excellent oxygen barrier, were added to the EVOH solutions in amounts of 0.1 to 1.0 wt %. The films obtained after annealing at 145 °C showed high contact transparency, with a good distribution of CNCs within the polymer matrix in contents up to 0.5 wt %. Variable-temperature ATR-FTIR spectroscopy showed that the selected annealing temperature enabled interfiber coalescence through thermally-induced molecular motions. The incorporation of CNCs reduced the crystallinity of EVOH and increased its thermal stability, delaying its thermal degradation. In terms of mechanical properties, the addition of CNCs resulted in an increase in the rigidity of the films, as well as a reduction in

ductility. For the highest content of CNCs, i.e. 1 wt %, there was a reduction in mechanical strength. Despite the great properties of EVOH and CNCs, both are very sensitive to moisture, which mainly affects their barrier properties. Therefore, different percentage of relative humidity (RH), i.e. 0, 20 and 80 %, were used during the oxygen barrier measurements to study the effect of moisture on their permeabilities. For the three % RH tested, oxygen permeability increased with increasing CNCs content. At 20 % RH, the lowest permeability values were obtained, as at this lower humidity, water molecules are able to fill the free volume of the matrix, reducing possible diffusion sites. Regarding the water vapor barrier, the addition of CNCs also led to an increase in permeability compared to pure EVOH.

Despite the positive results obtained by using electrospinning in the development of different PHAs materials, Block II dealt with polymer blending by melt compounding. Polymer blending is one of the most commonly used methods to improve certain limiting properties of polymers, to create new materials with more suitable characteristics for the desired application and to reduce costs and give value to products that would otherwise be discarded. Thus, in Chapter VI, blends of commercial PHB and waste-derived PHBV, characterized in Chapter I, were prepared by melt compounding. In addition, rice husk flour (RHF), from an agricultural by-product, was added as a filler in order to reduce the production costs of PHAs, revalorize waste and increase the biodegradability of the compound, forming so-called "green composites". Therefore, blends of PHB/PHBV and PHB/RHF were produced and then increasing amounts of PHBV were added to the latter blend in a range of 5-50 wt %. The amount of RHF was fixed at 10 wt %. To increase the compatibility between the biopolymers and the filler, a compatibilizer, triglycidyl isocyanurate (TGIC), and an initiator, dicumyl peroxide (DCP), were added. After the materials were melt-compounded and thermo-compressed into films, their morphological, thermal, mechanical and barrier properties were measured. RHF was well distributed within the polymeric matrices, with no voids or agglomerations, while the biopolymers visually showed good mixture without the presence of two phases. PHB/PHBV films were colorless while those containing RHF showed a brownish-yellow color. Through the thermal study, it was found that complete miscibility between the two bioplastics only occurred for contents up to 10 wt % PHBV. For higher contents, the films formed a two-phase system and also showed a two-phase crystallization. Moreover, it has been reported that the higher the 3HV content, as in this case 20 mol %, the more phase segregation is induced in PHB/PHBV blends (Saito, Inoue, and Yoshie 2001). The addition of PHBV to PHB/RHF blends increased their thermal stability, especially at higher contents. Contents of up to 10 wt % PHBV produced an improvement in the strength and ductility of the materials, counteracting the intrinsic brittleness of the PHB and that induced by RHF. Finally, the addition of PHBV resulted in increased permeability to water vapor and limonene, although the barrier was still in the same order of magnitude as PHB.

In line with the above, the Chapter VII consisted of the blends of two PHAs by melt compounding. In this case, the biopolymers used were a commercial PHBV, with 2-3 mol % 3HV, and the terpolyester poly(3-hydroxybutyrate-*co*-3-hydroxyvalerate-*co*-3-hydroxyhexanoate) [P(3HB-*co*-3HV-*co*-3HHx)], a PHA derived from fruit pulp. This had a composition of 68 mol % 3HB, 17 mol % 3HV, and 15 mol % 3-hydroxyhexanoate (3HHx). The terpolymer was extracted with chloroform following the route described in the Chapter I and then melt-mixed with the PHBV in contents from 10 to 50 wt % and thermo-compressed into films. The blends showed good compatibility with no evidence of phase segregation and the films were transparent with a yellowish brown color. Differential scanning calorimetry (DSC) and WAXS studies showed that the addition of the terpolymer to the PHBV resulted in a reduction of the crystallinity of the

blends, with a lower T_m and enthalpy of fusion (ΔH_m). This can be attributed to the fact that the crystallization of the 3HB fraction was impaired by the other two fractions present. Nevertheless, the blends preserved the crystalline morphology of the PHB crystals for all compositions. The thermal stability of the blends was negligibly affected by the incorporation of the terpolymer. The blends showed a more ductile and flexible mechanical behaviour with increasing 3HHx content, because of its plasticizing effect. Due to the lower crystallinity of P(3HB-*co*-3HV-*co*-3HHx), the blends showed lower barriers to water vapor, limonene and oxygen than PHBV, although they remained in the same order of magnitude.

Based on the development of numerous monolayers, both by electrospinning and melt compounding, in the previous seven chapters, the development of multilayer systems from them was carried out in Block III. In the field of food packaging, the use of multilayer structures has been seen as a promising technique to cover all the necessary functionalities that would be not possible to achieve with polymer monolayers in a cost-effective manner. In Chapter VIII, a multilayer system was developed based on commercial PHBV electrospun fibers as outer layers with an interlayer of CNCs. For this purpose, one of the electrospun PHBV layers was impregnated with a CNCs layer by manual coating. In addition, the PHBV layer was also impregnated with nanocomposites made of a CNCs solution with different hydrocolloids, i.e. a protein, gelatine (GE) and three polysaccharides, agar (AG), xanthan gum (XG), and gum arabic (GA), in order to increase the barrier properties. Glycerol was added as plasticizer. Morphological results showed better impregnations in those hydrocolloids with higher viscosity, i.e. CNCs and the CNCs+XG biocomposite, related to a higher chemical interaction between them and with the PHBV. This better impregnation of the fibers resulted in less porosity on the surface of the fiber mats. However, the CNCs+GE and CNCs+GA biocomposites, with a lower viscosity, showed worse impregnation of the fibers, leaving some visible porosity, indicating that the solutions could diffuse through the fibers. The CNCs+AG biocomposite, despite also having a low viscosity, showed good impregnation of the fibers, indicating good interaction with CNCs and PHBV. However, after thermal treatment, at 160 °C, all the multilayers showed good adhesion, with a compact structure and no interphases. This demonstrates the ability of fibers developed by electrospinning to act as adhesives, so-called hot-tack (HT), without the need for synthetic glues. The mechanical properties of the PHBV/PHBV system did not modify with the addition of either the CNCs or the CNCs/hydrocolloid biocomposites, all being governed by the mechanical behaviour of PHBV, which was the dominant fraction in the system. Finally, the barrier properties PHBV/PHBV system were altered by the impregnation of the composites. Thus, limonene permeance was reduced in all composites, especially in those containing CNCs and the hydrocolloids AG and XG, which showed the best impregnation previously. With respect to oxygen, the PHBV/CNCs/PHBV multilayer showed the best barrier, with a permeance reduction of 88 % compared to the PHBV/PHBV multilayer. The water vapor barrier, however, was not improved with any of the biocomposites, due to their hydrophilic nature.

The ninth and last chapter, in line with the previous one, consisted of the development of a fully bio-based and compostable high oxygen barrier multilayer. For this purpose, different outer structural layers based on PHAs were tested, i.e. a commercial PHBV film, an extruded PHBV film, and a blown film of a blend of PHB with poly(butylene adipate-*co*-terephthalate) (PBAT). The inner layers consisted of a 1 µm thick layer of CNCs, coated on one of the outer layers, which provided the high oxygen barrier, and a layer of electrospun fibers of a CW-derived PHBV that acted as HT, on another outer film. The two outer coated layers were laminated and the morphological, mechanical and barrier properties of the multilayer were evaluated. The three

multilayer structures developed showed good adhesion to each other, showing the efficacy of the electrospun fibers as adhesives. The films showed good transparency, with color provided by the outer layers. In terms of mechanical properties, the multilayer formed with the outer layer of a PHB/PBAT blend resulted in a system with improved toughness and ductility properties, while the other two preserved the brittleness and stiffness typical of PHAs. In terms of barrier properties, the addition of the CNCs layer resulted in a large reduction in oxygen permeance, between 71 % and 86 %, while water and limonene permeance hardly changed compared to the control samples without CNCs. Overall, the multilayer consisting of the outer layer of PHB/PBAT blend, with the two inner layers of CNCs and electrospun biomass-derived PHBV fibers provided the most balanced properties.

In conclusion, the results of this PhD thesis highlight the need and advantages of using waste-derived PHAs as substitutes for synthetic plastics to reduce the consumption of non-renewable resources, as well as to revalorize agro-industrial and urban by-products and to introduce bio-based and biodegradable materials into the market. Furthermore, this doctoral thesis points out the versatility of the electrospinning technique for the development of polymeric monolayers with improved properties through the combined use of nanoparticles or active substances that confer high barrier properties or antimicrobial activity. In addition, the production of multilayers by laminating monolayers developed by electrospinning and other techniques, such as melt compounding, allows the creation of structures with good optical and thermal properties, as well as mechanical performance adapted to the final application, and high barrier properties to water, limonene and oxygen. This could allow their use in rigid, semi-rigid or flexible food packaging, in the form of trays or flow packs, which would guarantee the quality and safety of food, as well as extending their shelf life, all within the principles of the Circular Bioeconomy.

References

Hernández-López, Mónica, Zormy Nacary Correa-Pacheco, Silvia Bautista-Baños, Leonor Zavaleta-Avejar, José Jesús Benítez-Jiménez, Marcos Antonio Sabino-Gutiérrez, and Pedro Ortega-Gudiño. 2019. "Bio-based composite fibers from pine essential oil and PLA/PBAT polymer blend. Morphological, physicochemical, thermal and mechanical characterization." *Materials Chemistry and Physics* 234:345-353. doi: https://doi.org/10.1016/j.matchemphys.2019.01.034.

Kunioka, Masao, Akira Tamaki, and Yoshiharu Doi. 1989. "Crystalline and thermal properties of bacterial copolyesters: poly(3-hydroxybutyrate-co-3-hydroxyvalerate) and poly(3-hydroxybutyrate-co-4-hydroxybutyrate)." *Macromolecules* 22 (2):694-697. doi: 10.1021/ma00192a031.

Martínez-Camacho, A. P., M. O. Cortez-Rocha, A. Z. Graciano-Verdugo, F. Rodríguez-Félix, M. M. Castillo-Ortega, A. Burgos-Hernández, J. M. Ezquerra-Brauer, and M. Plascencia-Jatomea. 2013. "Extruded films of blended chitosan, low density polyethylene and ethylene acrylic acid." *Carbohydrate Polymers* 91 (2):666-674. doi: https://doi.org/10.1016/j.carbpol.2012.08.076.

Muthuraj, Rajendran, Oscar Valerio, and Tizazu H. Mekonnen. 2021. "Recent developments in short- and medium-chain- length Polyhydroxyalkanoates: Production, properties, and applications." *International Journal of Biological Macromolecules* 187:422-440. doi: https://doi.org/10.1016/j.ijbiomac.2021.07.143.

Yadav, Bhoomika, Anita Talan, R. D. Tyagi, and Patrick Drogui. 2021. "Concomitant production of value-added products with polyhydroxyalkanoate (PHA) synthesis: A review." *Bioresource Technology* 337:125419. doi: https://doi.org/10.1016/j.biortech.2021.125419.

Zabihzadeh Khajavi, Maryam, Arezoo Ebrahimi, Mojtaba Yousefi, Shervin Ahmadi, Mehdi Farhoodi, Adel Mirza Alizadeh, and Musarreza Taslikh. 2020. "Strategies for Producing Improved Oxygen Barrier Materials Appropriate for the Food Packaging Sector." *Food Engineering Reviews* 12 (3):346-363. doi: 10.1007/s12393-020-09235-y.

Overall impact of research activities

The research activities developed during this PhD thesis have demonstrated how the use of agro-industrial by-products and residues can be used for the development of biodegradable materials for use in both food packaging applications and short-life products. This allows the valorization of wastes, which are incorporated into the production chain, thus reducing their negative impact on the environment and organisms, as well as the production of packaging that ensures food quality and safety, increasing the shelf life of the products. The European Union has been promoting, through both political directives and research projects, the elimination of petroleum-based plastics and their substitution by polymers derived from renewable resources or wastes. Thus, this PhD thesis has been framed within the scope of three European projects: RES URBIS, based on the conversion of urban biowaste into valuable bio-based products through a biowaste biorefinery, YPACK, whose objective was the development of a biodegradable and/or compostable food packaging using agro-industrial by-products, and USABLE, focused on the production of a bioplastic packaging, through the use of biomass feedstock derived from food processing side streams. In addition, a patent has been filed on the development of a thermoformable structural layer based on biodegradable polymers for use in food packaging. Therefore, the preparation and characterization of the biopolymers and blends studied herein and their development by electrospinning and melt compounding for the production of monolayers and multilayer with antimicrobial and high barrier properties contributed to the achievement of sustainable biodegradable packaging within the principles of the Circular Bioeconomy.

V. CONCLUSIONS

Conclusions

1. By-product-derived polyhydroxyalkanoate (PHA) samples need to be subjected to the extraction step prior to processing in order to remove impurities from the biomass.

2. Two extraction methods were evaluated, extraction with sodium hypochlorite (NaClO) and with chloroform, using a poly(3-hydroxybutyrate-*co*-3-hydroxyvalerate) (PHBV) derived from fruit pulp fermentation. The materials obtained after chloroform extraction showed higher yield and purity. Their biopapers presented improved properties, showing more transparency, lower crystallinity and rigidity, and higher barriers to water vapor and oxygen than those extracted with NaClO. Thus, the chloroform extraction route was that selected for the extraction of all the biomass-derived PHAs studied.

3. A PHBV derived from municipal biowaste (MBW) was characterized after being extracted with chloroform and processed by electrospinning. The resulting biopaper showed materials with transparency, low crystallinity and adequate phase morphology and molecular order. The films were rigid and brittle with a high barrier to vapors and gases.

4. The 3-hydroxyvalerate (3HV) content in PHBVs affected the performance of some of their properties such as crystallinity, melting temperature, mechanical and barrier properties. A cheese whey (CW)-derived PHBV with three different 3HV contents, i.e. 20, 40 and 60 mol %, was studied. With increasing 3HV content, crystallinity and melting temperature (T_m) decreased. While the samples with 20 and 60 mol % 3HV exhibited a poly(3-hydroxybutyrate) (PHB)-rich phase and a poly(3-hydroxyvalerate) (PHV)-rich phase, respectively, the sample with 40 mol % 3HV showed the coexistence of the two crystalline morphologies. The materials were tougher and more flexible as the 3HV content increased, also showing higher permeability to vapors and gases.

5. The coalescence mechanism of electrospun fibers was analyzed by combined SAXS and WAXS and ATR-FTIR experiments at variable temperature. It was concluded that coalescence may be due to temperature-induced molecular disorder or thermally induced molecular order.

6. Eugenol essential oil encapsulated in mesoporous silica nanoparticles, MCM-41 type, loaded on electrospun PHBV fibers, was developed by electrospinning. The addition of eugenol resulted in a plasticization of the fibers, reducing the crystallinity and ductility of PHBV, while MCM-41 increased its strength up to 10 wt %, after which a reduction occurred due to agglomeration. At the same time, the barrier to water vapor and limonene increased with the addition of the nanoparticles up to 15 wt %. Finally, the biopapers

displayed significant antimicrobial activity (R ≥1 and <3) against *Staphylococcus aureus* (*S. aureus*) and *Escherichia coli* (*E. coli*), for 10 and 15 wt % MCM-41 with eugenol contents, respectively, after 15 days in open and closed systems.

7. The addition of cellulose nanocrystals (CNCs) to a poly(ethylene-*co*-vinyl alcohol) (EVOH) matrix by electrospinning resulted in reduced crystallinity and thermal degradation of the polymer, as well as increased mechanical strength and reduced ductility. Moisture affected negatively the barrier to oxygen, especially to high relative humidity, i.e. 80 %, and the incorporation of CNCs did not improve either the water vapor barrier or the already high oxygen barrier capacity of pure EVOH.

8. Green composites were developed by melt compounding by the addition of a biomass-derived PHBV and rice husk flour (RHF) fillers to PHB. RHFs were well distributed in the matrix, without agglomerations, and the addition of PHBV led to an increase in thermal stability and mechanical properties compared to pure PHB, counteracting its brittleness and increasing its flexibility. The use of waste and agricultural by-products resulted in a cost-effective material and waste valorization.

9. The polymer blend between a commercial PHBV and a biomass-derived terpolyester, i.e. poly(3-hydroxybutyrate-*co*-3-hydroxyvalerate-*co*-3-hydroxyhexanoate) [P(3HB-*co*-3HV-*co*-3HHx)], was processed by melt compounding. The incorporation of 3-hydroxyhexanoate (3HHx) monomer into PHAs blends resulted in a change in polymer properties, such as lower crystallinity and T_m, more flexible and ductile materials, and a barrier to vapors and gases on the same order of magnitude as PHB or PHBV.

10. Multilayer systems were developed by using electrospun PHBV fibers as outer layers and an interlayer of CNCs, impregnated on one side of the fiber mats. The multilayer structures showed, after thermal treatment, excellent interlayer adhesion, no change in PHBV mechanical performance and improved barrier properties to limonene and especially to oxygen. The addition of hydrocolloids to the CNCs prior to impregnation of the PHBV fibers only significantly improved their barrier to limonene.

11. The use of polymeric fibers developed by electrospinning has been demonstrated as adhesives, called hot-tack (HT), after thermal treatment below the T_m of the polymer, which allowed the elimination of the synthetic glues normally used in the industry.

12. A fully bio-based, compostable multilayer with high oxygen barrier and flexible and ductile mechanical properties was developed by laminating an outer layer of a blown film of a PHB blend with poly(butylene adipate-*co*-terephthalate) (PBAT), and two inner layers consisting of a 1 µm layer of CNCs and an electrospun layer of biomass-derived PHBV fibers.

VI. ANNEXES

Annex A: List of publications

frontiers in Sustainable Food Systems

ORIGINAL RESEARCH
published: 17 July 2018
doi: 10.3389/fsufs.2018.00038

Preparation and Characterization of Electrospun Food Biopackaging Films of Poly(3-hydroxybutyrate-*co*-3-hydroxyvalerate) Derived From Fruit Pulp Biowaste

*Beatriz Melendez-Rodriguez[1], Jinneth L. Castro-Mayorga[1], Maria A. M. Reis[2], Chris Sammon[3], Luis Cabedo[4], Sergio Torres-Giner[1] and Jose M. Lagaron[1]**

[1] Novel Materials and Nanotechnology Group, Institute of Agrochemistry and Food Technology (IATA), Spanish Council for Scientific Research (CSIC), Paterna, Spain, [2] UCIBIO-REQUIMTE, Chemistry Department, Faculty of Sciences and Technology, Universidade NOVA de Lisboa, Caparica, Portugal, [3] Materials and Engineering Research Institute, Sheffield Hallam University, Sheffield, United Kingdom, [4] Polymers and Advanced Materials Group, Universitat Jaume I, Castellón, Spain

OPEN ACCESS

Edited by:
Miguel Cerqueira, Laboratório Ibérico Internacional de Nanotecnologia (INL), Portugal

Reviewed by:
Miriam Dupas Hubinger, Universidade Estadual de Campinas, Brazil
Guadalupe Virginia Nevárez-Moorillón, Autonomous University of Chihuahua, Mexico

***Correspondence:**
Jose M. Lagaron
lagaron@iata.csic.es

Specialty section:
This article was submitted to Sustainable Food Processing, a section of the journal Frontiers in Sustainable Food Systems

Received: *02 March 2018*
Accepted: *26 June 2018*
Published: *17 July 2018*

Citation:
Melendez-Rodriguez B, Castro-Mayorga JL, Reis MAM, Sammon C, Cabedo L, Torres-Giner S and Lagaron JM (2018) Preparation and Characterization of Electrospun Food Biopackaging Films of Poly(3-hydroxybutyrate-co-3-hydroxyvalerate) Derived From Fruit Pulp Biowaste. Front. Sustain. Food Syst. 2:38. doi: 10.3389/fsufs.2018.00038

In the present study, circular economy based and potentially low-cost poly(3-hydroxybutyrate-*co*-3-hydroxyvalerate) (PHBV) was produced by mixed microbial cultures derived from fruit pulp, an industrial by-product of the juice industry. Three different chemical routes, namely non-extraction, extraction with sodium hypochlorite (NaClO), and extraction with chloroform, in combination with filtering and centrifugation, were explored to purify the biopolymer and find the most optimal solution for its processing *via* electrospinning. The resultant ultrathin fiber mats of the different extracted PHBV materials were thermally post-processed at different temperatures in order to obtain continuous films adequate for food packaging applications. The resultant films were characterized in terms of morphology, crystallinity as well as thermal, mechanical, and barrier properties. The results showed that extraction with both chloroform and NaClO with a post-treatment of filtering and centrifugation of the PHBV-containing biomass were necessary refining steps to allow its processing by electrospinning. In particular, the PHBV extracted with chloroform presented the highest degree of purity, resulting in more transparent films with lower wettability and higher flexibility. The here-formulated electrospun films made of biomass derived from biowaste exhibit great potential as interlayers or coatings for food biopackaging applications.

Keywords: PHBV, electrospinning, packaging, biowaste, circular economy

INTRODUCTION

The growing concern for plastic waste disposal of petroleum-based materials has intensified the study and development of bio-based and biodegradable polymers, particularly those synthesized from agro-industrial residues (Babu et al., 2013). Polyhydroxyalkanoates (PHAs) comprise a family of biodegradable biopolyesters synthesized by hundred species of Gram-positive (G+) and Gram-negative (G−) bacteria (Rehm, 2003). PHAs provide a particularly good alternative to fossil-derived polymers, showing the highest potential to replace polyolefins in packaging

ACS APPLIED BIO MATERIALS

www.acsabm.org Article

Valorization of Municipal Biowaste into Electrospun Poly(3-hydroxybutyrate-*co*-3-hydroxyvalerate) Biopapers for Food Packaging Applications

Beatriz Melendez-Rodriguez, Sergio Torres-Giner,* Laura Lorini, Francesco Valentino, Chris Sammon, Luis Cabedo, and Jose Maria Lagaron*

Cite This: *ACS Appl. Bio Mater.* 2020, 3, 6110−6123 Read Online

ACCESS | Metrics & More | Article Recommendations | Supporting Information

ABSTRACT: The present study reports on the production and characterization of a new biopackaging material made of poly(3-hydroxybutyrate-*co*-3-hydroxyvalerate) (PHBV) derived from municipal biowaste (MBW) and produced by the mixed bacterial culture technology. After purification and extraction, the MBW-derived PHBV was processed by electrospinning to yield defect-free ultrathin fibers, which were thermally post-treated. Annealing at 130 °C, well below the biopolymer's melting temperature (T_m), successfully yielded a continuous film resulting from coalescence of the electrospun fibrillar morphology, the so-called biopaper, exhibiting enhanced optical and color properties compared to traditional melt compounding routes. The crystallinity and crystalline morphology were comprehensively studied as a function of temperature by attenuated total reflectance-Fourier transform infrared (ATR-FTIR) spectroscopy and combined time-resolved synchrotron small- and wide-angle X-ray scattering (SAXS and WAXS) experiments, which clearly indicated that the molecular order within the copolyester was improved up to a maximum at 130 °C, and then it decreased at the biopolymer's T_m. It was hypothesized that by annealing at the temperature at which the thermally induced molecular order is maximized, the fibers generated sufficient mobility to align alongside, hence reducing surface energy and porosity. The data suggest that this material shows a good balance between enhanced mechanical and improved barrier properties to vapors and gases in comparison to traditional paper and other currently used petroleum-derived polymers, thus presenting significant potential to be part of innovative food biopackaging designs for the protection and preservation of foods in a circular bioeconomy scenario.

KEYWORDS: *PHBV, electrospinning, biopapers, waste valorization, food packaging, circular bioeconomy*

1. INTRODUCTION

The potential of polyhydroxyalkanoates (PHAs) as biobased and biodegradable replacements for conventional bulk commodity plastic packaging while promoting sustainable development has long been recognized.[1] These biopolymers are mainly produced by the action of bacteria, both Gram-positive (G+) and Gram-negative (G−),[2] during the fermentation of sugar or lipids under famine conditions.[3] However, there is also an increasing number of archaea that are being used to produce PHAs.[4] The most studied PHA is poly(3-hydroxybutyrate) (PHB). The homopolyester shows thermal and mechanical properties similar to those of petrochemical polyolefins such as low-density polyethylene (LDPE) and polypropylene (PP).[5,6] However, its low ductility and toughness as well as its narrow processing window limit the use of PHB for packaging. For this reason, poly(3-

Received: June 7, 2020
Accepted: August 25, 2020
Published: August 25, 2020

https://dx.doi.org/10.1021/acsabm.0c00698
ACS Appl. Bio Mater. 2020, 3, 6110−6123

BioMACROMOLECULES

pubs.acs.org/Biomac

Article

Development and Characterization of Electrospun Biopapers of Poly(3-hydroxybutyrate-*co*-3-hydroxyvalerate) Derived from Cheese Whey with Varying 3-Hydroxyvalerate Contents

Beatriz Melendez-Rodriguez, Maria A. M. Reis, Monica Carvalheira, Chris Sammon, Luis Cabedo, Sergio Torres-Giner, and Jose Maria Lagaron*

Cite This: *Biomacromolecules* 2021, 22, 2935−2953

Read Online

ACCESS | Metrics & More | Article Recommendations

ABSTRACT: In the present study, three different newly developed copolymers of poly(3-hydroxybutyrate-*co*-3-hydroxyvalerate) (PHBV) with 20, 40, and 60 mol % contents in 3-hydroxyvalerate (3HV) were produced by the biotechnological process of mixed microbial cultures (MMCs) using cheese whey (CW), a by-product from the dairy industry, as feedstock. The CW-derived PHBV copolyesters were first purified and then processed by solution electrospinning, yielding fibers of approximately 2 μm in cross-section in all cases. The resultant electrospun PHBV mats were, thereafter, post-processed by annealing at different temperatures, below their maximum of melting, selected according to their 3HV content in order to obtain continuous films based on coalesced fibers, so-called biopapers. The resultant PHBV films were characterized in terms of their morphology, crystallinity, and mechanical and barrier properties to assess their potential application in food packaging. The CW-derived PHBV biopapers showed high contact transparency but a slightly yellow color. The fibers of the 20 mol % 3HV copolymer were seen to contain mostly poly(3-hydroxybutyrate) (PHB) crystals, the fibers of the 40 mol % 3HV copolymer a mixture of PHB and poly(3-hydroxyvalerate) (PHV) crystals and lowest crystallinity, and the fibers of the 60 mol % 3HV sample were mostly made of PHV crystals. To understand the interfiber coalesce process undergone by the materials during annealing, the crystalline morphology was also assessed by variable-temperature both combined small-angle and wide-angle X-ray scattering synchrotron and Fourier transform infrared experiments. From these experiments and, different from previously reported biopapers with lower 3HV contents, all samples were inferred to have a surface energy reduction mechanism for interfiber coalescence during annealing, which is thought to be activated by a temperature-induced decrease in molecular order. Due to their reduced crystallinity and molecular order, the CW-derived PHBV biopapers, especially the 40 mol % 3HV sample, were found to be more ductile and tougher. In terms of barrier properties, the three copolymers performed similarly to water and limonene, but to oxygen, the 40 mol % sample showed the highest relative permeability. Overall, the materials developed, which are compatible with the Circular Bioeconomy organic recycling strategy, can have an excellent potential as barrier interlayers or coatings of application interest in food packaging.

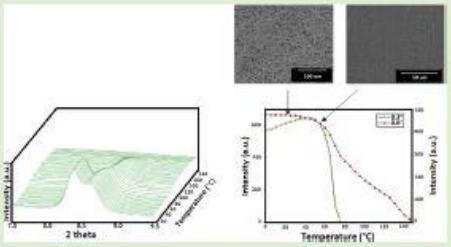

1. INTRODUCTION

Nowadays, the use of alternative materials to conventional plastics is increasingly important due to the environmental issues associated to the extensive use of single-use plastics. Thus, from political institutions, such as the European Union (EU), different strategies that have been developed focused on a better design of plastic products, the increase in recycling rates, and the promotion of Circular Economy processes.[1] For this reason, polyhydroxyalkanoates (PHAs), microbial biopolyesters produced during fermentation of lipids or sugar in famine conditions for energy and intracellular carbon storage compounds,[2] are currently seen as a proper green alternative to petroleum-derived polymers due to their renewable origin and biodegradability.[3] Within PHAs, the most studied biopolyester is poly(3-hydroxybutyrate) (PHB). This homopolymer shows similar characteristics in terms of thermal and mechanical properties that most common polyolefins, such as polyethylene (PE) and polypropylene (PP).[4] However, due to

Received: March 19, 2021
Revised: June 7, 2021
Published: June 16, 2021

https://doi.org/10.1021/acs.biomac.1c00353
Biomacromolecules 2021, 22, 2935−2953

nanomaterials

MDPI

Article

Electrospun Antimicrobial Films of Poly(3-hydroxybutyrate-*co*-3-hydroxyvalerate) Containing Eugenol Essential Oil Encapsulated in Mesoporous Silica Nanoparticles

Beatriz Melendez-Rodriguez [1], Kelly J. Figueroa-Lopez [1], Andrea Bernardos [2,3,4,5], Ramón Martínez-Máñez [2,3,4,5], Luis Cabedo [6], Sergio Torres-Giner [1] and Jose M. Lagaron [1,*]

1 Novel Materials and Nanotechnology Group, Institute of Agrochemistry and Food Technology (IATA), Spanish Council for Scientific Research (CSIC), Calle Catedrático Agustín Escardino Benlloch 7, 46980 Paterna, Spain; beatriz.melendez@iata.csic.es (B.M.-R.); kjfigueroal@iata.csic.es (K.J.E.-L.); storresginer@iata.csic.es (S.T.-G.)

2 Instituto Interuniversitario de Investigación de Reconocimiento Molecular y Desarrollo Tecnológico (IDM), Universitat Politècnica de València (UPV), Universitat de València (UV), camí de Vera s/n, 46022 Valencia, Spain; anberba@upv.es (A.B.); rmaez@qim.upv.es (R.M.-M.)

3 CIBER de Bioingeniería, Biomateriales y Nanomedicina (CIBER-BBN), Camino de Vera s/n, 46022 Valencia, Spain

4 Unidad Mixta de Investigación en Nanomedicina y Sensores, Universitat Politècnica de València (UPV), Instituto de Investigación Sanitaria La Fe, 46026 Valencia, Spain

5 Unidad Mixta UPV-CIPF de Investigación en Mecanismos de Enfermedades y Nanomedicina, Universitat Politècnica de València (UPV), Centro de Investigación Príncipe Felipe, 46012 Valencia, Spain

6 Polymers and Advanced Materials Group (PIMA), Universitat Jaume I, 12071 Castellón, Spain; lcabedo@uji.es

* Correspondence: lagaron@iata.csic.es

Received: 4 January 2019; Accepted: 2 February 2019; Published: 8 February 2019

check for updates

Abstract: The main goal of this study was to develop poly(3-hydroxybutyrate-*co*-3-hydroxyvalerate) (PHBV) films with long-term antimicrobial capacity of interest in food packaging applications. To this end, eugenol was first highly efficiently encapsulated at 50 wt.-% in the pores of mesoporous silica nanoparticles by vapor adsorption. The eugenol-containing nanoparticles were then loaded in the 2.5–20 wt.-% range into PHBV by electrospinning and the resultant electrospun composite fibers were annealed at 155 °C to produce continuous films. The characterization showed that the PHBV films filled with mesoporous silica nanoparticles containing eugenol present sufficient thermal resistance and enhanced mechanical strength and barrier performance to water vapor and limonene. The antimicrobial activity of the films was also evaluated against foodborne bacteria for 15 days in open vs. closed conditions in order to simulate real packaging conditions. The electrospun PHBV films with loadings above 10 wt.-% of mesoporous silica nanoparticles containing eugenol successfully inhibited the bacterial growth, whereas the active films stored in hermetically closed systems increased their antimicrobial activity after 15 days due to the volatile portion accumulated in the system's headspace and the sustained release capacity of the films. The resultant biopolymer films are, therefore, potential candidates to be applied in active food packaging applications to provide shelf life extension and food safety.

Keywords: PHBV; MCM-41; eugenol; antimicrobial properties; active packaging

polymers

MDPI

Article

Development and Characterization of Electrospun Fiber-Based Poly(ethylene-*co*-vinyl Alcohol) Films of Application Interest as High-Gas-Barrier Interlayers in Food Packaging

Beatriz Melendez-Rodriguez [1], Sergio Torres-Giner [1,†], Lorenzo Zavagna [1,‡], Chris Sammon [2], Luis Cabedo [3], Cristina Prieto [1] and Jose M. Lagaron [1,*]

[1] Novel Materials and Nanotechnology Group, Institute of Agrochemistry and Food Technology (IATA), Spanish Council for Scientific Research (CSIC), Calle Catedrático Agustín Escardino Benlloch 7, 46980 Valencia, Spain; beatriz.melendez@iata.csic.es (B.M.-R.); storresginer@upv.es (S.T.-G.); lorenzo@zavagna.it (L.Z.); cprieto@iata.csic.es (C.P.)

[2] Materials and Engineering Research Institute, Sheffield Hallam University, Sheffield S1 1WB, UK; c.sammon@shu.ac.uk

[3] Polymers and Advanced Materials Group (PIMA), School of Technology and Experimental Sciences, Universitat Jaume I (UJI), Avenida de Vicent Sos Baynat s/n, 12071 Castellón, Spain; lcabedo@uji.es

* Correspondence: lagaron@iata.csic.es; Tel.: +34-963-900-022

† This author is currently with the Research Institute of Food Engineering for Development (IIAD), Universitat Politècnica de València (UPV), Camino de Vera s/n, 46022 Valencia, Spain.

‡ This author is on leave from the Interuniversity National Consortium of Materials Science and Technology (INSTM), 50121 Florence, Italy.

check for updates

Citation: Melendez-Rodriguez, B.; Torres-Giner, S.; Zavagna, L.; Sammon, C.; Cabedo, L.; Prieto, C.; Lagaron, J.M. Development and Characterization of Electrospun Fiber-Based Poly(ethylene-*co*-vinyl Alcohol) Films of Application Interest as High-Gas-Barrier Interlayers in Food Packaging. *Polymers* **2021**, *13*, 2061. https://doi.org/10.3390/polym13132061

Academic Editor: Alexey Iordanskii

Received: 14 May 2021
Accepted: 21 June 2021
Published: 23 June 2021

Publisher's Note: MDPI stays neutral with regard to jurisdictional claims in published maps and institutional affiliations.

Abstract: In the present study, poly(ethylene-*co*-vinyl alcohol) with 44 mol % ethylene content ($EVOH_{44}$) was managed to be processed, for the first time, by electrospinning assisted by the coaxial technology of solvent jacket. In addition to this, different suspensions of cellulose nanocrystals (CNCs), with contents ranging from 0.1 to 1.0 wt %, were also electrospun to obtain hybrid bio-/non-bio nanocomposites. The resultant fiber mats were thereafter optimally annealed to promote interfiber coalescence at 145 °C, below the $EVOH_{44}$ melting point, leading to continuous transparent fiber-based films. The morphological analysis revealed the successful distribution of CNCs into $EVOH_{44}$ up to contents of 0.5 wt %. The incorporation of CNCs into the ethylene-vinyl alcohol copolymer caused a decrease in the crystallization and melting temperatures (T_c and T_m) of about 12 and 7 °C, respectively, and also crystallinity. However, the incorporation of CNCs led to enhanced thermal stability of the copolymer matrix for a nanofiller content of 1.0 wt %. Furthermore, the incorporation of 0.1 and 0.5 wt % CNCs produced increases in the tensile modulus (E) of ca. 38% and 28%, respectively, but also yielded a reduction in the elongation at break and toughness. The oxygen barrier of the hybrid nanocomposite fiber-based films decreased with increasing the CNCs content, but they were seen to remain high barrier, especially in the low relative humidity (RH) regime, i.e., at 20% RH, showing permeability values lower than 0.6×10^{-20} $m^3 \cdot m \cdot m^{-2} \cdot Pa^{-1} \cdot s^{-1}$. In general terms, an optimal balance in physical properties was found for the hybrid copolymer composite with a CNC loading of 0.1 wt %. On the overall, the present study demonstrates the potential of annealed electrospun fiber-based high-barrier polymers, with or without CNCs, to develop novel barrier interlayers to be used as food packaging constituents.

Keywords: EVOH; cellulose nanocrystals; electrospinning; high barrier; food packaging

1. Introduction

Polymers have been replacing the materials traditionally used in packaging, such as metal, glass, or cardboard, because they are more flexible, lighter, and habitually more cost-effective [1]. However, polymer-based materials present certain disadvantages, such as higher permeability and sorption to gases like oxygen or carbon dioxide, moisture,

materials

MDPI

Article

Reactive Melt Mixing of Poly(3-Hydroxybutyrate)/Rice Husk Flour Composites with Purified Biosustainably Produced Poly(3-Hydroxybutyrate-*co*-3-Hydroxyvalerate)

Beatriz Melendez-Rodriguez [1], Sergio Torres-Giner [1,*], Abdulaziz Aldureid [2], Luis Cabedo [2] and Jose M. Lagaron [1,*]

[1] Novel Materials and Nanotechnology Group, Institute of Agrochemistry and Food Technology (IATA), Spanish Council for Scientific Research (CSIC), Calle Catedrático Agustín Escardino Benlloch 7, 46980 Paterna, Spain

[2] Polymers and Advanced Materials Group (PIMA), Universitat Jaume I, 12071 Castellón, Spain

* Correspondence: storresginer@iata.csic.es (S.T.-G.); lagaron@iata.csic.es (J.M.L.)

Received: 31 May 2019; Accepted: 1 July 2019; Published: 4 July 2019

check for updates

Abstract: Novel green composites based on commercial poly(3-hydroxybutyrate) (PHB) filled with 10 wt % rice husk flour (RHF) were melt-compounded in a mini-mixer unit using triglycidyl isocyanurate (TGIC) as compatibilizer and dicumyl peroxide (DCP) as initiator. Purified poly(3-hydroxybutyrate-*co*-3-hydroxyvalerate) (PHBV) produced by mixed bacterial cultures derived from fruit pulp waste was then incorporated into the green composite in contents in the 5–50 wt % range. Films for testing were obtained thereafter by thermo-compression and characterized. Results showed that the incorporation of up to 20 wt % of biowaste derived PHBV yielded green composite films with a high contact transparency, relatively low crystallinity, high thermal stability, improved mechanical ductility, and medium barrier performance to water vapor and aroma. This study puts forth the potential use of purified biosustainably produced PHBV as a cost-effective additive to develop more affordable and waste valorized food packaging articles.

Keywords: PHB; PHBV; rice husk; green composites; biosustainability; waste valorization

1. Introduction

The current concern to reduce the use of petroleum-derived materials has led to the search for natural and biodegradable polymers. Polyhydroxyalkanoates (PHAs) is a family of linear polyesters produced in nature by the action of bacteria during fermentation of sugar or lipids in famine conditions [1]. PHAs represent a good alternative to conventional polymers in the frame of the circular economy since they are fully bio-based and biodegradable [2]. Among the different commercially available PHAs, the most widely studied is poly(3-hydroxybutyrate) (PHB). This isotactic homopolyester presents a relatively high melting temperature (T_m) and good stiffness and strength due to its high crystallinity (>50%). As a result, PHB articles present similar performance or even greater than some commodities plastics such as polypropylene (PP) and barrier properties close to those of polyethylene terephthalate (PET) [3]. PHB undergoes rapid and complete disintegration within a maximum period of 6 months through the action of enzymes and/or chemical deterioration associated with living microorganisms. Moreover, PHB is biodegradable not only in composting conditions but also in other environments such as marine water [4].

However, the use of PHB for packaging applications is limited due to its excessive brittleness and narrow processing temperature window [5]. To overcome these limitations, its copolymer with

polymers

MDPI

Article

Blends of Poly(3-Hydroxybutyrate-*co*-3-Hydroxyvalerate) with Fruit Pulp Biowaste Derived Poly(3-Hydroxybutyrate-*co*-3-Hydroxyvalerate-*co*-3-Hydroxyhexanoate) for Organic Recycling Food Packaging

Beatriz Meléndez-Rodríguez [1], Sergio Torres-Giner [1,†], Maria A. M. Reis [2], Fernando Silva [2], Mariana Matos [2], Luis Cabedo [3] and José María Lagarón [1,*]

[1] Novel Materials and Nanotechnology Group, Institute of Agrochemistry and Food Technology (IATA), Spanish Council for Scientific Research (CSIC), Calle Catedrático Agustín Escardino Benlloch 7, 46980 Paterna, Spain; beatriz.melendez@iata.csic.es (B.M.-R.); storresginer@iata.csic.es (S.T.-G.)
[2] UCIBIO-REQUIMTE-Applied Molecular Biosciences Unit, Chemistry Department, Faculty of Sciences and Technology, New University of Lisbon, 1099-085 Lisbon, Portugal; amr@fct.unl.pt (M.A.M.R.); fra.silva@campus.fct.unl.pt (F.S.); m.matos@campus.fct.unl.pt (M.M.)
[3] Polymers and Advanced Materials Group (PIMA), Universitat Jaume I (UJI), 12071 Castellón, Spain; lcabedo@uji.es
* Correspondence: lagaron@iata.csic.es; Tel.: +34-963-900-022
† This author is currently with the Research Institute of Food Engineering for Development (IIAD), Universitat Politècnica de València (UPV), Camino de Vera s/n, 46022 Valencia, Spain; storresginer@upv.es.

check for updates

Citation: Meléndez-Rodríguez, B.; Torres-Giner, S.; Reis, M.A.M.; Silva, F.; Matos, M.; Cabedo, L.; Lagarón, J.M. Blends of Poly(3-Hydroxybutyrate-*co*-3-Hydroxyvalerate) with Fruit Pulp Biowaste Derived Poly(3-Hydroxybutyrate-*co*-3-Hydroxyvalerate-*co*-3-Hydroxyhexanoate) for Organic Recycling Food Packaging. *Polymers* **2021**, *13*, 1155. https://doi.org/10.3390/polym13071155

Academic Editor: Justyna Możejko-Ciesielska

Received: 13 March 2021
Accepted: 26 March 2021
Published: 4 April 2021

Publisher's Note: MDPI stays neutral with regard to jurisdictional claims in published maps and institutional affiliations.

Abstract: In the present study, a new poly(3-hydroxybutyrate-*co*-3-hydroxyvalerate-*co*-3-hydroxyhexanoate) [P(3HB-*co*-3HV-*co*-3HHx)] terpolyester with approximately 68 mol% of 3-hydroxybutyrate (3HB), 17 mol% of 3-hydroxyvalerate (3HV), and 15 mol% of 3-hydroxyhexanoate (3HHx) was obtained via the mixed microbial culture (MMC) technology using fruit pulps as feedstock, a processing by-product of the juice industry. After extraction and purification performed in a single step, the P(3HB-*co*-3HV-*co*-3HHx) powder was melt-mixed, for the first time, in contents of 10, 25, and 50 wt% with commercial poly(3-hydroxybutyrate-*co*-3-hydroxyvalerate) (PHBV). Thereafter, the resultant doughs were thermo-compressed to obtain highly miscible films with good optical properties, which can be of interest in rigid and semirigid organic recyclable food packaging applications. The results showed that the developed blends exhibited a progressively lower melting enthalpy with increasing the incorporation of P(3HB-*co*-3HV-*co*-3HHx), but retained the PHB crystalline morphology, albeit with an inferred lower crystalline density. Moreover, all the melt-mixed blends were thermally stable up to nearly 240 °C. As the content of terpolymer increased in the blends, the mechanical response of their films showed a brittle-to-ductile transition. On the other hand, the permeabilities to water vapor, oxygen, and, more notably, limonene were seen to increase. On the overall, this study demonstrates the value of using industrial biowaste derived P(3HB-*co*-3HV-*co*-3HHx) terpolyesters as potentially cost-effective and sustainable plasticizing additives to balance the physical properties of organic recyclable polyhydroxyalkanoate (PHA)-based food packaging materials.

Keywords: polyhydroxyalkanoates; waste valorization; food packaging; Circular Bioeconomy; organic recycling

1. Introduction

The massive use of synthetic plastics in recent decades has caused a deep damage to the environment. Polymers derived from fossil hydrocarbons are habitually non-biodegradable, making them difficult to eliminate and being accumulated in landfills or in natural environments [1]. This environmental issue becomes particularly relevant for packaging applications, in which the articles are generally discarded after a short and

Carbohydrate Polymer Technologies and Applications 2 (2021) 100150

Contents lists available at ScienceDirect

Carbohydrate Polymer Technologies and Applications

journal homepage: www.sciencedirect.com/journal/carbohydrate-polymer-technologies-and-applications

Barrier biopaper multilayers obtained by impregnation of electrospun poly (3-hydroxybutyrate-*co*-3-hydroxyvalerate) with protein and polysaccharide hydrocolloids

Beatriz Melendez-Rodriguez [a], Marie-Stella M'Bengue [a,1], Sergio Torres-Giner [a,2], Luis Cabedo [b], Cristina Prieto [a], Jose Maria Lagaron [a,*]

[a] Novel Materials and Nanotechnology Group, Institute of Agrochemistry and Food Technology (IATA), Spanish Council for Scientific Research (CSIC), Calle Catedrático Agustín Escardino Benlloch 7, 46980 Valencia, Spain
[b] Polymers and Advanced Materials Group (PIMA), School of Technology and Experimental Sciences, Universitat Jaume I (UJI), Avenida de Vicent Sos Baynat s/n, 12071 Castellón, Spain

ARTICLE INFO

Keywords:
Nanocellulose
PHBV
Additives
Multilayers
Gas barrier
Food packaging

ABSTRACT

Multilayer biopapers composed of two electrospun layers of poly(3-hydroxybutyrate-co-3-hydroxyvalerate) (PHBV) were impregnated, at the inner side of one of the layers, with cellulose nanocrystals (CNCs) and their composites with hydrocolloids, to develop high-barrier fully biobased structures. The study aimed for the first time at comparing the impregnation of electrospun fibers with several biopolymer solutions. Thus, neat CNCs, and CNCs mixed as a minor fraction, that is, 2 wt%, with gelatin (GE), agar (AG), xanthan gum (XG), and gum arabic (GA) were assessed in their potential to improve the barrier properties of PHBV. Glycerol plasticizer was added to the composite formulations. The impregnated electrospun multilayer mats were subsequently annealed, below the PHBV melting point, to yield continuous films by an interfiber coalescence process, so-called biopapers, and thereafter characterized to evaluate their potential for high barrier food packaging applications. The morphological characterization revealed good interlayer adhesion, more noticeably for those containing CNCs and their nanocomposites with AG and XG. From their mechanical response, it was inferred that the material behavior was governed mainly by the rigidity of the PHBV substrates, and this could not be significantly improved by impregnation with any of the various hydrocolloids. Whereas the water vapor barrier was not seen to improve in any of the samples, the barrier to the organic vapor limonene, used as a standard for aroma barrier, was however improved in the samples impregnated with AG and XG composites. Interestingly, the oxygen barrier properties were significantly improved but only by impregnation with pure CNCs. This study reports for the first time a scalable impregnation technology approach to produce fully biobased barrier multilayers.

1. Introduction

In a context of global environmental problems, a change of perspective towards the use of petroleum derived materials has been gaining relevance in recent decades. The massive production of plastics, about 360 million tons per year, in combination to their non-biodegradable nature represent a serious end-of-life management problem (Geyer, Jambeck & Law, 2017). Every year, around eight billion kilograms of plastic waste reach the oceans from the coast, being 40% of which single-use items (Commission, 2018). Thus, the use of bio-based, biodegradable, and eco-friendly polymers as substitutes for traditional petrochemical ones is becoming increasingly important.

In this regard, cellulose is of great interest due to its biodegradability and abundancy (Huber et al., 2012). Cellulose is a polysaccharide

* Corresponding author.
E-mail addresses: beatriz.melendez@iata.csic.es (B. Melendez-Rodriguez), marie-stella.m-bengue@grenoble-inp.org (M.-S. M'Bengue), storresginer@upv.es (S. Torres-Giner), lcabedo@uji.es (L. Cabedo), cprieto@iata.csic.es (C. Prieto), lagaron@iata.csic.es (J.M. Lagaron).
[1] On leave from Grenoble INP – Pagora, UGA, International School of Paper, Print Media and Biomaterials, 461 Rue de la papeterie - CS 10065 - 38402 Saint-Martin d'Hères Cedex, France.
[2] This author is currently with the Research Institute of Food Engineering for Development (IIAD), Universitat Politècnica de València (UPV), Camino de Vera s/n, 46022 Valencia, Spain.

https://doi.org/10.1016/j.carpta.2021.100150
Received 23 May 2021; Received in revised form 24 August 2021; Accepted 7 September 2021
Available online 9 September 2021

nanomaterials

MDPI

Article

High-Oxygen-Barrier Multilayer Films Based on Polyhydroxyalkanoates and Cellulose Nanocrystals

Beatriz Melendez-Rodriguez [1], Sergio Torres-Giner [1,†], Inmaculada Angulo [2], Maria Pardo-Figuerez [1,3], Loïc Hilliou [4], Jose Manuel Escuin [5], Luis Cabedo [6], Yuval Nevo [7], Cristina Prieto [1] and Jose Maria Lagaron [1,*]

1 Novel Materials and Nanotechnology Group, Institute of Agrochemistry and Food Technology (IATA), Spanish Council for Scientific Research (CSIC), 46980 Valencia, Spain; beatriz.melendez@iata.csic.es (B.M.-R.); storresginer@upv.es (S.T.-G.); mpardo@iata.csic.es (M.P.-F.); cprieto@iata.csic.es (C.P.)
2 Gaiker Technology Centre, Basque Research and Technology Alliance (BRTA). Parque Tecnológico de Bizkaia, edificio 202, 48170 Zamudio (Bizkaia), Spain; angulo@gaikerres
3 Bioinicia R&D, Bioinicia S.L., 46980 Valencia, Spain
4 IPC/I3N, Institute for Polymers and Composites, Department of Polymer Engineering, University of Minho, 4800-058 Braga, Portugal; loic@dep.uminho.pt
5 Tecnopackaging S.L., Polígono Industrial Empresarium, 50720 Zaragoza, Spain; info@tecnopackaging.com
6 Polymers and Advanced Materials Group (PIMA), School of Technology and Experimental Sciences, Universitat Jaume I (UJI), 12071 Castellón, Spain; lcabedo@uji.es
7 Melodea Bio-Based Solutions, Faculty of Agriculture-Hebrew University, Rehovot 76100, Israel; yuval@melodea.eu
* Correspondence: lagaron@iata.csic.es; Tel.: +34-963-900-022
† Current address: Research Institute of Food Engineering for Development (IIAD), Universitat Politècnica de València (UPV), 46022 Valencia, Spain.

check for updates

Citation: Melendez-Rodriguez, B.; Torres-Giner, S.; Angulo, I.; Pardo-Figuerez, M.; Hilliou, L.; Escuin, J.M.; Cabedo, L.; Nevo, Y.; Prieto, C.; Lagaron, J.M. High-Oxygen-Barrier Multilayer Films Based on Polyhydroxyalkanoates and Cellulose Nanocrystals. *Nanomaterials* **2021**, *11*, 1443. https://doi.org/10.3390/nano11061443

Academic Editor: Hirotaka Koga

Received: 5 May 2021
Accepted: 26 May 2021
Published: 30 May 2021

Publisher's Note: MDPI stays neutral with regard to jurisdictional claims in published maps and institutional affiliations.

Abstract: This study reports on the development and characterization of organic recyclable high-oxygen-barrier multilayer films based on different commercial polyhydroxyalkanoate (PHA) materials, including a blend with commercial poly(butylene adipate-*co*-terephthalate) (PBAT), which contained an inner layer of cellulose nanocrystals (CNCs) and an electrospun hot-tack adhesive layer of poly(3-hydroxybutyrate-*co*-3-hydroxyvalerate) (PHBV) derived from cheese whey (CW). As a result, the full multilayer structures were made from bio-based and/or compostable materials. A characterization of the produced films was carried out in terms of morphological, optical, mechanical, and barrier properties with respect to water vapor, limonene, and oxygen. Results indicate that the multilayer films exhibited a good interlayer adhesion and contact transparency. The stiffness of the multilayers was generally improved upon incorporation of the CNC interlayer, whereas the enhanced elasticity of the blend was reduced to some extent in the multilayer with CNCs, but this was still much higher than for the neat PHAs. In terms of barrier properties, it was found that 1 µm of the CNC interlayer was able to reduce the oxygen permeance between 71% and 86%, while retaining the moisture and aroma barrier of the control materials.

Keywords: PHBV; nanocellulose; multilayers; barrier films; packaging

1. Introduction

Packaging materials based on biopolymers that can biodegrade in both industrial and home compost conditions currently represent an alternative to solve the environmental issue of plastic accumulation [1,2]. Polyhydroxyalkanoates (PHAs) are thermoplastic biopolyesters produced by various microorganisms, mainly bacteria, during fermentation of sugar or lipids under famine conditions as energy-reserve inclusions in the cytoplasm [3]. The most widely studied PHA is poly(3-hydroxybutyrate) (PHB), whose thermal and mechanical characteristics are similar to polypropylene (PP) [4]. However, PHB is brittle and presents a poor processing window due to its high crystallinity and low thermal stability.

Annex B: Additional works

JOURNAL OF AGRICULTURAL AND FOOD CHEMISTRY

Article

pubs.acs.org/JAFC

Nanoencapsulation of *Aloe vera* in Synthetic and Naturally Occurring Polymers by Electrohydrodynamic Processing of Interest in Food Technology and Bioactive Packaging

Sergio Torres-Giner,[†] Sabina Wilkanowicz,[‡] Beatriz Melendez-Rodriguez,[†] and Jose M. Lagaron*[,†]

[†]Novel Materials and Nanotechnology Group, Institute of Agrochemistry and Food Technology (IATA), Spanish Council for Scientific Research (CSIC), Calle Catedrático Agustín Escardino Benlloch 7, 46980 Paterna, Spain

[‡]Bioinicia R&D, Calle Algepser 65—Nave 3, Polígono Industrial Táctica, 46988 Paterna, Spain

ABSTRACT: This work originally reports on the use of electrohydrodynamic processing (EHDP) to encapsulate *Aloe vera* (AV, *Aloe barbadensis* Miller) using both synthetic polymers, i.e., polyvinylpyrrolidone (PVP) and poly(vinyl alcohol) (PVOH), and naturally occurring polymers, i.e., barley starch (BS), whey protein concentrate (WPC), and maltodextrin. The AV leaf juice was used as the water-based solvent for EHDP, and the resultant biopolymer solution properties were evaluated to determine their effect on the process. Morphological analysis revealed that, at the optimal processing conditions, synthetic polymers mainly produced fiber-like structures, while naturally occurring polymers generated capsules. Average sizes ranged from 100 nm to above 3 μm. As a result of their different and optimal morphology and, hence, higher AV content, PVP, in the form of nanofibers, and WPC, of nanocapsules, were further selected to study the AV stability against ultraviolet (UV) light exposure. Fourier transform infrared (FTIR) spectroscopy confirmed the successful encapsulation of AV in the biopolymer matrices, presenting both encapsulants a high chemical interaction with the bioactive components. Ultraviolet—visible (UV—vis) spectroscopy showed that, while PVP nanofibers offered a poor effect on the AV degradation during UV light exposure (~10% of stability after 5 h), WPC nanobeads delivered excellent protection (stability of >95% after 6 h). This was ascribed to positive interactions between WPC and the hydrophilic components of AV and the inherent UV-blocking and oxygen barrier properties provided by the protein. Therefore, electrospraying of food hydrocolloids interestingly appears as a novel potential nanotechnology tool toward the formulation of more stable functional foods and nutraceuticals.

KEYWORDS: *electrospinning, electrospraying, biopolymers, Aloe vera leaf juice, encapsulation, food technology, bioactive packaging*

INTRODUCTION

Aloe barbadensis Miller is one of the main species of *Aloe vera* (AV), which belongs to the family Liliaceae, and its history dates back to the 4th century B.C.[1] The term "aloe" derives from "*alloeh*" in Arabic and "*halaf*" in Hebrew, which means bitter shiny substance, while the epithet "vera" means true or genuine.[2] The plant of AV is endemic to hot and dry world areas, such as the Arabian Peninsula or Africa, and it is well-adapted to grow in desert or arid climates. Therefore, its tissues have highly evolved for the retention and storage of water by the formation of a dense gel, the so-called leaf juice, which contains approximately 0.985 g of water/g wet basis.[3]

Some of the functional properties of AV are related to its antioxidant activity, wound and burn healing, pain and edema reduction, digestion, and immune response.[4] There are also some technical reports about its antibacterial and antifungal activity, especially in the form of fresh juice, and anticancer properties.[5] In addition, the extract of AV leaf juice has been reported to lower blood glucose levels in normal and alloxan-induced diabetic mice.[6] A wide range of bioactive compounds are found in the AV leaves, such as anthraquinones (e.g., aloins A and B), carbohydrates (e.g., pectin, cellulose, glucomannan, and others), enzymes (e.g., amylase, lipase, and oxidase), inorganic compounds (e.g., calcium, magnesium, iron, and zinc salts), non-essential and essential amino acids, and vitamins (e.g., vitamins B1, B2, B6, and C, β-carotene, choline, folic acid, and α-tocopherol).[7,8] In addition, AV contains salicylic acid that, in combination with magnesium, is considered to work together to provide a natural analgesic effect on burns.[9,10]

Because the degradation of AV bioactive ingredients starts right after harvesting of the plant, both the whole leaf and inner gel fillet need to be rapidly processed into more stable products. Therefore, protection from chemical degradation of AV compounds is of high importance, and the use of encapsulation technologies represent a suitable solution. Various encapsulation technologies have been previously used to protect AV compounds from degradation, such as freeze drying, spray drying, hot-air drying, and coacervation. For instance, AV has been recently encapsulated in polyamide nanoparticles by the emulsion—diffusion technique, followed by freeze drying.[11] In another study, similar AV nanocapsules of a triblock copolymer made of poly(ethylene glycol) (PEG) and poly(butylene adipate) (PBA) were also prepared.[12] However, spray drying, freeze drying, and other more conventional or advanced processing technologies often require the use of extremely low or high temperatures, vacuum, or harsh solvents, which may add complexity or may not be scalable.

Received: March 28, 2017
Revised: May 9, 2017
Accepted: May 12, 2017
Published: May 12, 2017

DOI: 10.1021/acs.jafc.7b01393
J. Agric. Food Chem. 2017, 65, 4439−4448

Food Packaging and Shelf Life 17 (2018) 39–49

Contents lists available at ScienceDirect

Food Packaging and Shelf Life

journal homepage: www.elsevier.com/locate/fpsl

Melt processability, characterization, and antibacterial activity of compression-molded green composite sheets made of poly(3-hydroxybutyrate-*co*-3-hydroxyvalerate) reinforced with coconut fibers impregnated with oregano essential oil

S. Torres-Giner[a,*], L. Hilliou[b], B. Melendez-Rodriguez[a], K.J. Figueroa-Lopez[a], D. Madalena[c], L. Cabedo[d], J.A. Covas[b], A.A. Vicente[c], J.M. Lagaron[a]

[a] Novel Materials and Nanotechnology Group, Institute of Agrochemistry and Food Technology (IATA), Spanish Council for Scientific Research (CSIC), Paterna, Spain
[b] Institute for Polymers and Composites/I3N, University of Minho, Guimarães, Portugal
[c] CEB - Centre of Biological Engineering, University of Minho, Braga, Portugal
[d] Polymers and Advanced Materials Group (PIMA), Universitat Jaume I (UJI), Castellón, Spain

ARTICLE INFO

Keywords:
PHBV
Coir
Essential oils
Active packaging
Agro-food waste valorization

ABSTRACT

New packaging materials based on green composite sheets consisting of poly(3-hydroxybutyrate-*co*-3-hydroxyvalerate) (PHBV) and coconut fibers (CFs) were obtained by twin-screw extrusion (TSE) followed by compression molding. The effect of varying the CF weight content, *i.e.* 1, 3, 5, and 10 wt.-%, and the screw speed during melt processing, *i.e.* 75, 150, and 225 rpm, on both the aspect ratio and dispersion of the fibers was analyzed and related to the properties of the compression-molded sheets. Finally, the CFs were impregnated with oregano essential oil (OEO) by an innovative spray coating methodology and then incorporated into PHBV at the optimal processing conditions. The functionalized green composite sheets presented bacteriostatic effect against *Staphylococcus aureus* from fiber contents as low as 3 wt.-%. Therefore, the here-prepared CFs can be successfully applied as natural vehicles to entrap extracts and develop green composites of high interest in active food packaging to provide protection and shelf life extension.

1. Introduction

The use of agro-food residues for the preparation of polymer composites is gaining a significant attention due to their huge availability and low price, being at the same time a highly sustainable strategy for waste valorization. Natural fibers (NFs), particularly those obtained from plants, represent an environmentally friendly and unique choice to reinforce bioplastic matrices due to their relative high strength and stiffness (Yang, Kim, Park, Lee, & Hwang, 2006). The substitution of oil-derived polymers with bio-based polymers as the matrix component results in the term "green composites" (Zini & Scandola, 2011), which indicates that the composite as a whole, *i.e.* both matrix and reinforcement, originates from renewable resources. In this regard, the incorporation of NFs such as jute, sisal, flax, hemp, and bamboo fibers into biopolymers has been recently intensified (Bogoeva-Gaceva et al., 2007). Resultant green composites do not only offer environmental advantages over traditional polymer composites, such as reduced dependence on non-renewable energy/material sources, lower greenhouse gas and pollutant emissions, improved energy recovery, and end-of-life biodegradability of components (Joshi, Drzal, Mohanty, & Arora, 2004), but also a potential reduction of both product density and energy requirements for processing (Faruk, Bledzki, Fink, & Sain, 2014).

Polyhydroxyalkanoates (PHAs) comprise a family of biodegradable aliphatic polyesters produced by microorganisms. PHAs show the highest potential to replace polyolefins in a wide range of applications, including packaging, due to their high mechanical strength and water resistance (Bugnicourt, Cinelli, Lazzeri, & Alvarez, 2014). Among PHAs, poly(3-hydroxybutyrate) (PHB) and its copolymer with 3-hydroxyvalerate (HV), *i.e.* poly(3-hydroxybutyrate-*co*-3-hydroxyvalerate) (PHBV), have so far received the greatest attention in terms of pathway characterization and industrial-scale production. The use of PHA copolymers presents certain advantages since they have a lower melting point and higher flexibility than their homopolymers, which improves melt stability and broadens their processing window (Torres-Giner, Montanes, Boronat, Quiles-Carrillo, & Balart, 2016). Furthermore, the

* Corresponding author.
E-mail address: storresginer@iata.csic.es (S. Torres-Giner).

https://doi.org/10.1016/j.fpsl.2018.05.002
Received 30 December 2017; Received in revised form 29 March 2018; Accepted 2 May 2018

Polymer Testing 90 (2020) 106754

Contents lists available at ScienceDirect

Polymer Testing

journal homepage: http://www.elsevier.com/locate/polytest

NMR analysis and triad sequence distributions of poly (3-hydroxybutyrate-co-3-hydroxyvalerate)

H.N. Cheng [a,*], Atanu Biswas [b], Karl Vermillion [b], Beatriz Melendez-Rodriguez [c], Jose Maria Lagaron [c]

[a] Southern Regional Research Center, U.S. Department of Agriculture, Agricultural Research Service, 1100 Robert E. Lee Blvd., New Orleans, LA, 70124, USA
[b] National Center for Agricultural Utilization Research, U.S. Department of Agriculture, Agricultural Research Service, 1815 N. University St., Peoria, IL, 61604, USA
[c] Novel Materials and Nanotechnology Group, IATA, CSIC, Av. Agustin Escardino 7, Paterna, 46980, Valencia, Spain

ARTICLE INFO

Keywords:
NMR
PHBV
Poly(hydroxyalkanoates)
Sequence distribution
Shift reagent
Statistical models

ABSTRACT

Polyhydroxyalkanoates (PHAs) are considered promising "green" alternatives to synthetic polymers because they are bio-derived, biodegradable and biocompatible. The properties of bacterial PHA copolymers depend on their microstructures, which can be modified with the use of different fermentation processes and feed materials. Thus, it is desirable to have an improved testing method for the determination of PHA microstructures. In this work, a detailed NMR analysis of poly(3-hydroxybutyrate-co-3-hydroxyvalerate) microstructure was made. Previously only two of the hydroxyvalerate ^{13}C NMR peaks have been assigned at the triad level. In this work, three of the ^{13}C hydroxyvalerate peaks and two of the hydroxybutyrate peaks were found to be split into four peaks each due to comonomer sequence effects. Using eight copolymer samples with a wide compositional range, we were able to assign all these peaks to B-centered and V-centered triad sequences. Through curve deconvolution, the triad intensities were determined. These triad sequence intensities can then be analyzed via both the first-order Markovian and two-component Bernoullian models to obtain more in-depth information on copolymer composition and comonomer reactivities.

1. Introduction

In recent years there has been continuing interest in agro-based polymers that are biodegradable, eco-friendly, and sustainable as alternatives to synthetic polymers based on petroleum feedstocks [1,2]. The increasing awareness of the problems of single-use plastics and the presence of microplastics in the environment has reinforced the attention towards these materials [3,4]. Among the agro-based polymers, polyhydroxyalkanoates (PHAs) appear attractive [5,6]. These polyesters are derived from bacterial fermentation, typically under nutrient-deficient conditions. They are biodegradable, biocompatible and non-toxic. Currently they are being considered for use in packaging films, food containers, agricultural films and foils, and a range of medical and bioengineering applications [5–8].

The most well-known PHA is poly(β-hydroxybutyrate) (PHB). However, PHB exhibits high stiffness and crystallinity. In order to increase its flexibility and processing capabilities, PHBV, a copolymer of 3-hydroxybutyrate (B) and 3-hydroxyvalerate (V), has been developed [6–8] (Fig. 1). Increasing V content in PHBV reduces the stiffness, melting point, and crystallinity of the resulting polyester. PHAs with longer alkyl chains have also been developed [9–11]. Copolymers of B and higher alkyl hydroxyl esters have also been reported [12,13].

Because the physical properties of PHBV depend on the copolymer composition and comonomer sequence distribution, their analysis has been reported many times in the literature [14–21]. The copolymer composition (amount of B and V units present) can be readily determined by analyzing the NMR spectra in solution [14–16] or in the solid state [17].

For B and V comonomer sequence distribution, solution ^{13}C NMR is usually used because the ^{13}C peaks show more splitting due to sequence effects. Bluhm et al. [14] and Doi et al. [15] assigned the ester carbons of the ^{13}C spectra to diads (BB, BV, VB, VV), the B2 methylene carbons to diads (BB and BV), and V2 and V4 methylene carbons to V-centered triads (BVB, VVB, BVV, and VVV). In both papers, the sequence distribution of B and V units was found to be approximately random. In addition, Doi et al. [15] and Kamiya et al. [16] also fitted these observed

* Corresponding author.
E-mail address: hn.cheng@usda.gov (H.N. Cheng).

https://doi.org/10.1016/j.polymertesting.2020.106754
Received 16 June 2020; Received in revised form 12 July 2020; Accepted 17 July 2020
Available online 20 July 2020
0142-9418/Published by Elsevier Ltd.

molecules

MDPI

Article

Tailoring the Properties of Thermo-Compressed Polylactide Films for Food Packaging Applications by Individual and Combined Additions of Lactic Acid Oligomer and Halloysite Nanotubes

Sandra Rojas-Lema [1], Luis Quiles-Carrillo [1], Daniel Garcia-Garcia [1], Beatriz Melendez-Rodriguez [2], Rafael Balart [1] and Sergio Torres-Giner [2,*]

1 Technological Institute of Materials (ITM), Universitat Politècnica de València (UPV), Plaza Ferrándiz y Carbonell 1, 03801 Alcoy, Spain; sanrole@epsa.upv.es (S.R.-L.); luiquic1@epsa.upv.es (L.Q.-C.); dagarga4@alumni.upv.es (D.G.-G.); rbalart@mcm.upv.es (R.B.)

2 Novel Materials and Nanotechnology Group, Institute of Agrochemistry and Food Technology (IATA), Spanish National Research Council (CSIC), Calle Catedrático Agustín Escardino Benlloch 7, 46980 Paterna, Spain; beatriz.melendez@iata.csic.es

* Correspondence: storresginer@iata.csic.es; Tel.: +34-963-900-022

Academic Editors: Alfonso Jimenez and Maria del Carmen Garrigós
Received: 14 April 2020; Accepted: 22 April 2020; Published: 23 April 2020

Abstract: In this work, films of polylactide (PLA) prepared by extrusion and thermo-compression were plasticized with oligomer of lactic acid (OLA) at contents of 5, 10, and 20 wt%. The PLA sample containing 20 wt% of OLA was also reinforced with 3, 6, and 9 parts per hundred resin (*phr*) of halloysite nanotubes (HNTs) to increase the mechanical strength and thermal stability of the films. Prior to melt mixing, ultrasound-assisted dispersion of the nanoclays in OLA was carried out at 100 °C to promote the HNTs dispersion in PLA and the resultant films were characterized with the aim to ascertain their potential in food packaging. It was observed that either the individual addition of OLA or combined with 3 *phr* of HNTs did not significantly affect the optical properties of the PLA films, whereas higher nanoclay contents reduced lightness and induced certain green and blue tonalities. The addition of 20 wt% of OLA increased ductility of the PLA film by nearly 75% and also decreased the glass transition temperature (T_g) by over 18 °C. The incorporation of 3 *phr* of HNTs into the OLA-containing PLA films delayed thermal degradation by 7 °C and additionally reduced the permeabilities to water and limonene vapors by approximately 8% and 47%, respectively. Interestingly, the highest barrier performance was attained for the unfilled PLA film plasticized with 10 wt% of OLA, which was attributed to a crystallinity increase and an effect of "antiplasticization". However, loadings of 6 and 9 *phr* of HNTs resulted in the formation of small aggregates that impaired the performance of the blend films. The here-attained results demonstrates that the properties of ternary systems of PLA/OLA/HNTs can be tuned when the plasticizer and nanofiller contents are carefully chosen and the resultant nanocomposite films can be proposed as a bio-sourced alternative for compostable packaging applications.

Keywords: PLA; OLA; HNTs; ultrasound-assisted dispersion; nanocomposites; food packaging

Academic Editors: Alfonso Jimenez and María del Carmen Garrigós

1. Introduction

Most commercial plastic packaging is currently made of non-biodegradable polymers derived from petroleum that is currently causing disposal problems and leakage into the oceans [1]. To solve these environmental issues, recent studies have been directed towards the development osf food

Polymer Chemistry

ROYAL SOCIETY OF CHEMISTRY

PAPER

View Article Online
View Journal | View Issue

Cite this: Polym. Chem., 2021, 12, 1571

Organocatalyzed closed-loop chemical recycling of thermo-compressed films of poly(ethylene furanoate)†

Elena Gabirondo,[a] Beatriz Melendez-Rodriguez,[b] Carmen Arnal,[b] Jose M. Lagaron,[b] Antxon Martínez de Ilarduya,[c] Haritz Sardon *[a] and Sergio Torres-Giner *‡[b]

Received 25th November 2020,
Accepted 11th January 2021

DOI: 10.1039/d0py01623c

rsc.li/polymers

Monomers obtained from renewable feedstocks have emerged as a sustainable alternative to petroleum derived polymers. One of the biomass derived polyesters that has recently been gaining attention as an alternative to petrochemical polyethylene terephtalate (PET) for food and beverage packaging applications is poly(ethylene furanoate) (PEF). However, similar to PET, PEF is not biodegradable or compostable and its end-of-life options must be thus considered to avoid contributing to the accumulation of plastic waste. In this manuscript, PEF films were first produced using thermo-compression, an industrially relevant processing method, and their thermal, mechanical, and barrier properties were determined and compared to those of PET and other biopolyesters to ascertain their suitability for food packaging. Thereafter, the chemical glycolysis of PEF film waste was investigated using a sustainable and thermally stable acid–base organocatalyst. After succesfully deconstructing PEF into bis(2-hydroxyethyl)-furan-2,5-dicarboxylate (BHEF), the obtained BHEF diester was used to resynthesize PEF using the same catalyst to generate a new biopolyester with similar thermal properties to the virgin one in a closed-loop cycle.

Introduction

There are two main strategic goals in the development of biorefineries: the displacement of petroleum in favor of renewable raw materials and the establishment of a robust bio-based industry, the so-called Bioeconomy.[1] Based on this concept, chemicals from various vegetable feedstocks such as sugars, starch, lignocelluloses, vegetable oils, organic acids or glycerol have been proposed as renewable monomers for polymer production.[2] In particular, the dehydration of abundant 6-carbon sugars (*e.g.* fructose and galactose) to give furans is a well-known transformation for the preparation of furfurals such as 5-hydroxymethylfurfural (HMF) and 5-methoxy methyl furfural (MMF) with high selectivity (~80%) and conversion (~90%) rates.[3] The oxidation of HMF, MMF, and their ethers in air over different catalysts[4,5] yields furan-2,5-dicarboxylic acid (FDCA). This furanic compound has been identified as a strategic renewable building block to replace petroleum derived terephthalic acid (TPA) in the production of polyesters.[6] Although the current conversion of furfurals into FDCA only reaches yields of 50–60%, this process is based on mild process conditions and requires low process energy requirements.[7,8]

Petrochemical PET currently has the largest market volume in bottles for water or beverages and it is also widely used in film applications for food trays and lids with a total world production capacity of over 65 million tons of virgin polymer a year.[9] While most PET is derived from petroleum, PET can also be partly bio-sourced at ~30% by using bio-based monoethylene glycol (bio-EG). However, the TPA monomer still remains petroleum derived due to both technical and economic constraints.[10,11] Since the production of FDCA and bio-EG utilizes renewable sugars, poly(ethylene 2,5-furandicarboxylate), more commonly termed poly(ethylene furanoate) (PEF), currently represents an appealing bio-mass derived replacement to petrochemical PET.[12] In this regard, Eerhart *et al.*[13] showed that replacing PET with PEF would reduce the non-renewable energy use by 40–50% and the greenhouse gas (GHG) emis-

[a]Department of Polymer Science and Technology, Institute for Polymer Materials (POLYMAT), Faculty of Chemistry, University of the Basque Country (UPV/EHU), Paseo Manuel de Lardizabal 3, 20018 Donostia, Spain. E-mail: haritz.sardon@ehu.es
[b]Novel Materials and Nanotechnology Group, Institute of Agrochemistry and Food Technology (IATA), Spanish National Research Council (CSIC), Calle Catedrático Agustín Escardino Benlloch 7, 46980 Paterna, Valencia, Spain
[c]Departament d'Enginyeria Química, Universitat Politècnica de Catalunya, Barcelona School of Industrial Engineering (ETSEIB), Diagonal 647, Barcelona, 8028, Spain
†Electronic supplementary information (ESI) available. See DOI: 10.1039/d0py01623c
‡This author is now with the Research Institute of Food Engineering for Development (IIAD), Universitat Politècnica de València (UPV), Camino de Vera s/n, 46022 Valencia, Spain (storresginer@upv.es).

6 Bio-nanosystems Resorting to Electrohydrodynamic Processing

Sergio Torres-Giner, Beatriz Melendez-Rodriguez, Adriane Cherpinski, and Jose M. Lagaron

CONTENTS

6.1 Introduction to Electrohydrodynamic Processing 103
6.2 Functionalization Techniques by Electrohydrodynamic Processing 107
6.2.1 Blending 107
6.2.2 Coaxial 108
6.2.3 Emulsion 108
6.3 Electrohydrodynamic Processing of Food-Grade Polymers 109
6.4 Bio-Nanosystems in the Food Industry 111
6.4.1 Antioxidants 112
6.4.2 Nutraceuticals 114
6.4.3 Flavors 115
6.4.4 Antimicrobials 116
6.4.5 Enzymes 117
6.4.6 Probiotics 119
6.5 Conclusions and Future Trends 120
References 121

6.1 INTRODUCTION TO ELECTROHYDRODYNAMIC PROCESSING

Over the past decade, electrohydrodynamic processing (EHDP) has gained a great interest in both scientific community and industry for fabrication of ultrathin polymer structures in the field of food technology (Echegoyen et al. 2017). EHDP is a straightforward, versatile, and low-cost technique that employs a high-voltage electrostatic field into a polymer solution or melt *via* a metallic capillary orifice to fabricate ultrathin polymer structures with diameters ranging from below 100 nm to above some microns (Reneker and Chun 1996). Polymer micro-, submicro-, and nanostructures obtained by EHDP offer notable physicochemical characteristics,

1

Emerging Trends in Biopolymers for Food Packaging

Sergio Torres-Giner, Kelly J. Figueroa-Lopez, Beatriz Melendez-Rodriguez, Cristina Prieto, Maria Pardo-Figuerez, and Jose M. Lagaron

Novel Materials and Nanotechnology Group, Food Safety and Preservation Department, Institute of Agrochemistry and Food Technology (IATA), Spanish Council for Scientific Research (CSIC), Calle Catedrático Agustín Escardino Benlloch 7, Paterna 46980, Spain

1.1 Introduction to Polymers in Packaging

According to the Food and Agriculture Organization of the United Nations (FAO), approximately one-third of all food produced globally is lost or wasted [1]. Food waste is produced throughout the whole food value chain, from the household to manufacturing, distribution, retail, and food service activities. Taking into consideration the limited natural resources available, it is more effective to reduce food waste than to increase food production. For this reason, several efforts have been put for the development of more effective food packaging strategies [2, 3]. Packaging items have become essential to protect food from different environmental conditions. Depending on the type of food, the packaging article can be customized to prevent or inhibit microbial growth, avoid food decomposition by removing the entrance of light, oxygen, and moisture, or even to prevent spoilage from small insects. Additionally, novel packaging items can be monitored to give information about the quality of the packaged food, ultimately diminishing food waste during distribution and transport [4].

Common materials utilized for food packaging include glass, paper, metal, and plastic. The latter are nowadays more frequently used since they have a large availability at a relatively low cost and can display good characteristics for packaging items, such as mechanical strength, barrier properties, and transparency [4, 5]. The most commonly used petrochemical materials for packaging applications can be divided into various families:

- Polyolefins and substitutes of olefins, such as low-density polyethylene (LDPE) and linear low-density polyethylene (LLDPE), polypropylene (PP), polystyrene (PS), oriented polystyrene (OPS), polyvinyl alcohol (PVOH), polyvinyl chloride (PVC), and polyvinylidene chloride (PVDC). Polyolefins are frequently used in reusable bags, paper cups, and stand-up pouches, while substitutes of olefins such as PVC are popularly used in cling films and in some prepackaged meals.

Sustainable Food Packaging Technology, First Edition. Edited by Athanassia Athanassiou.